JOURNAL OF BIOLOGICAL REGULATORS & HOMEOSTATIC AGENTS
Volume 33, No. 3, May - June, 2019

CONTENTS

EDITORIAL

THE MAST CELL – NEUROFIBROMATOSIS CONNECTION

D. ANTONOPOULOS[1,3], I. TSILIONI[3], N.A.A. BALATSOS[1], K.I. GOURGOULIANIS[2] and T.C. THEOHARIDES[3,4,5,6]

[1]Department of Biochemistry and Biotechnology, University of Thessaly, Biopolis, Larissa, Greece; [2]Department of Pulmonary Medicine, University of Thessaly, Biopolis, Larissa, Greece; [3]Molecular Immunopharmacology and Drug Discovery Laboratory, Department of Immunology, Tufts University School of Medicine, Boston, MA, USA; [4]Sackler School of Graduate Biomedical Sciences, Tufts University School of Medicine, Boston, MA, USA; [5]Department of Internal Medicine, Tufts University School of Medicine and Tufts Medical Center, Boston, MA, USA; [6]Department of Psychiatry, Tufts University School of Medicine and Tufts Medical CenterBoston, MA, USA

Received March 31, 2019 – Accepted April 15, 2019

Neurofibromatosis type 1 (NF1) is an autosomal dominant disorder affecting 1/3000 individuals worldwide (1, 2). It results from inactivating germline mutations of the neurofibromin gene belonging to the Schwann cell lineage and it is fully penetrant by the age of 5 (3). Neurofibromin is a 2818 amino acid protein that is produced in many cell types, but its levels are especially high in the nervous system (4). Neurofibromin is a potent negative regulator of RAS signaling, acting by promoting the hydrolysis of RAS bound GTP to GDP, converting RAS to its inactivated RAS-GDP state (3). Loss of neurofibromin function causes uncontrolled RAS activity, which results in increased cell proliferation and survival, thus causing nerve tumors known as neurofibromas (3). Subsequent gain of function mutations in RAS effector genes may cause neurofibromas to develop into an aggressive type of sarcoma known as "malignant peripheral nerve sheath tumors" (MPNST), which are the main cause of mortality in NF1 (5).

Ras and its downstream pathway proteins such as Rho, Rac and CDC42 GTPases, and their effectors, are known to promote biogenesis of extracellular vesicles (EVs), as well as regulate cargo selection and its release (6). Aside from the intercellular interactions mediated by soluble factors secreted by the various cell types, transfer of bioactive molecules (e.g DNA, RNA, proteins) also occuring through EVs can protect them from degradation and transfer them to specific target cells, especially in neuropsychiatric diseases (7). Increasing evidence indicates that EVs are involved in cancer, but their role in NF1 has not yet been studied.

Neurofibroma lesions are composed of many cell types: neurofibromin null-Schwann cells, including mast cells, fibroblasts and macrophages (8) (Fig. 1). The interplay between these cell types plays a fundamental role in controlling the tumor microenvironment and ultimately determining neurofibroma progression (8). A case in point is mast cells, which derive from the bone marrow, proliferate in response to stem cell factor (SCF, KIT ligand) and mature in tissues (9). Neurofibromin null (*NF1* -/-) Schwann cells secrete SCF (10), which mobilizes mast cells to infiltrate the neurofibroma site (11). There, mast cells secrete many angiogenic and mitogenic mediators (12), including nerve growth factor (NGF) (13) together with chondroitin sulfate

Key words: mast cell; neurofibromatosis

Corresponding Author:
T.C. Theoharides, MS, MPhil, PhD, MD
Molecular Immunopharmacology and Drug Discovery,
Department of Immunology, Tufts University School of Medicine,
136 Harrison Avenue Boston, MA, 02111, USA
Tel.: +1 617 636 6866 - Fax: +1 617 636 2456
e-mail: theoharis.theoharides@tufts.edu

0393-974X (2019)

DISCLOSURE: ALL AUTHORS REPORT NO CONFLICTS OF INTEREST RELEVANT TO THIS ARTICLE.

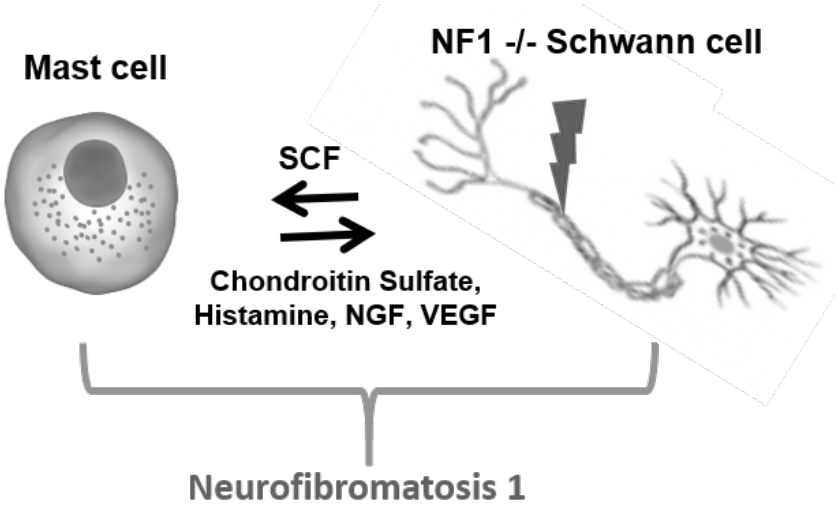

Fig. 1. *Diagrammatic representation of mast cell-Schwann cell interactions in the pathogenesis of Neurofibromatosis 1.*

(CS) (14) which binds to NGF and significantly increases its half-life (15). NGF can propagate tumor survival and proliferation (13), but can also have an autocrine action on mast cells to stimulate secretion of more biologically active mediators (16), completing a positive feedback autocrine circuit with mast cell-associated vascular endothelial growth factor (VEGF) (17), permitting neovascularization (5) and cancer growth (18). In addition, infiltrating mast cells secrete TGF-beta that mediates the recruitment and subsequent activation of fibroblasts in neurofibroma lesions, further contributing to the progression of the disease (19).

In fact, mast cells have been repeatedly shown to accumulate in tumor sites caused by many malignant diseases including pancreatic cancer; once they infiltrate, instead of degranulating and releasing TNF, they release VEGF and promote cancer growth (20, 21). Mast cells release EVs (22) that could contain molecules that affect Schwann cell growth. It is interesting that the main trigger of mast cell IgE, has been reported to be elevated in NF1 patients (23).

CONCLUSION

Unfortunately, available treatments for neurofibroma are still inefficient (24). Mast cells have been increasingly implicated in neuro-immune interactions (25, 26), hence inhibiting mast cells may prove to be a useful therapeutic approach. In fact, a number of drugs inhibiting mast cell symptoms or proliferation have been reported to be beneficial in NF1. For instance, the H1-histamine receptor antagonist ketotifen (27), the anti-allergic drug Tranilast (28), and the KIT inhibitor imatinib (24) were shown to reduce neurofibroma growth. Other potential options could include the natural flavonoid methoxyluteolin, which has been shown to inhibit human mast cells, and activation of the mammalian target of rapamycin (mTOR) (29), or the anti-inflammatory cytokine IL-37 (30-32).

REFERENCES

1. Gutmann DH, Ferner RE, Listernick RH, Korf BR, Wolters PL, Johnson KJ. Neurofibromatosis type 1. Nat Rev Dis Primers 2017; 3:17004.
2. Uusitalo E, Leppavirta J, Koffert A, et al. Incidence and mortality of neurofibromatosis: a total population study in Finland. J Invest Dermatol 2015; 135(3):904-6.
3. Cimino PJ, Gutmann DH. Neurofibromatosis type 1. Handb Clin Neurol 2018; 148:799-811.
4. Abramowicz A, Gos M. Neurofibromin in neurofibromatosis type 1 - mutations in NF1gene as a cause of disease. Dev Period Med 2014; 18(3):297-306.
5. Vasconcelos RAT, Guimaraes CP, Vieira TM, Noguera WS, Rapozo DCM, Acioly MA. Prognostic significance of mast cell and microvascular densities in malignant peripheral nerve sheath tumor with and without neurofibromatosis type 1. Cancer Med 2019; 8(3):972-81.

6. Sexton RE, Mpilla G, Kim S, Philip PA, Azmi AS. Ras and exosome signaling. Semin Cancer Biol 2019; 54:131-37.
7. Tsilioni I, Panagiotidou S, Theoharides TC. Exosomes in neurologic and psychiatric disorders. Clin Ther 2014; 36(6):882-88.
8. Carroll SL. The challenge of cancer genomics in rare nervous system neoplasms: malignant peripheral nerve sheath tumors as a paradigm for cross-species comparative oncogenomics. Am J Pathol 2016; 186(3):464-77.
9. Theoharides TC, Valent P, Akin C. Mast cells, mastocytosis, and related disorders. N Engl J Med 2015; 373(2):163-72.
10. Yang FC, Ingram DA, Chen S, et al. Neurofibromin-deficient Schwann cells secrete a potent migratory stimulus for Nf1+/- mast cells. J Clin Invest 2003; 112(12):1851-61.
11. Staser K, Yang FC, Clapp DW. Mast cells and the neurofibroma microenvironment. Blood 2010; 116(2):157-64.
12. Mukai K, Tsai M, Saito H, Galli SJ. Mast cells as sources of cytokines, chemokines, and growth factors. Immunol Rev 2018; 282(1):121-50.
13. Leon A, Buriani A, Dal TR, et al. Mast cells synthesize, store, and release nerve growth factor. Proc Natl Acad Sci U S A 1994; 91(9):3739-43.
14. Gross AR, Theoharides T.C. Chondroitin sulfate inhibits secretion of TNF and CXCL8 from human mast cells stimulated by IL-33. Biofactors 2018;1-13.
15. Brittis PA, Canning DR, Silver J. Chondroitin sulfate as a regulator of neuronal patterning in the retina. Science 1992; 255:733-736.
16. Kritas SK, Caraffa A, Antinolfi P, et al. Nerve growth factor interactions with mast cells. Int J Immunopathol Pharmacol 2014; 27(1):15-19.
17. Donelan J, Boucher W, Papadopoulou N, Lytinas M, Papaliodis D, Theoharides TC. Corticotropin-releasing hormone induces skin vascular permeability through a neurotensin-dependent process. Proc Natl Acad Sci USA 2006; 103:7759-64.
18. Ribatti D, Crivellato E, Roccaro AM, Ria R, Vacca A. Mast cell contribution to angiogenesis related to tumour progression. Clin Exp Allergy 2004; 34:1660-64.
19. Yang FC, Chen S, Clegg T et al. Nf1+/_ mast cells induce neurofibroma like phenotypes through secreted TGF-beta signaling. Hum Mol Genet 2007; 15(16):2421-37.
20. Theoharides TC. Mast cells and pancreatic cancer. N Engl J Med 2008; 358(17):1860-61.
21. Karamitopoulou E, Shoni M, Theoharides TC. Increased number of non-degranulated mast cells in pancreatic ductal adenocarcinoma but not in acute pancreatitis. Int J Immunopathol Pharmacol 2014; 27(2):213-20.
22. Skokos D, Botros HG, Demeure C, et al. Mast cell-derived exosomes induce phenotypic and functional maturation of dendritic cells and elicit specific immune responses in vivo. J Immunol 2003; 170(6):3037-45.
23. Geller M, Ribeiro MG, Araujo AP, de Oliveira LJ, Nunes FP. Serum IgE levels in neurofibromatosis 1. Int J Immunogenet 2006; 33(2):111-15.
24. Walker JA, Upadhyaya M. Emerging therapeutic targets for neurofibromatosis type 1. Expert Opin Ther Targets 2018; 22(5):419-37.
25. Skaper SD. Nerve growth factor: a neuroimmune crosstalk mediator for all seasons. Immunology 2017; 151(1):1-15.
26. Forsythe P. Mast Cells in Neuroimmune Interactions. Trends Neurosci 2019; 42(1):43-55.
27. Rodriguez-Jimenez P, Chicharro P, Munoz E, Dauden E. Long-term treatment of neurofibromatosis 1 with ketotifen. A report of three cases. Am J Med Genet A 2016; 170A(4):1092-94.
28. Yamamoto M, Yamauchi T, Okano K, Takahashi M, Watabe S, Yamamoto Y. Tranilast, an anti-allergic drug, down-regulates the growth of cultured neurofibroma cells derived from neurofibromatosis type 1. Tohoku J Exp Med 2009; 217(3):193-201.
29. Patel AB, Theoharides TC. Methoxyluteolin Inhibits Neuropeptide-stimulated Proinflammatory Mediator Release via mTOR Activation from Human Mast Cells. J Pharmacol Exp Ther 2017; 361(3):462-71.
30. Dinarello CA, Nold-Petry C, Nold M, et al. Suppression of innate inflammation and immunity by interleukin-37. Eur J Immunol 2016; 46(5):1067-81.
31. Tettamanti L, Kritas SK, Gallenga CE, et al. IL-33 mediates allergy through mast cell activation: Potential inhibitory effect of certain cytokines. J Biol Regul Homeost Agents 2018; 32(5):1061-65.
32. Mastrangelo F, Frydas I, Ronconi G, et al. Low-grade chronic inflammation mediated by mast cells in fibromyalgia: role of IL-37. J Biol Regul Homeost Agents 2018; 32(2):195-98.

EDITORIAL

OCCUPATIONAL ALLERGY: IS THERE A ROLE FOR NANOPARTICLES?

L. DI GIAMPAOLO[1-2], M. DI GIOACCHINO[1,3], R. MANGIFESTA[1], A. GATTA[3], N. TINARI[3], A. GRASSADONIA[3], Q. NIU[4], R. PAGANELLI[3], E. SABBIONI[1], T. OTSUKI[5] and C. PETRARCA[1]

[1]Allergy and Immunotoxicology & Occupational Biorepository - Ce.S.I. - Center of Excellence on Aging, Chieti, Italy; [2]Department of Medical, Oral and Biotechnological Sciences, G. d'Annunzio University, Chieti, Italy; [3]Department of Medicine and Science of Ageing, G. d'Annunzio University, Chieti, Italy; [4]Public Health School of Shanxi Medical University, Taiyuan, PR China; [5]Department of Hygiene, Kawasaki Medical School, Kurashiki, Japan

Received January 9, 2019 – Accepted February 26, 2019

All fields of industry are applying nanotechnologies for the development of advanced materials, therefore at present the number of workers exposed to nanosized materials are significantly increasing. Unfortunately, protective equipment for nanoparticles (NPs) is of uncertain efficacy so the risk of noxious effects, in particular allergic sensitization, on workers gives many concerns. At the same time, studies of allergic physiopathology demonstrated that the lack of prevention and treatment could result in invalidating diseases that, in case of professional etiology, might imply removal from the job and compensation. Therefore, a deeper knowledge of the role of NPs in inducing allergic diseases is mandatory to implement the risk assessment and preventive measures for nanosafety in the workplace. The possibility that NPs favor, exacerbate or directly induce allergy is being suggested by recent experimental investigations in cellular and animal models. Unfortunately, studies are heterogeneous and few data have received experimental confirmation, lacking reproducibility. What comes to attention is the uncertainty about the real plausibility of the observed experimental effects, as there are only a few reported cases of allergy onset or exacerbation for workers exposed to NPs. However, the potential for NPs to induce, favor or exacerbate allergies seems possible even though not completely demonstrated. This should be a greater incentive to carry out appropriate epidemiological studies that are lacking and really needed.

Nanomaterials, both engineered (intentionally designed with specific properties for a wide range of technological applications) and incidental (generally with poorly controlled sizes and shapes, and frequently made of a hodgepodge of different elements) are increasingly produced and used in various consumer and industrial products due to their peculiar properties. While enhanced functionality is achieved due to nanospecific properties, nanoparticles (NPs) can be released into the environment over the entire life cycle of nano-enabled products with potential harmful consequences. In fact, they can interact with biological substrates, possibly participating in the pathogenesis of some diseases, and are hypothesized to induce or facilitate the occurrence of immune-related disorders (1-3). Among these, allergy is the

Key words: nanomaterials; nanoparticles; allergy; occupational; workers; nanosafety; health surveillance; research

Corresponding Author:
Prof. Mario Di Gioacchino,
Department of Medicine and Science of Ageing,
G. d'Annunzio University,
Via dei Vestini, 66100 Chieti, Italy
Tel.: +39 871 541290/38
e-mail: mario.digioacchino@unich.it

0393-974X (2019)

most frequent as it affects about one-third of the general population, and subjects with an occupational cause have a prevalence ranging from 5 to 15% of those exposed. Moreover, diseases of occupational allergic etiology have a worse prognosis than non-professional ones; for example, occupational allergic asthma has a more severe pulmonary function decline that non-occupational allergic asthma, even when the causal agent has been removed or reduced (4).

Unfortunately, occupational health risks associated with nanomaterials are still undefined: only few studies are available regarding workplace air monitoring of nanoparticle production and little information is available on main exposure routes, potential exposure levels, and toxicity. While under normal circumstances NP emissions to the workplace are very limited, NP indoor concentrations are increased during bagging, packaging, or cleaning of process equipment or during accident situations in laboratories with accidental NP emissions.

NPs are present in biological fluids as aggregates and agglomerates, rather than isolated NPs, and they are hard to split apart because of their shape and electrostatic charge. Therefore, assessing these "multi-nanoparticle" entities by the current measuring devices is difficult and, most importantly, it is unknown to which extent they can break up into smaller units and release ions. Further difficulties come from the fact that airborne chemicals can be adsorbed onto NPs that can gain new bioactive functions, such as PM 0.5 (which include NPs) in industrial and traffic-influenced urban areas. It is well established that NPs can enter the human body (upon exposure) through inhalation, ingestion and absorption through the skin and reach tissues and cells through the circulation. Macrophages, epithelial and endothelial cells (the NP capturing cells) spread them into the blood stream and other cell types and tissues. 40% of pre-shift and 70% of the post-shift samples of exhaled breath condensate of production workers contain airborne titanium dioxide-NPs; 10% of the post-shift urine samples contained NPs, demonstrating that these NPs transit through the body (5). Many biologic properties (toxicity, immunomodulatory capacity) are dependent from ions released by NPs (6, 7). Biological activity of NPs, microparticles and ions of the same compound is different. In fact, BALB/c 3T3 fibroblasts undergo a higher degree of cell death when exposed to cobalt-NPs rather than microparticles and ions [Co(II)] (7, 8) whereas only micro- and NPs have morphological transforming potential (8). Moreover, also NP size (5 nm, 20 nm, 50 nm), aggregation tendency and capacity to form complexes with proteins (protein corona) contribute to determine the biological impact of NPs (2).

Allergy refers either to type I immune reaction characteristically mediated by a Th2 cytokine pattern or to type IV immune reaction where the Th1 cytokines are involved. Some metallic NPs have modulatory effects on the immune system (1, 2) and can influence the pattern of released cytokines, favoring or inhibiting Th2 or Th1 pattern of cytokines (3, 9, 10). Starting from data showing the increasing prevalence of occupational allergic diseases, the increasing application of nanomaterials in industries and the environment and the immunomodulatory effects of many nanoparticles, exploring the role of nanoparticles in favoring/inducing allergic sensitization in exposed workers is essential. In the last decade, many authors reviewed the relationship between NPs and the occurrence of allergic diseases, each underlying some aspect of these relationships. However, it is essential to have a general view of the problem in order to determine the plausibility of NP-induced (or favored) occupational allergy and the needs for future research.

Role of NPs in allergic sensitization

Allergic sensitization is a phenomenon starting from presentation of an antigen by dendritic cells and macrophages, acting as antigen presenting cells (APC), to T lymphocytes which, in the case of the type I immune reaction, proliferate and differentiate into Th2 cells, with upregulation of proallergenic cytokines IL4, IL13 and IL5 and reduction of regulatory cytokines, such as IL10, leading to allergen specific IgE production by B lymphocytes. In the case of the type IV immune reaction, T lymphocytes proliferate and differentiate in Th1 cytokine producing cells and cytotoxic T lymphocytes. These processes are induced by antigens of high molecular weight or

by low molecular weight haptens that bind to protein to form a complete antigen. Also NPs can interact with APCs (1), which detect and bind NPs by Toll-like receptors through which they deliver signals depending on NP size (2). NPs may act as haptens, since they bind to proteins and induce conformational changes exposing cryptic epitopes which might trigger immune responses, including allergy.

The possibility that NPs can interact with cells of the Th2 immune reactions has been reviewed recently (1, 2, 9, 11-13), and *in-vitro* and animal experiments suggest the possibility that NPs influence allergic sensitization. In animals, multi-walled carbon nanotube induces activation of alveolar macrophages and favors secretion of Th2 cytokines and the production of IgE by B lymphocytes. Fullerenes are able to activate the immune system with the final production of immunoglobulins. Subcutaneous or inhalant administration of carbon black-NPs (22 and 39 nm) to transgenic mice expressing the T cell receptor specific for the immunodominant peptide of ovalbumin (OVA) favors sensitization. In this animal model, carbon black-NPs and carbon nanofibres also showed a Th2 adjuvant effect, promoting allergic airway responses to allergens. The particle size correlates with the intensity of secondary responses induced in peptide-restimulated splenocytes *in vitro* that are characterized by increase of IL-4, IL-10 and IL-13, and reduced expression of Stat4, specific for Th1 cells.

There are many studies demonstrating that, besides a direct sensitization, NPs have an adjuvant effect, which may favor allergen sensitization. In fact, many NPs [carbon nanotubes (CNT), multi walled CNT (MWCNTs), silica-NPs, zinc oxide-NPs, nickel oxide-NPs], in particular when inhaled or instilled into the trachea, facilitate allergic sensitization and worsening of the allergic airway inflammation through the increase in Th2 cytokine pattern and activation of inflammatory cells.

The effects of other NPs are slightly more complex, seeming in some cases contradictory. In fact, TiO2-NPs, regarded as relatively non-toxic at the concentration of the occupational environments, favor allergic reactions only following parenteral or dermal exposure on compromised skin. In asthmatic rats, they inhibit IL4 release and the eosinophilic infiltration of the lung induced by allergens. On the contrary, in non-sensitized rats, intratracheally-instilled TiO_2-NPs provokes acute airway inflammation with transient IL-4 production, replaced by a durable Th1 response. In a mouse model, the same component instilled at 5-50 $mg \cdot kg^{-1}$ (150 μm aggregate mean size) induced a Th2-mediated chronic inflammation, showing a species-related bias of the immune response.

The adjuvant effect, as the direct effect, on Th2 sensitization is size dependent, in fact, subtoxic concentrations of 5 nm silver NPs (but not of 100 nm) induce *in-vitro* granule release by mast cells, with an increase in the level of intracellular Ca^{++} (via the generation of oxidative stress). The co-exposure of the same NPs and allergens, in mice with dermatitis, induces an increase in the number of tryptase-positive mast cells in the skin with early and severe clinical symptoms. These effects are not obtained with 100 nm silver NPs. In fact, NP size, beside their chemical composition, has an influence on the type of immune response, with bigger particles (>100 nm) more prone to induce a Th2 response, whereas smaller particles (~50 nm) induce rather a Th1 response.

Other NPs, such as Palladium and MWCNTs, induce secretion of high levels of IFN-γ, while inhibiting the tolerogenic cytokine IL-10, suggesting a potential role in the Th1-mediated mechanism of delayed allergic reactions (3, 10).

Nanoparticle worsening established allergy

In general, as shown above, NPs that favor allergic sensitization also interact with the major effector cells of allergy and therefore have the potential of worsening already established allergies. The above-cited reviews underlined that NP effects essentially depend on their chemical composition, their dose, shape and size and the timing of exposure.

The direct implication of NPs in the exacerbation of pre-existing type I allergy has been shown essentially in allergen-sensitized animals. Intratracheally administered silicon dioxide-NPs (non spherical, 10-20 nm, 140-180 $m^2 \cdot g^{-1}$) induced dose-dependent airway remodeling and worsening of the respiratory parameters along with

increase of IL-4 in the lung tissue. A very low dose (approx. 0.8 mg·kg-1) of intrapulmonary gold- or titanium dioxide-NPs modulate a non-IgE-mediated pulmonary inflammation and airway hyperreactivity (AHR) in a mouse model of diisocyanate-induced asthma.

In OVA-sensitized animals, but not in non-sensitized, inhaled Silver-NPs (3.3 $mg \cdot m^{-3}$) induced elevation of mediators and effectors of the allergic response (total IgE, Leukotriene 4, Th2 cells, IL-13 and oxidative stress) a significant increase in allergen-specific IgE and of vascular endothelial growth factor signaling pathway with mucus hypersecretion. Similarly, copper oxide NPs exacerbate asthma, in particular enhancing airway hyperreactivity, inflammatory cell counts, cytokines, IgE, and local reactive oxygen species production. In a murine model of diisocyanate-induced asthma, TiO2 and Au NP exposure led to a dramatic increase in AHR and in bronchoalveolar lavage (BAL) total cell counts along with a worsening of bronchial edema, epithelial damage and inflammation. However, conflicting evidence regarding the impact of Au NPs on pre-existing asthma has been reported; some authors demonstrated that Au NPs decrease inflammatory cell lung accumulation,—mucus production, and cytokine levels in a model of OVA-induced allergic asthma.

The timing of exposure is important as it determines the effect of NP exposure. TiO2/OVA-exposed mice, either during sensitization or between the OVA sensitization and challenge phases, have a worsening of AHR and eosinophilia along with an increase in Th2 cytokines IL-4, IL-13, and IL-5 and, but no effects were observed when TiO2 was given later.

Also the shape of NPs seems to influence their activity, in fact, in OVA-sensitized mice spherical and mesoporous (but no PEGylated) silica NPs induced bronchial inflammation, in particular, spherical NPs were generally the most inflammatory, causing enhanced eosinophilia and AHR when NPs were given during the challenge phase, whereas, mesoporous silica NPs were more inflammatory than spherical when repeatedly given during both sensitization and challenge (14).

A further important variable for the effect of NP on allergy, in particular allergic asthma, is the NP size. For example, 14-nm diameter carbon black NPs cause an increase in the number of lung dendritic cells, macrophages, and B cells in OVA-sensitized mice, whereas no effects were elicited in this model by the larger 56-nm NPs.

The literature on the effects of carbon nanotubes in animal models of allergic asthma is extensive. MWCNTs enhanced the development of airway fibrosis (airway collagen thickness) with IL-5 and the profibrotic cytokine platelet-derived growth factor-AA was significantly enhanced in a model of OVA-induced asthma. Other authors found that MWCNTs induced increase in bronchial hyperreactivity, eosinophilia, serum IgE, and IL-4 of bronchoalveolar lavage fluid in a similar animal model, with a more potent activity when administered with the allergen.

NPs may have a direct role in the development of bronchial asthma, since silicon dioxide-NPs are able to induce asthma-like symptoms with or without OVA immunization. Is eosinophil cell count in early childhood wheezing predictive of future asthma?

Nanoparticles and occupational allergic diseases

A great number of workers are exposed to NPs, in particular by inhalation and skin contact. To date, few studies have reported the potential sensitization/aggravating effects of NPs or NP-associated allergens. Epidemiological data show that palladium allergic contact dermatitis has increased in the last decades in people living in urban areas where NPs of "platinum group elements" and carbon particles are released by catalytic converters (15). Studies conducted on combustion-derived particles are somewhat conflicting. Volunteers exposed to diesel exhaust particulate (DEP) containing NPs (at $>10^6$ $particles \cdot cm^{-3}$, far exceeding the worst-case exposure for workers) showed transient lung and systemic inflammation, but no evidence of a unique toxicity for NPs and not supporting acute toxicity of NPs by virtue of their exclusive nano-size (at least within DEP) (13). On the contrary, there is also a good deal of evidence that CNTs, one of the most extensively studied nanomaterials in relation to asthma, can elicit allergic lung responses directly (11) or can promote asthma susceptibility (16) in people living in urban areas.

The interaction of allergens with engineered NPs, such as Au, Ag, ZnO, TiO2, SiO2, may occur at sites where such materials are handled, therefore (risk of) disease-aggravating conditions can be expected in occupational settings.

Apart from outdoor workers exposed to accidental airborne NPs (deriving from industries, vehicular traffic, various forms of combustion etc.) those in NP manufacturing or using them in different productions are exposed to potentially dangerous effects of engineered NPs. From an allergological point of view, exposed workers are at risk of developing nanoparticle-induced allergic pathologies, or exacerbating pre-existing allergic conditions. Moreover, it is conceivable that adverse health effects may develop in already hypersensitive populations, such as individuals with respiratory or cutaneous allergic diseases.

At present, data on the immune effects of occupational exposure to NPs are very limited and essentially based on limited case reports.

In 2009, polyacrylate-NP exposure was correlated with the appearance of pleural effusions and dyspnea experienced in seven healthy NP-occupationally exposed women. NPs were found in cells and chest fluid associated with lung inflammation, fibrosis and granuloma of the pleura (17).

Throat congestion, flushing of the face, rhinitis and erythema multiforme-like was diagnosed in a 22-year-old chemist involved in work leading to synthesis of dendrimers (nanosized particles used as drug carriers). Allergy testing resulted positive for nickel, and spirometry revealed bronchial hyperreactivity. Professional re-exposure after a 3-week period of absence from work and steroid treatment induced the recurrence of symptoms. (18).

A healthy 26-year-old non-smoking female occupationally exposed (without any personal protection) to dry nickel-NP (20 nm, 40-60 $m^2 \cdot g^{-1}$) powder developed throat congestion with postnasal drip, flushing of the face and skin reactions to earrings and belt buckle, never presented previously. The patch test was positive for nickel sulphate allergy (19).

An epidemiologic questionnaire-based study showed that sneezing (as a work-related effect) and allergic contact dermatitis (as worsened symptoms) were reported by workers handling various types of NPs (silver, iron, gold, titanium, silicon, carbon) (20).

A study on the prevalence of allergies was conducted in U.S. facilities handling carbon nanotubes and nanofibres (CNT/F, >5 μm long, <100 nm diameter). 18% of participant workers had evidence of CNT/F in sputum. Respiratory allergy appearance was positively associated to the relevance of the exposure ($p=0.040$) and number of years worked with CNT/F ($p=0.008$) (21).

A study on 416 workers in Taiwan exposed to nanomaterials found a significant association between NP exposure (in particular TiO_2) and fractional exhaled nitric oxide (FENO) in a multivariate linear regression analysis. Furthermore, asthma, allergic rhinitis, peak expiratory flow rate (PEFR), and NF-κB in exhaled breath condensate were also significantly associated with FENO (22).

DISCUSSION

Ambient air pollution has been associated with increase in allergic diseases: in particular some of their components, such as ozone, nitrogen dioxide and particulate matter (PM), can influence the immune system (23, 24). Epidemiological evidence suggests that both fine and ultrafine PM is associated with allergy and asthma, particle size being an important toxicological factor. Naturally then, with the advent of nanotechnology, physicians have become interested in examining the effects that engineered nanomaterials may have on the immune system.

Whatever form and chemical species they acquire inside the body, engineered NPs can induce oxidative stress attributable to their particulate physical form. The pro-inflammatory activity shown by most nanomaterials makes plausible the hypothesis that the occupational exposure might provide stimuli able to trigger pathological conditions and in particular immune related diseases.

Metals (e.g., cobalt, platinum, chromium, vanadium, nickel) are well known occupational sensitizers able to induce allergic asthma. Many

observations show that also nanosized metals, in particular in *in-vitro* and animal studies, own pro-sensitizing effects, suggesting their potential role in the development of professional immune disease-like allergy (both respiratory and cutaneous) as NPs can act as haptens or as a source of metal ions once inside the body. Pro-sensitizing effects might be worrying for all workers of industries producing nanomaterials, and in particular for those of pharmaceutical industries producing nanovaccines made of NPs loaded with immunogenic proteins to be used for immunotherapy or functionalized on the surface to generate immunoactivating compounds. Even more, animal studies show that NPs has a role in exacerbating allergic diseases.

However, both *in-vitro* and in-animal studies are heterogeneous and few data have received experimental confirmation. The evidence from *in-vitro* studies is that nanoparticles are able to interact with the immune system as they can modulate the cytokine/chemokine secretion and membrane receptor signaling in inflammatory cells, their cytotoxic activity and their number or activation state. Unfortunately, studies rarely compare the immune effects of NPs with the corresponding non-nano matter. For example the effects of metal NPs should be compared with those induced by the corresponding microparticles and ions, to better distinguish the role of dimension from the chemical nature of the NPs. Problematic aspects of studies on NP immune effects are summarized in Table I.

In general, some NPs have the potential to induce *in-vitro* immunosuppression, while others are associated with hypersensitive reactions (autoimmunity and allergies). Animal studies seem to confirm this possibility as the increases in Th2 cytokines are associated in mouse experiments with allergic manifestation. However, experimental results of NPs in animals are not definitive proof of their activity on humans and what is noticeable from the revision of the literature is the lack of human data. Published works refer essentially to case reports and there are no qualified epidemiological studies showing the immune-toxic effects of nanoparticles in the work setting. At present, the extent to which NPs represent a health problem at low levels for workers remains unexplored: it appears that NPs have few adverse effects on humans and it can be speculated that when NP exposure coincides with an infectious or malignant challenge, the odds of progressing into infection, hypersensitivity, or cancer can be changed. Likely, the enormous overcapacity of immune defense, the presence of compensatory mechanisms, and their fast restoration each contribute to limiting health threats for humans.

Studies on humans are difficult to assess essentially for two main reasons: challenge studies are not feasible on man, and in the environment NPs are contaminated with other numerous substances that modulate their activity.

Table I. *Problematic aspects of studies on NP-induced allergies.*

***In vitro* and in animal studies**	**Human studies**
Heterogeneity of experimental conditions	Difficulties in the characterization of NP exposure
Heterogeneity of used NPs (shape, size, composition)	Literature is based essentially on case reports of few patients
Few data have experimental confirmations	No long term epidemiological studies
Lack of reproducibility	No qualified epidemiological studies
Few studies compared NPs with related non- nano matter	No prospective observational studies
Extreme variability of target cells	
Short term exposure	

It is clear that data collected to date come from heterogeneous experimental studies that are affected by a bias due to the poor characterization of nanomatter once it reaches the human biologic matrices. In fact, although a precise characterization can be obtained for the manufactured nanomaterial products, upon interaction of nanoparticles with the organism the newly acquired properties are virtually not predictable and rather complex to measure (by using radioactive nanomaterials, for instance). This makes an unequivocal assessment of a cause-effect relationship difficult to obtain. Moreover, high doses and short time of exposure are applied in animal studies, whereas, the level of contamination expected in the workplace would resemble a chronic low dose exposure.

However, the workplace could represent an outstanding experimental setting because the level and the condition of exposure are well measurable and the health surveillance program for workers might provide the follow-up data to identify the onset and progression of possible occupational diseases. Among these, allergy, being one of the epidemics of the century and one of the most prevalent diseases in workers, should be carefully evaluated in terms of risks induced by NPs. For this purpose, only long-term observational studies will offer the possibility to determine the real allergic-related (and not allergic) risk from NPs. Health surveillance along with environmental monitoring will be the key phases in this endeavor.

REFERENCES

1. Petrarca C, Clemente E, Amato V, et al. Engineered metal based nanoparticles and innate immunity. Clin Mol Allergy 2015; 13:13. doi:10.1186/s12948-015-0020-1.
2. Alsaleh NB, Brown JM. Immune responses to engineered nanomaterials: Current understanding and challenges. Curr Opin Toxicol 2018; 10:8-14
3. Petrarca C, Perrone A, Verna N, et al. Cobalt nano-particles modulate cytokine in vitro release by human mononuclear cells mimicking autoimmune disease. Int J Immunopathol Pharmacol 2006; 19:11-14.
4. Di Giampaolo L, Cavallucci E, Braga M, et al. The persistence of allergen exposure favors pulmonary function decline in workers with allergic occupational asthma. Int Arch Occup Environ Health 2012; 85:181888.
5. Pelclova D, Barosova H, Kukutschova J, et al. Raman microspectroscopy of exhaled breath condensate and urine in workers exposed to fine and nano TiO2 particles: a cross-sectional study. J Breath Res 2015; 9:036008.
6. Petrarca C, Clemente E, Di Giampaolo L, et al. Palladium nanoparticles induce disturbances in cell cycle entry and progression of peripheral blood mononuclear cells: paramount role of ions. J Immunol Res 2014; 2014:295092.
7. Sabbioni E, Fortaner S, Farina M, et al. Interaction with culture medium components, cellular uptake and intracellular distribution of cobalt nanoparticles, microparticles and ions in Balb/3T3 mouse fibroblasts. Nanotoxicology 2014; 8:88-99.
8. Sabbioni E, Fortaner S, Farina M, et al. Cytotoxicity and morphological transforming potential of cobalt nanoparticles, microparticles and ions in Balb/3T3 mouse fibroblasts: an in vitro model. Nanotoxicology 2014; 8:455-64.
9. Meldrum K, Guo C, Marczylo EL, Gant TW, Smith R, Leonard MO. Mechanistic insight into the impact of nanomaterials on asthma and allergic airway disease. Part Fibre Toxicol 2017; 14:45.
10. Boscolo P, Bellante V, Leopold K, et al. Effects of palladium nanoparticles on the cytokine release from peripheral blood mononuclear cells of non-atopic women. J Biol Regul Homeost Agents 2010; 24:207-14.
11. Himly M, Mills-Goodlet R, Geppert M, Dusci A. Nanomaterials in the Context of Type 2 Immune Responses-Fears and Potentials. Front Immunol 2017; 8:471. doi: 10.3389/fimmu.2017.00471
12. Morimoto Y, Izumi H, Kuroda E. Significance of persistent inflammation in respiratory disorders induced by nanoparticles. J Immunol Res 2014; 962871. doi: 10.1155/2014/962871
13. Ihrie MD, Bonner JC. The toxicology of engineered nanomaterials in asthma. Curr Environ Health Rep. 2018; 5(1):100-9.
14. Park HJ, Sohn JH, Kim YJ, et al. Acute exposure to silica nano-particles aggravate airway inflammation:

different effects according to surface characteristics. Exp Mol Med 2015; 47:e173.
15. Santucci B, Valenzano C, de Rocco M, et al. Platinum in the environment: frequency of reactions to platinum-group elements in patients with dermatitis and urticaria. Contact Dermatitis 2000; 43:333-38.
16. Li N, Georas S, Alexis N, et al. A work group report on ultrafine particles (American Academy of Allergy, Asthma & Immunology): Why ambient ultrafine and engineered nanoparticles should receive special attention for possible adverse health outcomes in human subjects. J Allergy Clin Immunol. 2016; 138:386-96.
17. Song Y, Li X, Du X. Exposure to nanoparticles is related to pleural effusion, pulmonary fibrosis and granuloma. Eur Respir J 2009; 34:559-67.
18. Toyama T, Matsuda H, Ishida I, et al. A case of toxic epidermal necrolysis-like dermatitis evolving from contact dermatitis of the hands associated with exposure to dendrimers. Contact Dermatitis 2008; 59:122-23.
19. Journeay WS, Goldman RH. Occupational handling of nickel nanoparticles: a case report. Am J Ind Med 2014; 57:1073-76.
20. Liao HY, Chung YT, Lai CH, Lin MH, Liou SH. Sneezing and allergic dermatitis were increased in engineered nanomaterial handling workers. Ind Health 2014; 52:199-215.
21. Schubauer-Berigan MK, Dahm MM, Erdely A, et al. Association of pulmonary, cardiovascular, and hematologic metrics with carbon nanotube and nanofiber exposure among U.S. workers: a cross-sectional study. Part Fibre Toxicol 2018; 15:22.
22. Wu WT, Liao HY, Chung YT, et al. Effect of nanoparticles exposure on fractional exhaled nitric oxide (FENO) in workers exposed to nanomaterials. Int J Mol Sci 2014; 15:878-94
23. Baldacci S, Maio S, Cerrai S, et al. Allergy and asthma: effects of the exposure to particulate matter and biological allergens. Respir Med 2015; 109:1089-104
24. Boscolo P, Di Gioacchino M, Sabbioni E, et al. Lymphocyte subpopulations, cytokines and trace elements in asymptomatic atopic women exposed to an urban environment. Life Sci 2000; 67:1119-26.

EDITORIAL

IMPACT OF MAST CELLS IN SYSTEMIC LUPUS ERYTHEMATOSUS: CAN INFLAMMATION BE INHIBITED?

Al. CARAFFA[1], C.E. GALLENGA[2], S.K. KRITAS[3], G. RONCONI[4] and P. CONTI[5]

[1]School of Pharmacy, University of Camerino, Camerino, Italy; [2]Department of Biomedical Sciences and Specialist Surgery, Section of Ophthalmology, University of Ferrara, Ferrara, Italy; [3]Department of Microbiology and Infectious Diseases, School of Veterinary Medicine, Aristotle University of Thessaloniki, Macedonia, Greece; [4]Clinica dei Pazienti del Territorio, Fondazione Policlinico Gemelli, Rome, Italy; [5]Postgraduate Medical School, University of Chieti, Chieti, Italy

Received February 23, 2019 – Accepted April 17, 2019

Systemic lupus erythematosus (SLE), is a complex chronic inflammatory autoimmune disease, with rheumatological manifestations, which afflicts mainly women (1). SLE presents various heterogeneous clinical aspects and different pathogeneses and involves the production of anti-DNA autoantibodies which are deposited as immune complexes in various organs and tissues, provoking inflammation (2). These diseases cause multiple tissue and organ damage in arthritis, skin lesions, hematologic changes, renal and neurologic disorders, and others (Table I). In SLE, serum contains anti-nucleus antibodies and anti-DNA antibodies that can be important biomarkers for patients suffering from this disease (3).

Cytokines mediate inflammatory and immune reactions, they communicate between cells of the immune system and contribute to the pathogenesis of autoimmune diseases, including SLE (4). There is increasing evidence that cytokine IL-1 plays an important role in the development and pathogenesis of chronic autoimmune diseases, such as rheumatoid arthritis and SLE. IL-1 can activate TLR with release of other pro-inflammatory cytokines, therby mediating the pathogenesis of SLE which is the second most common disease after rheumatoid arthritis where TLR plays a key role. TLRs range from 1 to 13, most of which are expressed on the cell membrane; whereas TLR3, TLR7, TLR8, TLR9, TLR11, TLR12 and TLR13 are expressed intracellularly in endoplasmic reticulum, endosomes, endolysosomes, phagosomes, and lysosomes (5). It is important to note that TLR expression is enhanced in immune cells after exposure to pro-inflammatory cytokines. In addition, it must be pointed out that TLR7 is crucial, while the function of TLR9 is controversial. Therefore, IL-1 secretion, involved in inflammation, is due to TLR activation and subsequently to inflammasome which is a cytosolic protein complex important for the maturation of inflammatory caspase-1. In fact, caspase-1 cleaves the inactive pro-IL-1 into its mature form ready to be secreted (5).

Among the various immune cells that mediate inflammation in SLE, we also find the mast cells (MCs) which play a decisive role in this disease (6). It is well known that MCs and their histamine receptors can regulate both TH1 and TH2 cells. In

Key words: mast cell; systemic lupus erythematosus; IL-37; cytokines;inflammation

Corresponding Author:
Prof. Pio Conti,
Postgraduate Medical School,
University of Chieti,
Viale Unità d'Italia 73, Chieti, Italy
Tel./Fax: +39 0871 574136
e-mail: pconti@unich.it

0393-974X (2019)

Table I. *Diagnostic rules.*

Manifestations in
Skin: Facial erythema, Photosensitivity, oral ulcers, alopecia.
Joints: Pain, tenderness, swelling, arthritis, swelling, stiffness
Serous sites: Pleuritis, pericarditis, pericardial pain
Renal diseases: Proteinuria, red blood cell casts, cellular cast, renal disorders
Hematologic diseases: Hemolytic anemia, leukopenia, thrombocytopenia, lymphopenia
Immunologic disorders: LE cells, antiphospholipid antibody, low complement C3, C4, hemolytic anemia

SLE skin lesions, immune cells including MCs and T lymphocytes occur, infiltrate into the dermis and release pro-inflammatory cytokines, including IL-1 and TNF (7). Some studies have revealed that in SLE skin lesions, the number of MCs is increased, contributing to the inflammatory phenomenon and representing important cells in the pathophysiology of the disease, since they can also show a protective role (7). In SLE there are high levels of IgE that bind to MCs and basophilic granulocytes, and activate them to produce pro-inflammatory cytokines and to migrate in various tissues.

Mast cells

MCs derive from the hematopoietic precursor cells located in the bone marrow ($CD34^+/CD117^+/CD13^+$), and mature and reside in virtually all vascularized tissue (8). MCs are located perivascularly where they produce inflammatory mediators (including histamine), and pro-inflammatory cytokines (Table II) which participate in neuropsychiatric diseases and host response (8). In the brain, MCs are located near vessels, meninges, nerves, and thalamus and hypothalamus, and modulate the innate and adaptive immune response. They can migrate from the brain to the lymphoid organs and *vice versa*, and are good communicators with neurons and glial cells (9). MCs are capable of producing biologically active substances, including chemokines which recruit other cells and mediate inflammation. In addition, chemokines participate in inflammatory responses and CCL2 chemokines can be induced in MCs by IL-1, whose receptor is expressed by a variety of central nervous system (CNS) cells and tissues (10).

MCs of peripheral tissues generate immune mediators and communicate with spinal and encephalic dura mater, giving sensitivity to tissues. MCs are in communication with sensory nerves, and cross-talk with the cells of the microglia of the brain and spinal cord. One of the MC dysfunctions can affect the inflammatory pathway (11). MCs actively participate in neurodegenerative diseases including SLE. Clarifying the mechanism of MC activation and inhibition in SLE can help improve the therapeutic treatment of this autoimmune inflammatory disease (12).

IL-1 generated by several immune cells, such as macrophages, lymphocytes and MCs, has the ability to induce itself and it is involved in the release of other pro-inflammatory cytokines, which are very important effector molecules implicated in autoimmune disorders. IL-1 plays a key role in the induction and development of pathphysiology (13). IL-1, along with TNF, can induce the production of IFN-γ, an effect demonstrated in some inflammatory diseases. IFN-γ is a potential biomarker for SLE and its decrease is associated with severity and poor prognosis in patients with lupus.

Macrophages and MCs, together with other cells, express IL-1 receptors (IL-1R) and mediate primary immunity by responding to IL-1. This pro-inflammatory cytokine can act through TH1 cells, and can also amplify the response to TH2. The alteration of the TH1/TH2 equilibrium can lead to a greater susceptibility to SLE (5). In this disease,

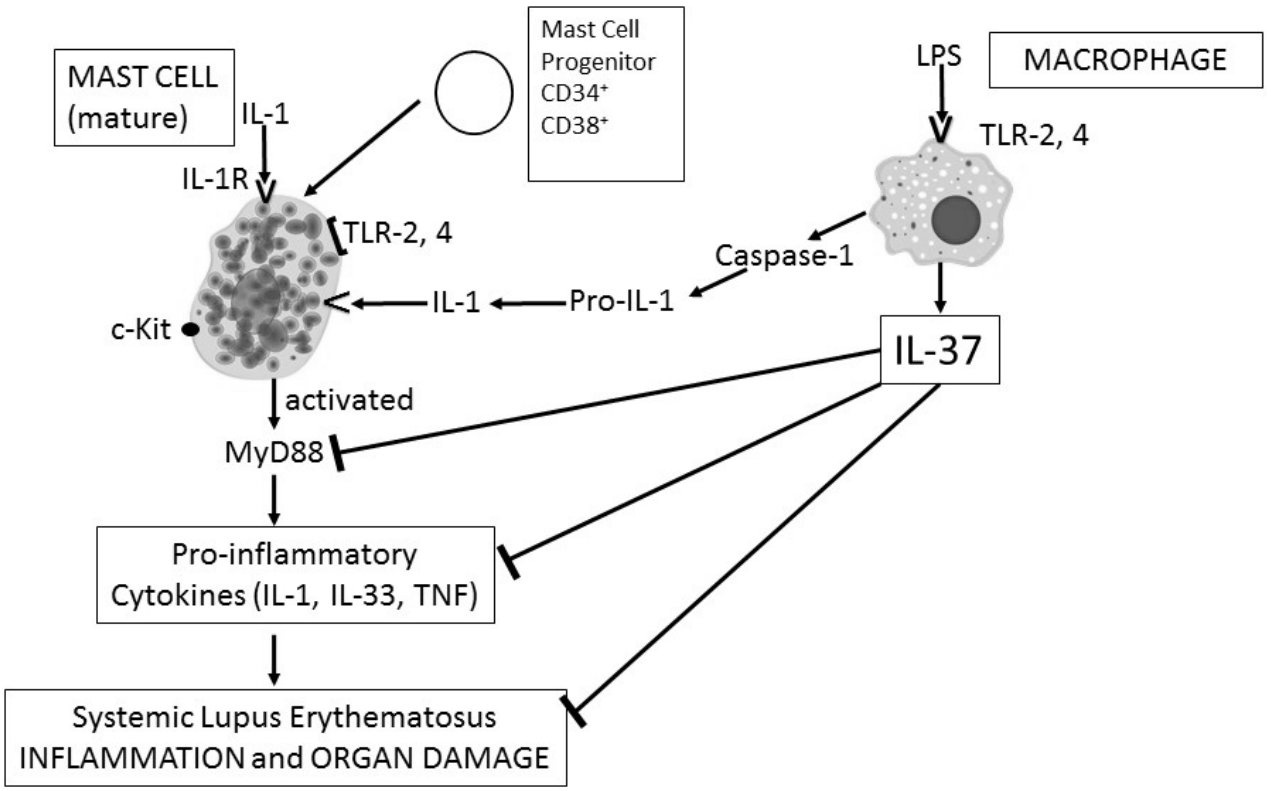

Fig. 1. *In systemic lupus erythematosus mature mast cells can be activated by IL-1, provoking the release of proinflammatory cytokines and causing inflammation and multi-organ damage, an effect that can be inhibited by IL-37 from activated macrophages.*

Table II. *Inhibitory effect of IL-37 in diseases.*

Diabetes, intestinal inflammation, multiple sclerosis,
inflammatory arthritis, allograft rejection,
fibromyalgia, arthritis, atherosclerosis, fibrosis,
endotoxemia, asthma, migraine, depression, autoimmunity,
allergy, mold inducing inflammation, ischemia,
hepatitis, neuroinflammation, cancer Inflammation.

the TH1/TH17 ratio is dysregulated, and a balance in favor of TH17 cells is increased and the cells are more responsive in SLE. Thus, IL-1 plays a potential role in the pathogenesis of SLE.

In addition, in SLE, the neurological manifestation is involved in which also MCs participate and mediate the phenomena of vasculitis and hemorrhagic inflammation, contributing to the pathogenesis of this disease (14). MCs are recalled by the release of MCP-1/CCL2 which is abundant in SLE and can be an important marker.

However, often the SLE diagnosis is not always easy and it would take more experiments on mice to clarify the true role of MC activation, in particular with IL-1.

To date, important studies on SLE therapy have missed the goal, even though some progress has been made. The classical therapy adopted for this disease is often based on the administration of cortisone and other immune suppressors (15). We believe

that understanding the imbalance of the IL-1 family members is fundamental for future therapeutic approaches. In this editorial, we propose a new therapeutic strategy based on MC-IL-1 inhibition with a natural cytokine inhibitor IL-37 (16).

IL-37

IL-F7 (most commonly called IL-37) is a member of the IL-1 family which binds IL-18 receptor alpha (IL-18Rα) chain and suppresses innate and acquired immunity (17). IL-37, is involved in the pathogenesis of the inflammatory autoimmune diseases including psoriasis, rheumatoid arthritis, fibromyalgia, Crohn's disease, SLE, and others (Table II).

It has been reported that IL-37 protects against inflammatory insults and blocks pro-inflammatory cytokines including IL-1, IL-33. IL-37 may also inhibit TNF with an indirect effect, since this highly pro-inflammatory cytokine can be induced by IL-1 (17).

This new IL-1 family member acts through the down-regulation on MyD88 in the nuclear biochemical cascade, which is necessary for the generation of pro-inflammatory cytokines, including IL-1 (18). In SLE, where there is strong local and systemic inflammation mediated by IL-1, the blocking of this cytokine could certainly reduce both inflammation and tissue damage, and bring relief to patients suffering from this autoimmune disease (19-20) (Fig. 1). However, treatments with this cytokine could also have side effects on the immune system as the precise doses of administration in humans and its exact functioning are not yet known.

REFERENCES

1. Tsokos GC Systemic lupus erythematosus. N Engl J Med 2011; 365(22):2110-21.
2. Jung JY, Bae CB, Suh CH. Promising biomarkers for systemic lupus erythematosus. Expert Opin Med Diagn 2013; 7(6):601-13.
3. Tsokos GC, Lo MS, Costa Reis P, Sullivan KE. New insights into the immunopathogenesis of systemic lupus erythematosus. Nat Rev Rheumatol 2016; 12(12):716-30.
4. Gottschalk TA, Tsantikos E, Hibbs ML. Pathogenic inflammation and its therapeutic targeting in systemic lupus erythematosus. Front Immunol 2015; 6:550.
5. Joosten LA, Abdollahi-Roodsaz S, Dinarello CA, O'Neill L, Netea MG. Toll-like receptors and chronic inflammation in rheumatic diseases: new developments. Nat Rev Rheumatol. 2016 Jun;12(6):344-57.
6. Kolkhir P, Pogorelov D, Olisova O, Maurer M. Comorbidity and pathogenic links of chronic spontaneous urticaria and systemic lupus erythematosus--a systematic review. Clin Exp Allergy 2016; 46(2):275-87.
7. Liew FY, Girard JP, Turnquist HR. Interleukin-33 in health and disease. Nat Rev Immunol 2016; 16(11):676-689.
8. Galli SJ, Kalesnikoff J, Grimbaldeston MA, Piliponsky AM, Williams CM, Tsai M. Mast cells as "tunable" effector and immunoregulatory cells: recent advances. Annu Rev Immunol 2005; 23:749-86.
9. Petra AI, Panagiotidou S, Stewart JM, Conti P, Theoharides TC. Spectrum of mast cell activation disorders. Expert Rev Clin Immunol 2014; 10(6):729-39.
10. Conti P, D'Ovidio C, Conti C, et al. Progression in migraine: Role of mast cells and pro-inflammatory and anti-inflammatory cytokines. Eur J Pharmacol 2019; 844:87-94.
11. Theoharides TC. Neuroendocrinology of mast cells: Challenges and controversies. Exp Dermatol 2017; 26(9):751-59.
12. Siiskonen H, Smorodchenko A, Krause K, Maurer M. Ultraviolet radiation and skin mast cells: Effects, mechanisms and relevance for skin diseases. Exp Dermatol 2018; 27(1):3-8.
13. Theoharides TC, Petra AI, Taracanova A, Panagiotidou S, Conti P. Targeting IL-33 in autoimmunity and inflammation. J Pharmacol Exp Ther 2015; 354(1):24-31.
14. Barile-Fabris L, Hernández-Cabrera MF, Barragan-Garfias JA. Vasculitis in systemic lupus erythematosus. Curr Rheumatol Rep 2014; 16(9):440.
15. Shih A, Jackson KC 2nd. Role of corticosteroids in palliative care. J Pain Palliat Care Pharmacother 2007; 21(4):69-76.
16. Gallenga CE, Pandolfi F, Caraffa A, Kritas SK, Ronconi G, Toniato E, Martinotti S, Conti P.

Interleukin-1 family cytokines and mast cells: activation and inhibition. J Biol Regul Homeost Agents 2019; 33(1):1-6.
17. Cavalli G, Dinarello CA. Suppression of inflammation and acquired immunity by IL-37. Immunol Rev 2018; 281(1):179-90.
18. Conti P, Caraffa A, Mastrangelo F, et al. Critical role of inflammatory mast cell in fibrosis: Potential therapeutic effect of IL-37. Cell Prolif 2018; 51(5):e12475.
19. Conti P, Caraffa A, Ronconi G, et al. Mast cells participate in allograft rejection: can IL-37 play an inhibitory role? Inflamm Res 2018; 67(9):747-55.
20. Conti P, Caraffa A, Ronconi G, et al. Impact of mast cells in depression disorder: inhibitory effect of IL-37 (new frontiers). Immunol Res 2018; 66(3):323-31.

EXPRESSION OF PTX3, HAS2 AND TNFAIP6 GENES IN RELATION TO REAL-TIME PROLIFERATION OF PORCINE ENDOMETRIAL LUMINAL EPITHELIAL CELLS IN PRIMARY CULTIVATION MODEL

K. WOJTANOWICZ-MARKIEWICZ[1], I. KOCHEROVA[2], M. JESETA[3], H. PIOTROWSKA-KEMPISTY[4], K.P. BRÜSSOW[1], M.T. SKOWROŃSKI[1], M. BRUSKA[2], D. BUKOWSKA[1], M. NOWICKI[5], B. KEMPISTY[2,3,5] and P. ANTOSIK[1]

[1]Veterinary Center, Nicolaus Copernicus University in Torun, Torun, Poland; [2]Department of Anatomy, Poznan University of Medical Sciences, Poznan, Poland; [3]Department of Obstetrics and Gynecology, University Hospital and Masaryk University, Brno, Czech Republic; [4]Department of Toxicology, Poznan University of Medical Sciences, Poznan, Poland; [5]Department of Histology and Embryology, Poznan University of Medical Sciences, Poznan, Poland

Received November 9, 2018 – Accepted February 28, 2019

Endometrial cells undergo very specific changes associated with reproductive processes. Cells prepare for embryo development by increasing their volume. Then, if fertilization fails, endometrial cells are liable for apoptosis, preparing new cells that are ready for subsequent processes related to the possibility of embryo implantation and the development of pregnancy. PTX3 and TNFAIP6 are absent or reduced in cultured COCs, resulting in a functional change in COC *in vitro*. In this work, we want to check how PTX3, HAS2 and TNFAIP6 behave in luminal epithelium primary cell culture. Cells obtained during slaughter from porcine specimens were cultured primarily *in vitro* for 7 days. Their proliferation patterns were then analysed using RTCA, with the expression of genes of interest evaluated with the use of immunofluorescence and RT-qPCR. The results of these changes in the expression of the genes of interest were analysed on each of the seven days of the porcine luminal primary cell culture. Our study showed the increased level of PTX3, HAS2 and TNFAIP6 expression at the same hours of primary culture. Rt-qPCR showed a higher level of expression of the PTX3 gene in the first 72 h, at the end of the lag phase (in the phase of stasis in which the cells adapt to the new environment and often die). In contrast, TNFAIP6 expression increases about 96 hours when the cells are in the full log phase (logarithmic phase growth) and continue this trend in the plateau phase. We did not observe such drastic changes in the HAS2 expression pattern, which leads us to hypothesize that PTX3 and TNFAIP6 are designed to maintain a constant level of HAS2 in the cell throughout its lifetime. The obtained results could become a point of reference for further *in vivo* and clinical research.

In our previous research, we used the model of porcine epithelial cells to study e.g. the expression and distribution of progesterone receptors (classical nuclear and membrane form, PGR, PGRMC1) in real time in the proliferation of luminal epithelium cells. We showed that the value of the proliferation index

Key words: pig; primary culture; genes expression; luminal epithelial cells

Corresponding Author:
Bartosz Kempisty PhD.,
Department of Anatomy,
Poznan University of Medical Sciences, ul. Święcickiego 6,
60-781 Poznań, Poland
Tel. 061 854 65 64, fax 061 854 65 68
e-mail: bkempisty@ump.edu.pl

0393-974X (2019)

of luminal epithelial cells differs significantly from the index of GC proliferation because the cells reach a log phase after only 120-144 hours of *in vitro* culture (IVC) (1, 2). In subsequent studies, we intend to check to what extent the key proteins/genes responsible for the proper course of ovulation affect the structure of the luminal epithelial cells.

Hyaluronan is the main component of the extracellular matrix of most tissues and organs, especially in the embryonic development phase. In the developing embryo, HA accumulates in the areas of cell migration and proliferation, playing an important role in the development of the craniofacial region, limbs, heart and nerves. The family of proteins that synthesize hyaluronan is HAS2 (hyaluronan synthase 2) (3, 4). Consisting of β-linked 1,4-disaccharides of β1,3-glucuronic acid in combination with N-acetylglucosamine, it is a characteristic component of the extracellular matrix in the early stages of morphogenesis, with its synthesis regulated spatially and temporally. The hyaluronan compound on the cell surface can affect cell behaviour, particularly in respect to the modulation of cell migration, adhesion, wound healing and tumour invasion (4, 5).

PTX3, which belongs to the pentraxins superfamily, is the protein taking part in the inflammatory process. The presence of PTX3 is recorded in the epithelium of the lung, epithelial mammary gland and the ovaries (6–8). PTX3 is an essential component of humoral innate immunity, sharing functional outputs, including complement activation, opsonization and, glycosylation-dependent regulation of inflammation, with immunoglobulins. Underlying mechanisms of PTX3 include binding of P-selectin and attenuated neutrophil recruitment at sites of inflammation. PTX3 released from activated leukocytes functioned locally to dampen neutrophil recruitment and regulate inflammation. Unlike CRP, which is produced by the liver in response to inflammatory mediators, PTX3 is synthesized locally at the inflammatory site. Antibodies have a glycosylation-dependent regulatory effect on inflammation (9–11). In addition, Ptx3 is produced by cumulus cells prior to ovulation, and the infertility of PTX3-deficient mice is caused by defects in ovulation and oocyte fertilization associated with the loss of cumulus investment during extrusion from the ovary (12). PTX3 is produced as a 10-20 multimeric subunit by macrophages and other types of cells or tissues after stimulation with primary inflammatory mediators lipopolysaccharide, interleukin 1 (IL1), or tumour necrosis factor α (TNFα) (10).

Tumour necrosis factor α-induced protein 6 (TNFAIP6 or TSG6) is a multifunctional protein usually associated with inflammation, which has the ability to specifically bind HA. TNFAIP6 is synthesized by cumulus and granulosa cells in the preovulatory follicle, and TNFAIP6-deficient mice are unable to form stable cumulus matrix and are sterile (13, 14). Covalent transfer of heavy chains from IαI to HA does not occur in TNFAIP6 –/– mice, indicating that TNFAIP6 is a key catalyst in this reaction. Oocytes, besides promoting cumulus matrix synthesis, inhibit hormone-induced proteolytic enzyme expression by mouse cumulus cells during matrix deposition, probably providing an additional mechanism for matrix stabilization. Indeed, synthesis of cumulus matrix ceases at ovulation and its degradation begins a few hours later, coinciding with an increase in protease production by the oocyte and the cumulus cells (15, 16).

Endometrial cells undergo very specific changes associated with reproductive processes. Cells prepare for embryo development by increasing their volume. Then, if fertilization fails, endometrial cells are liable for apoptosis, preparing new cells that are ready for subsequent processes related to the possibility of embryo implantation and the development of pregnancy. PTX3 and TNFAIP6 are absent or reduced in cultured COCs (cumulus-oocyte complex), resulting in a functional change in COC *in vitro* (17). In the present work, we wanted to check how PTX3, HAS2 and TNFAIP6 behave in luminal epithelium primary cell culture.

MATERIALS AND METHODS

Animals

In this study, crossbred gilts (n=45) at the age of about nine months and which displayed two regular oestrous cycles were collected from a commercial herd. All the animals were checked daily for estrus behaviour and were slaughtered after reaching the anestrus phase of the estrus cycle. The uteri were then transported to the laboratory within 30 min at 38°C.

Endometrial cell (EC) selection and culture

After slaughter, the uterine horns were washed twice with PBS (137 mM NaCl, 27 mM KCl, 10 mM Na_2HPO_4, 2 mM KH_2PO_4, pH 7.4) and immediately cut into small pieces (25-35 mg). Surface uterine epithelial cells were surgically removed using sterile surgical blades. The cell suspension obtained from this digestion was filtered through a mesh to remove non-dissociated fragments of tissue and then incubated with 0.05% collagenase I (Sigma Aldrich, Madison, USA) for 25 min at 38°C in a shaking water bath. Isolated cells were washed three times by centrifugation (10 min at 200 g) with Dulbecco's modified Eagle's medium (DMEM; Sigma Aldrich, Madison, USA) supplemented with gentamicin (20 μg/mL) and 0.1% BSA. The resulting luminal epithelial cells were filtered and washed three times by centrifugation (10 min at 200 g) with supplemented DMEM. The final pellet of luminal epithelial cells was resuspended in DMEM supplemented with 10% fetal calf serum (FCS; Sigma Aldrich, Madison, USA) and 10,000 U mL−1 penicillin G, 10 mg mL−1 streptomycin and 25 μg mL−1 amphotericin B (antibiotic-antimycotic solution; Sigma Aldrich, Madison, USA). The viability of the cells was 90-95%, as judged by trypan blue staining (Sigma Aldrich, Madison, USA). The cells were cultured at 38°C in a humidified atmosphere of 5% CO2. The culture medium was changed every 3 days (1, 18).

In-vitro endometrial cell cultivation using a real-time cell analyzer (RTCA)

The recovered endometrial cells were transferred into an E-Plate 16 of a real-time cell analyzer (RTCA, Roche-Applied Science, GmbH, Penzberg, Germany), which consisted of an RTCA analyzer, an RTCA SP station, and RTCA software. The cells were then cultured in 200 μl of standard porcine culture medium that consisted of Dulbecco's Modified Eagle's Medium (DMEM, Sigma-Aldrich, USA) as mentioned above. The cells were cultured for 0-168 h at 38.5°C under 5% CO_2. The cultivation medium was replaced every three days. After each period of cultivation, the cells were treated with trypsin (0.25% trypsin in a balanced salt solution, Sigma-Aldrich, St. Louis, MO, USA), and the collected pool of proliferating cells was used for RT-qPCR analysis. After each cultivation period, the cell index (CI) was used to evaluate the relative and quantitative changes in electrical cell impedance. The cell status was determined using RTCA software.

Confocal microscopy analysis of PTX3 and HAS2 expression and distribution in porcine luminal epithelial cells

The luminal epithelial cells were transferred into an X-well Lumox (94. 6150. 401, 4-well lumox Detachable, Sarstedt AG & Co. KG), The cells were then cultured in 1 ml of standard porcine culture medium that consisted of Dulbecco's Modified Eagle's Medium (DMEM, Sigma-Aldrich, USA) as mentioned above. The cells were cultured for 0-168 h at 38.5°C under 5% CO_2. The cultivation medium was replaced every three days. The cells were fixed using acetone-methanol (1:1) for 10 min at -20°C and washed three times in PBS/PVP (0.2%). To block nonspecific binding, samples were incubated in 3% BSA in PBS with 0.1% Tween 20 for 30 min at RT. The luminal epithelial cells were incubated for 1 h at room temperature (RT) with rabbit polyclonal anti- PTX3 antibody (sc 32866), and rabbit polyclonal anti- HAS2 (sc 66916), (both Santa Cruz Biotechnology, Santa Cruz, CA, USA) diluted 1:500 in PBS/1.5% BSA/0.1% Tween 20. After several washes with PBS/0.1% Tween 20, samples with the primary antibodies mentioned above were incubated for 1 h at RT with fluorescein isothiocyanate (FITC)-conjugated goat anti-rabbit IgG Ab and diluted 1:500 in PBS/0.1% Tween20. Following washing in PBS/0.1% Tween20, the luminal epithelial cells were stained with 0.1 μg/ml 4,6-diamino-2-phenylindole (DAPI; Santa Cruz Biotechnology, Santa Cruz, CA, USA) in mineral oil, mounted on glass slides in an antifade solution drop and examined under an LSN 510 confocal system in a Fluoview 10i microscope (Olympus). FITC was excited at 488 nm with an argon laser, and emissions were imaged through a 505-530 nm filter. All confocal microscopic images were analyzed using Imaris 7.2 software (BitPlane, Zurich, Switzerland) (19).

RNA extraction from porcine luminal epithelial cells

Total RNA was extracted from samples using TRI Reagent (Sigma, St Louis, MO, USA) and RNeasy MinElute Cleanup Kit (Qiagen, Hilden, Germany). The amount of total mRNA was determined from the optical density at 260 nm, and the RNA purity was estimated using the 260/280 nm absorption ratio (higher than 1.8) (NanoDrop spectrophotometer, Thermo Scientific, ALAB, Poland). The RNA integrity and quality were checked on a Bioanalyzer 2100 (Agilent Technologies, Inc., Santa Clara, CA, USA). The resulting RNA integrity numbers

(RINs) were between 8.5 and 10 with an average of 9.2 (Agilent Technologies, Inc., Santa Clara, CA, USA). The RNA in each sample was diluted to a concentration of 100 ng/μl with an OD260/OD280 ratio of 1.8/2.0. From each RNA sample, 500 ng of RNA was taken. The remaining amount of isolated RNA was used for the RT-qPCR study. Time quantitative polymerase chain reaction (RT-qPCR) analysis (18).

Real-time quantitative polymerase chain reaction (RT-qPCR) analysis

Total RNA was isolated from luminal epithelial cells each of the seven days of culture. The RNA samples were re-suspended in 20 μl of RNase-free water and stored in liquid nitrogen. RNA samples were treated with DNase I and reverse-transcribed (RT) into cDNA. RT-qPCR was conducted in a Light Cycler real-time PCR detection system (Roche Diagnostics GmbH, Mannheim, Germany) using SYBR® Green I as a detection dye, and target cDNA was quantified using the relative quantification method. The relative abundance of PTX3, TNFAIP6, and HAS2 transcripts in each sample were standardized to the internal standards. For amplification, 2 μl of cDNA solution was added to 18 μl of QuantiTect® SYBR® Green PCR (Master Mix Qiagen GmbH, Hilden, Germany) and primers (Table I). One RNA sample of each preparation was processed without the RT-reaction to provide a negative control for subsequent PCR (21, 22).

Statistical analysis

One-way ANOVA followed by the Tukey post-test was used to compare the real-time (RTCA) quantification results. The experiments were carried out with at least four replicates. The differences were considered to be significant at $^{*}P < 0.05$, $^{**}P < 0.01$ and $^{***}P < 0.001$. The statistical calculations were applied to compare the results in each investigated group to the highest normalized proliferation index at each time point. GraphPad Prism version 4.0 software (GraphPad Software, San Diego, CA, USA) was used for all statistical calculations.

RESULTS

The changes in cell morphology cultured *in vitro* for 168 h were analyzed by Nomarski system (Fig. 1).

RTCA analysis showed a specific pattern of cell proliferation, based on cell index analysis. The cell index was almost unchanged for the first 56 hours. Then, around hour 120, it remained at a similar constant level. The total increase in cell index varied between the cell samples. However, every population's index increased. During the analysis of the total period of culture using RTCA analyzer, we did not find statistically significant differences between individual samples. Differences in cellular indexes between the tested samples observed between 72 and 120 hours of breeding result from the fact that the samples are pooled samples from several individuals aged about 9 months The results of specific time periods are presented in Fig. 2.

Cells analysed during RTCA were subjected to immunofluorescent staining, using specific antibodies for HAS2, PTX3, with DAPI serving as positive control. The results of that analysis were analysed using confocal microscopy and are presented in Fig. 3.

As can be seen, intense, intracellular, extranuclear luminosity can be observed in all of the tests and

Table I. *Primer information and primer sequences used for the RT-qPCR analysis.*

Gene	Number	3′-5′	5′-3′
PTX3	X83601.1	ctagaggaagctgggactccg	agcctcaagtttcattggtgt
TNFAIP6	KJ892293.1	ctgactatgttgaaatatacgac	gtattctttccctgactgg
HAS2	KR063271.1	gaagtcatgtacacggcctt	agccatccagtatctcacac
ACTB	XM 003124280.3	cccttgccgctccgccttc	gcagcaatatcggtcatccat
HPRT	NM_001032376.2	ccatcacatcgtagccctc	acttttatatcgcccgttgac

time periods apart from the 24th hour of culture. While in that case, the fluorescence is not observable easily, it is present, as confirmed by the fluorescence graph. These results confirm the presence of all of the of the cellular antigens analysed, throughout the culture period.

Additionally, a region of interest intensity of fluorescence of specific antibodies was compared in different time periods of primary culture. The results are presented in the form of bar graphs and compiled in Fig. 4.

As can be seen on the graphs, most of the markers present distinct patterns of fluorescence intensity. HAS2 is the most intense at hour 48. At hour 120, an increase at around half of the highest value is observed, continuing till the end of the observation. Throughout the observation period, PTX3 immunofluorescence continuously increased, only at 144 hours a 50% decrease in fluorescence intensity was noted. The lowest fluorescence intensity was recorded in the first hours of the study, and the highest at 168 hours.

Finally, the levels of the studied markers were analysed using the RT-qPCR method. The results are presented in a form of a bar graph (Fig. 5).

As can be seen, the increase in the level of expression of the PTX3 gene is the highest in the first 48 h. The transcript levels of PTX3 at 48 h and 72 h were upregulated in relation to the starting point of culture. From 96 h, downregulation of mRNA expression occured and maintained a downward trend at the remaining time periods of cell culture. On the contrary, the expression of TNFAIP6 was the lowest in the first 48 hours, increasing in the next hours of testing. The transcript levels were downregulated in relation to the starting point of culture from 48 h to 96 h. Later, upregulation occured and maintained an upward trend until the end of observation. In turn, HAS2 was upregulated through the whole observation periods, with similar levels observed at 48 to 96 hours and a significant increase at 120 and 144 hours.

Concluding, we noted significant differences between the level of PTX3 expression in 48 and 72 h of cultures, in which the expression level increases in relation to 24 h of cultivation, and 96 to 144 hours in which the expression level dropped significantly. The opposite situation was observed in the levels of TNAIFP6 gene expression. In the case of this gene, the expression strongly diminished for 48 hours and then increased in the further culture periods. On the other hand, HAS2 expression throughout the culture was above the level from the 24-h sample.

DISCUSSION

In this study, we analysed the expression of PTX3, HAS2 and TNFAIP6 in luminal epithelial

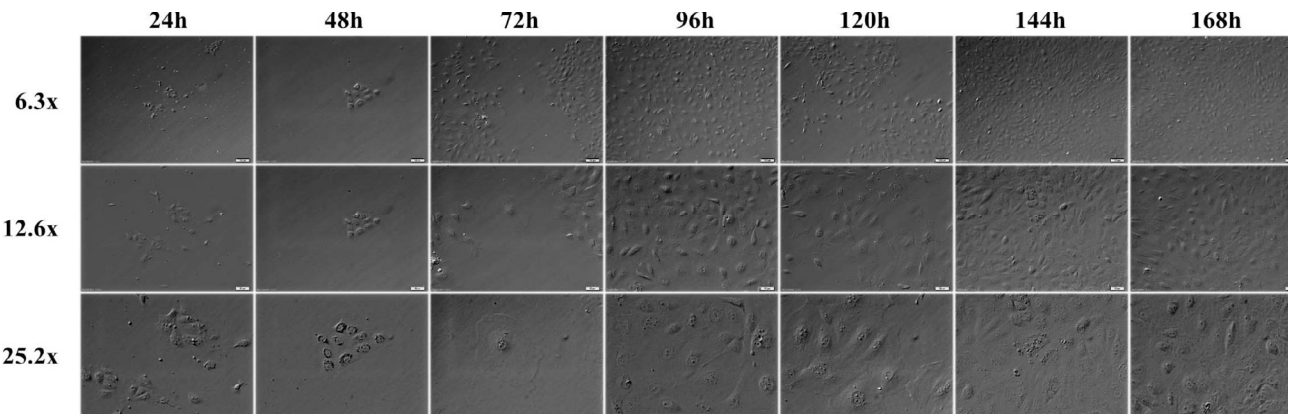

Fig. 1. *Changes in cell morphology during short-term (168 h) primary cell culture. The cells isolated from porcine luminal epithelium cell were cultured for 168 h. Each 24 h, cell growth, and morphology changes were documented under relief phase contrast with 10x, 20x, and 40x objective lenses (total magnifications: 6,3x, 12,6x, and 25,2x, resp.; M total = M objective × M video camera adapter).*

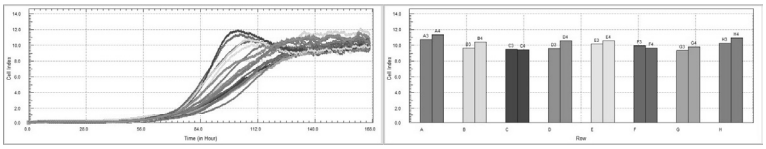

0-168h

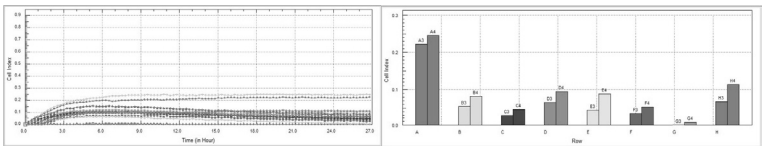

0-24h

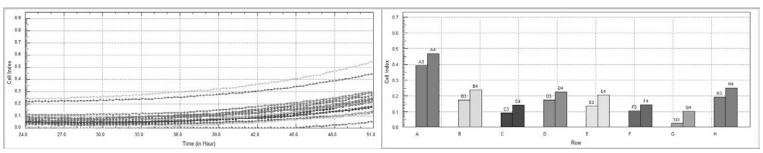

24-48h

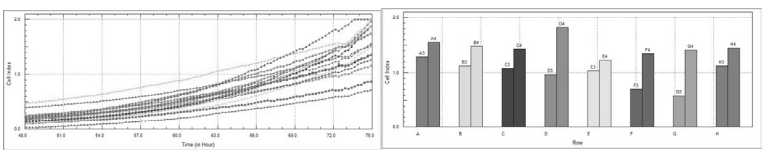

48-72h

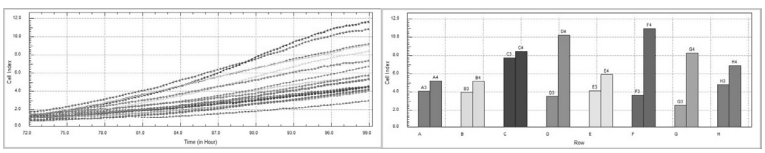

72-96h

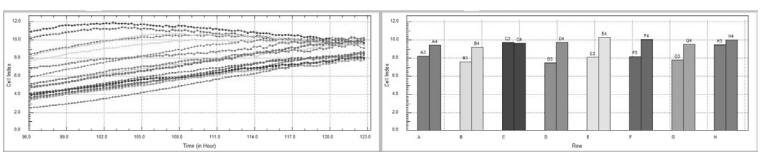

96-120h

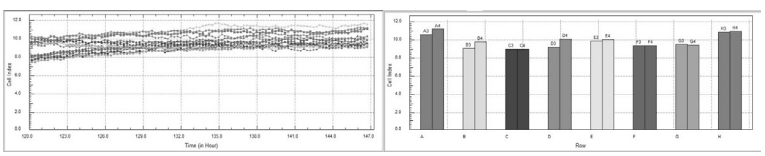

120-144h

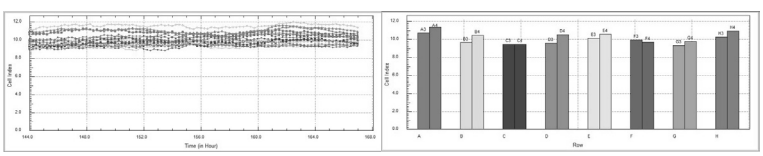

144h-168h

Fig. 2. *Real-time cell analysis (RTCA) results, in different time periods of primary culture, presented in form of a line graph, with starting and ending cell index plotted corresponding bar graphs. Each sample is drawn using a different color on both of the graphs.*

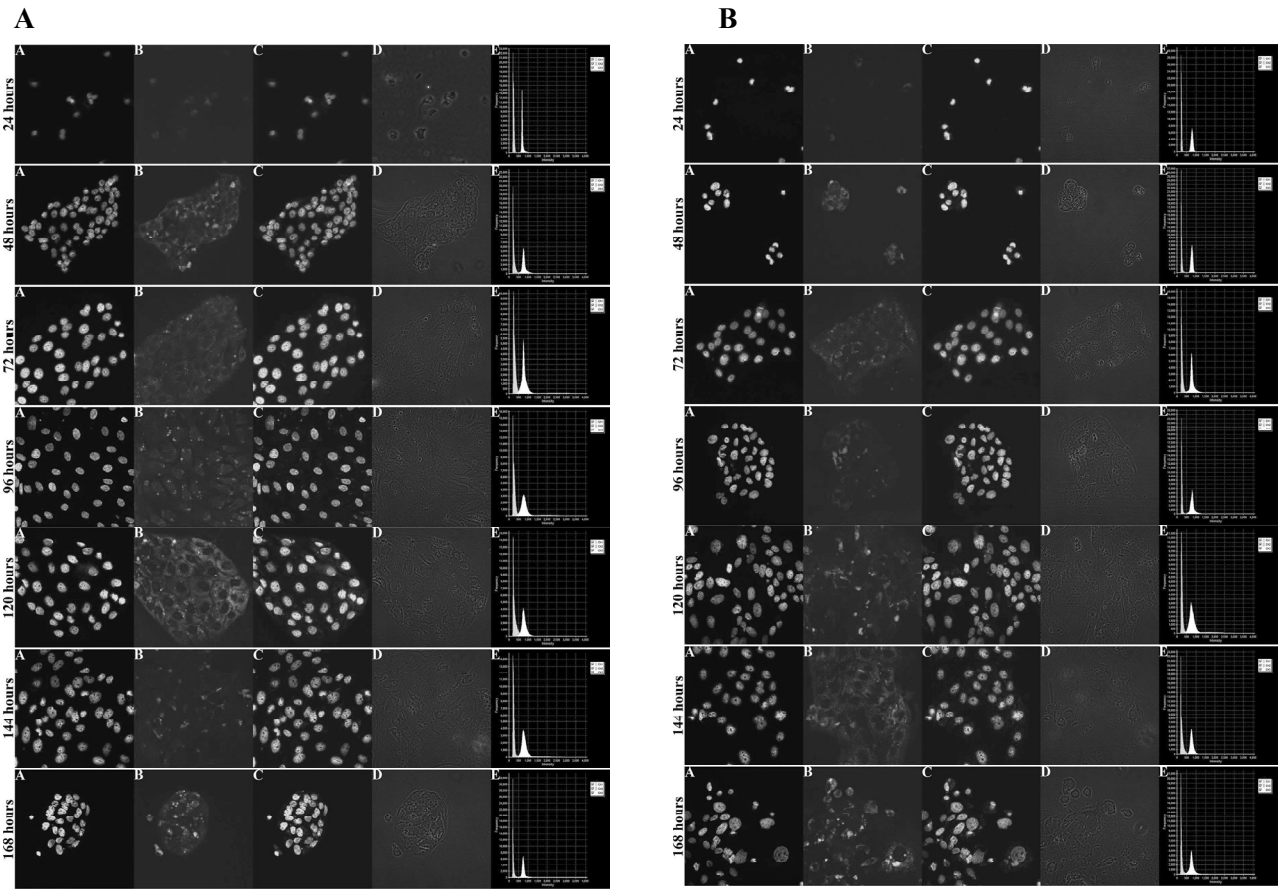

Fig. 3. ***A)*** *Immunofluorescence test results, with the primary antibody designed to detect PTX 3. A-positive control using DAPI; B-Results of PTX 3 detection using FitC; C-positive control using DAPI, presented together with PTX 3detection using FitC; D-negative control without the use of cytochrome; E-levels of fluorescence presented on a graph.* ***B)*** *Immunofluorescence test results, with the primary antibody designed to detect HAS 2. A-positive control using DAPI; B-Results of HAS 2 detection using FitC; C-positive control using DAPI, presented together with HAS 2 detection using FitC; D-negative control without the use of cytochrome; E-levels of fluorescence presented on a graph.*

cells, during seven days of primary cell culture *in vitro* without hormonal stimulation, using confocal microscopy analysis. The results showed an increased level of PTX3, HAS2 and TNFAIP6 protein expression during the time of the culture. Rt-qPCR showed a higher level of expression of the PTX3 gene in the first 72 h, which is the end of the lag phase (the phase of stasis in which the cells adapt to the new environment and often die). In contrast, the expression of TNFAIP6 increased around 96 hours, at the time when the cells were in the full log phase (the logarithmic growth phase), then continued to rise in the plateau phase. We did not observe such drastic changes in the HAS2 expression pattern, which leads us to suggest that PTX3 and TNFAIP6 are designed to maintain a constant level of HAS2 in the cell throughout its lifetime.

TNFAIP6 is required for the formation of covalent bonds between hyaluronan and heavy chains of the inter-α-trypsin inhibitor family proteins. TNFAIP6-deficient female mice showed severe fertility problems and impaired cumulus expansion (10, 15). Binding of the TNFAIP6 protein to hyaluronate was demonstrated by coprecipitation. Data indicate that the inflammatory cytokine (TNF or IL-1)-inducible, secretory TNFAIP6 protein is a member of the family of hyaluronate binding proteins, involved in cell-cell and cell-matrix interactions during inflammation and tumorigenesis. Comparative studies of the reverse transcription polymerase chain reaction performed by Fülöp have shown that TNFAIP6 mRNA is specifically expressed after induction of COC induced

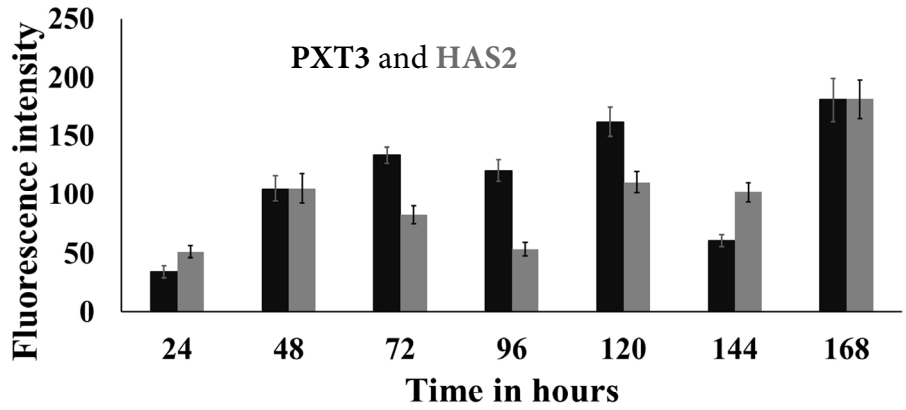

Fig. 4. R*egion of interest (ROI) fluorescence intensity measurement results, presented as a bar graph for different stages of primary culture.*

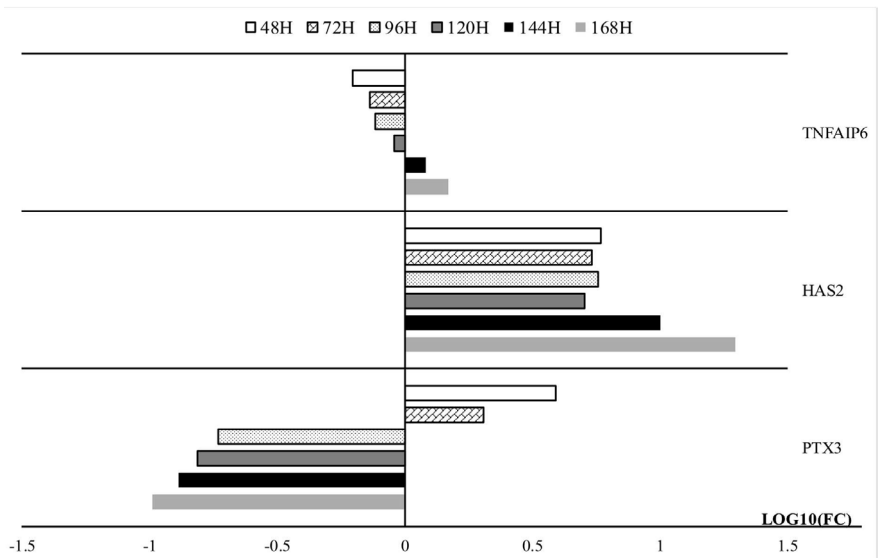

Fig. 5. *Results of RT-qPCR (Real Time-quantitative Polymerase Chain Reaction) validation of analyzed genes, presented in the form of bar graph. All the fold changes were described in relation to the transcript levels at 24 h of primary culture. LogFC was used to present the data, in order to improve the clarity and comparability of up and downregulation results. PTX 3- Pentraxin 3, HAS 2- Hyaluronan synthase 2, TNFAIP6- Tumour necrosis factor, alpha-induced protein 6.*

in vivo, identifying the first non-pathological process in which it plays an important role (3). Since TNFAIP6 binds to hyaluronan and interacts with an inter-α-trypsin inhibitor (IαI), a molecule that is necessary for COC matrix formation, this protein may have a structural role in the matrix or may increase the anti-lipolytic effect of IαI to protect the matrix from degradation (23, 24). The increase in LH also induces TNFAIP6 expression in granulosa cells. This process involves growth factor 9 derived from oocytes, and therefore TNFAIP6 synthesis proceeds under both autocrine and paracrine control. TNFAIP6 is usually expressed under inflammatory conditions, and its anti-inflammatory and chondroprotective effects in arthritis are well documented (25, 26).

PTX3 does not directly bind to hyaluronan, but binds to TNFAIP6, allowing crosslinking of hyaluronan chains as multimolecular complexes.

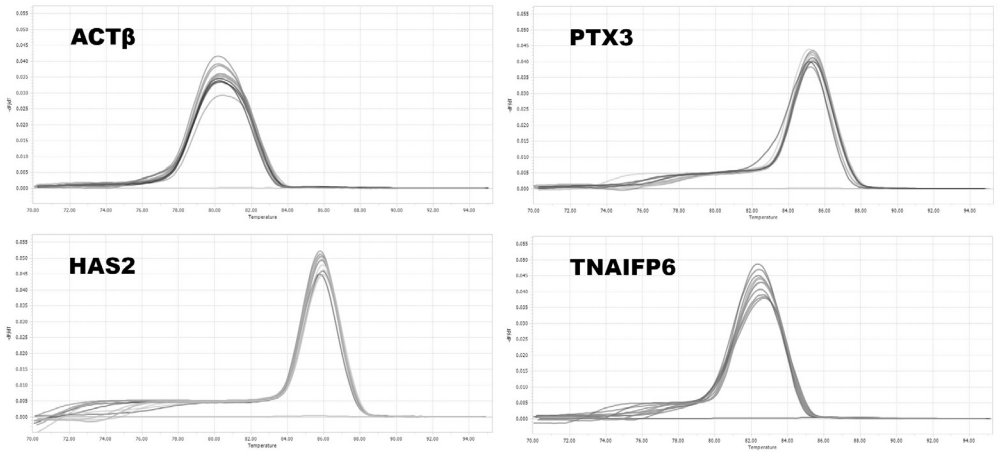

Fig. 6. *Dissociation curves that confirm the specificity of the amplification products obtained in the RT-qPCR analysis (ACTβ, PTX3, HAS2 and TNFAIP6).*

Expression of TNFAIP6 can be induced by TNFAIP1 and mechanical stimuli in vascular smooth muscle cells that lead to the synthesis and aggregation of proteoglycans. Modulation of the proteolytic network associated with inflammatory processes may be a mechanism in which TNFAIP6 inhibits inflammation. Activation of the TNFAIP6 gene by pro-inflammatory cytokines and the presence of TNFAIP6 protein in inflammatory lesions suggests its role in negative feedback control of the inflammatory response (27). Because this gene is significantly elevated in the identified endometrial stromal cells after 3 and 12 hours of exposure to trophoblast-secreted products, it is possible that it is involved in enabling invasive trophoblast migration through the stroma (27, 28).

In addition, PTX3 inhibits the mitogenic activity exerted by FGF 2 in bovine, mouse and human endothelial cells *in vitro*. This seems to be due to the ability of PTX3 to prevent binding of FGF2 to FGFR instead of the direct action of PTX3 on endothelial cells. In addition, PTX3 does not inhibit the proliferation of endothelial cells induced by various mitogens. It should be emphasized that PTX3 interacts with and inhibits the biological activity of FGF2 in doses comparable to those measured in the blood of patients affected by inflammatory diseases.

Various HAS (HAS1, HAS2 and HAS3) have been isolated and characterized in mammalian cells. Their biosynthesis occurs on the internal surface of the plasma membrane. However, HAS2 is responsible for the synthesis of HMW-HA (high molecular weight). HA exerts biological reactions through specific cell-surface receptors, forming co-receptor complexes with various receptor tyrosine kinases (5, 24). Studies show that HA and its dominant receptor, CD44, were expressed in early human DSCs (decidual stromal cells). The interaction of HMW-HA and CD44 contributes to the increase in DSC. This fact has been verified by the fact that HMW-HA promotes DSC proliferation and inhibits DSC apoptosis. In addition, there was no significant difference in DSC proliferation and apoptosis when subjected to pre-treatment with the HA antagonist peptide, anti-CD44 neutralizing antibody and combinations thereof (29).

According to Michael and colleagues, HAS2 belongs to one of the four genes contained in the ranking method evaluated for identifying good quality metaphase II (MII) oocytes that will ultimately provide a significantly better outcome regarding good blastocyst development and live birth (5).

Knudtsonin's research on humans shows the HA system is expressed in eutopic menstrual endometrial stromal cells (ESCs) and endometrial endothelial cells (EECs) from women with and without endometriosis. There are no differences in expression in HA production or degradation enzymes in EECs or ESCs

in women with or without endometriosis (30).

In summary, we have demonstrated the changes in the gene of interest expression on each of the seven days of porcine luminal cell primary culture. Our study shows the increased level of PTX3, HAS2 and TNFAIP6 expression at the same hours of primary culture. Rt-qPCR shows a higher level of expression of the PTX3 gene in the first 72 h, at the end of the lag phase (in the phase of stasis in which the cells adapt to the new environment and often die). In contrast, the expression of TNFAIP6 increases around 96 hours, at the time when the cells are in the full log phase (the logarithmic growth phase), and continues this trend in the plateau phase. We did not observe such drastic changes in the HAS2 expression pattern, which makes us presume that PTX3 and TNFAIP6 are designed to maintain a constant level of HAS2 in the cell throughout its lifetime.

In our research, we had a possibility to check the levels of expression of genes responsible for inflammation and protection against adhesion in endometrial cells, as well as the preservation of the expression of proteins necessary for the course of normal implantation of the embryo and the course of pregnancy. The obtained results could become a point of reference for further *in vivo* and clinical research.

ACKNOWLEDGEMENTS

Publication of this article was made possible by grant number UMO-2016/21/B/NZ9/03535 from the Polish National Science Centre

REFERENCES

1. Jankowski M, Dyszkiewicz-Konwińska M, Budna J, et al. Does migrative and proliferative capability of epithelial cells reflect cellular developmental competence? Med J Cell Biol 2018; 6(1):1-7.
2. Kempisty B, Ziółkowska A, Piotrowska H, et al. Short-term cultivation of porcine cumulus cells influences the cyclin-dependent kinase 4 (Cdk4) and connexin 43 (Cx43) protein expression-a real-time cell proliferation approach. J Reprod Dev 2013; 59(4):339-45.
3. Fülöp C, Kamath R V, Li Y, et al. Coding sequence, exon–intron structure and chromosomal localization of murine TNF-stimulated gene 6 that is specifically expressed by expanding cumulus cell–oocyte complexes. Gene 1997; 202(1–2):95-102.
4. Itano N, Kimata K. Expression cloning and molecular characterization of HAS protein, a eukaryotic hyaluronan synthase. J Biol Chem 1996; 271(17):9875-78.
5. Michael DR, Phillips AO, Krupa A, et al. The human hyaluronan synthase 2 (HAS2) gene and its natural antisense RNA exhibit coordinated expression in the renal proximal tubular epithelial cell. J Biol Chem 2011; 286(22):19523-32.
6. Garlanda C, Hirsch E, Bozza S, et al. Non-redundant role of the long pentraxin PTX3 in anti-fungal innate immune response. Nature 2002; 420(6912):182-86.
7. Jaillon S, Mancuso G, Hamon Y, et al. Prototypic long pentraxin PTX3 is present in breast milk, spreads in tissues, and protects neonate mice from Pseudomonas aeruginosa lung infection. J Immunol 2013; 191(4):1873-82.
8. Introna M, Alles V V, Castellano M, et al. Cloning of mouse ptx3, a new member of the pentraxin gene family expressed at extrahepatic sites. Blood 1996; 87(5):1862-72.
9. Deban L, Russo RC, Sironi M, et al. Regulation of leukocyte recruitment by the long pentraxin PTX3. Nat Immunol 2010; 11(4):328-34.
10. Han B, Mura M, Andrade CF, et al. TNFalpha-induced long pentraxin PTX3 expression in human lung epithelial cells via JNK. J Immunol 2005; 175(12):8303-11.
11. Moalli F, Jaillon S, Inforzato A, Sironi M, Bottazzi B, Mantovani A, Garlanda C. Pathogen recognition by the long pentraxin PTX3. J Biomed Biotechnol 2011; 2011:830421.
12. Varani S, Elvin JA, Yan C, et al. Knockout of pentraxin 3, a downstream target of growth differentiation factor-9, causes female subfertility. Mol Endocrinol 2002; 16(6):1154-67.
13. Lee GW, Lee TH, Vilcek J, et al. TSG-14, a tumor necrosis factor- and IL-1-inducible protein, is a novel member of the pentaxin family of acute phase proteins. J Immunol 1993; 150(5):1804-12.
14. Parkar AA, Kahmann JD, Howat SL, Bayliss MT, Day AJ. TSG-6 interacts with hyaluronan and aggrecan in a pH-dependent manner via a common functional

element: implications for its regulation in inflamed cartilage. FEBS Lett 1998; 428(3):171-76.
15. Wisniewski HG, Hua JC, Poppers DM, Naime D, Vilcek J, Cronstein BN. TNF/IL-1-inducible protein TSG-6 potentiates plasmin inhibition by inter-alpha-inhibitor and exerts a strong anti-inflammatory effect in vivo. J Immunol 1996; 156(4):1609-15.
16. Milner CM, Day AJ. TSG-6: a multifunctional protein associated with inflammation. J Cell Sci 2003; 116(Pt 10):1863-73.
17. Dunning KR, Watson LN, Zhang VJ, Brown HM, Kaczmarek AK, Robker RL, Russell DL. Activation of mouse cumulus-oocyte complex maturation in vitro through EGF-Like activity of versican1. Biol Reprod 2015; 92(5):116.
18. Kranc W, Jankowski M, Budna J, et al. Amino acids metabolism and degradation is regulated during porcine oviductal epithelial cells (OECs) primary culture in vitro – a signaling pathways activation approach. Med J Cell Biol 2018; 6(1):18-26.
19. Rybska M, Knap S, Jankowski M, et al: Characteristic of factors influencing the proper course of folliculogenesis in mammals. Med J Cell Biol 2018; 6(1):33-38.
20. Celichowski P, Nawrocki MJ, Dyszkiewicz-Konwińska MJ, et al. "Positive Regulation of RNA Metabolic Process" Ontology Group Highly Regulated in Porcine Oocytes Matured *In Vitro* : A Microarray Approach. Biomed Res Int 2018; 2018:1-10.
21. Nawrocki MJ, Celichowski P, Budna J, et al. The blood vessels development, morphogenesis and blood circulation are three ontologic groups highly up-regulated in porcine oocytes before in vitro maturation. Adv Cell Biol 2017; 5(2).
22. Tong X, Coulombe PA. Keratin 17 modulates hair follicle cycling in a TNFalpha-dependent fashion. Genes Dev 2006; 20(10):1353-64.
23. Varani S. Knockout of pentraxin 3, a downstream target of growth differentiation Factor-9, causes female subfertility. Mol Endocrinol 2002; 16(6):1154-67.
24. Chen L, Neville RD, Michael DR, et al. Identification and analysis of the human hyaluronan synthase 1 gene promoter reveals Smad3- and Sp3-mediated transcriptional induction. Matrix Biol 2012; 31(7-8):373-79.
25. Salustri A, Garlanda C, Hirsch E, et al. PTX3 plays a key role in the organization of the cumulus oophorus extracellular matrix and in in vivo fertilization. Development 2004; 131(7):1577-86.
26. Hernández EÁ, Kahl S, Seelig A, et al. Acute dietary fat intake initiates alterations in energy metabolism and insulin resistance. J Clin Invest 2017; 127(2):695-708.
27. Hess AP, Hamilton AE, Talbi S, et al. Decidual stromal cell response to paracrine signals from the trophoblast: amplification of immune and angiogenic modulators1. Biol Reprod 2007; 76(1):102-17.
28. Hesse M, Berg T, Wiedenmann B, Spengler U, Woitas RP, Magin TM. A frequent keratin 8 p.L227L polymorphism, but no point mutations in keratin 8 and 18 genes, in patients with various liver disorders. J Med Genet 2004; 41.
29. Zhu R, Wang S-C, Sun C, et al. Hyaluronan-CD44 interaction promotes growth of decidual stromal cells in human first-trimester pregnancy. PLoS One 2013; 8(9):e74812.
30. Knudtson JF, McLaughlin JE, Santos MT, Binkley PA, Tekmal RR, Schenken RS. The hyaluronic acid system is intact in menstrual endometrial cells in women with and without endometriosis. Reprod Sci 2018; 26(1):109-13.

EFFECT OF INSULIN-LIKE GROWTH FACTOR-1 ON PROMOTING HEALING OF SKIN ULCERS IN DIABETIC RATS

F. GONG*, F. ZHAO*, SL. CHENG, D. DING, BW. ZHANG, XL. LI and YL. HUANG

Department of Orthopaedics, People's Hospital of Autonomous Region of Ningxia Medical University, Yinchuan City, Ningxia Autonomous Region, China

Received December 16, 2018 – Accepted February 5, 2019

*These authors contributed equally to this work

To investigate the effect of exogenous insulin-like growth factor-1 (IGF-1) on the healing of skin ulcers in diabetic rats, male Sprague Dawleys (SD) rats with back skin ulcers were selected and divided into control group, model group and IGF-1 treatment group which received different doses of IGF-1 (0.5, 1.0, 1.5, and 2.0mg/L). The results showed that the healing speed of the skin ulcers was significantly affected by IGF-1, which reduced the size of wound (P<0.05). The expression of MMP-9 was enhanced while the expression of TIMP-1 was decreased in diabetic rats with skin ulcers. The IGF-1 treatment helped to restore the normal expression of both MMP-9 and TIMP-1 in diabetic rats with skin ulcers, and diabetic skin ulcers in the 1.5 mg/L IGF-1 group showed the best healing. Histological examination showed that after 20 days, fibroblasts in the IGF-1 experimental group with an appropriate concentration increased and the numbers of fibroblasts and capillaries were significantly higher than those of the other groups. Moreover, there were obvious wound surface contractions and re-epithelialization, and the new epithelium moved to the center of the wound faster. Therefore, it is concluded that an appropriate concentration of IGF-1 can significantly promote the healing of skin ulcers in diabetic rats.

With accelerated urbanization, population growth and aging, diabetes has become one of the primary diseases endangering human health worldwide (1). According to statistics, the number of diabetic patients (aged 20-79 years) reached 425 million in 2017, nearly triple the number of 151 million in 2000. By 2045, the number is expected to reach 629 million. The skin of diabetic patients is easily damaged, and in addition, diabetic vascular lesions may lead to ischemia and hypoxia of local tissues, while diabetic neuropathy may lead to local hypoesthesia (2). Therefore, as a chronic ulcer disease, diabetic skin ulcers is a common complication of diabetes. If diabetes is not treated timely, it will become more serious and may eventually lead to amputation, thus seriously affecting the quality of life of the patients. IGF-1 is one of the most widely distributed growth factors in the body and is secreted by almost all types of tissues and cells. Highly homologous with insulinogen, IGF-1 can promote cell differentiation and proliferation through its roles in the autocrine and paracrine systems (3, 4). It has been shown that IGF-1 is involved in the processes of wound inflammation, granulation tissue proliferation and re-epithelialization by improving the speed and quality of wound healing (5, 6). Topical IGF-1 has been used as a therapeutic

Key words: insulin-like growth factor-1; diabetes; skin ulcers; matrix metalloproteinase-9

Corresponding Author:
Dr Fei Zhao,
Department of Orthopaedics,
People's Hospital of Autonomous Region of Ningxia Medical University, Yinchuan City, 750001,
Ningxia Autonomous Region, China
e-mail: zhaofeinx198@126.com

0393-974X (2019)

agent to accelerate the healing of diabetic skin ulcers, to shorten the course, and reduce the cost of treatment. Due to the high cost of IGF-1 treatment and the possibility of inducing carcinogenesis at high doses, it is necessary to determine the minimum safe and effective concentration in the treatment of skin ulcers. Therefore, in this study, the effect of different concentrations of exogenous IGF-1 on the healing of skin ulcers in diabetic rats was observed, in order to determine the optimal concentration.

MATERIALS AND METHODS

Animals

Thirty male Sprague Dawley rats (aged 4-6 weeks, weight 70-180g, purchased from Nanjing Junke Bioengineering Co., Ltd., China) were used for this study. All rats were housed under a 12-hour light/dark cycle, and were given free access to food and water. The temperature and humidity of the animal facility were controlled at 22±2°C and 40-60%, respectively. The rats were allowed 1-week for acclimation prior to the experiment. The protocol was approved by the ethics committee of People's Hospital of Autonomous Region of Ningxia Medical University, and the experiment was carried out following the regulations of the State Science and Technology Commission on the management of laboratory animals.

Preparation of diabetic rat models

Rats were divided into three groups: control group (n=5), model group (n=5) and experimental group (n=20). Rats in the model and experimental groups were intraperitoneally injected with 60mg/kg of streptozotocin (STZ, Sigma company, USA) to induce diabetes. At 48 h after STZ injection, the level of blood glucose in the rats was above 16.7mmol/L, indicating the diabetes model was successfully established. Through the process of modeling, 20 diabetic rats were successfully obtained for subsequent establishment of the skin ulcer model.

Preparation of major liquids

2.10g of citric acid (Henan Shenghua Chemical Products Co., Ltd., China) was dissolved in 100mL of double distilled water (Shanghai regal Biology Technology Co, Ltd., China) to obtain the mother liquor of citric acid, which was also termed liquid A; 2.94 g of sodium citrate (Suzhou Kaixiang Fine Chemical Co, Ltd., China) was dissolved in 100 mL of double distilled water to obtain the mother liquor of sodium citrate, which was also called liquid B; 57 mL of liquid A and 43 mL of liquid B were then mixed together to obtain a 0.1mol/L citric acid buffer solution at PH4.4; prior to its application, STZ was dissolved in a pre-chilled citrate buffer to prepare an injectable solution at a concentration of 20mg/mL (prepared on ice in the dark). IGF-1 solutions (Nanjing Dian Biotechnology Co, Ltd., China) were prepared using a freeze-dried product at 15 min before use. During the preparation, each bottle of IGF-1 was dissolved in 1 ml of the sample diluent and mixed at room temperature for about 10 min to obtain an IGF-1 solution at a concentration of 10mg/L, which then underwent a series of dilutions to obtain IGF-1 solutions at concentrations of 2.0mg/L, 1.5mg/L, 1.0mg/L and 0.5mg/L, respectively.

Preparation and treatment of skin ulcer rats

Two weeks later, all rats (in the control, model and experimental groups) were intraperitoneally injected with chloral hydrate (Shanghai Xin Yu Biotech Co., Ltd., China). After general anesthesia, a 2cm x 2cm square wound was made on the back of each rat using a scalpel to generate a skin ulcer wound. After the skin wound was formed, 20 rats in the experimental group were randomly divided into 4 sub-groups (each of 5 animals) and 0.5, 1.0, 1.5, and 2.0 mg/L of IGF-1 (0.5mg/L group, 1.0 mg/L group, 1.5mg/L group, and 2.0mg/L group, respectively) were provided. In all treatment groups, 0.1 mL of IGF-1 solution was applied once a day to the wound surface using a piece of sterile gauze. The control group and the model group were given the same amount of normal saline. The treatment of IGF-1 was continued for 20 days.

Statistical analysis

The experimental data are expressed as mean ± standard deviation. SPSS19.0 software was used for statistical analysis. Student's *t*-test was used for the comparison between two groups, and $P < 0.05$ was considered statistically significant.

RESULTS

Macroscopic observation of skin ulcers

Fig. 1 shows representative images of skin ulcers

in the model group, 0.5mg/L group, 1.0 mg/L group, 2.0mg/L group, 1.5mg/L group and control group (left to right), respectively. In the model group, the ulcers worsened over time. The control group showed better healing of ulcers than that in the model group. After IGF-1 treatment, the wound healing was improved to various degrees. Overall, IGF-1 with a concentration of 1.5mg/L showed the best effect. The comparison of skin wounds in different groups is shown in Fig.1 and Fig. 2.

Observation of skin ulcer healing by electron microscopy

Rats in the normal control group healed normally and growth of fibroblasts was observed (Fig. 3). As the healing time increased, the number of inflammatory

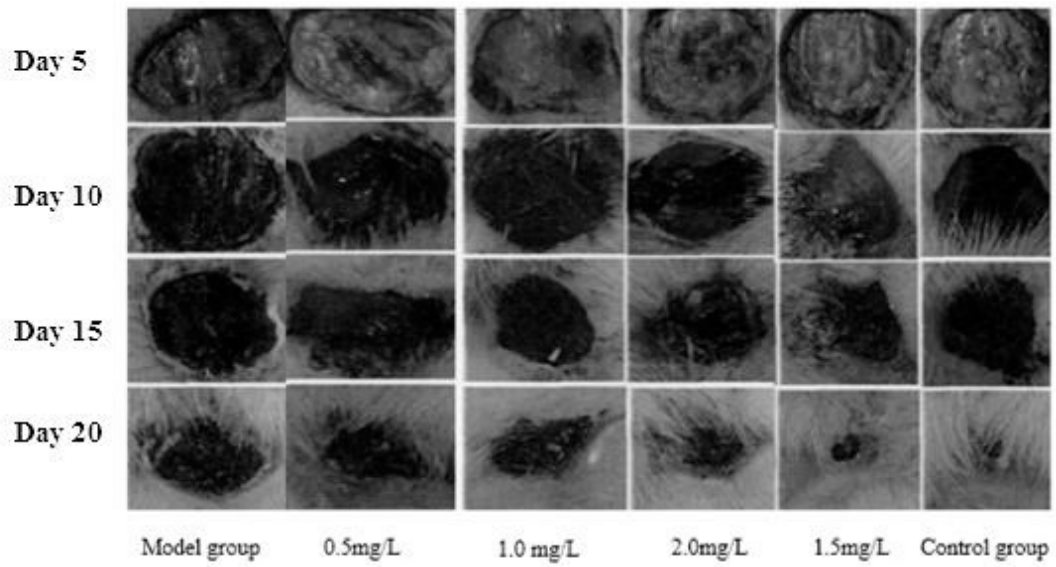

Fig. 1. *Observation of skin wounds in different groups on days 5, 10, 15 and 20 after modeling.*

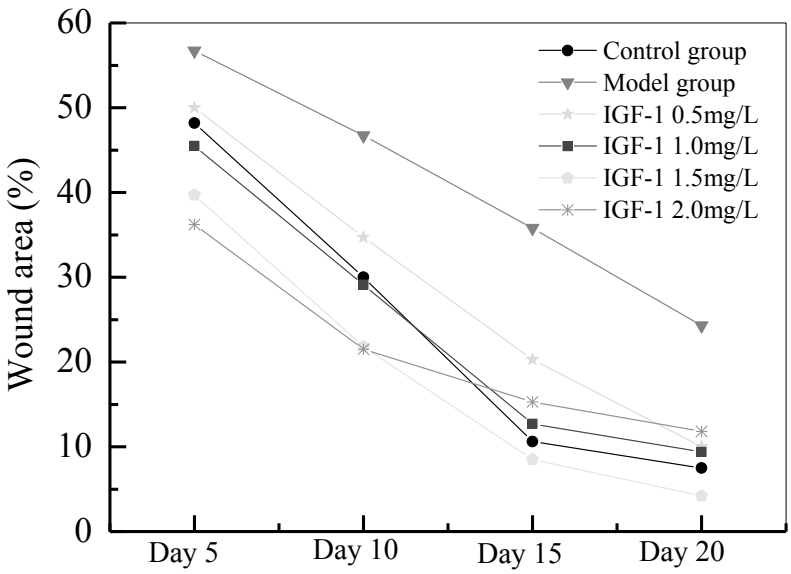

Fig. 2. *Comparison of skin wound areas in rats of different groups*

cells decreased and the tissue structure became clearer, along with increased amount of matrix and capillary tissues. The number of fibroblasts and neovascularization were significantly lower in the diabetes model group. Rapid granulation growth and a large number of fibroblasts and capillaries were observed in the groups treated by IGF-1. In addition, all IGF-1 treatment groups showed active proliferation of fibroblasts, with collagen fiber bundles arranged in a dense and orderly manner, indicating good healing. In particular, the number of fibroblasts in rats treated with 1.5mg/L IGF-1 was greater compared to other treatment groups, with better morphology. Although healing in the 2.0mg/L group was significantly faster than that in the 0.5mg/L and 1.0mg/L groups, the epidermal coverage in the 2.0mg/L group was worse than that in the 1.5mg/L group. Therefore, wound healing in the 1.5mg/L group was considered the best.

As shown in Fig. 4A, fibroblasts in the normal control group were orderly distributed and surrounded by closely arranged collagen fibers. Fibroblasts in the model group were less orderly distributed and their surrounding tissues showed signs of inflammation. On day 20 of IGF-1 intervention, more fibroblasts, regular cell morphology, enrichment of endoplasmic reticulum, mitochondria, lysosomes, Golgi complex and other cytoplasmic organelles, and a large number of neatly arranged collagen fibers were found in the IGF-1 treatment groups (Fig. 4B). Therefore, IGF-1 can promote wound healing compared with the normal control group.

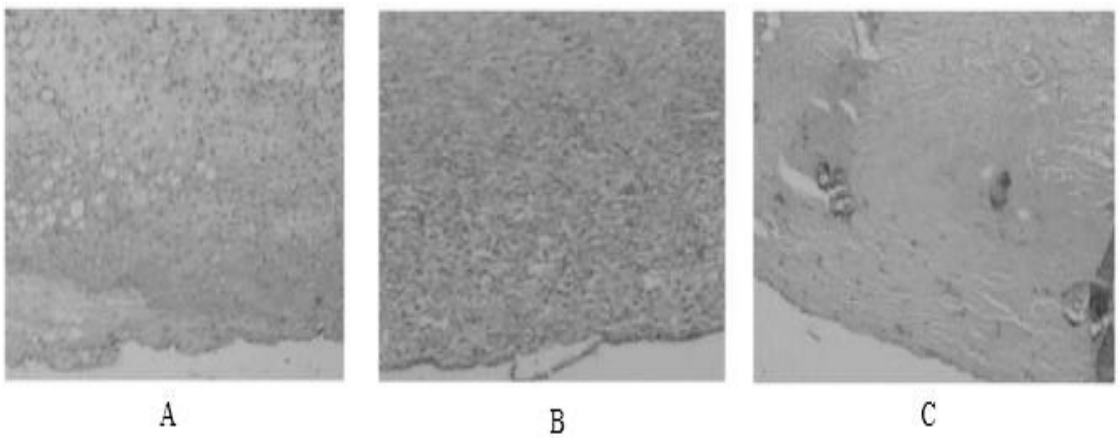

Fig. 3. *The expression of CD133 on the surface of transfected cell lines was detected by immunochemistry assays: **A**) Normal control group; **B**) Experimental group; **C**) diabetes model group) (×100).*

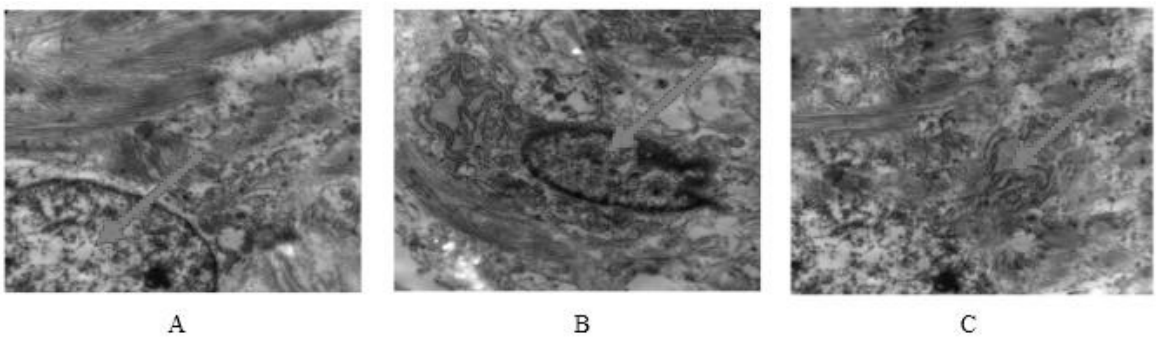

Fig. 4. *Morphological observation of fibroblasts on day 20 of skin ulcer treatment with exogenous insulin-like growth factor-1: **A**) Normal control group; **B**) Experimental group, and **C**) Diabetes model group) (×15 000).*

Expressions of MMP-9/Timp-1 in skin tissues of various groups

Compared with the control group, MMP-9 expressions in skin wounds significantly increased in the diabetes group and reached the peak on day 10 before it gradually decreased. The expression levels of MMP-9 in different IGF-1 dose groups were lower than those in the model group, suggesting that topical IGF-1 could alleviate skin ulcers. The expression level of MMP-9 also decreased in different IGF-1 dose groups. The effects of IGF-1 at concentrations of 0.5mg/L and 1.0mg/L were similar. At a concentration of 2.0 mg/L, the MMP-9 expression reached the peak on day 5 before it gradually decreased, but the MMP-9 expression remained higher than that in the control group and 1.5 mg/L group. Therefore, it was concluded that although a high dose of IGF-1 could temporarily relieve the skin ulcer, it was not suitable for long-term application. Therefore, 1.5mg/L was considered as the optimal dose of IGF-1, as shown in Table I. Fig. 5 shows the expression level of MMP-9/TIMP-1 on day 20 of exogenous IGF-1 treatment of skin ulcers.

Comparison of TIMP-1 expressions in skin tissues of different groups at different time points

After diabetes modeling, the expression of TIMP-1 in the skin wounds was significantly reduced. In the diabetes group, the expression of TIMP-1 reached the peak on day 10, and then gradually decreased, although the expression of TIMP-1 in the diabetes group was always lower than that in the control group. As the dose of IGF-1 increased, the expression of Timp-1 also increased. At concentrations of 0.5mg/L and 1.0mg/L, the expression of TIMP-1 was higher than that in the model group, although it was still lower than that in the control group on day 5 and day 10. On day 15 and day 20, although the expression of TIMP-1 in all groups decreased, TIMP-1 expressions in the 0.5mg/L and 1.0mg/L IGF-1 groups were higher than those in the control group. At a dose of 1.5mg/L, the difference was not significant compared

Table I. *Comparison of MMP-9 expressions in various groups at different time points ($\bar{x} \pm s$, gray value).*

Groups	Day 5	Day 10	Day 15	Day 20
Control group	28.35±2.11	34.80±1.27	20.67±2.13	11.32±1.21
Model group	26.24±1.32	37.16±2.41	32.37±1.23	25.22±2.14
0.5mg/L	21.45±2.08	30.41±1.77	23.24±2.05	24.02±2.08
1.0mg/L	22.28±1.66	25.22±2.35	21.16±2.32	22.86±2.07
1.5mg/L	26.94±1.08#	30.74±2.02*	19.57±2.11*	10.25±2.17*
2.0mg/L	27.06±2.10#	23.81±2.06	22.75±2.16	21.55±2.08

**P<0.05, compared with other dose groups; #P<0.05, compared with the control group*

Table II. *Comparison of Timp-1 expressions in different groups at different time points ($\bar{x} \pm s$, gray value).*

Groups	Day 5	Day 10	Day 15	Day 20
Control group	60.36±2.15*	80.08±3.01*	40.37±3.65*	10.17±5.21*
Model group	39.77±1.24	49.33±3.14	37.17±4.04	8.06±3.45
0.5mg/L	49.37±2.24	60.43±2.46	45.17±3.22	20.34±2.03
1.0mg/L	50.67±3.01	68.56±3.10	44.26±2.23	18.08±3.02
1.5mg/L	58.24±3.11*	78.62±5.06*	41.32±2.54*	12.19±3.17*
2.0mg/L	62.51±2.68	73.51±2.15	46.26±3.14	17.05±2.15

**P<0.05, compared with other dose groups*

with the control group. At an IGF-1 dose of 2.0mg/L, the effect of IGF-1 became significantly higher on day 5 and day 10, although no significant difference was observed among the three groups at later time points. Therefore, 1.5mg/L was considered as the optimal dose of IGF-1, as shown in Table II.

It was found that the expression of MMP-9 was higher in skin wounds of the diabetes mellitus model than the controls (Fig. 5). It was also found that the electrophoresis maps obtained under different processing methods were different.

DISCUSSION

Skin wound healing depends on the level of collagen synthesis in the wound (7). It has been shown that IGF-1 plays an important physiological role in wound healing. The main source of IGF-1 is outside the wound surface, which is closely related to the proliferation and activity of fibroblasts (8, 9). IGF-1, also known as somatomedin and highly homologous to proinsulin, is a single-chain basic polypeptide consisting of 70 amino acids (10). IGF-1 can induce the expression of basic fibroblast growth factor (bFGF), transforming growth factor-β (TGF-β) and other cytokines to promote production of fibronectin (11), to enhance synthesis and secretion of extracellular matrix, such as polyglucosamine and collagen, and to affect tissue remodeling upon wound repair (12). With the function of promoting insulin metabolism, IGF-1 mainly regulates body growth and development after birth by mediating the effect of growth hormone (G-H) (13). In G-H-deficient patients, IGF-1 can promote muscle and bone growth, promote brain development, and increase body weight. As an important growth factor, IGF also plays an important regulatory role in the proliferation, differentiation, and apoptosis of tissues and tumor cells via the autocrine and paracrine system (14, 15).

Changes in the expression of IGF-1 in wounds are associated with generation of fibroblasts and type I collagen. IGF-1 is closely involved in the regulation of type I collagen synthesis in the wound microenvironment. IGF-1 is intrinsically linked to the secretion of type I collagen and healing of wounds, while Type I and III collagens produced by fibroblasts are the main interstitial components in skin connective tissues (16). Type I and III collagens not only repair tissue defects, but also provide a scaffold for the migration of epidermal cells. Therefore, the proliferation and activation of fibroblasts in the wound directly affect wound healing (17, 18).

In this study, IGF-1 was used to repair diabetic wounds. The experimental results showed that, compared with the control group, IGF-1 significantly promoted healing of back ulcers in diabetic rats, manifested as a significantly reduced wound area and a significantly increased wound healing velocity. IGF-1 promoted the formation of new blood vessels on the wound surface as well as the growth and re-epithelialization of granulation tissues to achieve better wound healing than the control group. Clinically, many drugs based on insulin-like growth factors have been used in the treatment of diabetic ulcers by effectively improving local blood circulation, by promoting the regeneration of capillaries on the wound surface and by accelerating would healing. The advantages of this study were as follows. Firstly, it was verified that the

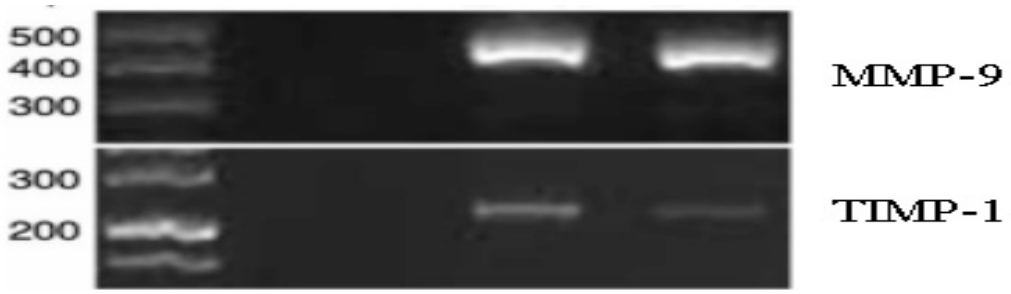

Fig. 5. *Electrophoresis detection of IGF-1 under MMP-9 and TIMP-1.*

application of exogenous IGF-1 can promote healing of skin ulcers in diabetic rats. Secondly, the optimal concentration of exogenous IGF-1 to promote healing of skin ulcers in diabetic rats was found to be 1.5mg/L, providing a theoretical basis for the application of insulin-like growth factor in clinical practice. The shortcoming of this study was that, when confirming whether IGF-1 was the result of the wound, the abnormal distribution of cell growth factor was not found in the localization, but the content of protein and its receptor was significantly lower than that of normal skin tissues. Accordingly, it can be considered that the main cause of delayed wound repair is the signal caused by altered expressions and functions of cytokine receptors and their downstream signaling molecules through factors affecting cell migration and nuclear gene expressions. Since the signaling process of cytokines and receptors is very complex, further studies are needed to elucidate the mechanism.

MMPs are involved in the process of wound matrix degradation and skin remodeling. The expression and activity changes of MMPs are closely related to wound healing fibrosis, scar formation and healing velocity of chronic wounds. It has been shown that the imbalance of MMPs/TIMPs is an important factor in the formation of chronic wounds (19, 20). During normal wound healing, MMPs/TIMPs play an important role in the removal of necrotic substances, cell migration and extracellular matrix degradation and remodeling. High expressions of MMPs promote cell migration and proliferation. The TIMP family inhibits the function of the MMP family and regulates the latter to function normally. They work together to maintain extracellular matrix homeostasis. In this experiment, it was found that after the establishment of diabetes models, MMP-9 and TIMP-1 were increased or decreased to different degrees compared with normal controls. However, after IGF-1 treatment, there were different trends, and the different dose groups changed differently. At a higher IGF-1 concentration of 2.0mg/L, the two indicators increased or decreased rapidly, and the effect was signigicant. Then, as time passed, the curative effect trend was not obvious, and the effect was equivalent to the smaller concentrations (0.5mg/L, and 1.0mg/L). At an IGF-1 concentration of 1.5mg/L, the trend of each indicator was the same as that of the normal control, and there was no significant difference. It was proved that the concentration of IGF-1 was suitable, and MMP-9/ TIMP-1 had a certain effect on skin lesions. It was shown that MMP-9/ TIMP-1 of normal skin maintained a stable level of dynamic balance (20, 21). When MMPs changed, its physiological antagonist TIMP also changed correspondingly. This balance change was not only conducive to the repair of local wounds, but also prevented excessive damage and accumulation of local substances.

To sum up, IGF-1 significantly accelerated the healing of skin ulcers in diabetic rats to a level higher than that in normal controls, and the effect of IGF-1 was greatest at a concentration of 1.5mg/L. This study showed that IGF-1 can be used as a safe and effective agent in the treatment of diabetic skin ulcers by significantly increasing healing speed and improving the quality of healing.

ACKNOWLEDGEMENTS

This work was supported by Ningxia Natural Science Foundation (NZ16182 and NZ16177).

REFERENCES

1. Alberti KG, Zimmet PZ. Epidemiology of diabetes-status of a pandemic and issues around metabolic surgery. Diabetes Care 2016; 39(6):878-83.
2. Rosenstein R, Hough A. Empagliflozin, Cardiovascular outcomes, and mortality in type 2 diabetes. N Engl J Med 2016; 374(11):1093-94.
3. Doré S, Pelletier JP, Dibattista JA, Tardif G, Brazeau P, Martel-Pelletier J. Human osteoarthritic chondrocytes possess an increased number of insulin-like growth factor 1 binding sites but are unresponsive to its stimulation. Possible role of IGF-1-binding proteins. Arthritis Rheum 1994; 37(2):253-63.
4. Rechler MM. Insulin-like growth factor binding proteins. Vitam Horm 2015; 29(5):713-22.
5. Wang XQ, Sarah L, Heather W, et al. Ganglioside GM3 depletion reverses impaired wound healing in diabetic rats by activating IGF-1 and insulin receptors. J Invest Dermatol 2014; 134(5):1446-55.
6. Schmidmaier G, Wildemann B, Gäbelein T, Heeger J,

Kandziora F, Haas NP, Raschke M. Synergistic effect of IGF-I and TGF-ß1 on fracture healing in ratsSingle versus combined application of IGF-I and TGF-ß1. Acta Orthop Scand 2003; 74(5):604-10.

7. Dangwal S, Stratmann B, Bang C, et al. Impairment of wound healing in patients with type 2 diabetes mellitus influences circulating MicroRNA patterns via inflammatory cytokines. Arterioscler Thromb Vasc Biol 2015; 35(6):1480-88.
8. Levine ME, Suarez JA, Brandhorst S, et al. Low protein intake is associated with a major reduction in IGF-1, cancer, and overall mortality in the 65 and younger but not older population. Cell Metab 2014; 19(3):407-17.
9. Balaji S, Lesaint M, Bhattacharya SS, et al. Adenoviral-mediated gene transfer of insulin-like growth factor 1 enhances wound healing and induces angiogenesis. J Surg Res 2014; 190(1):367-77.
10. Nakae J, Barr V, Accili D. Differential regulation of gene expression by insulin and IGF-1 receptors correlates with phosphorylation of a single amino acid residue in the forkhead transcription factor FKHR. EMBO J 2000; 19(5):989-96.
11. Brooker GJ, Kalloniatis M, Russo VC, Murphy M, Werther GA, Bartlett PF. Endogenous IGF-1 regulates the neuronal differentiation of adult stem cells. J Neurosci Res 2000; 59(3):332-41.
12. Stoll M, Bitterlich N, Cornelli U. Randomised, double-blind, clinical investigation to compare orlistat 60 milligram and a customized polyglucosamine, two treatment methods for the management of overweight and obesity. BMC Obes 2017; 4:4.
13. Jiang G, Wang W, Cao Q, et al. Insulin growth factor-1 (IGF-1) enhances hippocampal excitatory and seizure activity through IGF-1 receptor-mediated mechanisms in the epileptic brain. Clin Sci (Lond) 2015; 129(12):1047-60.
14. Jayesh P, Philip R, Singh IS. Multifactorial interaction of growth factors on Penaeus monodon, lymphoid cells and the impact of IGFs in DNA synthesis and metabolic activity in vitro. Cytotechnology 2015; 67(3):559-71.
15. Wang J, Shi M, Xi Y, et al. Recombinant human vascular endothelial growth factor receptor effectively inhibits angiogenesis in vivo. Mol Med Rep 2015; 11(5):3432-38.
16. Liao MH, Liu SS, Peng IC, Tsai FJ, Huang HH. The stimulatory effects of alpha1-adrenergic receptors on TGF-beta1, IGF-1 and hyaluronan production in human skin fibroblasts. Cell Tissue Res 2014; 357(3):681-93.
17. Armakolas A, Dimakakos A, Loukogiannaki C, et al. IL-6 is associated to IGF-1Ec upregulation and Ec peptide secretion, from prostate tumors. Mol Med 2018; 24(1):6.
18. Zhang Y, Li MX, Wang H, Zeng Z, Li XM. Metformin down-regulates endometrial carcinoma cell secretion of IGF-1 and expression of IGF-1R. Asian Pac J Cancer Prev 2015; 16(1):221-25.
19. Pirayesh A, Dessy LA, Rogge FJ, et al. The efficacy of a polyhydrated ionogen impregnated dressing in the treatment of recalcitrant diabetic foot ulcers: a multi-centre pilot study. Acta Chir Belg 2007; 107(6):675-81.
20. Muller M, Trocme C, Lardy B, Morel F, Halimi S, Benhamou PY. Matrix metalloproteinases and diabetic foot ulcers: the ratio of MMP-1 to TIMP-1 is a predictor of wound healing. Diabet Med 2008; 25(4):419-26.
21. Ulrich D, Noah EM, von Heimburg D, Pallua N.TIMP-1, MMP-2, MMP-9, and PIIINP as serum markers for skin fibrosis in patients following severe burn trauma. Plast Reconstr Surg 2003; 111(4):1423-31.
22. Ghomrasseni S, Dridi M, Gogly B, et al. Anetoderma: an altered balance between metalloproteinases and tissue inhibitors of metalloproteinases. Am J Dermatopathol 2002; 24(2):118-29.

GENE EXPRESSION REGULATING LIPOPOLYSACCHARIDE AND LIPID METABOLIC PROCESSES IN PORCINE ORAL MUCOSAL CELLS IN LONG-TERM PRIMARY *IN VITRO* CULTURE

A. BRYJA[1], M. DYSZKIEWICZ-KONWIŃSKA[1,2], P. CELICHOWSKI[3], I. KOCHEROVA[1], M.J. NAWROCKI[1], A. CHAMIER-GLISZCZYŃSKA[3], K. STEFAŃSKA[3], K. MEHR[4], P. ANTOSIK[5], D. BUKOWSKA[5], H. PIOTROWSKA-KEMPISTY[6], M. BRUSKA[1], M. NOWICKI[3] and B. KEMPISTY[1,3,7]

[1]Department of Anatomy, Poznan University of Medical Science, Poznań, Poland; [2]Department of Biomaterials and Experimental Dentistry, Poznan University of Medical Sciences, Poznań, Poland; [3]Department of Histology and Embryology, Poznan University of Medical Science, Poznań, Poland; [4]Department of Dental Prosthetics, Pomeranian Medical University in Szczecin, Szczecin, Poland; [5]Veterinary Center, Nicolaus Copernicus University in Torun, Toruń, Poland; [6]Department of Toxicology, Poznan University of Medical Science, Poznań, Poland; [7]Department of Obstetrics and Gynecology, University Hospital and Masaryk University, Brno, Czech Republic

Received October 24, 2018 – Accepted March 5, 2019

Lipids are an alternative energy source for cells and provide structural integrity in cell membrane and their metabolism is regulated with the use of different pathways, such as integrin signalling, oxidative stress, mechanical stress, and pH changes. All of those processes take place in the oral mucosa which is subject to different environmental impacts. In this study, porcine buccal pouch mucosal cells (pBPMCs) were used during long-term primary *in vitro* culture. The cultured cells were collected at 7, 15 and 30 days of IVC and subsequently transferred to RNA isolation. In the results of the following microarray analysis, we analyzed the genes detected, belonging to ontology groups, such as "cellular lipid metabolic process", "response to lipid" and "response to lipopolysaccharides. All of the genes involved in these ontological groups were expressed at higher levels at 7 days of IVC and substantially decreased in expression at days 15 and 30 of primary culture. We observed new genes, which may be recognized as markers in regulation of lipid metabolism in mucosal cells *in vitro*. The results suggested that the biochemical mechanism-involved lipids were accompanied by increased enzymatic activation and synthesis of crucial growth factors reaching high activity at day 7 of culture, which is also well documented as a stage of tissue regeneration period within oral mucosa. Therefore, this "biochemical fingerprint" may be an additional checkpoint of the integrity, resistance and easy adaptability of oral tissues, which are important conditions of success in tissue engineering and grafting for tissue reconstruction.

The biology of oral cavity cells and tissue has recently become a subject of huge interest among scientists and clinicians, especially regarding the topics of drug delivery and administration. It is a well-accepted theory that oral mucous membrane displays a crucial role for drug transport and/or

Key words: oral mucosa; lipopolysaccharides; lipid metabolic process; pig

Corresponding Author:
Bartosz Kempisty PhD,
Department of Histology and Embryology,
Department of Anatomy, Poznań University of Medical Sciences,
6 Święcickiego St., 60-781 Poznań, Poland
Tel./Fax: +48 61 8546418 / +48 61 8546440,
e-mail: bkempisty@ump.edu.pl

0393-974X (2019)

selective administration. Therefore, the permanent morphological, biochemical and/or metabolomic modification within the oral mucosa is the basis of possibilities for drug delivery. The continuous changes in the tissues of the oral region are also recognized as the marker of several diseases, as well as response to external damage factors such as radiotherapy and chemotherapy (1). Although the clinical symptoms of human diseases diagnosed in the oral tissues are well defined, the oral cells and tissue biology still requires further investigation. Pigs are often used as the model for biomedical research, however the experiments including porcine mucosal tissue, isolated, are performed for the first time in this study (2, 3). The porcine model was used to investigate the possibilities of buccal pouch mucosal cells in long-term *in vitro* culture (IVC). The porcine mucosal cells, primary culture model was used to analyse the gene expression profile involved in ontological groups, that are crucial for long-term *in vitro* culture, and cellular metabolic profile, as well as cell survival and/or apoptosis *in vitro*.

The cellular metabolic status is crucial for cell survival and lifespan. Recently, the proteomic and metabolomic profile of cells *in vitro* and/or *in vivo* is of high interest in the diagnosis of several human diseases. However, there are still few data regarding buccal pouch mucosal cell metabolic status during primary *in-vitro* culture. Furthermore, the cellular lipid metabolism profile is still undiscovered in these cells. Based on our recent observations, we suggested that the lipid metabolism may display a significant role in other processes such as cell proliferation, migration, differentiation, and sustaining of stemness plasticity in oral tissue architecture (4).

Although the morphological and biochemical changes within the mucosal tissue are well recognized in humans, the cellular transcriptomic, proteomic and metabolic status, during primary *in vitro* culture, is still unexplored (5). Using microarray assays and respective cell culture prepared *in vitro,* new genes were discovered that might be used in the future as the markers of physiological and pathophysiological processes in oral mucosal tissues. Therefore, in this study the complete transcriptomic analysis of genes expression profile involved in three ontological groups is presented, such as; "cellular lipid metabolic process", "response to lipids" and "response to lipopolysaccharide".

MATERIALS AND METHODS

Animals

For this study, a total of 35 pubertal crossbred Landrace gilts bred on a commercial local farm were

Table I. *Primers used for RT-qPCR analysis.*

Name	ID Number	Product Length (bp)	5'-3'	3'-5'
TGFB1	NM_214015.2	208	ACCATGCCAATTTCTGCCTG	GAACGCACGATCATGTTGGA
CCL2	NM_214214.1	185	TCTCCAGTCACCTGCTGCTA	TCTAGGTGGCTTATGGAGTC
SCARB1	NM_213967	155	GCCATTCAGGCCTATTCTGA	TGAAGAAGTGGGGTGTAGGG
PTGS2	NM_214321.1	184	AACATGGCATCACCCAATTT	GATCGATAGGGCTTCAGCAG
CXCL2	NM_001001861.2	237	CTGTGACCAAACGGAAGTCA	AGCCAAATGCATGAAACACA
UGCG	XM_021067532.1	173	AGAATGCTTCGTTGCCAGTT	CGACCGCGTAATCAAGTTTT
PDPN	XM_005665017.3	165	TTCATTGGTGCAATCATCGT	TTTCCACGGGTCATCTTCTC
LYN	XM_021089363.1	229	CTCCAGAGGCCATCAACTTC	CTCTCCTCCGCCTTCTCTTT
SPP1	NM_214023.1	220	ACTCCGATGAATCCGATGAG	TCCGTCTCCTCACTTTCCAC
ETS1	NM_001162886.1	208	CAGCCTGAAAGGTGTGGATT	ATCCGAGGTATAGCGGGACT
FABP5	NM_001039746.2	244	ATGGCAAAGACCTCACCATC	CGAGTGCAGGTGACATTGTT
SMPDL3A	XM_003480256.4	218	GTTTGTGGCACCTGCTGTTA	TTGGCTGCAAATCTTCAATG

used. They had a mean age of 155 days (range 140–170 days), and the mean weight was 100 kg (95-120 kg). All of the animals were housed under identical conditions and fed the same forage (depending on age and reproductive status). The experiments were approved by the Local Ethics Committee of the Poznan University of Life Sciences, Poland (permission no. 32/2012).

Cell isolation and culture

After slaughter, samples of buccal pouch mucosa were obtained within 40 min. and transported to the laboratory. The excised tissue was washed twice in Dulbecco's phosphate buffered saline (D-PBS; Sigma Aldrich, Madison, USA). The surface of the buccal pouch was surgically removed using sterile surgical blades. The tissue fragments were incubated with 0.05% collagenase I (Sigma Aldrich, Madison, USA) for 40 min. at 37°C and then were treated which 0.5% Trypsin/EDTA (Cascade Biologics, Portland, USA) for 10 min. The cell suspension obtained from this digestion was filtered through mesh and later was centrifuged (10 min. at 200 g) with Dulbecco's modified Eagle's medium (DMEM; Sigma Aldrich, Madison, USA). The final cell pellet was resuspended in DMEM supplemented with 10% fetal calf serum (FCS; Sigma Aldrich, Madison, USA) and 10 U/mL penicillin G, 10 mg/mL streptomycin, and 25 μg/mL amphotericin B. The cells were cultured at 37 °C in a humidified atmosphere of 5% CO_2. Once the oral mucosal cell cultures attained 70–80% confluency, they were passaged by digested with 0.025% Trypsin/EDTA (Cascade Biologics, Portland, USA), neutralized by a 0.0125% trypsin inhibitor (Cascade Biologics, Portland, USA), centrifuged, and resuspended at a seeding density of 2×10^4 cells/cm^2. The culture medium was changed every three days. Photos of two morphological types of cells (keratinocytes and fibroblasts) were taken prior to collection and are presented in Fig. 1.

Microarray expression analysis and statistics

Total RNA (100 ng) from each pooled sample was subjected to two rounds of sense cDNA amplification (Ambion® WT Expression Kit). The obtained cDNA was used for biotin labeling and fragmentation by Affymetrix GeneChip® WT Terminal Labeling and Hybridization (Affymetrix). Biotin-labeled fragments of cDNA (5.5 μg) were hybridized to the Affymetrix® Porcine Gene 1.1 ST Array Strip (48°C/20 h). Microarrays were then washed and stained according to the technical protocol using the Affymetrix GeneAtlas Fluidics Station. The array strips were scanned employing Imaging Station of the GeneAtlas System. Preliminary analysis of the scanned chips was performed using Affymetrix GeneAtlasTM Operating Software. All of the presented analyses and graphs were performed using Bioconductor and R programming languages. In order to correct background, normalize,

Table II. *Gene symbols, fold changes in expression, Entrez gene IDs and corrected P values of studied genes.*

Gene symbol	Fold change D15/D7	Fold change D30/D7	Adjusted P value D15/D7	Adjusted P value D30/D7	Entrez gene ID
UGCG	0.38384831	0.58498802	0.02377121	0.0709872	7357
SMPDL3A	0.41018006	0.36414373	0.03001935	0.02440647	10924
CCL2	0.25449428	0.68928442	0.04074382	0.40439092	6347
SCARB1	0.38123463	0.59461872	0.03463649	0.13432707	949
FABP5	0.29640512	0.26633887	0.02683568	0.02350151	2171
LYN	0.39674105	0.40740911	0.03463649	0.04233411	4067
CXCL2	0.15859884	0.36182524	0.02821057	0.10006067	2920
TGFB1	0.44379899	0.81544989	0.01501642	0.21660073	7040
PDPN	0.3878982	0.56600515	0.03422938	0.10331212	10630
SPP1	0.09199492	0.07015643	0.0162712	0.02301938	6696
ETS1	0.39786617	0.46500338	0.03111849	0.04747213	2113
PTGS2	0.17657895	0.3277974	0.03327215	0.08618281	5743

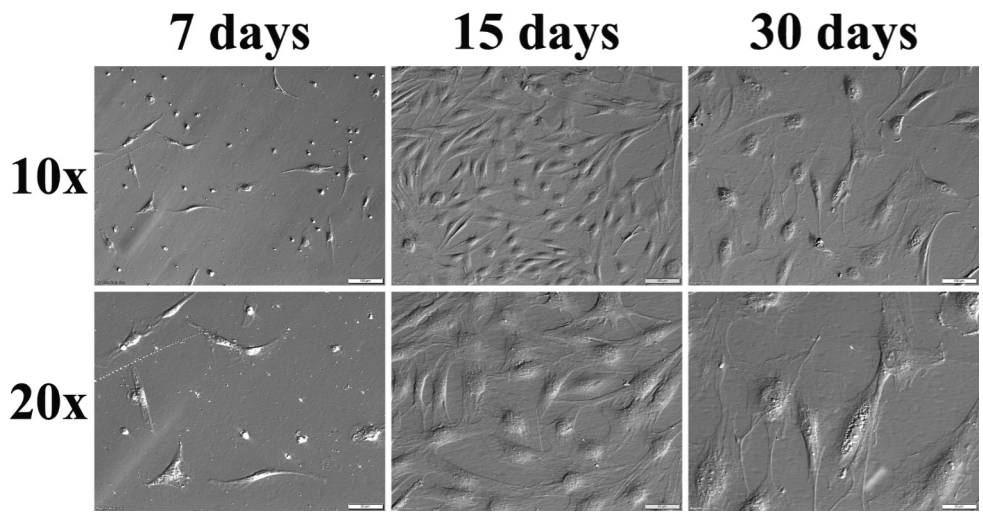

Fig. 1. *Photos of cells prior to material collection, taken using an inverted microscope, under relief contrast. Scale bars: 100 µm (10×), 50 µm (20×).*

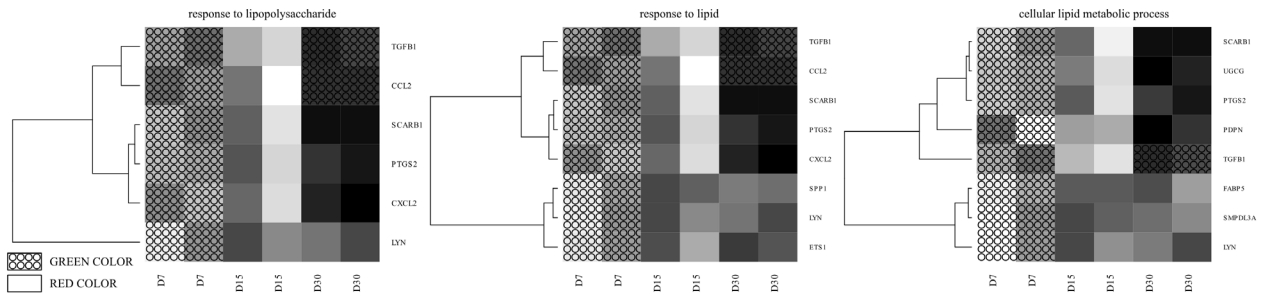

Fig. 2. *Heat map representation of differentially expressed genes belonging to the "response to lipids" (GO:0033993), "response to lipopolysaccharide" (GO:0032496) and "cellular lipid metabolic process" (GO:0044255) GO BP terms*

and summarize results, we used the Robust Multiarray Averaging (RMA) algorithm. To determine the statistical significance of the analyzed genes, moderated *t*-statistics from the empirical Bayes method were performed. The obtained P value was corrected for multiple comparisons using Benjamini and Hochberg's false discovery rate. The selection of significantly altered genes was based on a P value lower than 0.05 and expression higher than two-fold. The differentially expressed gene list (separated for up- and down-regulated genes) was uploaded to DAVID software (Database for Annotation, Visualization and Integrated Discovery) (6). Subsequently, the interaction was analyzed between the genes belonging to chosen GO terms with GOplot package (7). Finally, interactions between differentially expressed genes/proteins belonging to the chosen GO terms were investigated by STRING10 software (Search Tool for the Retrieval of Interacting Genes) (8). The list of gene names was used as a query for an interaction prediction. The search criteria were based on co-occurrences of genes/proteins in scientific texts (text mining), co-expression, and experimentally observed interactions. The results of such analyses generated a gene/protein interaction network where the intensity of the edges reflected the strength of the interaction score.

Real-time quantitative polymerase chain reaction analysis

Real-time quantitative polymerase chain reaction (RT-qPCR) was used to validate the expression of selected

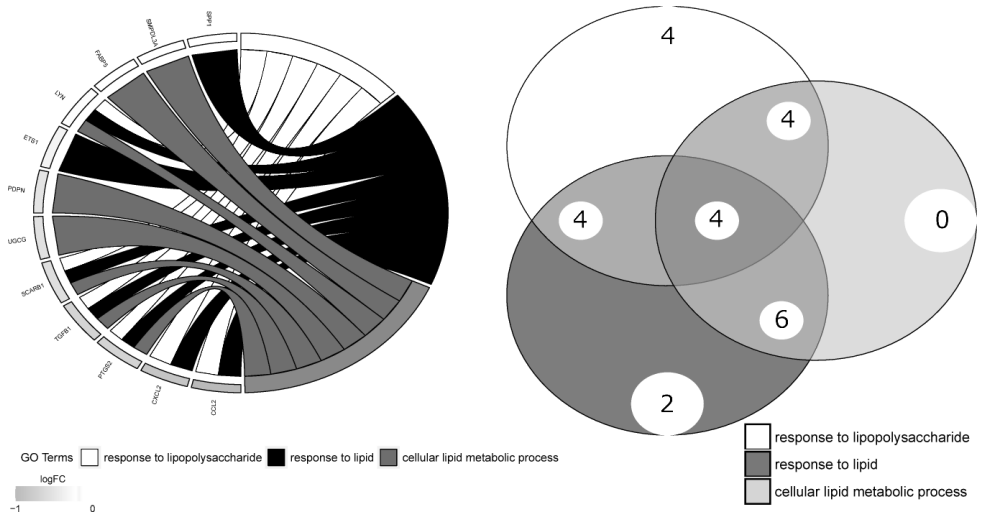

Fig. 3. ***A)*** *The representation of the mutual relationship between "response to lipids" (GO:0033993), "response to lipopolysaccharide" (GO:0032496) and "cellular lipid metabolic process" (GO:0044255) GO BP terms. The ribbons indicate which gene belongs to which categories. The genes were sorted by logFC from most to least changed gene.* ***B)*** *Venn diagram showing numbers of shared or exclusive genes between "response to lipids" (GO:0033993), "response to lipopolysaccharide" (GO:0032496) and "cellular lipid metabolic process" (GO:0044255) GO BP terms.*

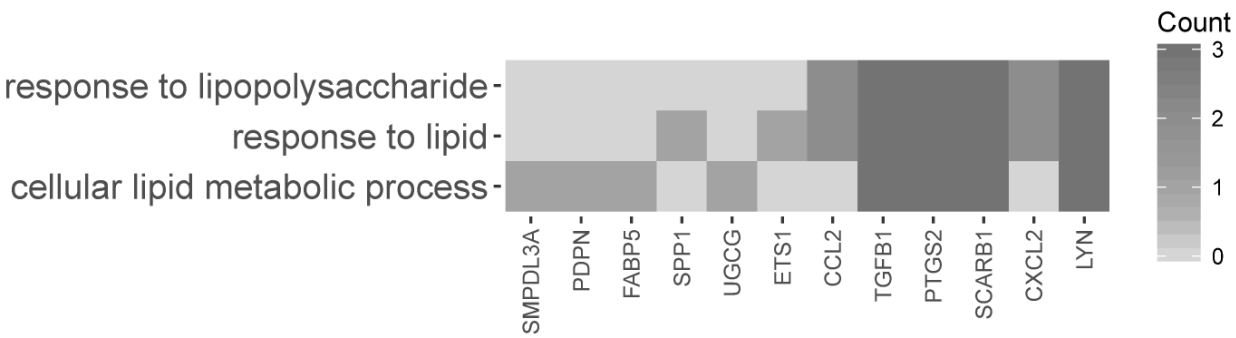

Fig. 4. *Heatmap showing the gene occurrence between "response to lipids" (GO:0033993), "response to lipopolysaccharide" (GO:0032496) and "cellular lipid metabolic process" (GO:0044255) GO BP terms.*

genes from the microarray analysis.

Total RNA was isolated from porcine buccal pouch mucosal cells using an RNeasy mini column from Qiagen GmbH (Hilden, Germany). The RNA samples were resuspended in 20 µl of RNase-free water and stored in liquid nitrogen. RNA samples were treated with DNase I and reverse-transcribed (RT) into cDNA. RT-qPCR was conducted in a LightCycler real-time PCR detection system (Roche Diagnostics GmbH, Mannheim, Germany) using SYBR® Green I as a detection dye, and target cDNA was quantified using the relative quantification method. For amplification, 2 µl of cDNA solution was added to 18 µl of QuantiTect® SYBR® Green PCR (Master Mix Qiagen GmbH, Hilden, Germany) and primers (Table I).

One RNA sample of each preparation was processed without the RT-reaction to provide a negative control for subsequent PCR.

RESULTS

Whole transcriptome profiling by Affymetrix microarray allow analyzing gene expression changes

between 7, 15 and 30 days of buccal pouch mucosa cells culture. Expression of 12257 transcripts was examined by Affymetrix® Porcine Gene 1.1 ST Array Strip. Genes with fold change higher than abs (2) and with corrected P value lower than 0.05 were considered as differentially expressed. This set of genes consists of 130 different transcripts. All the microarray data is available online at https://www.ncbi.nlm.nih.gov/geo/query/acc.cgi?acc=GSE112659.

The DAVID software analysis showed that differently expressed genes belong to 56 gene ontology groups. In this paper we focused on "response to lipids" (GO:0033993), "response to lipopolysaccharide" (GO:0032496) and "cellular lipid metabolic process" (GO:0044255) GO BP terms. These sets of genes were subjected to hierarchical clusterization procedure and are presented as heatmaps (Fig. 2). The gene symbols, fold changes in expression, Entrez gene IDs and corrected P values of these genes are shown in Table II.

Moreover, in gene ontology database genes that formed one particular GO group can also belong to other different GO term categories. By this reason we explored the gene intersections between selected GO BP terms. The relationship between these GO BP terms is presented as a well chart and Venn diagram (Fig. 3), as well as a heatmap (Fig. 4).

STRING interaction network was generated among differentially expressed genes belonging to each of the selected GO BP terms. Using such prediction method provided molecular interaction network formed between protein products of the studied genes (Fig. 5).

The three analyzed ontology groups include 12 genes, presenting three patterns of expression. TGFβ1 and CCL2 were significantly upregulated on day 7 of culture, which was followed then by large downregulation on day 15 and slight upregulation on day 30. SCARB1, PTGS2, CXCL2, UGCG, and PDPN expressed similar patterns on days 7 and 15. However, there was no change or little decrease in expression on day 30. Finally, LYN, SPP1, ETS1, FABP5, and SMDPL3A also continued the tendencies on days 7 and 15, which were followed by further

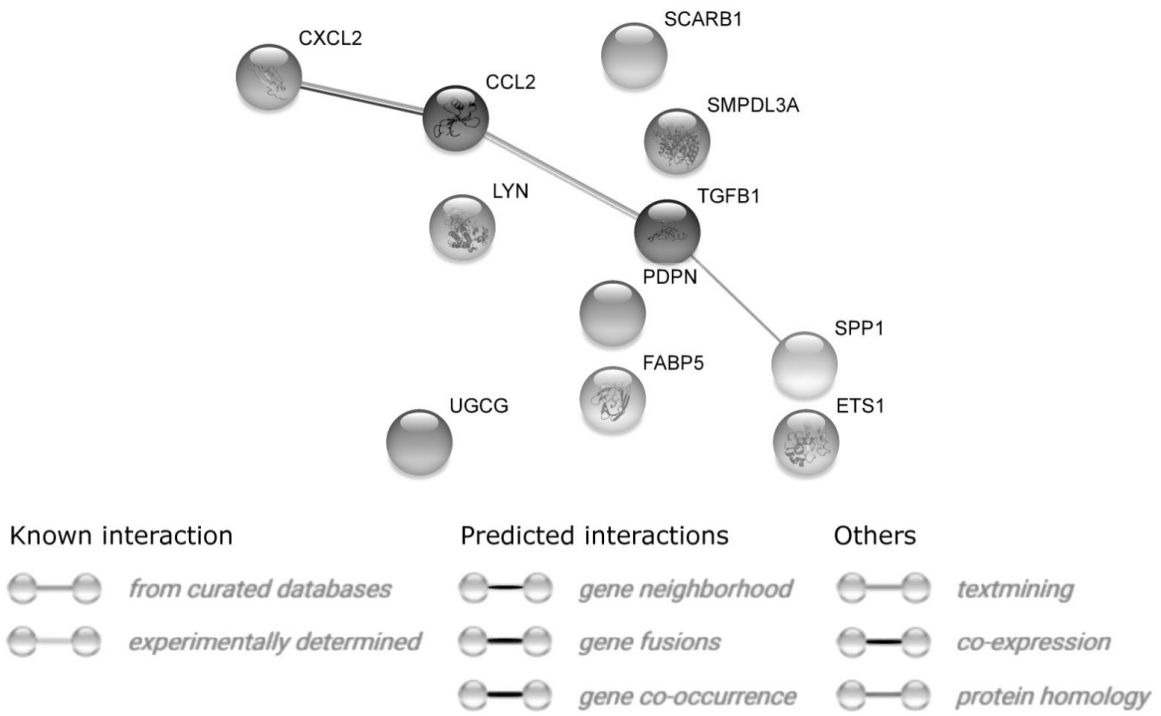

Fig. 5. *STRING-generated interaction network among differentially expressed genes belonging to the "response to lipids" (GO:0033993), "response to lipopolysaccharide" (GO:0032496) and "cellular lipid metabolic process" (GO:0044255)" GO BP terms. The intensity of the edges reflects the strength of interaction score.*

significant downregulation on day 30.

RT-qPCR analysis was conducted to validate the results of the microarray analysis (Fig. 6). Products obtained in the RT-qPCR analysis were presented as dissociation curves (Fig. 7). Overall, the direction of changes was confirmed in all but two examples (CCL2 and SMDPL3A). The pattern of changes is usually consistent between these methods, while the scale of changes varies (sometimes highly, like seen in PTGS2). The differences can be explained by the way in which both methods analyze transcript levels (microarray averages the probe scores for different transcript variants, while RT-qPCR analyses a single variant), as by the various processes of transcriptional modification that could have affected the results.

DISCUSSION

Oral mucosa can be characterized by its ability for undergoing fast and large-scale changes to its biochemical and morphological structure. External factors greatly influence that structure, which depends highly on proportions and interactions between different types of cells that can be found in the mucosa. These factors can be environmental, and mechanical as well as caused by specific drugs and chemical compounds. Because of the large capacity of oral mucosa to change, and its impressive regenerative abilities, there is a significant potential in development of methods to culture mucosal cells *in vitro* (2). Analysis of resulting cellular cultures

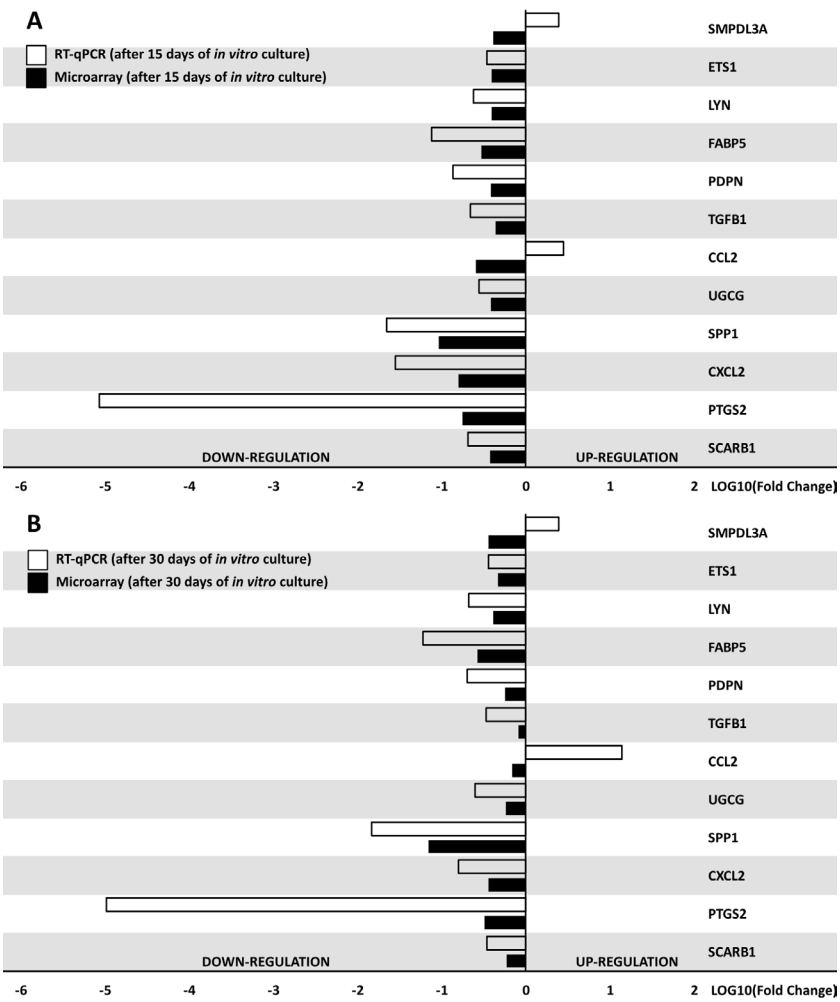

Fig. 6. *The results of RT-qPCR validation of the analysed genes, presented in a form of bar graph.* ***A****) RT-qPCR validation after 15 days of in vitro culture.* ***B****) RT-qPCR validation after 30 days of in vitro culture.*

can be used in research concerning oral cancers and epithelial stem cells. The results can also provide valuable insight into possible application of mucosal explants in tissue engineering and transplantology, and as a result provide ways to treat numerous diseases associated with epithelial tissue defects. The localization of the tissue also presents an advantage, as potential harvesting from a patient is proven to produce relatively little disability, resulting in better aesthetic outcomes, while high proliferation rates and capacity for differentiation much bigger than most of the epidermal cells makes oral mucosa a seemingly great source of epidermal cells (9). However, the modes of differentiation and proliferation of oral mucosa remain poorly understood, which calls for identification of markers of the processes that are part of their extraordinary plasticity. By labelling changes in genes that are expressed during long-term *in vitro* cultures and assigning them to ontology groups, it helps to better understand the cell functions and mechanism underlying their life cycle.

One of the analyzed genes was the cytokine, transforming growth factor beta 1 (TGFβ1). It is known to mediate fibroblast-myoblast differentiation, mostly working through the SMAD transduction pathway. It has also been proven to affect many cellular processes such as migration and proliferation. Additionally, the release of TGFβ1 is associated with events crucial to tissue repair which include chemoattraction of inflammatory cells, induction of angiogenesis and regulation of inflammatory mediators (10). Transcriptional regulation involving TGFβ1 varies depending on the target gene and cellular context and can be both negative and positive (11). TGFβ isoforms have also been defined as promoters of fibrotic growth. This causes them to be investigated as potential agents in forming of submucous fibrosis, as they increase the synthesis of matrix collagen and decrease its degradation (12). It has also been suggested that TGFβ1 can be a good marker for oral cancer, as cancer-associated fibroblast derived from oral squamous cell carcinoma have been observed to express TGFβ cytokines to promote their phenotype by weakening intercellular epithelial adhesion (13). Another gene, exhibiting similar mode of expression is C-C motif chemokine ligand 2 (CCL2), otherwise called Monocyte chemoattractant protein-1 (MCP-1), that is a part of two out of three ontological groups analyzed in this study – "response to liposaccharides" and "response to lipids". Chemokines are a part of

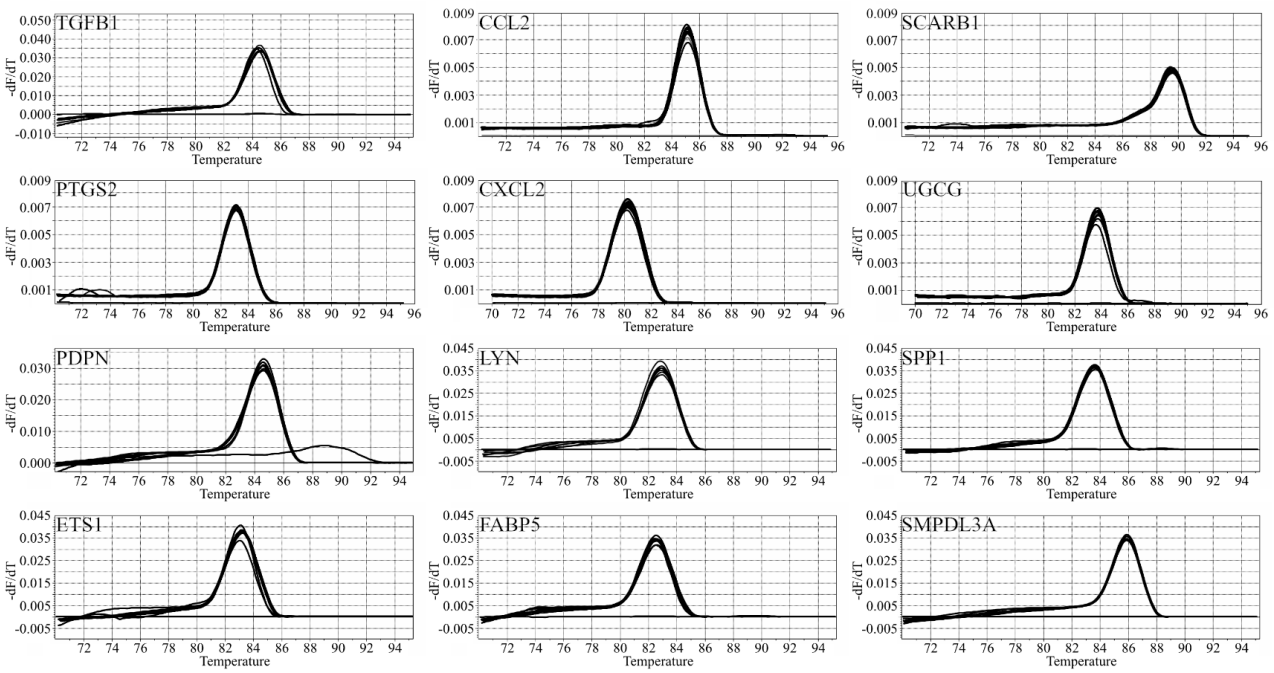

Fig. 7. *Dissociation curves that confirm of the amplification products obtained in the RT-qPCR analysis.*

the superfamily of cytokines that are involved in immunoregulatory and inflammatory responses. CCL2 is a chemotactic factor that attracts monocytes and basophils, but not neutrophils or eosinophils (14). It has been associated with pathogenesis of diseases associated with infiltration of monocytes, such as psoriasis, rheumatoid arthritis and atherosclerosis (15).

There are two genes that are part of all the analyzed ontology groups and exhibit the second of observed patterns of expression. SCARB1 and PTGS2 are both highly upregulated on day 7 of cell culture, downregulated on day 15 and exhibit no or minimal change of expression on day 30. The scavenger receptor class B type 1 (SCARB1) gene is a key factor in cholesterol transport pathway and plays an important role in lipid metabolism (16). It is the first reported HDL receptor (17). Its overexpression has resulted in extreme reduction in plasma HDL-C concentration (18), while its suppression is linked to significant increase of plasma HDL-C (19). It has also been reported to have a role in maintenance of LDL and VLDL plasma levels (20). Prostaglandin-endoperoxide synthase 2 (PTGS2), also known as cyclooxygenase 2 (COX2) is an essential rate-limiting enzyme in synthesis of prostaglandins from arachidonic acid. It acts both as dioxygenase and as a peroxidase and exists in 2 known forms PTGS1(COX1) and PTGS2(COX2). Expression of PTGS2 is induced by cytokines and growth factors, with inflammation serving as the main upregulatory event (21).

Macrophage inflammatory protein-2 (CXCL2/MIP-2) also exhibits the second observed pattern of expression. It is a chemokine, critical for neutrophil recruitment (22). It has been proven that lipopolysaccharides induce expression of CXCL2 in rat intestine *in vivo* (23). CXCL2 expression induces neutrophil influx, acting as a part of the inflammatory response to mediate bowel injury, one of the processes that allows the intestinal mucosa to play an important role in defense against pathogenic bacteria (22). There are two more genes that were upregulated on day 7, downregulated on day 15 and exhibited no, or very little change to expression on day 30 of *in-vitro* culture. UGCG (UDP-glucose ceramide glucosyltransferase) is a gene encoding ceramide glucosyltransferase. It encodes an enzyme catalyzing the first step of glycosylation, being a part of glycosphingolipid biosynthesis. Glycosphingolipids then function as membrane components that contain lipid and sugar moieties (24). The second gene, podoplanin (PDPN), which encodes a type-I integral membrane glycoprotein, is diversely distributed in human tissues. It is known that this protein performs multiple functions in development of organ systems such as heart, lung and lymphatic system as well as playing a part in inflammatory diseases and cancer metastasis. However, the exact mechanisms of action are still not well researched and are mostly unknown (25).

In the third detected pattern of expression, the genes were upregulated on day 7 and after were significantly downregulated through days 15 and 30. Proto oncogene LYN is the only one of these genes that is present in all of the analyzed ontological groups. It is a member of src-family protein tyrosine kinases (STKs). STKs are nonreceptor type tyrosine kinases that play an important role in regulation of leukocyte functions such as proliferation, cell migration, adhesion and phagocytosis (26). It is mainly expressed in hematopoietic cells, acting as an important signaling molecule of both positive and negative effects in differentiation of myeloid cells and B lymphocytes (27). Because of that fact it has been suggested that the gene could have a major role in development of leukemia and lymphoma. The research concerning this group of cancers is steadily providing evidence that confirms the role of LYN in several of their types (28). While rarely being a primary cause, it is often involved in signaling cascades, leading to neoplasia, hence oncogenesis. It has also been identified as a candidate gene in formation of precancerous lesions in oral buccal mucosa (29). ETS-1 was another proto-oncogene that followed the third observed pattern of expression. It is a founding member of the ETS transcription factor family. There are multiple functions attributed to this gene. It is confirmed to have a role in the immune response, as the loss of ETS-1 gene causes profound effects to the T, B and NK cells (30). It is also suspected to be involved in autoimmunity prevention. It is suggested that defects

in ETS-1 gene can be associated with autoimmune pathogenesis (31). It has also been proven to be present in a variety of tumors (32), especially those associated with the hematopoietic process (33). Secreted phosphoprotein 1 (SPP-1), otherwise called osteopontin also exhibited the last observed pattern of expression. It encodes a bone sialoprotein, that is presumed to be important in the development and functioning of a number of mammalian organs (34). It is involved in the attachment of osteoclast to the bone matrix (35), also functioning as a cytokine, upregulating the expression of interferon-gamma and interleukin-12 (36). Fatty-acid-binding protein 5 (FAB5) was another gene following that pattern of expression, while being a part of the "cellular lipid metabolic processes" ontology group. It is a part of a family of intracellular lipid binding proteins of low molecular mass. These proteins are involved in binding, storage and transport of hydrophobic ligands to the right cellular compartment (37). Upregulation of FAB5 has been detected in various types of cancer (38). The last gene detected, also showing increase of expression on day 7 of culture and decrease on day 15 and 30 is sphingomyelin phosphodiesterase acid-like 3A (SMPDL3A). It was originally identified in bladder tumors (39), and has since been shown to be involved in development of human macrophage cell lines, where it is regulated by liver X receptor (39). Apart from that, little more is known about its function. However, it has been proven that it is regulated by cholesterol, with macrophages expressing the genes after absorbing a significant amount (40).

In conclusion, we analyzed several genes that were detected using microarray analysis of long-term cell culture oral mucosal cells. All the genes were members of at least one of three ontology groups: "response to lipids", "response to liposaccharides" and "cellular lipid metabolic processes". There are several limitations to the study. The model used is a primary culture and, while it is the best reflection of the tissue conditions in an artificial environment, it needs to account for all the different types of cells present in the "mix". Additionally, as shown by the RT-qPCR validation of microarray results, this study should be considered as an entry level research, which needs follow-up focused on the analysis of protein expression, as it would more accurately describe the interactions that were detected in this study. However, detection and analysis of these genes, and changes of their expression during 30 days cell culture, provided us with insights about functioning of *in vitro* cultures of oral mucosal tissue and associated molecular processes that concern the topic of lipid metabolism.

ACKNOWLEDGEMENTS

This publication and its results are an outcome of a cooperation between Poznan University of Medical Sciences (Poznań, Poland) and Polish Ministry of Science and Higher Education, with Institute of Advanced Sciences Sp. z o.o. (Poznań, Poland), as a part of the "Professional PhD" programme.

REFERENCES

1. Borys S, Khozmi R, Kranc W, Bryja A, Dyszkiewicz-Konwińska M, Jeseta M, Kempisty B. Recent findings of the types of programmed cell death. Adv Cell Biol 2017; 5:43-49.
2. Bryja A, Dyszkiewicz-Konwinska M, Budna J, et al. The biomedical aspects of oral mucosal epithelial cell culture in mammals. J Biol Regul Homeost Agents 2017; 31:81-5.
3. Jankowski M, Dyszkiewicz-Konwińska M, Budna J, et al. Does migrative and proliferative capability of epithelial cells reflect cellular developmental competence? Med J Cell Biol 2018; 6:1-7.
4. Kranc W, Celichowski P, Budna J, et al. positive regulation of macromolecule metabolic process belongs to the main mechanisms crucial for porcine oocytes maturation. Adv Cell Biol 2017; 5:15-31.
5. Jankowski M, Dyszkiewicz-Konwińska M, Budna J, et al. The differentiation and transdifferentiation of epithelial cells in vitro – is it a new strategy in regenerative biomedicine? Med J Cell Biol 2018; 6:27-32.
6. Huang DW, Sherman BT, Tan Q, et al. DAVID Bioinformatics Resources: expanded annotation database and novel algorithms to better extract biology from large gene lists. Nucleic Acids Res 2007; 35:W169-75.
7. Walter W, Sanchez-Cabo F, Ricote M. GOplot: an R

package for visually combining expression data with functional analysis. Bioinformatics 2015; 31:2912-14.
8. Mering C von, Jensen LJ, Snel B, et al. STRING: known and predicted protein-protein associations, integrated and transferred across organisms. Nucleic Acids Res 2005; 33:D433-37.
9. Davis NG, Phillips A, Becker DL. Connexin dynamics in the privileged wound healing of the buccal mucosa. Wound Repair Regen 2013; 21:571-78.
10. Diegelmann RF, Evans MC. Wound healing: an overview of acute, fibrotic and delayed healing. Front Biosci 2004; 9:283-89.
11. Massague J. TGFbeta signalling in context. Nat Rev Mol Cell Biol 2012; 13:616-30.
12. Kamath VV, Krishnamurthy S, Satelur KP, Rajkumar K. Transforming growth factor-beta1 and TGF-beta2 act synergistically in the fibrotic pathway in oral submucous fibrosis: An immunohistochemical observation. Indian J Med Paediatr Oncol 2015; 36:111-16.
13. Cirillo N, Hassona Y, Celentano A, Lim KP, Manchella S, Parkinson EK, Prime SS. Cancer-associated fibroblasts regulate keratinocyte cell-cell adhesion via TGF-beta-dependent pathways in genotype-specific oral cancer. Carcinogenesis 2017; 38:76-85.
14. Gu L, Tseng SC, Rollins BJ. Monocyte chemoattractant protein-1. Chem Immunol 1999; 72:7-29.
15. Dewald O, Zymek P, Winkelmann K, et al. CCL2/ Monocyte Chemoattractant Protein-1 regulates inflammatory responses critical to healing myocardial infarcts. Circ Res 2005; 96:881–889.
16. Liu Y, Ordovas JM, Gao G, et al. The SCARB1 gene is associated with lipid response to dietary and pharmacological interventions. J Hum Genet 2008; 53:709-17.
17. Acton S, Rigotti A, Landschulz KT, Xu S, Hobbs HH, Krieger M. Identification of scavenger receptor SR-BI as a high density lipoprotein receptor. Science 1996; 271:518-20.
18. Kozarsky KF, Donahee MH, Rigotti A, Iqbal SN, Edelman ER, Krieger M. Overexpression of the HDL receptor SR-BI alters plasma HDL and bile cholesterol levels. Nature 1997; 387:414-17.
19. Rigotti A, Trigatti BL, Penman M, Rayburn H, Herz J, Krieger M. A targeted mutation in the murine gene encoding the high density lipoprotein (HDL) receptor scavenger receptor class B type I reveals its key role in HDL metabolism. Proc Natl Acad Sci USA 1997; 94:12610-15.
20. Ueda Y, Royer L, Gong E, Zhang J, Cooper PN, Francone O, Rubin EM. Lower plasma levels and accelerated clearance of high density lipoprotein (HDL) and non-HDL cholesterol in scavenger receptor class B type I transgenic mice. J Biol Chem 1999; 274:7165-71.
21. Wang D, DuBois RN. Prostaglandins and cancer. Gut 2006; 55:115-22.
22. Plaen IG de, Han X-B, Liu X, Hsueh W, Ghosh S, May MJ. Lipopolysaccharide induces CXCL2/macrophage inflammatory protein-2 gene expression in enterocytes via NF-kappaB activation: independence from endogenous TNF-alpha and platelet-activating factor. Immunology 2006; 118:153-63.
23. Remick DG, Newcomb DE, Bolgos GL, Call DR. Comparison of the mortality and inflammatory response of two models of sepsis: lipopolysaccharide vs. cecal ligation and puncture. Shock 2000; 13:110-16.
24. Ichikawa S, Sakiyama H, Suzuki G, Hidari KI, Hirabayashi Y. Expression cloning of a cDNA for human ceramide glucosyltransferase that catalyzes the first glycosylation step of glycosphingolipid synthesis. Proc Natl Acad Sci USA 1996; 93:4638-43.
25. Astarita JL, Acton SE, Turley SJ. Podoplanin: emerging functions in development, the immune system, and cancer. Front Immunol 2012; 3:283.
26. Lowell CA. Src-family kinases: rheostats of immune cell signaling. Mol Immunol 2004; 41:631-43.
27. Xu Y, Harder KW, Huntington ND, Hibbs ML, Tarlinton DM. Lyn tyrosine kinase: accentuating the positive and the negative. Immunity 2005; 22:9-18.
28. Ingley E. Functions of the Lyn tyrosine kinase in health and disease. Cell Commun Signal 2012; 10:21.
29. Chen DAN, Yang KAI, Zhang G, Mei JIE, Xiang LI. Screen and analysis of key disease genes for precancerous lesions of oral buccal mucosa induced by DMBA in golden hamsters. Oncol Lett 2011; 2:265-71.
30. Bories JC, Willerford DM, Grevin D, et al. Increased T-cell apoptosis and terminal B-cell differentiation induced by inactivation of the Ets-1 proto-oncogene. Nature 1995; 377:635-38.

31. Sullivan KE, Piliero LM, Dharia T, Goldman D, Petri MA. 3' polymorphisms of ETS1 are associated with different clinical phenotypes in SLE. Hum Mutat 2000; 16:49-53.
32. Yamaguchi E, Nakayama T, Nanashima A, Matsumoto K, Yasutake T, Sekine I, Nagayasu T. Ets-1 proto-oncogene as a potential predictor for poor prognosis of lung adenocarcinoma. Tohoku J Exp Med 2007; 213:41-50.
33. Garrett-Sinha LA. Review of Ets1 structure, function, and roles in immunity. Cell Mol Life Sci 2013; 70:3375-90.
34. Craig AM, Denhardt DT. The murine gene encoding secreted phosphoprotein 1 (osteopontin): promoter structure, activity, and induction in vivo by estrogen and progesterone. Gene 1991; 100:163-71.
35. Morinobu M, Ishijima M, Rittling SR, et al. Osteopontin expression in osteoblasts and osteocytes during bone formation under mechanical stress in the calvarial suture in vivo. J Bone Miner Res 2003; 18:1706-15.
36. Kahles F, Findeisen HM, Bruemmer D. Osteopontin: A novel regulator at the cross roads of inflammation, obesity and diabetes. Mol Metab 2014; 3:384-93.
37. Kawaguchi K, Kinameri A, Suzuki S, Senga S, Ke Y, Fujii H. The cancer-promoting gene fatty acid-binding protein 5 (FABP5) is epigenetically regulated during human prostate carcinogenesis. Biochem J 2016; 473:449-61.
38. Jeong C-Y, Hah Y-S, Im Cho B, et al. Fatty acid-binding protein 5 promotes cell proliferation and invasion in human intrahepatic cholangiocarcinoma. Oncol Rep 2012; 28:1283-92.
39. Noto PB, Bukhtiyarov Y, Shi M, McKeever BM, McGeehan GM, Lala DS. Regulation of sphingomyelin phosphodiesterase acid-like 3A gene (SMPDL3A) by liver X receptors. Mol Pharmacol 2012; 82:719-27.
40. Traini M, Quinn CM, Sandoval C, et al. Sphingomyelin phosphodiesterase acid-like 3A (SMPDL3A) is a novel nucleotide phosphodiesterase regulated by cholesterol in human macrophages. J Biol Chem 2014; 289:32895-913.

OXADIAZOLYL THIAZOLIDINEDIONE AS A NON-ADIPOGENIC PPAR-γ PARTIAL AGONIST AND ITS EFFECT ON GLUCOSE HOMEOSTASIS IN TYPE 2 DIABETES

N. THANGAVEL[1], M.A. BRATTY[1], S.A. JAVED[1], W. AHSAN[1] and H.A. HAZMI[2]

[1]Department of Pharmaceutical Chemistry, Faculty of Pharmacy, Jazan University, Jazan, Kingdom of Saudi Arabia; [2]Substance Abuse Research Centre, Jazan University, Jazan, Kingdom of Saudi Arabia

Received December 2, 2018 – Accepted March 5, 2019

The familiar glitazone anti-diabetics are thiazolidinedione derivatives, known to elicit action through full agonistic activity on PPAR-γ receptors. Full agonists are known for the side effect of weight gain, while partial agonists are weak to non-adipogenic compounds possessing anti-diabetic property. This work identified a new synthetic oxadiazolyl thiazolidinedione (OXTZD) as a ligand for PPAR-γ receptor with partial agonist activity and less transactivation potential compared to rosiglitazone through *in-vitro* PPAR-γ competitive binding assay and PPAR-γ transactivation-based luciferase reporter assay, respectively. OXTZD did not induce significant lipid accumulation when compared to differentiation control which contained insulin in PPAR-γ-dependent adipogenesis assay. *In-vivo* studies have proved that OXTZD effectively reduced blood glucose level in type 2 diabetic rats and also improved glucose tolerance and insulin sensitivity. After 15 days of oral treatment with OXTZD, rats did not gain weight, suggesting that OXTZD was effective in suppressing the weight gain. Molecular docking of OXTZD to PPAR-γ, predicted hydrogen bonds with SER342, ARG288, and CYS285 residues in arm III of the ligand binding domain which are unique to the partial agonists. Results of *in-vitro*, *in-vivo*, and docking studies were in good correlation to the fact that OXTZD is a PPAR-γ partial agonist having glucose-lowering property and lacks the side effect of weight gain. In conclusion, OXTZD could be developed as a therapeutic agent for diabetes and/or serve as a lead compound for further drug design studies targeting PPAR-γ for effective management of type 2 diabetes without inducing weight gain.

Type 2 diabetes is a chronic metabolic disorder which has invariably affected all age groups of the global population. Features of type 2 diabetes include hyperglycemia and insulin resistance (1). There exists a direct correlation of hyperglycemia with chronic ailments such as atherosclerosis, retinopathy, nephropathy, and neuropathy (2). Thiazolidinedione containing anti-diabetic drugs such as rosiglitazone and pioglitazone act by their full agonistic effect on Peroxisome Proliferator-Activated Receptor-γ (PPAR-γ) (3). PPAR-γ is an intracellular ligand-dependant protein which belongs to the group of nuclear receptors. Activation of PPAR-γ leads to insulin-sensitization and glucose-homeostasis, causing a decrease in blood sugar level in patients with type 2 diabetes (4-5). Nonetheless, their effectiveness is hampered by the various side-effects such as obesity and cardiovascular toxicities (6-7). It is important to separate the insulin-sensitizing and glucose-lowering effect of full agonists from

Key words: thiazolidinedione; PPAR-γ partial agonist; Type 2 diabetes; docking; in-vitro; in-vivo

Corresponding Author:
Prof. Neelaveni Thangavel,
Department of Pharmaceutical Chemistry,
Faculty of Pharmacy, Jazan University,
Jazan, P.O. Box 114, KSA- 45142
Tel: +966 017 329 5000
e-mail: venipsgcop2004@yahoo.co.in

0393-974X (2019)

their side effects. Partial PPAR-γ agonists are one such class of compounds with high binding affinity but produce less transactivation of PPAR-γ leading to glucose-lowering effect without side effects (8). Hence, partial agonists are considered to be safer alternatives to full agonists of PPAR-γ (9). Structurally diverse compounds are able to induce partial PPAR-γ activity. Various modes of binding interactions have been proposed for partial agonists (10-12). Distinct binding profile of partial agonists to PPAR-γ results in the different conformation of the receptor-agonist complex which induces an alteration in the recruitment of co-activators and repressors causing controlled expression of target genes in comparison to full agonists (13). The structural parameters necessary for PPAR-γ full or partial agonistic activity are almost common. Recent research has proved that derivatives of thiazolidinedione may exert partial PPAR-γ activity (14-15). Comparative structural features of rosiglitazone, recent thiazolidinedione containing partial agonists, and the OXTZD under study are provided in (Fig. 1). This study aims to evaluate the newer synthetic OXTZD as a PPAR-γ modulator by measuring its *in-vitro* binding affinity to PPAR-γ ligand binding domain (PPAR-γ -LBD) and the degree of transactivation of PPAR-γ. The effect of OXTZD on adipogenesis was also studied using *in-vitro* assay protocols. The effect of OXTZD on glucose homeostasis in intra-peritoneal streptozotocin (STZ)-induced type 2 diabetes in rats, oral glucose

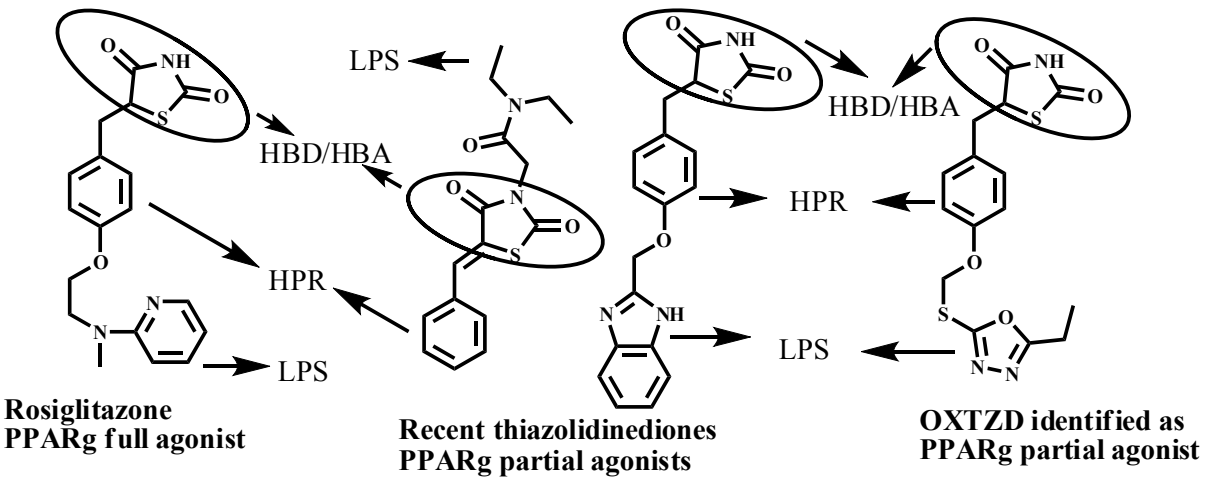

HBD/HBA : Hydrogen bond donor/Hydrogen bond acceptor
HPR : Hydrophobic ring
LPS : Lipophilic substituent

Fig. 1. *Comparative structural features of PPAR-γ full/partial agonists. Thiazolidinedione ring is important for agonist activity due to its ability to form hydrogen bonds with amino acid residues of the ligand binding domain of PPAR-γ. Other common pharmacophores include a hydrophobic ring linked to thiazolidinedione and a lipophilic substituent linked to the hydrophobic ring.*

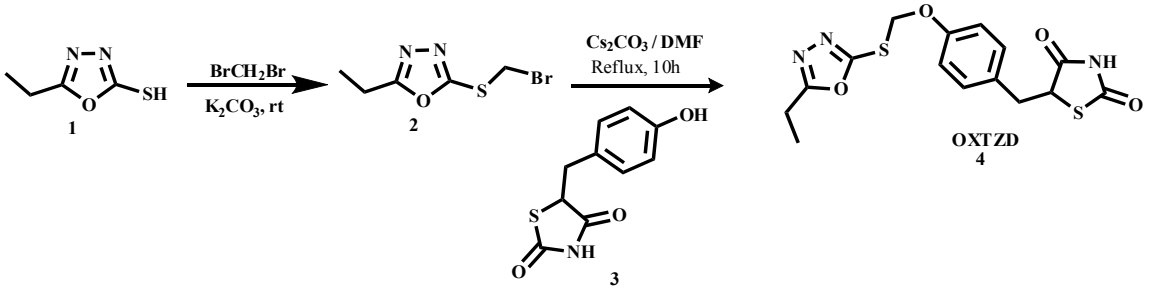

Fig. 2. *Scheme of synthesis of OXTZD. OXTZD was obtained in a moderate yield. The synthetic method was successful as evident from the structure of OXTZD confirmed by spectral analysis.*

load to treated rats, and sub-cutaneous insulin load to treated rats were also studied. In addition, molecular docking of OXTZD to 3D model of PPAR-γ -LBD was performed to probe the inter-molecular interactions.

MATERIALS AND METHODS

Materials

PolarScreen™ PPAR-γ competitor assay, Green, kit and Luciferase assay kit was purchased from Life technologies, Thermo Fisher Scientific Inc and Promega, respectively. Dulbecco's modified Eagle's medium (DMEM), fetal calf serum (FCS), fetal bovine serum (FBS), benzylpenicillin, glutamine, streptomycin was obtained from Gibco, Thermo Fisher Scientific Inc. 5-ethyl-1,3,4-oxadiazole-2-thiol was procured from Aurora Fine Chemicals LLC. All other chemicals, reagents, and solvents including rosiglitazone were purchased from Sigma-Aldrich. Test compounds and rosiglitazone were dissolved in DMSO and the final working solutions were optimized to contain ≤ 0.2% of DMSO.

Synthesis and characterization of OXTZD

The scheme of synthesis is given in Fig. 2. Melting point (mp) was recorded in open capillaries on Techne Stuart digital melting point apparatus and are uncorrected. IR spectrum was recorded on Shimadzu IR Spirit instrument using KBr pellet technique. ^{1}H and ^{13}C NMR spectra were determined in $CDCl_3$ with a Bruker AVII 400 MHz spectrometer, chemical shifts are given in parts per million (δ) downfield from tetramethylsilane as internal standard. Mass spectra were recorded using Thermo fisher scientific HF-mass spectrometer.

Potassium carbonate anhydrous (1 g, 7.23 mmol) was added to a mixture of 5-ethyl-1,3,4-oxadiazole-2-thiol (1) (0.65 g, 5 mmol) and dibromo methane (1 ml, 5 mmol) in 30 ml of water. The mixture was stirred at room temperature for 3 h and concentrated under vacuum to yield 2-(bromomethylthio)-5-ethyl-1,3,4-oxadiazole (2). The residue obtained was shaken with water and filtered at the pump. Compound (2) was obtained as white solid; yield 85%; mp 123°C; R*f* 0.55; IR (KBr) cm^{-1} 690 (-CH_2Br), 750 (-C-S-C-); ^{1}H NMR ($CDCl_3$): δ 4.96 (s, 2H, -CH_2Br); ^{13}C NMR ($CDCl_3$): δ 37.2 (-CH_2Br), 20.0 (-CH_2), 10.3 (-CH_3); ESI MS *m/z* (%): 223 (M^+)

Caesium carbonate anhydrous (3.90 g, 12.00 mmol) was added to a solution of 5-[(4-hydroxyphenyl) methyl]-1,3-thiazolidine-2,4-dione (3) (1.5 g, 6.71 mmol) in dimethyl formamide (20 ml). The resultant mixture was stirred at room temperature for 20 min, followed by the addition of 2-(bromomethylthio)-5-ethyl-1,3,4-oxadiazole (2) (6.71 mmol). The mixture obtained was refluxed for 10 h. Evaporation of the solvent produced a solid mass which was broken down by the addition of 30 ml of water. The aqueous mixture was shaken with 10 ml of ethyl acetate and the organic layer was collected. Extraction was repeated twice with equal proportions of ethyl acetate. Combined organic layers were washed with 1M aqueous solution of NaCl and dried over sodium sulfate anhydrous. The remaining organic solvent was removed in vacuo to yield a solid residue. The residue obtained was purified by column chromatography on silica gel (60-120 mesh size) by gradient elution with ethyl acetate-hexane. The compound thus obtained, OXTZD (4) was identified by TLC using ethyl acetate: hexane in the ratio of 2:1. The chemical name of OXTZD is (5-(4-((5-ethyl-1,3,4-oxadiazol-2-ylthio) methoxy) benzyl)-1,3-thiazolidine-2,4-dione).

OXTZD was obtained as white solid; yield 60%; mp 135; R*f* 0.40; (KBr) cm^{-1} 1256 (-aryl-O-), 1076 (-alkyl-O-), 755 (-C-S-C-); ^{1}H NMR ($CDCl_3$): δ 5.58 (s, 2H, -OCH_2); ^{13}C NMR ($CDCl_3$): 76.9 (-C-OR), ESI MS *m/z* (%): 365 (M^+). Peaks related to the absorption of the -OCH_2- bond created by the applied synthetic method are presented here and the rest of the spectra was also in good agreement with the structure of OXTZD. Spectral absorption characteristics of OXTZD are displayed in Fig. 3.

In-Vitro Assays

PPAR-γ competitive binding assay

Quantification of binding of OXTZD to PPAR-γ was carried out by measuring the decrease in fluorescence polarization value when OXTZD displaces fluormone, a PPAR-γ selective fluorescent ligand, from PPAR-γ -LBD tagged with glutathione *S*-transferase [PPAR-γ-LBD (GST)]. This was carried out using PolarScreen™ PPAR-γ competitor assay, Green kit, applying the protocol provided by the manufacturer. Shortly, 10 µl of solutions containing 0.001 µM to 100 µM of OXTZD in DMSO was mixed with 10 µl of PPAR-γ-LBD (GST) and fluormone tracer in nuclear receptor buffer, and incubated in the dark at room temperature for 2 h. Fluorescence polarization was measured at 485/535nm as excitation/emission wavelengths using omega fluorescence polarization plate

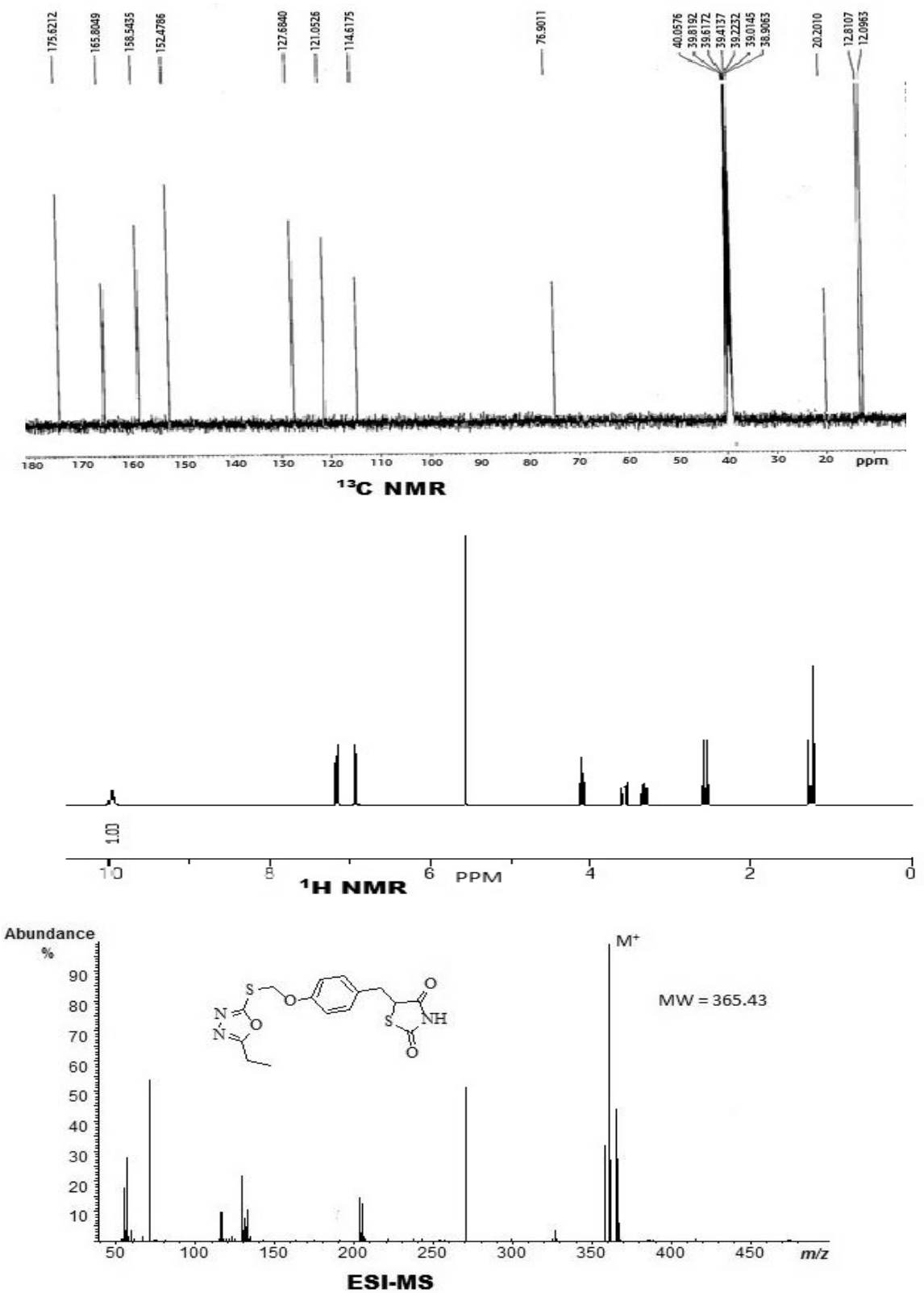

Fig. 3. *Spectral characteristics of OXTZD. ^{13}C NMR and ^{1}H NMR spectra. Chemical shifts exhibited in parts per million (δ) downfield from tetramethylsilane as internal standard was measured. ESI MS: (mass to charge ratio) m/z vs % abundance was used to confirm the structure. Spectral data obtained was in accordance with the structure of OXTZD.*

reader. Rosiglitazone (0.001 μM to 10 μM) was used as positive control. DMSO alone with PPAR-γ - fluormone complex was used as negative control, fluormone tracer alone, and buffer alone were used as other assay controls. Percentage normalized polarization v*s* log concentration (nM) of agonists was plotted to calculate IC_{50}. IC_{50} describes the compound's relative affinity to PPAR-γ LBD. Results were the mean ± standard error of the mean (SEM) of three replicate measurements. Non-linear regression was used for curve fitting.

PPAR-γ transactivation-based luciferase reporter assay

Transactivation of PPAR-γ by OXTZD was measured using the luciferase assay system, Promega. In brief, HEK-293 cells (ATCC) sub-cultured in DMEM were transfected with 2.5 μl of PPRE-Luc reporter plasmid, 6.67 μl of PPAR-γ, 1 μl of renilla, and 20 μl of lipofectamine. After 6 h of transfection, cells were treated with varying concentrations of OXTZD (0.05 μM to 5 μM) for 24 h. Cells were opened up and collected using cell culture lysis buffer. Luciferase reporter activity was measured as luminescence in a luminometer according to the manufacturer's instructions. Rosiglitazone (0.01 μM to 2 μM) was used as the standard drug. DMSO was used as the control. Neither OXTZD nor rosiglitazone interfered with the background luminescence. The luminescence measured represents the relative luciferase activity. Luciferase activity was proportional to the PPAR-γ transactivation potential of the compound. The observed luciferase activity was normalized to the control group without the test compound/ standard drug. Normalized luciferase activity was plotted against the log concentration of agonists in nM. The graph obtained was used to calculate EC_{50} of OXTZD. Values are the mean of three independent determinations with the standard error of the mean. Non-linear regression was used for curve fitting.

PPAR-γ dependent adipogenesis assay

3T3-L1 adipoblasts (ATCC) were cultured in 10% FCS+FBS in DMEM by incubation at 37°C in 10% CO_2 to less than 70% confluency. The cells were sub-cultured in 10% FBS-DMEM. Two days post-confluency, adipogenesis was stimulated by sub-cultivation of cells at low density in a DMEM growth medium containing 2 mM glutamine, 100U/ml benzylpenicillin, 100μg/ml streptomycin, and 10% FBS. This combination of antibiotics along with insulin stimulates adipogenesis through activation of transcription factors inducing transcription of PPAR-γ (16). Two days post-confluency, adipocyte differentiation was carried out by treating the cells with DMEM containing 10% FCS + 1μg/mL insulin (differentiation medium with insulin (DMI) as control). Additional groups of cells were also treated with DMI + OXTZD or Rosiglitazone (positive control) at 1, 5, and 10 μM concentrations, and DMEM+10% FCS (negative control). 0.2% DMSO+ DMI was also maintained as blank. The medium was changed every two days with fresh DMEM+10% FBS. The quantity of accumulated lipids, a measure of PPAR-γ-dependent adipogenesis, was measured after eight days using OilRed O staining. The media were aspirated, and 10% formaldehyde was added to the cells as a fixating agent, allowed to stand for 30 min followed by the addition of 70 μl of OilRed O solution (0.3 g in a mixture of 60 ml of isopropanol and 40 ml of water). Cells were washed with water, and the dye was eluted with 100 μl of isopropanol per well. The assay plates were incubated on a plate shaker for 15 min. Eluted dye was transferred from the wells to a clean assay plate, and was quantified at 550 nm using a omega microplate reader. The results were the mean of three independent determinations.

In-Vivo Studies

Anti-diabetic activity

Protocols for animal experimentation were approved by the institutional animal ethics committee. Healthy albino Wistar rats of both sexes weighing 150-200 g were obtained from the animal house of the central research lab, College of Pharmacy, Jazan University. Animals were acclimatized for one month prior to the study. A freshly prepared solution of streptozotocin (STZ) in 0.1M citrate buffer of pH 4.5 was used to induce type 2 diabetes. Single intraperitoneal injection of STZ at a dose of 60mg/kg body weight was administered to rats fasted over-night. Rats with blood glucose concentration greater than 270 mg/dl after 48 h of STZ injection were considered diabetic and used for the study. Rosiglitazone was used as the standard drug. Standard drug and OXTZD were suspended in 0.25% aqueous carboxymethyl cellulose (CMC). OXTZD (30 mg/kg) and the standard drug (5 mg/kg) were administered by oral gavage. Three groups containing twelve diabetic rats per group were administered with 0.25% CMC (vehicle control), rosiglitazone (standard), and OXTZD (test**)** once daily for 15 days. Every measurement of

glucose concentration was performed on the blood sample withdrawn from retro-orbital plexus of the eyes of the rats using a capillary tube at days 0, 3, 7, and 15. Glucose concentration in blood was measured using Accu-Chek blood glucose meter. Results are presented as mean ± SEM of data obtained from three individual determinations. Body weight was also monitored during the 1st and 15th day.

Oral glucose tolerance test (OGTT)

After 15 days of treatment of the diabetic rats with OXTZD and rosiglitazone, oral glucose tolerance test was performed. The animals divided into three groups (vehicle control, standard, and test) were fasted overnight. Glucose (50% solution at a dose of 3 g/kg) was administered orally to the animals. Blood glucose levels were measured as described above at 0, 30, 60, and 120 min intervals. Results were expressed as mean ± SEM of three repeated determinations.

Insulin tolerance test (ITT)

After 15 days of treatment with OXTZD and rosiglitazone insulin tolerance test was performed. Rats fasted overnight were administered with human recombinant insulin at a dose of 1IU/kg subcutaneously. Concentrations of glucose in blood were estimated before insulin injection (0min) and at 30, 60, and 90 min after insulin injection. Glucose levels were reported as mean ± SEM of three repeated measurements.

Statistical analysis

The data generated were modelled, and curve fitting was performed in GraphPad Prism v8.0.0. For *in-vivo* studies and adipogenesis assay, two-way ANOVA followed by Tukey's multiple comparisons test were applied to compare the means between two groups. $P<0.05$ was considered significant and $P<0.01$ was considered highly significant.

Molecular docking

Binding modes of OXTZD were studied by docking to PDB 2PRG receptor using Auto Dock 4.2. 2PRG is the 3D structure of ligand binding domain and co-activator assembly of human PPAR-γ co-crystallized with rosiglitazone. Prior to docking, 2PRG structure was edited in Discovery Studio Client 2016. Polypeptide chain A was retained, chain B, water, and rosiglitazone molecules were deleted. The resultant protein structure was energy minimized using optimize geometry option. The receptor file was saved in PDB format and loaded to Auto Dock and transformed to PDBQT file which describes charges of atoms, types of atoms etc. Binding site in the ligand binding domain was defined by creating a grid of 60X60X60 with grid space of 0.375 Å and scaling factor of 1.0 Å.

Structure of OXTZD was constructed and subjected to energy minimization using Chem3D Ultra 10.0 applying MM2 simulations and the low energy conformation produced was saved in PDB format and subsequently loaded to Auto Dock. These structures were reformed into PDBQT files which represent the topology of ligands including the rotatable bonds, atomic charges etc. All rotatable bonds were permitted. Prepared OXTZD was docked to the binding site inside the grid set on the prepared 2PRG receptor. Rigid receptor-flexible ligand docking formed the basis of this docking. Docking procedure involved the identification of the best binding pose among 50 possible conformations on the basis of binding energy. To assess the predictive ability of docking protocol, rosiglitazone was redocked to the native co-crystallized rosiglitazone using rigid re-docking.

RESULTS

PPAR-γ competitive binding assay to evaluate the binding efficacy of OXTZD to the receptor resulted in the plot of log concentration-response curve (Fig. 4). Rosiglitazone, a full agonist binds to PPAR-γ with an IC_{50} of 0.19 μM. The half maximal binding concentration (IC_{50}) of OXTZD was 11.66 μM. OXTZD binds competitively to PPAR-γ in a concentration- dependent pattern. OXTZD displaces fluormone tracer bound to PPAR-γ-LBD and the free fluormone has low polarization value than the bound form. The reduction in polarization values as a result of OXTZD binding to PPAR-γ-LBD stands as a proof for its binding ability though weaker than rosiglitazone. The concept that partial agonists activate PPAR-γ despite their low binding capacity encouraged us to test the transactivation activity of OXTZD. PPAR-γ transactivation potential of OXTZD was assessed by luciferase reporter assay on HEK-293 cells. The log dose-response curve (Fig. 5) for transactivation assay indicated that OXTZD was able to elicit PPAR-γ transactivation with an EC_{50} of 3.11 μM. The OXTZD induced maximal transactivation activity of 3.17±0.6-

fold, was less than the 12.5±0.5-fold transactivation produced by rosiglitazone at its maximum effective dose of 1 μM. OXTZD-induced transactivation occurs at concentrations greater than 1 μM. Rosiglitazone activated the receptor with an EC_{50} value of 0.44 μM. Taken together, OXTZD can be considered as a partial agonist of PPAR-γ producing sub-maximal transactivation.

The hypothesis that partial agonists exhibit a less pronounced effect on adipogenesis was tested by the incubation of 3T3-L1 adipocytes with OXTZD. Lipids concentrated in adipocytes were stained with OilRed O dye. Spectrophotometric quantification of the eluted dye serves as a measure of accumulated intra-cellular lipids. Rosiglitazone-induced adipogenesis was very high when compared to DMI control and was dose-dependent (Fig. 6). One can visually distinguish the difference in lipid accumulation between the groups through the intensity of the color developed.

OXTZD did not produce a marked increase in intra-cellular lipids when compared to DMI. No enhancement in the accumulation of lipids above the basal level (DMI control) was observed even at the highest tested dose of 10 μM of OXTZD. This suggests that OXTZD is a non-adipogenic modulator of PPAR-γ.

Having proved that OXTZD is a partial agonist of PPAR-γ, it is necessary to test whether it has the ability to regulate glucose homeostasis in type 2 diabetes similar to other modulators of the receptor. Fig. 7 indicates that the oral administration of OXTZD for 15 days to type 2 diabetic rats resulted in a pronounced reduction in fasting blood glucose levels when compared to the animals in the vehicle control group ($P < 0.05$) at 3, 7, and 15 days. In addition, it was also efficient enough to produce a comparable reduction in fasting blood glucose to that of the standard drug, rosiglitazone ($P < 0.05$).

Further studies were carried out to determine the effect of OXTZD on glucose tolerance and insulin sensitivity by OGTT and ITT, respectively. Results of OGTT (Fig. 8) demonstrate the improvement in glucose tolerance accomplished by OXTZD at 60 and 120 min after an oral glucose load to diabetic rats.

The improvement in glucose tolerance caused by OXTZD, 30mg/kg in treated animals, was significant ($P < 0.05$) when compared to the animals in rosiglitazone and vehicle control groups. Rosiglitazone and OXTZD significantly improved insulin tolerance or insulin sensitivity (Fig. 9) after 30, 60, and 90 min of subcutaneous injection of 1 IU/kg of human recombinant insulin. Improved insulin sensitivity was indicated by the decline in blood

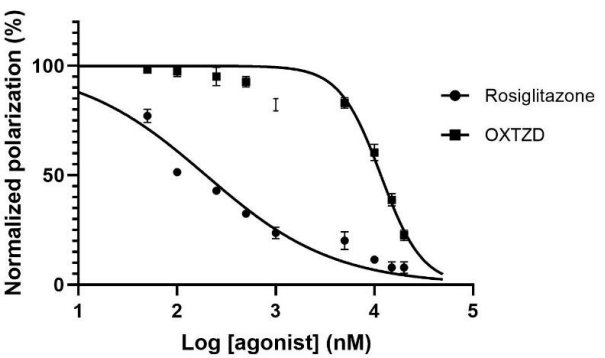

Fig. 4. *PPAR-γ competitive binding assay; Each data point is the mean ± standard error of mean (SEM) of three replicate measurements; DMSO was used as the control. The measured fluorescence polarization was normalized to %. The observed decrease in % fluorescence polarization for OXTZD and rosiglitazone indicate that they displace the bound fluormone tracer ligand and bind competitively to PPAR- γ. The IC_{50} of OXTZD was higher than rosiglitazone indicating its partial agonist activity.*

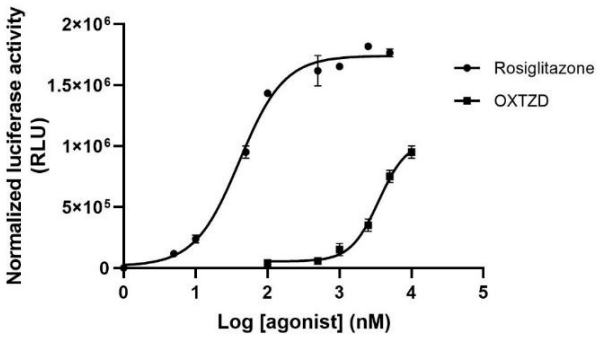

Fig. 5. *PPAR-γ transactivation-based luciferase reporter assay on HEK-293 cells. Readings were the mean ±SEM of three replicate measurements; DMSO was the control. Measured and normalized luciferase activity in relative luminescence units (RLU) was plotted against logarithmic concentration of OXTZD and rosiglitazone to calculate the $EC_{50;}$ EC_{50} of OXTZD was higher than rosiglitazone which shows that OXTZD possesses a weak PPAR-γ transactivation potential and partial agonist activity.*

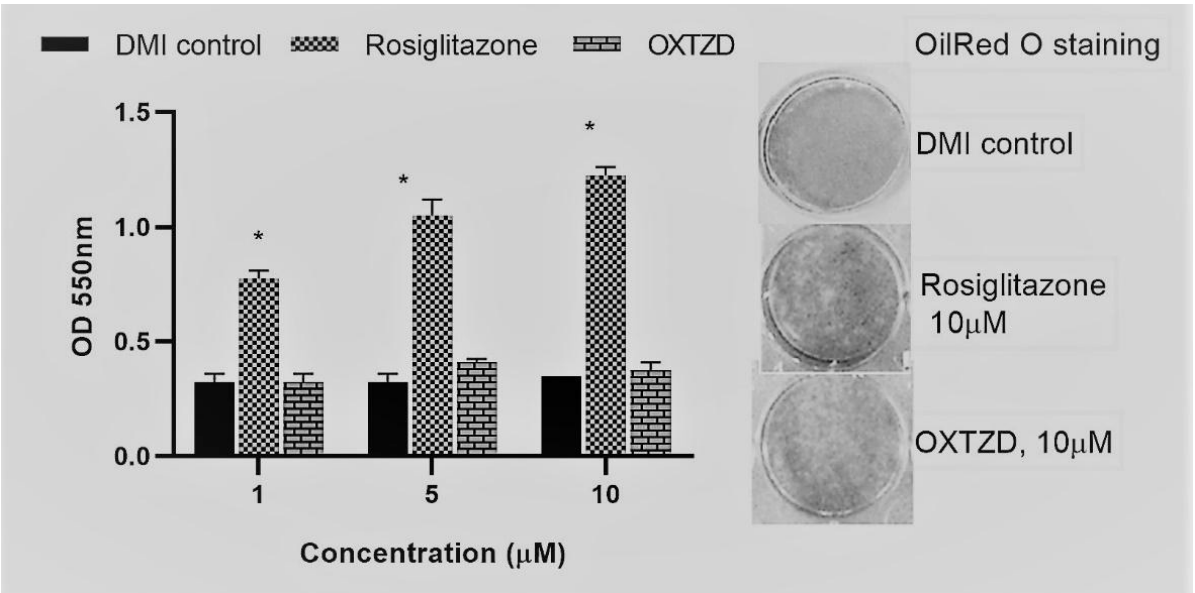

Fig. 6. *Results of PPAR-γ dependent adipogenesis assay. Each bar in the graph is the mean ± SEM of three independent determinations: two-way ANOVA followed by Tukey's test; * indicates P < 0.01 compared to DMI control; OXTZD did not induce significant adipogenesis compared to DMI control. The 3T3-L1 adipocytes were stained with OilRed O solution; Rosiglitazone well, developed an intense color compared to OXTZD and DMI control indicating its adipogenic activity. OXTZD did not induce adipogenesis.*

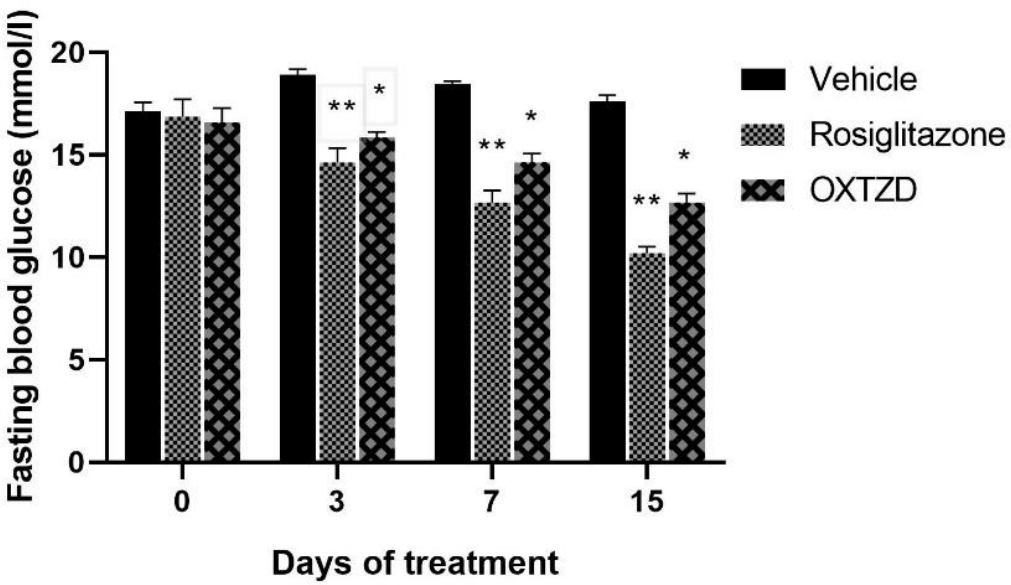

Fig. 7. *Results of in-vivo anti-diabetic activity (n = 12 rats/group). Bar graph is the compilation of results of three independent determinations (mean ± SEM); 0.25% aqueous carboxy methyl cellulose was the vehicle control, standard drug rosiglitazone, 5mg/kg and OXTZD 30mg/kg were given orally; Two-way ANOVA followed by Tukey's test. * indicates P < 0.05, ** indicates P < 0.01 compared to vehicle; OXTZD produced statistically significant blood glucose-lowering effect compared to rosiglitazone, P < 0.05.*

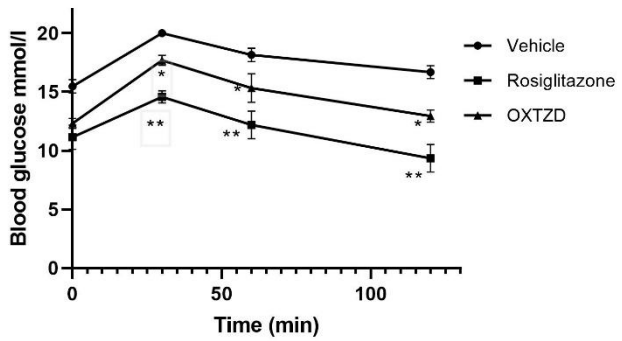

Fig. 8. *Results of OGTT after 15 days of treatment with OXTZD, 30mg/kg (n = 12 rats/group). Each data point is the mean ± SEM of three individual experiments; 0.25% aqueous carboxy methyl cellulose was the vehicle control; Two-way ANOVA followed by Tukey's test; * indicates P < 0.05 and ** P < 0.01 compared to vehicle; Also, OXTZD improved the glucose tolerance after oral administration of 3g/kg of glucose to treated rats, statistically significant, P < 0.05 compared to rosiglitazone.*

glucose levels in animals of the rosiglitazone and OXTZD group from that of animals in the vehicle control group ($P < 0.01$).

The most beneficial effect of OXTZD on mean body weight of the treated animals was that it did not increase the body weight (Fig. 10) when compared to animals in the vehicle control group ($P < 0.05$), while rosiglitazone induced weight gain by a small measure higher than the vehicle. Results of the *in-vivo* studies were in correlation with the *in-vitro* studies.

Partial agonists are said to bind to PPAR-γ-LBD in an entirely different mode from that of full agonists (17). In order to predict the binding mode and OXTZD-PPAR-γ interactions, molecular docking to 2PRG was performed. OXTZD binds to 2PRG in a U-shaped conformation (Fig. 11) with the binding energy of -9.89 kcal/mol and rosiglitazone binds with ΔG of -10.82 kcal/mol.

The binding site residues for OXTZD include MET348, VAL339, LEU333, CYS285, MET329, ALA292, ARG288, SER342, and ILE341. OXTZD binding interactions with 2PRG differed from that of rosiglitazone (18). Widely assessed interactions for characterizing full/partial agonists are the polar hydrogen bonds. OXTZD established three hydrogen bonds, with SER342, CYS285, and ARG288, respectively, (Fig. 12) which is unique for the partial agonists (19). It also formed several other significant hydrophobic interactions with the binding site residues. Hydrogen bonds were formed between the oxygen of -O-CH_2- linker, L2 and the amino group of SER342, oxygen of oxadiazole and the amino group of ARG288, and keto oxygen of thiazolidinedione and the hydrogen of sulfhydryl group of CYS285. The docking protocol was valid with an RMSD value of 1.01 when native rosiglitazone was redocked to PPAR-γ. Collectively, results illustrate that OXTZD is an efficacious partial agonist of PPAR-γ able to reduce blood glucose with beneficial effects on adipogenesis and weight gain in diabetic rats.

DISCUSSION

OXTZD, chemically named (5-(4-((5-ethyl-1,3,4-oxadiazol-2-ylthio) methoxy) benzyl)-1,3-thiazolidine-2,4-dione) was synthesized and confirmed to contain the structure shown in Fig. 1. This study would be the first report on oxadiazolyl thiazolidinedione derivative as a partial agonist of PPAR-γ. OXTZD has less binding affinity to PPAR-γ compared to the full agonist rosiglitazone. This could be explained by the absence of hydrogen bonding interactions with the arm I residues of PPAR-γ-LBD on docking of OXTZD to PPAR-γ and a higher binding energy than rosiglitazone. Full agonists interact with

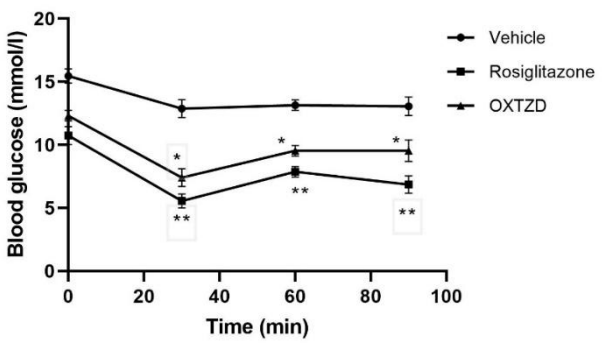

Fig. 9. *Results of ITT, (n = 12 rats/group). Each data point is the mean ± SEM of three individual experiments; 0.25% aqueous carboxy methyl cellulose was the vehicle control; Two-way ANOVA followed by Tukey's test; * indicates P < 0.05, ** indicates P < 0.01 when compared to rosiglitazone and vehicle respectively; OXTZD improved the insulin tolerance of treated rats to subcutaneous insulin, 1IU/kg, when administered orally at a dose of 30mg/kg.*

AF-2 helix of arm I in PPAR-γ-LBD, and establish a network of hydrogen bonds with its residues like TYR473, HIS323, HIS449 etc., stabilizing the H-12 helix resulting in increased binding affinity, and PPAR-γ transactivation compared to partial agonists (20). The active conformation of OXTZD did not occupy arm I leading to lower binding than rosiglitazone. The decreased binding ability of OXTZD might be one of the reasons for the sub-maximal transactivation of the receptor as indicated by the luciferase reporter assay. Another justification is the binding mode and nature of binding interactions predicted by docking. The binding site of OXTZD was defined by the residues present in arm II and arm III of PPAR-γ-LBD. Arm II residues which contribute to the putative binding site of OXTZD were MET348, VAL339, ILE341, and MET329; arm III residues include LEU333, CYS285, ALA292, ARG288, and SER342. It has been suggested that the potent partial agonists adopt a conformation so as to interact with arm II and establish a polar hydrogen bond with SER342 or other residues of arm III especially, CYS285 and ARG288 (21). The bound conformation of OXTZD was shown to interact through hydrogen bonds with SER342, CYS285, and ARG288. Furthermore, OXTZD was found to bind in a mode distinct from the recent thiazolidinediones (14, 15) having PPAR-γ partial agonist activity. Interestingly, benzylidene thiazolidinedione formed four hydrogen bond contacts through oxygen atoms of two keto groups in thiazolidinedione (Fig. 1). Authors have predicted that one of the hydrogen bonds was between benzylidene thiazolidinedione and TYR327 of arm I, and the rest of the bonds were with SER342, ARG288, and L340 constituting arm II (14). Thus, the established binding modes of OXTZD suggest the importance of thiazolidinedione and oxadiazole motifs linked through -O-CH_2- linker. Associating these binding interactions with the *in-vitro* binding affinity and transactivation activity substantiates the claim that OXTZD functions as an effective PPAR-γ partial agonist. PPAR-γ partial agonists, due to their less agonistic and transactivation potency, possess a different side effect profile from that of full agonists. The characters of partial agonists are believed to range from weak to non-adipogenic, which would decrease the common side effect of obesity caused by full agonists like rosiglitazone and pioglitazone (22). Thus, it was essential to study the adipogenic potential of OXTZD. From the results of PPAR-γ-dependent adipogenic assay using OilRed O staining, we understood that OXTZD was non-adipogenic in nature as it did not increase lipid accumulation as opposed to the DMI control group. Given the advantages of OXTZD as a partial agonist, we proceeded to verify its *in-vivo* blood glucose-lowering activity, which is indispensable for its development as a clinically useful agent. From the results of *in-vivo* anti-diabetic activity in diabetic rats, OGTT and ITT in treated rats, it was evident that OXTZD has the ability to reduce the fasting blood glucose level, improve oral glucose tolerance, and also increase insulin sensitivity in the diabetic state. In addition, OXTZD also lacks the obesity side effect as understood from the observations on body weight following the treatment with OXTZD.

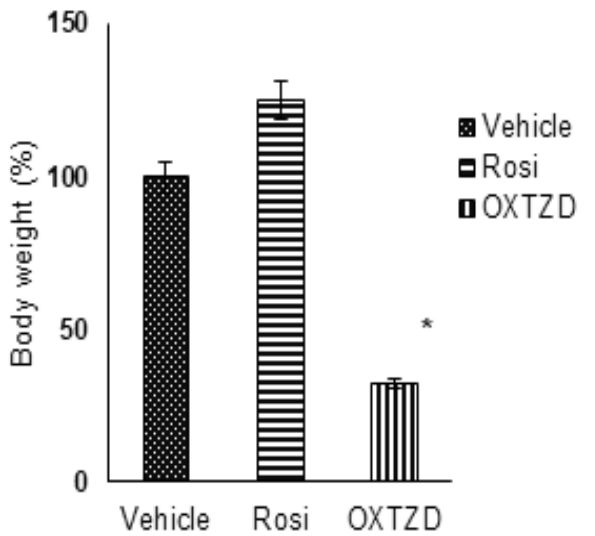

Fig. 10. *Effect of OXTZD on body weight after 15 days of treatment (n = 12 rats/group). Each bar represents the mean ±SEM of three individual determinations; Two-way ANOVA followed by Tukey's test; * indicates P < 0.05 statistically significant suppression in body weight compared to vehicle (0.25% aqueous carboxy methyl cellulose) control.*

To conclude, this study furnishes evidence for the partial PPAR-γ agonist activity of a novel synthetic oxadiazolyl thiazolidinedione, OXTZD. The blood glucose-lowering effect of OXTZD in type 2 diabetes, with a potential non-adipogenic property,

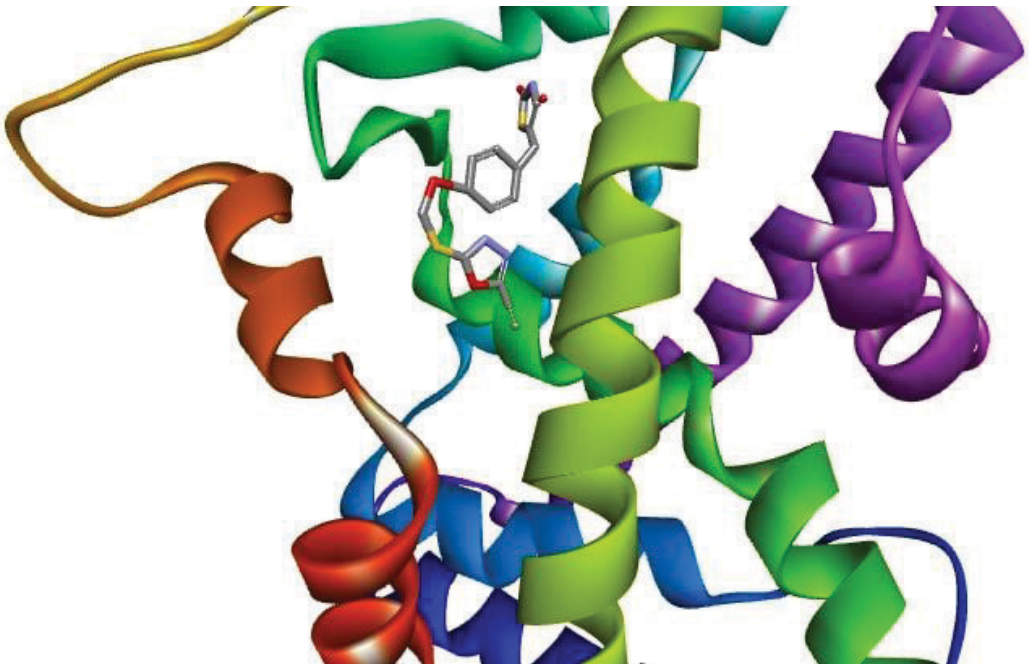

Fig. 11. *The conformation of OXTZD-PPAR-γ complex. OXTZD-2PRG complex obtained by docking was viewed in Discovery Studio Client 2016; OXTZD binds to arm II and III of the Y-shaped binding cavity of PPAR-γ-LBD.*

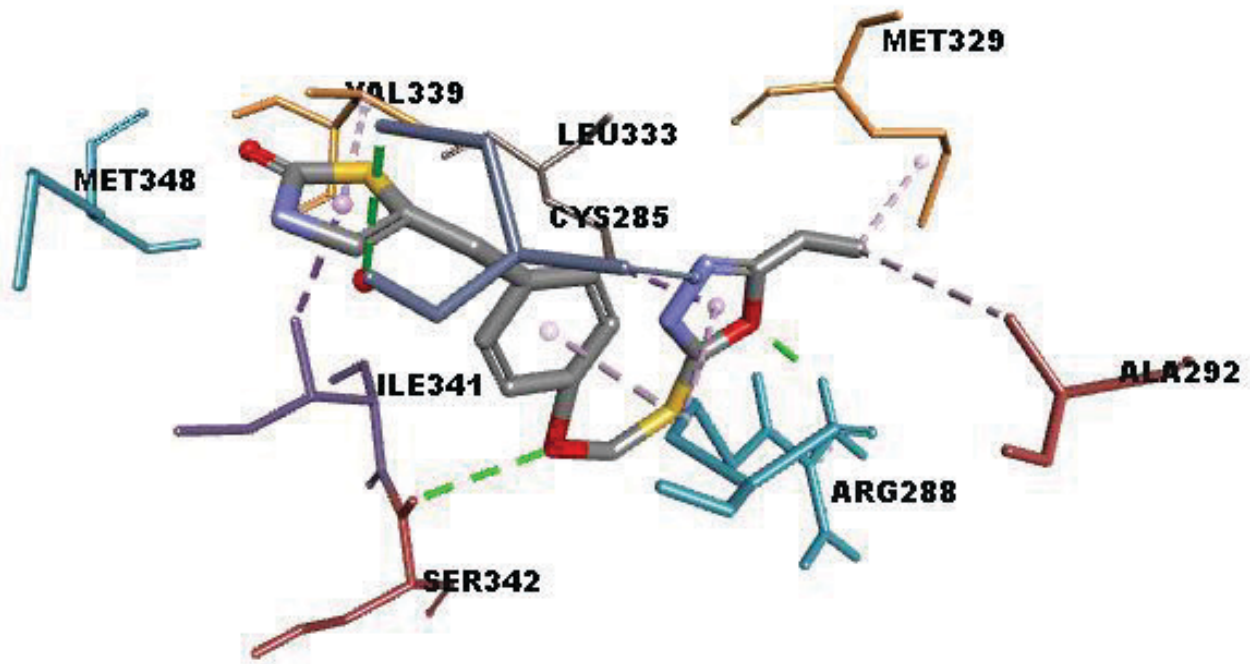

Fig. 12. *Binding interactions of OXTZD with PPAR-γ viewed in Discovery Studio Client 2016. Bonds in green are hydrogen bonds between OXTZD and SER342, ARG288, and CYS285 of arm II and III; also seen are the other π-alkyl and alkyl-alkyl hydrophobic interactions between OXTZD and the residues in arm II and arm III.*

was mediated through the restricted binding to, and transactivation of PPAR-γ. OXTZD is a promising lead for further structural modifications to develop anti-diabetic drugs targeting PPAR-γ, simultaneously maintaining insulin sensitivity with a better side effect profile compared to rosiglitazone. At the same time, OXTZD can be promoted to the next stages of study for development into a therapeutic agent.

ACKNOWLEDGEMENTS

This work was supported by the Deanship of research and scientific affairs, Jazan University, Jazan, Kingdom of Saudi Arabia, Research Grant. No: JUP7/2014-2015; 37/7/00118.

REFERENCES

1. Henry RR, Erickson D, Ciaraldi TP. PPAR γ agonists and the future for insulin sensitizers: A report of a debate and presentations on the subject at the 72nd Scientific Sessions of the American Diabetes Association, Philadelphia, 8-12 June, 2012. Br J Diabetes Vasc Dis 2012; 12:206-10.
2. Clymer JW. Current developments in thiazolidinediones. Adv Health Sci Res 2011; 1:1-6.
3. Nishizuka M, Imagawa M. PPARgamma target genes and the molecular mechanism of transcriptional control by PPARgamma. Nihon rinsho 2010; 68:189-93.
4. Derosa G, Maffioli P. Peroxisome proliferator-activated receptor-γ (PPAR-γ) agonists on glycemic control, lipid profile and cardiovascular risk. Curr Mol Pharmacol 2012; 5:272-81.
5. Olefsky JM. Treatment of insulin resistance with peroxisome proliferator–activated receptor γ agonists. J Clin Investig 2000; 106:467-72.
6. Aghamohammadzadeh N, Niafar M, Dalir Abdolahinia E, et al. The effect of pioglitazone on weight, lipid profile and liver enzymes in type 2 diabetic patients. Ther Advan Endocrinol Metab 2015; 6:56-60.
7. Kus V, Flachs P, Kuda O, et al. Unmasking differential effects of rosiglitazone and pioglitazone in the combination treatment with n-3 fatty acids in mice fed a high-fat diet. PLoS One 2011; 6:e27126.
8. Kim J, Han D, Kim J, et al. PPAR γ partial agonist, KR-62776, inhibits adipocyte differentiation via activation of ERK. Cell Mol Life Sci 2009; 66:1766-81.
9. Kung J, Henry RR. Thiazolidinedione safety. Expert Opin Drug Saf 2012; 11:565-79.
10. Zhang F, Lavan BE, Gregoire FM. Selective modulators of PPAR-γ activity: molecular aspects related to obesity and side-effects. PPAR Res 2007; 2007:32696
11. Rocchi S, Picard F, Vamecq J, et al. A unique PPARγ ligand with potent insulin-sensitizing yet weak adipogenic activity. Mol Cell 2001; 8:737-47.
12. Feldman P, Lambert M, Henke B. PPAR modulators and PPAR pan agonists for metabolic diseases: the next generation of drugs targeting peroxisome proliferator-activated receptors?. Curr Top Med Chem 2008; 8:728-49.
13. Doshi LS, Brahma MK, Bahirat UA, Dixit AV, Nemmani KV. Discovery and development of selective PPARγ modulators as safe and effective antidiabetic agents. Expert Opin Investig Drugs 2010; 19:489-512.
14. Yasmin S, Capone F, Laghezza A, et al. Novel benzylidene thiazolidinedione derivatives as partial PPARγ agonists and their antidiabetic effects on Type 2 diabetes. Sci Rep 2017; 7:14453.
15. Darwish KM, Salama I, Mostafa S, Gomaa MS, Helal MA. Design, synthesis, and biological evaluation of novel thiazolidinediones as PPARγ/FFAR1 dual agonists. Eur J Med Chem 2016; 109:157-72.
16. Ruiz-Ojeda F, Rupérez A, Gomez-Llorente C, Gil A, Aguilera C. Cell models and their application for studying adipogenic differentiation in relation to obesity: a review. Int J Mol Sci 2016; 17:1040.
17. Guasch L, Sala E, Castell-Auví A, et al. Identification of PPARgamma partial agonists of natural origin (I): development of a virtual screening procedure and in vitro validation. PLoS One 2012; 7:e50816.
18. Thangavel N, Al MB, Javed S, Ahsan W, Al HH. Critical insight into design of PPAR-γ agonists by virtual screening techniques. Curr Drug Discov Technol 2018. doi: 10.2174/1570163815666180227164028.
19. Liu C, Feng T, Zhu N, et al. Identification of a novel selective agonist of PPARγ with no promotion of adipogenesis and less inhibition of osteoblastogenesis. Sci Rep 2015; 5:9530.

20. Farce A, Renault N, Chavatte P. Structural insight into PPARγ ligands binding. Curr Med Chem 2009; 16:1768-89.
21. Guasch L, Sala E, Valls C, et al. Structural insights for the design of new PPARgamma partial agonists with high binding affinity and low transactivation activity. J Comput Aided Mol Design 2011; 25:717-28.
22. Agrawal R, Jain P, Dikshit NS. Balaglitazone: a second generation peroxisome proliferator-activated receptor (PPAR) gamma (γ) agonist. Mini Rev Med Chem 2012; 12:87-97.

THE ROLE OF miR-186 AND ZNF545 IN INHIBITING THE PROLIFERATION OF MULTIPLE MYELOMA CELLS

S. DENG[1], JJ. XIANG[1], HP. GE[1], ZP. HU[1], JP. SHEN[1], SY. LIN[1] and YQ. ZENG[2]

[1]Department of Hematology, The First Affiliated Hospital of Zhejiang Chinese Medical University, Hangzhou, Zhejiang Province, China; [2]Department of Orthopedics, Tongde Hospital of Zhejiang Province, Hangzhou, Zhejiang Province, China

Received December 16, 2018 – Accepted February 26, 2019

This study aimed to investigate the mechanism underlying the inhibitory effect of tumor suppressor gene miR-186 and zinc finger protein 545 (ZNF545) on the proliferation of multiple myeloma (MM) cells. CD138 magnetic beads were used to isolate different types of myeloma cell lines (KM3, U266, RPMI-8226, and H929), which were then infected by lentivirus carrying the miR-186 gene. Using uninfected myeloma cells as the control, MTT [3-(4,5-dimethyl-2-thiazolyl)-2,5-diphenyl-2-H-tetrazolium bromide, Thiazolyl Blue Tetrazolium Bromide] assay was performed to calculate the rate of cell proliferation at different time points. In addition, the correlation between the expression of Jagged 1 and miR-186 was analyzed by real-time Polymerase Chain Reaction (PCR). Furthermore, the effect of 5-Aza-2-deoxycytidine and acetylase inhibitor Trichomycin A (TSA) on the expression of ZNF545 and proliferation/apoptosis of MM cells was investigated using Reverse Transcription-Polymerase Chain Reaction (RT-PCR), Western blotting (WB), MTS [3-(4,5-dimethylthiazol-2-yl)-5-(3-carboxymethoxyphenyl)-2-(4-sulfophenyl)-2H-tetrazolium] cell proliferation assay, and Annexin V-FITC/PI staining. Compared with the control group, the proliferation of miR-186-overexpressing U266 and RPMI-8226 cells was significantly decreased. In cell cloning experiments, miR-186 decreased the number of U266 and RPMI-8226 clones while reducing the protein expression of Jagged 1. The expression level of ZNF545 in myeloma patients was also reduced to some extent. ZNF545 protein also promoted the apoptosis of myeloma cells. By inhibiting the proliferation of myeloma cells, miR-186 gene and ZNF protein may be used as tumor suppressors in the treatment of myeloma.

Multiple myeloma (MM) is a common type of blood malignancy and its incidence has been rising in recent years. MM is derived from malignant plasma cells of bone marrow and can quickly spread to many organs, thus causing multiorgan failures in MM patients (1-2). The pathogenesis of MM is complex, in which many factors, such as heredity and gene variation, are involved. Clinically, MM is characterized by anemia, impaired renal function and osteolytic damage. Protease inhibitors can inhibit the growth of tumor cells to a certain extent. However, in order to cure myeloma, it is necessary to inhibit the growth of tumor cells from a genetic point of view.

Most miRNA genes are found in the chromosomal

Key words: MM; miR-186; ZNF545; cell proliferation; inhibition

Corresponding author:
Dr Yuqing Zeng,
Department of Orthopedics,
Tongde Hospital of Zhejiang Province,
No.234 Gucui Road, Xihu District, Hangzhou,
Zhejiang Province, 310012, China
e-mail: zengyuqing0571@163.com

0393-974X (2019)

region of tumor cells, i.e., there is a certain correlation between miRNA expressions and the development of tumors (3). In a study of chronic lymphoblastic leukemia, Quesada, et al. (4) found that the regulation of miRNA expressions could effectively affect the development of tumors. Borel, et al. (5) further analyzed the expression of miRNAs in patients with hepatocellular carcinoma and showed the abnormal expression of multiple miRNAs, i.e., the expression of miR-224 and miR-182 was up-regulated while the expression of miR-214 and miR-145 was down-regulated. Beside miRNAs, epigenetics also regulated the growth of tumors (6). As an epigenetic mechanism of regulation, DNA methylation plays an important role in early detection and diagnosis of tumors (7). It was confirmed previously that tumor cells were associated with an abnormal level of DNA methylation, whereas transferase inhibitors could be used to effectively treat tumors by regulating the level of DNA methylation (8).

In terms of MM, previous studies have confirmed the abnormally high expression of several miRNAs in MM patients (9). In addition, using gene chip analysis and real-time Polymerase Chain Reaction (PCR), Seckinger, et al. (10) showed a strong correlation between chromosomal ectopic regulation and abnormal expressions of multiple miRNAs in MM patients. As a zinc finger protein, KRAB-containing zinc finger protein (KRAB-ZFP) (11) plays an important role in the growth of tumors. The abnormal methylation of KRAB-ZFP DNA also participates in the occurrence and metastasis of tumors. Therefore, the status of DNA methylation of KRAB-ZFP gene may be used as a biomarker for the early detection and clinical diagnosis of tumors.

As a kind of miRNA, miR-186 (12) shows abnormal chromosomal expressions in cancer cells. It has also been confirmed that (13) miR-186 reduces the expression of several genes in myeloma cells. Furthermore, the regulation of miR-186 expressions could inhibit the growth of myeloma cells. On the other hand, as demonstrated by Fan, et al., the mutations in ZNF545 (14), a member of KRAB-ZFP proteins, affected the expression of tumor suppressor genes and subsequently affect the occurrence and growth of glioblastoma. Therefore, this study was carried out to further clarify the mechanisms underlying the inhibitory effect of miR-186 and ZNF545 on the proliferation of MM cells.

MATERIALS AND METHODS

Cell lines

MM cell lines, including U266, KM3, RPMI-8226 and H929, were purchased from the American Type Culture Collection (ATCC) and cultured in an RPMI-1640 medium supplemented with 10% fetal bovine serum and 1% penicillin streptomycin. The cells were cultured in a 37°C incubator containing 3% CO_2 and saturated humidity. In addition, 293T cells were used for lentiviral packaging and were cultured in DMEM supplemented with 10% fetal bovine serum. The strain used for the packaging of plasmids was Escherichia coli DH5α. Primer sequences used for real-time PCR were as follows: (p53-F, TCAACAAGATGTTTTGCCAACTG), (p53-R, ATGTGCTGTGACTGCTTGTAGATG), (β-actin-F, CCTGTGGCATCCACGAAACT), and (β-actin-R, GAAGCATTTGCGGTGGACGAT). BALB/c-nu nude mice aged 5-7 weeks were purchased from Beijing Witonglihua Laboratory Animal Technology Co., Ltd, which multiple myeloma cell RPMI-8226 was injected subcutaneously into the right armpit of mice, we needed to measure body condition of mice and tumor size of mice regularly, when all the experiments were done, the mice were sacrificed and the tumor tissues were taken out for experimental analysis.

Design of miR-186's Primers

Firstly, a pMD18-T vector (a special vector for efficient cloning of PCR products) and the gene fragment of miR-186(Guangzhou RiboBio Company, China) were digested by double enzyme digestion and resolved by gel electrophoresis. Subsequently, a ligation system containing 9.0 μl of miR-186 gene, 2 μl of T4 DNA ligase, 2 μl of T4 buffer, and 6.0 μl of pMD18-T (0.1μg/μl) was incubated overnight at 5°C to carry out the ligation reaction, and the products of ligation were transformed into *E. coli*. After culturing, multiple colonies were picked and subjected to electrophoresis (Bio-Rad, USA) to select colonies carrying the correct gene sequence. Subsequently, plasmids were extracted from bacterial culture according to the instruction of a plasmid extraction kit (QIAGEN, Germany).

Preparation of lentiviral vectors

An empty phU6-MCS-PGK-EGEP vector was digested

by double enzyme digestion along with the recombinant plasmid of miR-186 gene. The digestion products were ligated in a system containing T4 DNA ligase, T4 buffer and pMD18-T vectors (consistent with the primer design method of gene miR-186), and the ligation reaction was carried out overnight at 5°C. The ligation products were transformed into *E. coli*. After culturing, multiple colonies were picked and subjected to electrophoresis to select colonies carrying the correct gene sequence. Subsequently, lentiviral vectors were extracted from bacteria culture and used to infect 293T cells. After 6 h of infection, the bacteria were transferred into a complete culture medium (Bio-Rad, USA). After 2 days of culture, the supernatant of bacteria culture was centrifuged to obtain different concentrations of lentiviral concentrates.

Lentivirus preparation and infection of target cells

293T cells in the logarithm growth were trypsinized (15), collected, seeded and grown to over 85% confluency. After replacing the medium using a serum-free medium for virus infection, the virus solution was added to the culture medium. Seven h later, the cells were washed with phosphate-buffered saline (PBS) and 10 mL of cell culture medium containing 10% fetal bovine serum (Gibco, USA) were added onto the cells. Finally, cell supernatant was collected at night and centrifuged at 3500g for 15 min to collect infected virus, which was then filtered and stored in an EP tube.

U266, RPMI-8226, KM3, and H929 cells in the logarithm growth were seeded in culture dishes (Gibco, USA) before a small amount of lentivirus and 3 mL of 10% fetal bovine serum cytosol and coagulant amine were added, so that the concentration of cytosol was 6mg/mL. After 24 h of culture, the supernatant was removed and replaced with a normal culture medium containing 10% fetal bovine serum. The status of cell infection was then observed under a fluorescence microscope (Leica, Germany).

Bacterial liquid culture and identification of ZNF545 plasmids

A vial of *E. coli* DH5α culture was taken out from the cryogenic freezer to transfer 60 μl of bacterial culture into an EP tube. Subsequently, 15 μl of plasmid solution containing pcDNA3.1 (Promega Company, USA) and pcDNA3.1-ZNF545 plasmids was mixed into the bacterial culture and incubated at 50 in a water bath. After the mixture was cooled on ice for 3 min, it was centrifuged and incubated for five more h before 150 μl of bacterial solution was transferred onto a LA agarose plate containing penicillin. After 15 h of inverted culture, several colonies were picked using a small sterile pipette tip and placed in a sterile Falcon tube containing 5 ml of LA bacterial culture. After another 15 h of culture, plasmids were extracted from the colonies and the integrity of isolated plasmids was detected by agarose gel electrophoresis and PCR (ABI, USA).

Plasmid extraction and infection in MM cells

The bacterial culture medium containing gene ZNF545 was centrifuged to collect the pellet. Thereafter, 300 μl of RNase solution was added to the pellet on a rotary oscillator, followed by the addition of 300 μl pyrolysis solution and 300 μl neutralization solution, respectively. After 3 min of incubation on ice, the mixture was loaded onto a centrifugal column and centrifuged. According to the instruction of the centrifugal column, it was eluted with 80 μl of TE buffer to collect the plasmid.

Myeloma cells were seeded into a 96-well plate and cultured until 75% of confluence. Subsequently, 4μl of Lipofectamine 2000 liposomes were mixed with 4 μg of plasmids and incubated at room temperature for 15 min After aspirating cell culture medium from the 96-well plate, the mixture of Lipofectamine 2000 and plasmids was added onto the cells. After 5 h of transfection, the mixture was removed and replaced with the complete culture medium.

Proliferation of miR-186-infected cells was detected by MTT assay

Myeloma cell lines U266, RPMI-8226, KM3 and H929 were selected and infected with miR-186. Different culture media were cultured for 72 h, and a small amount of culture solution was taken out at different time points. 5mg/ml MTT solution (Shanghai Biyuntian Biotechnology Research Institute, China) was then added to the cells and mixed evenly. After another 5 h of culture, the MTT solution (16) was removed and replaced with 150 ul of dimethyl sulfoxide in each well. The solution was then fully dissolved and placed on a plate reader to detect the value of optical density and to plot the cell proliferation curve.

Detection of Jagged 1 expressions after miR-186 infection

Primier 5.0 was used to detect the expression of Jagged 1(Sigma Company, USA) in cells infected with miR-186. The primers were designed as follows: (upstream of Jagged

1, 5'-AAGTGTGCCTCAAGGAGTATC-3'), (downstream of Jagged 1, 5'-ACTGTCAGGTTGAACGGTGTC-3'), (upstream of β-actin, 5'-GGAAATCGTGCGTGACAT-3'), and (downstream of β-actin, 5'-AAGGAAGGCTGGAAGAGTG-3'). The expression of target gene (17) was identified by SYBR Green infiltration.

Firstly, protein samples were extracted (Invitrogen, USA) and vortexed on ice for 15 min. The supernatant was then transferred into centrifugal tubes and the concentration of extracted protein was determined. Subsequently, 10 μl of each protein sample was resolved by a 13% separating gel and then blotted onto a PVDF membrane. Subsequently, the membrane was blocked with a blocking solution containing 5% BSA, washed with PBS for several times, and then visualized to analyze the profile of cell proliferation (18).

Detection of cell proliferation after ZNF545 infection

Different myeloma cell lines, including U266, RPMI-8226, KM3 and H929, were placed in different 96-well plates and subjected to the MTS assay at different time points within a period of 72 h. At specified time points, the original culture medium was discarded and replaced with 150μl of complete culture medium containing 20% MTS (19). After culturing at 35 , the absorbance in each well was detected by a plate reader. At last, the cell proliferation curve was plotted.

Detection of apoptosis in cells infected with ZNF545

Digestive manipulation of trypsin was carried out on myeloma cells infected with ZNF545, and the cells were then placed in centrifugal tubes, washed by PBS and centrifuged. The supernatant was then removed and replaced with 400 μl of binding buffer in each tube. Subsequently, reagents of Annexin V-FITC/PI double staining(BD Company, USA) (20) were added into the tubes and incubated for 20 min, followed by the addition of 100 μl of binding buffer into each tube. After packing the solution of bone marrow cell lines into 4 EP tubes, the tubes were analyzed by flow cytometry(BD, USA) to calculate the apoptosis rate of different cells.

Statistical analysis

SPSS17.0 statistical software was used for data analysis. The experimental data were expressed as $\bar{x}\pm s$. The *t*-test was used for comparison among different groups and a probability value of $P<0.05$ was considered statistically significant.

RESULTS

Experimental results of the proliferation of MM cells

Infection of myeloma cells with miR-186 was carried out prior to the MTT test. As shown in Fig. 1, A and B, the growth ability of cells in the U266/miR-186 and RPMI-8226/miR-186 groups was significantly reduced compared with the U266/Control, RPMI-8226/Control, U266/miR-186 and RPMI-8226/miR-186 groups ($P<0.05$). In Fig. 1C and compared with the H929/Control group, the growth ability of H929/miR-186 cells was significantly enhanced ($P<0.05$). In the plate cloning experiment, compared with the U266/Control and RPMI-8226/Control groups, the cloning ability of U266/miR-186 and RPMI-8226/miR-186 groups was significantly reduced ($P<0.05$), as shown in Fig. 1D. Compared with the H929/Control group, the cloning ability of H929/miR-186 group was significantly enhanced ($P<0.05$), as shown in Fig. 1E.

Effects of miR-186 on the expression of Jagged 1 in MM cells

As shown in Fig. 2A, there was no significant difference in the levels of Jagged 1 protein among control cells and miR-186-infected U266 and RPMI 8226 cells ($P > 0.05$). From the results of WB assays (Fig. 2B) and compared with the control group, the levels of Jagged 1 protein in miR-186-infected U266, H929 and RPMI-8226 cells were significantly decreased ($P < 0.05$), indicating that the high expression of miR-186 could inhibit the expression of Jagged 1 protein.

Effects of ZNF545 on the proliferation of MM cells

As can be seen in Fig. 3A, it was found that the expression of ZNF545 was down-regulated in U266, RPMI-8226, H929 and KM3 cells, but the infection with pcDNA3.1-ZNF545 plasmids effectively restored the expression of ZNF545. Using soft agar and plate cloning methods, it was found that, compared with the Vector group, the cloning ability of ZNF545-infected myeloma cells was reduced to a certain degree ($P < 0.05$) (Fig. 3, B and C). MTS test also showed that the proliferation ability of selected myeloma cell lines (U266, RPMI-8226, KM3, and H929) decreased significantly after ZNF545 infection ($P < 0.05$), as shown in Fig. 3D.

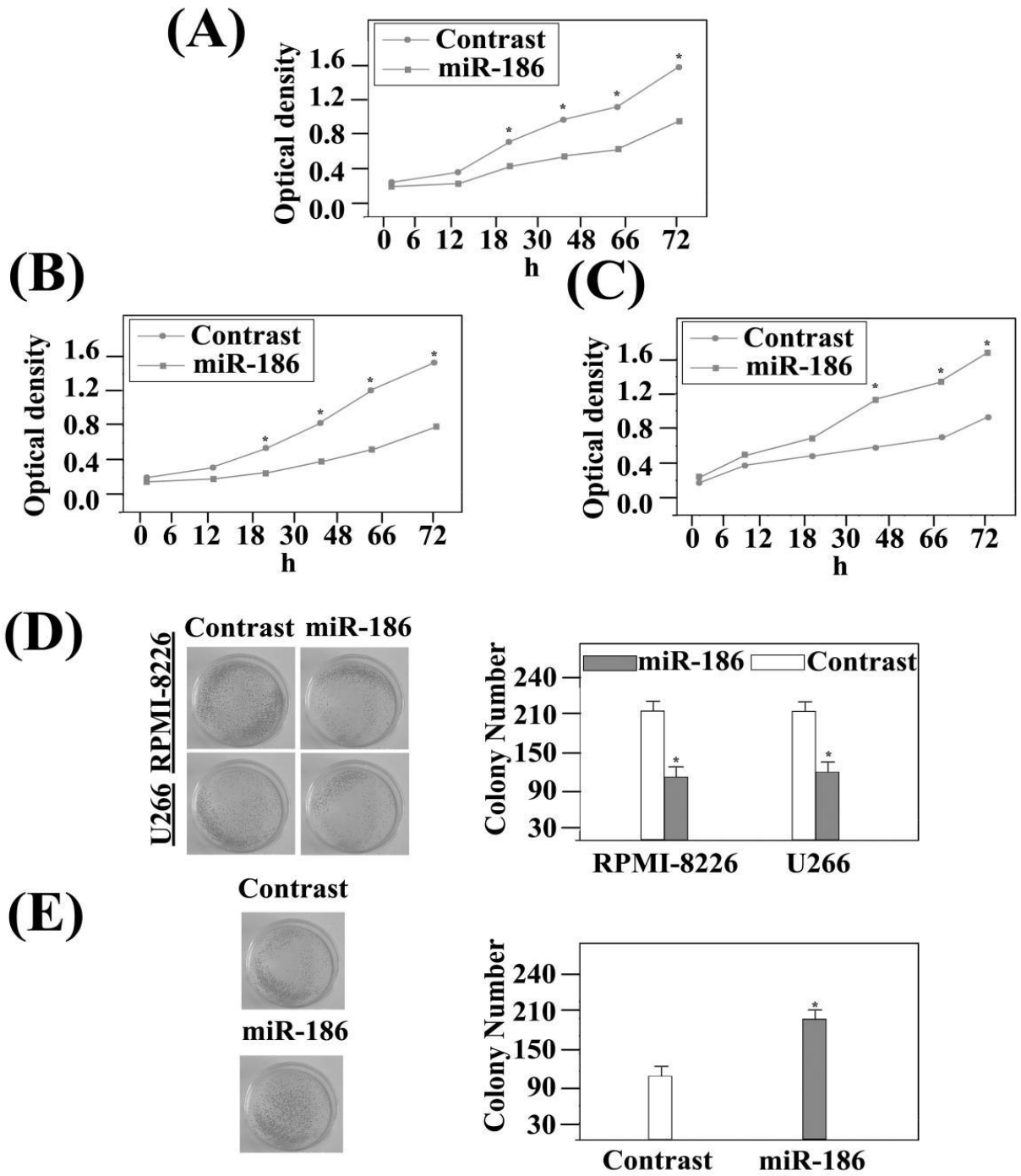

Fig. 1. *The effects of miR-186 on the proliferation of MM cells.* ***A****) MTT method was used to evaluate the effects of miR-186 on the growth of U266 cells.* ***B****) MTT method was used to evaluate the effects of miR-186 on the growth of RPMI-8226 cells.* ***C****) MTT method was used to evaluate the effects of miR-186 on the growth of H929 cells.* ***D****) plate cell cloning analysis was carried out to evaluate the effects of miR-186 on the proliferation of U266 and RPMI-8226 cells.* ***E****) plate cell cloning analysis was carried out to evaluate the effects of miR-186 on the proliferation of H929 cells, *P<0.05.*

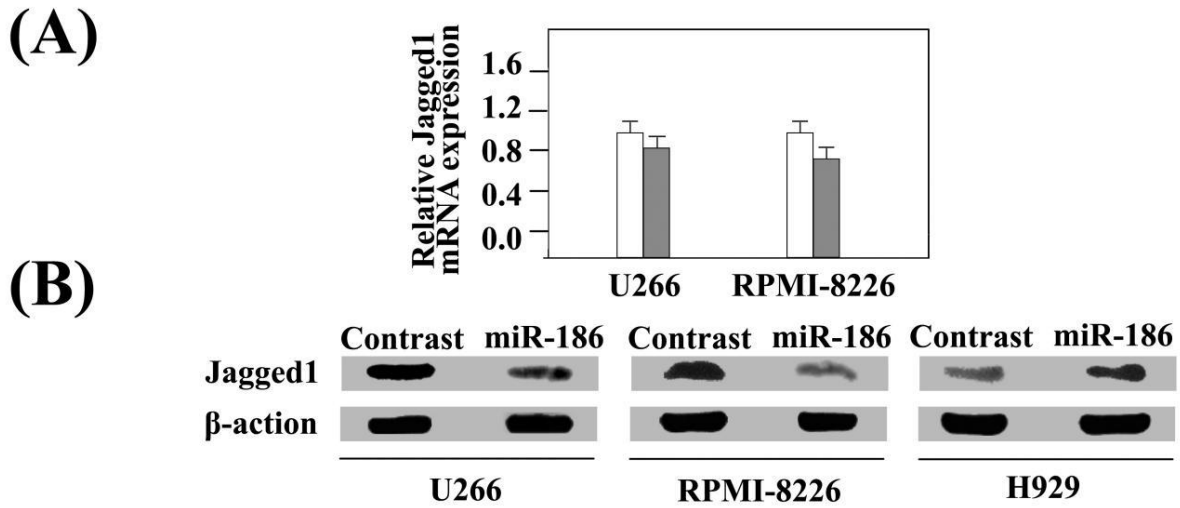

Fig. 2. *The effects of miR-186 on the expression of Jagged 1. **A**) the effects of miR-186 on the expression of Jagged 1, and (**B**) the effects of miR-186 on the expression of Jagged 1protein, P<0.05*

Effects of ZNF545 on the apoptosis of MM cells

WB assay was used to demonstrate that the expression of ZNF545 protein was increased after the myeloma cells were infected with pcDNA3.1-ZNF545 plasmids (Fig. 4A). In flow cytometry assays shown in Fig. 4B, the number of apoptotic KM3, U266 and RPMI-8226 cells was increased significantly after the cells were infected with pcDNA3.1-ZNF545 plasmids ($P < 0.05$). Cleaved-caspase 3, cleaved-caspase 6 and cleaved-caspase 8 antibodies were then used to detect caspase activity after ZNF545 infection, respectively. As shown in Fig. 4C, the activity of caspase was significantly increased after ZNF545 infection.

DISCUSSION

As a kind of miRNA, miR-186 showed abnormal chromosomal expressions in tumor cells. It has been confirmed that miR-186 reduces the expression of some genes in myeloma cells. Regulation of gene expression by miR-186 can inhibit the growth of myeloma cells. At the same time, as demonstrated by Fan, et al., the mutations in ZNF545, a member of KRAB-ZFP proteins, affected the expression of tumor suppressor genes and subsequently affected the occurrence and growth of glioblastoma.

MTT method was used here to test the proliferation ability of myeloma cells infected with miR-186 gene, which significantly inhibited the proliferation ability of myeloma cells after 24 h of culture. In the plate cell cloning experiment, it was also proved that miR-186 could inhibit the proliferation of myeloma cells. In order to further investigate the effect of miR-186 on the proliferation of myeloma cells, the expression of Jagged 1, a target gene of miR-186, was measured in MM cells by RT-PCR and Western blot. The results showed that the high expression of miR-186 could decrease the protein levels of Jagged 1 in U266 and RPMI-8226 cells, while the protein level of Jagged 1 was increased significantly in miR-186-infected H929 cells.

P53 tumor suppressor protein is located in the TP53 gene region of 17p13.1, which can ensure integrity of the gene and promote stability of the genome. Many reports also mention that p53 transcriptional activity can promote inhibitory growth of cancer cells, and it has been confirmed that many cellular proteins can affect the transcription of p53 protein; the accumulation of p53 protein can promote the activation of downstream pathways and activate growth-related factors. Therefore, the signal pathway of p53 protein is significant for the treatment of cancer, and many anti-cancer experiments are designed to promote the re-activation of p53 gene.

The expression of p53, a tumor suppressor, in tumor cells is closely related to their stability. The activation of p53 plays an important role in inhibiting tumor development. KRAB-ZFP proteins is directly involved in the transcription of p53, i.e., KRAB-ZFP proteins can regulate the expression of p53. In this study, the expression of ZNF545, a member of KRAB-ZFP proteins, was studied. Through cell proliferation, flow cytometry and caspase enzyme assays, it was demonstrated that ZNF545 could inhibit

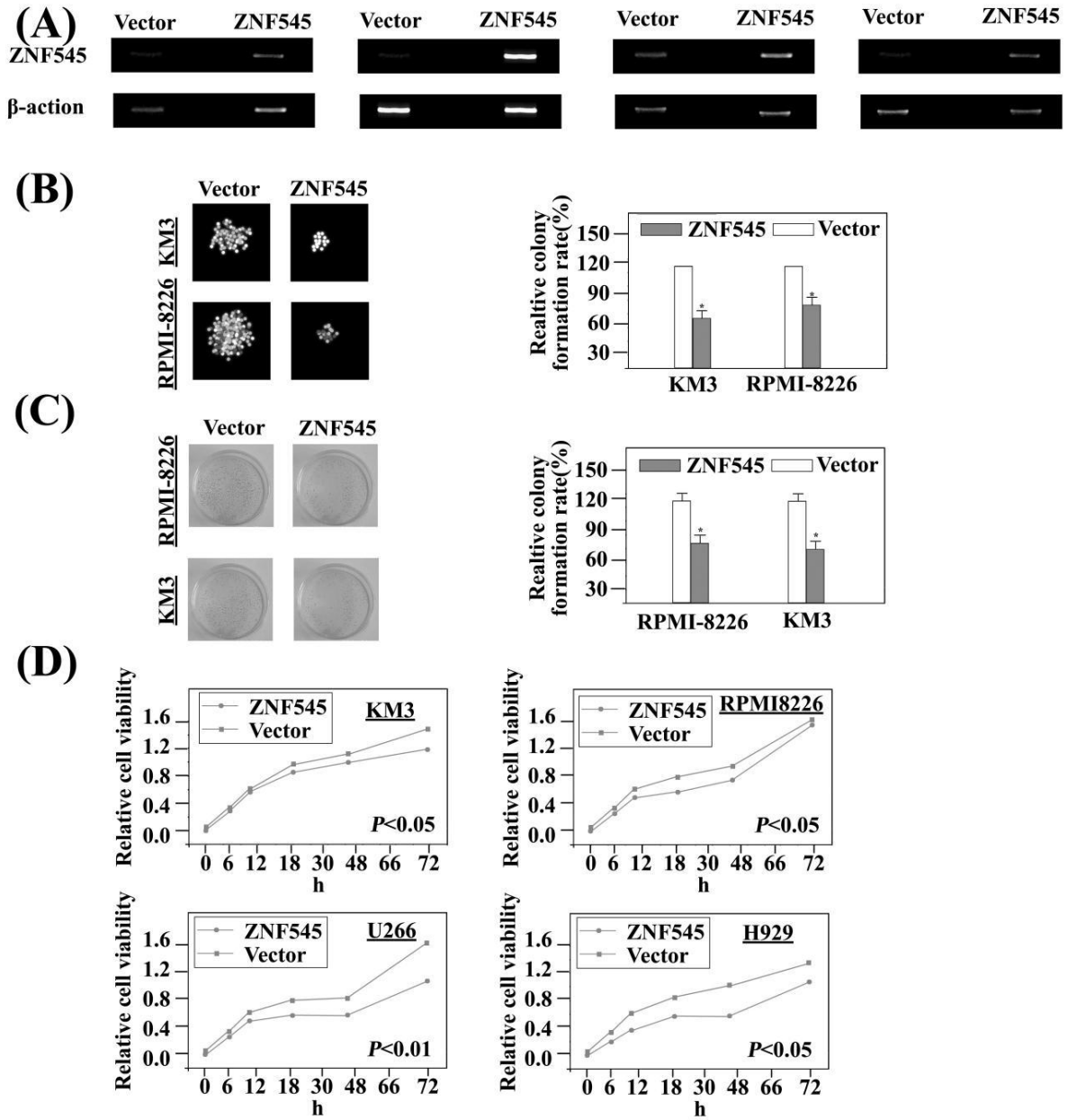

Fig. 3. *The effect of exogenous ZNF545 on the proliferation of myeloma cells.* ***A)*** *RT-PCR was used to evaluate the effect of ZNF545 on the proliferation of myeloma cells.* ***B)*** *soft agar cloning experiment was used to evaluate the effect of ZNF545 on the proliferation of myeloma cells.* ***C)*** *plate cloning experiment was used to evaluate the effect of ZNF545 on the proliferation of myeloma cells.* ***D)*** *MTS proliferation experiment was used to evaluate the effect of ZNF545 on the proliferation of myeloma cells, *P<0.05*

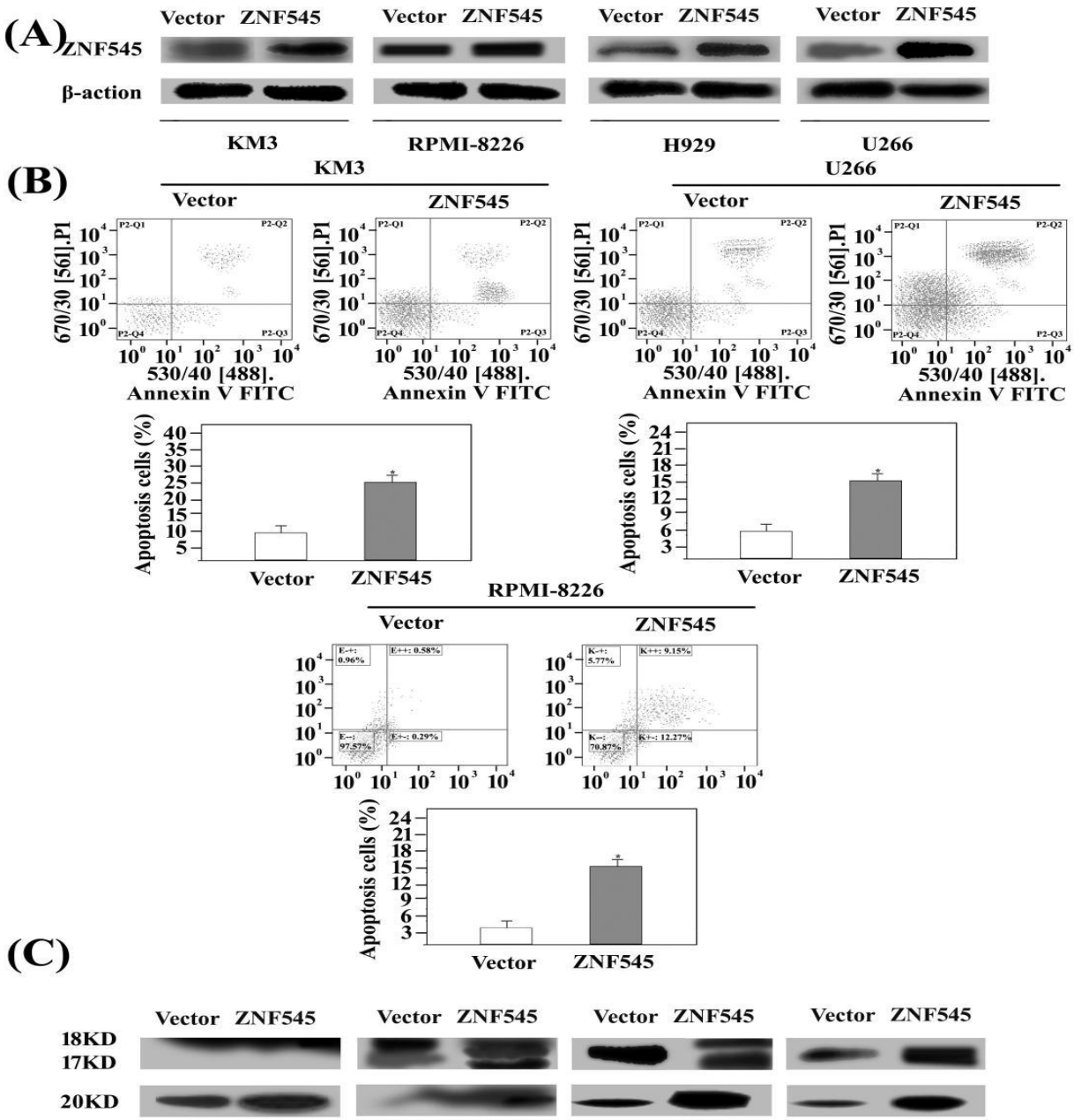

Fig. 4. *The effect of exogenous ZNF545 on the apoptosis of myeloma cells.* ***A)*** *WB method was used to evaluate the effects of exogenous ZNF545 in myeloma cells.* ***B)*** *Flow cytometry was used to evaluate the effect of ZNF545 on the growth of myeloma cells.* ***C)*** *Caspase activity demonstrated the pro-apoptotic effect of ZNF545 on myeloma cells, *P<0.05.*

the proliferation of myeloma cells and hence might be used as a gene to inhibit tumor development.

In summary, as markers for inhibited growth of myeloma cells, miR-186 and ZNF545 provide a new choice for cancer treatment in the future.

ACKNOWLEDGEMENTS

This work was supported by Zhejiang Province Natural Science Foundation Project (Grant/Award, Number: LQ18H080003); Zhejiang Province,

Medical and Health General Research Program (Grant/Award, Number: 2016KYA151); Zhejiang Province, Chinese Medicine Research Fund Project (Grant/Award Number: 2016ZA080).

REFERENCES

1. Anagnostopoulos A, Weber D, Rankin K, Delasalle K, Alexanian R. Thalidomide and dexamethasone for resistant multiple myeloma. Br J Haematol 2003; 121(5):768-71.
2. Hussein MA, Saleh M, Ravandi F, Mason J, Rifkin RM, Ellison R. Phase 2 study of arsenic trioxide in patients with relapsed or refractory multiple myeloma. Br J Haematol 2004; 125(4):470-6.
3. Nowak DM, Gajecka M. Nonrandom distribution of mirnas genes and single nucleotide variants in keratoconus loci. PLoS One 2015; 10(7):e0132143.
4. Quesada V, Conde L, Villamor N, et al. Exome sequencing identifies recurrent mutations of the splicing factor SF3B1 gene in chronic lymphocytic leukemia. Nat Genet 2011; 44(1):47-52.
5. Borel F, Konstantinova P, Jansen PL. Diagnostic and therapeutic potential of miRNA signatures in patients with hepatocellular carcinoma. J Hepatol 2012; 56(6):1371-83.
6. Heard E, Martienssen RA. Transgenerational epigenetic inheritance: myths and mechanisms. Cell 2014; 157(1):95-109.
7. Soppe WJ, Jasencakova Z, Houben A,et al. DNA methylation controls histone H3 lysine 9 methylation and heterochromatin assembly in Arabidopsis. EMBO J 2002; 21(23):6549-59.
8. Corces-Zimmerman MR, Hong WJ, Weissman IL, Medeiros BC, Majeti R. Preleukemic mutations in human acute myeloid leukemia affect epigenetic regulators and persist in remission. Proc Natl Acad Sci USA 2014; 111(7):2548-53.
9. Sun Z, Zhang T, Hong H, Liu Q, Zhang H. miR-202 suppresses proliferation and induces apoptosis of osteosarcoma cells by downregulating Gli2. Mol Cell Biochem 2014; 397(1-2):277-83.
10. Seckinger A, Meiner T, Moreaux J, et al. miRNAs in multiple myeloma - a survival relevant complex regulator of gene expression. Oncotarget 2015; 6(36):39165-83.
11. Wolf G, Yang P, Fchtbauer AC, et al. The KRAB zinc finger protein ZFP809 is required to initiate epigenetic silencing of endogenous retroviruses. Genes Dev 2015; 29(5):538-54.
12. Kim SY, Lee YH, Bae YS. miRr-186, miR-216b, miR-337-3p, and miR-760 cooperatively induce cellular senescence by targeting α, subunit of protein kinase ckii in human colorectal cancer cells. Biochem Biophys Res Commun 2012; 429(3-4):173-9.
13. Shaer A, Azarpira N, Karimi MH. Differentiation of human induced pluripotent stem cells into insulin-like cell clusters with miR-186 and miR-375 by using chemical transfection. Appl Biochem Biotechnol 2014; 174(1):242-58.
14. Fan Y, Zhan Q, Xu H, et al. Epigenetic identification of ZNF545 as a functional tumor suppressor in multiple myeloma via activation of p53 signaling pathway. Biochem Biophys Res Commun 2016; 474(4):660-66.
15. de Wied D, Greven HM, Lande S, Witter A. Dissociation of the behavioural and endocrine effects of lysine vasopressin by tryptic digestion. Br J Pharmacol 1972; 45(1):118-22.
16. Chun J, Kim YS. Platycodin D inhibits migration, invasion, and growth of MDA-MB-231 human breast cancer cells via suppression of EGFR-mediated Akt and MAPK pathways. Chem Biol Interact 2013; 205(3):212-21.
17. Sarkar FH, Sakr WA, Li YW, Sreepathi P, Crissman JD. Detection of human papillomavirus (HPV) DNA in human prostatic tissues by polymerase chain reaction (pcr). Prostate 1993; 22(2):171-80.
18. Gürtler A, Kunz N, Gomolka M, et al. Stain-free technology as novel normalization tool in western blot analysis. Anal Biochem 2013; 433(2):105-11.
19. Appel EA, Rowland MJ, Loh XJ, Heywood RM, Watts C, Scherman OA. Enhanced stability and activity of temozolomide in primary glioblastoma multiforme cells with cucurbit[n]uril. Chem Commun (Camb) 2012; 48(79):9843-5.
20. Xie Q, Sun Z, Chen M, Zhong Q, Yang T, Yi J. IL-8 up-regulates proliferative angiogenesis in ischemic myocardium in rabbits through phosphorylation of Akt/GSK-3β(ser9) dependent pathways. Int J Clin Exp Med 2015; 8(8):12498-508.

AROTINOID TROMETAMOL INHIBITS ARSENIC TRIOXIDE-STIMULATED KERATINOCYTE PROLIFERATION VIA THE Wnt, Shh, AND BONE MORPHOGENETIC PROTEIN SIGNALING PATHWAYS

X. ZHOU[1*], L. YAN[2*], X.L. BU[3], X.G. XU[4], X.L. BI[1] and J. GU[1]

[1]Department of Dermatology, Changhai Hospital, Naval Medical University, Shanghai, P. R. China; [2]New Drug Research Center, School of Pharmacy, Naval Military Medical University, Shanghai, P. R. China; [3]Department of Dermatology, Gongli Hospital, Naval Military Medical University, Shanghai, P. R. China; [4]Department of Dermatology, Changzheng Hospital,Naval Military Medical University, Shanghai, P. R. China

Received December 22, 2018 – Accepted March 15, 2019

[*]These Authors contributed equally to this work

Arsenic acts as a human carcinogen and contributes to skin cancer via mechanisms that remain largely unknown. Recent evidence implicates the perturbation of Wnt, Shh and BMP signals as a potential mechanism. We initiated studies to examine gene expression changes in these signaling pathways. Meanwhile, the antagonistic effect of retinoic acid was explored. In this study, HaCaT and NHEK cells were treated with arsenic trioxide (As_2O_3) alone or in combination with arotinoid trometamol (retinoic acid receptor agonist). Flow cytometric analysis, PCR array and Western blot were used to determine the potential mechanism and signaling pathways associated with arsenic carcinogenesis. The results showed that low concentration As_2O_3 could stimulate keratinocyte proliferation, and arotinoid trometamol inhibited the process via regulating the expression of about 20 genes. These genes included components of Wnt signaling (CSNK1A1L, CTNNB1, SFRP1, Wnt10B, Wnt11, Wnt16, Wnt5A, Wnt8A), Shh signaling (C6orf138, HHIP, PTCHD1) and BMP signaling pathway (BMP2, BMP7). The changes of some differentially expressed genes of these signaling pathways in As_2O_3 treatment group were counteracted by the subsequent arotinoid trometamol treatment. Our data suggest that dysregulation and cross-talk of Wnt, Shh and BMP signals play great roles in the process of arsenic-induced carcinogenesis, which could be antagonized by arotinoid trometamol.

Prolonged ingestion of arsenic, through contaminated water, food and drugs, contributes to increased incidence of skin, lung and bladder cancer. Hyperkeratosis is considered as one of the manifestations of non-malignant disease related to chronic arsenic exposure (1, 2). However, the mechanisms of arsenical keratosis and arsenic-related skin cancer are not well understood. The proposed mechanisms include growth factor overproduction, chromosomal aberrations, oxidative stress and perturbation of signaling pathways (3-5). In particular, the Wnt, sonic hedgehog (Shh) and bone morphogenetic protein (BMP) signaling pathways have been implicated in the progression and maintenance of skin tumors in recent years (6).

Key words: arotinoid trometamol; arsenic trioxide; keratinocyte; Wnt; Shh; BMP; PCR array

Corresponding Author:
Dr Xinling Bi,
Department of Dermatology,
Changhai Hospital, Naval Medical University,
Shanghai 200433, P. R. China
Fax: 021-31161561;
e-mail: bixinling@163.com

0393-974X (2019)

Wnt signaling has been described as acting through two or more distinct signaling mechanisms. Most Wnt isoforms signal through the so-called Wnt/β-catenin pathway. Recent studies have demonstrated that squamous cell carcinoma of the oral cavity express a set of Wnt genes, and Wnt signaling is predominantly activated. Furthermore, a few isoforms, including Wnt4, Wnt5A and Wnt5B, often signal through a β-catenin independent or non-canonical pathway (7). Hedgehog proteins exert biological effects by binding to the Hh ligand PTCHED. This binding relieves PTCHED inhibition of Smo, allowing Smo to induce downstream Gli activators and inhibiting the formation of Gli repressors. The Shh pathway is best known for being up-regulated in a majority of basal cell carcinomas (8). Similarly, BMP signaling is also involved in controlling a variety of pathobiological processes in the skin, including wound healing, psoriasis, and carcinogenesis. Moreover, BMP signaling might interact with the Wnt and Shh signaling pathways (6, 9). Based on our previous studies, we hypothesized that dysregulation of Wnt, Shh and BMP signaling might be involved in the mechanisms of arsenic-related hyperkeratosis and skin cancer.

Retinoic acid can be applied topically and systemically to treat keratosis and malignancies associated with arsenic (10). Arotinoid trometamol (AT), developed by Chongqing Huapont Pharm. Co., Ltd, is a retinoic acid receptor agonist with a chemical structure similar to (E)-4-[2-(5,6,7,8-tetrahydro-5,5,8,8-tetramethyl-2-naphthylenyl)-1-propenyl] benzoic acid (TTNPB). Previous studies from our group have shown that low concentrations of arsenic stimulated keratinocyte proliferation, which is associated with the mechanisms of carcinogenesis (11). Herein, we tested whether arotinoid trometamol could inhibit arsenic trioxide (As_2O_3)-stimulated keratinocyte proliferation. In addition, using Human Signaling RT² Profiler™ PCR Array, we determined the gene expression changes in keratinocytes treated with low concentrations of As_2O_3 alone or combined with arotinoid trometamol. The results showed that dysregulation and cross-talk of the Wnt, Shh and BMP signaling pathways played important roles in the arsenic-induced carcinogenesis.

MATERIALS AND METHODS

Cell lines and reagents

Cells of the human keratinocyte line HaCaT were purchased from American Type Culture Collection and were maintained in Dulbecco's modified essential medium (Gibco/BRL, USA) supplemented with 10% fetal calf serum (Life Technologies, Gaithersburg, MD), 2 mM glutamine (Life Technologies, USA) and 100 U/mL of penicillin/streptomycin at 37°C in a humidified atmosphere containing 5% CO_2. Normal human epidermal keratinocytes (NHEKs) were isolated from adolescent foreskin. The obtained keratinocytes were cultured in keratinocyte serum-free medium (Invitrogen) with recombinant epidermal growth factor (0.2 μg/mL) and bovine pituitary extract (20 μg/mL) (12). As_2O_3 (Sigma Chemical Co, St. Louis, MO, USA) was dissolved in 0.1 M NaOH and diluted in 0.9% phosphate-buffered NaCl solution (PBS) to generate a 50 mM stock solution. Arotinoid trometamol (99.7% pure) was supplied by Chongqing Huapont Pharm. Co., Ltd. (Chongqing, China).

Cell proliferation assays

HaCaT and NHEK cells were evaluated for their proliferation using ^{3}H-thymidine uptake. Briefly, cells were seeded in 96-well plates at 5×10^3/well in complete media and were allowed to grow for an additional 24 h. Following a 24 h starvation period in serum-free media, the cells were then grown in media with different concentrations of As_2O_3 for 12 days. After the treatments, the cells in each well were labeled for 24 h with 1 μCi of ^{3}H-TdR. Then, the cells were harvested, and the incorporated radioactivity was measured using a liquid scintillation counter. The experiments were carried out at least three times.

Flow cytometric analysis

HaCaT and NHEK cell cycle distribution was determined using a Cycle Test™ PLUS DNA Reagent Kit (Becton Dickinson, USA) according to the manufacturer's instructions. The cells were treated with 2 nM As_2O_3 for 4 weeks. The group of HaCaT cells stimulated by arsenic was then treated with arotinoid trometamol (0.1 μm) for different time periods. All the cells were trypsinized and then were stained with propidium iodide. The percentages

of cells in the different phases of the cell cycle were measured with a FACScalibur flow cytometer (Becton Dickinson, San Jose, CA, USA) and were analyzed using CELLQuest software. The experiments were carried out at least three times.

MTT Assay

Growth inhibition of keratinocytes was determined by measuring the MTT dye absorbance of living cells. Cells (10^4/well) were seeded in 96-well microtiter plates (Becton Dickinson, USA) and were allowed to grow to 75% confluence. HaCaT cells stimulated by 2 nM As_2O_3 for 4 weeks were then treated with arotinoid trometamol (0.1 μM) for 24 h, 36 h and 48 h; then, 20 μL of MTT (Sigma) solution (5 mg/mL in PBS) was added. After 4 h of incubation, the supernatant was aspirated, and 150 μL of DMSO was added to each well. The absorbance of the formazan formed in viable cells was measured with an automated microplate reader at a wavelength of 540 nm. The experiments were carried out at least three times.

PCR array analysis

A group of HaCaT cells were continuously treated with 2 nM As_2O_3 for 4 weeks. Another group of HaCaT cells were treated with As_2O_3 (2 nM) for 4 weeks, then treated with arotinoid trometamol (0.1 μm) for 48 h. Total RNA was isolated using TRIZOL Reagent (Invitrogen Life Technologies). The concentration and purity of the RNA were determined with NanoDrop® ND-1000. First-strand cDNA was synthesized using SuperScript III Reverse Transcriptase, oligo (dT) 18 and dNTP Mix (Invitrogen). cDNA was added to the Human Signaling RT² Profiler™ PCR Array (SuperArray, USA), and then a real-time PCR cycling program was run. The data were analyzed with the ΔΔCt method, calculating the ΔΔCt for each gene across two groups and the change fold for each gene from As_2O_3-treated or As_2O_3-AT-treated to the control group as $2^{-\Delta\Delta Ct}$. These experiments were repeated three times independently. Genes with fold changes >2.0 and *p*-values less than 0.05 were considered to indicate differentially expressed genes, which were selected for further analysis.

Western blot analysis

HaCaT cells were treated with As_2O_3 (2 nM) for 4 weeks, and then cells were treated with arotinoid trometamol (0.1 μM) for 48 h. After that, HaCaT cells were then washed with cold PBS and lysed on ice for 30 min in lysis buffer containing 1% Nonidet P-40, 30 mM Tris-HCl (pH 7.4), 0.5 mM EDTA (pH 8.0), 150 mM NaCl, 10% glycerol, 1 mM sodium orthovanadate, 40 mM NaF, and a mixture of protease inhibitors (Merck). Protein concentrations were determined with a Bio-Rad protein assay kit (Bio-Rad, Hercules, CA, USA). Total cellular protein (50 μg) was electrophoresed on 12% SDS polyacrylamide gels and transferred to nitrocellulose membranes. The membranes were blocked with 10% nonfat milk in phosphate-buffered saline (PBS, Invitrogen) containing 0.1% Tween 20 (PBST). Polyclonal primary antibodies specific for CSNK1A1L, CTNNB1, BTRC, SIAH1, Wnt11, Wnt2B and Wnt5A were purchased from Sigma, Inc. (St. Louis, MO, USA). Antibodies specific for GAS1, SMO, LRP2, HHIP, BMP2, BMP6 and BMP7 were purchased from Proteintech (Rocky Hill, NJ, USA). β-actin (Sigma, Inc) were used as the internal control. The membranes were incubated with appropriate primary antibodies (1:500-1:1000) at 4°C overnight and followed by incubating with horseradish peroxidase-conjugated secondary antibodies (mouse IgG antibody, 1:10000 dilution) for 1 h at room temperature. Protein bands were revealed using an enhanced chemiluminesence kit (Amersham Bioscience, Sweden). The experiments were carried out at least three times.

Statistical analysis

All of the analyses were performed using SPSS statistics software, version 17.0. All of the values are presented as the mean ± SD. Analysis of variance (ANOVA) was performed when appropriate. Statistical significance was tested using Dunnett's test, and *p* values less than 0.05 were considered significant.

RESULTS

Arsenic trioxide stimulate keratinocyte proliferation

Several researches have indicated that chronic exposure to arsenic induces proliferation and aberrant mitosis of keratinocytes (13, 14). In the present study, HaCaT and NHEK cells were incubated with low concentration of arsenic for 4 weeks. As expected, As_2O_3 (1 to 20 nM) significantly stimulated keratinocyte proliferation in comparison

to the control group. But higher concentrations (>40 nM) of As_2O_3 did not cause a further increase in cell growth in either HaCaT or NHEK cells (Fig. 1A). In addition, after exposure to 2 nM As_2O_3 for 6, 9, and 12 days, there was a constitutive increase in [^{3}H]TdR incorporation into keratinocytes (data not shown). Interestingly, HaCaT cells were more sensitive to As_2O_3-induced proliferation than NHEK cells were.

This enhanced proliferation was consistent with changes in the cell cycle. PI-stained DNA was determined by flow cytometry at different time points. After 2 nM As_2O_3 induction for 12 d, the S-phase fraction increased from 20.43% to 42.37% in HaCaT. Similarly, the S population gradually increased from 18.52% to 39.87% in NHEKs (Fig. 1B). These data suggested that 2 nM As_2O_3 induced cell cycle transition from phase G1 to S. Taken together, these results demonstrated that arsenic compounds can stimulate cell proliferation by affecting cell cycle progression.

Arotinoid trometamol inhibits As_2O_3-induced keratinocyte proliferation

To investigate the biological role of retinoic acid in arsenic-stimulated cell proliferation, cell growth inhibition assay was performed. We have excluded

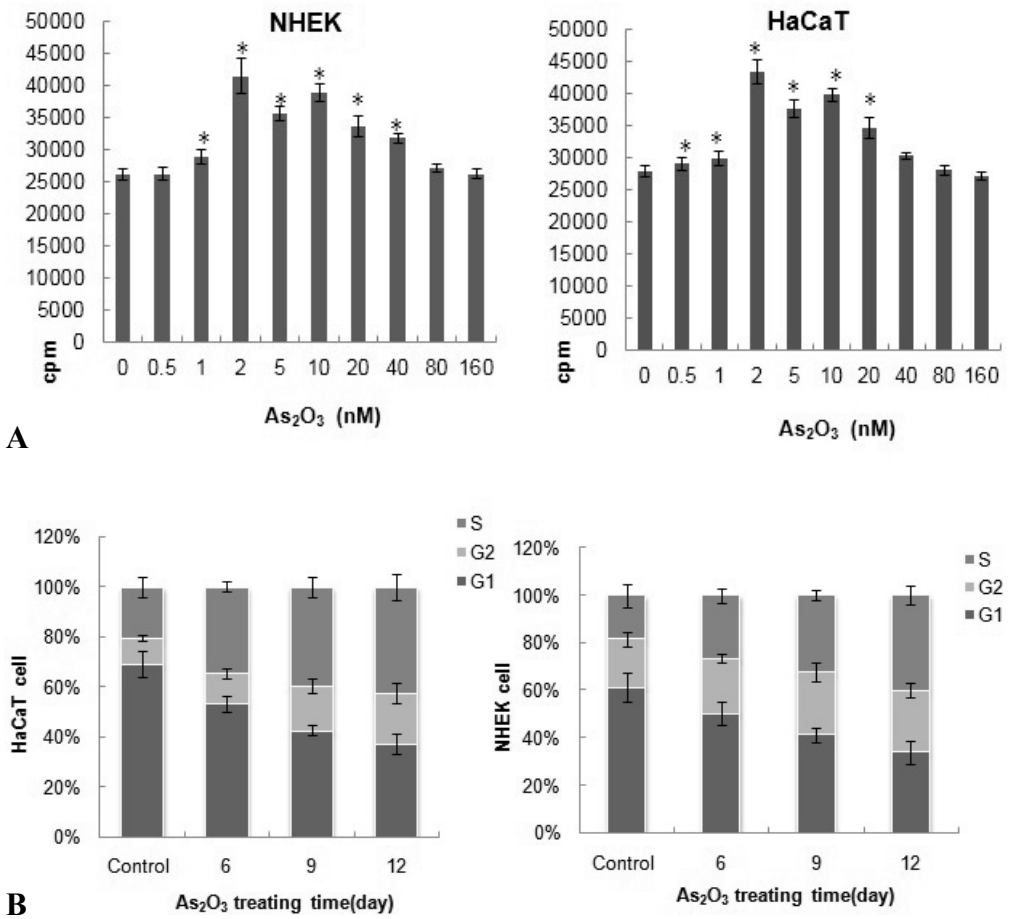

Fig. 1. *Low concentrations of As_2O_3 exposure induces keratinocytes proliferation. **A)** NHEK, HaCaT cells were grown in media with various concentrations of As_2O_3. 4 weeks later, cells were labeled for 24 h with 1μCi ^{3}H-TdR. Incorporated radioactivity was counted in a liquid scintillation spectrometer and cultures were performed in triplicate. **B)** Flow cytometric analysis of cell cycle distribution in keratinocytes. Cells were cultured with 2nM As_2O_3 for different times as described in "Materials and Methods". Cell cycle distribution was analyzed by flow cytometry.*

proliferation inhibition related to cytotoxicity. As expected, arotinoid trometamol inhibited keratinocyte proliferation in a dose-dependent manner when compared with the control group (Fig. 2A). Almost no proliferation inhibition was observed if the concentrations of arotinoid trometamol were less than 10^{-2} μM (Fig. 2A). The IC_{50} value of arotinoid trometamol against HaCaT cells after 24 h of incubation was approximately 0.8 μM. In NHEKs, the concentration of arotinoid trometamol required for 50% growth inhibition was approximately 3 μM. These results indicated that arotinoid trometamol inhibited As_2O_3-induced keratinocyte growth in a dose-dependent manner.

The effects of arotinoid trometamol on the cell cycle were further determined. HaCaT cells were treated with 2 nM As_2O_3 for 4 weeks and then treated with arotinoid trometamol for 24 h, 36 h, and 48 h. As shown in Fig. 2B, arotinoid trometamol treatment caused 43.82% of the cells being arrested in the G1 phase after 24 h, and 57.25% after 48 h. Meanwhile, this process was accompanied by a concomitant decrease in the proportion of S-phase cells. No significant changes were observed in the G2/M phase of the cell cycle in HaCaT cells. These results suggest that the inhibitory effects of arotinoid trometamol might be due, at least in part, to cell cycle arrest in the G1 phase.

PCR array analysis identifies changed expression in genes of the Wnt, Shh and BMP signaling pathways

To further investigate the pathways involved in arsenic-induced proliferation and differentiation, gene expression in response to As_2O_3 was evaluated by Human Signaling RT² Profiler™ PCR Array. The array includes genes of the Wnt, Shh and BMP signaling pathways, as well as other associated genes involved in cell proliferation and differentiation. The results showed that 13 genes were aberrantly expressed after chronic arsenic exposure. Of these 13 genes, 5 were found to be up-regulated and 8 were down-regulated over 2-fold (Table I). These genes included components of the Wnt (CSNK1A1L, CTNNB1, SFRP1, Wnt10B, Wnt11, Wnt16, Wnt5A, Wnt8A), hedgehog (C6orf138, HHIP, PTCHD1) and BMP (BMP2, BMP7) signaling pathways. Our data also showed that, despite the differential expression level not changing by more than 2-fold, arsenic treatment up-regulated MAPK1 gene expression with fold change of 1.58. This result was consistent with previously published data that arsenic exposure activated the MAPK pathway via ERK phosphorylation (13). Furthermore, after

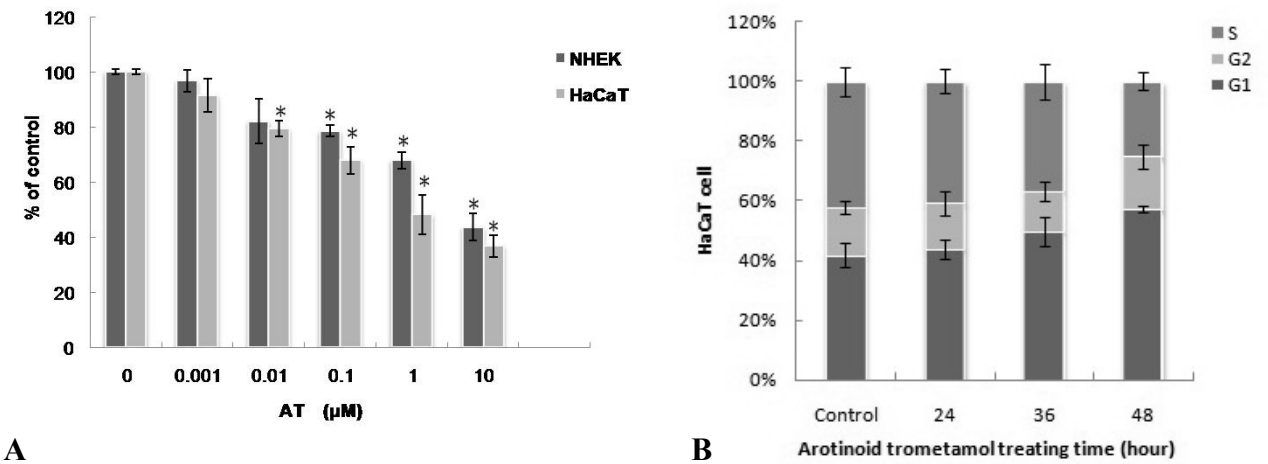

Fig. 2. *Arotinoid trometamol inhibited As_2O_3-induced proliferation of NHEK, HaCaT cell lines.* ***A****) Cell growth inhibition was assessed by MTT assay. Results represent means ± SD of three independent experiments with triplicate wells.* ***B****) Flow cytometric analysis of cell cycle distribution in keratinocytes. HaCaT Cells stimulated by As_2O_3 were cultured with 0.1 μM arotinoid trometamol for various times as described in "Materials and Methods". Cell cycle distribution was analyzed by flow cytometry.*

Table I. *Differentially expressed genes in HaCaT cells stimulated by As_2O_3.*

Gene	RefSeq	Description	Fold (Regulation)
Wnt pathway			
CSNK1A1L	NM_145203	Casein kinase 1, alpha 1-like	4.17
CTNNB1	NM_001904	B-Catenin (cadherin-associated protein), beta 1, 88kDa	2.58
Wnt10B	NM_003394	Wingless-type MMTV integration site family, member 10B	2.56
Wnt11	NM_004626	Wingless-type MMTV integration site family, member 11	-3.16
Wnt16	NM_057168	Wingless-type MMTV integration site family, member 16	-3.32
Wnt2B	NM_004185	Wingless-type MMTV integration site family, member 2B	-1.96
Wnt8A	NM_058244	Wingless-type MMTV integration site family, member 8A	-2.82
Wnt5A	NM_003392	Wingless-type MMTV integration site family, member 5A	-3.56
SFRP1	NM_003012	Secreted frizzled-related protein 1	2.76
Shh pathway			
HHIP	NM_022475	Hedgehog interacting protein	-2.39
LRP2	NM_004525	Low density lipoprotein-related protein 2	-1.98
C6orf138	NM_001013732	Chromosome 6 open reading frame 138	-2.47
PTCHD1	NM_173495	Patched domain containing 1	-2.98
BMP pathway			
BMP2	NM_001200	Bone morphogenetic protein 2	-4.22
BMP7	NM_001719	Bone morphogenetic protein 7	3.27
Others			
MAPK1	NM_002745	Mitogen-activated protein kinase 1	1.58

being stimulated by As_2O_3, keratinocyte was then treated by arotinoid trometamol. The altered gene expression of the WNT, Shh and BMP signaling pathways was also analyzed by PCR array analysis. As shown in Table II, 21 genes were observed to be differentially expressed over 2-fold, such as components of the WNT (BTRC, SFRP1, SIAH1, GSK3B, Wnt10B, Wnt11, Wnt2B, Wnt5B, Wnt6, Wnt9A, and PRKACA), hedgehog (PTCHD1, PTCHD2, GAS1, LRP2 and SMO) and BMP (BMP6 and BMP7) signaling pathways. Although BMP7, CSNK1A1L, and CTNNB1 genes were 2.63-, 1.76-, and 1.92-fold upregulated, respectively, after the treatment with arotinoid trometamol, these genes showed a reduced trend when compared to the fold change after As_2O_3 treatment, which was 3.27-, 4.17-, and 2.58-fold. Additionally, the expression of KCTD11 and metastasis suppressor 1 (MTSS1) were increased by 2.61- and 3.15-fold over control cells; both genes are important regulators of multi-cellular organism development. As a hedgehog antagonist, the expression of KCTD11 is reduced in human tumors. MTSS1, a novel metastasis suppressor gene, plays important roles in anti-cancer metastasis. Thus, their up-regulation verified the anti-tumor effects of arotinoid trometamol.

More importantly, our data showed that many differentially expressed genes in the Wnt, Shh and BMP signaling in the arsenic treatment group were counteractively expressed by the subsequent arotinoid trometamol treatment, such as CSNK1A1L, CTNNB1, SIAH1 in Wnt signaling, SMO in Shh signaling, and BMP2 in BMP signaling pathways. This finding could, in part, explain how arotinoid

Table II. *Differentially expressed genes in HaCaT cells treated with arotinoid trometamol followed by As_2O_3.*

Gene	RefSeq	Description	Fold (Regulation)
WNT pathway			
CSNK1A1L	NM_145203	Casein kinase 1, alpha 1-like	1.76
CTNNB1	NM_001904	Catenin (cadherin-associated protein), beta 1, 88kDa	1.92
BTRC	NM_033637	Beta-transducin repeat containing	3.48
Wnt10B	NM_003394	Wingless-type MMTV integration site family, member 10B	4.28
Wnt11	NM_004626	Wingless-type MMTV integration site family, member 11	2.06
Wnt2B	NM_004185	Wingless-type MMTV integration site family, member 2B	10.23
Wnt5A	NM_003392	Wingless-type MMTV integration site family, member 5A	-1.71
Wnt5B	NM_032642	Wingless-type MMTV integration site family, member 5B	2.18
Wnt6	NM_006522	Wingless-type MMTV integration site family, member 6	2.10
Wnt9A	NM_003395	Wingless-type MMTV integration site family, member 9A	3.74
SFRP1	NM_003012	Secreted frizzled-related protein 1	7.04
PRKACA	NM_002730	Protein kinase, cAMP-dependent, catalytic, alpha	2.01
GSK3B	NM_002093	Glycogen synthase kinase 3 beta	3.15
Shh pathway			
PTCHD1	NM_173495	Patched domain containing 1	-3.58
PTCHD2	NM_020780	Patched domain containing 2	2.16
LRP2	NM_004525	Low density lipoprotein-related protein 2	4.31
NPC1L1	NM_013389	NPC1 (Niemann-Pick disease, type C1, gene)-like 1	1.92
SMO	NM_005631	Smoothened homolog (Drosophila)	-2.44
GAS1	NM_002048	Growth arrest-specific 1	3.00
SIAH1	NM_003031	Seven in absentia homolog 1 (Drosophila)	8.75
BMP pathway			
BMP2	NM_001200	Bone morphogenetic protein 2	1.27
BMP6	NM_001718	Bone morphogenetic protein 6	4.86
BMP7	NM_001719	Bone morphogenetic protein 7	2.63
Others			
MAPK1	NM_002745	Mitogen-activated protein kinase 1	1.06
MTSS1	NM_014751	Metastasis suppressor 1	3.15
KCTD11	NM_001002914	Potassium channel tetramerisation domain containing 11	2.61
ERBB4	NM_005235	V-erb-a erythroblastic leukemia viral oncogene homolog 4 (avian)	5.03

trometamol inhibited As_2O_3-induced keratinocyte proliferation. The expression changes of BMP7, Wnt11, Wnt16 and BTRC after treatment with As_2O_3 or arotinoid trometamol were not consistent with data published earlier; these findings could be due to different experimental conditions.

Arotinoid trometamol inhibits the As_2O_3-enhanced Wnt signaling pathway in keratinocytes

PCR array analysis revealed that chronic exposure to As_2O_3 significantly modulated the gene expression levels of Wnt proteins, receptors and modulators, leading to activation of Wnt signaling. As shown in

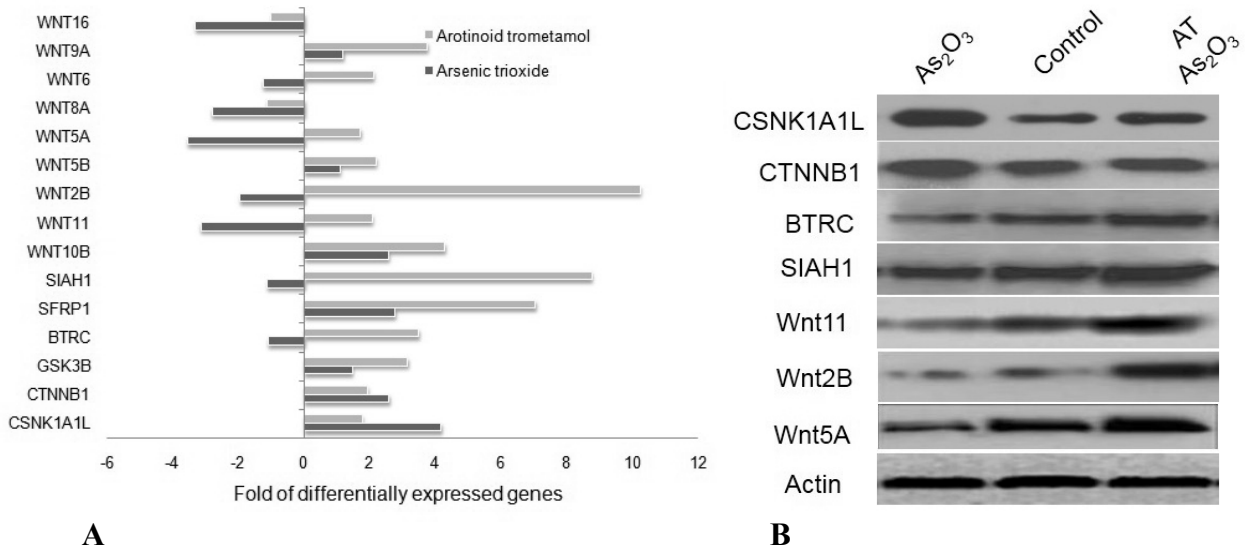

Fig. 3. *Arotinoid trometamol inhibited the As_2O_3-enhanced Wnt signaling pathway in keratinocytes.* ***A****) Epidermal keratinocytes were treated with As_2O_3 (2 nM) for 4 weeks, and then cells were treated with arotinoid trometamol (0.1 μM) for 48 h. PCR array analysis identify gene expression changes of Wnt signaling pathway.* ***B****) The cell lysates were prepared and analyzed by Western blot using antibodies against CSNK1A1L, CTNNB1, BTRC, SIAH1, Wnt11, Wnt2B and Wnt5A. Representative examples of three experiments are shown.*

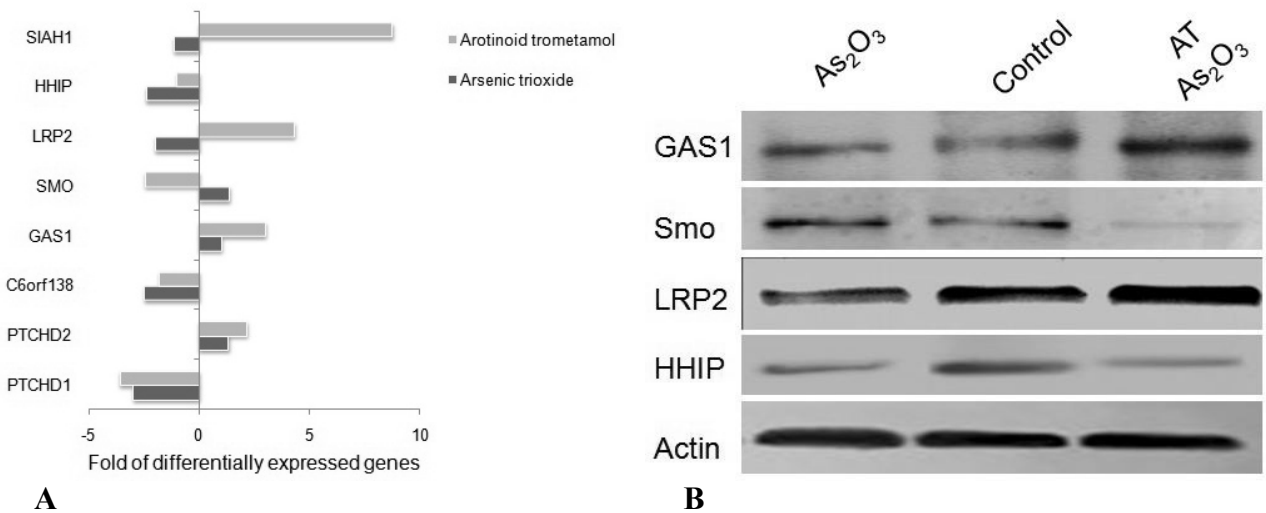

Fig. 4. *Effects of As_2O_3 and arotinoid trometamol on Shh signaling in keratinocytes.* ***A****) Epidermal keratinocytes were treated with As_2O_3 (2 nM) for 4 weeks, and then cells were treated with arotinoid trometamol (0.1 μM) for 48 h. PCR array analysis identified gene expression changes of Shh signaling pathway.* ***B****) The cell lysates were prepared and analyzed by Western blot using antibodies against GAS1, SMO, LRP2 and HHIP. Representative examples of three experiments are shown.*

Fig. 3A, As_2O_3 treatment up-regulated CSNK1A1L and CTNNB1 expression (4.17 and 2.58 fold, respectively), and down-regulated SIAH1 (-1.13 fold). These genes participate in Wnt signaling, and their expression changes could enhance DNA synthesis and cell growth which might be related to cancer development. In contrast, arotinoid trometamol treatment strongly counteracted the effects of As_2O_3 treatment. The expression of CSNK1A1L and CTNNB1 was reduced to 1.76- and 1.92-fold,

respectively. SIAH1 was up-regulated (8.75-fold). In particular, Wnt5A was up-regulated from -3.56- to 1.71-fold. Although the expression of BTRC, Wnt2B, and SFRP1 also had obvious changes, their function is unclear in the carcinogenesis of skin. The final effect of arotinoid trometamol on Wnt signaling was pathway inhibition, which could be enhanced by up-regulation of GSK3B (from 1.45- to 3.15-fold).

To validate our PCR array findings that the effects of As_2O_3 and arotinoid trometamol on the proliferation and differentiation of keratinocytes were associated with the Wnt signaling pathway, we then analyzed the expression of the above-mentioned genes by Western blot. As shown in Fig. 3B, the protein expression of CSNK1A1L and CTNNB1 was increased in the As_2O_3-treated cells compared with the controls. Wnt5A was slightly down-regulated. In contrast, the addition of arotinoid trometamol significantly down-regulated the expression of CSNK1A1L, CTNNB1 proteins, and up-regulated Wnt5A protein, suggesting that the Wnt pathway was inactivated. Meanwhile, increased protein levels of SIAH1 exerted a growth-suppressive effect on keratinocytes.

Effects of As_2O_3 and arotinoid trometamol on Shh signaling in keratinocytes

SMO was down-regulated at mRNA and protein levels by arotinoid trometamol treatment (Fig. 4, A, B). Other transcripts for Shh including SHH, PTCH1, and GLI, were not expressed differentially after treatment with As_2O_3 or arotinoid trometamol according to PCR array analysis. Although PTCHD1 mRNAs was markedly down-regulated by As_2O_3 and arotinoid trometamol treatment, PTCHD2 mRNA was slightly up-regulated after arotinoid trometamol treatment; the roles of these gene expression changes need to be further explored. In addition, As_2O_3 treatment did not cause significant expression alteration of GAS1, but arotinoid trometamol treatment up-regulated its expression (from 1- to 3-fold, Fig. 4, A, B). GAS1 is known to be a putative tumor suppressor gene, blocking entry to the S phase and preventing cycling of normal and transformed cells. In contrast, arotinoid trometamol treatment antagonized the down-regulation of HHIP expression caused by As_2O_3 (from -2.39 to -1-fold, Fig. 4, A, B). HHIP was found to bind to SHH directly and attenuate Shh signaling. Thus these results suggested that As_2O_3 could activate, but arotinoid trometamol inhibit Shh signaling to some extent.

Arotinoid trometamol activates the As_2O_3-inhibited BMP signaling

Previous reports have shown that BMP2 and BMP6 inhibited keratinocyte growth and induced terminal differentiation. We observed that As_2O_3 treatment decreased the expression of BMP2 in cultured

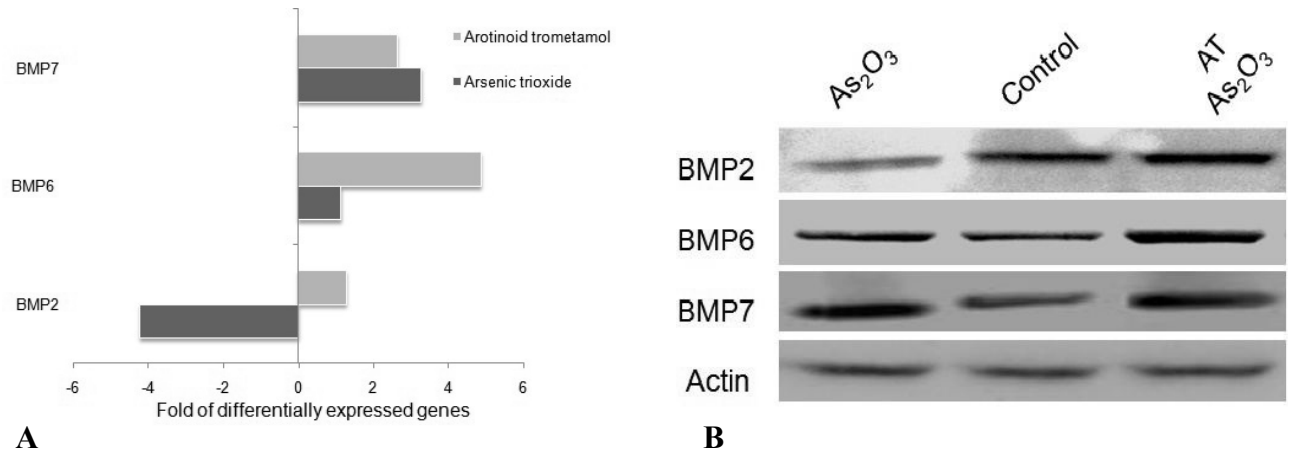

Fig. 5. *Activation of As_2O_3-inhibited BMP signaling by arotinoid trometamol.* ***A****) Epidermal keratinocytes were treated with As_2O_3 (2 nM) for 4 weeks, and then cells were treated with arotinoid trometamol (0.1 μM) for 48 h. PCR array analyses identified gene expression changes of BMP signaling pathway.* ***B****) The cell lysates were prepared and analyzed by Western blot using antibodies against BMP2, BMP6 and BMP7. Representative examples of three experiments are shown.*

keratinocytes (-4.22-fold) at mRNA level (Fig. 5A), as well as the protein level (Fig. 5B). Conversely, arotinoid trometamol treatment significantly up-regulated BMP2 expression (from -4.22- to 1.27-fold). Although As_2O_3 treatment did not significantly alter the mRNA and protein expression levels of BMP6, arotinoid trometamol treatment caused strong up-regulation of BMP6 expression (Fig. 5). These changes in gene expression were helpful in explaining the role of BMP signaling pathways in the control of tumor development. In addition, BMP7, a typical and powerful member of the BMP family, can inhibit the growth and colony-forming potential of a number of head and neck squamous cell carcinomas (HNSCCs). However, our data showed that As_2O_3 up-regulated and arotinoid trometamol slightly down-regulated its gene and protein expression (Fig. 5), therefore further studies are needed to elucidate these mechanisms. Meanwhile, BMP2, BMP6 and BMP7 are also involved in the hedgehog signaling pathway to exert their regulatory functions.

DISCUSSION

Humans exposed to environmental arsenic have increased incidences of lung, skin, and bladder cancers compared to unexposed persons. Although this link is well established, the mechanisms by which arsenicals induce neoplasms are not yet completely understood (15). The data in this study demonstrated that low-concentration of As_2O_3 stimulated HaCaT and NHEK proliferation, which were inhibited by arotinoid trometamol. PCR array and Western blot analyses showed that Wnt, Shh, and BMP signaling pathways were involved in the process of skin carcinogenesis. We presented evidence that arotinoid trometamol treatment counteracted the effects of As_2O_3 by regulating the signaling network.

We previously reported that exposure to low concentrations of arsenic in a chronic manner, which is considered to mimic the human exposure situation more closely, can significantly enhance keratinocyte proliferation, accompanied by alterations in cell cycle progression. Interestingly, HaCaT cells were more sensitive to arsenic-induced proliferation than NHEKs (11). Here, we observed the notable time- and dose-dependent antagonism of arotinoid trometamol in keratinocytes treated with arsenic trioxide. Arrest of the G1 phase and a decrease in the proportion of the S-phase were associated with the response to retinoic acid treatment.

Wnt, Shh and BMP signaling pathways are required for the changes in cell proliferation and cell cycle progression caused by arsenic and arotinoid trometamol. The Wnt signaling pathway is involved in many normal cell physiological processes and in carcinogenesis. Increased Wnt signaling is observed in SCCs, and it plays an important role in the maintenance of tumor-like properties in epidermal cancer stem cells (16). In particular, Ahlborn et al. reported that multiple transcripts of the Wnt signaling pathway were significantly altered by sodium arsenite exposure to K6/ODC mouse skin (17). It was also suggested that Wnt5A was transcriptionally activated during arsenic-induced malignant transformation (18). But Popp et al. reported the contrary conclusion that Wnt5A suppressed keratinocytes proliferation and promoted the differentiation by increased biosynthesis of keratin-1 and loricrin (19). Our results were consistent with their studies. Reduced expression of Wnt11 and Wnt2B after arsenic treatment was dramatically increased by the effects of arotinoid trometamol. Increasing SIAH-1 expression after arotinoid trometamol treatment can induce cell cycle arrests, tumor suppression through beta-catenin degradation. SFRP1 acts as a biphasic modulator of Wnt signaling, promoting Wnt-induced effects at low concentrations and counteracting them at higher concentrations (20). SFRP1 was highly up-regulated (7.04-fold) by arotinoid trometamol, and Wnt signaling was inhibited in this study. Although As_2O_3 in certain concentrations can inhibit human cancer cell growth and tumor development in mice by blocking the hedgehog/GLI pathway (21), other studies have suggested that long-term low-concentration of arsenic exposure could promote cancer partly through the activation of hedgehog signaling. For example, the expression of PTCH1 and GLI1 is frequently measured to evaluate the presence or absence of Shh pathway activity. Arsenic could activate hedgehog signaling by decreasing

the stability of GLI3, the repressor of Shh pathway (22). Here, we provide an important insight into the etiology of arsenic-induced human carcinogenesis. Although the levels of GLI3, PTCH1 and GLI1 did not change significantly, differential expression of mRNAs and the proteins of PTCHD2 and GAS1 blocked entry to S phase and prevented cycling of normal and transformed cells. Furthermore, our data, showing down-regulation of SMO expression by arotinoid trometamol, could partly explain its anti-tumor effects.

Bone morphogenetic proteins are known to induce the formation of bone and cartilage (23). Recent studies showed they play pivotal roles in the regulation of skin development, including the control of cellular proliferation and differentiation, epithelial-mesenchymal interactions, melanogenic activity and tissue remodeling (24). BMPs are also involved in controlling a variety of pathobiological processes in the skin, including psoriasis, wound healing and carcinogenesis (25-27). BMP6 markedly stimulated melanogenesis, increased melanosome transfer from melanocytes to keratinocytes (28), and inhibited epidermal proliferation. BMP2 inhibited keratinocyte growth and induced terminal differentiation and epithelial-to-mesenchymal transition (27). We observed that As_2O_3 treatment decreased the gene expression of BMP2 in cultured keratinocytes, and arotinoid trometamol treatment significantly up-regulated its expression. In addition, arotinoid trometamol caused strong up-regulation of BMP6 expression. In actuality, the tumor-suppressing activity of the BMPs in the skin epithelium might be mediated at least in part via stage-dependent antagonizing of the Wnt and Shh signaling pathways. Inhibition of BMP signaling by noggin results in abnormal activation of Wnt and Shh signaling, promoting skin tumor formation (6). More recent observations have demonstrated the crosstalk of BMP, Shh and Wnt signaling during the development of hair follicles and skin tumorigenesis, confirming the previous data showing positive regulation of Shh expression by BMP antagonists (29, 30). We also showed that arotinoid trometamol dose-dependently inhibited keratinocytes proliferation stimulated by As_2O_3. These data provide compelling evidence that retinoid acid could be used to treat cancer and hyperkeratosis associated with arsenic. Furthermore, dermatologists and hematologists have found that the incidence of skin tumors is not higher in acute promyelocytic leukemia (APL) or lymphoma patients treated with As_2O_3. The potential reason is that retinoic acid and As_2O_3 combination therapy is common (31, 32). Retinoic acid might counteract the carcinogenetic effects of As_2O_3 on skin.

In conclusion, our study indicated that low concentrations of As_2O_3 can significantly enhance keratinocyte proliferation and differentiation. Multiple signaling pathways, including Wnt, Shh, and BMP, contribute to the development of arsenic-associated malignancy. These signaling pathways are also responsible for the effects of arotinoid trometamol treatment.

ACKNOWLEDGEMENTS

This work was sponsored by Shanghai Pujiang Program (18PJD053); Bright Future grant (Association of Dermatovenereology of Integrated Traditional and Western Medicine 2018) and Naval Military Medicine Program of Changhai hospital (2018JS001). We would like to show our sincere gratitude to Prof. Mi Qing-sheng, who kindly provided advice on the study design and experimental procedures.

REFERENCES

1. Argos M, Parvez F, Rahman M, et al. Arsenic and lung disease mortality in Bangladeshi adults. Epidemiology 2014; 25:536-43.
2. Bailey K, Xia Y, Ward WO, et al. Global gene expression profiling of hyperkeratotic skin lesions from inner Mongolians chronically exposed to arsenic. Toxicol Pathol 2009; 37:849-59.
3. Yajima I, Kumasaka MY, Ohnuma S, et al. Arsenite-mediated promotion of anchorage-independent growth of HaCaT cells through placental growth factor. J Invest Dermatol 2015; 135:1147-56.
4. Zhang Z, Wang X, Cheng S, et al. Reactive oxygen species mediate arsenic induced cell transformation and tumorigenesis through Wnt/beta-catenin pathway

in human colorectal adenocarcinoma DLD1 cells. Toxicol Appl Pharmacol 2011; 256:114-21.
5. Singh KP, Kumari R, Treas J, DuMond JW. Chronic exposure to arsenic causes increased cell survival, DNA damage, and increased expression of mitochondrial transcription factor A (mtTFA) in human prostate epithelial cells. Chem Res Toxicol 2011; 24:340-49.
6. Sharov AA, Mardaryev AN, Sharova TY, et al. Bone morphogenetic protein antagonist noggin promotes skin tumorigenesis via stimulation of the Wnt and Shh signaling pathways. Am J Pathol 2009; 175:1303-14.
7. Iwai S, Yonekawa A, Harada C, et al. Involvement of the Wnt-beta-catenin pathway in invasion and migration of oral squamous carcinoma cells. Int J Oncol 2010; 37:1095-103.
8. Youssef KK, Van Keymeulen A, Lapouge G, et al. Identification of the cell lineage at the origin of basal cell carcinoma. Nat Cell Biol 2010; 12:299-305.
9. Steinert S, Kroll TC, Taubert I, et al. Differential expression of cancer-related genes by single and permanent exposure to bone morphogenetic protein 2. J Cancer Res Clin Oncol 2008; 134:1237-45.
10. Chatterjee A, Chatterji U. All-trans retinoic acid protects against arsenic-induced uterine toxicity in female Sprague-Dawley rats. Toxicol Appl Pharmacol 2011; 257:250-63.
11. Bi X, Gu J, Guo Z et al. Different pathways are involved in arsenic-trioxide-induced cell proliferation and growth inhibition in human keratinocytes. Skin Pharmacol Physiol 2010; 23:68-78.
12. Kumar R, Parsad D, Kanwar A, Kaul D. Development of melanocye-keratinocyte co-culture model for controls and vitiligo to assess regulators of pigmentation and melanocytes. Indian J Dermatol Venereol Leprol 2012; 78:599-604.
13. Chowdhury R, Chatterjee R, Giri AK, Mandal C, Chaudhuri K. Arsenic-induced cell proliferation is associated with enhanced ROS generation, Erk signaling and CyclinA expression. Toxicol Lett 2010; 198:263-71.
14. Wu CH, Tseng YS, Kao YT, Sheu HM, Liu HS. Low concentration of arsenic-induced aberrant mitosis in keratinocytes through E2F1 transcriptionally regulated Aurora-A. Toxicol Sci 2013; 132:43-52.
15. Lee CH, Wu SB, Hong CH, et al. Aberrant cell proliferation by enhanced mitochondrial biogenesis via mtTFA in arsenical skin cancers. Am J Pathol 2011; 178:2066-76.
16. Malanchi I, Peinado H, Kassen D et al. Cutaneous cancer stem cell maintenance is dependent on beta-catenin signalling. Nature 2008; 452:650-653.
17. Ahlborn GJ, Nelson GM, Ward WO, et al. Dose response evaluation of gene expression profiles in the skin of K6/ODC mice exposed to sodium arsenite. 2008/01/15 ed; 2008.
18. Jensen TJ, Wozniak RJ, Eblin KE, Wnek SM, Gandolfi AJ, Futscher BW. Epigenetic mediated transcriptional activation of Wnt5A participates in arsenical-associated malignant transformation. Toxicol Appl Pharmacol 2009; 235:39-46.
19. Popp T, Steinritz D, Breit A, et al. Wnt5a/beta-catenin signaling drives calcium-induced differentiation of human primary keratinocytes. J Invest Dermatol 2014; 134:2183-91.
20. Saini S, Liu J, Yamamura S, Majid S, Kawakami K, Hirata H, Dahiya R. Functional significance of secreted Frizzled-related protein 1 in metastatic renal cell carcinomas. Cancer Res 2009; 69:6815-22.
21. Beauchamp EM, Ringer L, Bulut G, et al. Arsenic trioxide inhibits human cancer cell growth and tumor development in mice by blocking Hedgehog/GLI pathway. J Clin Invest 2011; 121:148-60.
22. Fei DL, Li H, Kozul CD, et al. Activation of Hedgehog signaling by the environmental toxicant arsenic may contribute to the etiology of arsenic-induced tumors. Cancer Res 2010; 70:1981-88.
23. Wu SQ, Ma SZ, Zhang C, Li DQ, Gao CZ. Effects of human parathyroid hormone on bone morphogenetic protein signal pathway following spinal fusion in diabetic rats. J Biol Regul Homeost Agents 2017; 31:111-17.
24. Romagnoli M, Belguise K, Yu Z, et al. Epithelial-to-mesenchymal transition induced by TGF-beta1 is mediated by Blimp-1-dependent repression of BMP-5. Cancer Res 2012; 72:6268-78.
25. Fessing MY, Atoyan R, Shander B, Mardaryev AN, Botchkarev VV, Jr., Poterlowicz K, Peng Y, Efimova T, Botchkarev VA. BMP signaling induces cell-type-specific changes in gene expression programs of human keratinocytes and fibroblasts. J Invest Dermatol 2010; 130:398-404.
26. Ahmed MI, Mardaryev AN, Lewis CJ, Sharov AA,

Botchkareva NV. MicroRNA-21 is an important downstream component of BMP signalling in epidermal keratinocytes. J Cell Sci 2011; 124:3399-404.
27. Yan C, Grimm WA, Garner WL, Qin L, Travis T, Tan N, Han YP. Epithelial to mesenchymal transition in human skin wound healing is induced by tumor necrosis factor-alpha through bone morphogenic protein-2. Am J Pathol 2010; 176:2247-2258.
28. Singh SK, Abbas WA, Tobin DJ. Bone morphogenetic proteins differentially regulate pigmentation in human skin cells. J Cell Sci 2012; 125:4306-19.
29. Suzuki K, Yamaguchi Y, Villacorte M, et al. Embryonic hair follicle fate change by augmented beta-catenin through Shh and Bmp signaling. Development 2009; 136:367-72.
30. Katoh M. Transcriptional regulation of Wnt2B based on the balance of Hedgehog, Notch, BMP and Wnt signals. Int J Oncol 2009; 34:1411-15.
31. Lallemand-Breitenbach V, Zhu J, Chen Z, de The H. Curing APL through PML/RARA degradation by As2O3. Trends Mol Med 2012; 18:36-42.
32. Bazarbachi A, Suarez F, Fields P, Hermine O. How I treat adult T-cell leukemia/lymphoma. Blood 2011; 118:1736-45.

EFFECTS OF Sca-1(+) BONE MARROW MESENCHYMAL STEM CELLS ON LUNG ISCHEMIA-REPERFUSION INJURY

Y. LI, F. WANG, L. YANG, JY. ZHAO and LY. ZHANG

Department of Thoracic Surgery, The Second Affiliated Hospital of Harbin Medical University, Harbin, Heilongjiang, China

Received January 16, 2019 – Accepted March 15, 2019

This study aimed to explore the effect of Sca-1$^+$ bone marrow stromal stem cells (BMSCs) on lung ischemia reperfusion injury in mice. Five healthy Sprague-Dawley rats were selected to isolate and purify their Sca-1$^+$ BMSCs using a Sca-1+ magnetic sorting kit in conjunction with whole bone marrow culture. In addition, 21 male C57BL/6J mice were divided into 3 groups (7 mice in each group), namely sham group (group A), I/R group (group B) and BMSCs group (group C). A pulmonary ischemia reperfusion injury model was established by ligating the left pulmonary portal vessel for 60 min and reperfusion for 240 min, after which the right pulmonary portal vessel was blocked to measure arterial partial pressure of oxygen (PaO_2) and arterial partial pressure of carbon dioxide ($PaCO_2$). Subsequently, the mice were sacrificed to determine their superoxide dismutase (SOD) activity, malondialdehyde (MDA) content and myeloperoxidase (MPO) activity in the lung tissue. The histological changes were observed by light microscopy, while an enzyme-linked immunosorbent assay (ELISA) was used to detect the changes in plasma expressions of tumor necrosis factor-α (TNF-α) and interleukin-10 (IL-10) in the mice. In addition, plasma expressions of TNF-α and B-cell lymphoma-2 (bcl-2) in the mice were detected by immunohistochemistry, while the apoptosis of transplanted lung cells was detected by a TdT-mediated dUTP Nick-End Labeling (TUNEL) method. Compared with group A, group B showed a decreased level of PaO_2 and SOD activity but an increased level of MDA content and MPO activity ($P<0.01$), indicating that group B had significant ischemia reperfusion injury compared to group A. In conclusion, BMSCs significantly reduced lung ischemia-reperfusion injury and improved lung function through their anti-oxidation, anti-inflammatory and anti-apoptosis properties.

As a major cause of postoperative respiratory dysfunction and death, lung ischemia-reperfusion injury (LIRI) is mainly diagnosed in the early stage of lung transplantation and extracorporeal circulation surgery (1, 2). With the improvement of surgical methods and the application of potent immunosuppressive agents, lung transplantation has been widely used in the treatment of end-stage lung diseases. However, clinical data show that LIRI is still a long-term problem with no easy solutions. After lung transplantation, nearly 30% of patients still suffer from lung function insufficiency, while 15~20% of patients suffer from serious lung damage and require continuous treatments of positive pressure ventilation and medications. Sometimes, an extracorporeal membrane lung is needed to improve ventilation in these patients, while some patients may experience multiple organ failure and even death (3).

As stem cells with multi-directional differentiation ability, BMSCs can expand easily *in vitro* to quickly

Key words: Sca-1$^+$ BMSCs; lung ischemic-reperfusion injury; apoptosis; antioxidant

Corresponding Author:
Dr Linyou Zhang,
Department of Thoracic Surgery,
The Second Affiliated Hospital
Harbin Medical University, NO.246 Xuefu Road,
Nangang District, Harbin, 150001, Heilongjiang, China
e-mail: lyzhang_harbinmed@163.com

0393-974X (2019)

produce enough cells for treatments. In addition, BMSCs can promote the repair of damaged tissues and hence are important constituents of cell replacement therapy (4, 5). For example, stem cell antigen-1 (SCA-1) is a surface antigen of stem cells and progenitor cells. In this study, Sca-1$^+$ BMSCs were obtained using a Sca-1$^+$ magnetic sorting kit (Stem Cell company, Canada) and then injected into mice with LIRI to explore the effect of Sca-1$^+$ BMSCs on LIRI. It is expected that this study can provide a new therapeutic strategy for clinical treatment of LIRI and improvement of early lung functions after lung transplantation.

MATERIALS AND METHODS

Animals

Twenty-one healthy male C57BL/6J mice with an age of 6-8 weeks and a body weight of 16-24 g were purchased from Beijing Huafukang Biotechnology Co., Ltd., China. In addition, 5 healthy SD (Sprague-Dawley) rats with an age of 4 weeks and a body weight of 98□105 g were purchased from Shanghai Bangyao Biotechnology Co., Ltd., China. All animals were housed under a 12-hour light/dark cycle and were given free access to food and water. The temperature and humidity of the animal facility were controlled at 22±2°C and 40-60%, respectively. The animals were allowed for 1 week of acclimation prior to the experiment. Five healthy SD rats were used for BMSC isolation, and 21 male C57BL/6J mice were grouped as follows: Group A: n=7, after the thoracotomy, no operation was performed to close the chest; Group B: n=7, at the time of reperfusion, 0.5 ml of phosphate buffer was injected through the tail vein; Group C: n=7, BMSCs (1.0×10^6 BMSCs were dissolved in 0.5 ml of cell culture medium) were injected into the tail vein of each mouse. The protocol was approved by the ethics committee of The Second Affiliated Hospital of Harbin Medical University, and the experiment was carried out following the regulations of the State Science and Technology Commission on the management of laboratory animals.

Establishment of an LIRI model

Mice were intraperitoneally injected with 0.1mg/g ketamine +0.01mg/g xylazine (Shanghai Hengdu biological Co., Ltd., China) for anesthesia. After tracheotomy, mechanical ventilation was performed by tracheal intubation with a tidal volume of 0.6 ml, a ventilation frequency of 120 times/min, an inspiration and expiration ratio of 1:2, and an inspired oxygen fraction of 100%. The left chest of the mouse was depilated and the local skin was disinfected, while the 4th and 5th intercostal space was bluntly separated to fully expose the left pulmonary hilum. Then, 5 U/g heparin was injected through the tail vein (Shanghai Kanglang Biological Technology Co., Ltd., China). After 5 min, the left pulmonary hilum was blocked with a vascular clamp at the end of expiration, and the left lung remained ischemic for 60 min before the vascular forceps were released to free the blockage. Finally, the left lung was reperfused for 240 min.

Isolation and identification of mouse BMSCs

After the mice were anesthetized and sacrificed by cervical dislocation, they were disinfected with 75% ethanol (Qingdao Jieshikang Biological Technology Co., Ltd., China) and their lower limbs were washed 3 times under aseptic conditions with the phosphate buffer. The epiphyses of the femur and tibia were cut off to expose the bone marrow cavity, so that the bone marrow was collected using a culture medium (GIBCO, USA) containing penicillin and streptomycin (Wuhan Hualianke Biological Technology Co., Ltd., China). Mononuclear cells were then isolated under aseptic conditions using a lymphocyte separation medium to obtain Sca-1$^+$ BMSCs using a Sca-1$^+$ magnetic sorting kit (Stem Cell, Canada), and the isolated BMSCs were cultured in Dulbecco's modified eagle medium (GIBCO, USA) containing low glucose. Finally, the BMSCs were subcultured to the third generation for identification and implantation assays.

Detection of malondialdehyde (MDA) content, superoxide dismutase (SOD) activity, and myeloperoxidase (MPO) activity

At 4 hours after reperfusion, mice were anesthetized with 10% chloral hydrate (Pharmaceutical Factory of Fujian Medical University Union Hospital, China) (4 ml/kg), and placed in a supine position and mechanically ventilated (related parameters: oxygen concentration: 1.0, tidal volume: 10 ml/kg, respiratory rate: 80 times/min). The median thoracotomy of each mouse was performed by removing the anterior chest wall and blocking the right pulmonary hilum for 5 min, so that the abdominal aortic blood was collected for arterial blood gas analysis. An enzyme-linked

immunosorbent assay (ELISA) was performed using the plasma of centrifuged inferior vena cava blood samples. The samples of transplanted lung tissues were then divided into two parts:

The upper 1/2 part of the specimens was immersed in 10% formalin (Shanghai Sanshu Biological Technology Co., Ltd., China) and embedded in paraffin for HE (hematoxylin-eosin) staining, immunohistochemical assays, and TUNEL detection of apoptosis; the lower 1/2 part of the specimens was fixed in liquid nitrogen for 3 minutes and then stored at -80°C for ELISA and protein assays. After the storage, some tissues from the left lung were dried, weighed, placed in a tissue grinder (Shanghai Jingxin Industrial Development Co., Ltd., China), mixed with 2 ml of physiological saline (Shanghai Shfeng Biological Technology Co., Ltd., China), and ground into a tissue homogenate in an ice bath. After centrifugation at 1000r/min for 10 min in a refrigerated centrifuge (Gene, USA), the supernatant was diluted to 5% homogenate using physiological saline, and the contents of SOD, MDA, and MPO in lung tissue samples were detected by SOD, MDA and MPO assay kits (Nanjing Jiancheng Bioengineering Institute, China), respectively.

Histopathologic examination

Routine light microscopy: The left lung specimens of 0.8cm × 0.8cm × 0.8cm in size were fixed with 10% formalin, dehydrated with gradient ethanol, embedded with paraffin at a low temperature, sectioned, stained with HE, and observed and photographed under a microscope.

Qualitative and quantitative analysis of TNF-α and IL-10

Tumor necrosis factor-α (TNF-α) and Interleukin 10 (IL-10) detection kits (R&D Systems, China) were used for the detection of TNF-α and IL-10 according to kit instructions. Finally, absorbance values of the samples were measured at a wavelength of 450 nm using ELISA (Bio-Rad, USA).

Immunohistochemical detection of TNF-α and IL-10 expressions in lung samples

Paraffin sections were routinely dewaxed, washed with gradient alcohol and placed in distilled water for 10 min. The sections were then incubated at room temperature for 10 min with newly prepared 3% hydrogen peroxide (Bei Jing Think-Far Technology Co. Ltd., China) to inactivate endogenous enzymes, followed by the addition of 0.01 ml citric acid buffer solution (Shanghai Youyu Biotechnology Co. Ltd., China) (pH 7.2-7.6) on the sections, which were then placed in a microwave oven and heated to boiling twice to repair antigens. In the next step, 5% bovine serum albumin (BSA) blocking solution (Cell Signaling Technology Inc, USA) was added dropwise on the sections and the incubation was carried out at room temperature for 20 min after which excess liquid was removed without washing. Subsequently, the sections were incubated with corresponding mice anti-rat TNF-α or IL-10 monoclonal antibodies (Santa Cruz, USA) at 4°C overnight, followed by incubation at 37°C for 20 min with HRP-labeled goat anti-mice IgG antibodies (Sigma, USA). After 2 min × 3 times of PBS (pH 7.2-7.6) washing, the sections were incubated at 37°C for 20 min with a streptavidin-biotin-peroxidase complex (SABC) (Beijing Solarbio Science & Technology Co. Ltd., China), and the color of the sections was developed at room temperature using a BAD reagent (Wuhan Boster Biological Technology Co. LTD., China). Finally, the sections were lightly counterstained with hematoxylin, dehydrated, sealed with neutral gum, and observed under a microscope.

Apoptosis of lung cells and expressions of anti-apoptosis gene B-cell lymphoma 2 protein (bcl-2)

The level of apoptosis of lung cells was detected by a Terminal-deoxynucleoitidyl Transferase Mediated Nick End Labeling (TUNEL) method and visualized by light microscopy. Apoptotic cells were identified by brown-yellow particles in the nucleus. Evaluation method for apoptosis index: each specimen was observed under a microscope and the number of apoptotic cells in 5 high power fields (× 400) was calculated. Apoptosis index (AI)= number of TUNEL positive cells/total number of cells × 100%. A double-blind method was used to calculate the mean apoptosis index of each lung tissue sample as its apoptosis index. Immunohistochemistry assays were then used to detect the expression, location and intensity of bcl-2 in transplanted lung tissues

Statistical analysis

All data were expressed as mean±standard deviation and processed with SPSS 12.0 statistical software. One-way analysis of variance (One-way ANOVA) was used for comparison among different groups, and $P<0.05$ was considered statistically significant.

RESULTS

Analysis of MDA content, MPO activity, SOD activity, PaO_2 and $PaCO_2$ in lung tissues

As shown in Fig. 1, and compared with group A, SOD activity in group B was significantly decreased along with an increased MDA content and MPO activity ($P<0.01$). Compared with group B, the content of MDA and the activity of MPO in the lung tissue of group C decreased significantly ($p<0.01$), along with significantly increased SOD activity ($p<0.01$). Compared with group A, PaO_2 significantly decreased while $PaCO_2$ significantly increased in group B. In addition, PaO_2 in group C was significantly higher than that in group B ($p<0.01$), along with a significantly lower level of $PaCO_2$ ($p<0.01$).

Histopathologic examination

As shown in Fig. 2 and after 4-hour reperfusion, the transplanted lung in group B showed poor elasticity under the naked eye, along with obvious pulmonary congestion, swelling, and foamy secretion in the trachea. Under the light microscope, the transplanted lung in group B showed thickened alveolar septum, edema and infiltration of inflammatory cells dominated by neutrophils. In addition, there were edema fluid, red blood cells and exuded inflammatory cells in some alveolar space in the transplanted lung of group B, with neutrophil seizures in the capillary lumen. Compared with group B, the level of alveolar interstitial edema in the alveolar cavity of group C was significantly reduced, along with reduced inflammatory cell infiltration, reduced edema fluid and fewer red blood cells.

Qualitative and quantitative analysis of TNF-α and IL-10 expressions

The immunohistochemical positive signal of TNF-α was mainly located in the cytoplasm and was brownish yellow (DAB staining) (Fig. 3, A, B,

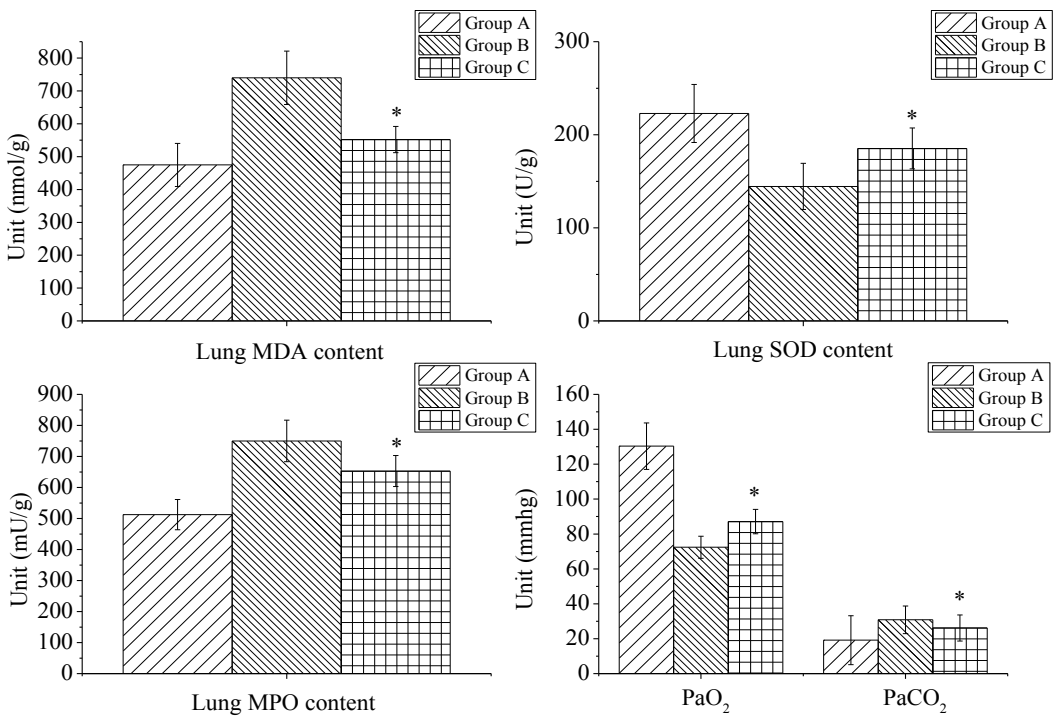

Fig. 1. *MDA content, MPO activity and SOD activity in lung tissues of each group (*Group C was compared with Group B, P < 0.01)*

C). The expression of TNF-α was mainly distributed in the alveolar septum as well as inflammatory cells and exudates in the alveolar cavity. In addition, the expression of TNF-α was significantly increased in group B and decreased in group C (Fig. 3).

The concentration of TNF-α in group A was the lowest (10.91±1.49 pg/ml). Compared with group B (50.15±4.57 pg/ml), the concentration of TNF-α in group C (37.30±4.93pg/ml) decreased significantly ($P < 0.01$). The IL-10 expression in group A was the lowest (8.26±2.81pg/ml). Compared with group B (25.43±1.85pg/ml), the IL-10 expression decreased significantly in group A ($P < 0.01$) (34.57±2.99 pg/ml) but increased significantly in group C ($P < 0.01$) (Fig. 3).

Levels of lung cell apoptosis and the expression of bcl-2

As shown in Fig. 4, A-C, the positive signals of TUNEL staining were mainly located in the nucleus. In addition, apoptotic cells were scattered in the lung tissue, with a reduced cell size, a brownish yellow color, a condensed nucleus, periphery

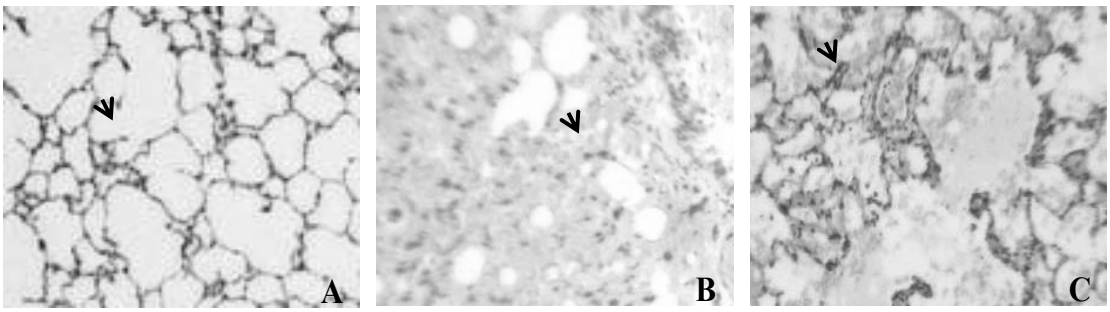

Fig. 2. *Morphological changes in each group after 4-hour reperfusion (hematoxylin-eosin staining (HE)× 100).* ***A****) Group A, sham-operated group;* ***B****) Group B, during reperfusion, 0.5 mL of phosphate buffer was injected through the tail vein;* ***C****) Group C, BMSCs were injected into the tail vein on the basis of group B.*

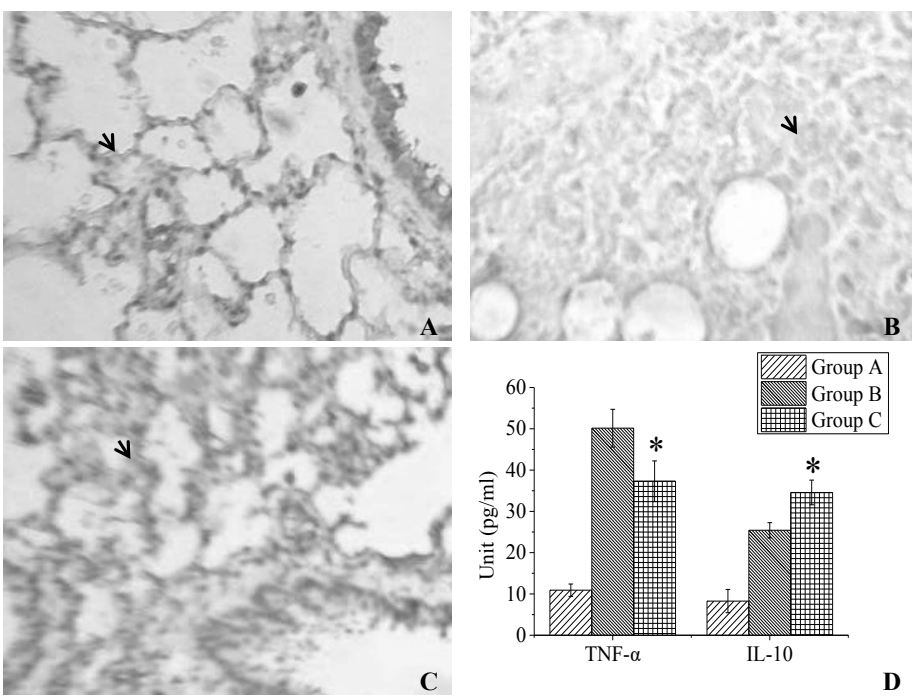

Fig. 3. *Expression levels of plasma TNF-α and IL-10.* ***A****) expression level of TNF-α in group A (×100);* ***B****) expression level of TNF-α in group B (×100);* ***C****) expression level of TNF-α in group C (×100);* ***D****) expression levels of TNF-α and IL-10 in each group (×100). *Group C was compared with Group B, $P < 0.01$.*

chromatin accumulation and nuclear fragmentation. The apoptotic cells were mainly alveolar epithelial cells, while a few apoptotic cells were infiltrating inflammatory cells. Compared to other groups, group B showed a significantly increased number of apoptotic cells and more common nuclear fragmentation. The apoptosis index of group C was significantly lower than that of group B ($P < 0.01$) (Fig. 4D).

The positive signals of immunohistochemical staining of Bcl-2 were mainly located in the cytoplasm, and the cells with positive expressions of Bcl-2 were brown-yellow. In group C, the strong positive expression of Bcl-2 was mainly located in the bronchiole epithelium as well as type I and type II alveolar epithelium. Furthermore, the expression of bcl-2 in the transplanted lung tissues of groups A and B was significantly lower than that of group C (Fig. 5).

DISCUSSION

In this study, the protective effect of BMSCs against lung ischemia-reperfusion injury (LIRI) was studied in mice by establishing a mouse model of lung ischemia-reperfusion injury. The results of blood gas analysis showed that PaO_2 in group C was significantly increased ($P<0.01$) along with significantly decreased $PaCO_2$ ($P<0.01$), indicating that the transplantation of BMSCs could effectively inhibit LIRI, improve the gas exchange capacity of transplanted lungs, and improve lung functions. In addition, the results of pathological examination also showed that the degree of pathological damages was significantly reduced in group C, along with alleviated alveolar interstitial edema and neutrophil infiltration.

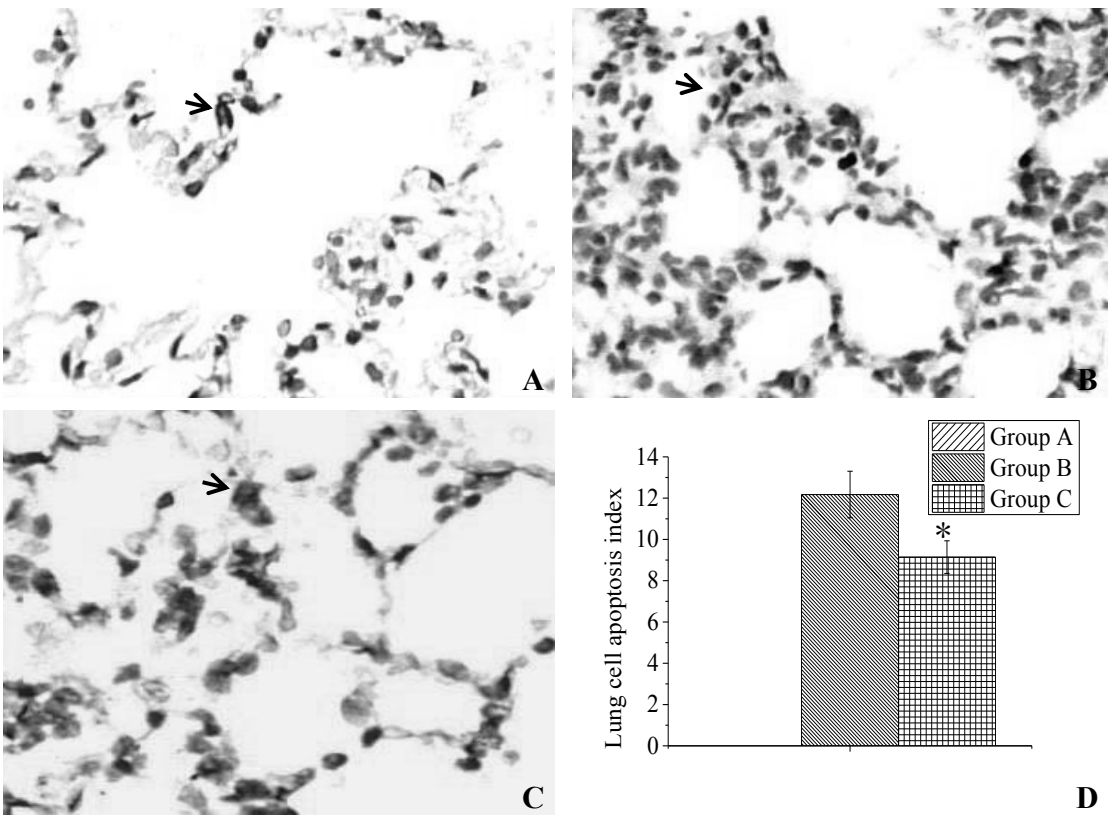

Fig. 4. *Apoptosis of lung cells after 4-hour reperfusion in each group.* ***A)*** *TUNEL staining of group A (×200);* ***B)*** *TUNEL staining of group B (×200);* ***C)*** *TUNEL staining of group C (×200);* ***D)*** *apoptosis index of lung cells in each group.* ******* *Group C was compared with Group B, $P < 0.01$.*

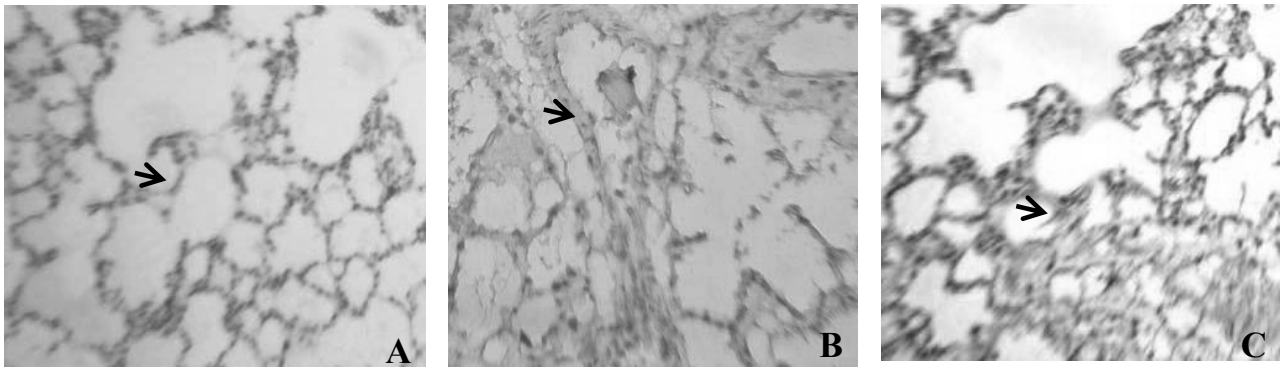

Fig. 5. *Expressions of bcl-2 in lung tissues of each group after 4-hour reperfusion.* ***A****) group A;* ***B****) group B;* ***C****) group C.*

SOD can remove superoxide anions and protect cells from damage. The level of SOD activity indirectly reflects the ability of the body in removing oxygen free radicals (6, 7). In addition, MDA is a lipid peroxide formed by the attack of unsaturated fatty acids by oxygen free radicals, and the level of MDA indirectly reflects the severity of free radical attacks in the body (8, 9). Furthermore, MPO activity reflects the extent of neutrophil infiltration, whereas neutrophil inhibitors can reduce lung injury, improve lung compliance and reduce pulmonary edema by reducing neutrophil infiltration (10, 11). In this study, it was found that BMSCs can enhance the scavenging ability of reactive oxygen species, thus reducing the lipid peroxidation of biofilms, reducing the production of superoxide ions and other toxic chemicals by increasing SOD activity, decreasing MDA content and MPO activity, and reducing the infiltration of neutrophils.

Featured by microvascular expansion, hyperemia, increased interstitial permeability, increased secondary interstitial edema, increased pulmonary vascular resistance and gas exchange impairment, lung ischemia-reperfusion injury is closely related to the overexpression and activation of a series of enzymes as well as the massive release of inflammatory cytokines induced by the interaction between neutrophils and the vascular endothelium (12, 13). In lung ischemia-reperfusion injury, TNF-α is the first released cytokine and acts as the initiator of many other cytokines. BMSCs can promote the secretion of anti-inflammatory cytokines such as IL-10 while inhibiting the secretion of inflammatory cytokines such as TNF-α (14). In addition, IL-10 can inhibit the activation, migration and adhesion of inflammatory cells and reduce the infiltration of neutrophils by inhibiting the secretion of TNF- α, IL-1 and other inflammatory cytokines by polykaryocytes or phagocytes (15). The results of this study showed that, compared with group B, the expression of TNF-α was significantly down-regulated in group C, along with significantly up-regulated expressions of IL-10.

As the most important anti-apoptotic gene, Bcl-2 can prevent the onset of apoptosis (16, 17). In this study, the expression of bcl-2 protein in group C was higher than that in group B, indicating that BMSCs could inhibit and reduce ischemia-reperfusion-induced apoptosis by up-regulating the expression of bcl-2 protein in lung tissues. Furthermore, the TUNEL assay of this study showed that BMSCs decreased apoptotic index by decreasing the number of apoptotic cells.

To sum up, BMSCs can reduce the extent of lung ischemia reperfusion injury in mice by scavenging oxygen free radicals, inhibiting inflammatory responses in the lung tissues, and inhibiting apoptosis.

ACKNOWLEDGEMENTS

This work was supported by Harbin Science and Technology Bureau (2016RAXYJ104).

REFERENCES

1. Liu S, Xu J, Fang C, Shi C, Zhang X, Yu B, Yin Y. Over-expression of heat shock protein 70 protects mice against lung ischemia/reperfusion injury through SIRT1/AMPK/eNOS pathway. Am J Transl Res 2016; 8(10):4394-404.
2. Laubach VE, Sharma AK. Mechanisms of lung ischemia-reperfusion injury. Curr Opin Organ Transplant 2016; 21(3):246-52.
3. Trulock EP, Edwards LB, Taylor DO, Boucek MM, Keck BM, Hertz MI. The Registry of the International Society for Heart and Lung Transplantation: twenty-first official adult lung and heart-lung transplant report--2004. J Heart Lung Transplant 2004; 23(7):804-15.
4. Hoganson DM, Meppelink AM, Hinkel CJ, et al. Differentiation of human bone marrow mesenchymal stem cells on decellularized extracellular matrix materials. J Biomed Mater Res A 2014; 102(8):2875-83.
5. Garca-Garca A, de Castillejo CL, Mndez-Ferrer S. BMSCs and hematopoiesis. Immunol Lett 2015; 168(2):129-35.
6. Yuan L, Liu S, Tu W, Zhang Z, Bao J, Dai Z. Biomimetic superoxide dismutase stabilized by photopolymerization for superoxide anions biosensing and cell monitoring. Anal Chem 2014; 86(10):4783-90.
7. Ghneim HK, Al-Sheikh YA, Alshebly MM, Aboul-Soud MA. Superoxide dismutase activity and gene expression levels in Saudi women with recurrent miscarriage. Mol Med Rep 2016; 13(3):2606-12.
8. Tsikas D. Assessment of lipid peroxidation by measuring malondialdehyde (MDA) and relatives in biological samples: Analytical and biological challenges. Anal Biochem 2017; 524:13-30.
9. Ademosun AO, Oboh G. Anticholinesterase and antioxidative properties of water-extractable phytochemicals from some citrus peels. J Basic Clin Physiol Pharmacol 2014; 25(2):199-204.
10. Yuan Q, Jiang YW, Ma TT, Fang QH, Pan L. Attenuating effect of Ginsenoside Rb1 on LPS-induced lung injury in rats. J Inflamm (Lond) 2014; 11(1):40.
11. Zhao M, Li C, Shen F, Wang M, Jia N, Wang C. Naringenin ameliorates LPS-induced acute lung injury through its anti-oxidative and anti-inflammatory activity and by inhibition of the PI3K/AKT pathway. Exp Ther Med 2017; 14(3):2228-34.
12. Yaidikar L, Thakur S. Punicalagin attenuated cerebral ischemia-reperfusion insult via inhibition of proinflammatory cytokines, up-regulation of Bcl-2, down-regulation of Bax, and caspase-3. Mol Cell Biochem 2015; 402(1-2):141-48.
13. Xu L, Li Y, Fu Q, Ma S. Perillaldehyde attenuates cerebral ischemia-reperfusion injury-triggered overexpression of inflammatory cytokines via modulating Akt/JNK pathway in the rat brain cortex. Biochem Biophys Res Commun 2014; 454(1):65-70.
14. Yang Z, Zhang XR, Zhao Q, et al. Knockdown of TNF-α alleviates acute lung injury in rats with intestinal ischemia and reperfusion injury by upregulating IL-10 expression. Int J Mol Med 2018; 42(2):926-34.
15. Sutter AG, Palanisamy AP, Ellet JD, Schmidt MG, Schnellmann RG, Chavin KD. Intereukin-10 and Kupffer cells protect steatotic mice livers from ischemia-reperfusion injury. Eur Cytokine Netw 2014; 25(4):69-76.
16. Huang DC, O'Reilly LA, Strasser A, Cory S. The anti-apoptosis function of Bcl-2 can be genetically separated from its inhibitory effect on cell cycle entry. EMBO J 1997; 16(15):4628-38.
17. Yang T, Xu F, Sheng Y, Zhang W, Chen Y. A targeted proteomics approach to the quantitative analysis of ERK/Bcl-2-mediated anti-apoptosis and multi-drug resistance in breast cancer. Anal Bioanal Chem 2016; 408(26):7491-503.

MiR-17-5p MODULATES MITOCHONDRIAL FUNCTION OF THE GENIOGLOSSUS MUSCLE SATELLITE CELLS THROUGH TARGETING Mfn2 IN HYPOXIA

W. QIN[1], YBH. ZHANG[1], BL. DENG[2], J. LIU[1], HL. ZHANG[1] and ZL. JIN[1]

[1]Department of Orthodontics, State Key Laboratory of Military Stomatology and National Clinical Research Center for Oral Diseases and Shaanxi Clinical Research Center for Oral Diseases, School of Stomatology, The Fourth Military Medical University, Xi'an, Shannxi, China; [2]Department of Orthodontics, Lianbang Dental Hospital of Xincheng District, Xi'an, Shaanxi, China

Received January 13, 2019 – Accepted March 19, 2019

The root cause of obstructive sleep apnea-hypopnea syndrome (OSAHS) is repeated hypoxia during sleep. The genioglossus is one of the most important upper airway dilatation muscles and is important for maintaining normal oxygen supply during sleep. Hypoxia can directly affect the energy metabolism level of the genioglossus muscle, thereby weakening muscle function. MicroRNAs (miRNAs) can regulate mitochondrial function at the post-transcriptional level and achieve recovery or even enhancement of genioglossus function, but the specific mechanism is still unclear. In this study, an intermittent hypoxic cell model was established to detect the effects of hypoxia on the proliferation and apoptosis of Genioglossus muscle satellite cells (GG MuSCs), and the damage to the mitochondrial structure and function was assessed by transmission electron microscopy and mitochondrial membrane potential. Then, miR-17-5p was upregulated and downregulated by miRNA mimics and inhibitors, respectively, and bioinformatics analysis was used to predict and validate the target genes of miR-17-5p. The results showed that the hypoxic environment affected the proliferation of GG MuSCs and mitochondrial membrane potential, which promoted the occurrence of apoptosis and mitochondrial edema. After upregulation of miR-17-5p, cell proliferative capacity and mitochondrial function were restored. Bioinformatics prediction and gene and protein level analyses found that Mfn2 may be a target gene of miR-17-5p.

Obstructive sleep apnea-hypopnea syndrome (OSAHS) is a serious multiorgan, multisystem respiratory disorder that leads to hypoventilation, sleep disorder, and altered aerobic metabolism throughout the body (1). Hypoxia/hypoventilation plays a crucial role in the pathogenesis of OSAHS. Strategies to improve ventilation have always been the focus of severe OSAHS research (2). Among the many possible treatments for OSAHS, therapy to improve genioglossus function has been a hot research topic (3).

The genioglossus muscle is known as the "safety muscle" for upper airway respiratory function (4). Its unique anatomical position and muscle contraction directly indicate that treatment of the genioglossus muscle can effectively open the obstructed airway and restore aerobic function during sleep breathing, which in turn improves and even ameliorates OSAHS

Key words: microRNA; hypoxia; mitochondria; muscle satellite cells

Corresponding Author:
Dr Zuolin Jin,
Department of Orthodontics,
State key Laboratory of Military Stomatology
and National Clinical Research Center for Oral Diseases
and Shanxi Clinical Research Center for Oral Diseases,
School of Stomatology, The Fourth Military Medical University,
145 West Changele Road, Xi'an, Shaanxi, 710032, China
Tel.: +86 2984776138 - Fax: +86 29 83223047
e-mail: zuolinjin007@163.com

0393-974X (2019)

(5). The normal function of the genioglossus muscle depends on the normal supply of energy, that is, the balance of mitochondrial aerobic metabolism and glycolysis.

MicroRNAs (miRNAs) have been found to regulate mitochondrial aerobic metabolism and glycolysis in recent years. By silencing or inhibiting the transcription of target genes, miRNAs can participate in the regulation of all aspects of biological activities, including mitochondrial aerobic metabolism and glycolysis (6). Since Kulshreshtha discovered hypoxia-regulated miRNAs in 2006, these hypoxic miRNAs have been shown to have significant regulatory roles in the tumor hypoxic microenvironment, mitochondrial dynamics, myocardial ischemia/hypoxia, mitochondrial kinetics, divisional fusion, and metabolic functions (7-8). Based on our previous research, we found that the miR-17 family may affect the mitochondrial metabolism of the genioglossus muscle in a hypoxic environment. Therefore, the main purpose of this experiment was to determine the influence of miR-17-5p on the function of the genioglossus muscle in hypoxic conditions and to conduct a preliminary exploration of the target genes of miR-17-5p. In this study, we investigated the influence of miR-17-5p on the regulation of the biological characteristics and mitochondrial function of GG MuSCs in a hypoxic environment and the related mechanisms.

MATERIALS AND METHODS

Rat genioglossus muscle satellite cell culture

Three-week-old SD rats were used. All animal procedures were performed according to the protocol approved by the Animal Care Committee of the Fourth Military Medical University. After sacrifice, the genioglossus muscles were separated and shredded. Type I collagenase (Sigma, USA) was added, and digestion was performed in a 37°C incubator for 45 min. Then, twice the volume of the existing solution was added to terminate the DMEM reaction (HyClone, USA). The filtrate was collected, the supernatant was removed by centrifugation, and a single cell suspension was obtained by adding DMEM and cultured in a culture flask. The high-purity genioglossus muscle satellite cells were obtained by a differential adherence technique, and the primary cultured cells were fused to 60% for cell passage (9).

MTT

The cells were isolated by trypsinization and resuspended, and the cell suspension was collected and quantified. The cell suspension was added to a 96-well plate at 150 cells per well, and 6 wells were set as a blank control. The cells were incubated in a constant temperature incubator, and the solution was changed after 24 h. After adherence of the cells, 20 μl of MTT solution (Sigma, USA) was added to each well, the cells were incubated in a 37°C incubator for 4 h, and the supernatant in the wells was carefully aspirated. Then, 180 μl of DMSO (Sigma, USA) was added to each well, and the samples were gently vortexed for 5 min to dissolve the purple crystals thoroughly. The absorbance value of each well at 490 nm was measured, and the average value was calculated. The above operation was repeated every 24 h, and the data were used to generate a growth curve.

Differentiation of rat genioglossus muscle satellite cells

Cells were cultured in 6-well plates until they reached 60% confluence. Then, these cells were incubated with serum-free medium and adipogenesis medium (50 nM dexamethasone, 35 mg/ml indometacin, and 5 mg/ml insulin, Sigma, USA) for 6 d, and the media were changed every other day. Then, 6-well plates were washed 3 times with PBS, the cells were fixed with 4% paraformaldehyde for 30 min and washed 3 times with PBS, oil red O solution was added (5 g oil red O was dissolved in 100 ml of isopropanol) and the cells were stained for 20 min. The cells were washed 3 times with PBS and allowed to dry. Observation was performed using an inverted microscope.

Identification of GG MuSCs

The cells were fixed with paraformaldehyde (ShengGong, China) for 30 min, combined with a 0.25% Triton membrane, incubated for 20 min in a 37°C incubator, incubated with 3% hydrogen peroxide for 15 min, and then mixed with 100% sheep serum in the incubator for 30 min. The liquid in the well plate was aspirated, and primary antibody diluted with goat serum (murine anti-multi-species monoclonal antibody myosin, Santa Cruz, USA) was added. The samples were refrigerated overnight at 4°C, and after rewarming, biotin-labeled secondary

antibody (goat anti-mouse IgG-FITC, Santa Cruz, USA) was added, incubated at 37°C for 45 min, combined with 1 μg/ml of Hochest (Santa Cruz, USA) and placed in the incubator for 15 min. Finally, a photograph was taken under a fluorescence microscope.

RT-PCR

The RNA was isolated from cell cultures using TRIzol (TaKaRa, Japan). The reverse transcription reaction of total RNA was carried out with 2 μg in a 20 μL system. cDNA synthesis was performed using the SYBR® PrimeScriptTM miRNA RT-PCR Kit (TaKaRa, Japan), and a negative control group without the RNA template and miRNA PrimeScript RT Enzyme Mix was used to identify sample contamination. qPCR was performed using an ABI7500 (Applied Biosystems) machine for 45 cycles, and the fold change for all the samples was calculated by the $2^{-\Delta\Delta Ct}$ method. U6 was used as housekeeping gene for miRNA qPCR.

The primer sequences used were as follows:

Rno-miR-17-1-3p, 5'ACUGCAGUGAAGGCACUUGUGG3'; Rno-miR-17-2-3p, 5'ACUGCACUGCAAGCACUUCUUAC3'; Rno-miR-17-5p, 5'CAAAG UGCUU ACAGU GCAGG UAG3'; U6, forward 5'GCTTC GGCAG CACAT ATACT AAAAT3' and reverse 5'CGCTT CACGA ATTTG CGTGT CAT3'.

The target miR-17 was screened by comparing the expression changes of the three molecules in hypoxic and normoxic genioglossus tissues.

Hypoxia time determination

A three-gas incubator was used to establish a model of intermittent hypoxic cells. Cells were randomly grouped into the hypoxic 0 h, 3 h, 6 h, 12 h and 24 h groups according to the hypoxic incubation time. Screening for hypoxic time was performed by detecting differences in the expression levels of miR-17-5p at different hypoxic times.

Transient transfection of miR-17-5p

Cells in the logarithmic growth phase were used. The miR-17 mimic transfection concentration was 100 nmol per well, the miR-17 inhibitor transfection concentration was 200 nmol per well, three replicate wells were set in each group, and a blank control with only transfection reagent was used at the same time. Then, 12.5 μl of pre-miR-17 and 25 μl of anti-miR-17 stock solution (concentration 20 μM) were diluted with 150 μl of 1×riboFECTTM CP Buffer (RiboBio, China), mixed gently, and incubated for 5 min at room temperature, and 15 μl of riboFECTTM was added. CP Reagent was mixed, placed at room temperature for 30 min, and incubated in a CO_2 incubator for 12 h before RT-PCR.

Experimental grouping

The cells were divided into the following 6 groups: Normoxia (N, 21% O_2), Normoxia+pre-miR-17-5p (N+pre), Normoxia+anti-miR-17-5p (N+anti), Hypoxia (H, 10% O_2), Hypoxia+pre-miR-17-5p (H+pre), and Hypoxia+anti-miR-17-5p (H+anti).

Effect of miR-17-5p on proliferation and apoptosis

The transiently transfected cells were inoculated and subjected to MTT assays to calculate cell proliferation. Apoptosis detection was performed as follows: cells were collected, resuspended, and centrifuged, the supernatant was discarded, and 200 μl of mixed buffer was added and mixed by pipetting. Then, 5 μl of Annexin V-FITC and PI (ShengGong, China) were added in sequence, the cells were stained for 10 min, 490 μl of binding buffer was added, and the effect of miR-17-5p on apoptosis was detected by flow cytometry.

Effect of miR-17-5p on mitochondrial structure and function

The cells underwent transient transfection and were divided into experimental and control groups. The mitochondrial structure of the genioglossus muscle satellite cells of the two groups was observed by transmission electron microscopy. The mitochondrial membrane potential was detected, and the MitoTracker probe (Invitrogen, USA) working solution was preheated in a 37°C water bath. The mitochondrial membrane potential probe working solution was added, incubated at 37°C for 25 min, separated by trypsinization, centrifuged, resuspended, and washed. The cells were collected, and the mean fluorescence intensity of the MitoTracker probe was measured by flow cytometry.

Target gene expression

Using TargetScan, DIANA LAB and other target gene prediction software, we predicted that Mfn2 and Arl2 may be target genes of miR-17-5p. After transfection of pre-miR-17-5p and anti-miR-17-5p, a PCR reaction was carried out. The specific primer (RiboBio, China) sequences are as

follows: Mfn2, F: 5'GTCCAAGGTCAGGGGTATCA3' and R: 5'ATCAGCATCCAGGCAAAACT3'; Arl2, F: 5'GGGAGGACATCGACACCA3' and R: 5'AGGACCGCAGGGACTTCT3'; β-actin, F: 5'TGGCACCCAGCACAATGAA3' and R: 5' CTAAGTCATAGTCCGCCTAGAAGCA3'.

Western blot analysis

GG MuSCs were washed with PBS and lysed in mRIPA buffer (50 mmol/l Tris pH 7.5, 1% NP-40, 0.30% deoxycholate, 150 mmol/LlNaCl, and protease inhibitors). After 45 min of incubation, the cell lysates were cleared by centrifugation at 12,00 g for 5 min at 4°C, and the protein concentrations of the supernatants were determined using Bio-Rad protein assay solution (Bio-Rad, Hercules, CA, USA). Typically, 30 to 50 proteins were separated by SDS-PAGE and transferred onto PVDF membranes. Proteins were detected with specific antibodies (Mfn2 mouse IgG from Santa Cruz, Arl2 mouse IgG from Santa Cruz, GAPDH mouse IgG from Santa Cruz-USA). The bands were quantified with ImageJ software.

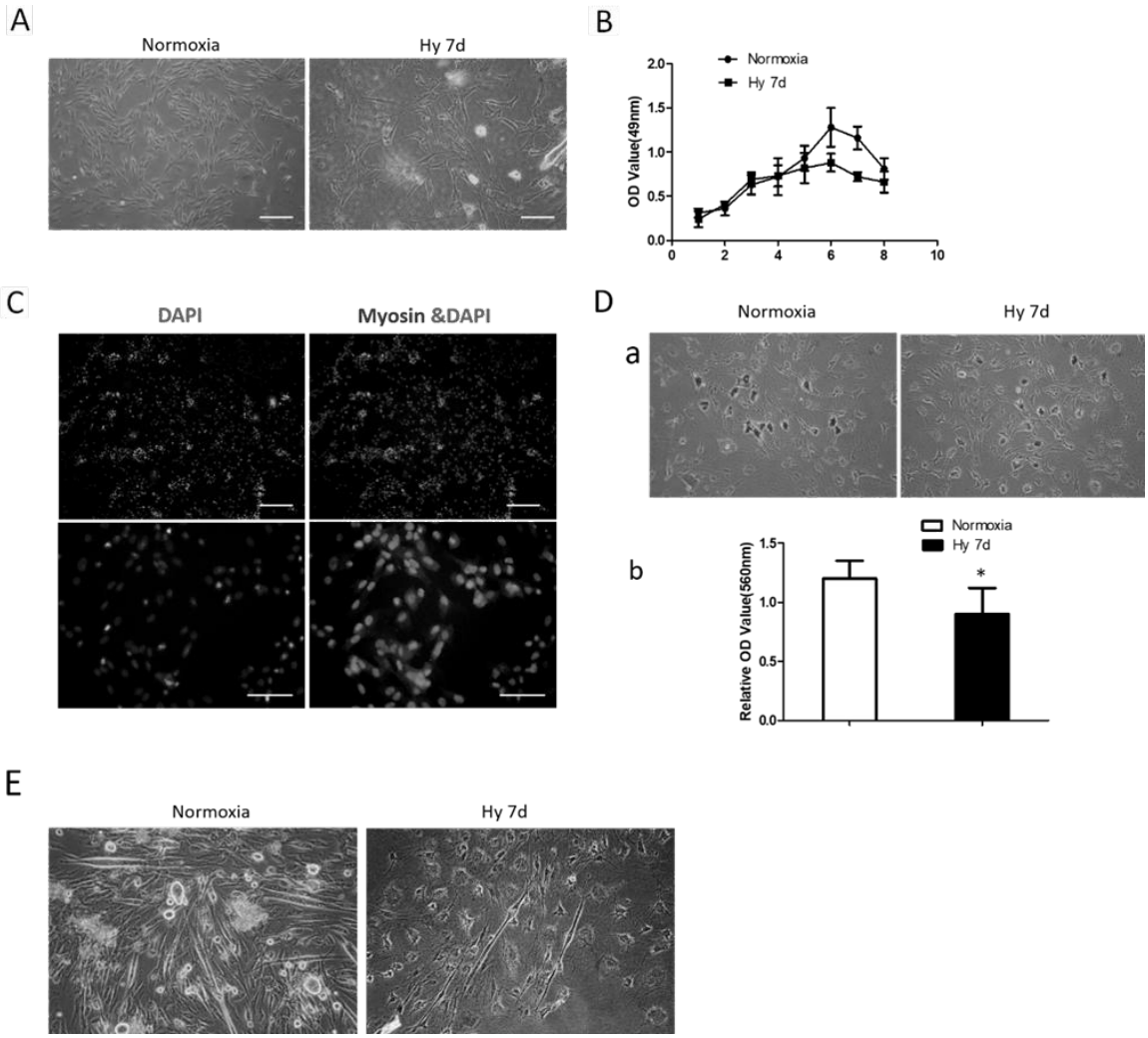

Fig. 1. *The function of GG MuSCs decreases significantly in hypoxia.* ***A****) Morphology of GG MuSCs (scale bar=100 μm);* ***B****) cell growth curve by MTT.* ***C****) Immunofluorescence identification of GG MuSCs(myosin);* ***D****) a: Adipogenic differentiation was evaluated by Oil Red O staining (after 28 days of adipogenic induction) (scale bar = 200 μm); b: Quantitative data for Alizarin Red S staining Oil Red O staining (*: p <0.05);* ***E****) Muscular tube forming. The myoblast capacity of hypoxic group was lower than that of normoxic group*

Statistical analysis

SPSS19.0 software was used for statistical analysis of the data, which are presented as the mean±SEM. One-way ANOVA and the LSD-t test were used for comparisons between treatment and control groups. Significant differences were set at p values of 0.05 and 0.01.

RESULTS

The function of GG MuSCs decreases significantly in hypoxia

GG MuSCs are long fusiform cells and arranged in a directional manner. After myogenic induction and adipogenic induction, the formation of myotubes and lipid droplets was observed, but the formation of these was less in the hypoxia group (Fig. 1, D and E). After immunofluorescence staining, the cells were observed by fluorescence microscopy, and the positive cells were red (Fig. 1C). Five fields were randomly selected, and the percentage of positively stained cells was statistically analyzed, all of which reached more than 95%, indicating that the satellite cells of the genioglossus muscle were highly pure (Fig. 1).

Determination of miR-17 and hypoxic time

The RT-PCR results showed that miR-17-5p expression was the most significant in the hypoxic group and was more than twice as high as that in the normoxic group (Fig. 2A). Therefore, we selected miR-17-5p for further analysis. The relative expression of miR-17-5p at different hypoxic times was detected by RT-PCR, and the expression of miR-17-5p was significantly decreased in the hypoxic 12-h group (Fig. 2B). Therefore, we defined hypoxic stimulation for 12 h as the most sensitive time for miR-17-5p analysis and used these conditions in subsequent experiments (Fig.2).

Effects of upregulation and downregulation of miR-17-5p on cell proliferation and apoptosis

After transfection of anti-miR-17-5p, the survival rate of muscle satellite cells was lower in the hypoxia group than the normoxia group; after pre-miR-17-

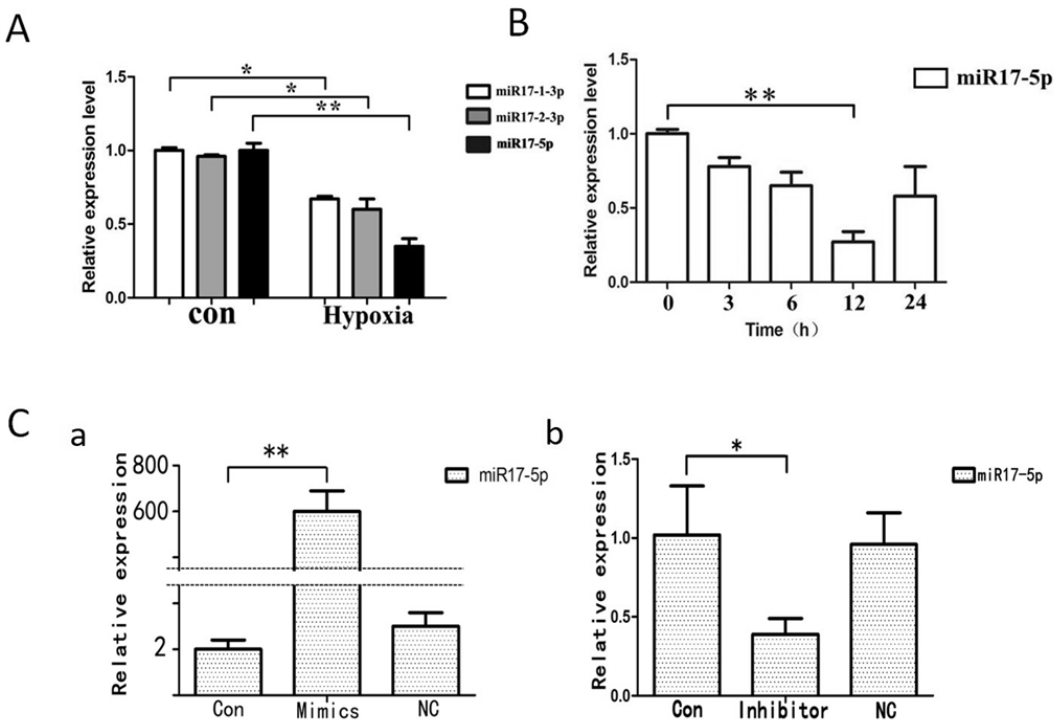

Fig. 2. *Screening and transfection of miR17-17-5p.* ***A)*** *Relative expression level of miR-17 family;* ***B)*** *Differences in the expression levels of miR-17-5p at different hypoxic times;* ***C)*** *a: Changes in the expression of miR-17-5p were detected after upregulation; b: Changes in the expression of miR-17-5p were detected after downregulation. (*p < 0.05, ** p < 0.01)*

5p transfection, the survival rate of muscle satellite cells increased significantly (Fig. 3A), indicating that upregulation of miR-17-5p has a protective effect on the proliferation of genioglossus muscle satellite cells. Flow cytometry showed that there was no significant difference in the apoptosis rate between the normoxia group, normoxic+pre-miR-17-5p group and normoxic+anti-miR-17-5p group (P>0.05). The apoptosis rate of GG MuSCs in the hypoxic group was significantly higher than that in the normoxia group (P<0.05). After transfection with anti-miR-17-5p, the apoptosis rate of GG MuSCs was lower in the hypoxic group than the normoxia group (P<0.05); after transfection with pre-miR-17-5p, the apoptosis rate of GG MuSCs in rats was higher than that in the normoxia group but decreased in the hypoxic group (P>0.05) (Fig. 3B).

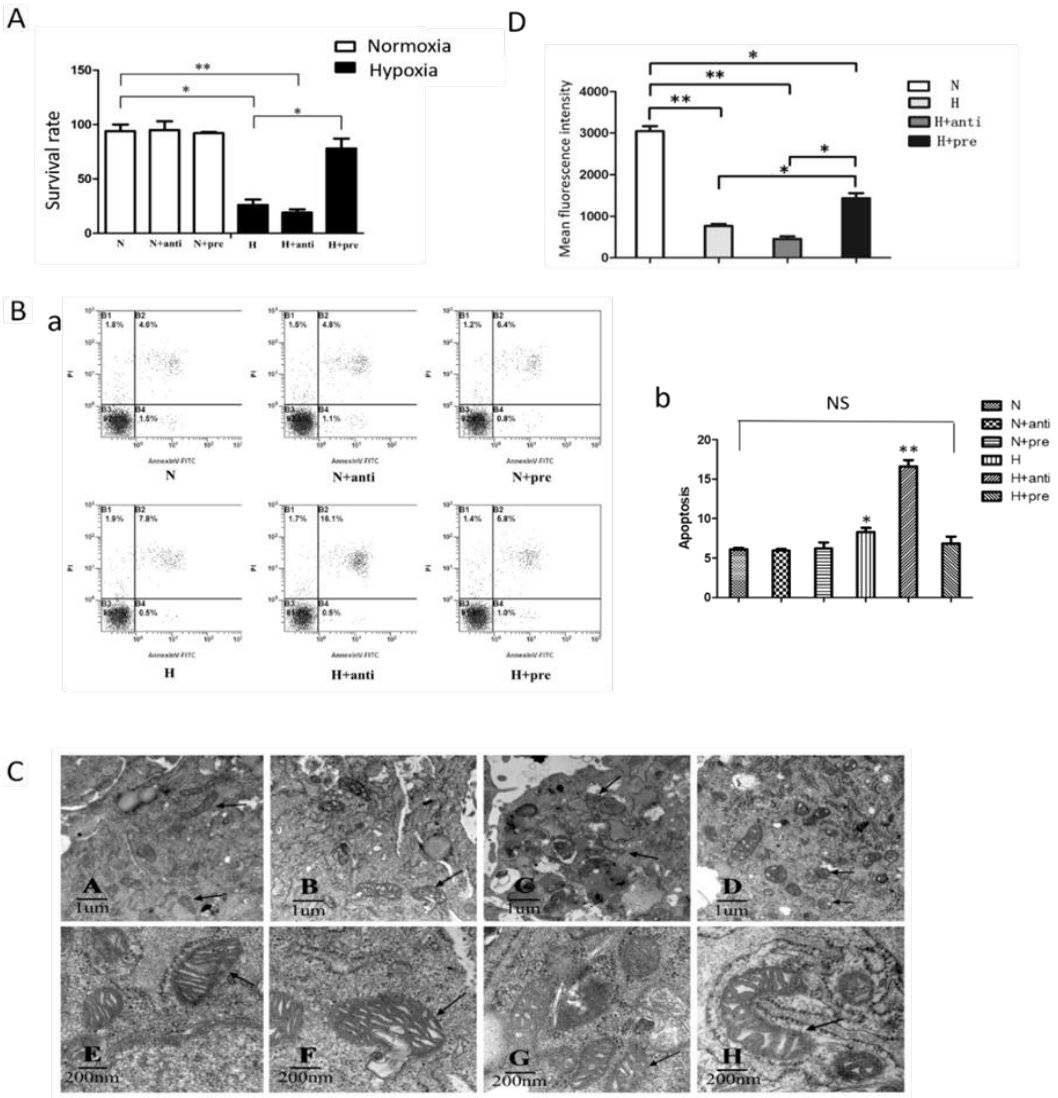

Fig. 3. *Effects of upregulation and downregulation of miR-17-5p on cell capacity and mitochondrial structure and function.* ***A****) MTT analysis revealed that upregulation of miR-17-5p could rescue the survival rate of GG MuSCs in hypoxia;* ***B****) a: Apoptosis rate was increased in hypoxia group compared with normoxia group. Upregulation of miR-17-5p can decrease the apoptosis rate of GG MuSCs in hypoxia (apoptosis rate was lower in H+Pre group compared with H group; b: Quantitative data of Apoptosis);* ***C****) normoxia group (A, E); hypoxia group (B, F); H+anti group(C,G); H+pre group(D, H);* ***D****) Quantitative data of Mitochondrial membrane potential. (*p < 0.05, ** p < 0.01, NS: p > 0.05)*

Effects of upregulation and downregulation of miR-17-5p on cell mitochondrial structure and function

Transmission electron microscopy showed that the mitochondria in the H group were dilated *in vivo* and *in vitro*, the matrix was scarce, the electron density decreased, the mitochondria became shorter and shorter, the membrane was incomplete, and there was often a break at the edge of the proximal membrane. Compared with the H group, the H+anti group had more mitochondria with more structural damage, and the degree of damage was more serious. At high magnification, the mitochondria had a balloon-like appearance, suggesting that the mitochondria had severe pathological edema. Compared with the H group, the H+pre group had fewer mitochondria and decreased mitochondrial edema. At high magnification, almost no balloon-like mitochondria were found. These findings suggested that the damage to the mitochondrial structure was reduced (Fig. 3C).

The flow cytometry results showed that the mean fluorescence intensity of the mitochondrial membrane potential in group H decreased by 3.5 times compared with that in group N ($P<0.01$), and the H+anti group showed a decrease of 4.5 times compared with group N ($P<0.01$) and the H+pre group. The fluorescence intensity was still lower than that of the normoxic group, but it was restored compared with that of the H group (Fig. 3D). The average fluorescence intensity was 2.09 times that of the H group ($P<0.05$) (Fig. 3).

Target gene prediction

The results of RT-PCR and Western blot analyses showed that the expression levels of Arl2 and Mfn2 were increased in the hypoxic group, but Arl2 did not change significantly at the protein level. The Mfn2 gene level in the hypoxic group was higher than that in the normoxic group; the level increased 4.3 times, and the protein level also increased by 3.5 times; these

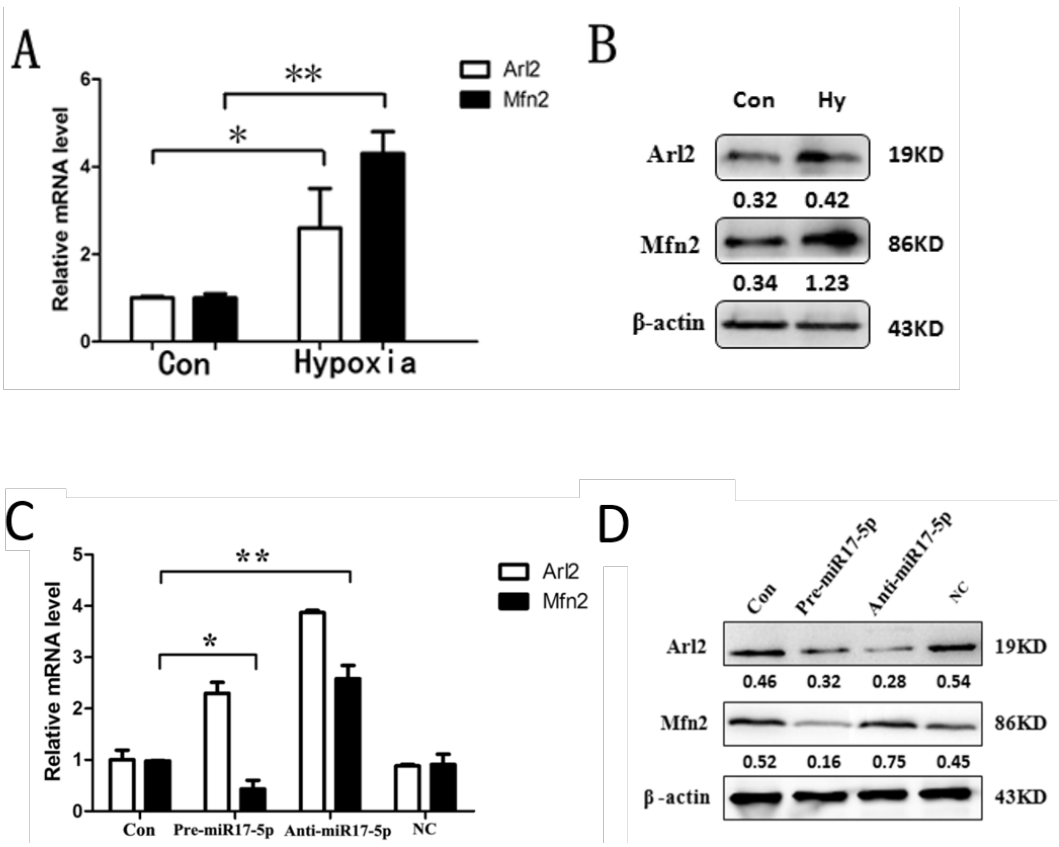

Fig. 4. *Mfn2 expression increased in hypoxia group and changed with miR-17-5p.* ***A, C****) The relative expression levels of Arl2 and Mfn2 genes;* ***B, D****) The protein levels of Arl2 and Mfn2 were measured by Western blot. The expression levels were normalized to β-actin. Data represent mean±standard deviation, *p < 0.05, ** p < 0.01, n=3.*

findings are consistent (Fig. 4, A/B). miR-17-5p was upregulated and downregulated by the transfection of mimics and inhibitors, respectively, and the Arl2 and Mfn2 genes and proteins were detected. The results showed that the mRNA level of Arl2 increased after transfection of pre-miR-17-5p and anti-miR-17-5p, and the protein level decreased, but the trends of change did not match; Mfn2 at the gene or protein level was inversely proportional to the expression of miR-17-5p, and the results were statistically significant (Ppre=0.024; Panti=0.033). Therefore, we initially determined that the gene that affects the mitochondrial fusion function of Mfn2 is the target gene of miR-17-5p (Fig.4).

DISCUSSION

The genioglossus muscle satellite cells are important for maintaining the long-term structure and function of the genioglossus muscle (10). These cells show strong division and proliferation and are considered to be the best *in-vitro* cell model for studying abnormal skeletal muscle OSAHS (11). The survival rate of each group was detected by MTT colorimetric assays. The survival rate of the hypoxia group was significantly lower than that of the normoxia group, indicating that hypoxia inhibited the proliferation of GG MuSCs.

Apoptosis is a normal physiological process of cells (12). After transfection of pre-miR-17-5p in hypoxic cells, flow cytometry showed that the apoptotic rate was restored, and after transfection of anti-miR-17-5p in hypoxic cells, flow cytometry analysis showed that the apoptotic rate increased, indicating that upregulation of miR-17-5p can protect cells in a hypoxic environment. We compared the proliferation and apoptosis of the normal control group with those of the normoxic group and the normoxic group after transient transfection and found that the proliferation and apoptosis levels of the normoxia group were similar to those of the other groups, due to the CP transfection reagent applied in this experiment. The experiment had essentially no side-effects.

The mitochondria are mainly composed of a two-layer membrane structure formed by the outer membrane (13). Proton pumps are present on the inner membrane and pump the protons in the matrix into the outer chamber, thus forming the transmembrane potential of the mitochondrial inner and outer membranes (14). The potential can be negative and positive, and the formation of the potential chemical gradient is extremely important for driving ATP synthesis. Therefore, mitochondrial membrane potential levels can effectively respond to mitochondrial energy metabolism (15). At the same time, it is precisely because of the transmembrane potential that positively charged fluorescent dyes can interact with it. The fluorescent probe selected in this experiment was positively charged. The average fluorescence intensity of the fluorescent probe was detected by flow cytometry. Changes in potential levels indirectly reflect the production capacity of mitochondria in muscle satellite cells (16).

Protection of the mitochondrial structure can be performed to investigate the upregulation of miR-17-5p. In this experiment, TargetScan, DIANA LAB and other software programs were used to screen miR-17-5p and mitochondria-related functional target genes. After statistical analysis, the intersection of various software programs was used to identify two mitochondrial function-related genes, Arl2 and Mfn2, which may be our target gene. Mfn2 belongs to the mitochondrial fusion protein gene family, which plays an important role in the process of mitochondrial fusion and division (17). When the Mfn2 gene was knocked out, the mitochondrial fusion efficiency was significantly reduced, and fusion did not occur, resulting in mitochondrial rupture and fragmentation (18).

RT-PCR and Western blot analyses showed that only the change in Mfn2 was consistent with the transient transfection results of miR-17-5p, and it changed significantly at the gene and protein levels. Finally, we predicted the relationship between miR-17-5p and Mfn2. The mitochondrial fusion-related gene is a target gene for miR-17-5p that is involved in mitochondrial function. However, the identification of this gene also requires the construction of a luciferase reporter gene plasmid and other methods for further exploration, which will be the focus of our future research.

In conclusion, upregulation of miR-17-5p can

play a protective role in mitochondrial function. Bioinformatics analysis and gene and protein analyses were used to identify Mfn2 as a target gene in our research.

ACKNOWLEDGEMENTS

This study was supported by the National Natural Science Foundation of China (NO.81500851).

REFERENCES

1. Bearpark H, Elliott L, Grunstein R, et al. Occurrence and correlates of sleep disordered breathing in the Australian town of Busselton: a preliminary analysis. Sleep 1993; 16(8 Suppl):S3-S5.
2. Barbe F, Barcelo A, Montserrat JM. Sleep apnoea syndrome: a look at ethnicity, pathogeny and potential therapheutic approaches. Sleep Med Rev 2005; 9(6):415-18.
3. Lewis MR, Ducic Y. Genioglossus muscle advancement with the genioglossus bone advancement technique for base of tongue obstruction. J Otolaryngol 2003; 32(3):168-173.
4. Boyd JH, Petrof BJ, Hamid Q, Fraser R, Kimoff RJ. Upper airway muscle inflammation and denervation changes in obstructive sleep apnea. Am J Respir Crit Care Med 2004; 170(5):541-46.
5. Kuna ST. Respiratory-related activation and mechanical effects of the pharyngeal constrictor muscles. Respir Physiol 2000; 119(2-3):155-61.
6. Osaki M, Okada F, Ochiya T. miRNA therapy targeting cancer stem cells: a new paradigm for cancer treatment and prevention of tumor recurrence. Ther Deliv 2015; 6(3):323-37.
7. Kulshreshtha R, Ferracin M, Wojcik SE, et al. A microRNA signature of hypoxia. Mol Cell Biol 2007; 27(5):1859-67.
8. Kulshreshtha R, Ferracin M, Negrini M, Calin GA, Davuluri RV, Ivan M. Regulation of microRNA expression: the hypoxic component. Cell Cycle 2007; 6(12):1426-31.
9. Liu W, Wen Y, Bi P, Lai X, Liu XS, Liu X, Kuang S. Hypoxia promotes satellite cell self-renewal and enhances the efficiency of myoblast transplantation. Development 2012; 139(16):2857-65.
10. Attia M, Maurer M, Robinet M, et al. Muscle satellite cells are functionally impaired in myasthenia gravis: consequences on muscle regeneration. Acta Neuropathol 2017; 134(6):869-88.
11. Wang H, Zhang D, Jia S, et al. Effect of Sustained hypoxia on autophagy of genioglossus muscle-derived stem cells. Med Sci Monit 2018; 24:2218-24.
12. Elmore S. Apoptosis: a review of programmed cell death. Toxicol Pathol 2007; 35(4):495-16.
13. Picard M, Taivassalo T, Gouspillou G, Hepple RT. Mitochondria: isolation, structure and function. J Physiol 2011; 589(Pt 18):4413-21.
14. Smirnov AY, Mourokh LG, Nori F. Forster mechanism of electron-driven proton pumps. Phys Rev E Stat Nonlin Soft Matter Phys 2008; 77(1 Pt 1):11919.
15. Ge H, Zhang F, Shan D, et al. Effects of mitochondrial uncoupling protein 2 inhibition by genipin in human cumulus cells. Biomed Res Int 2015; 2015:323246.
16. Kotake Y, Ohta S. MPP+ analogs acting on mitochondria and inducing neuro-degeneration. Curr Med Chem 2003; 10(23):2507-16.
17. Fang X, Chen X, Zhong G, Chen Q, Hu C. Mitofusin 2 downregulation triggers pulmonary artery smooth muscle cell proliferation and apoptosis imbalance in rats with hypoxic pulmonary hypertension via the PI3K/Akt and mitochondrial apoptosis pathways. J Cardiovasc Pharmacol 2016; 67(2):164-74.
18. Zhang D, Ma C, Li S, et al. Effect of Mitofusin 2 on smooth muscle cells proliferation in hypoxic pulmonary hypertension. Microvasc Res 2012; 84(3):286-96.

SHORT CHAIN FATTY ACIDS CONTRIBUTE TO GUT MICROBIOTA-INDUCED PROMOTION OF COLONIC MELATONIN RECEPTOR EXPRESSION

B. WANG, L. ZHANG, SW. ZHU, JD. ZHANG and LP. DUAN

Department of Gastroenterology, Peking University Third Hospital, Beijing, China

Received February 13, 2019 – Accepted March 22, 2019

Melatonin plays an important role in various gut functions through melatonin receptors. The gut microbiota/gut hormone axis has recently received increasing attention. However, the relationship between the gut microbiota and melatonin receptors has not yet been evaluated. We aimed to determine the effect of the gut microbiota on colonic melatonin receptor expression in germ-free (GF) rats and to further explore the potential mechanism in Caco-2 cells. In this study, GF rats were transplanted with fecal samples from a healthy human donor. Subsequently, 16S rRNA sequencing was performed to analyze the microbial communities. Colon tissue was collected for immunohistochemical analysis. The correlations between melatonin receptor expression and the gut microbiota were assessed. Melatonin receptor expression in Caco-2 cells was detected by Western blot. We found that fecal microbiota transplantation significantly increased the expression of colonic melatonin receptors in GF rats. The amount of fecal Short chain fatty acids (SCFAs) was significantly higher in fecal microbiota transplantation (FMT) rats than in GF rats. SCFA-producing bacteria, such as *Alistipes* and *Blautia,* were positively correlated with colonic melatonin receptor expression in FMT rats. Additionally, acetate and propionate significantly increased melatonin receptor-1 expression in Caco-2 cells. Therefore, the gut microbiota may promote melatonin receptor expression, and the mechanism may involve the action of SCFAs. This finding may facilitate the development of new therapeutic treatments for various gastrointestinal disorders.

Melatonin is a hormone that has been widely found in vertebrates (1). Melatonin was first discovered in the pineal gland and participates in many biological processes, such as the circadian rhythm, mood regulation, reproduction and immunity (2). Additionally, melatonin has been confirmed to be synthesized in enterochromaffin cells in the gastrointestinal (GI) mucosa (3). Melatonin exerts protective effects, such as immune enhancement, antioxidant activity and regulation of disturbed motility, on the GI tract (4). These biological actions are mainly mediated by membrane receptors (5).

Melatonin receptor-1 (MT1) and melatonin receptor-2 (MT2) are two mammalian melatonin receptor subtypes (6). Both MT1 and MT2 receptors belong to the G-protein-coupled receptor family. MT1 receptor activation results in adenylate cyclase inhibition and phospholipase C-β activation, while MT2 receptor activation mediates the stimulation of phosphoinositide hydrolysis and the inhibition of adenylate cyclase and the soluble guanylate cyclase pathway (7-9).

The gut microbiota plays a pivotal role in the regulation of GI homeostasis (10). Perturbations of the gut microbiota have been associated with many

Key words: gut microbiota; fecal microbiota transplantation; melatonin receptor; short chain fatty acids

Corresponding Author:
Dr LP. Duan,
No.49 North Garden Rd.,
Haidian District,
Beijing, China
Tel.: +86 10 82806003 - Fax: +86 10 82801250
e-mail: duanlp@bjmu.edu.cn

0393-974X (2019)

DISCLOSURE: ALL AUTHORS REPORT NO CONFLICTS OF INTEREST RELEVANT TO THIS ARTICLE.

GI diseases, such as celiac disease, inflammatory bowel disease, and functional bowel disorders (11-15). Additionally, accumulating evidence has suggested that the gut microbiota/gut hormone interactions play a role in the pathophysiology of gastrointestinal disorders (16). The secretion of glucagon-like peptide-1 (GLP-1) (17) and serotonin (18), which are important gut hormones in gut homeostasis, has been confirmed to be affected by the gut microbiota. Gut microbiota metabolites consisting of short chain fatty acids (SCFAs) could stimulate GLP-1 expression *in vitro* (19, 20). Indigenous spore-forming bacteria have been confirmed to promote 5-HT biosynthesis in the colon. The structure of the gut microbiota composition can be modulated by diet (21). Moreover, the importance of microbiota-derived metabolites, especially SCFAs, has been increasingly recognized in the homeostatic interactions between the gut microbiota and the host (22). However, the relationship between the gut microbiota and the melatonin receptor has not yet been evaluated. Therefore, we conducted this study to determine the effect of the gut microbiota on colonic melatonin receptor expression in germ-free (GF) rats and to further explore the underlying mechanism in Caco-2 cells.

MATERIALS AND METHODS

Animal experiments

GF Sprague-Dawley (SD) rats (male) were born and bred in the Department of Animal Laboratory Science Department at the Peking University Health Science Center. At six weeks of age, the GF rats were divided into two groups (fecal microbiota transplantation (FMT) group (n=5) and GF group (n=5) and subjected to FMT by gavage (the fecal microbiota obtained from one healthy human was transplanted into the FMT group, and sterile saline was transplanted into the GF group). Rats in the same group received the fecal microbiota from the same sample, and transplantation was performed only once. Twenty-four days after the FMT, fecal samples were collected from rats for further analyses of the microbiota. Then, the rats were sacrificed with anesthesia. Colon tissue samples were collected and fixed in 10% buffered formalin. The animal experiments were approved by the Ethics Committee of the Peking University Health Science Center (LA2016230)

Immunohistochemistry

Colon tissue sections were cut with a Leica microtome to a thickness of 4 μm. The sections were deparaffinized using the routine method. The sections were incubated in 3% hydrogen peroxide in methanol for 15 min to quench endogenous peroxidase activity. After blocking with goat serum for 30 min, the sections were incubated with rabbit anti-MT1 (1:500, orb11085, Biorbyt) and rabbit anti-MT2 (1:500, ab203346, Abcam) overnight at 4°C. Then, the sections were incubated with anti-rabbit secondary antibody (Zhongshan Golden Bridge) for 30 min at room temperature. Diaminobenzidine was used as a chromogen for color development.

Ten fields from each slide were randomly selected under a Leica DM 2500 microscope at magnification of 400×, photographed by a Nikon DS-Vi1 camera, and then exported via Nikon NIS-Elements imaging software. The integrated optical density (IOD) of positive staining substances was measured using the image-Pro Plus 6.0 software.

16S rRNA sequencing of gut microbiota

Microbial DNA was extracted from fecal samples using the E.Z.N.A.® Soil DNA Kit (Omega Bio-Tek, Norcross, GA, USA) following the manufacturer's protocols. The hypervariable regions (V3 to V4) of the bacterial 16S ribosomal RNA gene were amplified using two primers (338F (5'-ACTCCTACGGAGGCAGCAG-3') and 806R (5'-GACTACHVGGGTWTCTAAT)). Purified amplicons were pooled in equimolar amounts, and paired-end sequencing (2x300) was conducted using the Illumina MiSeq platform (Illumina, San Diego, USA).

Quantification of fecal SCFAs

Fecal SCFAs (acetate, propionate, butyrate) of FMT and GF rats were detected with ultra-performance liquid chromatography coupled to tandem mass spectrometry (UPLC-MS/MS).

Cell culture and treatments

Caco-2 cells were obtained from the American Type Culture Collection (Rockville, MD, USA) and maintained in minimum essential medium supplemented with 10% fetal bovine serum (FBS) (Gemini) and 1% penicillin/streptomycin (Gibco) at 37°C in a humidified atmosphere of 5% CO_2. Cells were subcultured every 2 days. In the

experiments, cells were seeded in 60-mm dishes, allowed to attach and treated with sodium acetate (0 to 40 mM, Sigma-Aldrich), sodium propionate (0 to 20 mM, Sigma-Aldrich) and sodium butyrate (0 to 10 mM, Sigma-Aldrich) for 24 h.

Western blot analysis

Proteins from Caco-2 cells were extracted with RIPA extraction buffer mixed with a protease inhibitor cocktail. The lysates were centrifuged at 12,000 rpm for 10 min. A BCA protein assay kit was used to quantify the protein concentration. Equal amounts of protein (30 μg) were electrophoresed in 12% sodium dodecyl sulfate polyacrylamide gels and transferred onto nitrocellulose membranes under a constant current of 250 mA for 90 min. The membranes were blocked with 5% nonfat dried milk at 25°C and incubated with rabbit anti-MT1 antibody (1:1,000, orb11085, Biorbyt) and rabbit anti-MT2 antibody (1:1,000, ab203346, Abcam) separately overnight at 4 . β-actin was used as the internal reference protein. The primary antibodies were detected using anti-rabbit or mouse secondary antibodies and were visualized with an infrared imaging system (LI-COR Biosciences, Lincoln, USA). The band intensity relative to that of β-actin was calculated, and the results were expressed as fold change from control values.

Statistical analysis

The results are presented as the mean± SEM. The data for MT1 and MT2 expression in rats were analyzed with a nonparametric Mann-Whitney test. The data for MT1 and MT2 expression in Caco-2 cells were analyzed with a one-way analysis of variance (ANOVA) followed by an LSD post-test. Statistical significance was determined when the P value was less than 0.05. The statistical analyses were performed using SPSS software version 24.0 (SPSS Inc., Chicago, IL, USA). The associations between the colonic melatonin receptor expression in FMT rats and bacterial taxa were visualized and identified by heatmaps of Spearman rank correlation coefficients using the pheatmap package in R.

RESULTS

Effect of the gut microbiota on colonic melatonin receptor expression

The expression of melatonin receptors in the colon of rats was detected 24 days after FMT by immunohistochemistry. Immunoreactive melatonin receptors were localized mostly on colonic epithelial cells. MT1 expression was significantly higher in FMT rats than in GF rats (IOD mean: 452.80±120.40 versus 65.80±13.12, p = 0.0079) (Fig. 1, a-c). MT2 expression was also significantly higher in FMT rats than tin GF rats (IOD mean: 229.30±143.30 *vs* 53.75±1.94, p=0.0079) (Fig. 1, d-f).

Fecal microbiota profiles of FMT rats

Five fecal specimens from FMT rats were used for 16S rRNA sequencing to evaluate the gut microbiota composition after FMT. The microbiota composition at the genus level was revealed by a community heatmap (Fig. 2a), and the percent of community abundance is shown in Table I. We found that *Bacteroides*, *Paraprevotella*, and *Parabacteroides* were most abundant in the FMT rats. Additionally, the community bar plot analysis showed different composition ratios of the bacterial genera, which indicates differences in the abundance of genera in the FMT rats (Fig. 2b).

Fecal SCFAs (acetate, propionate, butyrate) of FMT and GF rats

The amount of fecal SCFAs (acetate, propionate, butyrate) was significantly higher in FMT rats than in GF rats (Fig. 3).

Association between colonic melatonin receptor expression and gut microbiota

In the view of the correlation analyses conducted in the FMT rats that analyzed the correlation between microbial composition at the genus level and melatonin receptor expression (Fig. 4), *Alistipes* was positively correlated with colonic MT1 expression and *Blautia* was positively correlated with colonic MT2 expression.

Effect of SCFAs on melatonin receptor expression in Caco-2 cells

To further investigate the effect of SCFAs on colonic melatonin receptor (MT1 and MT2) expression, Caco-2 cells were incubated with sodium acetate (0 to 40 mM), sodium propionate (0 to 20 mM) and sodium butyrate for 24 h. The effect of SCFAs on melatonin receptor protein expression was determined by Western blotting.

As is shown in Fig. 4a, treatment with 40 mM sodium acetate significantly increased the expression of MT1. Sodium acetate also increased MT1 expression in Caco-2 cells at concentrations of 20 mM and 10 mM, but the increases were not significant. Treatment with 10, 20, or 40 mM sodium acetate increased the expression of MT2, but the increase was not significant (Fig. 5a).

Treatment with sodium propionate at concentrations ranging from 5 to 20 mM significantly increased the expression MT1 in Caco-2 cells (Fig. 5b). MT2 expression was also increased by sodium propionate, but the increase was not significant. No significant variation in MT1 and MT2 expressions were detected in butyrate-treated cells (Fig. 5c).

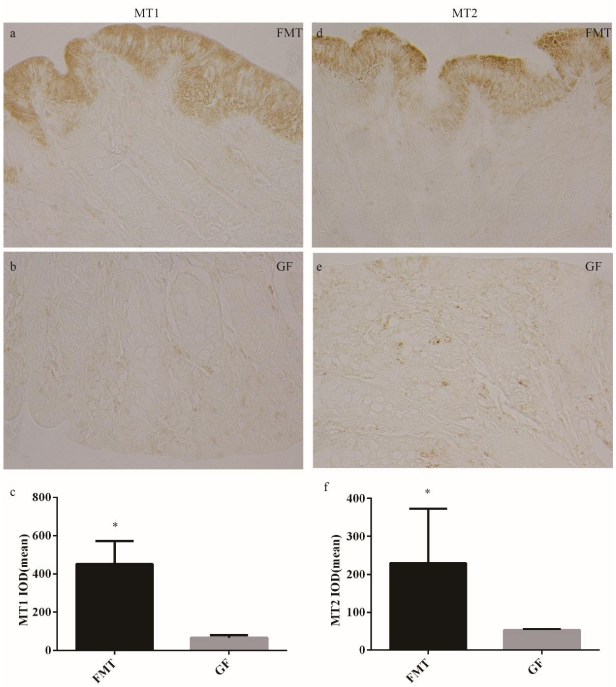

Fig. 1. *Effect of FMT on the expression of colon melatonin receptors.* ***a)*** *Immunohistochemical staining of MT1 in the colon of FMT rats.* ***b)*** *Immunohistochemical staining of MT1 in the colon of GF rats.* ***d)*** *Immunohistochemical staining of MT2 in the colon of FMT rats. e. Immunohistochemical staining of MT2 in the colon of GF rats. (a, b, d, e magnification: 400×).* ***c, f)*** *the expressions (presented as the mean IOD of positively stained substances) of both MT1 and MT2 were significantly higher in the FMT rats than in the GF rats. The line in the scatter plots (c, f) indicates the mean value. The results are presented as the means±SEM.*
** $0.01 < p \leq 0.05$*
MT1: melatonin receptor-1; MT2: melatonin receptor-2; FMT: fecal microbiota transplantation; GF: germ-free; IOD: integrated optical density

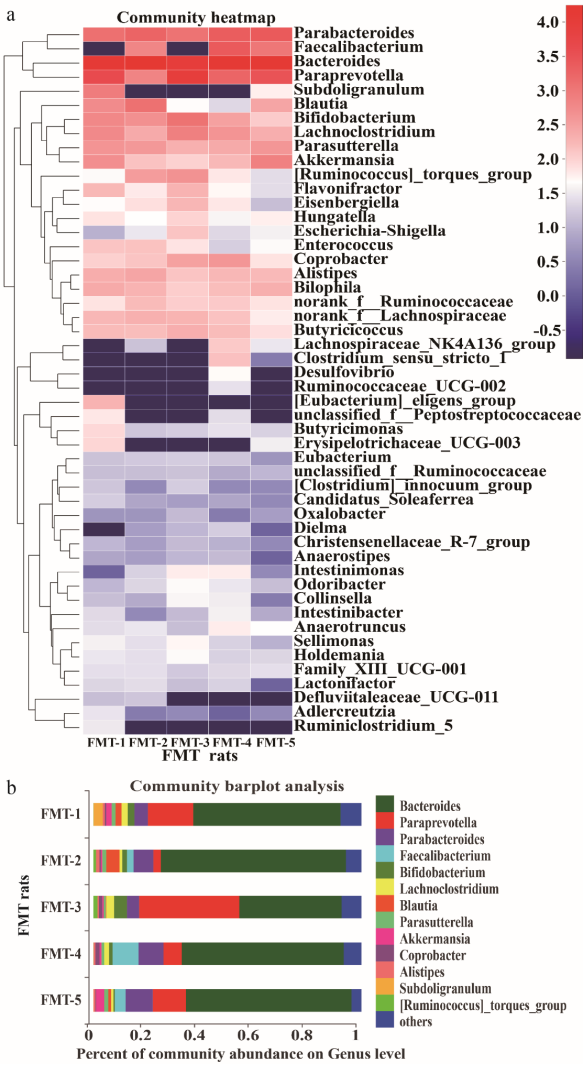

Fig. 2. *Variation of fecal microbiota in FMT rats at the genus level.* ***a)*** *Bacteroides, Paraprevotella, and Parabacteroides were most abundant in FMT rats based on the community heatmap.* ***b)*** *A community bar plot analysis showed different composition ratios of bacterial genera. FMT: fecal microbiota transplantation.*

DISCUSSION

In the present study, we found that the gut microbiota could stimulate colonic melatonin receptor

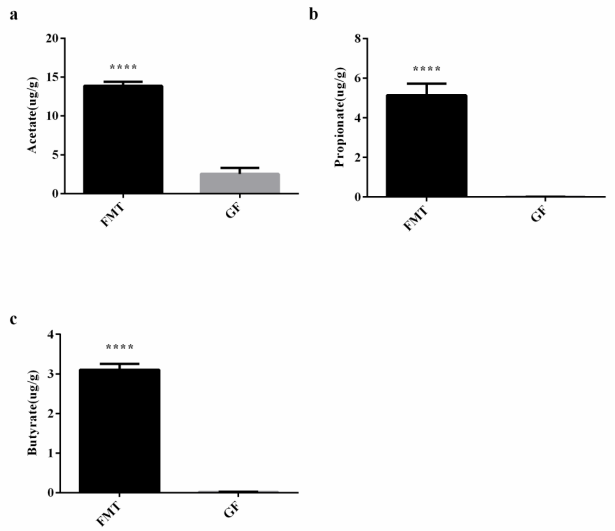

Fig. 3. *Fecal SCFAs (acetate, propionate, butyrate) of FMT and GF rats.* ***a****) The amount of fecal acetate in FMT and GF rats.* ***b****) The amount of fecal propionate in FMT and GF rats.* ***c****) The amount of fecal butyrate in FMT and GF rats. The results are presented as the means±SEM. ****$p \leq 0.000$; FMT: fecal microbiota transplantation; GF: germ-free.*

expression in GF rats, which further confirmed the role of the gut microbiota/gut hormone axis. To our knowledge, this study is the first to investigate the effect of the gut microbiota on melatonin receptor expression.

The gut microbiota is of vital importance in the development of GI functions, such as intestinal barrier function, GI mucosal immunology, and the gut-brain axis (23). Because melatonin has been confirmed to play a crucial role in gut motility and immunity (4), the promotion of colonic melatonin receptor expression by the gut microbiota suggests that the gut microbiota may affect gut motility and immunity through functional pathways involving melatonin.

Increasing evidence has indicated that metabolites of the gut microbiota could affect the physiology of the host (24). SCFAs, which are fermented from indigestible dietary fiber by the gut microbiota, are crucial and are the best-studied metabolites of the gut bacteria (25). SCFAs have been shown to affect GI metabolism and function. Acetate, propionate, and butyrate are the main SCFAs in the gut and have been suggested to enhance the integrity of the intestinal epithelium (26), increase mucus production (27), affect gut motility and immunity (28) and stimulate the release of gut hormones and neuropeptides (29). According to our study, the SCFA contents (acetate, propionate, butyrate) were significantly higher in the FMT group than in the GF group, which is consistent with other studies (30, 31). In addition, the correlation analyses performed in FMT rats showed that *Alistipes* (32, 33) and *Blautia* (34), both of which are SCFA-producing (including acetate and propionate) bacteria, were positively correlated with colonic melatonin receptor expression. Therefore, we focused on SCFAs as candidate promotors of melatonin receptor expression.

Furthermore, to verify the effect of SCFAs on

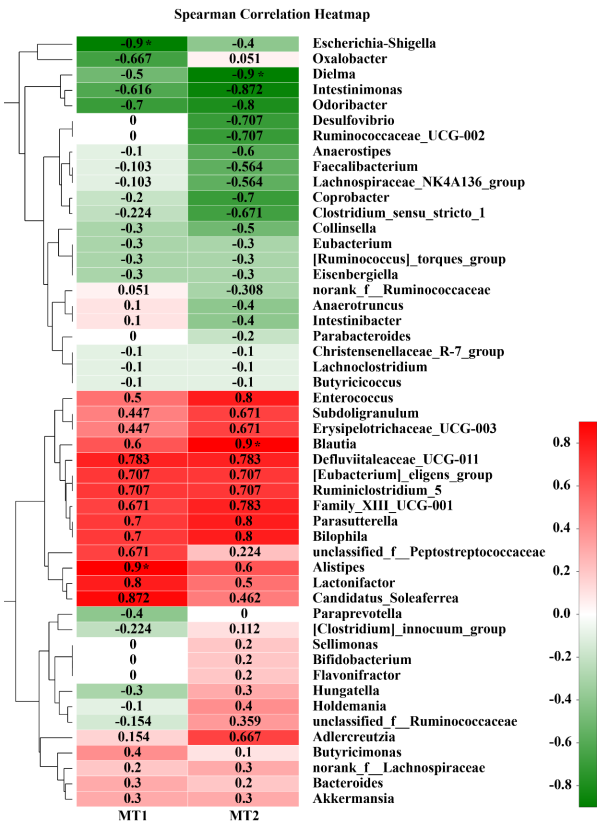

Fig. 4. *Relationship between colonic melatonin receptor expression and the gut microbiota. Heat maps of Spearman's rank correlation coefficients between colonic melatonin receptor expression and the gut microbiota at the genus level. Spearman's correlation coefficients are presented on the actual bar. *$0.01 < p \leq 0.05$*

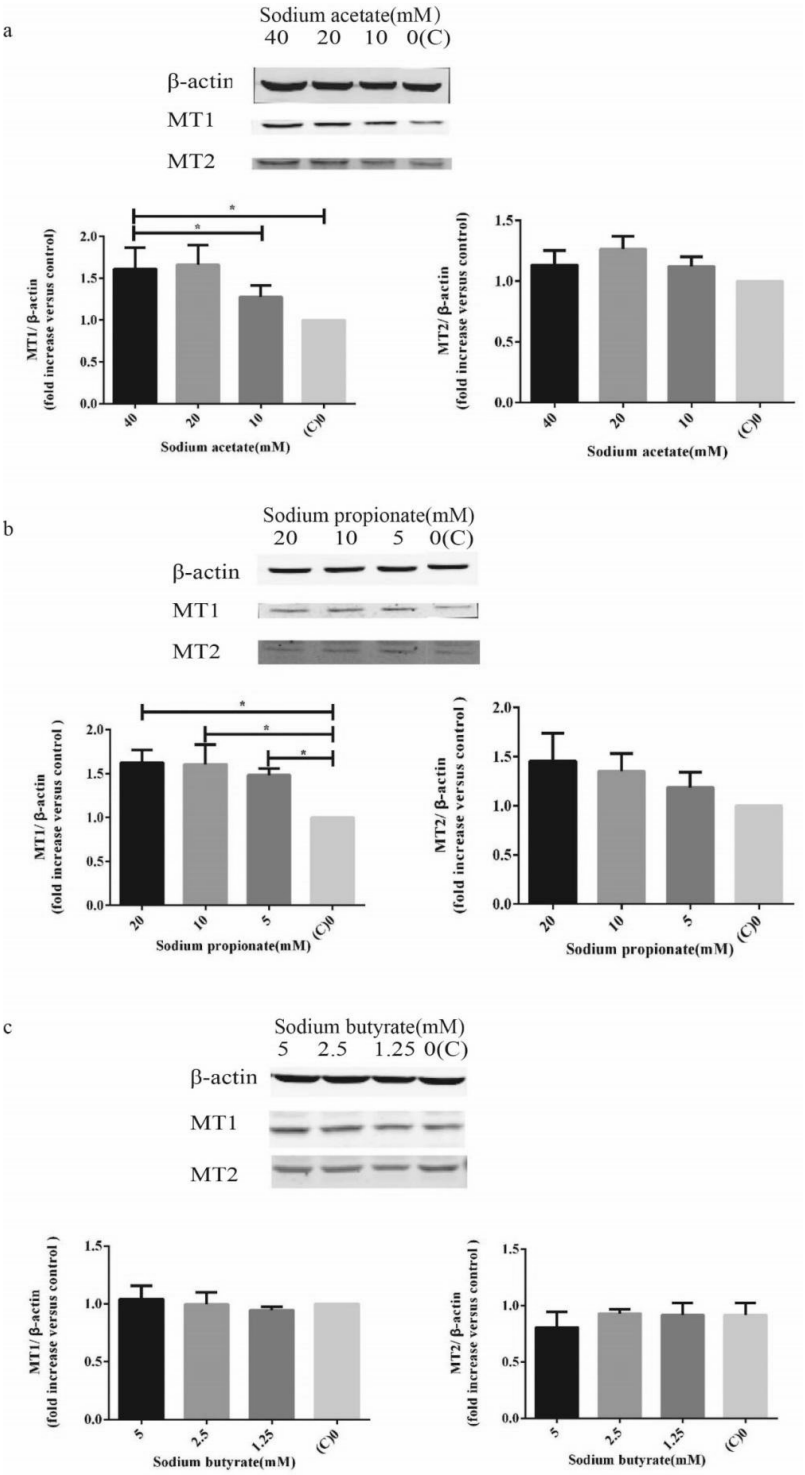

Fig. 5. *Effect of short chain fatty acids on melatonin receptor expression in Caco-2 cells.* ***a****) Relative MT1 and MT2 quantification by Western blot analysis of protein extract of control or sodium acetate-treated Caco-2 cells.* ***b****) Relative MT1 and MT2 quantification by Western blot analysis of protein extract of control or sodium propionate-treated Caco-2 cells.* ***c****) Relative MT1 and MT2 quantification by Western blot analysis of protein extract of control or sodium butyrate-treated Caco-2 cells. The results are presented as the means±SEM of four experiments performed in duplicate.*
**0.01 < p ≤ 0.05. MT1: melatonin receptor-1; MT2: melatonin receptor-2*

Table I. *Percent of community abundance at the genus level in FMT rats (the top 12 most abundant core bacteria genera).*

Genus	Abundance (%)				
	FMT-1	FMT-2	FMT-3	FMT-4	FMT-5
Bacteroides	54.9	69.1	38.4	60.5	61.7
Paraprevotella	16.8	2.8	37.2	7.0	12.3
Parabacteroides	5.1	7.1	4.6	9.1	10.2
Faecalibacterium	0	2.6	0	10.0	4.1
Bifidobacterium	2.4	1.9	4.8	1.2	0.5
Lachnoclostridium	2.3	0.9	3.1	1.7	0.9
Blautia	2.2	5.0	0.2	0	1.1
Parasutterella	1.7	1.5	0.8	1.0	1.6
Akkermansia	2.0	0.5	0.4	0.7	2.9
Coprobacter	0.4	0.5	1.2	1.6	0.3
Alistipes	0.9	1.1	0.5	0.7	0.7
Subdoligranulum	3.5	0	0	0	0

melatonin receptor expression, we treated Caco-2 cells (an intestinal epithelial cell line) with SCFAs at different concentrations. The results were in line with the findings from the animal experiments. Both acetate and propionate increased melatonin receptor expression in a dose-dependent manner, while the effect of butyrate on melatonin receptor expression was not significant.

However, although SCFAs represent potential microbial metabolites that can promote melatonin receptor expression, additional mechanisms by which gut microbiota affect melatonin receptor expression may exist. Further studies on animals lacking SCFA receptors are needed to elucidate a cause and effect mechanism of melatonin receptor expression.

In conclusion, our study is the first to demonstrate that the gut microbiota may promote melatonin receptor expression via acetate and propionate. SCFAs may be one mechanism by which gut microbiota promote melatonin receptor expression. In addition, our study further emphasized the existence of the gut microbiota/gut hormone axis. These findings may help in the development of new therapeutic target for GI disorders.

ACKNOWLEDGEMENTS

This study was supported by National Natural Science Foundation of China (81670491).

The authors are grateful to all subjects who participated in this study. The authors appreciate the technical support of the Medical Research Center of Peking University Third Hospital and the Clinical Stem Cell Center of Peking University Third Hospital, as well as the support of the Department of Laboratory Animal Science, Peking University Health Science Center, for animal experiments.

REFERENCES

1. Mukherjee S, Maitra SK. Gut melatonin in vertebrates: chronobiology and physiology. Front Endocrinol (Lausanne) 2015; 6:112.
2. Brzezinski A. Melatonin in humans. N Engl J Med 1997; 336:186-195.
3. Bubenik GA. Thirty four years since the discovery of gastrointestinal melatonin. J Physiol Pharmacol 2008; 59 Suppl 2:33-51.

4. Mozaffari S, Rahimi R, Abdollahi M. Implications of melatonin therapy in irritable bowel syndrome: a systematic review. Curr Pharm Des 2010; 16:3646-3655.
5. Chen CQ, Fichna J, Bashashati M, Li YY, Storr M. Distribution, function and physiological role of melatonin in the lower gut. World J Gastroenterol 2011; 17:3888-3898.
6. von Gall C, Stehle JH, Weaver DR. Mammalian melatonin receptors: molecular biology and signal transduction. Cell Tissue Res 2002; 309:151-162.
7. Bondi CD, McKeon RM, Bennett JM, et al. Mt1 melatonin receptor internalization underlies melatonin-induced morphologic changes in chinese hamster ovary cells and these processes are dependent on gi proteins, mek 1/2 and microtubule modulation. J Pineal Res 2008; 44:288-298.
8. Chan AS, Lai FP, Lo RK, Voyno-Yasenetskaya TA, Stanbridge EJ, Wong YH. Melatonin mt1 and mt2 receptors stimulate c-jun n-terminal kinase via pertussis toxin-sensitive and -insensitive g proteins. Cell Signal 2002; 14:249-257.
9. Ho MK, Yung LY, Chan JS, Chan JH, Wong CS, Wong YH. Galpha(14) links a variety of g(i)- and g(s)-coupled receptors to the stimulation of phospholipase c. Br J Pharmacol 2001; 132:1431-1440.
10. Lin L, Zhang J. Role of intestinal microbiota and metabolites on gut homeostasis and human diseases. BMC Immunol 2017; 18:2.
11. Nagao-Kitamoto H, Kitamoto S, Kuffa P, Kamada N. Pathogenic role of the gut microbiota in gastrointestinal diseases. Intest Res 2016; 14:127-138.
12. Gorkiewicz G, Moschen A. Gut microbiome: a new player in gastrointestinal disease. Virchows Arch 2018;472:159-172.
13. Ni J, Wu GD, Albenberg L, Tomov VT. Gut microbiota and ibd: causation or correlation? Nat Rev Gastroenterol Hepatol 2017; 14:573-584.
14. Sundin J, Ohman L, Simren M. Understanding the gut microbiota in inflammatory and functional gastrointestinal diseases. Psychosom Med 2017; 79:857-867.
15. Marasco G, Di Biase AR, Schiumerini R, et al. Gut microbiota and celiac disease. Dig Dis Sci 2016; 61:1461-1472.
16. Fukui H, Xu X, Miwa H. Role of gut microbiota-gut hormone axis in the pathophysiology of functional gastrointestinal disorders. J Neurogastroenterol Motil 2018;24:367-386.
17. Yang M, Fukui H, Eda H, et al. Involvement of gut microbiota in association between glp-1/glp-1 receptor expression and gastrointestinal motility. Am J Physiol Gastrointest Liver Physiol 2017; 312:G367-G373.
18. Yano JM, Yu K, Donaldson GP, et al. Indigenous bacteria from the gut microbiota regulate host serotonin biosynthesis. Cell 2015; 161:264-276.
19. Psichas A, Sleeth ML, Murphy KG, et al. The short chain fatty acid propionate stimulates glp-1 and pyy secretion via free fatty acid receptor 2 in rodents. Int J Obes (Lond) 2015; 39:424-429.
20. Yadav H, Lee JH, Lloyd J, Walter P, Rane SG. Beneficial metabolic effects of a probiotic via butyrate-induced glp-1 hormone secretion. J Biol Chem 2013; 288:25088-25097.
21. Makki K, Deehan EC, Walter J, Backhed F. The impact of dietary fiber on gut microbiota in host health and disease. Cell Host Microbe 2018; 23:705-715.
22. Sun M, Wu W, Liu Z, Cong Y. Microbiota metabolite short chain fatty acids, gpcr, and inflammatory bowel diseases. J Gastroeterol 2017; 52:1-8.
23. Di Mauro A, Neu J, Riezzo G, Raimondi F, Martinelli D, Francavilla R, Indrio F. Gastrointestinal function development and microbiota. Ital J Pediatr 2013; 39:15.
24. Rooks MG, Garrett WS. Gut microbiota, metabolites and host immunity. Nat Rev Immunol 2016; 16:341-352.
25. Koh A, De Vadder F, Kovatcheva-Datchary P, Backhed F. From dietary fiber to host physiology: short-chain fatty acids as key bacterial metabolites. Cell 2016; 165:1332-45.
26. Chen G, Ran X, Li B, et al. Sodium butyrate inhibits inflammation and maintains epithelium barrier integrity in a tnbs-induced inflammatory bowel disease mice model. EBioMedicine 2018; 30:317-325.
27. Willemsen LE, Koetsier MA, van Deventer SJ, van Tol EA. Short chain fatty acids stimulate epithelial mucin 2 expression through differential effects on prostaglandin e(1) and e(2) production by intestinal myofibroblasts. Gut 2003; 52:1442-1447.
28. Priyadarshini M, Kotlo KU, Dudeja PK, Layden BT. Role of short chain fatty acid receptors in intestinal physiology and pathophysiology. Compr Physiol 2018;

8:1091-1115.
29. Farzi A, Frohlich EE, Holzer P. Gut microbiota and the neuroendocrine system. Neurotherapeutics 2018; 15:5-22.
30. Hoverstad T, Midtvedt T. Short-chain fatty acids in germfree mice and rats. J Nutr 1986; 116:1772-1776.
31. Maier BR, Onderdonk AB, Baskett RC, Hentges DJ. Shigella, indigenous flora interactions in mice. Am J Clin Nutr 1972; 25:1433-1440.
32. Brown CT, Davis-Richardson AG, Giongo A, et al. Gut microbiome metagenomics analysis suggests a functional model for the development of autoimmunity for type 1 diabetes. Plos One 6 2011; 6:e25792.
33. Li J, Sung CY, Lee N, Ni Y, Pihlajamaki J, Panagiotou G, El-Nezami H. Probiotics modulated gut microbiota suppresses hepatocellular carcinoma growth in mice. Proc Natl Acad Sci U S A 2016; 113:E1306-E1315.
34. Zhang X, Zhao Y, Zhang M, et al. Structural changes of gut microbiota during berberine-mediated prevention of obesity and insulin resistance in high-fat diet-fed rats. Plos One 2012; 7:e42529.

MOLECULAR MECHANISMS OF LONG CHAIN NON-CODING RNA CTBP1-AS IN REGULATION OF INVASION AND MIGRATION OF BREAST CANCER CELLS

HB. CUI[1] and CZ. GENG[2]

[1]Department of Thyroid Breast Surgery, Cangzhou Central Hospital, Cangzhou, China; [2]Breast Center, Fourth Hospital of Hebei Medical University, Tianshan Road, Shijiazhuang, China

Received February 25, 2019 – Accepted March 29, 2019

This study aimed to investigate the role of long-chain non-coding RNA CTBP1-AS in breast cancer progression and cell invasion as well as migration. Clinical data of breast cancer patients (N = 155) in our hospital was collected for further analysis. qRT-PCR was used to detect LncRNA CTBP1-AS expression levels in human normal breast epithelial cell (MCF-10A) and breast cancer cells (MCF-7, BT-549, MDA-MB-231 and MDA-MB-435). LncRNA CTBP1-AS knock-down and overexpressed lentivirus vectors were constructed to transfect breast cancer cells. Colony formation assay was employed to detect cell proliferative abilities. Flow cytometry was performed to detect cell apoptosis ratio. Wound healing scratch assay was used to detect cell migration, and Transwell matrigel assay was used to detect cell invasion. Bioinformatics analysis was performed to predict the downstream targets of LncRNA CTBP1-AS, which were further validated by dual-luciferase reporter gene system. The results showed that LncRNA CTBP1-AS was aberrantly overexpressed in breast cancer tissues and breast cancer cells compared to the control group. Moreover, the expression levels of LncRNA CTBP1-AS were positively related with tumor size, histological grade and the expression levels of Ki-67 and Her2. Further analysis showed that LncRNA CTBP1-AS expression levels negatively correlated with patient survival time and clinical prognosis. Of note, overexpressed LncRNA CTBP1-AS promoted breast cancer cell proliferation and invasion as well as migration, and decreased cell apoptosis ratio. Bioinformatics analysis and dual-luciferase reporter gene system results validated that microRNA-940 was the downstream target of LncRNA CTBP1-AS. Interestingly, overexpressed microRNA-940 abrogated the effects of LncRNA CTBP1-AS on cell proliferation, apoptosis, and invasion. In conclusion, overexpressed LncRNA CTBP1-AS promoted breast cancer cell proliferation, invasion as well as migration, inhibited cell apoptosis and accelerated breast cancer development by sponging microRNA-940.

Breast cancer is the second leading cause of cancer death in women (1). It was reported that approximately 230,000 women worldwide are newly diagnosed with invasive breast cancer every year, and about 40,000 of whom die from breast cancer (2). With the development of first-line endocrine therapy, the five-year survival rate of hormone receptor-positive breast cancer patients has been significantly improved (3). Moreover, improvement of the traditional cancer therapies (surgery, radiotherapy and chemotherapy) significantly increase overall patient survival. However, as a result of breast

Key words: LncRNA CTBP1-AS; breast cancer; mir-940; cell invasion; cell migration

Corresponding author:
Geng Cuizhi, Ph.D.,
Breast Center, Fourth Hospital,
Hebei Medical University,
No. 169 of Tianshan Road,
Shijiazhuang, 050011, China
e-mail: drgengcuizhi666@163.com

0393-974X (2019)

cancer cell invasion and metastasis, the therapeutic efficacy of the above treatments is largely limited (4). Therefore, it is necessary to find the occurrence and the underlying molecular mechanisms of breast cancer cell invasion and metastasis, which might help to provide new potential therapeutic agents.

LncRNA CTBP1-AS is a long noncoding RNA, which has been reported to participate in the development of multiple cancers, such as prostate cancer (5), hepatocellular carcinoma (6), colorectal cancer (6), gastric cancer (6) and lung cancer (6). For example, researchers have found that androgen-responsive long noncoding RNA CTBP1-AS promoted the development of prostate cancer (7). LncRNA CTBP1-AS has been proved to play an important role in the regulation of cancer cell invasion and migration (6). However, to date, there are no studies reporting the relationship between LncRNA CTBP1-AS and breast cancer. Recent studies found that LncRNAs could regulate cell functions and disease development by sponging miRNAs (8). Of note, LncRNA CTBP1-AS has been reported to sponge miRNAs (9). For example, LncRNA CTBP1-AS regulated oncogenic process in osteosarcoma cells by sponging and inhibiting expressions of microRNA-485-3p (9). microRNA-940 was proved to play a crucial role in cancer development (10, 11), and miRNA-940 inhibited cell growth and migration in triple-negative breast cancer (12). Notably, our bioinformatics analysis predicted that microRNA-940 was the downstream target of LncRNA CTBP1-AS.

Taken together, it is reasonable to hypothesise that overexpressed LncRNA CTBP1-AS might promote breast cancer progression by targeting microRNA-940.

MATERIALS AND METHODS

Patients

Breast cancer patients (N = 155) who received treatment from January 2016 to January 2018 in the Affiliated Hospital of Harbin Medical University were selected. According to the histology grade, 20 of them were in G1 stage, 116 were in G2 stage and 19 were in G3 stage (Table II). The breast cancer tissue samples and adjacent normal tissues were collected from the selected patients for further analysis. The specimens were immediately stored in liquid nitrogen and stored in at -80°C. The study was approved by the ethics committee of Affiliated Hospital of Harbin Medical University. All patients had signed informed consent before surgery.

Cell culture and grouping

Human breast cancer cell lines (MCF-7, BT-549, MDA-MB-231, MDA-MB-435) and human normal breast epithelial cell line (MCF-10A) were purchased from American Type Culture Collection (ATCC) and preserved in our laboratory. The frozen cells were quickly transferred into a 37°C water bath and shaken continuously. The cells in the cryopreservation tube were transferred into 15 ml Eppendorf (EP) tube and centrifuged at 400 rpm for 5 min. After centrifugation, the supernatant was discarded immediately and the complete culture medium was next added to the tube. The cells were then cultured at 37°C in an incubator under the conditions of saturated humidity containing 5% CO_2.

Cell transfection

The LncRNA CTBP1-AS overexpressed and knock-down lentivirus vectors were designed and constructed by Sangon Biotech Corporation (Shanghai, China). LncRNA CTBP1-AS overexpressed vectors were used to transfect BT-458 cells, and LncRNA CTBP1-AS knock-down vectors were employed to transfect MDA-MB-435 cells. The Lipofectamine RNAiMAX Reagent (Invitrogen, Carlsbad, CA, USA) was used to transfect vectors into cells according to the instructions of the manufacturer. Briefly, The groups were set as follows. Down-regulation group: shRNA (transfection reagent + meaningless non-specific control sequence), shCTBP1-AS (transfection reagent and pGLV3-shCTBP1-AS); over-expression group: pGLV5 (transfection reagent + meaningless non-specific control sequence), pGLV5-CTBP1-AS (transfection reagent and pGLV5-CTBP1-AS). All chemicals, buffer, and culture mediums were purchased from Sigma, USA or Cell Signaling USA.

RNA extraction

Tissue RNA extraction: The tissue samples were evenly stirred in tissue liquid by an ultrasonic homogenizer at 4°C. Tissue suspension was incubated at

37°C for 5 min. Then 200 ml of chloroform was added to the tissue samples. After that, the tissue suspension was centrifuged for 5 min at 12,000 rpm. The supernatant was then carefully collected and transferred into a new 1.5 ml centrifugal tube, after which 250 ml of 75% alcohol was added into the tube for further experiments.

Cellular RNA extraction: The cells were cultured under the standard conditions (37°C, 5% CO_2) and collected when the confluence reached about 70-80%. After that, cells were diluted by phosphate buffer saline (PBS) and the cellular RNA was extracted by Trizol kit (Invitrogen, USA) according to the manufacturer's protocol. In brief, the single cell suspension was transferred into a completely precooled EP tube and incubated at 37°C for 5 min. Furthermore, 200 mL of chloroform was added into the cell suspension and kept at 37°C for 3 min. The supernant was then collected by centrifugation at 12,000 rpm for 30 s and incubated at -20°C for 1 h. Afterwards, ethanol (75%) was added to precipitate the total mRNA, which was dissolved by Diethyl Pyrocarbonate (DEPC) liquid and refrigerated at -80°C for further experiments.

Quantitative PCR detection

Reverse transcription of extracted RNA *in vitro* was carried out to obtain the product of complementary DNA (cDNA). Using the obtained cDNA as template, fluorescent quantitative PCR was carried out to quantify the relative expression levels of the target genes, which were normalized to the internal reference (U6 mRNA levels). Briefly, the ΔCT values were detetced by the Fluorescent Quantitative PCR instrument purchased from Thermo Fisher Scientific (USA). The gene expression levels were evaluated according to the $2^{-\Delta\Delta CT}$ method. In addition, the primers of the involved genes were designed and constructed by Sangon Biotech (Shanghai, China). The primer sequences are shown in Table I.

Cell counting Kit-8 (CCK-8) experiment

Cells were digested with trypsin to form a single cell suspension. The cell concentration was regulated to 1×10^3/ml and 100 ml was added to A 96-well cell culture plate. The remaining pore was added into the aseptic medium. The cells were collected at 24, 48, 72 and 96 h after implantation. Three replication holes were obtained from each group. Cell proliferation was evaluated by CCK-8 assay kit (Yeasen Corporation, Shanghai, China) according to the manufacturer's instructions. In brief, 20 μl of CCK-8 solution was added to each pore and incubated with cells for 2 h. Optical density (OD) value was determined by enzyme immunoassay at the end of culture. The blank cell-free control pore was taken as zero by adding only culture medium, and the experiment was repeated three times.

Cell scratch test

The cells were digested with appropriate trypsin and diluted by Dulbecco's modified eagle medium (DMEM) to the concentration of 1×10^4/ml. The cell suspension was then seeded in the 24-well plate and cultured in an incubator with humidity air containing 5% CO_2 at 37°C. The sterile micro-pipette head (10 ml) was added with a rigid scar and a word "10" in the 24-hole plate. Each scar has a hole. The scraping area was observed and scratched under inverted microscope at 0, 12 and 24 h, respectively. The scratch healing rate was calculated to evaluate the ability of cell migration. Each experiment repeated at least three times.

Detection and analysis of luciferase

The cells were counted and inoculated into the cell plate at 24 h before the transfection. When the degree of cell

Table I. *The primer sequences of qRT-PCR.*

Primer	Upstream sequence (5'-3')	Downstream sequence (5'-3')	Expanding
LncRNA	GTAAGCTTCCTACTC	GAACATCAGAGTAGGAAGCTTA	215bp
GAPDH	GCACCGTCAAGGCTGAGAA	TGGTGAAGACGCCAGTGGA	141bp
U6	CTCGCTTCGGCAGCA	AACGCTTCACGAATTTG	

fusion in the orifice plate was 50-60%, the culture medium was sucked out. After washing three times with PBS, the medium was added into the poreS at 300 mL per pore and cultured in the incubator. The transfection reagent was prepared at a ratio of 1:50 and placed at room temperature for 5 min. After that, MicroRNA (1 μl), microRNA inhibitor (1 μl) and plasmid (0.5 μg) were added to the EP tube respectively at room temperature for 5 min. The above liquids were placed in the same EP tube at room temperature for 20 min. The transfection reagent (100 μl) was added into the orifice plate to fully mix it with the culture medium in the orifice plate and put into the incubator for further culture. After 4-6 h of transfection, the transfection reagent was removed and a new medium was added to the orifice plate. Luciferase activity was detected strictly in accordance with Promega's kit. Relative luciferase activity = luciferase (R) / firefly luciferase (F).

Statistical analysis

SPSS 21.0 statistical software was used for the statistical analysis. *Chi*-squared test was used to compare the counting data in the group. T-test or variance analysis were used to compare the mean of the two groups. $P < 0.05$ was used for statistical significance.

RESULTS

Correlation of LncRNA CTBP1-AS expressions and breast cancer progression

To investigate the aberrant expression of LncRNA CTBP1-AS in clinical tissues, qRT-PCR was used to detect LncRNA CTBP1-AS expression levels in breast cancer and adjacent normal tissues. The gel electrophoresis results showed that we successfully reversely transcribed LncRNA CTBP1-AS to

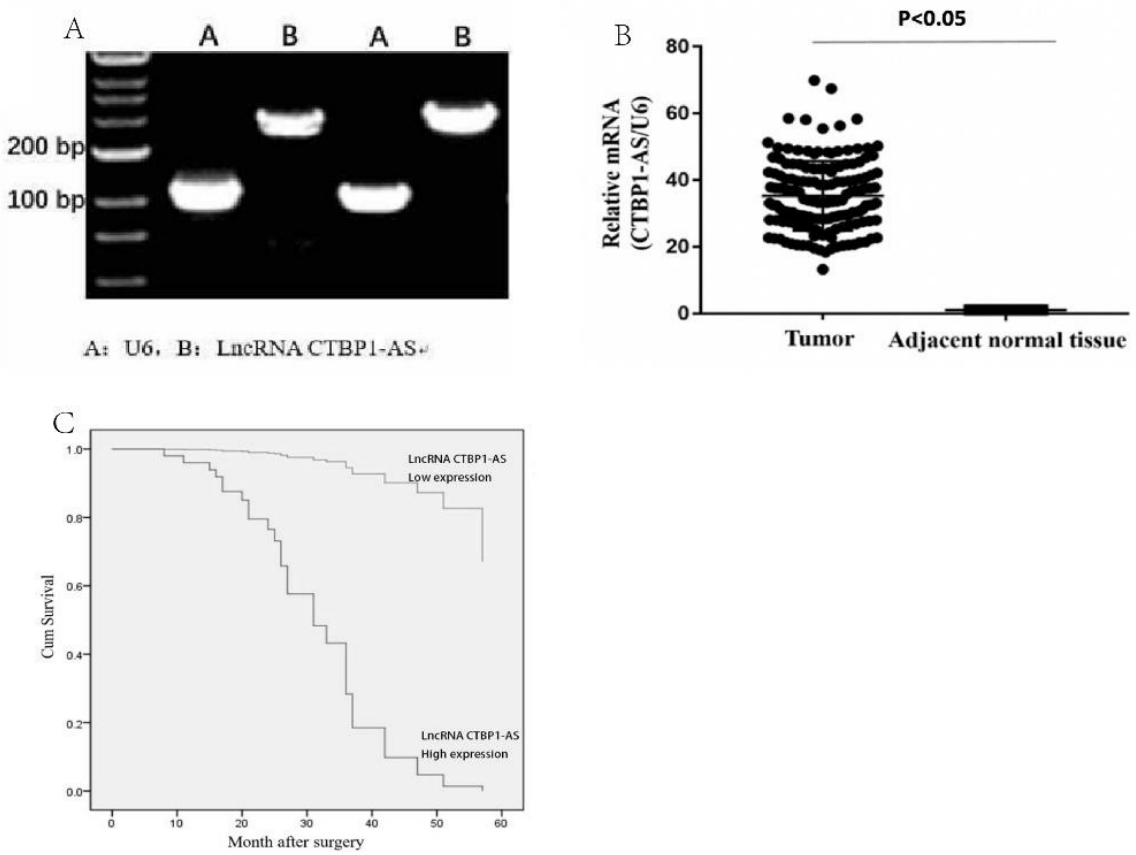

Fig. 1. LncRNA CTBP1-AS expression levels in clinical tissues was detected by qRT-PCR. ***A)*** *Gel electrophoresis image of U6 and LncRNA CTBP1-AS.* ***B)*** *Relative expression of LncRNA CTBP1-AS in 155 Breast cancer tissues and matched adjacent normal tissues. *P< 0.05, compared to controls.* ***C)*** *LncRNA CTBP1-AS expression and survival analysis of breast cancer patients.*

Table II. *Relationship between the LncRNA CTBP1-AS and clinical characteristic of breast cancer patients*

Characteristics	Number (%)	Expression		χ^2	P
		Low(23)	High(132)		
Age(years)					
<60	110/155(70.97)	14	96	0.823	0.364
≥61	45/155 (29.03)	9	36		
Tumor size					
pT1	24/155 (15.48)	5	19		
pT2	103/155(66.45)	6	97	21.771	0.000**
pT3/pT4	28/155(18.07)	12	16		
Histology grade					
G1	20/155 (48.8)	5	15		
G2	116/155(51.2)	10	106	14.332	0.000**
G3	19/155(48.8)	8	11		
Lymph node status					
pN0	83/155 (56.1)	15	68	1.478	0.224
pN1-3	72/155(44.0)	8	64		
ER expression					
Positive	98/155(75.6)	12	86	1.419	0.234
Negative	57/155(24.4)	11	46		
PR expression					
Positive	88/155(75.6)	14	74	0.185	0.667
Negative	67/155(24.4)	9	58		
Ki67 expression					
≤14%	93/155(75.6)	9	84	4.901	0.027*
>15%	62/155(24.4)	14	48		
Her-2 expression					
Positive	101/155(75.6)	6	95	18.164	0.000**
Negative	54/155(24.4)	17	37		

complementary DNA (cDNA) (Fig. 1A). Further qRT-PCR results showed that LncRNA CTBP1-AS was aberrantly overexpressed in breast cancer tissues compared to the adjacent normal tissues ($P < 0.05$) (Fig. 1B). Further analysis of the expression of LncRNA CTBP1-AS on the prognosis of breast cancer patients showed that the prognosis of breast cancer patients was related with the expression of LncRNA CTBP1-AS ($P < 0.01$). Specifically, LncRNA CTBP1-AS expression levels were negatively correlated with the prognosis of breast cancer patients ($P < 0.01$) (Fig. 1C).

Furthermore, statistical analysis of the expression of LncRNA CTBP1-AS and clinical indicators showed that the expression level of LncRNA CTBP1-AS was closely related to tumor size (p=0.000), histological grade (p=0.000), Ki67 expression (p=0.027) and Her-2 expression (p=0.000) (Table II).

Expression of LncRNA CTBP1-AS in breast cancer cell lines

We next explored the expression levels of LncRNA CTBP1-AS in breast cancer cell lines (MCF-7, BT-549, MDA-MB-231, MDA-MB-435) and human normal breast epithelial cell line (MCF-10A). The qRT-PCR results showed that LncRNA CTBP1-AS was significantly overexpressed in breast cancer cell lines in contrast with MCF-10A cells ($P<0.05$) (Fig. 2), which was in accordance with our clinical results and indicated that LncRNA CTBP1-AS may play an oncogenic role in the development of breast cancer.

The effects of LncRNA CTBP1-AS on breast cancer cell proliferative ability

Since LncRNA CTBP1-AS levels were lowest in BT-549 cells and highest in MDA-MB-435 cells compared to other breast cancer cells (MCF-7 and MDA-MB-231) (Fig. 2), we next explored the effects of LncRNA CTBP1-AS on breast cancer cell proliferation by transfecting BT-549 cells with LncRNA CTBP1-AS overexpressed and MDA-MB-435 cells with knock-down vectors, respectively. The colony formation assay results showed that knock-down of LncRNA CTBP1-AS inhibited MDA-MB-435 cell proliferation ($P<0.05$) (Fig. 3A). On the contrary, overexpressed LncRNA CTBP1-AS promoted BT-549 cell proliferation ($P<0.05$) (Fig.

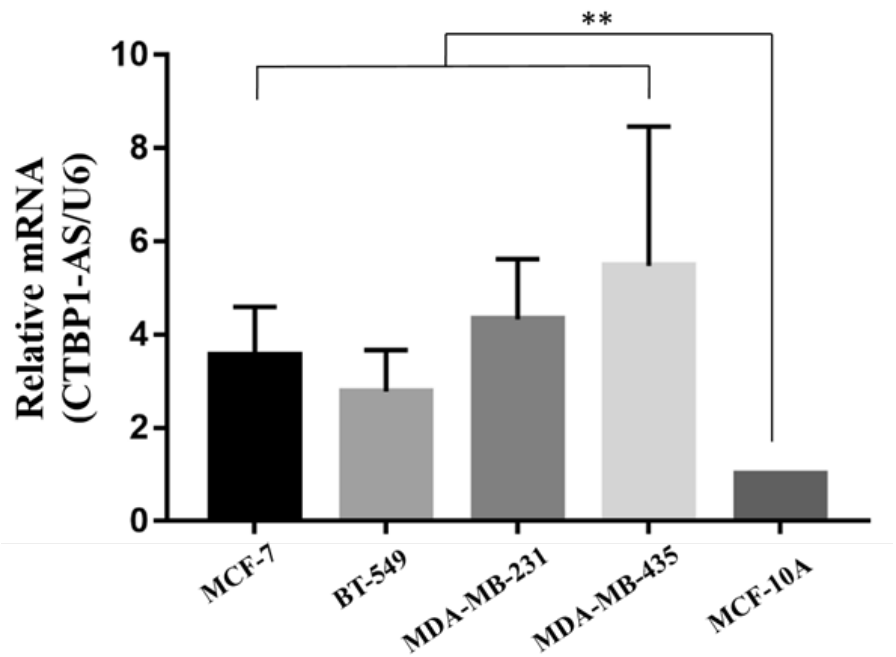

Fig. 2. *Relative expression of LncRNA CTBP1-AS in 31 breast cancer cell lines. **P < 0.01 compared to controls.*

3B). These results suggest that LncRNA CTBP1-AS increased breast cancer cells proliferation abilities.

Influences of LncRNA CTBP1-AS on breast cancer cells apoptosis

Flow cytometry was used to detect the effects of CTBP1-AS expression on breast cancer cell apoptosis ratio. The results showed that knock-down of CTBP1-AS increased MDA-MB-435 apoptosis ratio ($P < 0.05$) (Fig. 4A), while overexpressed CTBP1-AS significantly decreased BT-549 cell apoptosis ratio compared to the control group ($P < 0.05$) (Fig. 4B), which indicated that CTBP1-AS promoted breast cancer cells apoptosis.

Wound healing scratch assay was performed to evaluate cell migration

The wound healing scratch assay results showed that the migration ability of MDA-MB-435 cells was significantly reduced by down-regulation of CTBP1-AS compared with the control group ($P < 0.05$). Similarly, overexpression of CTBP1-AS increased the healing ability of BT-459 cells compared with the control group ($P < 0.05$) (Fig. 5). The results indicated that CTBP1-AS increased breast cancer cells migration ability.

Breast cancer cells' invasive abilities were influenced by CTBP1-AS

Transwell matrigel assay results showed that the invasive ability of MDA-MB-435 cell line was significantly decreased by knocking down CTBP1-AS compared to the control group ($P < 0.05$). Furthermore, overexpression of CTBP1-AS increased the invasive ability of BT-549 cells compared with the control group ($P < 0.05$) (Fig.6).

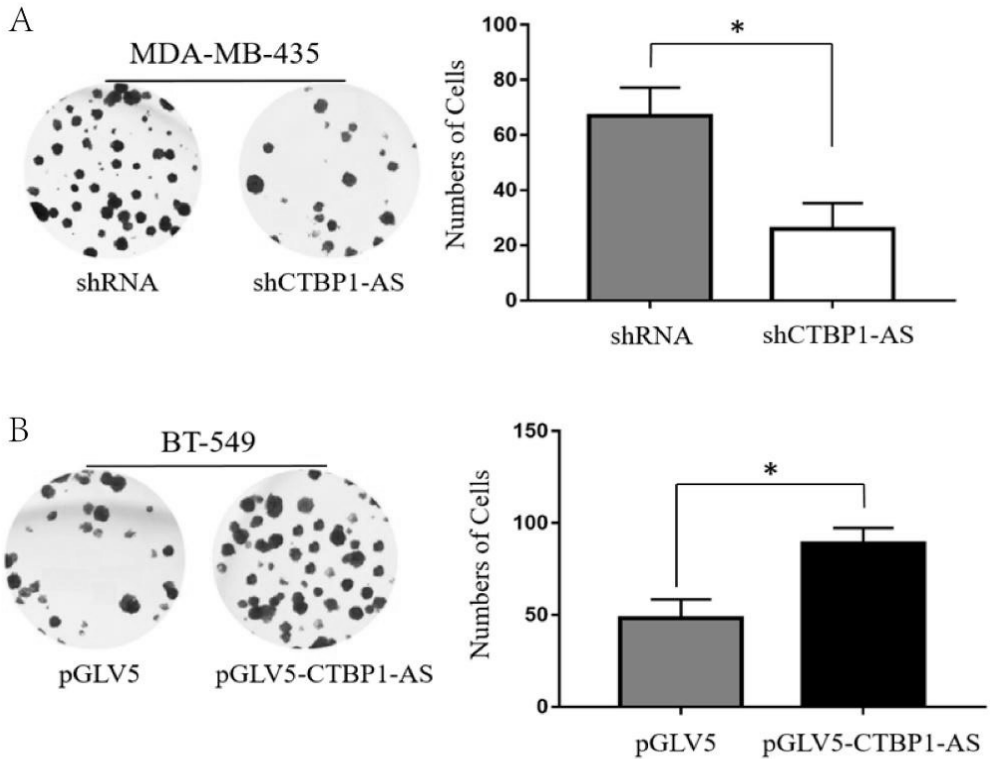

Fig. 3. *Colony formation assays for breast cancer cells downregulated or overexpressed CTBP1-AS. (left) Microphotographs of colonies; (right) the mean of the colony numbers on triplicate plates from a representative experiment (conducted thrice); bars, SD.* ***A****) shRNA: MDA-MB-45 cells transfected with scrambled control shRNA; shCTBP1-AS: MDA-MB-45 cells transfected with shRNA#3;* ***B****) pGLV5:BT-549 cells transfected with scrambled pGLV5;PGLV5-CTBP1-AS:BT-549 cells transfected with pGLV5#3. *P<0.05 compared to controls. *P<0.05, as determined using Student's t-test.*

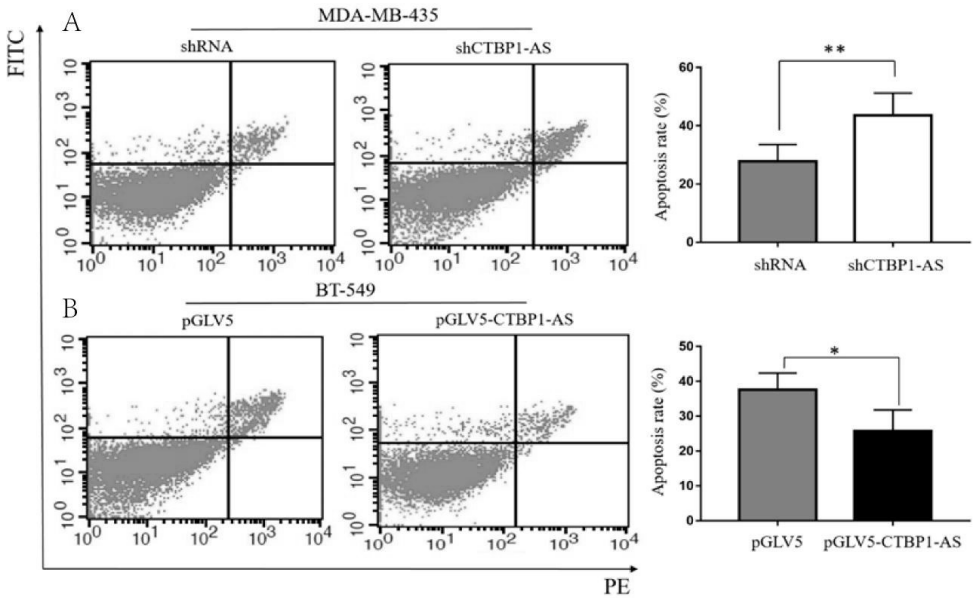

Fig. 4. *CTBP1-AS down-regulation or up-expression affected on apoptosis of breast cancer cells with flow cytometry. bars, SD.* ***A)*** *shRNA: MDA-MB-45 cells transfected with scrambled control shRNA; shCTBP1-AS: MDA-MB-45 cells transfected with shRNA#3;* ***B)*** *pGLV5:BT-549 cells transfected with scrambled pGLV5;PGLV5-CTBP1-AS:BT-549 cells transfected with pGLV5#3. *P < 0.05 compared to controls. *P<0.05, as determined using Student's t-test.*

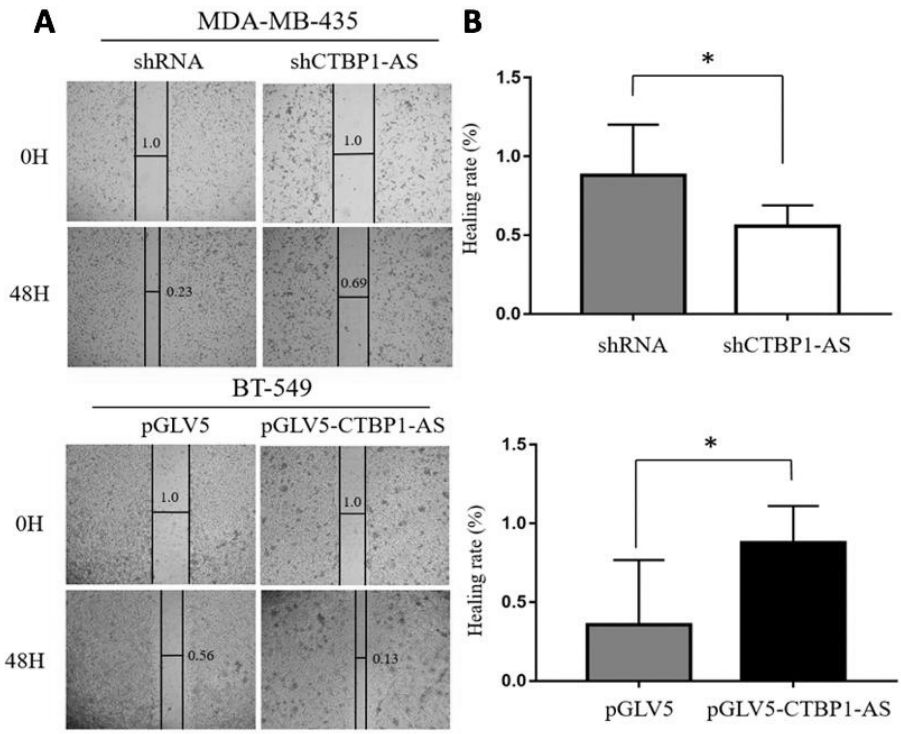

Fig. 5. *Wound-healing assay tested breast cancer cell migration after down- or up-regulation of CTBP1-AS.* ***A)*** *photography (×10).* ***B)*** *healing rate in different time points. shRNA: MDA-MB-45 cells transfected with scrambled control shRNA; shCTBP1-AS: MDA-MB-45 cells transfected with shRNA#3;pGLV5:BT-549 cells transfected with scrambled pGLV5; PGLV5-CTBP1-AS:BT-549 cells transfected with pGLV5#3 bars, SD. *P<0.05compared to controls.*

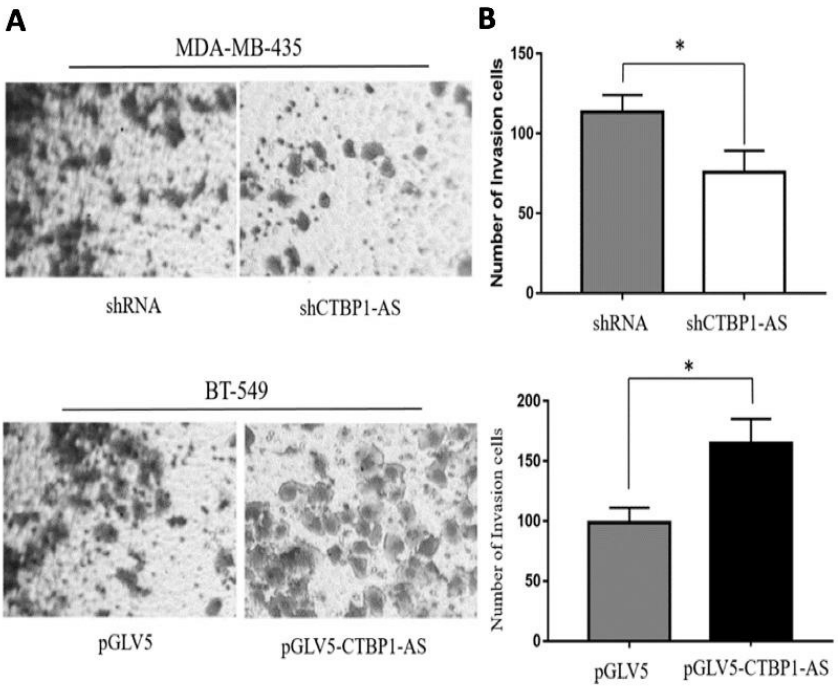

Fig. 6. *Transwell matrigel assay tested H1299 invasion after up-regulation of LncRNA CTBP1-AS.* ***A****) photography (×10).* ***B****) cells number through the matrigel membrance. shRNA: MDA-MB-45 cells transfected with scrambled control shRNA; shCTBP1-AS: MDA-MB-45 cells transfected with shRNA#3;pGLV5:BT-549 cells transfected with scrambled pGLV5; PGLV5-CTBP1-AS:BT-549 cells transfected with pGLV5#3 *P<0.05, compared to controls.*

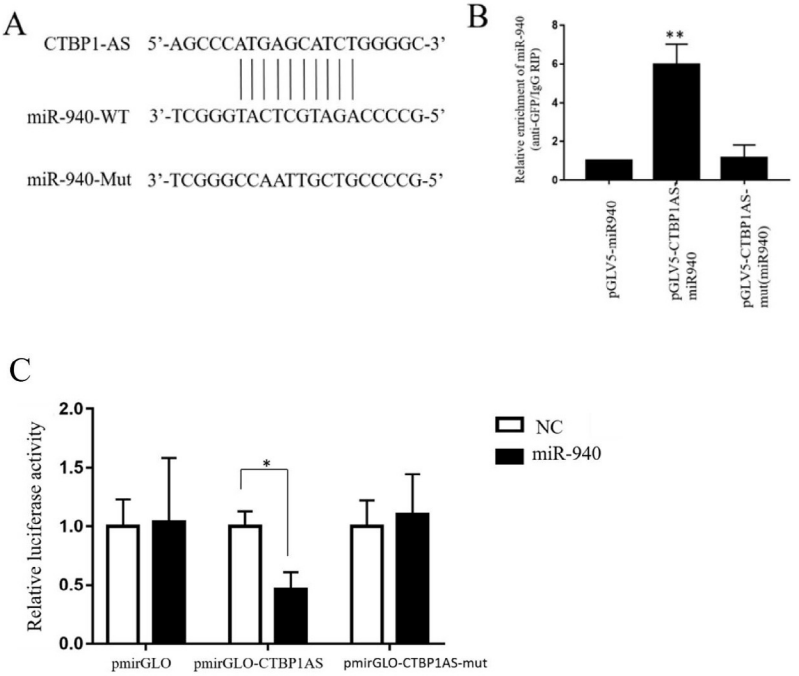

Fig. 7. *Target gene prediction and RNA immunoprecipitation.* ***A****) the downstream target gene of LncRNA CTBP1-AS was miR-940.* ***B****) cells transfected with pGLV5-CTBP1AS-micro940 were highly enriched with microRNA-940 comparing with that of blank plasmid and binding site mutant pGLV5-CTBP1AS-mut.* ***C****) Luciferase reporter assay indicated that overexpression of LncRNA CTBP1-AS repressed the luciferase activity in H1299 cells transfected with WT-MIR-940-3'-UTR. bars, SD. *P<0.05 compared to controls.*

These results suggest that breast cancer cell invasion could be promoted by CTBP1-AS.

microRNA-940 was the downstream target of LncRNA CTBP1

The bioinformatics analysis (StarBASE and DIANA TOOLS) predicted that microRNA-940 was the downstream target of LncRNA CTBP1-AS (Fig. 7A). RNA immunoprecipitation showed that the cells transfected with pGLV5-CTBP1AS-micro940 were highly enriched with microRNA-940 ($P < 0.05$) (Fig.7B). However, the concentration of microRNA-940 in the transfected blank plasmid pGLV5-micro940 and the binding site mutant pGLV5-CTBP1AS-mut (micro940) was lower (Fig. 7B). In addition, the dual luciferase reporter gene experiment was used to verify the relationship between microRNA-940 and CTBP1-AS. The results showed that overexpression of microRNA-940 resulted in a significant decrease in luciferase activity in pmirGLO-CTBP1AS transfected cells ($P<0.05$). However, there was no significant effect on luciferase activity of transfected mutant vectors ($P > 0.05$) (Fig.7C), which proved that microRNA-940 was a downstream target gene of LncRNA CTBP1-AS.

DISCUSSION

Related studies have found that human transcriptome contains not only about 21,000 codable proteins but also 10,000-32,000 LncRNAs, 11,000 pseudogenes and 9,000 microRNAs (13). According to the molecular length of non-coding RNA, it can be divided into two categories (14): i) Short-chain non-coding RNAs less than 200 nt, such as microRNAs involved in post-transcriptional RNA degradation or translation inhibition, and tRNA (transfer RNA, transporting RNA) involved in RNA translation, etc. ii) More than 200 nt of LncRNA has been found to be involved in many biological processes, such as chromatin modification, transcriptional regulation, microRNA function regulation, RNA stability and protein function regulation. LncRNA plays an important role as a new potential key regulator of normal cell development, and abnormal expression of LncRNA may play a key role in tumorigenesis (15). Many LncRNAs play an important role in the pathogenesis of breast cancer and may be used as diagnostic markers and therapeutic targets. Therefore, studying the function of microRNA will lead to a better understanding of the occurrence of breast cancer and open the door for better management of effective diagnosis and treatment strategies. Because of the high activity of ribonuclease, RNA is easily degraded outside the cell. At present, the body fluids of tumors in many patients include blood, serum, plasma, urine, lymph nodes and gastric juice (16-20). Askarian detected high expression of ZFAS1 in mammary ducts of mice, but low expression in breast tumors. ZFAS1 was involved in regulating acinar development and epithelial cell differentiation in mammary glands (21). Zhang found that the serum DNA content of HOTAIR in breast cancer patients was 2.5 times higher than that in normal patients, which could become one of the diagnostic indicators of breast cancer (22). Takayama found that CTBP1-AS was mainly localized in the nucleus and its expression was up-regulated in prostate cancer (7). In addition, CTBP1-AS promoted the growth of hormone-dependent and castration-resistant tumors. It could directly inhibit CTBP1 expression by recruiting RNA-binding transcription inhibitor PSF and histone deacetylase (7). The expression of LncRNA CTBP1-AS in 155 breast cancer tissues was significantly higher than that in adjacent tissues. LncRNA CTBP1-AS was closely related to tumor size, Ki67 expression and Her-2 expression. Meanwhile, the expression of LncRNA CTBP1-AS in breast cancer cell lines was significantly higher than that in normal breast epithelial cell lines.

One of the main characteristics of malignant tumors is distal metastasis, which often indicates poor prognosis and therapeutic effect. Zhang found that down-regulation of LncRNA HOTAIR expression in breast cancer cells could reduce cell apoptosis and invasion by destroying epithelial-mesenchymal transformation (22). Askarian-Amiri found that knocking out LncRNA ZFAS1 in breast ductal cancer cells inhibited cell migration (21). In the present study, we demonstrated that LncRNA CTBP1-AS can accelerate the movement of breast cancer cells, increase the invasive ability and

promote the occurrence of distal invasion in both vertical and horizontal directions.

LncRNA can function through transcriptional or post-transcriptional mechanisms. Franco found that there were complex interactions among different types of RNA, including protein-coding RNA and pseudogenes, LncRNA and circRNA, which had no protein-coding function. They contain some common binding sites of microRNAs, which can competently bind to common microRNAs with cancer-promoting or anti-cancer effects through microRNAs response elements (MREs), thereby eliminating or reducing the inhibition of microRNAs on other target genes, and playing a role in inhibiting or promoting cancer progression (23). The discovery of competitive endogenous RNA (ceRNA), including LncRNA, cyclic RNA and pseudogenes, has revealed a completely new post transcriptional regulation. It reveals the complexity of ncRNA regulation in various important non-coding RNA species in cancer (24, 25). Zadeh found that the up-regulation of microRNA-21 in primary breast cancer samples was associated with advanced clinical stage, lymph node metastasis and poor prognosis (26). In addition, microRNA-21 has been shown to inhibit many tumor suppressor genes, including TPM1, p53, and PDCD4 (27, 28). Su found that the expression of microRNA-205 in breast cancer was significantly lower than that in normal tissues, and inhibited cell proliferation and invasion by targeting HER3 and VEGF-A directly. It also shows that EMT processes are negatively regulated by targeting ZEB1 and ZEB2 (29). Liu W found that the expression of microRNA-940 in breast cancer patients was significantly lower than that in adjacent tissues, which was closely related to lymph node metastasis and TNM staging (30). It has been reported that the expression of microRNA-940 is closely related to the prognosis of breast cancer patients and is an independent prognostic factor for breast cancer (30).

In this study, we found that LncRNA CTBP1-AS can recognize the 3'-UTR characteristic target sequence of microRNA-940 through luciferase activity detection, which proved that microRNA CTBP1-AS was the target gene of LncRNA CTBP1-AS. In addition, qRT-PCR and other experiments showed that LncRNA CTBP1-AS could negatively regulate the expression of microRNA-940 in breast cancer tissues and cells. Finally, we constructed a plasmid that overexpressed microRNA-940. It was found that the overexpression plasmid of miR-940 partially antagonized the effects of LncRNA CTBP1-AS on the proliferation, migration and invasion of lung cancer cell lines. Our results confirmed that the mechanism of action of LncRNA CTBP1-AS in breast cancer cells is to inhibit the proliferation, migration and invasion of cancer cells by directly inhibiting the expression of the target gene microRNA-940, which could induce apoptosis.

To sum up, we found that the expression of LncRNA CTBP1-AS in breast cancer tissues and cells was significantly up-regulated, which was related to the size of tumors and prognosis of patients. At the cellular level, we verified that LncRNA CTBP1-AS regulates the proliferation and invasiveness of cancer cells by targeting the expression of microRNA-940 which showed that it participates in the occurrence and development of breast cancer, and may provide new ideas and molecular targets for clinical diagnosis and treatment.

REFERENCES

1. Merino Bonilla JA, Torres Tabanera M, Ros Mendoza LH. Breast cancer in the 21st century: from early detection to new therapies. Radiologia 2017; 59(5):368-79.
2. Biehler-Gomez L, Giordano G, Cattaneo C. The appearance of breast cancer metastases on dry bone: Implications for forensic anthropology. J Forensic Leg Med 2019; 61:5-12.
3. Montagna G, Anderson D, Bochenek-Cibor J, et al. How to become a breast cancer specialist in 2018: The point of view of the second cohort of the Certificate of Competence in Breast Cancer. Breast 2019; 43:18-21.
4. Kang KH, Hwan SK, Kyubo K, et al. Effect of time interval between breast-conserving surgery and radiation therapy on outcomes of node-positive breast cancer patients treated with adjuvant doxorubicin/ cyclophosphamide followed by taxane. Cancer Res Treat 2016; 48(2):483-90.

5. Liu Z, Hao C, Song D, Zhang N, Bao H, Qu Q. Androgen receptor coregulator CTBP1-AS is associated with polycystic ovary syndrome in Chinese somen: A preliminary study. Reprod Sci 2015; 22(7):829-37.
6. Li J, Li Z, Zheng W, Li X, Wang Z, Cui Y, Jiang X. LncRNA-ATB: An indispensable cancer-related long noncoding RNA. Cell Prolif 2017; 50(6).
7. Takayama K, Horie-Inoue K, Katayama S, et al. Androgen-responsive long noncoding RNA CTBP1-AS promotes prostate cancer. EMBO J 2013; 32(12):1665-80.
8. Paraskevopoulou MD, Hatzigeorgiou AG. Hatzigeorgiou, Analyzing MiRNA-LncRNA Interactions. Methods Mol Biol 2016; 1402:271-86.
9. Du K, Zhang X, Lou Z,et al. MicroRNA485-3p negatively regulates the transcriptional co-repressor CtBP1 to control the oncogenic process in osteosarcoma cells. Int J Biol Sci 2018; 14(11):1445-56.
10. Gu GM, Zhan YY, Abuduwaili K, Wang XL, Li XQ, Zhu HG, Liu CL. MiR-940 inhibits the progression of NSCLC by targeting FAM83F. Eur Rev Med Pharmacol Sci 2018; 22(18):5964-71.
11. Li P, Xiao Z, Luo J, Zhang Y, Lin L. MiR-139-5p, miR-940 and miR-193a-5p inhibit the growth of hepatocellular carcinoma by targeting SPOCK1. J Cell Mol Med 2019; 23(4):2475-88.
12. Hou L, Chen M, Yang H, et al. MiR-940 inhibited cell growth and migration in triple-negative breast cancer. Med Sci Monit 2016; 22:3666-72.
13. Bhan A, Soleimani M, Mandal SS. Long noncoding RNA and cancer: a new paradigm. Cancer Res 2017; 77(15):3965-81.
14. Soudyab M, Iranpour M, Ghafouri-Fard S. The role of long non-coding RNAs in breast cancer. Arch Iran Med 2016; 19(7):508-17.
15. Ji P, Diederichs S, Wang W, et al. MALAT-1, a novel noncoding RNA, and thymosin beta4 predict metastasis and survival in early-stage non-small cell lung cancer. Oncogene 2003; 22(39):8031-41.
16. Li J, Wang Y, Yu J, Dong R, Qiu H. A high level of circulating HOTAIR is associated with progression and poor prognosis of cervical cancer. Tumour Biol 2015; 36(3):1661-5.
17. Crea, F, Watahiki A, Quagliata L, et al. Identification of a long non-coding RNA as a novel biomarker and potential therapeutic target for metastatic prostate cancer. Oncotarget 2014; 5(3):764-74.
18. Wang XS, Zhang Z, Wang HC, et al. Rapid identification of UCA1 as a very sensitive and specific unique marker for human bladder carcinoma. Clin Cancer Res 2006; 12(16):4851-58.
19. Melo CP, Campos CB, Rodrigues Jde O, et al. Long non-coding RNAs: biomarkers for acute leukaemia subtypes. Br J Haematol 2016; 173(2):318-20.
20. Zheng Q, Wu F, Dai WY, et al. Aberrant expression of UCA1 in gastric cancer and its clinical significance. Clin Transl Oncol 2015; 17(8):640-46.
21. Askarian-Amiri ME, Crawford J, French JD, et al. SNORD-host RNA Zfas1 is a regulator of mammary development and a potential marker for breast cancer. RNA 2011; 17(5):878-91.
22. Zhang L, Song X, Wang X, et al. Circulating DNA of HOTAIR in serum is a novel biomarker for breast cancer. Breast Cancer Res Treat 2015; 152(1):199-208.
23. Franco-Zorrilla JM, Valli A, Todesco M, et al. Target mimicry provides a new mechanism for regulation of microRNA activity. Nat Genet 2007; 39(8):1033-7.
24. Thomson DW, Dinger ME. Endogenous microRNA sponges: evidence and controversy. Nat Rev Genet 2016; 17(5):272-83.
25. Calin GA, Dumitru CD, Shimizu M, et al. Frequent deletions and down-regulation of micro- RNA genes miR15 and miR16 at 13q14 in chronic lymphocytic leukemia. Proc Natl Acad Sci U S A 2002; 99(24):15524-29.
26. Zadeh MM, Ranji N, Motamed N. Deregulation of miR-21 and miR-155 and their putative targets after silibinin treatment in T47D breast cancer cells. Iran J Basic Med Sci 2015; 18(12):1209-14.
27. Yang C, Wang G, Yang J, Wang L. Long noncoding RNA NBAT1 negatively modulates growth and metastasis of osteosarcoma cells through suppression of miR-21. Am J Cancer Res 2017; 7(10):2009-19.
28. Wang Z, Yao W, Li K, Zheng N, Zheng C, Zhao X, Zheng. Reduction of miR-21 induces SK-N-SH cell apoptosis and inhibits proliferation via PTEN/PDCD4. Oncol Lett 2017; 13(6):4727-33.
29. Su CM, Lee WH, Wu AT, Lin YK, Wang LS, Wu CH, Yeh CT. Pterostilbene inhibits triple-negative breast cancer metastasis via inducing microRNA-205 expression and negatively modulates epithelial-

to-mesenchymal transition. J Nutr Biochem 2015; 26(6):675-85.
30. Liu W, Xu Y, Guan H, Meng H. Clinical potential of miR-940 as a diagnostic and prognostic biomarker in breast cancer patients. Cancer Biomark 2018; 22(3):487-93.

A 10-YEAR RETROSPECTIVE COMPARATIVE HUMAN STUDY ON SCREW-RETAINED *VERSUS* CEMENTED DENTAL IMPLANT ABUTMENTS

B. SINJARI, G. D'ADDAZIO, T. TRAINI, G. VARVARA, A. SCARANO, G. MURMURA and S. CAPUTI

Department of Medical Oral and Biotechnological Sciences, University 'G. d'Annunzio' of Chieti–Pescara, Chieti, Italy

Received January 29, 2019 – Accepted April 1, 2019

The aim of this 10-year retrospective study was to evaluate the long-term reliability, survival rate and mechanical and biological complications of single-crown implant rehabilitations with two different types of fixture-abutment connections: screw-retained abutments (SRAs) with internal hexagonal connection, and cemented retained abutments (CRAs). A total of 300 single implant-supported crowns were analysed, which had been inserted between 2004 and 2007. Patients were classified according to two groups: the SRA group (n = 150) and the CRA group (n = 150). The primary outcome was marginal bone loss (MBL) on peri-apical radiographs. Bleeding on probing (BOP) and probing depth (PD) were also evaluated. Moreover, prosthetic complications were recorded. Analysis of variance (ANOVA) was used to evaluate the differences between the groups. The overall implant failure rate was 4.2%. The overall positive BOP index was 81.9% of the sites under investigation, as 83.4% for SRA and 80.4% for CRA. Moreover, >5 mm PD demonstrated a rate of 21.0% for CRA, and 13.8% for SRA. The primary outcome of mean MBL was 2.09±1.07 mm for SRA and 1.54±1.20 mm for CRA. Analysis of variance of MBL showed statistical significance for the difference between these two groups (P <0.001). For the mechanical aspects, an overall 12.5% of complications occurred. No implant or abutment fractures were recorded. Although complications occurred, the results from this 10-year retrospective study show that these two methods have positive long-term follow-up. With MBL significantly greater for the SRA group than the CRA group, the clinical use of CRA is encouraged in terms of the lower bone resorption rate.

Nowadays, dental implants represent an efficient option for replacement and restoration of missing teeth in a safe and predictable way. This means that, overall, they can provide great benefits for the patient quality of life (1). A large number of studies have indicated early implant success rates of 94.6%, and an overall mean success rate after >10 years of function of 89.7% (1, 2).

On the other hand, failures and complications of implant-supported rehabilitations have been widely described (2). These can be either mechanical or biological, and can occur during the surgical stages or during function. Specifically, the early complications can include surgical trauma, intra-operative infection or contamination, loss of primary stability, and fibro-integration. The later complications have been described as marginal bone loss (MBL) around the implants, peri-implant infection, prosthetic overload,

Key words: peri-implant bone resorption; fixture-abutment connection; long-term follow-up; implant survival rate; screw retained abutment; cemented retained abutment

Corresponding Author:
Dr Bruna Sinjari,
Department of Medical Oral and Biotechnological Sciences,
University 'G. d'Annunzio' of Chieti–Pescara,
Via dei Vestini, 31 - 66100 Chieti (CH), Italy
Tel.: +39 392 7471479 - Fax: +39 0871 3554070
e-mail: b.sinjari@unich.it

0393-974X (2019)

occlusal changes and other mechanical complications related to these implant prosthetic restorations (2, 3). Despite the changes that have occurred in implantology over the years, MBL appears to occur in the peri-implant area following implant placement and loading, and as such, it appears to be one of the most important factors for implant survival (2-4). Indeed, in 1986, Albrektsson et al. (3) studied and included MBL in the success criteria for long-term osseo-integration of implants. They indicated that a MBL of up to 1 mm in the first year and successive annual mean MBL of 0.2 mm during the following years can be considered as physiological (3, 4). Several studies have investigated the possibility of reducing MBL rates over the years. Indeed, MBL appears to be influenced not only by mechanical factors, but also by cellular and biological ones. (3) Different implant surface treatments have been developed to improve osteoblast and fibroblast adhesion on the implant surface (5). On the contrary, however, these surfaces should not allow bacteria adhesion, to diminish their peri-implant tissue colonization (6). Moreover, a previous human study showed that the risk of MBL can be decreased by use of chlorhexidine gel inside the connection, which significantly reduces MBL during the first year (7). On the other hand, mechanical and technical risks have an important role in implant dentistry, as they can lead to increases in interventions and increased repair rates, thus also influencing chair time, economical costs, and even patient quality of life (8).

These risk rates might also be influenced by the material used for a restoration (9). The type of implant abutment connection and system stability have key roles in the long-term implant success rate. Therefore, over the years, different implant-abutment connections have been developed to further improve performance, clinical simplicity and long-term outcomes of implant therapies (8-12). The transition from one-piece to biphasic implants has simplified procedures, although on the other hand, each of the connections provide advantages and disadvantages in clinical use (13). Regarding this, screw loosening and abutment fractures are among the major complications of biphasic implant supported rehabilitations (10). At the same time, the presence of two different components can lead to development of a microgap on the fixture–abutment interface (13, 14). The presence of such microgaps, that have been described as microscopic spaces between an implant and its corresponding abutment, can also allow bacterial microinfiltration and micromovement and component damage, which will all influence the long-term success rates (14). Several studies have been looking for different solutions to minimise these complications (14, 15). Indeed, for a number of years, the more commonly used types of connections were external and internal hexagon or octagon connections (8, 16).

The external hexagon connection was the first solution to be developed and studied (17). Although, it was simple to use and was considered a valid solution for a long time, higher screws loosening rates and higher marginal bone loss were reported, compared to other solutions (17). Subsequently, the internal hexagon connection was developed to improve the mechanical coupling and system stability (16). This solution reduced the incidence of microgaps, and also demonstrated better distribution of mechanical stress on the implant surface (17)

However, more recently, different types of internal connections have been developed, such as cone morse, cemented and hybrid. Short-term studies have shown excellent results for the seals provided by cemented connections and morse-type connections, compared to classic internal hexagon connections (8, 14, 15). In an *in-vitro* study, Assenza et al. (15) demonstrated that cemented connections can provide total sealing of the connections, to ensure reduction in the incidence of microgaps between the two components, and thus better control of bacterial leakage. On the other hand, incorrect removal of cement residues can cause peri-implant inflammatory reactions (18). Hexagonal internal connections, however, have shown improved follow-up, with very satisfactory results in terms of reliability and survival rates (16). On this basis, it is important to determine the long-term reliability of alternative solutions to hexagonal connections.

Thus, although, different types of implant abutment connections have been developed, there remains a lack of knowledge as to which of these might have better long-term follow-up. Therefore, the aim of this 10-year retrospective study was to evaluate the long-term follow-up for mechanical and biological

complications of single-crown implant rehabilitations with two different types of connections: screw-retained abutments (SRAs) with internal hexagonal connection, and cemented retained abutments (CRAs).

MATERIALS AND METHODS

A total of 300 single implant supported restorations were divided according to the two different types of connections. The 300 patients selected for the present study received single implant supported restorations between 2004 and 2007 in the Department of Medical, Oral and Biotechnological Sciences, University of Chieti–Pescara (Italy).

The patients enrolled (i.e., samples) were divided into two groups based on the implant-abutment connection type: the SRA group, with an internal hexagon connection with SRA (LEADER Italia s.r.l., Cinisello Balsamo, MI, Italy), and the CRA group, with an internal CRA (Bone System, Milan, Italy). No selection was made regarding the surface treatments. The concept of platform switching was not applied to these two groups to avoid variables related to this. Thus, the fixtures and abutments were of the same size (i.e., platform matched). In the CRA group , the system used provided a collar positioned inside the fixture, with a press-to-fit system. A titanium full-milled abutment without a retention screw was cemented onto the collar. Both of the groups had single prosthetic crowns cemented onto the corresponding implant abutments.

At 10 years of follow-up, the patients were called for radiographic and clinical evaluation. All of the data regarding the patients were recorded, including age, sex, medical condition, smoking and parafunctions. Also, data on implant, peri-implant tissues, prosthetic information and conditions of the periodontal hygiene control were also collected. The patients for this retrospective study were chosen following inclusion and exclusion criteria previously described (4, 19). Moreover, the patients with periodontitis and severe parafunctions were excluded; they were rehabilitated with a single implant-supported rehabilitation. All of the patients signed an informed written consent and received information on the risks of implant therapy.

At the time of insertion, all of the selected implants were inserted by experienced surgeons under standard conditions concerning bone quality, density and residual bone, according to the Cawood and Owell (1988) classification (20). No guided bone regeneration or post-extraction techniques were performed. All of the 300 implants were submerged and positioned at bone level. The prosthetic phases were performed according to best practice protocols, and the abutments were tightened or cemented according to the manufacturer's indications (16). Moreover, the cementation system has been described in detail in a previous study (21). All of the implants had follow-up of at least 10 years. The patients underwent the follow-up visit, during which they were evaluated using clinical and radiological examinations. The implant success rates were evaluated according to the clinical and radiographic criteria of Misch (2): (i) absence of implant mobility; (i) absence of pain; (iii) absence of recurrent peri-implant infection; and (iv) radiographic crestal bone loss, all of which were recorded using specific Case Report Forms.

The following periodontal parameters were considered and evaluated: bleeding on probing (BOP), probing depth (PD), and regular annual control visits over the years. A cut-off of 5 mm was taken in terms of the PD, which was considered as a negative outcome (i.e., PD >5 mm). The highest values were recorded on the specific Case Report Forms. PD was determined using a periodontal probe (PCP15; North Carolina, USA), with all effort to maintain the recommended pressure strength on 25 g, with the probe placed parallel to the major axis of the implant, and with the analysis of the 4-point probing. The BOP was analysed 15 s later.

To compare radiographic modifications of the peri-implant marginal bone, intra-oral radiography was carried out as a routine procedure, using the parallel-ray technique, and immediately after implant insertion. To measure the crestal bone remodelling, as previously described (4), an intra-oral analogic radiograph was taken and processed using digital software, as the method was considered to be high precision for these scientific evaluations, with a precision of <0.1 mm. The mean distance between the mesial and distal regions was used as the primary outcome for this study. In every radiograph, the distance from the top of the fixture and the mesial and distal crestal bone levels was measured to the first bone to implant contact. The mean distance between the mesial and distal regions was calculated for the data analysis. Also, these were calibrated with the known implant lengths and diameters, to guarantee correct measurements, even if an implant

Table I. *Health scale for dental implants according to the Misch classification (3).*

Implant quality scale group	Clinical condition
I. Success (optimum health)	(a) No pain or tenderness upon function
	(b) Zero mobility
	(c) 2 mm radiographic bone loss from initial surgery
	(d) No exudates history
II. Satisfactory survival	(a) No pain on function
	(b) Zero mobility
	(c) 2–4 mm radiographic bone loss
	(d) No exudates history
III. Compromised survival	(a) May have sensitivity on function
	(b) No mobility
	(c) Radiographic bone loss 4 mm (<1/2 of implant body)
	(d) Probing depth 7 mm
	(e) May have exudates history
IV. Failure	Any of the following:
(clinical or absolute failure)	(a) Pain on function
	(b) Mobility
	(c) Radiographic bone loss 1/2 length of implant
	(d) Uncontrolled exudate
	(e) No longer in mouth

Table II. *Patient characteristics according to both study groups at the beginning of the study.*

Characteristic	SRA group	CRA group
(n)	150	150
Gender (male) [n (%)]	101 (67.3)	96 (64.0)
Mean age (years)	61.42 ±9.41	62.31 ±9.89
Age range (years)	36-74	39-75
Site of treatment (mandible) [n (%)]	78 (52.0)	84 (56)
Smoker (<10 cigarettes per day) [n (%)]	81 (54.0)	79 (52.6)

Table III. *Summary and comparisons of the general data across the two study groups regarding patients enrolled in the study at 10 years of follow up.*

General data	SRA group	CRA group
(n)	145	143
Gender (male) [n (%)]	99 (68.3)	93 (65.0)
Mean age (years)	61.06 ±9.35	63.33 ±9.95
Implant failure (Misch group IV) [n (%)]	5 (3.4)	7 (4.9)
Probing depth [n (%)]	20 (13.8)	30 (21.0)
Bleeding on probing (+)[n (%)]	121 (83.4)	115 (80.4)
Mean marginal bone loss [mm]	2.09 ±1.07	1.54 ±1.20
Annual control visit (yes) [n (%)]	33 (22.8)	41 (28.7)
Unscrew/ abutment decement[n (%)]	9 (6.2)	12 (8.4)
Ceramic fracture[n (%)]	11 (7.6)	4 (2.8)

Table IV. *Statistical analysis comparing the different MBL values between the two study groups.*

Group	(n)	Mean marginal bone loss [mm]	Std error [mm]	Lower 99% [mm]	Upper 99% [mm]
SRA	145	2.097	0.095	1.851	2.342
CRA	143	1.547	0.095	1.300	1.794
Source	**DF**	**Sum of squares**	**Mean square**	**F ratio**	**Prob > F**
Treatments	1	21.75508	21.7551	16.719	<0.0001
Error	286	372.14936	1.3012		
C. total	287	393.90444			

was at a slight angle on the radiograph (4). Based on this measure, computer-assisted calibration was performed and the linear measurements of MBL were taken using ImageJ 1.48 v. (Bethesda, MD, USA). The patients and their related collected data were divided according to the classification proposed by Misch and colleagues in 2008 (2). According to Misch, the International Congress of Oral Implantologists Pisa consensus conference Implant Quality of Health Scale was used (2). The latter includes four implant categories, divided as follows: Group I, considered as success and optimum health conditions, with no pain, no clinical implant mobility, and MBL <2.0 mm; Group II, considered as 'survival', with 'satisfactory' health status, with possible history of clinical problems, but no pain, no clinical implant mobility, and MBL from 2.0 mm to 4.0 mm; Group III, also considered in the 'survival' category, but with 'compromised' health status, with MBL >4 mm, but bone loss <50% of implant length, PD <7 mm and often accompanied by BOP; Group IV, considered as clinical or absolute failure, where the implant needed to be removed

(for further details, see Table I).

Finally, all prosthetic complications were recorded, such as abutment decementation, screw loosening, prosthetic fracture and crown decementation.

The null hypothesis was that there were no differences for mean MBL for the long-term follow-up between the use of these two implant-abutment connection types. Therefore, the primary outcome was the mean MBL for the single implant supported restorations.

The secondary outcomes were: (i) implant failure, which was described as mobility or any infection defining implant removal; (ii) prosthetic failure or complications, when it was impossible to place the ceramic restoration or when its loss was due to fracture or secondary implant failure; (iii) the gingival index, as plaque score and BOP score recorded during the control visit; (iv) any complications and adverse events reported over the years defined by the study.

The data are presented as means ±standard deviation. Statistical analyses were performed using the SPSS software (version 24.0; IBM Corporation, Armonk, NY, USA) and the Excel software (version 15.39; Microsoft, Redmond, WA, USA). Analysis of variance (ANOVA) was used to evaluate the differences between the groups. Tukey-Kramer tests were used as *post-hoc* tests after a one-way ANOVA, to investigate the difference for MBL in the two groups. Yates *chi*-squared tests were used to compare the differences between the groups, as divided using the Misch classification. The significance was set to $p = 0.05$.

RESULTS

During the control visits, the 300 patients were evaluated according to the inclusion and exclusion criteria. The mean age of the patients was 64.2 years (range, 36-75 years). Among these 300 patients enrolled, 197 were male and 103 females (65.6%, 34.4%, respectively). Smokers represented 53% of the sample, with <10 cigarettes per day. The initial information regarding the patients is given in Table II.

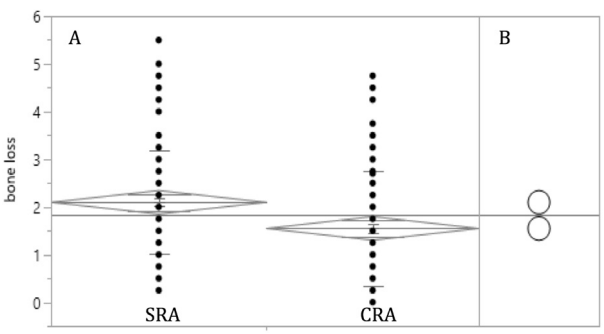

Fig. 1. *SRA and CRA groups at 10 years of follow-up. **A**) Mean marginal bone loss. **B**) Tukey-Kramer tests (P <0.01).*

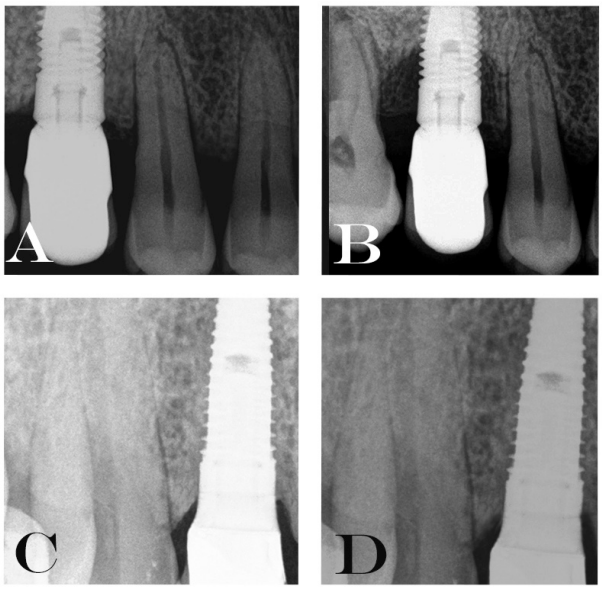

Fig. 2. *Representative radiographs from the SRA and CRA groups. Screw-retained abutment restoration (SRA group) at baseline (**A**) and at 10 years of follow-up (**B**). Cemented retained abutment restoration (CRA group) at baseline (**C**) and at 10 years of follow-up (**D**).*

At 10 years of follow-up, the overall survival rates for CRA and SRA was 95.8%. According to the Misch classification (2), a total of 4.2% of the implants failed, and these were removed. These were specifically five restorations in the SRA group A and seven in the CRA group. All of the failed implants were excluded from the further measurements and statistical analysis. Therefore the data analysed for statistical purposes referred to 288 patients, as 145 implants for the SRA group, and 143 implants for the CRA group.

The data collected provided information regarding both the degree of bone resorption and the periodontal hygienic status of the samples, as given in Table III. The BOP showed a cumulative positive index at 81.9% of the total sites under investigation, overall for both groups. Specifically, the SRA group showed BOP of 83.4%, and the CRA group

of 80.4%. The difference between these two groups regarding BOP was not statistically significant (P >0.005). Moreover, PD >5mm for the peri-implant soft tissues analysis demonstrated a rate of 21.0% for the CRA group, and 13.8% for the SRA group. In terms of the PD, there was no statistical difference between these two groups.

For the primary endpoint of MBL, the means after 10 years of follow-up were 2.09±1.07 mm for the SRA group, and 1.54±1.20 mm for the CRA group (Tables III, IV; Fig. 1). The radiographs shown in Fig. 2 illustrate the differences between the groups at implant insertion and at 10 years of follow-up.

According to the Misch classification (2), the patients were classified as follows (see also Table I):

- Group I (optimum health conditions): SRA, 54 patients (37.2%); CRA, 88 patients (61.5%).
- Group II ('survival' category, with satisfactory health status): SRA, 79 patients (54.5%); CRA, 45 patients (31.5%).
- Group III ('survival' category, with compromised health status): SRA, 12 patients (8.3%); CRA, 10 patients (7.0%).
- Group IV (failed implants): SRA, 5 patients (3.5%); CRA, 7 patients (4.9%).

Among the groups analysed, statistically significant differences emerged regarding the MBL, as shown in Table IV and Fig. 1. ANOVA showed significant difference between the groups (P <0.001). Tukey-Kramer tests also showed statistically significant difference between the groups (Fig. 1). Comparing the distribution of the patients between these groups, there were statistically significant differences between the patients of the SRA and CRA groups who were

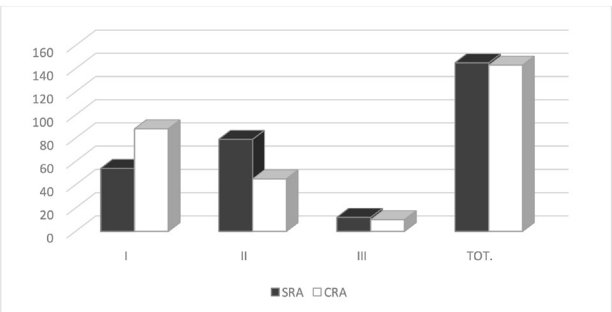

Fig. 3. *Distribution of the patients between the SRA and CRA groups according to the Misch classification (Groups I-IV).*

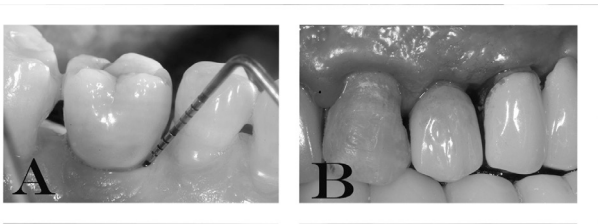

Fig. 4. *Representative clinical images from the SRA and CRA groups at 10 years of follow up.* ***A)*** *Implant supported restoration in the CRA group during PD (4 mm). No PD and BOP were present for this case.* ***B)*** *Implant supported restoration from the SRA group, where BOP after probing was present.*

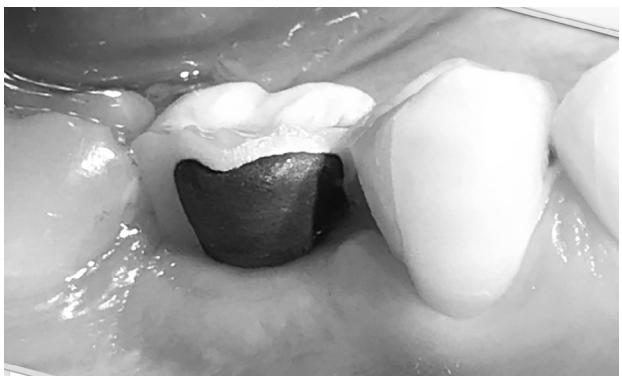

Fig. 5. *Representative clinical image demonstrating a ceramic fracture of the implant supported restoration in the CRA group at 10 years of follow-up.*

included in groups I and II according to the Misch classification (2). On the contrary, there were no statistically significant differences in the SRA *versus* CRA comparison of patients who were included in group III of Misch. The results of the statistical analysis between the groups (Table V, Figs. 3 and 4) provide exemplary clinical images from patients belonging to group I (CRA group) and group III (SRA group) of Misch.

Finally, for the prosthetic complications, these were seen to be divided according to unscrewing or abutment decementation, and to fracture and/or chipping of ceramic restoration (Fig. 5). For the latter, an overall total of 12.5% of prosthetic complications occurred. For unscrewing or abutment decementation, the total for the SRA group was 6.2%, and for the CRA group, 8.4%. Moreover, for ceramic fractures,−these were seen for SRA as 7.6%, and for CRA as 2.8%. No implant or abutment fractures had occurred. In terms

of the prosthetic complications, there was no statistical difference between the SRA and CRA groups.

DISCUSSION

Several studies have evaluated survival rates, biological and mechanical complications and marginal bone loss for different types of implant-supported restorations, although not for different types of implant abutment connection systems (22, 23). To the best of our knowledge, this is the first study that compares the roles of these two types of implant abutment connections at 10 years of follow-up.

Specifically, in the present study, an internal hexagon screw-retained connection was compared with a cemented connection. Over the years, different connections have been proposed and compared with the aim of reducing the microgap, and MBL and biological and mechanical complications (8). Conical connections were promised to reduce the microgap, and therefore to minimise bacterial infiltration (14). However, it was demonstrated that bacterial infiltration also occurs for conometric connections (24). With regard to cemented connections, some short-term studies have shown excellent marginal sealing between the components, which thus reduces the possibility of bacterial colonisation and abutment micromovement (15, 21). The present retrospective study demonstrates excellent survival rates for both the SRA and CRA types of connection, with some differences seen for the mechanical and biological complications at this long-term follow-up (10 years). Here, the total overall implant failure was 4.2%. This rate is consistent with the literature, which shows survival rates at 10 years or more of 95.9% and 95.7% (19, 25).

Implant complications have been classified as mechanical (i.e., prosthetic) and biological (i.e., relative to the health of the peri-implant tissues). The present data show that these two types of complications occur differently across these SRA and CRA groups studied. In more detail, high BOP and PD scores were recorded for both groups, with a cumulative rate of 81.9%. These data are in agreement with the literature, which has shown BOP values >80% at long-term follow-up (25). It is reasonable to suppose that this is not due to the type of connection used, but to the patient oral hygiene and the frequency of their control visits. More than 70% of the patients investigated did not undergo regular check-ups for many reasons (e.g., distance from the structure, personal commitments, economic difficulties). In this regard, it is advisable to keep all implant-supported implants under long-term control, regardless of the type of connection used.

The PD values were recorded considering a cut-off >5 mm, and in this case no significant differences were seen for PD between the SRA and CRA groups. Oral hygiene conditions once more justify these similar data. Moreover, it has been shown that if PD increases around implants, if it is not accompanied by symptoms, it has little diagnostic relevance. The presence of such pockets might indicate a lack of initial bone, and not necessarily a peri-implant pathology (26). In the same way, it has been shown that PD >5 mm or >6 mm can be a prognostic indicator, although this must necessarily be associated with other criteria for pathology indication (26)

The MBL analysis over long-term follow-up can be considered a predictable healthy state factor of implant rehabilitations (26). At 10 years, the CRA group showed more advantageous results than the SRA group. Indeed, following the division of the samples into the three groups according to Misch (2), there was a significant difference ($P < 0.005$) in the sample distributions across the SRA and CRA groups. A total of 61.5% of the CRA group was classified in group I of Misch. These rehabilitations can be considered a success and under optimal health conditions. On the other hand, most patients in the SRA group (54.5%) were classified into group II of Misch. This category represented the implant 'survival' phase, albeit without symptoms and clinical problems. Moreover, the mean MBL data showed that the patients in the CRA group showed lower values than for the SRA group. In the 10 years of follow-up, the patients in the CRA group showed mean bone loss of 1.54 mm, *versus* 2.09 mm for the SRA group.

It is important to stress that platform switching rehabilitations were not considered in the present study. As previously demonstrated, this concept allowed the reduction of the peri-implant marginal bone loss over the years (8). The difference between

the SRA and CRA groups was statistically significant, probably due to the different connection used, taking into consideration that all of the other variables were similar across both of these groups. Therefore, internal hexagon rehabilitations were clinically more susceptible and subject to greater risk in terms of the survival rate (7).

The low degree of bone resorption in the CRA group might be due to the type of connection. It is reasonable to suppose that the presence of a microgap, due to the flat-to-flat relationship between the abutment and the fixture present in the SRA method, was responsible for the greater bacterial accumulation described as the main cause of the peri-implant bone resorption process (27). Moreover, the space described as a microgap with the SRA method might act as a reservoir for bacteria (15, 21, 28). This accumulation can cause bone resorption due to the release of bacterial or host products (28). The CRA method, on the other hand, has a press fitting connection due to the transmucosal collar, and a cemented abutment, which can guarantee a greater seal, and therefore a lower incidence of such complications (28). According to this study, this connection can maintain the fixture-abutment seal over time (follow-up, >10 years), thus reducing peri-implant bacterial colonisation. *In-vitro* studies have shown how the cemented method can provide satisfactory results compared to the screw-retained connections, in terms of bacterial infiltration into the connection (21).

Mechanical complications were manifested in a more varied way between the SRA and CRA groups. Indeed, although all of the prosthetic clinical phases respected standardised protocols for the realization of these prosthetic crowns, the prevalence of unscrewing or abutment decementation was similar between the two groups. This demonstrates that unscrewing or decementation are the first, in order of frequency, post-surgical complications during single implant rehabilitations (29). Using the correct tightening or cementation protocol can help to reduce the incidence of this prosthetic complication. This problem increases the chair time and the possibility of need for repair, especially due to the difficulty in removing the prosthetic restoration without damaging it (30).

Other complications occurred with lower frequency, such as ceramic fracture. This is consistent with the literature, and can be considered as a normal event in such rehabilitations, probably due to mechanical separation of the ceramic part, occlusal adjustments or wear of materials (30).

In conclusion, the bone resorption rates here defined a valid method of investigation into such long-term follow-up. The comparisons between the SRA and CRA methods showed that the CRA method ensures better results in terms of bone resorption, and therefore implant survival rates. From the prosthetic point of view, both methods show excellent results in terms of performance and reliability. Finally, from the periodontal point of view, both methods showed high BOP and PD rates, which were similar (no statistically significant differences), which demonstrates the need for strict control of the patients, with the aim of improving their oral hygiene to ensure greater success of their implant-prosthetic rehabilitation.

The results from this 10-year retrospective study show that both the SRA and CRA methods have positive long-term follow-up, although there were complications encountered for both groups. MBL and peri-implant PD were greater in the SRA group than the CRA group. On this basis, the possibility of having better coupling between the parts in the CRA methodology encourages the clinical use of this type of connection.

REFERENCES

1. Simonis P, Dufour T, Tenenbaum H. Long-term implant survival and success: a 10-16-year follow-up of non-submerged dental implants. Clin Oral Implants Res 2010; 21:772-77.
2. Misch CE, Perel ML, Wang HL et al. Implant success, survival and failure: the International Congress of Oral Implantologists (ICOI) Pisa consensus conference. Implant Dent 2008; 17:5-15.
3. Albrektsson T, Zarb GA, Worthington P, Erikson AR. The long-term efficacy of current used dental implants: a review and proposed criteria of success. Int J Oral Maxillofac Implants 1986; 1:11-25.
4. Traini T, Berardini M, Congedi F, Sinjari B, Trisi P, Caputi S. Impact of second stage surgery on bone remodeling around new hybrid titanium implants: a

prospective clinical study in humans. Implant Dent 2017; 26(1):121-28.
5. Sinjari B, Traini T, Caputi S, Mortellaro C, Scarano A. Evaluation of fibrin clot attachment on titanium laser-conditioned surface using scanning electron microscopy. J Craniofac Surg. 2018; 29(8):2277-81.
6. Di Giulio M, Traini T, Sinjari B, Nostro A, Caputi S, Cellini L. *Porphyromonas gingivalis* biofilm formation in different titanium surfaces, an *in-vitro* study. Clin Oral Implants Res. 2016; 27(7):918–925.
7. Sinjari B, D'Addazio G, De Tullio I, Traini T, Caputi S. Peri-implant bone resorption during healing abutment placement: the effect of a 0.20% chlorhexidine gel vs. placebo – a randomized double-blind controlled human study. Biomed Res Int 2018; 2018:5326340.
8. Caricasulo R, Malchiodi L, Ghensi P, Fantozzi G, Cucchi A. The influence of implant-abutment connection to peri-implant bone loss: a systematic review and meta-analysis. Clin Implant Dent Relat Res 2018; 20(04):653-64.
9. Bramanti E, Cervino G, Lauritano F, et al. FEM and Von Mises analysis on prosthetic crowns structural elements: evaluation of different applied materials. Sci World J 2017; 2017:1029574.
10. Kitagawa T, Tanimoto Y, Odaki M, Nemoto K, Aida M. Influence of implant/ abutment joint designs on abutment screw loosening in a dental implant system. J Biomed Mater Res B Appl Biomater 2005; 75:457-63.
11. Cicciù M, Cervino G, Bramanti E, et al. FEM analysis of mandibular prosthetic overdenture supported by dental implants: evaluation of different retention methods. Comput Math Methods Med 2015; 2015:943839.
12. Cicciù M, Bramanti E, Matacena G, Guglielmino E, Risitano G. FEM evaluation of cemented-retained *versus* screw-retained dental implant single-tooth crown prosthesis. Int J Clin Exp Med 2014; 7(4):817-25.
13. Gehrke SA, Delgado-Ruiz RA, Prados Frutos JC, Prados-Privado M, Dedavid BA, Granero Marín JM, Calvo Guirado JL. Misfit of three different implant-abutment connections before and after cyclic load application: an *in-vitro* study. Int J Oral Maxillofac Implants 2017; 32(4):822-29.
14. Scarano A, Valbonetti L, Degidi M, Pecci R, Piattelli A, de Oliveira PS, Perrotti V. Implant-abutment contact surfaces and microgap measurements of different implant connections under 3-dimensional X-ray microtomography. Implant Dent 2016; 25(5):656-62.
15. Assenza B, Tripodi D, Scarano A, Perrotti V, Piattelli A, Iezzi G, D'Ercole S. Bacterial leakage in implants with different implant–abutment connections: an *in-vitro* study. J Periodontol 2012; 83(4):491-97.
16. Esposito M, Maghaireh H, Pistilli R, Grusovin MG, Lee ST, Trullenque-Eriksson A, Gualini F. Dental implants with internal *versus* external connections: five-year post-loading results from a pragmatic multicentre randomised controlled trial. Eur J Oral Implantol 2016; 9(2):129-41.
17. de Medeiros RA, Pellizzer EP, Vechiato Filho AJ, Dos Santos DM, da Silva EV, Goiato MC. Evaluation of marginal bone loss of dental implants with internal or external connections and its association with other variables: a systematic review. J Prosthet Dent 2016; 116(4):501-6.e5.
18. Staubli N, Walter C, Schmidt JC, Weiger R, Zitzmann NU. Excess cement and the risk of peri-implant disease - a systematic review. Clin Oral Implants Res 2017; 28(10):1278-90.
19. Papaspyridakos P, Barizan Bordin T, Kim YJ, et al. Implant survival rates and biologic complications with implant-supported fixed complete dental prostheses: a retrospective study with up to 12-year follow-up. Clin Oral Implants Res 2018; 29(8):881-93.
20. Cawood JJ, Howell RA. A classification of the edentulous jaws classes I to IV. Int J Oral Maxillofac Surg 1988; 17:232-79.
21. Assenza B, Artese L, Scarano A, et al. Screw vs cement-implant-retained restorations: an experimental study in the beagle. Part 2. Immunohistochemical evaluation of the peri-implant tissues. J Oral Implantol 2006; 32(1):1-7.
22. Wittneben JG, Joda T, Weber HP, Brägger U. Screw-retained vs. cement-retained implant-supported fixed dental prosthesis. Periodontol 2000 2017; 73(1):141–151.
23. Lemos CA, de Souza Batista VE, Almeida DA, Santiago Júnior JF, Verri FR, Pellizzer EP. Evaluation of cement-retained *versus* screw-retained implant-supported restorations for marginal bone loss: a systematic review and meta-analysis. J Prosthet Dent

2016; 115(4):419-27.
24. Schmitt CM, Nogueira-Filho G, Tenenbaum HC, Lai JY, Brito C, Döring H, Nonhoff J. Performance of conical abutment (Morse Taper) connection implants: a systematic review. J Biomed Mater Res A 2014; 102(2):552-74.
25. Zitzmann NU, Berglundh T. Definition and prevalence of peri-implant disease. J Clin Periodontol 2008; 35 (8):286-91.
26. Renvert S, Persson GR, Pirih FQ, Camargo PM. Peri-implant health, peri-implant mucositis, and peri-implantitis: case definitions and diagnostic considerations. J Clin Periodontol 2018; 45(20):S278–S285.
27. Rismanchian M, Hatami M, Badrian H, Khalighinejad N, Goroohi H. Evaluation of microgap size and microbial leakage in the connection area of four abutments with Straumann (ITI) implant. J Oral Implantol 2012; 38(6):677-85.
28. Assenza B, Scarano A, Leghissa G, Carusi G, Thams U, Roman FS, Piattelli A. Screw- vs cement-implant-retained restorations: an experimental study in the Beagle. Part 1. Screw and abutment loosening. J Oral Implantol 2005; 31(5):242-46.
29. Wittneben JG, Buser D, Salvi GE, Bürgin W, Hicklin S, Brägger U. Complication and failure rates with implant-supported fixed dental prostheses and single crowns: a 10-year retrospective study. Clin Implant Dent Relat Res 2014; 16(3):356-64.
30. Parnia F, Yazdani J, Fakour P, Mahboub F, Vahid Pakdel SM. Comparison of the maximum hand-generated torque by professors and postgraduate dental students for tightening the abutment screws of dental implants. J Dent Res Dent Clin Dent Prosp 2018; 12(3):190-95.

LIPID PEROXIDATION AS A PREDICTIVE BIOMARKER OF THE EARLY STAGE OF CANCER

B. BOBROWSKA-KORCZAK[1], D. SKRAJNOWSKA[1], A.K. KISS[2], R. WRZESIEN[3], W. BIELECKI[4], A. ORZOŁ[1], P. ZEBROWSKI[1] and S. BIALEK[5]

[1]Department of Bromatology, Medical University of Warsaw, Warsaw, Poland; [2]Department of Pharmacognosy and Molecular Basis of Phytotherapy, Medical University of Warsaw, Warsaw, Poland; [3]Central Laboratory of Experimental Animals, Medical University of Warsaw, Warsaw, Poland; [4]Department of Pathology and Veterinary Diagnostics, Faculty of Veterinary Medicine, Warsaw University of Live Sciences, Warsaw, Poland; [5]Department of Biochemistry and Clinical Chemistry, Medical University of Warsaw, Warsaw, Poland

Received January 23, 2019 – Accepted April 3, 2019

Prostate cancer continues to be a major cause of morbidity and mortality in men around the world. The data concerning the antioxidant status and the degree of lipid peroxidation at the moment of the initiation of cancer is limited. The aim of this research is to assess the effect of selected minerals (zinc, selenium, iron, copper and calcium) on the growth of the neoplastic process and the concentrations of selected biomarkers of the oxidative damage in rats with implanted prostate cancer cells. It was found that the diet supplementation with selected minerals (zinc, selenium, iron, copper and calcium) affect the occurrence of prostate tumor growth in the examined rats. The intraperitoneal implantation of prostate cancer cells resulted in the occurrence of prostatic adenoma in 71% of the examined rats. In the rats that were additionally supplemented with selenium and with copper, the cancer cell aggregates constituted, respectively, 25% and 38% of the cases. As a result of implantation of cancer cells, the level of biomarkers of lipid peroxidation increased both in the urine and in tissues of the examined animals (rat group without supplementation). No relationship was found between the process of lipid peroxidation due to the supplementation with selenium and copper, and the lower incidence of cancer and the induction of apoptosis. The reduced activity of antioxidative enzymes (catalase, superoxide dismutase and glutathione peroxidase) creates favorable conditions for the formation of cancer cell aggregates, which was shown in the rats whose diet was supplemented with iron. In summary, we conclude that lipid peroxidation represents a fruitful approach to early stage cancer prevention. Supplementation of rats with trace elements correlated with the risk of developing cancer, but the mechanisms of this action is complicated and dose-dependent.

Stationary concentration and the rate of reaction of reactive oxygen species (ROS) which cause damage to cell structure depend on the steady-state balance between the rate of ROS production and the concentrations of low molecular weight antioxidants and the activity of defense enzymes. An increased rate of production of reactive oxygen species in the body, or deficiencies in defense mechanisms against

Key words: cancer; biomarkers lipid peroxidation; cancer initiation; cancer cell; trace elements

Corresponding Author:
Dr. Dorota Skrajnowska,
Department of Bromatology,
Medical University of Warsaw,
Banacha 1, 02-097 Warsaw, Poland
Tel./fax: +48225720785
e-mail: dorota.skrajnowska@wum.edu.pl

0393-974X (2019)

DISCLOSURE: ALL AUTHORS REPORT NO CONFLICTS OF INTEREST RELEVANT TO THIS ARTICLE.

ROS provoke dangerous reactions in the organism which are induced by ROS (defined as oxidative stress). Oxidative stress has been recognized as a contributing factor to many diseases, including different kinds of cancers (1, 2).

Prostate cancer continues to be a major cause of morbidity and mortality in men around the world (3). Elevated levels of lipid peroxidation products have been detected in prostate cancer patients as opposed to healthy ones (4-6). However, the data concerning the antioxidant status and the degree of lipid peroxidation at the moment of cancer initiation are limited. Additionally, the present work provides new information for understanding the role of trace elements (including Se, Zn, Ca, Fe, Cu) in cancer risk management.

The aim of the study was to evaluate the effect of the early stage of neoplastic process and the effect of trace element supplementation on the concentration of selected biomarkers of oxidative damage to fats and the activity of antioxidant enzymes.

MATERIALS AND METHODS

Male Sprague-Dawley rats (n = 88) were obtained from the Animal Laboratory, Department of General and Experimental Pathology from the Medical University of Warsaw. The study was approved by the Ethics Committee, Medical University of Warsaw, and all experiments were carried out in compliance to the current laws of the country. The animals were kept under standard conditions with 12-h light-dark cycle at a temperature 22°C. They had free access to food (standard diet: Labofeed H, Zurawia 19, 89–240 Kcynia, Poland) and water. The diet was composed of the following compounds (per 1 kg): protein (210 g), fat (39.2 g), fibre (43.2 g), ash (55 g), carbohydrates (300 g), vitamin A (15,000 IU), vitamin D3 (1000 IU), vitamin E (90 mg), vitamin K3 (3 mg), vitamin B1 (21 mg), vitamin B2 (16 mg), vitamin B6 (17 mg), vitamin B12 (80 μg), pantothenic acid (30 mg), folic acid (5 mg), nicotinic acid (133 mg), Ca (10 g), P (8.17 g), Mg (3 g), K (9.4 g), Na (2.2 g), Cl (2.5 g), S (1.9 g), Fe (250 mg), Mn (100 mg), Zn (76.9 mg), Cu (21.3 mg), Co (2.0 mg), I (1.0 mg), and Se (0.5 mg).

Experimental procedure

The experiment was conducted over 90 days.

After the adaptation period (10 days – rats' age 60 to 70 days), the animals (n=88) were randomly divided into two experimental groups. In group 1 (study group), the rats were implanted with prostate cancer cells, and in group 2 (control group) the rats were accommodated under the same conditions as those in Group 1, fed the same diet, but with no implanted cancer cells. The cancer cells (LNCaP) were implanted intraperitoneally in the amount $1x10^6$ (in PBS 0.4 ml) in the rats at age 90 days. The certified line of androgen-dependent human prostate cancer cells was obtained from ATTC bank (American Type Culture Collection, Menassas, VA).

The animals from both groups (study and control) were provided with the minerals by oral gavage in a solution:

- zinc 4.6 mg/ml (1.85 mg Zn (II)/day/rat) (as $ZnSO_4x7H_2O$ in aqueous suspension) (n=15),
- copper 0.639 mg/ml (0.256 mg Cu (II)/day/rat) (as $CuSO_4x5H_2O$ in aqueous suspension) (n=15),
- selenium 0.018 mg/ml (0.0072 mg Se/day/rat) (as Na_2SeO_4 in aqueous suspension) (n=15),
- iron 7.5 mg/ml (3 mg Fe (II)/day/rat) (as $FeSO_4x7H_2O$ in aqueous suspension) (n=15),
- calcium 0.075 g/ml (0.03 g Ca/day/rat) (as $CaCl_2x6H_2O$ in aqueous suspension) (n=15).

The rats were fed extra supplements suspended in water, 0.4 mL daily, from 70 days until 150 days of age when they were sacrificed by decapitation. The animals fed with only the standard diet (without supplementation) received 0.4 mL of water (n=13). The doses of trace elements were selected based on the values used in the Labofeed H diet (extrapolated on the rats' body weight). According to the level of trace elements in the Labofeed diet, the rats were fed, via gavage, extra supplements of the following: double dose of Zn and Cu or one dose of Fe or a quarter dose of Ca. The doses of selected minerals were chosen based on their levels in dietary supplements that are commonly used by people and can be available at any pharmacy.

In order to obtain rat urine samples the animals were placed in individual metabolic cages for 24 hours. In the case of the group of rats that were fed only the standard diet (with no supplementation) the samples of urine for determination of the level of 8-isoprostaglandin $F_{2\alpha}$ (8-isoPGF$_{2\alpha}$) were collected on week 13, 14, 15, 18 and 21 of the animals' lifetime. In the case of the remaining (supplemented) groups the kinetics of the level of

8-isoPGF$_{2\alpha}$ was assessed in the rat urine collected at week 14 and 21 (that is, at the beginning of the experiment just after implantation of prostate cancer cells, and at the end of the experiment when the tumors appeared). The blood and tissues for the experiment was collected within week 21 of the rats' lifetime, during their decapitation. In order to obtain serum the blood was centrifuged for 15 min at 3500 rpm. The obtained material was stored at the temperature of -70°C until the analysis was performed.

Histopathology

The rats were sacrificed by decapitation at 150 days of age, and tumors were evaluated histopathologically. The tissues were recorded in a buffered formalin solution, then they were dehydrated, sealed in paraffin and cut into scraps 4 μm thick. The hematoxylin and eosin staining of tissue and cell sections was applied and the sections were evaluated using a BX43 Olympus research microscope.

Determination of 8-isoprostaglandin F$_{2\alpha}$

The level of 8-isoprostaglandin F$_{2\alpha}$ in rat serum and urine was detected by the ELISA method using the commercially available kit (8-isoprostane EIA Kit, Cayman Chemical Company, Ann Arbor, MI) according to the manufacturer's instruction. The concentration of 8-isoPGF$_{2\alpha}$ in urine was standardized by conversion to creatinine level. The latter was examined in urine samples with creatinine test (Hydrex, Warsaw, Poland) based on Jaffe's reaction (in alkaline environment creatinine forms a colored complex with picric acid). The final results were expressed as ng/mg creatinine.

Determination of the malonic dialdehyde

The level of malonic dialdehyde (MDA) was determined in the tissue (liver, heart, kidney) samples homogenized in 0.9% cold NaCl solution, by the aid of TBA (thiobarbituric acid) method (7). The result were evaluated from standard curve (0.25; 0.63; 1.25; 1.88; 2.5; 3.75; 5; 7.5; 10 nmol/ml) and expressed as nmol/g tissue.

Determination of catalase, superoxide dismutase and glutathione peroxidase activities

The serum activities of catalase, superoxide dismutase and glutathione peroxidase were measured using commercial microplate assay kits for rats (Catalase Assay Kit Catalog No. 707002; SOD Assay Kit Catalog No. 706002; Glutathione Peroxidase Assay Kit Catalog No. 703102) obtained from Cayman Chemical Company Ann Arbor, MI. For determination of the enzyme activities, a Bio-Tek Instruments spectrophotometer (JNC, Highland Park, Box 998, Winooski UT 05404 – 0998, USA) was used.

Statistical analysis

The Statistica 12.0 software (StatSoft, USA) was used for statistical analysis. The normal distribution of the data was tested using the Shapiro-Wilk method. For the normal data, the Student's *t*-test and ANOVA, followed by Tukey's test with unequal sample size were used for analysis. The non-normal data was analyzed with Mann-Whitney U nonparametric test. In order to verify the results of tumor incidence, in the implanted prostate cancer cells rats, the relative risk (RR) calculation was used. The results were considered statistically significant when $p<0.05$.

RESULTS

As a result of the performed studies the effect of supplementation with selected trace elements on the occurrence of tumor hyperplasia in rats was examined (Table I). The tumors were located subcutaneously, mainly in lymph nodes. In the case of the rats that were provided a standard unsupplemented diet intraperitoneal implantation of prostate cancer cells resulted in the occurrence of prostatic adenoma in 71% of the examined rats (Table I). The greatest proliferation of tumor cells and the greatest number of their aggregates in lymph nodes were found in the rats whose diet was supplemented with iron. In the case of rats that were additionally supplemented with selenium, as well as, which was particularly interesting, with copper, the cancer cell aggregates constituted, respectively, 25% (2/8) and 38% (3/8) of the cases. The histopathological studies showed that the cells in the epithelium displayed prostate gland cell characteristics, with the possibility of tumor growth, but with no signs of inflammation (Fig. 1). In non-implanted groups spontaneous cancers were not observed.

The animals were implanted with cancer cells on day 90 of their lifetime, i.e. at week 13. A statistically significant difference in the level of 8-isoPGF2α in the urine of rats that were fed only

Table I. *Tumor induction in relation to supplementation.*

Type of supplementation	Tumor incidence (%) (number of animals that developed tumors)
Standard diet	5/7 (71%)
Zn (4.6 mg/ml)	4/8 (50%)
Cu (0.639 mg/ml)	3/8 (38 %)
Se (0.018 mg/ml)	2/8 (25%)[a] (p=0.001)
Fe (7.5 mg/ml)	8/8 (100%)[a] (p=0.05)
Ca (0.075 g/ml)	7/8 (88%)

[a]*: groups implanted with cancer cells; group fed standard diet* vs *groups fed diet with addition of trace elements (p≤0.05).*

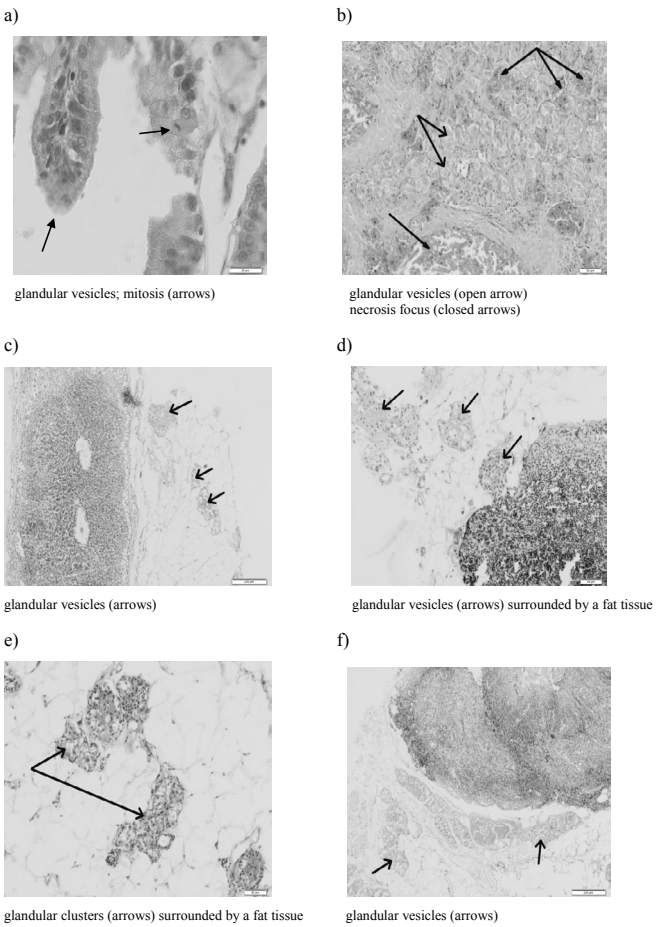

Fig. 1. *Hematoxylin-eosin-stained sections of anterior prostate from rats implanted LNCaP cells.* ***a****) Rats fed standard diet - without supplementation;* ***b****) rats fed diet supplemented with selenium;* ***c****) rats fed diet supplemented with iron;* ***d****) rats fed diet supplemented with copper;* ***e****) rats fed diet supplemented with calcium;* ***f****) rats fed diet supplemented with zinc.*

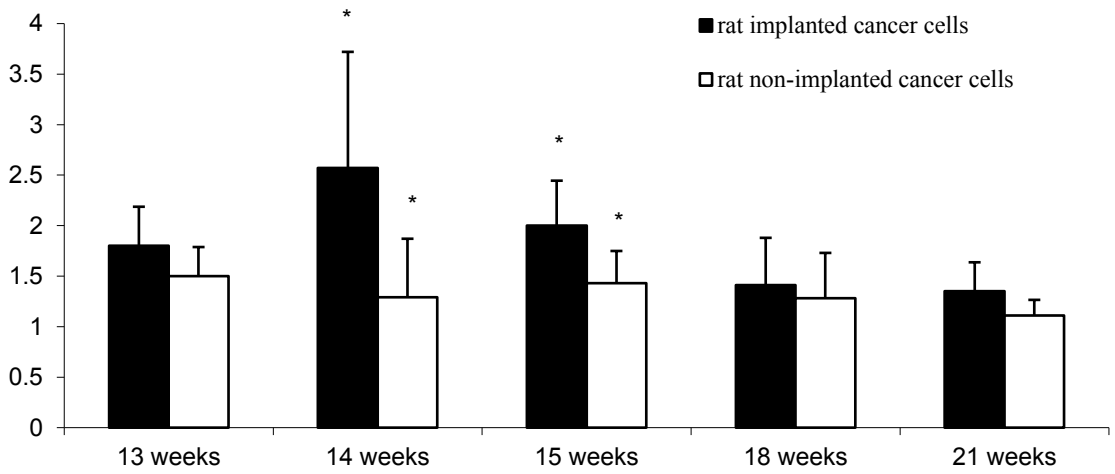

Fig. 2. *Urinary 8-isoPGF2α (ng/mg creatinine) (means ± standard deviation) in rats fed only the standard diet (without supplementation) in early-onset prostate cancer (13-14-15-18-21 week of rodent's age). *: statistically significant results (p<0.05) of a comparison of the 8-isoPGF2α level in the urine of the implanted versus non-implanted rats, in analogous time.*

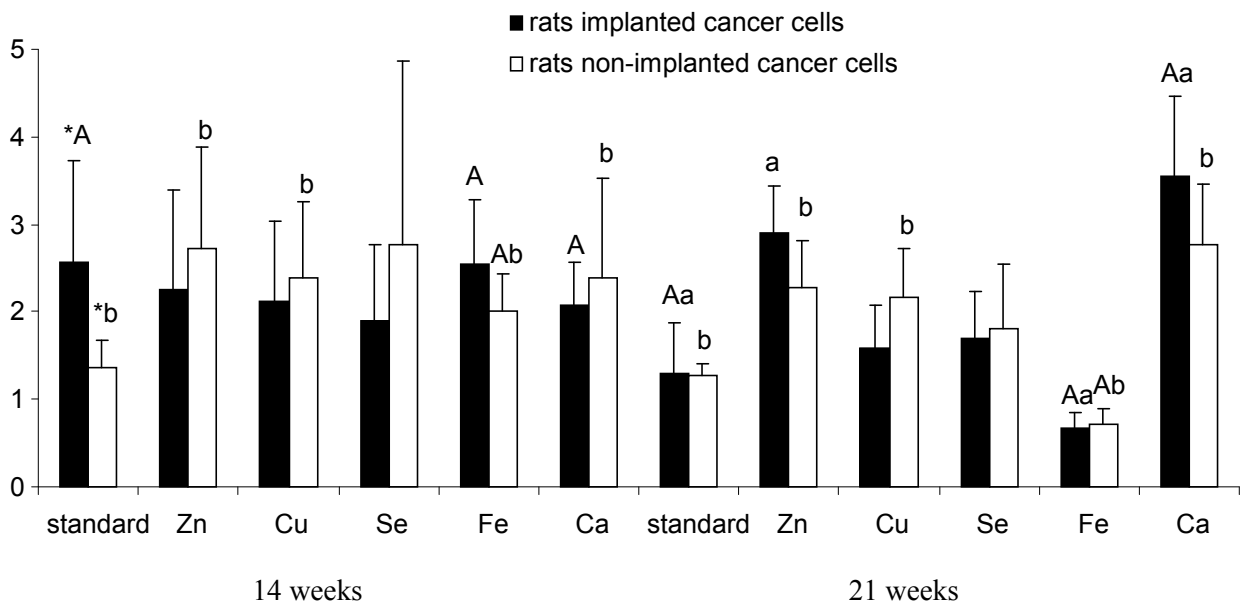

Fig. 3. *The effect of rat supplementation on the content of 8-isoPGF2α (pg/mL) (means ± standard deviation) in rat urine (14→21 week). * – groups implanted cancer cells rats vs groups non-implanted cancer cell rats, fed the same diet, in the same period (p<0.05). A – 14 vs 21 week (rats fed the same diet, implanted or non-implanted cancer cells) (p<0.05). a - groups implanted cancer cells; group fed standard diet versus groups fed diet with addition of trace elements (p<0.05). b - groups non-implanted cancer cells; group fed standard diet versus groups fed diet with addition of trace elements (p<0.05).*

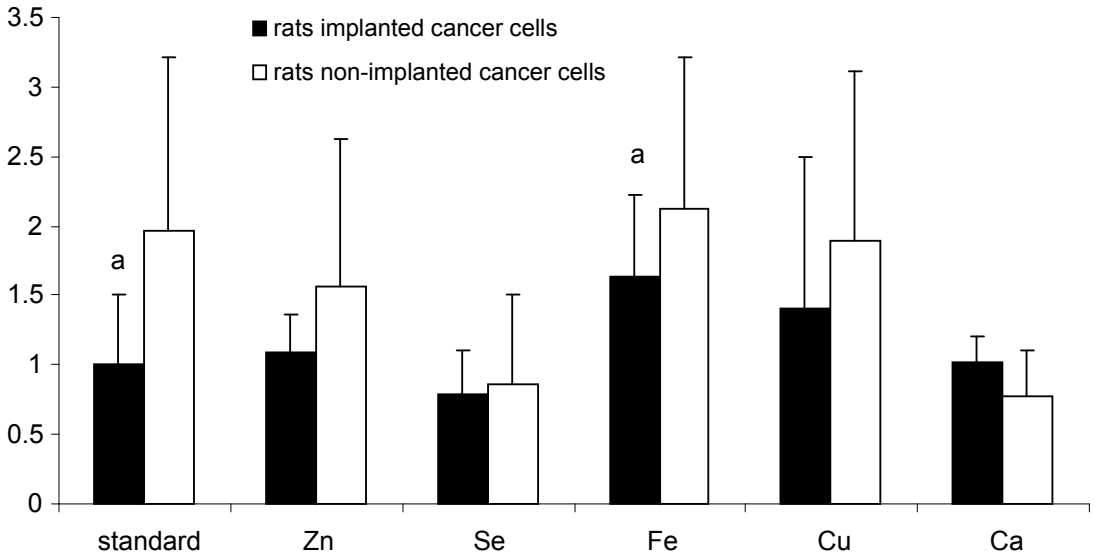

Fig. 4. *The effect of rat supplementation on the content of 8-isoPGF2α (pg/mL) (means ± standard deviation) in rat serum (21 week).*

the standard diet (without supplementation) was observed on week 14 and 15 of the rats' lifetime, that is 1 and 2 weeks after implementation of cancer cells (Fig. 2). On week 21 of the rats' lifetime the concentration of 8-isoPGF2α both in the serum and in the urine did not differ statistically (in groups of rats without supplementation) (Figs. 2-4). No statistically significant differences were found in the level of 8-isoPGF2α on week 14 between the rats with implanted cancer cells that were fed the standard diet and those supplemented with selected elements (Fig. 3). Taking into account the results of studies of the level of 8-isoPGF2α collected at week 21 of the animals' lifetime, a statistically significant level was found to be lower in the rats that were additionally supplemented with iron, as compared with those that received only the standard diet (Fig. 3). In the case of rats that were implanted cancer cells and supplemented with Zn and Ca, a statistically significant increase of the level of 8-isoPGF2α was found, as compared with the unsupplemented rats.

In the case of the rats that received only the standard diet, a statistically significant increase of MDA was found in the heart and kidneys, collected on the day of their decapitation which occurred at week 21 of the rats' lifetime (Fig. 5) (as compared with the non-implanted rats, obtaining the same supplementation). The level of MDA in the liver of rats implanted with cancer cells in comparison with the non-implanted animals was, respectively, 119.21±17.46 *vs* 99.60± 11.51 ($p = 0.06$) (rats fed only the standard diet, without supplementation). It was found that the rats that were treated with cancer cells and supplemented with calcium were characterized by a lower level of MDA in the liver and kidneys, as compared with the animals that were fed only the standard diet. The rats treated with cancer cells and supplemented with iron and selenium were characterized by a higher statistically significant level of MDA in the heart, in comparison with the rats that were fed the same diet but were not treated with cancer cells.

A statistically significant lower activity of both catalase and glutathione peroxidase was found in the case of rats that were implanted with cancer cells and supplemented with iron, as compared with the rats that received the same diet but were not implanted with cancer cells (respectively: 33.18±8.19 *vs* 50.56±6.12 nmol/min/ml; 1.42±0.05 *vs* 1.49±0.05 $p<0.05$) (Fig. 6). Additionally, the rats

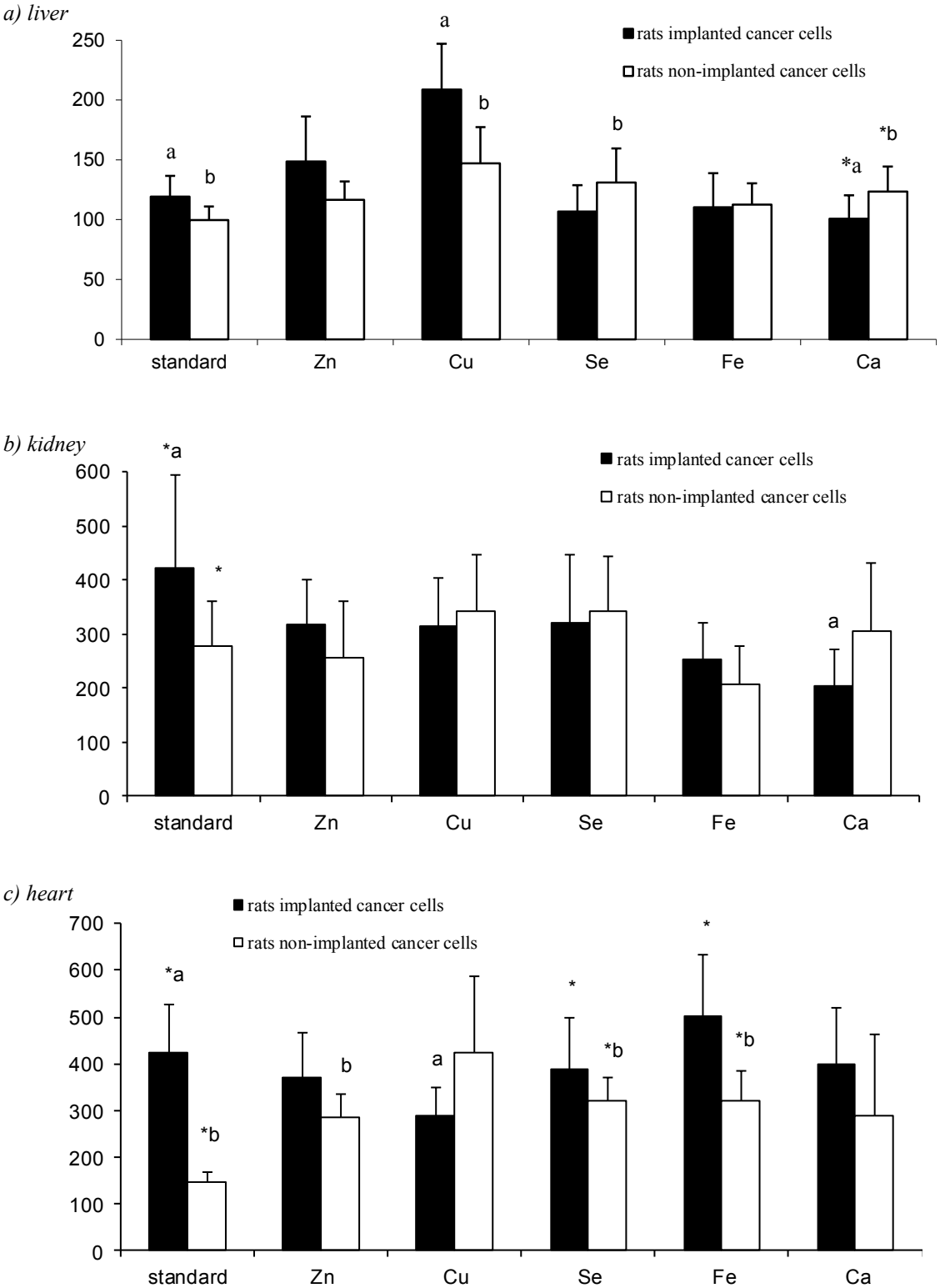

Fig. 5. *Effect of the cell implanted on MDA (nmol/g tissue) levels in different rat organs. *: rats with implanted cancer cells* vs *rats with no implanted cancer cells rats, fed the same diet ($p<0.05$). a: groups with implanted cancer cells; group fed standard diet* vs *groups fed diet with addition of trace elements ($p<0.05$). b: non-implanted cancer cells group; group fed standard diet* vs *groups fed diet with addition of trace elements ($p<0.05$).*

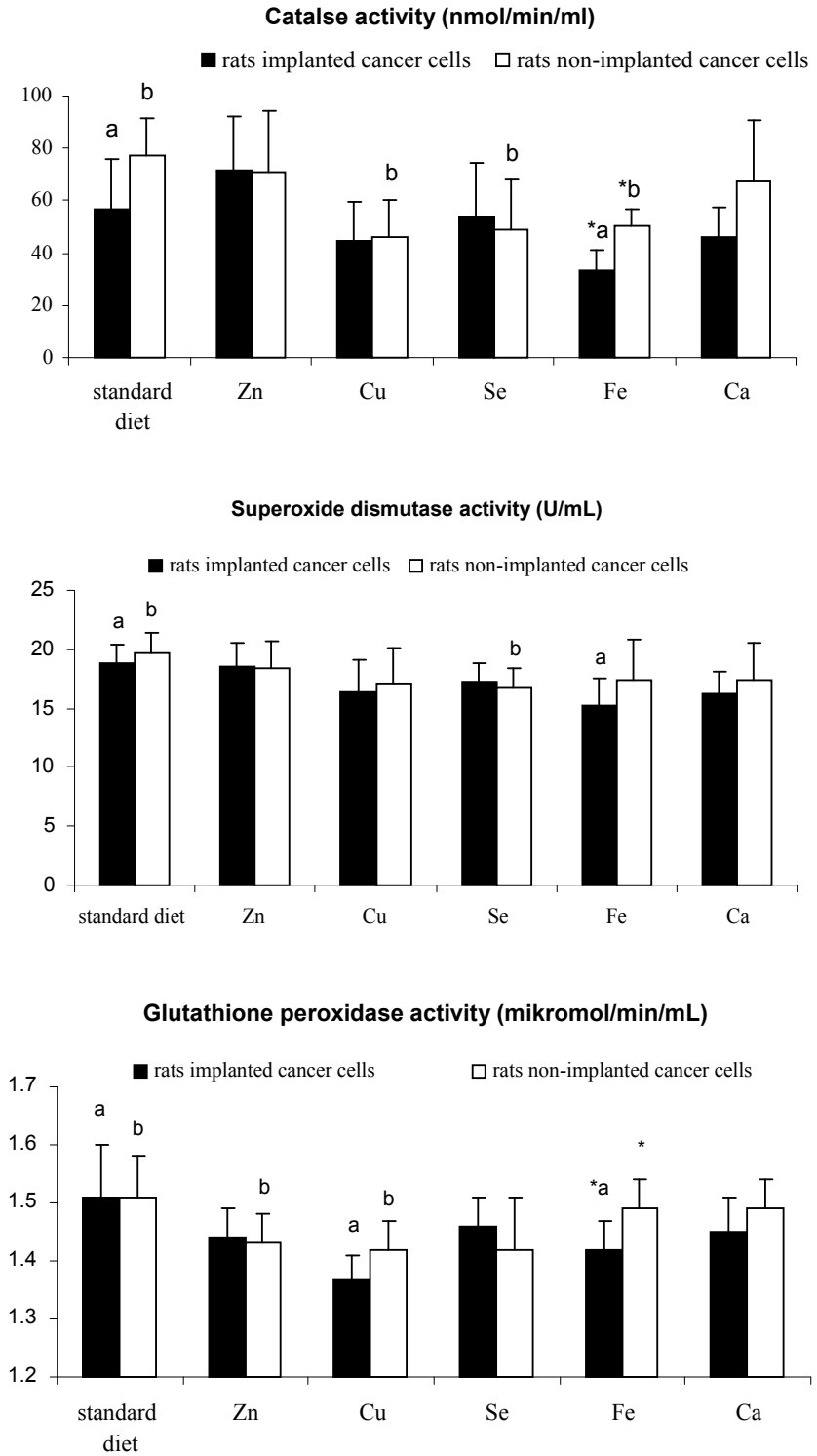

Fig. 6. *The effect of rat supplementation on the catalase (nmol/min/ml), superoxide dismutase (U/mL) and glutathione peroxidase (μmol/min/mL) activities in rat serum (mean ± standard deviation). *: groups of rats implanted with cancer cells* vs *groups of rats not implanted with cancer cells, fed the same diet ($p<0.05$). a - groups implanted with cancer cells; group fed standard diet* vs *groups fed diet with addition of trace elements ($p<0.05$). b - groups non-implanted with cancer cells; group fed standard diet* vs *groups fed diet with addition of trace elements ($p<0.05$).*

treated with cancer cells and supplemented with iron were characterized by a statistically significant lower activity of catalase, superoxide dismutase and glutathione peroxidase, in comparison with those that obtained only the standard diet. In the case of rats that were not implanted with cancer cells, a significantly lower catalase activity was found in the animals that were supplemented with copper, selenium and iron, in comparison with those that obtained only the standard diet. A statistically significant activity of superoxide dismutase was noted to be lower in the animals that were supplemented with selenium, as compared with the unsupplemented ones (groups not implanted with cancer cells). In the case of rats that were non-implanted with cancer cells a significantly lower glutathione peroxidase activity was observed in the animals that were supplemented with zinc and copper, in comparison with those that obtained only the standard diet.

DISCUSSION

Lipid peroxidation (LPO) is the best known biological process proceeding by a free radical chain reaction mechanism. The effect of LPO products in the cell is the modification of physical properties of cell membranes, which consists mainly in changing their permeability. Lipid peroxidation also results in inhibition of the activity of membrane enzymes and transporting proteins. Additionally, some products formed due to lipid peroxidation are factors which corrupt oxidative phosphorylation in mitochondria, which means they weaken the relationship between electron transport chain (cell respiration) and mitochondrial ATP synthase. The products of lipid peroxidation, that is malondialdehyde and isoprostanes, exhibit mutagenic and carcinogenic activity, as well as affecting the rate of cell proliferation. An enhanced level of LPO products was found in the course of many diseases, including different types of cancer, diabetes, atherosclerosis, AIDS, various inflammatory states and Alzheimer's disease (1-3, 9).

On the other hand, lipid peroxidation (or lipid peroxidation-related mechanisms), especially in the early stage of carcinogenesis, can be a protective factor for the prevention of cancer. Generation of lipid peroxidation products in cells may lead to their growth arrest and death, which is inhibited by antioxidants. Evidence suggests a role of lipid peroxidation products in the control of cell proliferation and in the induction of differentiation, maturation and apoptosis. Lipid peroxidation and ROS are triggers and essential mediators of apoptosis, which eliminate precancerous and cancerous, virus-infected and otherwise damaged cells (10-13). In the investigations carried out as a result of implantation of cancer cells the level of biomarkers of lipid peroxidation increased both in the urine and in tissues of the examined animals (rat group without supplementation) (Fig. 2, Fig. 5). It can be supposed that the obtained results are an example of chemoprevention via the mechanism that was activated due to oxidative stress. Lipid peroxidation can trigger the process of apoptosis, activating the intrinsic suicide pathway present within all cells. Apoptosis is a fundamental mechanism that regulates cell and tissue homeostasis and eliminates cancer cells (14-15).

Carcinogenesis, oxidative stress and apoptosis are associated with the effect of environmental factors (including diet). As a result of the present study, the occurrence of tumor hyperplasia was found in 25% of the rats whose diet was supplemented with selenium (in the group of rats that received only the standard diet it was 71%) ($p=0.001$). In the case of rats whose diet was supplemented with copper the occurrence of tumor cell proliferation was found only in 3 out of 8 rats (38%). Induction of apoptosis is considered an important cellular event that can account for the cancer preventive effects of Se and Cu. In the performed studies no relationship was found between the process of lipid peroxidation due to the rats' supplementation with selenium and copper, and the lower incidence of cancer and the induction of apoptosis. However, the mechanisms of apoptosis activation is dependent on the concentration, chemical forms, time of exposure to trace elements and cell type (16-20). Tumor inhibition by sodium selenite in human colon cancer cell lines HCT116 and SW620 is associated with activation of c-Jun NH2 terminal kinase (JNK).

Sodium selenite are able to downregulate β-catenin signaling pathway through inhibiting Akt kinase in colorectal cancer cells and colon xenograft tumors (16). Selenium compounds strongly inhibit the growth of mammalian tumor cells at cell cycle phases specific for each compound. Selenite treatment (10 μM) of human lymphocytes resulted in accumulation in the S-phase with irreversible growth inhibition, whereas selenate-treated (250 μM) lymphocytes accumulated in the G2 phase with reversible inhibitory effects (17). Although, it was found that all selenium compounds inhibited cell proliferation and induced cell death, selenite and selenide induced both DNA single (51-59%) and double-strand breaks (4.8-14.6%) in a concentration-dependent manner (1-5 μM); no DMBA damage was observed for the organic forms, methylselenocyanate (2-7 μM) and methylselenocysteine (20-100 μM) (17). What is interesting, selenite has been shown to be a more effective antioxidant when compared to selenate, but selenite can also oxidatively damage DNA under conditions of oxidative stress. This prooxidant effect is not observed with selenate.

Copper is an essential trace element needed to ensure cell function. There is no consensus about the cell death pathway induced by Cu. The results suggested that Cu induces the activation of apoptosis through caspase-dependent and independent pathways (21, 22). Copper is generally considered as a prooxidant metal which participates in Fenton-like reaction. One of the mechanisms of the precancerous copper activity involves its ability to produce a strongly reactive hydroxyl radical responsible for oxidative damage to DNA strands and also peroxidation of cell membrane lipids (23, 24). However, in the performed investigations the addition of copper to the rats' diet resulted in an increase of MDA level in the livers only. The mechanisms of copper can be directed against cancer cells in a dose-dependent manner, what was also confirmed in our study.

The greatest proliferation of cancer cells and the greatest number of their aggregates in lymph nodes were found in the rats whose diet was supplemented with iron (100%). The increased levels of iron in the body are associated with increased cancer risk, as was confirmed in our study (25). The mechanisms by which iron has such roles have been debated for decades. Iron may accelerate tumor initiation by enhancing the formation of free radicals, as well as function as a nutrient that fosters tumor cell proliferation (25). What is interesting, in the performed investigations in the urine of rats supplemented with iron, a statistically significant reduction of the level of 8-isoPGF2α was found. In the applied model, both the inhibition of the cancer process in the case of rats that were supplemented with selenium and copper, and the increased intensity of the cancer process in the case of rats that were supplemented with iron, probably occurred in a way that was independent of the process of lipid peroxidation. Supplementation of rats with trace elements correlated with the risk of developing cancer, but the mechanisms of this action is complicated and important mechanistic details are still unknown. Studying the role of iron and cancer has been revealed that proteins involved in iron metabolism may be multifunctional and can contribute to malignancy in ways that are independent of their primary role in iron metabolism (25). Cancer cells undergo intensive cell division and need a considerable amount of iron for their development. In the case of breast cancer, the neoplastic cells have 5- to 15-fold more transferrin receptors (TFR1) than the cells of healthy mammary glands, which favors the uptake of higher amounts of iron. TFR1 is highly expressed in many cancers, including breast cancer, leukemia, lymphoma bladder cancer, lung cancer, glioma and others. Another type of transferrin receptor, known as TfR2, was recently discovered,. They are present in many cancer cells and can additionally increase iron absorption (25-27). Some members of the STEAP family of metalloreductases, which participate in iron uptake by reducing endosomal ferric iron to ferrous iron, are also overexpressed in cancer, including STEAP1, STEAP2 and STEAP3. Overexpression of lipocalin 2, which is involved in an alternative pathway of iron uptake, in breast cancer cells increases proliferation and increases angiogenesis in corneal pocket angiogenesis assay. Iron also initiates the process of carcinogenesis by a damaging effect on macrophages or an overexpression of IL-6 and IL-8

stimulating the tumor angiogenesis (26). Moreover, as shown in our research, in the case of the rats supplemented with iron, a statistically significant reduction of catalase, superperoxide dismutase and glutathione peroxidase activity was found.

In summary, we conclude that lipid peroxidation represents a fruitful approach to early stage cancer prevention. The mechanism of anti- and pro-neoplastic activity of mineral components is complicated and it depends on the dose of the supplemented compound.

REFERENCES

1. Freitas M, Baldeiras I, Proenca T, Alves V, Mota-Pinto A, Sarmento-Ribeiro A. Oxidative stress adaptation in aggressive prostate cancer may be counteracted by the reduction of glutathione reductase. FEBS 2012; 2:119-28.
2. Griffiths RH, Moller L, Bartosz G, et al. Biomarkers. Mol Aspects Med 2002; 23:101-208.
3. Montuschi P, Barnes PJ, Roberts LJ. Isoprostanes: markers and mediators of oxidative stress. FASEB J 2004; 18:1791-800.
4. Caliskan-Can E, Miser-Salihoglu E, Atalay C, Yalcintas-Arslan U, Simsek B, Yardim-Akaydin S. DNA damage and lipid peroxidation in several types of cancer. FABAD J Pharm Sci 2010; 35:125-32.
5. Sandhya B, Manoharan S, Lavanya GS, Manmohan CR. Lipid peroxidation and antioxidant status in prostate cancer patients. Indian J Sci Technol 2010; 3(1):83-86.
6. Brys M, Morel A, Forma E, Krzeslak A, Wilkosz J, Rozanski W, Olas B. Relationship of urinary istprostanes to prostate cancer occurence. Mol Cell Biochem 2013; 372:149-53.
7. Tukozkan N, Erdamar H, Seven I. Measurement of total malondialdehyde in plasma and tissues by high-performance liquid chromatography and thiobarbituric acid assay. Firat Tip Dergisi 2006; 11(2):88-92.
8. Pramanik KC, Boreddy SR, Srivastava SK. Role of mitochondrial electron transport chain complexes in capsaicin mediated oxidative stress leading to apoptosis in pancreatic cancer cells. PloS One 2011; 5:1-16.
9. Crakowski JL. Isoprostanes: an emerging role in vascular physiology and disease? Chem Phys Lipids 2004; 128:75-83.
10. Gago-Dominquez M, Castelao JE, Pike MC, Sevanian A, Haile RW. Role of lipid peroxidation in the epidemiology and prevention of breast cancer. Cancer Epidemiol Biomarkers Prev 2005; 14(12):2829-39.
11. Barrera G. Oxidative stress and lipid peroxidation products in cancer progression and therapy. ISRN Oncology 2012; doi:10.5402/2012/137289.
12. Custovic Z, Zarkovic K, Cindric M, et. al. Lipid peroxidation product acrolein as a predictive biomarker of prostate carcinoma relapse after radical surgery. Free Rad Res 2010; 44:497-504.
13. Aydin A, Arsova-Sarafinovska Z, Sayal A, et. al. Oxidative stress and antioxidant status in non-metastatic prostate cancer and benign prostatic hyperplasia. Clin Biochem 2006; 39:176-79.
14. Gollapudi S, Ghoneum M. MGN-3/Biobran, modified arabinoxylan from rice bran, sensitizes human breast cancer cells to chemotherapeutic agent, daunorubicin. Cancer Detect Prev 2008; 32:1-6.
15. Pelicano H, Carney D, Huang P. ROS stress in cancer cells and therapeutic implication. Drug Resist Updat 2004; 7:97-110.
16. Sanmartin C, Plano D, Sharma AK, Palop JA. Selenium compounds, apoptosis and other types of cell death: an overview for cancer therapy. Int J Mol Sci 2012; 13:9649-72.
17. Ramoutar RR, Brumaghim J. Antioxidant and anticancer properties and mechanisms of inorganic selenium, oxo-sulfur, and oxo-selenium compounds. Cell Biochem Biophys 2010; 58:1-23.
18. Abdulah R, Miyazaki K, Nakazawa M, Koyama H. Chemical forms of selenium for cancer prevention. J Trace Elem Med Biol 2005; 19:141-50.
19. Ramoutar RR, Brumaghim J. Antioxidant and anticancer properties and mechanisms of inorganic selenium, oxo-sulfur, and oxo-selenium compounds. Cell Biochem Biophys 2010; 58:1-23.
20. Zeng H, Combs GF. Selenium as an anticancer nutrient: roles in cell proliferation and tumor cell invasion. J Nutr Biochem 2008; 19:1-7.
21. Kawakami M, Inagawa R, Hosokawa T, Saito T, Kurasaki M. Mechanism of apoptosis induced by copper in PC12 cells. Food Chem Toxicol 2008;

46(6):2157-61.
22. Santos S, Silva AM, Matos M, Monteiro SM, Alvaro AR. Copper induced apoptosis in Caco-2 and Hep-G2 cells: expression of caspases 3, 8 and 9, AIF and p53. Comp Biochem Physiol C Toxicol Pharmacol 2016; 185:138-46.
23. Formigari A, Irato P, Santon A. Zinc, antioxidant system and metallothionein in metal mediated-apoptosis: biochemical and cytochemical aspects. Comp Biochem Phys 2007; 146:443-45.
24. Gupte A, Mumper RJ. Elevated copper and oxidative stress in cancer cells as a target for cancer treatment. Cancer Treat Rev 2009; 35:32-46.
25. Torti SV, Torti FM. Iron and cancer: more ore to be mined. Nat Rev Cancer 2013; 13(5):342-55.
26. Gurzau ES, Negau C, Gurzau AE. Essentials metals-case study on iron. Ecotoxicol Environ Safe 2003; 56(1):190-96.
27. Bogdan AR, Miyazawa M, Hashimoto K, Tsuji Y. Regulators of iron homeostasis: new players in metabolism, cell death and disease. Trends Biochem Sci 2016; 41(3):274-86.

LETTER TO THE EDITOR

EFFECT OF GENERAL ANESTHESIA COMBINED WITH EPIDURAL ANESTHESIA ON PERIOPERATIVE IMMUNE FACTORS IN CERVICAL CANCER

G-D. LIU, G-Q. LIANG, H. WANG and Y. ZHOU

Department of Anesthesiology, Zhuhai People's Hospital, Zhuhai, China

Received November 26, 2018 – Accepted February 13, 2019

To the Editor,

Cervical cancer (CC) is a common malignant tumor that seriously threatens the health and life of female patients (1). At present, surgical resection remains as the preferred treatment for CC (2). Surgery is an invasive procedure, and surgical stress increases immunosuppression in CC patients, which can lead to serious immune injury and increase the risk of CC metastasis and recurrence (3). Some studies have revealed that besides reducing the stress reaction caused by surgery and alleviating the immunosuppression caused by surgery stress, anesthesia could also affect the immune function of CC patients (4). Some anesthesia methods even produce immunosuppression, affecting the patient's recovery (5). The present study compares the effects of general anesthesia combined with epidural anesthesia (GACWEA) and general anesthesia (GA) alone on immune factors during the CC perioperative period, in order to explore the best anesthesia mode and provide a reference for choosing a reasonable anesthesia method for CC surgery.

MATERIALS AND METHODS

Study subjects

The present study was approved by the Ethics Committee of Zhuhai People's Hospital, Zhuhai, China. The patients or their family members provided an informed consent. A total of 126 CC patients, who underwent surgery in the hospital from June 2016 to May 2017, were selected for the study. The sample size was calculated by statistical software. Inclusion criteria for the patients were: diagnosed by pathological biopsy and met the diagnostic criteria for CC; without a history of hormone treatment; without a history of radiochemotherapy; provided an informed consent; and those with American Society of Anesthesiologists (ASA) grade I-II. Exclusion criteria: patients with a history of immune diseases; contraindications to epidural anesthesia and GA; patients who had received analgesic or narcotic drugs in the previous 60 days; patients with dysfunction of the heart, liver, kidney and other organs; patients with an allergic constitution; characteristic populations (pregnant and lactating women, and patients with neurological and psychiatric diseases). All CC patients were randomly divided into two groups: GACWEA group (n= 66) and GA group (n= 60).

Method

After entering the operating room, venous access was established in all patients in the two groups. All patients initially underwent epidural anesthesia. Then, L1-2 was selected as the puncture point, and 5 ml of lidocaine (2%) was given after puncture. After 5 min, the anesthesia plane was tested to confirm the success of the epidural anesthesia. Then, in both groups of patients, anesthesia was induced

Key words: general anesthesia; epidural anesthesia; cervical cancer; perioperation; immune factors

Corresponding Author:
Dr G-D. Liu,
Department of Anesthesiology,
Zhuhai People's Hospital, No. 79 of Kangning Road,
Xiangzhou District, Zhuhai 519000, China
Tel.: +86 756 2158628 - Fax: +86 756 2158626
e-mail: guideliudr@21cn.com

0393-974X (2019)

with 0.3 μg/kg of sufentanil, 1.5-2.5 mg/kg of propofol and 0.1 mg/kg of vecuronium bromide. Mechanical ventilation with parallel endotracheal intubation was given. In both groups, the inhalation of 0.8 MAC of sevoflurane was given to maintain anesthesia. An intravenous injection of vecuronium bromide was intermittently given to maintain satisfactory muscle relaxation. In addition, in the GACWEA group, 2% lidocaine was pumped into the epidural space at a rate of 4-6 ml/h. In the GA group, remifentanil was given for target-controlled analgesia, and the target plasma concentrations of remifentanil were 3.5, 5.0 and 3.0 ng/ml before skin incision, abdominal inspection and abdominal closure, respectively. During the operation, the bispectral index (BIS) was used to monitor the depth of anesthesia, which was maintained within 40-60. After the operation, the endotracheal tube was removed after the patient was fully awake, had become hemodynamically stable and recovered spontaneous breathing, and the normal muscle strength and reflex returned to normal levels. Both groups of patients were given patient-controlled epidural analgesia at the end of the operation, and 30 μg of sufentanil + 300 mg of ropivacaine were added to the 250-ml electronic analgesia pump. A single dose was 2 ml, the continuous infusion rate was 5 ml/h, and locking time was 15 min.

Observation indexes

Ramsay sedation score and visual analog scale (VAS) pain score at six hours, 12 hours, one day and two days after the operation were evaluated in the two groups. In addition, elbow venous blood was extracted at T0 (five minutes before anesthesia), T1 (immediately after the operation), T2 (one day after the operation), T3 (three days after the operation), and T4 (five days after the operation). Furthermore, the levels of T-lymphocyte subsets, such as CD3+, CD4+, CD8+, CD4+/ CD8+, interleukin-6 (IL-6) and natural killer (NK) cells, were detected. Ramsay sedation score: agitated, non-cooperative state, 1 point; quiet, cooperative state, 2 points; sleepy, complies with instructions, 3 points; asleep, able to be woken up, 4 points; non-responsive state, 5 points. VAS pain score : A 10-cm long line segment was drawn on a piece of white paper. One end of the line segment was set as 0, which represents no pain, while the other end of the line segment was set as 10, which represents severe pain. That is, 0-10 represents the different degrees of pain. The patient was asked to make a mark on the corresponding position of the line segment to represent his own degree of pain. The levels of $CD3^+$, $CD4^+$, $CD8^+$ and NK cells were detected using a FACSCanto II flow cytometer (Becton, Dickinson and Company, USA). IL-6 level was detected using enzyme-linked immunosorbent assay (ELISA) (Millipore, USA). The test was carried out accordingly to the manufacturer's instructions.

Statistical analysis

Data were analyzed using statistical software SPSS19.0. Quantitative data were expressed as mean±standard deviation (x±SD). Qualitative data were expressed as case number and rate. Intergroup comparison was conducted using univariate analysis of variance. Repeated measurement variance analysis was used to compare the index at different time points in each group. Qualitative data were analyzed using *Chi*-squared test. The non-normally distributed continuous data were compared using non-parametric tests. $P<0.05$ was considered statistically significant.

RESULTS

Comparison of general data between the two groups of patients

The 126 patients were aged 34-68 years, (average 52.26±5.19 years). The course of disease ranged within 1-8 months, with an average course of disease of 3.87±0.05 months. Their weight ranged within 49-76 kg, with an average body weight of 55.43±5.69 kg. Furthermore, 97 patients (76.98%) were positive for HPV, while 29 patients (23.02%) were negative for HPV. Moreover, adenocarcinoma was found in 91 patients (72.22%), squamous cell carcinoma was found in 20 patients (15.87%), and squamous adenocarcinoma was found in 15 patients (11.91%). ASA grades: 84 patients (66.67 %) were at grade I, and 42 patients (33.33 %) were at grade II. The difference between the two groups was not statistically significant ($P>0.05$), Table I.

Comparison of T-lymphocyte subset levels at different time points

The levels of T-lymphocyte subsets $CD3^+$, $CD4^+$ and $CD4^+/CD8^+$ in the two groups were significantly lower at T1, T2 and T3 than at T0, and the difference was statistically significant ($P<0.05$). The levels of

Table I. *Comparison of the results between the two groups of patients.*

INDEX	GACWEA group (n=66)	GA group(n=60)	χ^2/t/u	*p*
Age (years)	52.35±5.38	52.02±5.27	0.3472	0.7290
disease course (months)	3.85±0.14	3.88±0.16	1.1224	0.2639
Weight (kg)	54.98±5.41	55.64±5.77	0.6626	0.5088
HPV (positive/negative)	51/15	46/14	0.0065	0.9357
PATHOLOGICAL TYPE (adenocarcinoma/adenocarcinoma/adeno-squamous carcinoma)	47/11/8	44/9/7	0.0800	0.9608
ASA grades (grade I/II)	43/23	41/19	0.3769	0.7063
6h (Ramsay Sedation Scale score)	3.79±0.36	3.82±0.39	0.4490	0.6542
12h (Ramsay Sedation Scale score)	3.33±0.26	3.38±0.27	1.0585	0.2919
1d (Ramsay Sedation Scale score)	2.73±0.22	2.79±0.23	1.4962	0.1371
2d (Ramsay Sedation Scale score)	1.76±0.19	1.82±0.21	1.6838	0.0947
6h (VAS pain score)	3.81±0.39	3.84±0.41	0.4208	0.6746
12h (VAS pain score)	2.38±0.36	2.40±0.38	0.3033	0.7622
1d (VAS pain score)	2.07±0.31	2.16±0.35	1.5306	0.1284
2d (VAS pain score)	1.74±0.16	1.80±0.20	1.8672	0.0642

Table II. *Comparison of levels of T-lymphocyte subsets in the two groups at different time points (*x±*s).*

Time	GACWEA GROUP (N=66)				GA GROUP (N=60)			
	CD3+(%)	CD4+(%)	CD8+(%)	CD4+/CD8+	CD3+(%)	CD4+(%)	CD8+(%)	CD4+/CD8+
T_0	69.24±7.21	38.27±3.84	28.44±3.18	1.35±0.31	69.27±7.24	38.30±3.85	28.46±3.21	1.35±0.33
T_1	60.57±6.41[a]	30.62±3.58[a]	26.49±2.63	1.16±0.28	61.25±6.45[a]	31.53±3.62[a]	27.38±2.68	1.15±0.26[a]
T_2	58.52±6.29[a]	28.43±3.17[a]	24.67±2.26	1.15±0.20[a]	51.78±5.29[ab]	24.60±2.59[ab]	23.58±2.83[a]	1.04±0.28[ab]
T_3	64.62±6.59[a]	35.82±3.67[a]	27.18±2.77	1.32±0.29	59.18±6.53[ab]	31.44±3.59[ab]	27.01±2.69	1.16±0.27[ab]
T_4	68.62±7.17	37.64±3.71	28.04±3.11	1.34±0.30	67.61±7.03	37.69±3.73	28.18±3.17	1.34±0.31

.[a]Compared with T_0, $p < 0.05$; [b]Compared with GACWEA group, $p < 0.05$

Table III. *Comparison of levels of IL-6 and NK cells in the two groups at different points (x±s)*

Time	GACWEA group (n=66)		GA group (n=60)	
	IL-6(pg/ml)	NK cells(%)	IL-6(ng/L)	NK cells(%)
T_0	57.68±5.88	19.47±2.26	57.81±5.93	19.46±2.28
T_1	95.73±9.61[a]	18.33±2.72	103.73±9.69[ab]	18.12±2.74
T_2	103.73±10.52[a]	17.89±2.74	128.87±13.04[ab]	16.58±2.42
T_3	84.75±8.68[a]	18.37±2.11	100.28±10.71[ab]	17.29±2.14
T_4	59.68±6.72	19.02±1.79	70.74±7.28[ab]	18.87±1.80

[a]*Compared with* T_0, $p < 0.05$; [b]*Compared with GACWEA group,* $p < 0.05$.

T-lymphocyte subsets $CD3^+$, $CD4^+$ and $CD4^+/CD8^+$ in the two groups gradually recovered from T3 to T4, which returned to a level close to the pre-operative level at T4. At T2 and T3, the levels of $CD3^+$, $CD4^+$ and $CD4^+/CD8^+$ were significantly lower in the GA group than in the GACWEA group, and the differences were statistically significant (P<0.05), Table II.

Comparison of Ramsay sedation scores at six hours, 12 hours, one day and two days after the operation between the two groups

The Ramsay sedation score in the two groups gradually decreased with time after the operation, The differences in Ramsay sedation scores at six hours, 12 hours, one day and two days after the operation between the two groups were not statistically significant (P>0.05), Table I.

Comparison of VAS pain scores at six hours, 12 hours, one day and two days after the operation between the two groups

The VAS pain score in the two groups gradually decreased with time after the operation. The difference in VAS pain scores at six hours, 12 hours, one day and two days after the operation between the two groups were not statistically significant (P>0.05), Table I.

Comparison of levels of IL-6 and NK cells at different time points in the two groups

The IL-6 level in the two groups was significantly higher at T1, T2 and T3 than at T0, and the difference was statistically significant (P<0.05). The IL-6 level in the two groups gradually decreased from T2 to T4, and the IL-6 level returned to a level close to the pre-operative level at T4. Furthermore, IL-6 levels at T1, T2, T3 and T4 were significantly higher in the GA group than in the GACWEA group, and the differences were statistically significant (P<0.05). The level of NK cells in the two groups was significantly lower at T1, T2 and T3 than at T0, and the difference was statistically significant (P<0.05). The level of NK cells in the two groups gradually recovered from T3 to T4, and returned to a level close to the pre-operative level at T4. At T2 and T3, the level of NK cells was significantly lower in the GA group than in the GACWEA group, and the

difference was statistically significant ($P<0.05$). The details are presented in Table III.

DISCUSSION

Studies have revealed that anesthesia is an important method to reduce surgical stress response (6-8). It has been reported that anesthesia can lead to different degrees of immunosuppression and stress reactions in patients, and exert influence on T lymphocytes and NK cells (9). However, immune function is not only affected by the anesthesia itself, but also anesthetic drugs, anesthetic methods and anesthetic depth (10). Therefore, we conducted this study to investigate the effect of GACWEA on perioperative immune factors in patients who had undergone cervical cancer surgery.

The levels of T-lymphocyte subsets, such as $CD3^+$, $CD4^+$, $CD8^+$, $CD4^+/CD8^+$, and changes in IL-6 and NK cells at different time points after the operation were compared between the GACWEA group and GA group, and these indexes at different time points after the operation were compared with preoperative indexes in both groups. The results also revealed that the effects of anesthesia methods and drugs on immune function were different and GACWEA coulf improve the inhibition of cellular immunity caused by surgical trauma. The mechanism is that GACWEA can effectively block injury signals from entering into the central nervous system through the peripheral nerve, and block the dominant role of the sympathetic nerve on the adrenal medullary, reducing stress response. In addition, GACWEA can also effectively reduce the dosage of anesthetic drugs, avoiding the occurrence of cellular immunosuppression caused by their heavy use.

In summary, compared with GA, GACWEA can effectively alleviate the immunosuppression of surgical stress in CC patients, and has little impact on inflammatory cytokines, which is worthy for application in the clinic.

REFERENCES

1. Dizon DS, Mackay HJ, Thomas GM, et al. State of the science in cervical cancer: where we are today and where we need to go. Cancer 2014; 120:2282-88.
2. Gu JJ, Yin L, Wu J, Zhang N, Huang T, Ding K, He X. Inhibitory effect of cetuximab combined with cisplatin on nasopharyngeal carcinoma cell lines and its molecular mechanism. China Cancer 2016; 25:303-8.
3. Chen WQ, Wang K, Tang J, et al. Cervical esophagostomy improves the life quality of patients with dysphagia induced by radiotherapy for nasopharyngeal carcinoma. Chin J Otorhinolaryngol Head Neck Surg 2016; 51:179-82.
4. Yang KH, Hu Y, Li Y, Peng CX. Two different methods of anesthesia for laparoscopic colon perioperative cellular immunity and cytokines of patients with colon cancer. J Clin Exp Med 2016; 15:173-76.
5. Cata JP, Bauer M, Sokari T, Ramirez MF, Mason D, Plautz G, Kurz A. Effects of surgery, general anesthesia, and perioperative epidural analgesia on the immune function of patients with non-small cell lung cancer. J Clin Anesth 2013; 25:255-62.
6. Xiao J, Luo XL, Li WC, Yang HL, Hu T. Effects of different concentrations of dexmedetomidine on immunity and cognitive dysfunction in senile patients with lower thoracic and lumbar operation under general anesthesia. Lab Med Clin 2016; 13:775-78.
7. Wu J, Wang WJ. Effect of different anesthesia methods on perioperative immune function in small cell lung cancer. J Mod Oncol 2016; 24:1630-33.
8. Cho JS, Lee MH, Kim SI, et al. The effects of perioperative anesthesia and analgesia on immune function in patients undergoing breast cancer resection: a prospective randomized study. Int J Med Sci 2017; 14:970-76.
9. OuyangYB, Stary CM, White RE, Giffard RG. The use of microRNAs to modulate redox and immune response to stroke. AnTioxid Redox Sidnal 2015; 22:187-202.
10. Wang YW. Effects of 2 different anesthesia protocols on perioperative cellular immunity and IL-6 in patients who underwent laparoscopic radical colectomy. Pr J Cancer 2015; 30:355-58.

LETTER TO THE EDITOR

IDENTIFICATION OF THE SULFOTRANSFERASE ISO-ENZYME PRIMARILY RESPONSIBLE FOR THE BIO-ACTIVATION OF TOPICAL MINOXIDIL

J. M[C]COY[1], A. GOREN[1,2], T. NACCARATO[1], M. KOVACEVIC[2], M. SITUM[3], V.L. SKUDAR[4] and T. LOTTI[2]

[1]Applied Biology, Inc., Irvine, CA, USA; [2]Department of Dermatology and Venereology, University of Rome "G.Marconi", Rome, Italy; [3]Department of Dermatology and Venereology, University Hospital Center "Sestre milosrdnice", Zagreb, Croatia; [4]Department of Dermatology and Venereology, Zagreb School of Medicine, University of Zagreb, Croatia

Received November 6, 2018 – Accepted February 14, 2019

To the Editor,

Pattern hair loss (i.e., androgenetic alopecia) is a common condition afflicting approximately fifty percent of men and women by the age of fifty (1). Currently, topical minoxidil is the only US FDA approved drug for the treatment of pattern hair loss in men and women. Unfortunately, clinical studies have demonstrated that less than 40% of patients respond to topical minoxidil therapy (2). Therefore, developing novel therapies for hair loss or adjuvant therapies for improving the efficacy of minoxidil is of clinical importance. Topical minoxidil is a pro-drug, converted to its active form, minoxidil sulfate, via sulfotransferase enzymes located in hair follicles (3, 4). Previously, we demonstrated that the activity of sulfotransferase enzymes in hair follicles is a major determinant for minoxidil response (5). As such, inducing the expression of sulfotransferase in hair follicles may significantly alter the clinical response rate to topical minoxidil.

Buhl et al. (6) demonstrated the hair shaft (hair shaft, cortex, medullar, inner root sheath) accounted for only 9% of the minoxidil sulfonating activity of the hair follicle and that the hair sheath (dermal papilla, outer root sheath, cavernous sinus and connective tissue) accounted for 91% of the minoxidil sulfonating activity. Eight members of the SULT1 family are known to exhibit substrate specificity toward minoxidil. Of these, only three have been detected in human scalp tissues (7). SULT1A1, SULT1A3, and SULT1E1 have also been found in cultured kerotioncytes, as well as scalp tissue biopsies (7). SULT1A1 and SULT1A3 are phenol sulfotransferase (PST) enzymes responsible for metabolism of various planar phenol xenobiotics. SULT1E1 (estrogen sulfotransferase) is the leading enzyme candidate responsible for cholesterol sulfonation in the skin; however, SULT1E1 shows substrate specificity toward minoxidil, as well.

An important first step in identifying compounds that may alter minoxidil sulfonation rates in the hair follicle would be to identify which of the three sulfotransferases found in the scalp are predominately responsible for converting minoxidil to minoxidil sulfate. In order to identify the iso-enzyme primarily responsible for the bio-activation of minoxidil in hair follicles, we compared the enzymatic activity of plucked human hair samples to recombinant human SULT1A1, SULT1A3, and SULT1E1 enzymes.

Key words: pattern hair loss; minoxidil; alopecia; sulfotransferase

Corresponding Author:
John McCoy, PhD
Applied Biology, 17780 Fitch,
Suite 192, Irvine, CA 92614, USA
Tel.: +1 (949) 387-4526
e-mail: johnm@appliedbiology.com

0393-974X (2019)

MATERIALS AND METHODS

Plucked human hair samples from 16 volunteers (8 men and 8 women) were collected at a hospital dermatology department (Department of Dermatology and Venereology, Clinical Hospital Center Sestre Milosrdnice, Zagreb, Croatia). Each Subject signed an informed written consent prior to participating in the study. Each subject's plucked hairs were trimmed just above the bulb so that the smallest amount of hair containing the bulb was obtained. Four hair bulbs from each subject were inserted into an individual well on a 96-well plate. Subsequently, 200 uL of solution containing a colorimetric sulfotransferase activity assay, previously described (5), was added to each well. In addition, purified recombinant hSULT1A1, hSULT1A3, and hSULT1E1 were obtained (R&D systems, Minneapolis, MN, USA). 2 ug of each enzyme were combined with the activity assay and placed into separate wells on the 96-well plate. A spectrophotometer (Biotek Powerwave HT Microplate Spectrophotometer, Winooski, VT, USA) was used to measure the optical density at 405 nm (OD 405) over a period of 24 hours. Absorbance data was recorded for each well every 20 min. A total of 73 data points were recorded for each sample.

RESULTS

The raw kinetic data over 24 hours was analyzed. To account for sulfotransferase enzyme variability in human samples, the kinetic data from the 16 human samples were averaged. The Pearson correlation coefficient (MedCalc v18.5) was used to determine the best fit between the enzymatic activity of the human hair samples and each recombinant SULT enzyme. The correlation in enzymatic activity between the human samples and the SULT1A1 enzyme was $r=0.9712$, $p<0.001$ with (95CI: 0.9544, 0.9819). The correlation in enzymatic activity between the human samples and the SULT1E1 enzyme was $r=0.8135$, $p<0.001$ with (95CI: 0.7178, 0.8791). The correlation in enzymatic activity between the human samples and the SULT1A3 enzyme was 0.7728, $p<0.001$ with (95CI: 0.6601, 0.8515). In addition, the enzyme kinetics (OD 405) for each recombinant SULT enzyme was plotted against the average of the pooled human hair samples (Fig. 1).

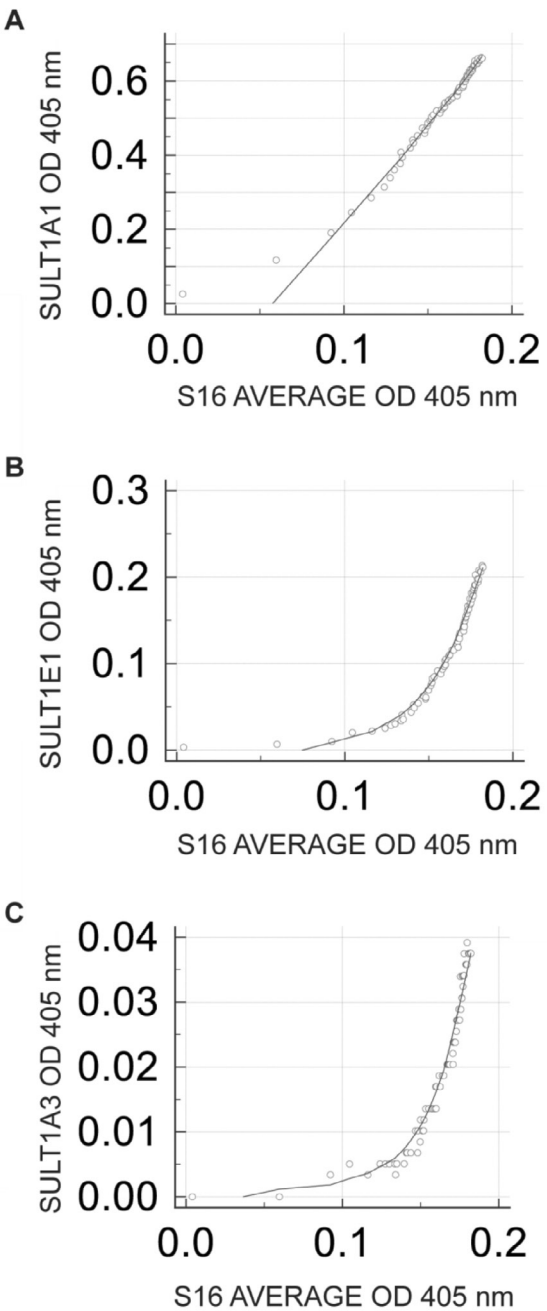

Fig. 1. *Plot of enzyme kinetics (OD 405) for each recombinant SULT enzyme versus the average of the pooled human hair samples. SULT1A1 vs human samples (**A**). SULT1E1 vs human samples (**B**). SULT1A3 vs human samples (**C**).*

DISCUSSION

Three of the eight members of the SULT1 family are present in the hair root sheath and scalp: SULT1A1, SULT1A3, and SULT1E1. The results of

this study indicate that SULT1A1 is likely the most significant contributor to the activation of minoxidil in human hair follicles ($r=0.9712$, $p<0.001$). The activity of sulfotransferase enzymes in hair follicles is a major determinant of minoxidil response; thus, pattern hair loss patients who are non-responders to topical minoxidil could potentially benefit from the up-regulation of the SULT1A1 enzyme expressed in human hair follicles. Utilizing the results of this study, we are developing a topical minoxidil adjuvant therapy that up-regulates the follicular SULT1A1 enzyme.

REFERENCES

1. Hoffmann R, Happle R. Current understanding of androgenetic alopecia. Part II: clinical aspects and treatment. Eur J Dermatol 2000; 10(5):410-17.
2. Olsen EA, Whiting D, Bergfeld W, et al. A multicenter, randomized, placebo-controlled, double-blind clinical trial of a novel formulation of 5% minoxidil topical foam versus placebo in the treatment of androgenetic alopecia in men. J Am Acad Dermatol 2007; 57(5):767-74.
3. Baker CA, Uno H, Johnson GA. Minoxidil sulfation in the hair follicle. Skin Pharmacol 1994; 7(6):335-39.
4. Anderson RJ, Kudlacek PE, Clemens DL. Sulfation of minoxidil by multiple human cytosolic sulfotransferases. Chem Biol Interact 1998; 109(1-3):53-67.
5. Goren A, Shapiro J, Roberts J, et al. Clinical utility and validity of minoxidil response testing in androgenetic alopecia. Dermatol Ther 2015; 28(1):13-16.
6. Buhl AE, Waldon DJ, Baker CA, Johnson GA. Minoxidil sulfate is the active metabolite that stimulates hair follicles. J Invest Dermatol 1990; 95(5):553-77.
7. Dooley TP, Haldeman-Cahill R, Joiner J, Wilborn TW. Expression profiling of human sulfotransferase and sulfatase gene superfamilies in epithelial tissues and cultured cells. Biochem Biophys Res Commun 2000; 277(1):236-45.

LETTER TO THE EDITOR

EXPRESSION AND CLINICAL SIGNIFICANCE OF p16 AND Ki-67 IN MALIGNANT MELANOMA OF THE CONJUNCTIVA

FF. SU[1] and JL. CHEN[2]

[1]Department of Ophthalmology, Jingzhou Central Hospital, Jingzhou City, Hubei Province, China;
[2]Department of Ophthalmology, Shibei Hospital, Jing'an District, Shanghai, China

Received November 26, 2018 – Accepted January 25, 2019

To the Editor,

Malignant melanoma (MM) is a tumor with highly invasive and metastatic potential and poor prognosis (1). MMs of the eye include those of the choroid, eyelid, and conjunctival (CMM) (2). The differential diagnosis includes mainly conjunctival melanocytic nevi (CMN) but also conjunctival papillomas determined by HPV infection (3), and other types of benign or malignant tumors of the conjunctiva. The most common feature of CMN is the presence of cysts in the lesion, which recur more quickly after biopsy and occur in uncommon sites (e.g. palpebral conjunctiva or fornix conjunctiva) (4). There are still no definite clinical symptoms that can accurately predict malignant transformation of CMN.

The p16 (p16Ink4A, CDKN2A) protein is encoded by the INK4a-ARF gene (5) and can directly participate in tumor suppression by negatively regulating cell growth and proliferation. The P16 gene can reduce the proliferation of cancer cells by inhibiting their division and by inducing their death (6). Ki-67 protein is a large protein located in the nucleus (7). Since its half-life is short and its changes of expression are consistent with the phase changes in intracellular DNA replication, this protein has become a reliable indicator for the detection of tumor cell proliferation activity (8). The present study examines the difference between the pathological features of CMN and CMM in correlation with the expression of p16 and Ki-67.

MATERIALS AND METHODS

Clinical data

A total of 34 cases of pathologically confirmed CMM (experimental group) and 34 cases of CMN (control group) were recruited from February 2015 to November 2017 in Jingzhou Central Hospital. All enrolled patients provided surgically resected tumor specimens. The detailed medical records and clinical research data of the enrolled patients were collected. Clinical data were provided by the patient or his/her family. The patient's informed consent was obtained for the acquisition of the specimen, and the present study was approved by the Ethics Committee of Jingzhou Central Hospital.

After the tumor tissue was surgically removed, a paraffin block was prepared and used as a spare. The present study was based on the clinical staging of the American Joint Committee on Cancer (AJCC) conjunctival malignant melanoma (9), as following:

Stage T0 - No evidence of primary tumor

Stage T1 - Bulbar conjunctival malignant melanoma; T1a: less than 1 quadrant; T1b: greater than 1 quadrant but less than 2 quadrants; T1c: greater than 2 quadrants but less than 3 quadrants; T1d: greater than 3 quadrants

Key words: conjunctival malignant melanoma; conjunctival nevus; P16; Ki-67, biomarkers

Corresponding author:
Dr Jili Chen,
Department of Ophthalmology, Shibei Hospital,
No. 4500 Gonghe New Road,
Jing'an District,
Shanghai 200435, China
e-mail: chenjilicornea@163.com

0393-974X (2019)

Stage T2 - Conjunctiva, fornix conjunctiva and/or lacrimal caruncle malignant melanoma; T2a: less than 1 quadrant, without invasion of lacrimal caruncle; T2b: more than 1 quadrant, without invasion of lacrimal caruncle; T2c: less than 1 quadrant, invasion of lacrimal caruncle; T2d: more than 1 quadrant, invasion of lacrimal caruncle

Stage T3 - Local invasion of malignant melanoma; T3a: invasion of the eyeball; T3b: invasion of the eyelid; T3c: invasion of the orbit; T3d: Invasion of paranasal sinuses

Stage T4 - Malignant melanoma invades the central nervous system

The criteria for enrollment were the following: the patient was diagnosed with an *in situ* CMM tumor; primary CMM was considered only in the absence of previous CMM resection; patients were not suffering from other unknown diseases.

Exclusion criteria: metastasis of the conjunctiva from the primary eyelid, malignant melanoma in the eye or malignant melanoma of the other parts of the body to the conjunctiva and orbital nevus pigmentation were not included in the present study. Ocular surface inflammation and other tumor cases.

All pathological specimens were fixed in 4% buffered formaline, processed and embedded in paraffin according to routine procedures. Hematoxylin-eosin (HE) staining was used for the pathological diagnosis of the samples according to the standard protocol (1).

Immunohistochemical staining

p16 and Ki-67 expression was evaluated by immunohistochemistry on serial sections (4 μm) using the primary antibodies: mouse anti-human p16 monoclonal antibody (Shanghai Fusheng Industrial Co., Ltd., Shanghai, China) and mouse anti-human Ki-67 monoclonal antibody (Shanghai Fusheng Industrial Co., Ltd., Shanghai, China).

The immunohistochemical staining positive reaction was considered when the cytoplasm and/or nucleus of the cells were bright red under the microscope. Ten high magnification fields (40X objective) were randomly observed in each slice. Based on the percentage of the stained cells from the total number of cells, they were classified as: negative (-) (<5%), weakly positive (+) (6-25%), moderately positive (++) (26-75%), and strongly positive (+++) (> 75%) (10).

Statistical analysis

The data of the present study were analyzed by SPSS19.0 software. The differences in expression rates between groups were tested using *chi*-squared test, and correlation analysis was performed using Spearman correlation. The relationship between each factor and the clinical stage and prognosis of CMM was compared. $P<0.05$ was considered statistically significant.

RESULTS

Clinical stage and recurrence of the tumor

A significant difference in the recurrence of different clinical stages of AJCC tumors was noted ($P<0.05$). The higher recurrence rate was observed in stage 2 conjunctival malignant melanoma, 17 cases, compared with 5 cases in stage 3 and only 2 cases in stage 1.

Histopathological examination

Under HE staining, CMM was divided into epithelioid cell type, spindle cell type and mixed cell type (Fig. 1A). Local tumor necrosis could be observed under the microscope. In mixed cell type CMM, vascular walls were destroyed, whereas some entered the lumen (Fig. 1D). Nuclear fission was noted in the tumor (Fig. 1E). The infiltration of inflammatory cells was local or diffused (Fig. 1C).

Expression of p16 and Ki67

The expression of p16 in CMM is shown in Fig. 2A. The red nuclei represent the positive expression site of p16, and some melanin particles can still be observed. Based on the aforementioned criteria for the percentage of positive immunohistochemical detection, it could be observed that the expression of p16 in CMM differed between the two groups. The experimental group showed a decreased expression of p16, as 20 cases were negative for p16 expression compared with only 2 cases in the control group ($P<0.001$). In the control group there were 2 cases with negative p16 expression, 7 cases with low p16 expression, 9 cases with moderate p16 expression and 16 cases with high p16 expression compared with 20 cases of negative p16 expression, 7 cases of low p16 expression, 7 cases with moderate p16 expression and no case of high p16 expression in the experimental group. The expression of p16 in CMN is shown in Fig. 2B.

There was no significant difference in the expression of p16 among epithelial cell type, spindle cell type, and mixed cell type of CMM (χ^2=0.209, P=0.881). p16 overexpression was correlated with less advanced clinical stages of CMM (χ^2=9.182, P=0.01). Spearman correlation analysis indicated that r = -0.603, P = 0.005, which pointed towards a strong correlation. Loss of p16 expression in CMM is associated with tumor recurrence (χ^2=4.673, P=0.025). The Spearman correlation analysis indicated that r = -0.441, P = 0.025, indicating a negative correlation.

Ki-67 was highly expressed in the experimental group compared with the control group (Fig. 3, A,B). In the experimental group, there were 7 cases with negative Ki-67 expression, 8 cases with low Ki-67 expression, 7 cases with moderate Ki-67 expression and 12 cases with high Ki-67 expression compared with 25 cases with negative Ki-67 expression, 9 cas-

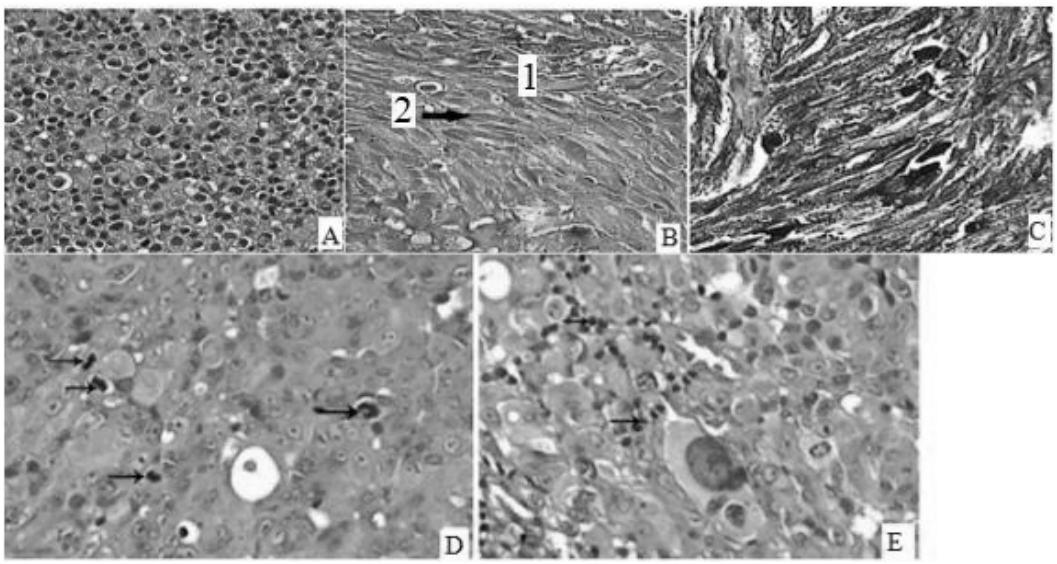

Fig. 1. ***A)*** *HE staining of epithelioid cell type: the cells are round, the nucleolus is obvious, visible mitosis;* ***B)*** *HE staining of mixed cell type in which both epithelial and spindle cells are present. The arrow 1 indicates the epithelium. The arrow 2 indicates spindle cell;* ***C)*** *HE staining of spindle cell type: the cells are fusiform, spindle-shaped, with prominent nucleoli, and the cytoplasm is rich in pigment particles);* ***D)*** *Mitotic figures in the tumor, 200X;* ***E)*** *Distribution of inflammatory cells in the tumor, 200X).*

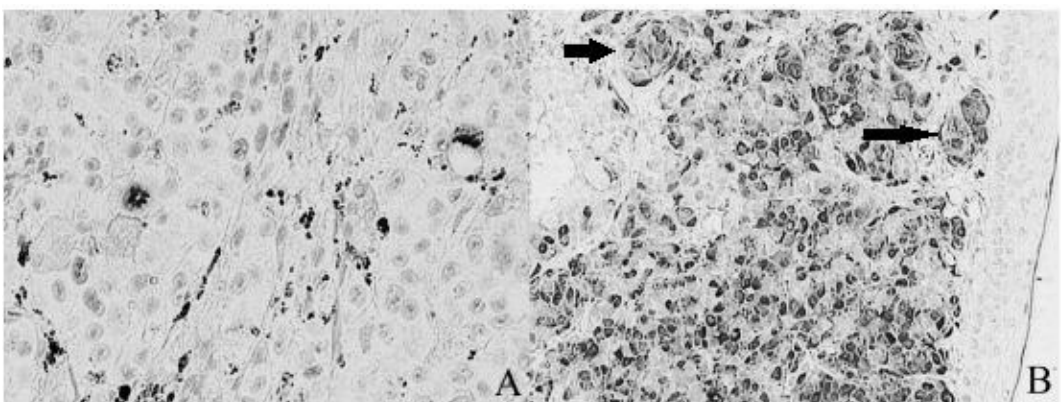

Fig. 2. *p16 expression in CMM and CMN.* ***A)*** *p16 expression in the experimental group, 200X;* ***B)*** *p16 expression in the control group, positive cells indicated by arrows include the positive cell nuclei and part of their cytoplasm . 100X).*

es of low Ki-67 expression and 12 cases of the high/moderate Ki-67 expression in control group. Ki-67 expression was associated with the recurrence of the disease in the experimental group. In the experimental group there were 10 non-recurrent cases and 24 recurrent cases. In non-recurrent cases 8 had low Ki-67 expression and 2 cases medium-high Ki-67 expression. In recurrent cases 7 with had negative/low Ki-67 expression and 17 had medium-high Ki-67 expression. Spearman correlation analysis showed that r=0.485, P=0.026. Ki-67 expression was positively correlated with recurrence in the experimental group.

Spearman correlation analysis indicated that r =-0.793, P<0.05, showing that the expressions of p16 and Ki-67 were negatively correlated in the experimental group (χ^2=15.382, P=0.018) (Table I).

DISCUSSION

P16 is a tumor suppressor gene involved in the negative regulation of the cell cycle, and participates in the development of a variety of tumors. The results of the present study demonstrated that the positive expression rate of p16 in the experimental group was significantly lower than that in the control group. Mouriaux et al. (11) found negative expression of p16 in 66% of cases of choroid neoplasms which is in agreement with the present study results.

In the current study, CMM was divided into p16 non-/low-expression group and middle-high expression group. The prognosis of these two groups is negatively correlated with p16 expression, p16 overexpression associates with good prognosis while absence or

Table I. *Correlation between p16 and Ki-67 expression in experimental groups*

Ki-67	p 16				χ^2	P value
	-	+	++	+++		
-	0	2	5	0		
+	3	3	2	0		
++	5	2	0	0	15.382	0.018
+++	12	0	0	0		

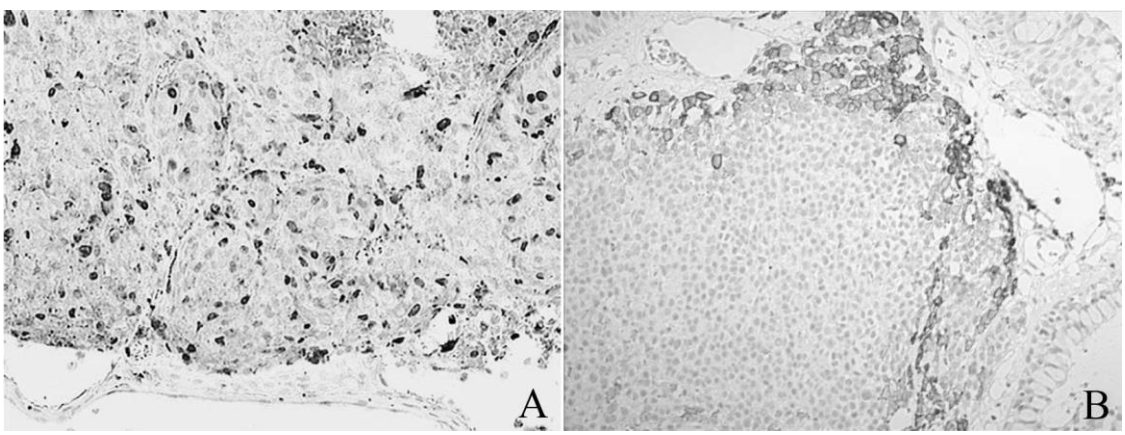

Fig. 3. *Ki-67 immunohistochemistry in CMM and CMN. **A)** Immunohistochemical staining of Ki-67 in the experimental group, positive cells showed either nuclear or nuclear and cytoplasmic positivity, 100X; **B)** Control group Ki-67 immunohistochemical staining, 100X)*

low p16 expression associates with a poorer prognosis.

Ki-67 is an excellent marker, which marks the active proliferation of tumor cells. Yoshioka et al. (12) suggested that the high Ki-67 expression is correlated with low overall survival rate after surgery in breast cancer. The results demonstrated that Ki-67 is not directly related to the tumor stage but with prognosis, indicating that the tumor stage is not necessarily positively associated with the prognosis.

Loss of p16 expression and overexpression of Ki-67 is associated with the recurrence of CMM, which suggested that the determination of p16 and Ki-67 expression could be used as markers for prognosis of CMM. However, the mechanism of p16 involvement in the pathogenesis of CMM and the inactivation mechanism of the P16 gene require further investigation.

REFERENCES

1. Gerami P, Jewell SS, Pouryazdanparast P, et al. Copy number gains in 11q13 and 8q24 [corrected] are highly linked to prognosis in cutaneous malignant melanoma. J Mol Diagn 2011; 13(3):352-58.
2. Andres C, Andres-Belloni B, Hein R, et al. iDermatoPath - a novel software tool for mitosis detection in H&E-stained tissue sections of malignant melanoma. J Eur Acad Dermatol Venereol 2017; 31(7):1137-47.
3. Boda D, Docea AO, Calina D, et al. Human papilloma virus: Apprehending the link with carcinogenesis and unveiling new research avenues (Review). Int J Oncol 2018; 52(3):637-55.
4. Larsen AC. Conjunctival malignant melanoma in Denmark. Epidemiology, treatment and prognosis with special emphasis on tumorigenesis and genetic profile. Acta Ophthalmol 2016; 94(8):842.
5. Rajasekaran R, Priya Doss CG, Sudandiradoss C, Ramanathan K, Sethumadhavan R. In silico analysis of structural and functional consequences in p16INK4A by deleterious nsSNPs associated CDKN2A gene in malignant melanoma. Biochimie 2008; 90(10):1523-29.
6. Zoroquiain P, Fernandes BF, Gonzalez S, Novais GN, Schalper KA, Burnier MN Jr. p16ink4a expression in benign and malignant melanocytic conjunctival lesions. Int J Surg Pathol 2012; 20(3):240-45.
7. Park SG, Lee JH, Lee WA, Han KM. Biologic correlation between glucose transporters, hexokinase-II, Ki-67 and FDG uptake in malignant melanoma. Nucl Med Biol 2012; 39(8):1167-72.
8. Özgün, E, SeçKiN S, ErgöçEn S. The importance of Ki-67 in differential diagnosis of intradermal melanocytic nevus, dysplastic nevus and malignant melanoma, and comparison of Ki-67 with prognostic factors of malignant melanoma. Türkiye Klinikleri Dermatoloji Dergisi 2009; 19(4):184-92.
9. AJCC-UICC Ophthalmic Oncology Task Force. Malignant melanoma of the conjunctiva. In: Edge SE, Byrd DR, Carducci MA, Compton CA, eds. AJCC Cancer Staging Manual. 7th ed. New York, NY: Springer: 539-546, 2009.
10. Docea AO, Mitrut P, Grigore D, Pirici D, Calina DC, Gofita E. Immunohistochemical expression of TGF beta (TGF-beta), TGF beta receptor 1 (TGFBR1), and Ki67 in intestinal variant of gastric adenocarcinomas. Rom J Morphol Embryol 2012; 53(3 Suppl):683-92.
11. Mouriaux F, Maurage CA, Labalette P, Sablonniere B, Malecaze F, Darbon JM. Cyclin-dependent kinase inhibitory protein expression in human choroidal melanoma tumors. Invest Ophthalmol Vis Sci 2000; 41(10):2837-43.
12. Yoshioka T, Hosoda M, Yamamoto M, et al. Prognostic significance of pathologic complete response and Ki67 expression after neoadjuvant chemotherapy in breast cancer. Breast Cancer 2015; 22(2):185-91.

LETTER TO THE EDITOR

PERSONALIZED NUTRITIONAL SUPPORT THERAPY ON POSTOPERATIVE NUTRITIONAL STATUS AND IMMUNE FUNCTION IN PATIENTS WITH GASTROINTESTINAL MALIGNANT TUMORS

MJ. YUAN, WQ. YUAN and WC. KONG

Gastrointestinal Surgery, Hangzhou First People's Hospital Affiliated to Medical School of Zheiiang University, Hangzhou, China

Received December 19, 2018 – Accepted January 25, 2019

To the Editor,

As a type of malignant tumor, gastrointestinal tumors (1) are usually manifested as gastric cancer (2) and gastrointestinal cancer (3). Tumor resection and drug chemotherapy are conventional ways to treat gastrointestinal tumors (4). However, resection of the digestive tract tumor will change the original structure of the digestive system (5). At the same time, fasting and gastrointestinal decompression can also cause a decreased electrolyte concentration. Therefore, the nutrition needed by patients cannot be absorbed properly, resulting in malnutrition and decreased immune function.

Patients suffering from gastrointestinal tumors are under tremendous psychological stress, therefore, it is necessary to pay attention to their physical/mental health and nutritional status after tumor resection (1), i.e., to improve their quality of life. Many cancer patients often suffer from anorexia and tend to avoid outdoor activities due to anxiety, which is not conducive to condition improvement. In terms of improving the quality life of post-operational patients, Ding et al believes that the postoperative nutritional status of patients should be improved (5). Motamedi et al. (6) demonstrated that more than 20% of patients died of malnutrition after tumor resection. It has been further confirmed that many patients with digestive tract diseases lacked access to a reasonable diet (7).

with digestive tract diseases lived in regions with more difficult living conditions and hence lacked access to a reasonable diet. In this study, the value of personalized nutritional treatment in patients with gastrointestinal cancer was discussed from the perspective of nutritional status and immune function.

MATERIALS AND METHODS

Patients

This study enrolled 120 patients with gastrointestinal malignancies who underwent elective treatment or palliative resection plus chemotherapy in Hangzhou First People's Hospital Affiliated to Medical School of Zheiiang University from September 2015 to August 2017. Inclusion criteria for the patients were: (i) age ≥ 18 years; (ii) grade I, II and III tumors and a survival period of ≥ 6 months. Tumor grade was determined by endoscopy, imaging and pathological classification according to the latest standards of the American Cancer Council (AJCC); (iii) elective treatment or palliative resection in the oncology department and completed 5 cycles of chemotherapy in the follow-up; (iv) agreement to participate in this study. SEE-P-B/AO scoring mechanism was adopted to score the nutritional status of the patients.

Key words: gastrointestinal malignant tumor; personalized nutritional support; nutritional status; immune function; SEE-P-B/AO

Corresponding Author:
Dr Wenqin Yuan,
Gastrointestinal Surgery,
Hangzhou First People's Hospital
Affiliated to Medical School, Zheiiang University,
No.261 Huansha Road, Hangzhou 310006, China
e-mail: wenqin_yuan2010@163.com

0393-974X (2019)

Exclusion criteria were: (i) age < 18 years or > 75 years; (ii) weight could not be determined; (iii) unclear consciousness or mental illness; (iv) not agreed to participate in the study. Informed consent was signed by all patients or their families and this study was approved by the Ethics Committee of Hangzhou First People's Hospital Affiliated to Medical School of Zheiiang University. The patients completed the postoperative evaluation of nutrition and immune function under the supervision of an assessor, and their results were analyzed by a reviewer.

Grouping and evaluation methods

The patients were randomly divided into two groups, with 60 cases in each group. The Patient Information Sheet was designed to show the patient condition, which included basic information, BMI (kg/m^2), upper-arm circumference (cm), skin wrinkle thickness of triceps brachii (mm), albumin (g/L), serum prealbumin (g/L) and hemoglobin (g/L). The assessment of nutritional status and immune function of the patients was based on the Patient Self-Assessment Indicator Analysis Guide (SEE-P-B/AO), weight, nutrition intake, nutritional symptoms, function and physical examination were selected as reference indicators, as it can judge the nutritional status of patients according to the numerical results.

Methods of personalized nutrition support

The weight, age and lifestyle of each patient were recorded and discussed by endocrinology experts and dietitians. When the intestinal intake was less than 60% of normal value, the patients would be given the parenteral nutrient solution, which was administrated through deep veins, while the patients were still allowed oral food intake at the same time. The amount of extraintestinal heat card was preferably 30kcal/(kg.d). For patients treated with oral hypoglycemic agents, regular short-acting insulin was given daily for 3 days prior to surgery to adjust their levels of blood glucose. In patients with preoperative instability of blood glucose, fast-acting insulin was given to them as soon as possible according to the value of their blood glucose. Crystal and colloid supplementation was given within 72 h after surgery, and an all-in-one nutrient solution was given via parenteral administration. After the gastrointestinal function of the patients was restored, a small amount of liquid food was given before the diet gradually returned to normal. At the same time, the amount of all-in-one nutrient solution was reduced.

Methods used for assessment of nutritional status

The weight and height of each patient were measured in the fasting state to calculate the BMI value. When the thickness of the triceps skin wrinkles in each patient was measured, the upper arm of the patient was relaxed before the measurement was taken at about 2 cm above the dorsal side of the left upper arm. When the circumference of the upper arm was measured, the upper arm of the patient was relaxed before a soft tape measure was used to read the value around the middle of the left upper arm. According to the relevant criteria for malnutrition (5), a BMI value of ≤ 18.5 indicated that the patient was underweight. The reference value for the thickness of the triceps skin wrinkles was 8.3 mm for men and 15.5 mm for women. The reference value for the upper arm circumference was 27.8 cm for men and 25.4 cm for women. If the value of a patient was less than 90% of the reference value, the patient was malnourished.

Nutritional protein and other nutritional indicators: serum levels of albumin, prealbumin, and hemoglobin were measured under fasting using venous blood taken within 24 h of patient admission. According to the relevant standards of malnutrition (albumin $\leq$ 35g/L, male hemoglobin $\leq$ 120g/L, female hemoglobin $\leq$ 110g/L), the status of malnutrition in each patient was determined. According to the SEE-P-B/AO, the nutritional status of each patient should be assessed jointly by the patient and medical staffs. Weight changes, eating disorders, illness recovery, and physical functions were assessed by the patient (A-type points). Changes in disease and nutritional needs (B-type points), changes in physical metabolic stress (C-type points), and physical changes (D-type points) were assessed under the supervision of the medical staff. Finally, the SEE-P-B/AO score was obtained by summing up the scores of A, B, C, and D type points. A higher score indicated a more serious status of malnutrition.

Test of immunologic function

Flow cytometry was used to detect the ratios of $CD3^+$, $CD4^+$, and $CD8^+$ T cells and the levels of intrinsic factors IL-2, IL-10, IgG, and IgA in peripheral blood mononuclear cells. Each subtype of cells was frozen at -70°C and then activated in a water bath at 50°C (Shanghai Shengke Instrument Equipment Co., Ltd., China). Subsequently, the

frozen liquid on the surface was removed by centrifugation (Thermo Fisher Scientific Co., Ltd., China). The expression of surface antigen markers, CD4, CD8, CD27, and CD28(FITC mouse anti-human CD4, APC-cy7 mouse anti-human CD8, PE-PECY7 mouse anti-human CD27, Percp mouse anti-human CD28 (BD Company, USA), in 1 x 10^6 cells was measured by flow cytometry (FACS canto II, BD Company, USA).

Determination of IL-2/IL-10/IgG/IgA expressions by enzyme-linked immunosorbent assay (Interleukin-2 ELISA detection reagent Interleukin-10 ELISA detection reagent were bought from Wuhan Huamei Biological Engineering Co., Ltd., China, Microplate reader was bought from Thermo Fisher Scientific Co., Ltd., USA): A certain amount of antibody was added to a 96-well plate and dried. Subsequently, 280 μL of assay diluent was added into each well and the plate was stirred at 200 rpm before being incubated for 1 h (CO_2 incubator from Thermo Fisher Scientific Co., Ltd., China). After incubation, the above operation was repeated before two duplicate wells were set for each sample. After the plate was stirred at 200 rpm, it was further incubated for 2 h and dried. In the next step, 100μL/well of the detection antibody was added and the plate was stirred at 200 rpm before it was incubated for 1 h and blot dried. Subsequently, 100μL/well of avidin-HRP (Avidin-horse radish peroxidase) was added and the plate was stirred at 200 rpm before it was incubated for 0.5 h for color development (electron microscope from Olympus company, Japan). When the color reached a desired level, 150μL/well of stop solution was added to detect the corresponding OD value in each well.

Statistical analysis

Statistical analysis was performed using SPSS 17.0

Table I. *Comparison of biochemical indicators between the routine treatment group and personalized nutrition treatment group.*

Index	Time	Routine treatment group	Personalized Nutrition Treatment Group
Albumin(g/L)	1 day before surgery	38.88±3.65	38.15±3.64
	1 week after surgery	31.28±3.26#	32.34±3.08#*
	1 month after surgery	33.65±3.33#	35.37±3.15#*
	3 months after surgery	35.67±2.96#	36.68±3.28*
	5 months after surgery	36.12±3.04#	38.57±3.24*
Serum prealbumin(g/L)	1 day before surgery	247.25±36.85	252.12±37.37
	1 week after surgery	132.85±42.85#	152.64±41.37#*
	1 month after surgery	158.96±38.65#	187.57±37.78#*
	3 months after surgery	187.69±38.99#	232.75±38.67*
	5 months after surgery	202.67±38.21#	238.37±37.92*
Hemoglobin(g/L)	1 day before surgery	140.78±16.85	135.96±17.36
	1 week after surgery	105.63±18.37#	111.75±18.26#*
	1 month after surgery	112.69±21.64#	128.37±17.86#*
	3 months after surgery	119.67±20.08#	131.62±19.38*
	5 months after surgery	128.34±19.35#	136.43±18.76*

**compared between the routine treatment group and personalized nutrition treatment group* (P<0.05); *#compared with* 1 *day before surgery* (P<0.05).

Table II. *Changes in the proportion of immune cell subsets measured at 1 day before the surgery and 10 days post-surgery.*

Parameter	Mode of nutrition treatment	1 day before the surgery	10 days after the surgery	*P*
CD4(%)	routine treatment	38.84±7.85	36.25±7.26	no statistical significance
	personalized nutrition treatment	37.34±6.87	42.56±6.36	<0.05
	P	no statistical significance	<0.05	
CD8 (%)	routine treatment	24.84±5.34	23.87±4.27	no statistical significance
	personalized nutrition treatment	24.36±3.68	23.67±3.69	no statistical significance
	P	no statistical significance	no statistical significance	
NK (%)	routine treatment	13.85±4.78	14.47±4.36	no statistical significance
	personalized nutrition treatment	14.05±2.77	18.67±5.17	<0.05
	P	no statistical significance	<0.05	
NKT (%)	routine treatment	7.08±3.14	8.27±5.19	no statistical significance
	personalized nutrition treatment	7.64±3.36	11.39±5.17	<0.05
	P	no statistical significance	<0.05	
CD4/CD8	routine treatment	1.67±0.32	1.58±0.28	no statistical significance
	personalized nutrition treatment	1.56±0.33	1.82±0.32	<0.05
	P	no statistical significance	<0.05	

statistical software. Experimental data were expressed as x±s. Comparison of data between two different groups was performed using an independent sample *t*-test. Repeated measurements were analyzed by one-way analysis of variance. $P < 0.05$ indicated that the difference was statistically significant.

RESULTS

Comparison of nutritional indicators between groups

There was no significant difference between the personalized treatment group and the conventional treatment group in their serum levels of albumin, prealbumin, and hemoglobin obtained 1 day before the surgery (P>0.05) (Table I). However, the nutritional indicators of the personalized treatment group were significantly better than those of the conventional treatment group at 1 week, 1 month, 3 months, and 5 months after surgery ($P < 0.05$). In addition, in the personalized treatment group, the serum levels of albumin, prealbumin, and hemoglobin obtained at 1 week post-surgery were significantly higher than those obtained at 1 month post-surgery ($P < 0.05$).

Comparison of ratios of immune cell subpopulations and immune functions between groups

The proportion of $CD4^+$/NK/NKT (natural killer T) cells in the personalized treatment group increased after the surgery (Table II). At the same time, the ratio of $CD4^+/CD8^+$ cells in the personalized treatment group was significantly higher than that in the conventional treatment group ($P < 0.05$). As shown in Fig. 1A, there was no significant change in the expression levels of CD4CTLA4, CD4PD-1, CD8CTLA4, and CD8PD-1 in the personalized treatment group throughout the treatment (P>0.05). As shown in Fig. 1B, the expression levels of CD4CD27/CD4CD28/CD8CD27 in the personalized treatment group were significantly increased after the treatment ($P < 0.05$).

Comparison of serum expressions of inflammatory cytokines between groups throughout the treatment

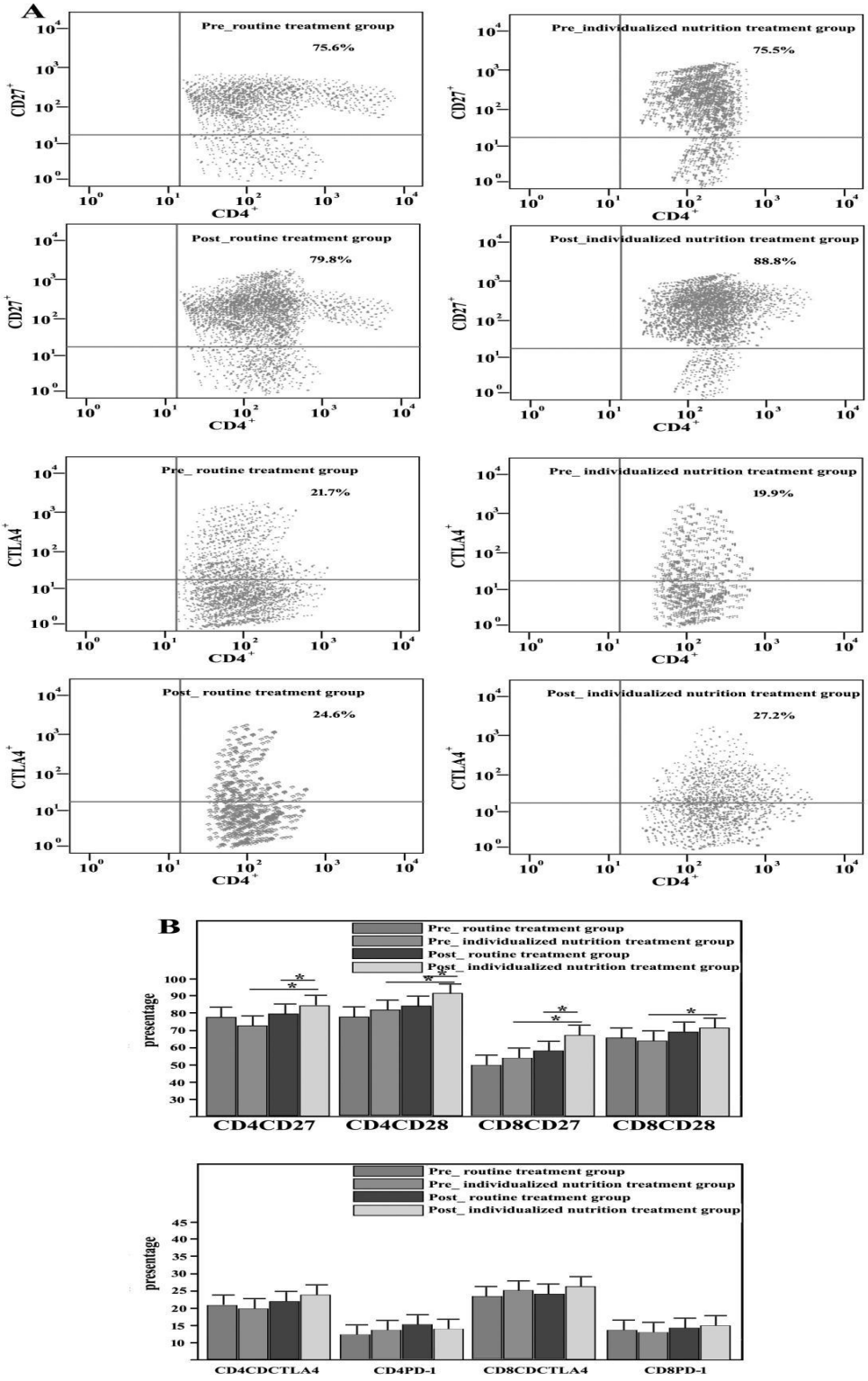

Fig. 1. *Immune functions in different groups of patients measured before and after the administration of enteral nutrition. **A**) The proportions of $CD3^+CD4^+$, $CD3^+CD8^+$ and natural killer cells in the peripheral blood of patients receiving enteral nutrition treatment were measured at 1 day before the surgery and 10 days after the surgery; **B**) expressions of $CD3^+CD4^+$, $CD3^+CD8^+$ and CD27/CD28, *P<0.05.*

Table III. *Changes in serum levels of related factors before/after enteral nutrition treatment.*

Parameter	Mode of nutrition treatment	1 day before the surgery	10 days after the surgery	*P*
IL-2(pg/mL)	routine treatment	224.78±118.2	232.14±128.64	no statistical significance
	personalized nutrition treatment	214.67±126.75	268.96±110.67	<0.05
	P	no statistical significance	<0.05	
IgG(pg/mL)	routine treatment	181.7±48.67	213.85±65.2	<0.05
	personalized nutrition treatment	184.75±64.37	256.37±66.8	<0.05
	P	no statistical significance	<0.05	
IgA(pg/mL)	routine treatment	166.27±84.3	238.6±127.6	<0.05
	personalized nutrition treatment	182.6±115.7	175.4±86.7	no statistical significance
	P	no statistical significance	<0.05	
IL-10(pg/mL)	routine treatment	268.6±84.6	267.6±63.9	no statistical significance
	personalized nutrition treatment	283.5±77.6	223.9±68.9	<0.05
	P	no statistical significance	<0.05	

The expression levels of IL-2 and IgG in the personalized treatment group were significantly increased by day 10 post-surgery, while the expression levels of IgA and IL-10 were significantly decreased ($P < 0.05$) (Table III). In the personalized treatment group, the expression levels of IL-2 and IgG were significantly increased while the expression level of IL-10 was significantly decreased ($P < 0.05$). By comparing the data obtained at 10 days before with that after the surgery, there was no significant difference in the expression level of IgA in the personal treatment group ($P>0.05$).

DISCUSSION

For patients with gastrointestinal malignancies, personalized nutritional support is often given during postoperative chemotherapy (8). During the five-month period studied here, the nutritional status and immune function of the patients were significantly improved. The scoring mechanism of SEE-P-B/AO was introduced in this study, which confirmed the hypothesis that a personalized nutritional support program exerts a positive effect on postoperative physical conditions of patients with gastrointestinal malignancies who have been treated with chemotherapy.

During this study, chemotherapy showed an obvious impact on the health of patients, however, further study is needed to verify whether personalized nutrition support treatment alleviates chemotherapy-induced physical dysfunction (9). In addition, a personalized nutrition therapy can improve the postoperative quality of life of patients to a certain extent, thus improving their emotional status. However, further study is needed to verify whether the treatment of personalized nutrition support is directly related to patient emotion (10).

REFERENCES

1. Liu X, Qiu H, Liu J, et al. A novel prognostic score,

based on preoperative nutritional status, predicts outcomes of patients after curative resection for gastric cancer. J Cancer 2016; 7(14):2148-56.
2. Ding D, Feng Y, Song B, Gao S, Zhao J. Effects of preoperative and postoperative enteral nutrition on postoperative nutritional status and immune function of gastric cancer patients. Turk J Gastroenterol 2015; 26(2):181-85.
3. Motamedi MAK, Barzin M, Ebrahimi M, Ebrahimi R, Khalaj A. Severe fatal protein malnutrition and liver failure in a morbidly obese patient after mini-gastric bypass surgery: case report. Int J Surg Case Rep 2017; 33:71-74.
4. Kohl KD, Ciminari ME, Chediack JG, Leafloor JO, Karasov WH, McWilliams SR, Caviedes-Vidal E. Modulation of digestive enzyme activities in the avian digestive tract in relation to diet composition and quality. J Comp Physiol B 2017; 187(2):339-351.
5. Fischer M, JeVenn A, Hipskind P. Evaluation of muscle and fat loss as diagnostic criteria for malnutrition. Nutr Clin Pract 2015; 30(2):239-48.
6. Tang MX, Zhang YH, Hu L, Kwak-Kim J, Liao AH. CD14++ CD16+ HLA-DR+ monocytes in peripheral blood are quantitatively correlated with the severity of pre-eclampsia. Am J Reprod Immunol 2015; 74(2):116-22.
7. Hudson RS, Yi M, Esposito D, et al. Microrna-106b-25 cluster expression is associated with early disease; recurrence and targets caspase-7 and focal adhesion in human prostate cancer. Oncogene 2013; 32(35):4139-47.
8. El Abd OH, Amadera JE1, Pimentel DC, Pimentel TS. Intravascular flow detection during transforaminal epidural injections: a prospective assessment. Pain Physician 2014; 17(1):21-27.
9. Romero I, Bast RC Jr. Minireview: human ovarian cancer: biology, current management, and paths to personalizing therapy. Endocrinology 2012; 153(4):1593-602.
10. Berger AM, Gerber LH, Mayer DK. Cancer-related fatigue: implications for breast cancer survivors. Cancer 2012; 118(8 Suppl):2261-69.

LETTER TO THE EDITOR

KINETIC INTERACTION BETWEEN ALBENDAZOLE AND FLORFENICOL IN HEALTHY ADULT FEMALE BEETAL GOATS

M.A. NAEEM[1,2], N.A. KARROW[3], M.M. ASHRAF[2] and J. WU[4]

[1]State Key Laboratory of Agricultural Microbiology, College of Veterinary Medicine, Huazhong Agricultural University, Wuhan, P.R.China; [2]Institute of Pharmacy, Physiology and Pharmacology, University of Agriculture, Faisalabad, Pakistan; [3]Department of Animal Biosciences, University of Guelph, Guelph, Ontario, Canada; [4]College of Animal Science, Tarim University, Alar City, Xinjiang P.R. China

Received February 4, 2019 – Accepted March 5, 2019

To the Editor,

Simultaneous administration of two or more drugs can lead to unexpected interactions, sometimes adverse reactions (1). Pharmacodynamic and pharmacokinetic drug interactions are commonly studied in pharmacology (2). Pharmacodynamic interactions take place at the receptor site or cellular level directly, whereas, pharmacokinetic interactions take place at absorption, metabolism and elimination levels (2). Florfenicol is a synthetic broad-spectrum antibiotic that has structural similarity to thiamphenicol (3). It provides antibacterial activity against chloramphenicol- and thiamphenicol-resistant microorganisms such as *Staphylococcus aureus*, *Escherichia coli* and *Salmonella typhimurium* (3). Albendazole shows potent enzyme induction properties and induces the hepatic cytochome P450 enzymatic system (4). Consequently, albendazole may elicit drug interaction when administered with florfenicol. In veterinary clinics of Pakistan, albendazole is frequently prescribed as a broad-spectrum anthelmintic along with other antibiotics for a combination therapy (poly-pharmacy). However, poly-pharmacy has always generated drug interactions (5).

The beetal breed of goat in Pakistan has been considered superior to all other breeds with respect to its well-developed size and high milk yield (6). Moreover, the kinetic interaction data of albendazole and florfenicol, plus dosage regimen for florfenicol, in beetal breeds in plain areas of Pakistan are not available. Keeping in view the above-mentioned importance of drug interactions during combination therapy, the present study was designed to compute pharmacokinetic parameters for florfenicol, including dosage regimen, by performing a florfenicol and albendazole co-administration field experiment.

MATERIALS AND METHODS

Drugs

An injectable solution (300 mg mL^{-1}) of florfenicol (Nuflor®, Merck and Co. Madison, NJ07940, USA), and an albendazole oral drench (112.5 mg mL^{-1}) (Selbazole®, SelmorePharma, Pakistan) were used for the experiment. A florfenicol standard of analytical grade (Sigma-Aldrich) was used to generate the standard curve via high performance liquid chomatography (HPLC).

Experimental animals

Ten healthy adult female beetal goats (22-36 months of age and 38-43 kg body weight) were used for this experimental trial. The design and procedures

Key words: drug-interactions, disposition kinetics, dosage regimen, pharmacokinetics

Corresponding Author:
Dr. Juyuan Wu,
College of Animal Science, Tarim University,
Alar City, Xinjiang 843300, P.R. China
Tel.: +86 13779826829
e-mail:wjyn-w@126.com

0393-974X (2019)

were approved by the ethics committee of the University of Agriculture, Faisalabad, Pakistan. All the animals were fed dry wheat straw and green fodder of the season with free access to drinking water at the experimental area of the livestock farm.

Experimental trial

One of the jugular veins of each animals was canulated under aseptic conditions with a plastic canula to collect blood samples. A control/blank blood sample was collected in each experiment prior to drug administration, then florfenicol was administered as per the manufacturer's recommendation at a dose of 20 mg Kg^{-1} body weight into the right neck muscle during the first phase of the experiment. Blood samples were collected at 0.5, 1, 1.5, 2, 2.5, 3, 3.5, 4, 4.5, 5, 6, 7, 8, 10 and 12 h intervals; each animal was given a wash out period of 2 weeks. In the second phase, an oral dosage of albendazole drench was administered as per the manufacturer's recommendation at the dose of 7.5 mg Kg^{-1} body weight; after 2 h, the same recommended dose of florfenicol was then administered intramuscularly. Blood samples were collected in plastic centrifuge tubes by following the same time interval as mentioned above. Serum was separated by centrifugation at 5,000 rpm for 5 min and then stored at -20°C until analysis.

Analytical procedure

For plotting a standard curve, the florfenicol standard was dissolved in methanol to prepare a stock solution of 1 mg mL^{-1} (0.1% w/v). Spike serum samples (1 to 10 µg mL^{-1}) were prepared in drug-free control goat serum at concentrations of 10, 3.5, 3.0, 2.5, 1.25, 1.0, 0.1 and 0.025 µg mL^{-1} for preparation of a standard curve. These spike samples were extracted and analyzed in the same manner as unknown samples and were stored at -20°C until analysis. For HPLC analysis, samples were filtered though Micropore membrane discs (0.45 µm), and 20 µL was injected into the HPLC. A standard curve was prepared using linear regression by plotting peak area (y-axis) *versus* florfenicol serum concentration (x-axis). Linear equation (y= 443.25x + 25.076) and regression co-efficient (R2= 0.9995) were calculated while plotting standard curve. Florfenicol concentrations in unknown samples were determined by standard curve interpolation.

Serum sample preparation

A total of 300 µg of each serum sample was added to an Eppendorf tube, then 300 µg of methanol was added. This solution was vortexed for 5 min, then centrifuged for 10 min at 12,000 rpm. The organic layer was transferred to another clean Eppendorf tube, filtered, and loaded onto the HLPC column.

Chomatographic analysis

The concentration of serum florfenicol was determined by reverse-phase HPLC, performed at room temperature, using a previously published method (7). An HPLC system (HPLC Sykam-S 1122, Sykum GmbH, Gewerbering 1586922 Eresing, Germany) containing a stainless-steel separation column, packed with YMC pack A-312 (Thermo Hypersil-Keystone, BDS-C_{18} with 250 x 4.6 mm dimensions and 5 µm particle size) was used for sample separation. This system was equipped with a pre-column (Guard-Pak™) filled with a µBondapak™ C_{18} cartridge (Thermo Hypersil, England) and UV/ Visible detector (Sykam, S-3210) set at 275 nm. The mobile phase consisted of a mixture of 0.05 M NaAc buffer (adjusted with concentrated glacial acetic acid to pH 6.0) and acetonitrile–methanol (92:4:4, v/v/v), which was run in the system at flow rate of 1 mL/ min. Equal volumes (about 20 ul) of the standard and serum samples were injected separately into HPLC. A chomatogram was recorded with computer software (Peak Simple Chromatography Data System, Buck Scientific Inc., East Norwalk. USA), and the areas of major peaks for both were measured to calculate serum concentrations of drug against peak area. Separation of florfenicol was achieved at 37ºC, using isocratic mode.

Validation method

The analytical procedure was validated by calculating limit of detection (LOD), limit of quantification (LOQ), accuracy and precision. LOD and LOQ were calculated using formulae 3*SD/ slope and 10*SD/slope, respectively. Where SD represents standard deviation and slope mean slope

of standard curve obtained in the linear equation. Accuracy of the method was obtained by calculating the percent recovery (%R) of florfenicol. Here in the analysis, three consecutive standard concentrations of florfenicol were used: 2.5 µg mL^{-1}, 3.0 µg mL^{-1}, 3.5 µg mL^{-1}, and the %R was obtained by using the formula; (recovered concentration/injected concentration) x 100. Precision of the assay was assessed in respect to both repeatability and reproducibility and 3 µg mL^{-1} standard concentration of florfenicol was selected for its calculation. The precision was obtained five times within the same day for intra-day variation and next three days for inter-day variation. The precision was checked by using the formula [(Standard deviation/ Mean) x 100 %].

Statistical analysis

In each experiment, serum concentration *versus* time data of florfenicol was used to calculate disposition kinetic parameters using two-compartment open model with the computer program MW/ PHARM (version 3.02) by F. Roumbout in cooperation with the University Center for Pharmacy, Department of Pharmacology and Therapeutics, University of Gronigen and Medi/ Ware (Netherlands) (copyright 1987-1991). The mean and standard error of mean (SEM) for each concentration and parameter was calculated. Significance was determined using Student's *t*-test (8). Differences between pharmacokinetic variables, including maximum concentration given by drug (C_{max}), time at which C_{max} of drug in serum obtained (T_{max}), absorption rate constant (K_{abs}), absorption half-life ($t_{1/2abs}$), extrapolated zero time concentration of drug in elimination phase (B), elimination rate constant (β), elimination half-life ($t_{1/2\beta}$), volume of distribution (V_d) and total body clearance of drug (Cl_B), area under curve (AUC), mean residence time (MRT) and concentrations of florfenicol at different time points both alone and in combination with albendazole, were considered significant when $P<0.05$ (8).

Dosage regimen

Based on the calculated pharmacokinetic

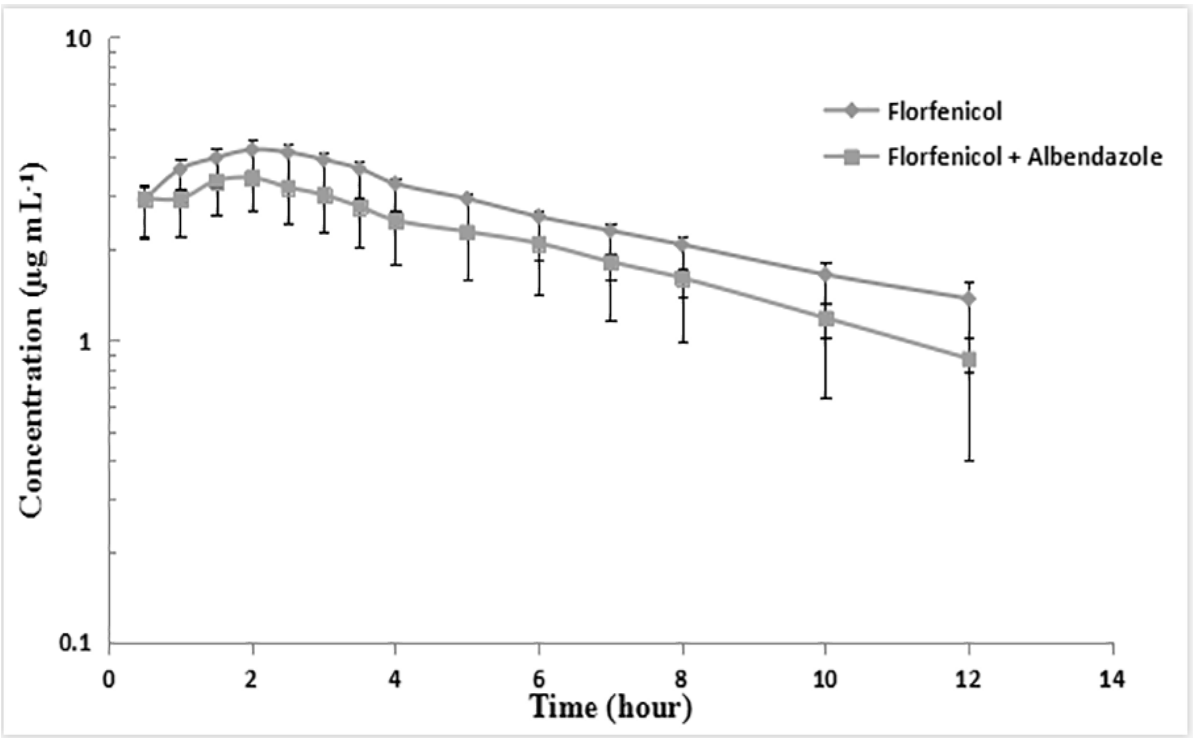

Fig. 1. *Mean±SEM (Mean±Standard error of mean) concentrations (µg mL^{-1}) of florfenicol alone and along with albendazole versus time on a semilogarithmic scale in ten healthy adult female beetal goats.*

Table I. *Mean±SEM serum concentrations (µg mL^{-1}) of Florfenicol alone and along with albendazole in ten healthy adult female beetal goats.*

Time (hs)	Florfenicol alone (µg mL^{-1})	Florfenicol with Albendazole (µg mL^{-1})
0.5	2.90±0.37	1.98±0.28*
1	3.66±0.31	2.93±0.23*
1.5	3.99±0.33	3.35±0.21*
2	4.25±0.35	3.43±0.21*
2.5	4.17±0.29	3.19±0.19*
3	3.94±0.23	3.01±0.18*
3.5	3.68±0.19	2.76±0.18*
4	3.28±0.15	2.48±0.17*
5	2.93±0.11	2.28±0.13*
6	2.55±0.11	2.08±0.12*
7	2.29±0.12	1.81±0.11*
8	2.06±0.14	1.60±0.13*
10	1.64±0.16	1.18±0.14*
12	1.37±0.19	0.87±0.15*

**Significantly (P<0.05) different from respective value; SEM: Standard error of mean*

Table II. *Mean±SEM values for kinetic parameters of Florfenicol alone and with Albendazole in ten healthy adult female beetal goats.*

Parameters	Units	Florfenicol alone	Florfenicol with albendazole
C_{max}	µg mL^{-1}	4.22±0.32	3.29±0.21*
T_{max}	h	1.86±0.16	1.98±0.16^{NS}
K_{abs}	h^{-1}	1.59±0.13	1.36±0.23^{NS}
$t_{1/2abs}$	h	0.47±0.04	0.69±0.16^{NS}
B	µg mL^{-1}	5.29±0.46	4.85±0.51^{NS}
β	h^{-1}	0.13±0.02	0.17±0.03^{NS}
$t_{1/2\beta}$	h	6.56±0.94	5.06±0.77^{NS}
V_d	L Kg^{-1}	4.05±0.35	4.49±0.39^{NS}
Cl_B	L h^{-1} Kg^{-1}	0.47±0.04	0.69±0.06*
AUC	µg h mL^{-1}	32.36±1.48	24.66±1.51*
MRT	h	10.13±1.36	8.30± 1.00^{NS}

** Significantly (P<0.05) different from respective value; NS: non-significantly (P>0.05) different from respective value (µg: microgram; mL: milliliter; L: liter, Kg: kilogram); SEM: Standard error of mean.*

Table III. *Dosage regimen of florfenicol alone and along with albendazole at various dosing interval in adult healthy female beetal goats.*

Dosing Intervals	**Drugs** →	Florfenicol		Florfenicol + Albendazole	
	MIC ↓	Priming Dose	Maintenance Dose	Priming Dose	Maintenance Dose
8 h	0.25	2.865	1.852	4.373	3.251
	1	11.46	7.408	17.49	13
	2	22.92	14.82	34.99	26.01
	4	45.83	29.63	69.98	52.02
	6	68.75	44.45	104.9	78.02
	8	91.67	59.27	139.9	104
12 h	0.25	4.82	3.81	8.63	7.51
	1	19.27	15.22	34.53	30.04
	2	38.54	30.44	69.06	60.08
	4	77.09	60.89	138.1	120.2
	6	115.6	91.34	207.2	180.2
	8	154.2	121.8	276.2	240.3
24 h	0.25	22.93	21.92	66.39	65.27
	1	91.72	87.67	265.6	261.1
	2	183.4	175.3	531.1	522.2
	4	366.67	350.67	1062.3	1044.3
	6	550.31	526.01	1593.4	1566.4
	8	773.74	701.34	2124.5	2088.6

parameters, an optimal dosage regimen of florfenicol alone and with albendazole was calculated using healthy adult goats. The calculations were based on the range of the therapeutic concentrations *i.e.* 0.25-8 μg mL^{-1}. Priming and maintenance dosage regimens were calculated at 8, 12 and 24 h time intervals, with minimum inhibitory/therapeutic concentration (MIC) range 0.25-8.0 μg mL^{-1} of florfenicol. MIC of 2 μg mL^{-1} at a 12-h time interval was used for the calculation of dosage regimen, as given in Table III. Based on MIC or C°P, V_d, ß and different time intervals, optimal dosage regimens, both priming and maintenance doses, of florfenicol alone and with albendazole were calculated in adult goats by using Baggot's formula (9). There equations are given as:

Priming dose= P = C°P (min). V_d ($e^{ßt}$)

whereas,

Maintenance dose= M = C°P (min). V_d ($e^{ßt-1}$)

RESULTS

The values for serum concentration of florfenicol alone and in combination with albendazole against time after intramuscular administration in beetal goats are shown in Fig.1 and Table I. During HPLC method validation, The LOD and LOQ were 0.225 and 0.749, respectively. The average percentage of recovery was found to be 103.6%, 92.34% and 99.43% for 2.5 μg mL^{-1}, 3.0 μg mL^{-1} and 3.5 μg mL^{-1}, respectively. The precision of both intra- and inter-day was < 5%. The concentration value of intramuscularly administered florfenicol alone was 4.25±0.35 μg mL^{-1} at 2 h, which declined progressively to 1.37±0.19 at 12 h. The concentration of florfenicol with albendazole was 3.43±0.21 μg mL^{-1} at 2 h and declined to 0.87±0.15 at 12 h. This reflected a significant ($P<0.05$) decrease (approximately 19.3%) in concentration for florfenicol at 2 hours when administered with albendazole; however, a 36.5% decrease in florfenicol concentration at 12 hours post-medication was also noted. The pharmacokinetic parameter values of florfenicol alone and after co-administration with albendazole in ten healthy adult female beetal goats are presented in Table II. It is evident that administration of albendazole rendered a significant ($P<0.05$) change in the values of kinetic parameters of florfenicol *i.e.* decreasing trend in maximum concentration C_{max} 4.22±0.32 μg mL^{-1} to 3.29±0.21 μg mL^{-1} (22%)and area under curve AUC 32.36±1.48 to 24.66±1.51, whereas, increasing trend in total body clearance Cl_B 0.47±0.04 $Lh^{-1}Kg^{-1}$ to 0.69 0.06 $Lh^{-1}Kg^{-1}$ (46.9%). However, a non-significant ($P>0.05$) increasing trend was observed for time to attain maximum serum drug concentration T_{max} 1.86±0.16 to 1.98±0.16 h (6.5%), absorption half-life $t_{1/2}$ abs 0.47±0.04 to 0.69±0.16 h (46.9%), elimination rate constant β 0.13±0.02 to 0.17±0.03 h^{-1} (30.8%), volume of distribution V_d 4.05±0.35 to 4.49±0.39 L Kg^{-1} (10.9%) and a non-significant ($P>0.05$) decreasing trend in absorption rate constant K_{abs} 1.59±0.13 to 1.36±0.23 h^{-1}(46.8%), extrapolated zero time drug concentration B 5.29±0.46 to 4.85±0.51 μg mL^{-1} (8.32%), elimination half-life $t_{1/2}$ β 6.56±0.94 to 5.06±0.77 h (22.9%) and mean residence time MRT 10.13±1.36 to 8.30±1.00 h.

Regarding dosage regimen of florfenicol, by administration alone, the calculated priming dose of florfenicol at 2 μg mL^{-1}, MIC was 38.54 mg Kg^{-1} body weight instead of 20 mg Kg^{-1} body weight, whereas, the maintenance dose was 30.44 mg Kg^{-1} body weight. Similarly, in combination with albendazole, 69.06 mg Kg^{-1} body weight was calculated as the priming dose and 60.08 mg Kg^{-1} body weight as the maintenance dose according to estimated pharmacokinetic parameters of this study, as shown in Table III.

DISCUSSION

In the current study, to understand the kinetic interaction between albendazole and florfenicol in goats, field trial was employed. Florfenicol serum concentrations at different time points were best fitted by a two-compartment open model by intramuscular administration. After obtaining serum samples, HPLC was performed to obtain concentration of florfenicol at different time points. Total concentration of the drugs was analyzed, regardless of tissue compartment, protein binding and extent of metabolism. The peak concentration of florfenicol in goat serum decreased from 4.22±0.32 to 3.3±0.21 μg mL^{-1} (Table II) after its concurrent administration with albendazole (Fig. 1). It has been reported that besides drug-drug interactions, changes in maximum serum concentration may also be influenced by both environmental and species variations (10). Besides enzyme induction, the change in pharmacokinetic parameters of florfenicol may also be attributed to genetic differences among animals (11). In the present study, a decrease in the elimination half-life of florfenicol may be due to the higher value of β after administration with albendazole, as the half-life of a drug remains reciprocal to the value of β. However, the half-life of a drug is a derived parameter that changes as a function of both total body clearance Cl_B and volume of distribution V_d (12); an increase in V_d of florfenicol in the present study may be attributed to a decrease in the value of B, and in turn, an increase in Cl_B of florfenicol has been shown through increased values of V_d and β, when administered with albendazole (12) In short, the pharmacokinetic parameters revealed a significant decrease in maximum concentration and total body clearance of florfenicol by its co-administration

with oral albendazole drench. These findings led us to a dose adjustment of florfenicol alone and in combination therapy with albendazole.

ACKNOWLEDGEMENTS

This work was supported by Huazhong Agricultural University Scientific and Technological Self-innovation Foundation (Program No. 52204-13002) and University of Agriculture, Faisalabad, Pakistan and for providing chemicals, equipment and technical guidelines at their research labs.

REFERENCES

1. Tannenbaum C, Sheehan NL. Understanding and preventing drug–drug and drug–gene interactions. Expert Rev Clin Pharmacol 2014; 7(4):533-44.
2. Cascorbi I. Drug interactions--principles, examples and clinical consequences. Dtsch Arztebl Int 2012; 110(8):546-55.
3. Birdane YO, Birdane FM. Pharmacokinetics of florfenicol following intravenous and intramuscular administration in dogs. Vet Med 2015; 60(6):323-29.
4. Escobargarcia D, Camachocarranza R, Pérez I, Dorado V, Arriagaalba M, Espinosaaguirre JJ. S9 induction by the combined treatment with cyclohexanol and albendazole. Mutagenesis 2001; 16(6):523-28.
5. Dookeeram D, Bidaisee S, Paul JF, et al. Polypharmacy and potential drug–drug interactions in emergency department patients in the Caribbean. Int J Clin Pharm 2017; 39(5):1-9.
6. Prasad H, Tewari HA, Sengar OPS. Milk yield and composition of the beetal breed and their crosses with Jamunapari, Barbari and Black Bengal breeds of goat. Small Rumin Res 2005; 58(2):195-99.
7. Alcorn J, Dowling P, Woodbury M, Killeen R. Pharmacokinetics of florfenicol in North American elk (Cervus elaphus). J Vet Pharmacol Ther 2010; 27(5):289-92.
8. Steel RGD, Torrie JH. Principles and procedures of statistics, a biometrical approach: McGraw-Hill; 1997 p. 234.
9. Baggot JD. Principles of drug disposition in domestic animals: the basis of veterinary clinical pharmacology 1977.
10. Javed I, Iqbal Z, Khan MZ, et al. Disposition kinetics and optimal dosage of ciprofloxacin in healthy domestic ruminant species. Acta Vet Brno 2009; 78(1):155-62.
11. Anke-Hilse MVDZ, Daly AK. Pharmacogenetics and individualized therapy. Clin Pharmacol Ther 2012; 92(6):215-50.
12. Hussain T, Javed I, Muhammad F. Disposition kinetics of enrofloxacin following intramuscular administration in goats. Pak Vet J 2014; 34(3):293-96.

LETTER TO THE EDITOR

FOUR METHODS FOR IDENTIFYING AMBIGUOUS *STREPTOCOCCUS PNEUMONIAE* ISOLATES: THE EXPERIENCE FROM A SWEDISH UNIVERSITY HOSPITAL

G. KAZDAGLIS[1,2], J. LUCIN[1], K. KERTAT[1] and S. PERSIS[1]

[1]Department of Medical Microbiology, Linköping University hospital, Sweden; [2]Department of Hygiene, Faculty of Medicine, Aristotle University of Thessaloniki, Greece

Received December 17, 2018 – Accepted February 28, 2019

To the Editor,

Streptococcus pneumoniae is a Gram-positive, alpha-hemolytic, facultative anaerobic coccus. It is the most common cause of community acquired pneumonia in adults and infants, and a major cause of morbidity and mortality. It is also a frequent cause of otitis media and sinus infections. It spreads through close person-to-person contact via respiratory droplets. It presents as pneumonia, bacteremia, or meningitis (1).

The *S. pneumoniae* bacterium has more than 90 serological types. All strains of *Streptococcus pneumoniae* are provided with a polysaccharide capsule. To date, 90 distinct capsular types have been described, six of them very recently. Some of the types are antigenically related to each other and such related types are included together in groups, for example, 9A, 9L, 9N and 9V, while types without a close antigenic relationship to other types are given numbers only - for example, types 1, 2, 3, 4, 5. All of the six recently described types are antigenically related to previously known types. The capsular polysaccharides are composed of repeating units of oligosaccharides and for most of them the exact chemical structure is known. The extent of cross-reactivity between types within the respective groups may differ—for example, types 6A and 6B have identical chemical composition except for one of the bonds between two sugars and are extensively cross-reactive, while types 19F and 19A are clearly less cross-reactive (1). Although most of these serotypes cause disease, only a small subset of them are involved in the majority of invasive pneumococcal disease cases. In outpatient settings, current clinical practice guidelines for pneumonia recommend amoxicillin for children and macrolides or doxycline for adults while for the cases that require hospitalization or for patients with presumptive pneumococcal meningitis, initial treatment should include a broad-spectrum cephalosporin and/or vancomycin before antibiotic susceptibility results are available. Identification of *S. pneumoniae* therefore, is essential for the proper management of respiratory patients (2). Methods that may be used for the identification of *S. pneumoniae* include: optochin disk susceptibility (3), bile solubility test, latex agglutination, DNA probe (4, 5).

Given that the understanding of the epidemiology of pneumococcal infections is based on the geographic spread of the different serotypes and their variable invasiveness, the identification of specific *S. pneumoniae* serotypes is very important (6). In addition, data regarding the prevalence of the various *S. pneumoniae* serotypes is critical to the development of pneumococcal vaccines (7). It is therefore desirable to choose inexpensive and easy to perform methods for testing for alpha-hemolytic *Streptococcus* in

Key words: Streptococcus pneumoniae, Pneumococcus, *bile solubility test, PCR*

Corresponding Author:
Georgios Kazdaglis, MD, PhD,
Department of Hygiene, Faculty of Medicine,
Aristotle Univesity of Thessaloniki
54124, Thessaloniki, Greece
Tel.: +30 6975063876 - Fax: +30 2310673926
e-mail: georgioskazdaglis@live.com

0393-974X (2019)

properly collected respiratory and blood samples. For this reason, we compared the results of the optochin disk susceptibility test, of the latex (agglutination) test, of the bile solubility test and of DNA probes in order to determine the most advantageous method of testing for *S. pneumoniae*.

MATERIALS AND METHODS

The Clinical Microbiology Department at Linköping University Hospital routinely uses the optochin disk susceptibility test, the agglutination test and the polymerase chain reaction (PCR) to identify *S. pneumoniae*. All routinely used tests are properly validated. Airway pathogens are grown on blood agar plates together with a Thermo Fisher Scientific Inc®optochin-disc (Fig. 1). However, real-time Polymerase Chain Reaction (PCR) is used for the identification of airway pathogens only upon the request of the attending physician. In addition, when required, bile solubility testing is performed by the local Public Health Authority to the jurisdiction of which the Linköping University Hospital belongs.

Optochin discs are used for diagnostic purposes based on the optochin ability to increase the *S. pneumoniae* fragility. The cocci cannot grow around the patch and thus an inhibition zone is formed. An inhibition zone ≥ 14 mm is classified as positive result. Inhibition zones between 7 and 14 mm are indeterminate results, while inhibition zones ≤ 7 are considered as negative results (3).

Agglutination (antibody-antigen reactions) tests detect serotype specific capsular antigens of *S. pneumoniae*. The aggregates are detected macroscopically within 1 minute (6). The Oxoid DrySpot™ Pneumo Test is a latex agglutination test used for the detection of *S. pneumoniae* capsular antigen which is isolated from culture plates and blood culture. The detection is based on the agglutination (in the presence of sufficient amount of antigen) of antibody sensitized blue latex particles which represent most of the recognized serological types of pneumococci (8, 9) and are dried on cards. The test is deemed positive when the latex agglutinates form visible clumps in the presence of bacterial suspension of phosphate buffer that contains bacterial colonies. The Phadebact® pneumococcus co-agglutination test, on the other hand, contains Pneumococcal Reagent and Pneumococcal Control. When a sample of pneumococci is mixed with the Pneumococcal Reagent, specific antigens on the cell surface bind to the corresponding specific antibodies and form a coaglutination lattice that is visible to the naked eye.

In real-time PCR, data is collected during the exponential growth (log) phase of PCR when the quantity of the PCR product is directly proportional to the amount of template nucleic acid. The progress of the amplification reaction (amount of the PCR product) is monitored by the use of a fluorescent reporter molecule. In every amplification cycle, the increase in fluorescence intensity is proportional to the increase in the amplification product concentration. A common starting point (baseline correction) is then determined for the plots of fluorescence *vs* cycle number for all the samples and a threshold for fluorescence, above the background but within the linear phase of amplification, is chosen for all the plots. The cycle number at which an amplification plot crosses this threshold is the threshold cycle (or "Ct"). The Ct value correlates with the starting target concentration of the sample; the larger the amount of initial DNA template in the sample, the earlier the Ct value is for that sample (Fig. 2A). In the case of *S. pneumoniae*, the absence of fluorescence means that no *S. pneumoniae* DNA is detected in the sample and, therefore, the curve remains flat (2) (Fig. 2 A, B).

Finally, the bile (sodium deoxycholate) solubility test distinguishes *S. pneumoniae* from all other alpha-hemolytic streptococci by specifically lysing *S. pneumoniae*. Other bacterial cells are not lysed and, when present, give their suspension a turbid appearance. Clearing of the suspension upon addition of sodium deoxycholate indicates the presence of *S. pneumoniae* (positive outcome). Additionally, the bile test lends itself to optical reading by an optical densitymeter (10). Partial clearing (partial solubility) of the suspension is not considered positive for pneumococcal identification, while partially soluble strains of alpha-hemolytic streptococci that have optochin zones of inhibition <14 mm are not considered pneumococci (11).

For the purposes of the present study, 60 *alpha-hemolytic* isolates from nasopharynx, sputum, broncho-alveolar lavage, and blood were tested. All samples were obtained from patients of Linköping University hospital during the 2015-2016 season. All patients gave their informed consent in order to be included in the study while, in the case of deceased patients, written consent was obtained from their family or their next of kin.

As is the case with all laboratory tests routinely used in the Linköping University Hospital, the bile solubility test, the agglutination test (drySPOT and Thermo Fisher

Scientific Inc®), and real-time PCR (in-house validated technique) were performed by strictly adhering to the test kit manufacturer's instructions. For the internal control of all tests *S. pneumoniae* ATCC33400 and *Streptococcus mitis* NCTC10712 were used.

RESULTS

Sixty isolates from nasopharynx samples, sputum, broncho-alveolar lavage, and blood samples were prepared and tested for presence of *S. pneumoniae* and the results were compared using the four different methods mentioned above. Presence of *S. pneumoniae* was confirmed in 40 isolates using the optochin test. Other alpha-hemolytic streptococci were identified in 11 of the isolates. The results for 9 of the isolates were ambiguous. The 9 isolates for which the optochin test results were ambiguous were also tested using bile solubility and agglutination tests. Although the results were ambiguous as well, when tested with real time PCR they were negative for the presence of S. *pneumoniae*.

DISCUSSION

Given that *S. pneumoniae* is the most common cause of community acquired pneumonia and a major

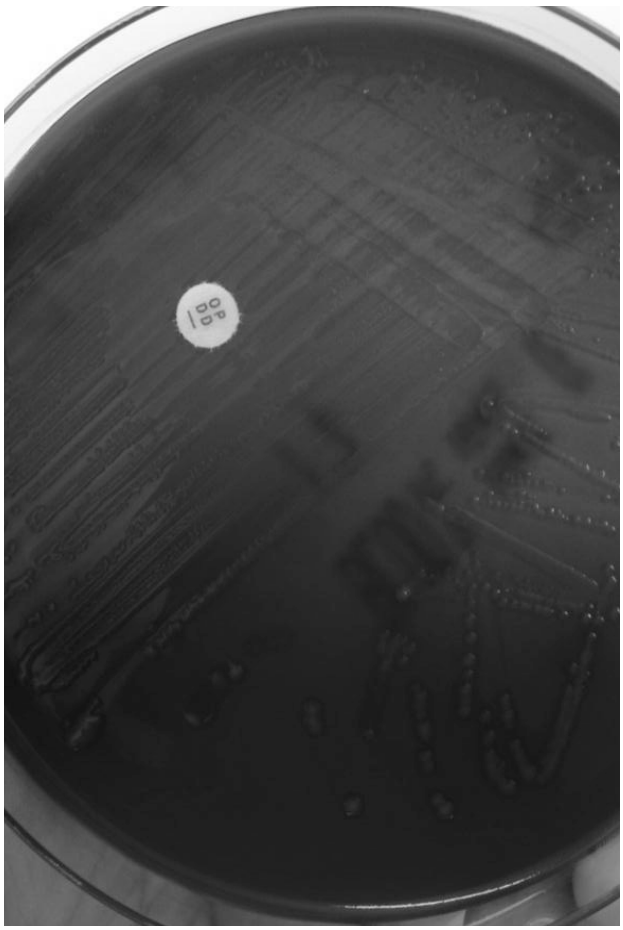

Fig. 1. S. pneumoniae *in blood agar plate with optochin disc.*

Table I. *Advantages and disadvantages of the identification methods.*

Test	Accuracy (1 to 4; Low-to-high)	Cost of Reagents (1 to 4; Low-to-high)	Total time required for obtaining results	Operator's working time Required for obtaining results
Optochin	3	1	24 hours	15 minutes
Agglutination	1	1	10 minutes	1 minute
PCR	4	4	3 hours	1 hour
Bile solubility	2	1	2 hours	15 minutes

Table II. *Results of the identification methods.*

Strains	Optochin	Bile solubility test	Agglutination	PCR
S.pneumoniae	40	Not tested	Not tested	Not tested
Other alpha-hemolytic streptococci	11	Not tested	Not tested	Not tested
Ambiguous *S.pneumoniae*	9	9	9	9 Negative for *S.pneumoniae*

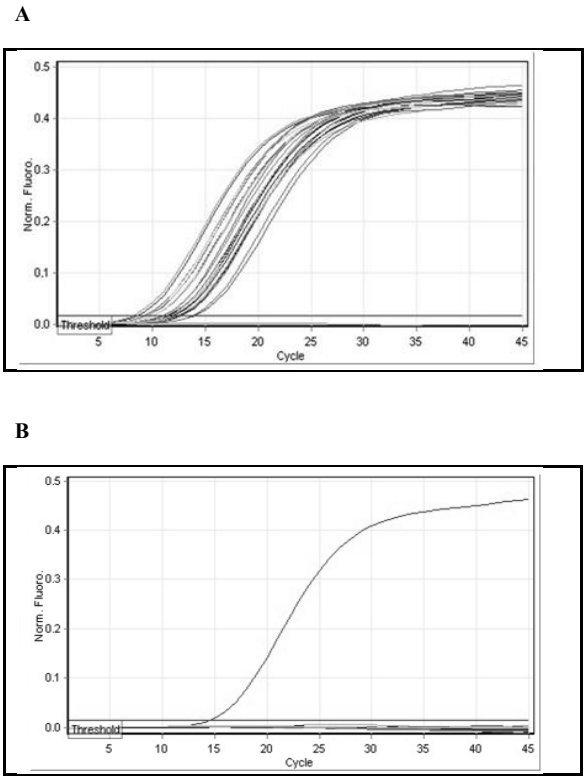

Fig. 2. ***A)*** *Positive PCR for* S. pneumonia. ***B)*** *Negative PCR for* S. pneumoniae. *Presence of alpha- hemolytic streptococcus*.

cause of morbidity and mortality, it is of paramount importance for Public Health Authorities to rely on its unambiguous identification, both for treating the individual patients and for mounting containment measures. Real life considerations, however, require that not only effectiveness but also financial and operational aspects of the health care system must be taken into consideration when making a choice of a test to be used for *S. pneumoniae* detection. Table I summarizes a few of the most relevant characteristics of the four methods used for the identification of *S. pneumoniae* based on the cumulative experience of the Linköping University hospital. It is evident from Table I that different tests present different effectiveness, ease of use, and demand on hospital resources. Although the sample size is sufficient to permit conclusions, no investigation was made concerning the resistance of the strains. However, according to the importance of *S. pneumoniae* sensitivity, we intend to further investigate this issue. Similar periodical studies by major University Hospitals and Health Authority administrations are strongly recommended in order to increase effectiveness of diagnostic methods used in tertiary hospitals.

In summary, alpha-hemolytic Streptococcus from appropriately collected samples (respiratory, blood) should be initially tested with the optochin disk susceptibility test, which is the most inexpensive and easy to perform method. If colony morphology is consistent, latex test and bile solubility test can be performed to further confirm the results. However, despite its cost and greater demand for hospital resources, real-time PCR emerges as the only secure method for evaluating equivocal results.

REFERENCES

1. Rodrigo C, Lim WS. The relevance of pneumococcal serotypes. Curr Infect Dis Rep 2014; 16(4):403.
2. Chandler LJ, Reisner BS, Woods GL, Jafri AK. Comparison of four methods for identifying Streptococcus pneumoniae. Diagn Microbiol Infect Dis 2000; 37(4):285-87.
3. Gardam MA, Miller MA. Optochin revisited: defining the optimal type of blood agar for presumptive identification of Streptococcus pneumoniae. J Clin Microbiol 1998; 36(3):833-34.
4. Schlegel L, Prostak JM, Spicq C, Sissia G, Frémaux A, Geslin P. Presumptive tests and molecular hybridization for the identification of untypable strains of Streptococcus pneumoniae. Pathol Biol (Paris) 1998; 46(6):459-63.
5. Mundy LS, Janoff EN, Schwebke KE, Shanholtzer CJ, Willard KE. Ambiguity in the identification of Streptococcus pneumoniae. Optochin, bile solubility, quellung, and the AccuProbe DNA probe tests. Am J Clin Pathol 1998; 109(1):55-61
6. Sorensen RU, Edgar JDM. Overview of antibody-mediated immunity to S. pneumoniae: pneumococcal infections, pneumococcal immunity assessment, and recommendations for IG product evaluation. Transfusion 2018; 58 Suppl 3:3106-3113.
7. Chan WY, Entwisle C, Ercoli G, et al. A novel, multiple-antigen pneumococcal vaccine protects

against lethal Streptococcus pneumoniae challenge. Infect Immun 2018; 10. pi: IAI.00846-18.

8. Henrichsen, J. Six newly recognized types of Streptococcus pneumoniae. J Clin. Microbiol 1995; 33:2759-62.
9. Lee P, Wetherall BL. Cross-reaction between Streptococcus pneumoniae and group C streptococcal latex reagent. J Clin Microbiol 1987; 25:152-53.
10. Slotved HC, Facklam RR, Fuursted K. Assessment of a novel bile solubility test and MALDI-TOF for the differentiation of Streptococcus pneumoniae from other mitis group streptococci. Sci Rep 2017; 7(1):7167.
11. Mundy LS, Janoff EN, Schwebke KE, Shanholtzer CJ, Willard KE. Ambiguity in the identification of Streptococcus pneumoniae. Optochin, bile solubility, quellung, and the AccuProbe DNA probe tests. Am J Clin Pathol 1998; 109(1):55-61.

LETTER TO THE EDITOR

ASPARTATE AMINOTRANSFERASE TO PLATELET RATIO INDEX VALUE IN PREDICTING LIVER FIBROSIS IN PATIENTS WITH HEPATITIS B VIRUS INFECTION

JS. MEI[1*], Q. LI[2*], XF. LIAO[2], GH. SUN[2], X. DING[2], ZX. WANG[2], YL. OUYANG[2], T. JIANG[2] and CB. LI[2]

[1]Cardiothoracic Surgery, The Second Clinical Medical College of Yangtze University, Jingzhou, China; [2]Department of Clinical Laboratory, The Second Clinical Medical College of Yangtze University, Jingzhou, China

Received November 29, 2018 – Accepted February 26, 2019

[*]These authors contributed equally to this work

To the Editor,

Hepatitis B virus (HBV) infection affects more than 240 million individuals worldwide. Of those with chronic HBV who do not receive treatment, 15-40% progress to cirrhosis and liver failure and liver cancer (1). Patients with chronic HBV infection and without clinical symptoms, with normal liver function or with mild impairment of liver function are not eligible for active antiviral treatment (2). However, research has shown that most of the patients have varying degrees of inflammatory response and fibrosis (3).

Moreover, chronic liver disease patients have liver fibrosis for a long period before developing liver cirrhosis (LC) (4), therefore, early active and regular antiviral therapy is an effective measure to prevent chronic HBV from progressing to cirrhosis or hepatocellular carcinoma. Double therapy with Pegylated Interferon and Ribavirin or nucleotide analogs represent a therapeutic approach of treatment (1, 5). Complications may occur if vitamin K-dependent coagulopathies are associated (6).

In recent years, non-invasive evaluation of LF has become a hot topic for many researchers. Aspartate aminotransferase (AST) and aspartate aminotransferase to platelet ratio index (APRI) have been shown to be useful for non-invasive diagnosis of LF/LC (7). This study aimed to evaluate the correlation between APRI and LF in patients with chronic hepatitis B and chronic hepatitis B virus carriers whose ALT/AST levels were less than 2-fold increased in an attempt to identify a non-invasive tool for early diagnosis of LF and for selection of optimum time for antiviral therapy.

MATERIALS AND METHODS

Patients

Two hundred and eighty patients with chronic hepatitis B virus infection who were hospitalized in The Second Clinical Medical College of Yangtze University and underwent liver biopsy between October 2016 and August 2018 were enrolled in the study.

Inclusion criteria for the patients were: i) diagnosis of chronic hepatitis B virus infection in accordance with the Guidelines for the Prevention and Treatment of Chronic Hepatitis B formulated by the 2010 Chinese Medical Association; ii) hospitalized in The Second

Key words: aspartate aminotransferase; aspartate aminotransferase to platelet ratio index; hepatitis B virus; liver fibrosis; liver cirrhosis

Corresponding Author:
Dr Chengbin Li,
Department of Clinical Laboratory,
The Second Clinical Medical College,
Yangtze University, No. 1 Renmin Road,
Jingzhou District, Jingzhou, 434020, China
e-mail: li_chengbin001@163.com

0393-974X (2019)

Clinical Medical College of Yangtze University and performed liver biopsy, liver function and blood routine, coagulation function, five hepatitis B quantification and hepatitis B virus determination one week before liver biopsy; iii) ALT and AST values less than 2-fold the upper limit of normal detection (40U/L); iv) had not undergone treatment with nucleoside (acid) analogs or interferon antiviral and other anti-enzymatic drugs; v) no obvious drinking history or drug use history that may cause liver function damage in the past six months; vi) no non-alcoholic fatty liver; vii) no genetic metabolism-related liver diseases; viii) no other hepatotropic viruses.

Exclusion criteria for the patients: hepatic cirrhosis, elderly, treatment with analogs of Interferon.

The study was approved by Ethics Committee of The Second Clinical Medical College of Yangtze University, China and all patients signed the informed consent to participate in the study.

Routine blood test

LH750 blood cell analyzer (Beckman Kurt Trading Co., Ltd., USA) was used for routine blood tests, including white blood cells, red blood cells, hemoglobin and Platelet (PLT).

Blood biochemical examination

Automatic biochemical analyzer (Shanghai Wuxi Medical Devices Co., Ltd., China) was used for detection of albumin, globulin, albumin to globulin ratio (A/G) (1-2.5), total bilirubin (2-20umol/L), ALT and AST, alkaline phosphatase (45-132U/L), γ-glutamyl transpeptidase (GGT) (7-50U/L), lactate dehydrogenase (LDH) (109-245U/L) and prealbumin (160-350U/L), dual-channel semi-automatic hemagglutination analyzer (German Mercer, Germany) was used to detect the hemostatic series, including activated partial thromboplastin time (APTT) (23-37 s), plasma prothrombin time (PT) (9-13 s), prothrombin time activity (75-100%), plasma thrombin time (TT) (16-18s), and fibrinogen content (200-400mg/dl).

Hepatitis B serological markers examination

Five quantitative hepatitis B (HBVM) (HBsAg [hepatitis B surface antigen], HBsAb [hepatitis B surface Antibody], HBeAg [hepatitis B e antigen], HBeAb [hepatitis B e Antibody], and HBcAb [hepatitis B core Antibody]) were detected by ELISA (Enzyme Linked Immunosorbent Assay Method, Xiamen Haifei Biotechnology Co., Ltd., China). The positive minimum detection limit of HBeAg was 1.0 S/CO.

Quantitative detection of hepatitis B virus

Real-time fluorescence quantitative PCR (Real-time fluorescent quantitative polymerase chain reaction kit (qPCR kit, Somerfield Technology Company, USA) was used to detect HBV-DNA. The lowest detection limit was 1 x 10^3copies/mL.

Pathological diagnosis of liver tissue

Liver tissue specimens were collected by standard ultrasound-guided liver biopsy procedure and then were fixed with 10% neutral formalin and dehydrated with alcohol, embedded with paraffin, and stained with hematoxylin-eosin staining and reticular fiber for morphological evaluation. At least three intact portal sections were selected and observed under light microscope. Collagen staining of liver tissue for evaluating the degree of fibrosis was carried out by Masson trichrome staining kit (Beijing Solebo Technology Co., Ltd., China) and dyeing procedure according to the instructions. Liver tissue samples were graded according to pathological grading (G) and staging (S). Grade 0 – no portal/periportal inflammation; grade 1 – portal inflammation with lobular degeneration but no necrosis; grade 2 – mild portal/periportal necrosis with lobular degeneration with focal necrosis or acidophil bodies; grade 3 – moderate portal/periportal necrosis with lobular degeneration, severe focal cell damage; grade 4 – severe portal/periportal necrosis with lobular degeneration including bridging necrosis. The stages according to fibrosis: stage 0 – no fibrosis; stage 1 – enlarged, fibrotic portal tracts; stage 2 – periportal or portal-portal septa were observed but the architecture was intact; stage 3 – presence of fibrosis with architectural distortion but without staging of cirrhosis; stage 4 – probable or definitive cirrhosis.

Statistical analysis

Statistical software SPSS 19.0 was used to

analyze the data. The data was represented by the mean ± standard deviation (x±*s*), and the Student's *t*-test was used to compare the two groups. A value of P<0.05 was considered statistically significant. The correlation between APRI and pathological staging of LF was analyzed by Spearman's correlation. ROC curve was used to calculate the optimal cut-off points of APRI corresponding to the stages of hepatic fibrosis in stage S2 (marked hepatic fibrosis) and stage S4 (cirrhosis).

RESULTS

Clinical and pathological characteristics of the patients

Of the 280 patients with chronic hepatitis B virus infection [218 males (77.86%) and 62 females (22.14%) with an average age of 37.47±12.57 and a median course of disease of 6 years] 238 cases (85%) were HBV-DNA positive, 42 cases (15%) were HBV-DNA negative, 157 cases (56.07%) were HBeAg positive and 123 cases (43.93%) were HBeAg negative.

LF staging: S0 stage 17 cases, S1 stage 98 cases, S2 stage 77 cases, S3 stage 46 cases, and S4 stage 42 cases. Stage S0-S1 of LF was used as mild fibrosis group: 115 cases; Stage S2-S3 as obvious fibrosis group: 123 cases; and Stage S4 as LC group: 42 cases. The data showed that the severity of LF increases with age, PLT decreases with the severity of LF and AST increases gradually with the severity of LF.

Diagnostic value of APRI for obvious LF and LC

ROC curve was used to calculate the optimal cut-off point of APRI corresponding to stage S2 (marked hepatic fibrosis) and stage S4 (cirrhosis) (Fig. 1). The pathological liver stage of the patients was in line with obvious LF changes when APRI≥0.272. The area under the ROC curve (AUR) was 0.641, sensitivity was 48.27%, specificity was 75.66%, and positive predictive value was 73.92% (P=0.0001), indicating that 73.92% of the patients had LF when APRI was above 0.272; when APRI≥0.309, ROC curve coincided with changes of LC. The AUR was 0.769, sensitivity was 68.71%, specificity was 76.79%, and the negative predictive value was 93.28% (P=0.0001). If APRI<0.309, there was a possibility of 93.28% excluding LC, as shown in Table I. The ROC curves of obvious LF and LC are shown in Fig. 1, A and B.

Optimal cut-off point of APRI in LF and LC of different HBV-DNA loads

According to different HBV-DNA levels, HBV-DNA positive patients were divided into two groups: 1×10^3~1×10^5copies/mL and 1×10^6~1×10^8copies/mL. In the group where HBV-DNA was 1×10^3~1×10^5copies/mL, APRI≥0.179 was the optimal cut-off point of obvious LF, the AUR was 0.679, the sensitivity was 79.33%, the specificity was 61.03%, and the positive predictive value was 80.62% (P=0.0004); APRI≥0.282 was the optimal cut-off point of LC, the AUR was 0.757, the sensitivity was 69.15%, the specificity was 73.18%, and the negative predictive value was 89.18% (P=0.0001). In the group where HBV-DNA was 1×10^6~1×10^8copies/mL, APRI≥0.274 was the optimal cut-off point of obvious LF, the AUR was 0.651, the sensitivity

Table I. *Optimal cut-off point of APRI for obvious LF and LC.*

Groups	APRI	AUR	95%CI	Sensitivity (%)	Specificity (%)	PPV (%)	NPV (%)	P
Obvious fibrosis group	0.272	0.641	0.586~0.690	48.27	75.66	73.92	50.66	0.0001
LC group	0.309	0.769	0.722~0.813	68.71	76.79	33.68	93.28	0.0001

AUR: area under the ROC curve; CI: confidence interval; PPV: positive predictive value; NPV: negative predictive value

was 53.19%, specificity was 79.82%, and the positive predictive value was 73.41%(P=0.0005); APRI≥0.325 was the optimal cut-off point of LC, the AUR was 0.847, the sensitivity was 85.98%, the specificity was 81.22%, and the negative predictive value was 98.37%(P=0.0001), as shown in Table II.

Optimal cut-off point of APRI for HBeAg and HBV-DNA positive or not

According to HBeAg positive or not, ROC was used to determine the optimal cut-off point of APRI in patients with obvious LF and LC. Among 157 HBeAg positive patients, APRI≥0.282 was the optimal cut-off point for obvious LF, the AUR was 0.627, the sensitivity was 45.97%, the specificity was 80.87%, and the positive predictive value was 72.88% (P=0.0014); APRI≥0.288 was the optimal cut-off point for LC, the AUR was 0.751, the sensitivity was 71.52%, the specificity was 72.56%, and the negative predictive value was 94.92% (P=0.0001). Among 123 HBeAg negative patients, APRI≥0.179 was the optimal cut-off point

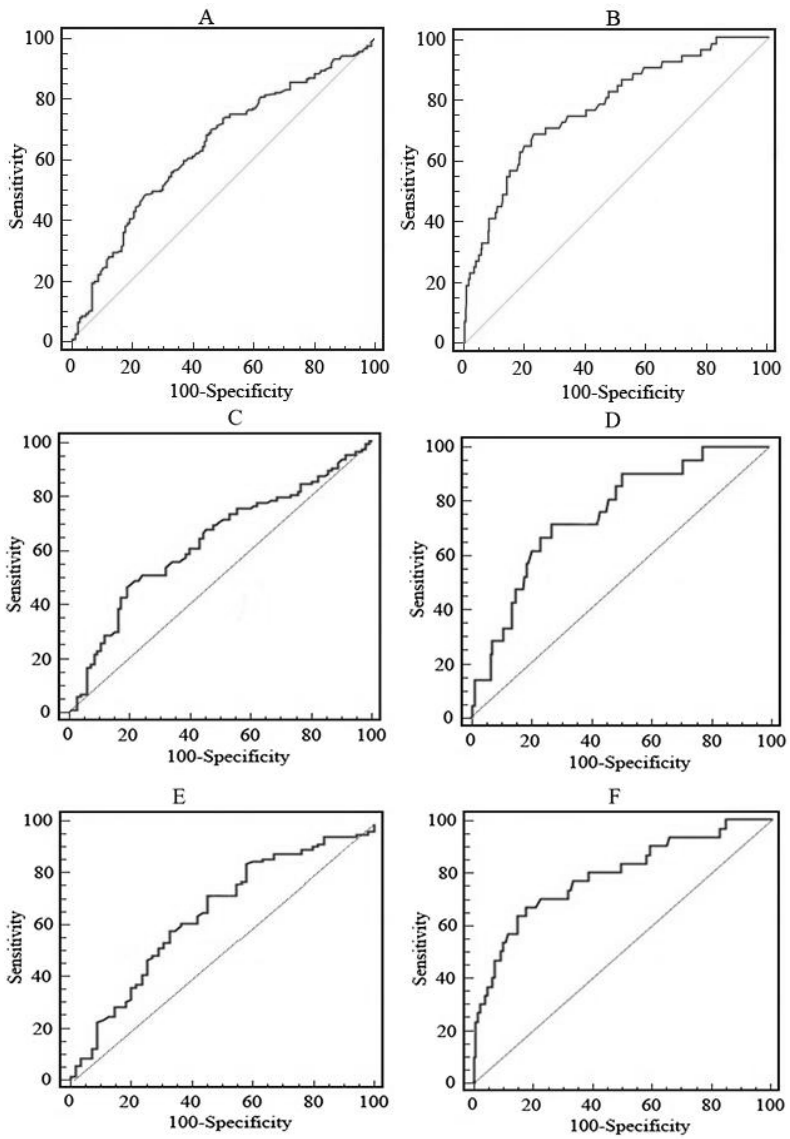

Fig. 1. *ROC curve of APRI. A) obvious LF group, AUR is 0.641; B) LC group, AUR is 0.769; C) obvious LF group, AUR is 0.627; D) LC group, AUR is 0.751; E) obvious LF group, AUR is 0.656; F) LC group, AUR is 0.792 (longitudinal axis is sensitivity, and horizontal axis is 100- specificity.*

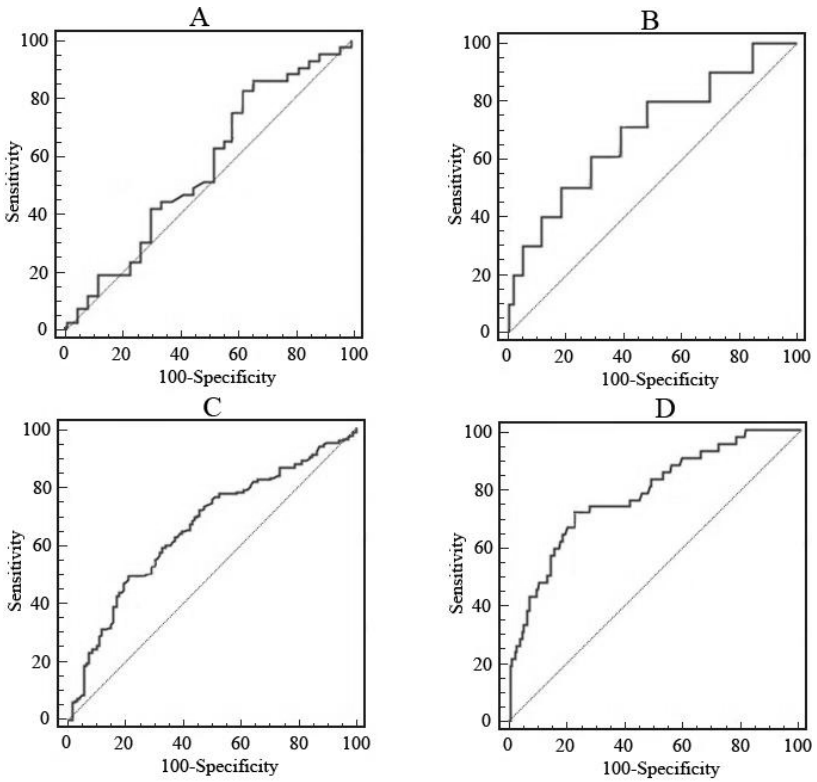

Fig. 2. *ROC curve. A) ROC curve of obvious LF group APRI in HBV-DNA negative patients, the AUR was 0.573; B) ROC curve of LC group APRI in HBV-DNA negative patients, the AUR was 0.683; C) ROC curve of obvious LF group APRI in HBV-DNA positive patients, the AUR was 0.661; D) ROC curve of LC group APRI in HBV-DNA negative patients, the AUR was 0.78.*

for obvious LF, the AUR was 0.656, the sensitivity was 76.31%, the specificity was 53.19%, and the positive predictive value was 74.39% (P=0.0005); APRI≥0.348 was the optimal cut-off point for LC, the AUR was 0.792, the sensitivity was 66.68%, the specificity was 81.93%, and the negative predictive value was 92.04% (P=0.0001), as shown in Table II. In HBeAg positive patients, the ROC curves of obvious LF group and LC group can be seen in Fig. 1C and Fig. 1D, while in HBeAg negative patients, the ROC curves of obvious LF group and LC group can be seen in Fig. 1, E and F.

The optimal cut-off point for APRI in patients with obvious LF and LC was determined by ROC based on whether HBV-DNA was positive or not (negative if HBV-DNA was below the detection value). Among 238 cases of HBV-DNA positive patients, APRI≥0.272 was the optimal cut-off point for obvious LF, the AUR was 0.661, the sensitivity was 52.18%, the specificity was 77.28%, and the positive predictive value was 75.66% (P=0.0001); APRI≥0.309 was the optimal cut-off point for LC, the AUR was 0.781, the sensitivity was 71.52%, the specificity was 76.18%, and the negative predictive value was 94.16% (P=0.0001). Among 42 cases of HBV-DNA negative patients, APRI≥0.154 was the optimal cut-off point for obvious LF, the AUR was 0.573, the sensitivity was 82.78%, the specificity was 41.33%, and the positive predictive value was 69.15% (P=0.3541); APRI≥0.256 was the optimal cut-off point for LC, the AUR was 0.683, the sensitivity was 69.29%, the specificity was 69.31%, and the negative predictive value was 93.19% (P=0.0387), as shown in Table II. In HBV-DNA negative patients, the ROC curves of obvious LF group and LC group can be seen in Fig. 2, A and B, while in HBV-DNA positive patients, the ROC curves of obvious LF group and LC group can be seen in Fig. 2, C and D.

Table II. *Data results table.*

		APRI	AUR	95%CI	Sensitivity (%)	Specificity (%)	PPV (%)	NPV (%)	P
A					1×10^3~1×10^5copies/mL group				
	Obvious fibrosis group	0.179	0.679	0.587~0.764	79.33	61.03	80.62	58.93	0.0004
	LC group	0.282	0.757	0.667~0.831	69.15	73.18	42.03	89.18	0.0001
					1×10^6~1×10^8copies/mL group				
	Obvious fibrosis group	0.274	0.651	0.563~0.716	53.19	79.82	73.41	61.33	0.0005
	LC group	0.325	0.847	0.786~0.895	85.98	81.22	30.84	98.37	0.0001
B	HBeAg	APRI	AUR	95%CI	Sensitivity (%)	Specificity (%)	PPV (%)	NPV (%)	P
					Positive				
	Obvious fibrosis group	0.282	0.627	0.559~0.702	45.97	80.87	72.88	56.88	0.0014
	LC group	0.288	0.751	0.682~0.810	71.52	72.56	25.18	94.92	0.0001
					Negative				
	Obvious fibrosis group	0.179	0.656	0.577~0.729	76.31	53.19	74.39	54.19	0.0005
	LC group	0.348	0.792	0.718~0.851	66.68	81.93	45.62	92.04	0.0001
C	HBV-DNA	APRI	AUR	95%CI	Sensitivity (%)	Specificity (%)	PPV (%)	NPV (%)	P
					Negative				
	Obvious fibrosis group	0.154	0.573	0.443~0.685	82.78	41.33	69.15	62.03	0.3541
	LC group	0.256	0.683	0.583~0.808	69.29	69.31	28.11	93.19	0.0387
					Positive				
	Obvious fibrosis group	0.272	0.661	0.602~0.715	52.18	77.28	75.66	54.18	0.0001
	LC group	0.309 0.781		0.723~0.824	71.52 76.18		33.89	94.16	0.0001

A: Optimal cut-off point of APRI corresponding to different HBV-DNA loads in obvious LF and LC; B: Optimal cut-off point of APRI for LF and LC with or without HBeAg positive; C. Optimal cut-off point of APRI corresponding to LF and LC whether

In addition, Spearman's correlation analysis showed that APRI was positively correlated with staging of LF ($r=0.373$, $P<0.001$).

DISCUSSION

The progression of chronic HBV infection can cause LF which, if left untreated, can lead to LC (1). In recent years, non-invasive evaluation of LF has concerned clinicians, and APRI has been shown to be of clinical value in evaluating the degree of LF (7). The results of this study showed that 73.92% of the patients with LF stage S2 had APRI≥0.272, with an AUR of 0.641. When LF stage was S4 (LC stage), the AUR was 0.769, and the negative predictive value was 93.28% when APRI≥0.309. The value of AUR for APRI was >0.5, indicating that the use of APRI in evaluating LF has a great applied value.

Currently, the difficulty of non-invasive diagnosis model of LF and LC is represented by differentiation between non-significant LF (S0-S1) and LC (S4). The sensitivity of APRI optimal cut-off point is not high enough, as past reports showed that older age and high viral load are risk factors for LF (8, 9). HBV-DNA is HBV replication that can stimulate the immune response of the body, making the degree of pathological changes increase. In addition, the level of HBV-DNA is related to the appearance and high mortality determined by LC and hepatocellular carcinoma (10). Studies show that in chronic HBV infections with normal or mildly abnormal transaminases, increased age is associated with obvious LF (11, 12). The present study shows that the severity of LF increases with age. The corresponding APRI can be determined according to different age groups and HBV-DNA levels, so as to improve the clinical application value of APRI in evaluating the degree of LF. Furthermore, the sensitivity, specificity, and negative predictive value of APRI in evaluating LC are all improved after viral load grouping.

REFERENCES

1. Tang LSY, Covert E, Wilson E, Kottilil S. Chronic hepatitis B infection: A review. JAMA 2018; 319(17):1802-13.
2. Koo YX, Tay M, Teh YE, Teng Det al. Risk of hepatitis B virus (HBV) reactivation in hepatitis B surface antigen negative/hepatitis B core antibody positive patients receiving rituximab-containing combination chemotherapy without routine antiviral prophylaxis. Ann Hematol 2011; 90(10):1219-23.
3. Lee YH, Bae SC, Song GG. Hepatitis B virus (HBV) reactivation in rheumatic patients with hepatitis core antigen (HBV occult carriers) undergoing anti-tumor necrosis factor therapy. Clin Exp Rheumatol 2013; 31(1):118-21.
4. Li Q, Li W, Huang Y, Chen L. The gamma-glutamyl transpeptidase-to-platelet ratio predicts liver fibrosis and cirrhosis in HBeAg-positive chronic HBV infection patients with high HBV DNA and normal or mildly elevated alanine transaminase levels in China. J Viral Hepat 2016; 23(11):912-19.
5. Kamal AM, Mitrut P, Docea AO, et al. Double therapy with pegylated interferon and ribavirin for chronic hepatitis C. A pharmacogenetic guide for predicting adverse events. Farmacia 2017; 65(6):877-84.
6. Wojciechowski VV, Călina D, Tsarouhas K, et al. A guide to acquired vitamin K coagulophathy diagnosis and treatment: the Russian perspective. DARU 2017; 25:10.
7. Shin WG, Park SH, Jang MK, et al. Aspartate aminotransferase to platelet ratio index (APRI) can predict liver fibrosis in chronic hepatitis B. Dig Liver Dis 2008; 40(4):267-74.
8. Chrysanthos NV, Papatheodoridis GV, Savvas S, Kafiri G, Petraki K, Manesis EK, Archimandritis AJ. Aspartate aminotransferase to platelet ratio index for fibrosis evaluation in chronic viral hepatitis. Eur J Gastroenterol Hepatol 2006; 18(4):389-96.
9. Chen CJ, Yang HI, Su J, et al. REVEAL-HBV Study Group. Risk of hepatocellular carcinoma across a biological gradient of serum hepatitis B virus DNA level. JAMA 2006; 295(1):65-73.
10. Chou YC, Yu MW, Wu CF, Yang SY, et al. Temporal relationship between hepatitis B virus enhancer II/ basal core promoter sequence variation and risk of hepatocellular carcinoma. Gut 2008; 57(1):91-97.
11. Chen G, Lin W, Shen F, Iloeje UH, London WT, Evans AA. Past HBV viral load as predictor of mortality and morbidity from HCC and chronic liver disease in a prospective study. Am J Gastroenterol 2006; 101(8):1797-803.

12. Wang CC, Lim LY, Deubner H, et al. Factors predictive of significant hepatic fibrosis in adults with chronic hepatitis B and normal serum ALT. J Clin Gastroenterol 2008; 42(7):820-26.

LETTER TO THE EDITOR

INFLAMMATORY RESPONSES AND BIOLOGICAL CHARACTERISTICS OF HUMAN OSTEOSARCOMA CELLS AND UMBILICAL CORD BLOOD MONONUCLEAR CELLS IN CO-CULTURED MICROENVIRONMENT

Q. ZHANG, L. CAO, YP. WU and XD. MIAO

Foot and Ankle Group of Department of Orthopaedics, The Second Hospital Affiliated to Zhejiang University School of Medicine, Hangzhou, Zhejiang University, China

Received December 19, 2018 – Accepted February 5, 2019

To the Editor,

Human osteosarcoma (HOS) is the most common type of primary malignant osteosarcoma (1, 2). The microenvironment of HOS can promote the growth, proliferation, invasion and metastasis of HOS (3, 4). A long-term chronic inflammatory response has been shown in the microenvironment of HOS, and a large number of inflammatory factors, including cytokines, growth factors, chemokines, reactive oxygen species and prostaglandins, are secreted by HOS cells to promote their growth (5). Bian et al. (6) found that inflammatory gene polymorphisms play a key role in the occurrence and progression of HOS.

Inflammatory factors in the umbilical cord blood, including TGF-β1, IL-6 and IL-10, are multidirectional cytokines (7, 8). TGF-β1 can promote the proliferation and metastasis of tumor cells through the TGF-β/Smad signaling pathway, thus promoting the secretion of some cytokines to mediate immune regulation (9). HOS cells and human umbilical cord blood mononuclear cells were co-cultured *in vitro*. Subsequently, ELISA was used to detect the changes in cytokine concentrations and to study the effects of such changes on the migration, invasion and proliferation of HOS cells to further clarify the interaction between HOS cells and immune cells, thus providing a scientific basis for the treatment of HOS.

MATERIALS AND METHODS

Culture of HOS cells

HOS cells (the HOS cell line was provided by The Second Hospital Affiliated to Zhejiang University School of Medicine, Hangzhou, China) were centrifuged at 1000 rmp for 5 min. The supernatant was then removed and the cells were resuspended in 5 mL of DMEM medium (Gibco, USA) containing 10% fetal bovine serum (Hyclone Corporation, USA). The cells were mixed evenly and then transferred into a culture flask. After labeling the flask, the cells were cultured at 37°C under 5% CO_2 in an incubator (Thermo, USA). When the tumor cells reached 80% confluency, the supernatant was removed and the cells were digested with 0.25% trypsin (Gibco, USA). Subsequently, the tumor cells were divided equally into three culture flasks. After labeling the flasks, the cells were cultured at 37°C under 5% CO_2.

Extraction of mononuclear cells from umbilical cord blood

Umbilical cord blood was collected from full-term fetuses delivered at The Second Hospital Affiliated to Zhejiang University School of Medicine, Hangzhou, China. Five samples (15-20 mL each) of umbilical cord blood were

Key words: HOS; nuclear cells; microenvironment; biological characteristics

Corresponding Author:
Dr Xudong Miao,
Foot and Ankle Group,
Department of Orthopaedics, The Second Hospital Affiliated to Zhejiang University, School of Medicine,
No.88 Jiefang Road, Hangzhou, 31000, China
e-mail: shj1hao@zju.edu.cn

0393-974X (2019)

DISCLOSURE: ALL AUTHORS REPORT NO CONFLICTS OF INTEREST RELEVANT TO THIS ARTICLE.

collected using vacuum anticoagulant tubes (BD Company, USA). 15 mL of umbilical cord blood was collected and diluted with RPMI-1640 solution (Gibco, USA) at a volume ratio of 1:1, followed by the addition of a 1/2 volume human lymphocyte separating solution Histopaque 1077 (Shanghai Dingguo, China). In the next step, the cells were centrifuged at 2500 rmp centrifugal machine (Beijing Medical Centrifuge Factory, China) for 20 min. The liquid in the tube separated into four layers. The cells in the middle albuginea layer were taken and washed twice with the RPMI-1640 solution. After 10 min of centrifugation at 2000 rmp, the cells were collected and resuspended in the RPMI-1640 solution to a concentration of 1.0×10^6 cells/mL.

Establishment of an in vitro co-culture model of HOS cells and mononuclear cells

When the HOS cells reached 80% confluency, the density of HOS cells was adjusted to 3.0×10^5/mL and the cells were seeded into 6-well plates at 1 mL per well, followed by the addition of 1.0×10^6/mL mononuclear cells into each well on top of the HOS cells (experimental group). In the control group, the two kinds of cells were cultured separately. After 3 days of culture, 1 mL/well of culture medium was added every day until the culture was terminated. After 3, 5 and 7 days of culture, the supernatant was collected to measure the expression of cytokines IL-6, IL-10 and TGF-β using ELISA kit (Bio Legend, USA). Finally, the adherent tumor cells were collected and their biological characteristics were measured by Transwell and MTT (Shanghai Dingguo Biotechnology Co., Ltd., China) assays.

Changes in the migration profile of HOS cells

HOS cells were cultured for 3, 5 and 7 days before they were harvested. After adjusting the cell concentration to 50×10^4 cells/mL, 200 μL of cell suspension was added into each Transwell chamber not coated by Matrigel (BD Corporation, USA), i.e. approximately 1.0×10^5 cells per chamber. At the same time, 500 mL of DMEM medium containing 10% fetal bovine serum was added into each lower chamber. After 24 h of routine culture, the cells were removed from the upper surface of the membrane by a wet cotton swab, stained with crystal violet for 30 min, washed with distilled water for 1 min, and photographed at 200x magnification.

Changes in the invasive ability of HOS cells

Pre-cooled serum-free DMEM medium was mixed with Matrigel matrix glue at a ratio of 3:1. The diluted Matrigel was injected into the bottom chamber of Transwell (50 μL diluted Matrigel in each chamber). After incubating HOS cells at 37°C for 2 h, the HOS cells were inoculated into the Transwell chamber, cultured for another 48 h, fixed with 4% formaldehyde (Shanghai Dingguo Biotechnology Co., Ltd., China) for 15 min, and stained with 1% crystal violet (Shanghai Dingguo Biotechnology Co., Ltd., China) for 30 min. After being washed with distilled water, the Transwell microporous membrane was photographed at 200x magnification by using Olympus IX70 Inverted Phase Difference Microscope (Olympus, Japan).

Changes in the proliferation of HOS cells

HOS cells were cultured for 3, 5 and 7 days, and harvested to prepare single cell suspensions. Subsequently, the cells were seeded into 96-well plates at 10,000 cells/well with 100 μL per well. The cells were then cultured under 5% CO_2 at 37°C for 1-4 days. At 24 h, 48 h, 72 h and 96 h of culture, 20 μL of MTT solution was added into each well and incubated for 4 h. Then, the supernatant was carefully discarded before 150 μL of DMSO (Biotechnology Co., Ltd., China) was added into each well. The plate was oscillated for 10 min so that the crystals were fully dissolved. The absorption value of each well was detected at a wavelength of 490 nm to determine the proliferation profiles of the cells in Enzyme-linked Immunoassay (Awareness, USA).

Statistical analysis

SPSS19.0 software was used for data statistics. Measurement data were expressed in the form of (mean ± SD). All data were tested for normality. Duncan's new multiple range test (MRT) was used to compare two groups. $P < 0.05$ indicated the difference was significant.

RESULTS

Morphological changes of HOS cells and monocytes in the co-culture model

On the first day of co-culture, the tumor cells started to attach to the wall (Fig. 1A). A large number of lymphocytes were located around the tumor cells and the vitality of the tumor cells was poor. On the third day of co-culture, the number of immune cells decreased and the HOS cells attached more tightly to the wall. However, large gaps were visible among cells

(Fig. 1B). By the fifth day of co-culture, the number of immune cells continued to decrease and the number of HOS cells increased significantly (Fig. 1C). Overall, the number of monocytes decreased gradually, but the difference was not significant on days 1, 3 and 5, while the number of HOS cells increased gradually, and the basic immune cells were all engulfed by HOS cells at the later stage of culture.

Changes in TGF-β concentrations

Changes in the concentration of TGF-β secreted by HOS cells, IL-6 and IL-10 are shown in Fig. 2. HOS cells can secrete high levels of cytokine TGF-β by themselves, while umbilical cord blood mononuclear cells barely express TGF-β. The concentration of TGF-β in the experimental group was significantly higher than that in the HOS group on day 3 of co-culture ($P < 0.05$). There was no significant difference between the two groups on day 5 of co-culture, although the concentration of TGF-β in the experimental group was still higher than that in the HOS group. On day 7 of co-culture, the concentration of TGF-β in the experimental group was significantly lower than that in the HOS group ($P < 0.05$).

Changes in the concentrations of IL-6 and IL-10

The content of IL-6 and IL-10 in the co-culture group was significantly higher than that in the control

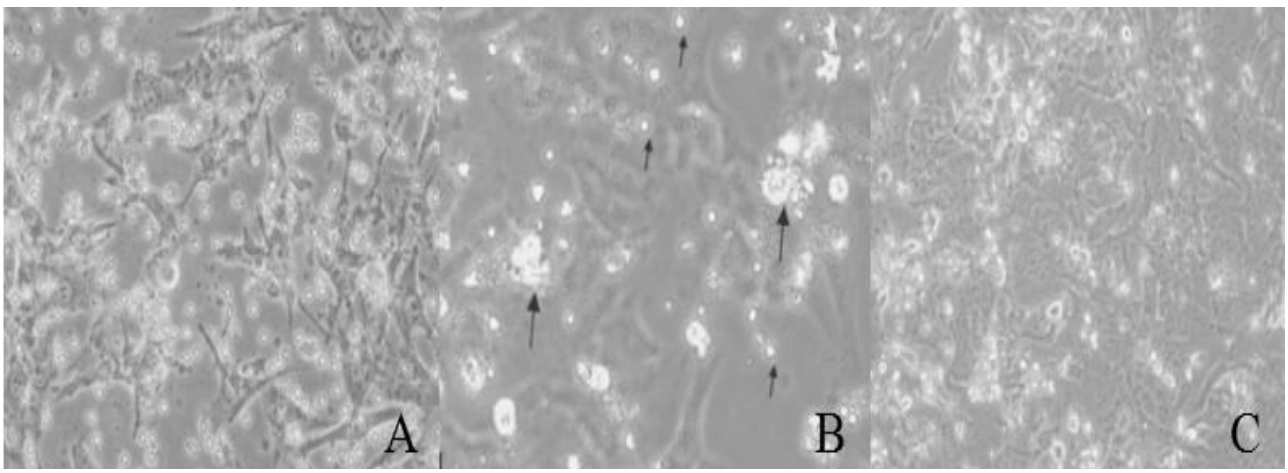

Fig. 1. *Dynamic changes of HOS cells and immune cells. **A**) day 1 of co-culture; **B**) day 3 of co-culture; **C**) day 5 of co-culture) (200x magnification)*

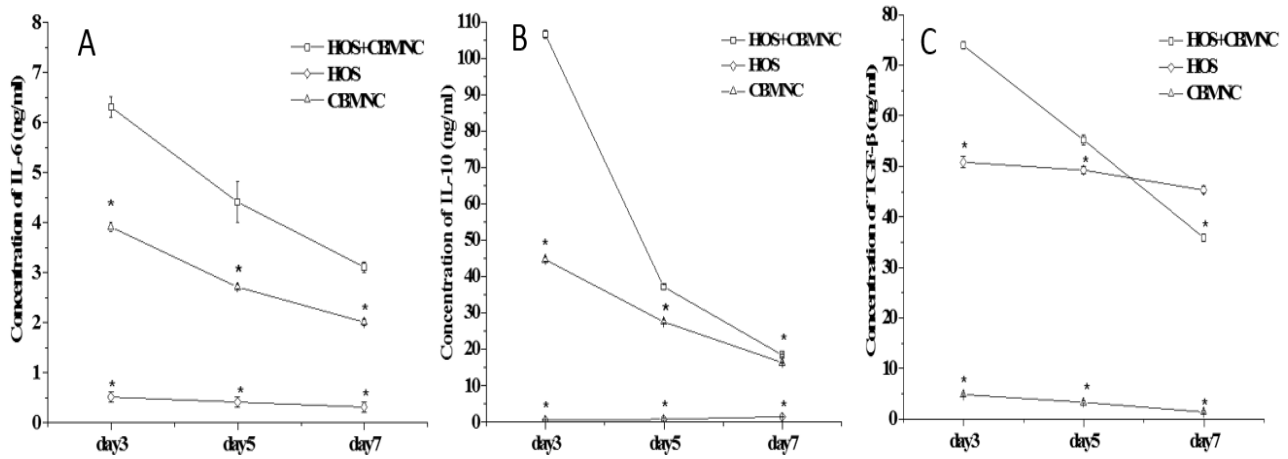

Fig. 2. *Changes of IL-6 (**A**), IL-10 (**B,**) and TGF-β (**C**) concentrations.*

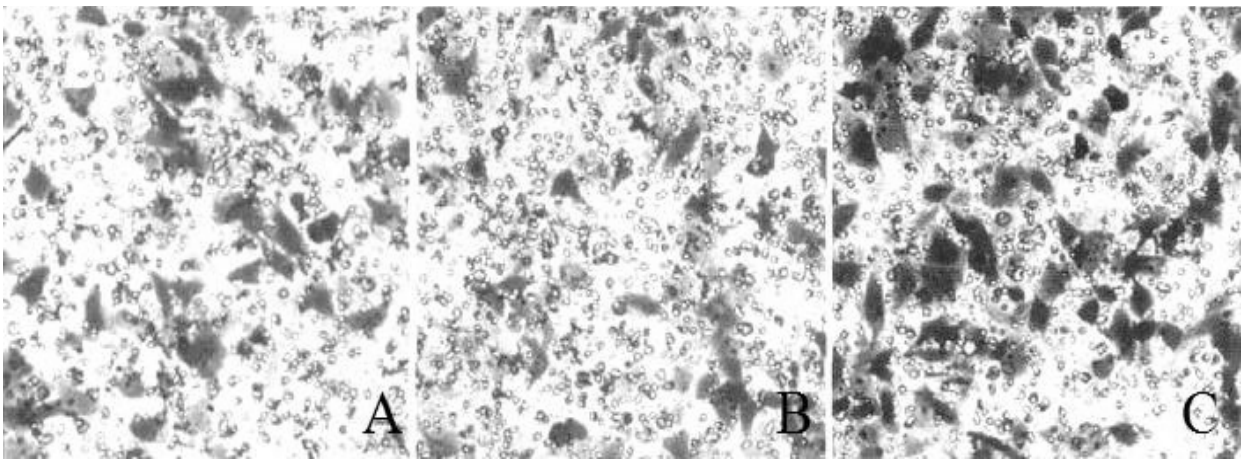

Fig. 3. *Migration of HOS cells in the co-culture model: **A**) 3 days; **B**) 5 days, **C**) 7 days (magnification, x200).*

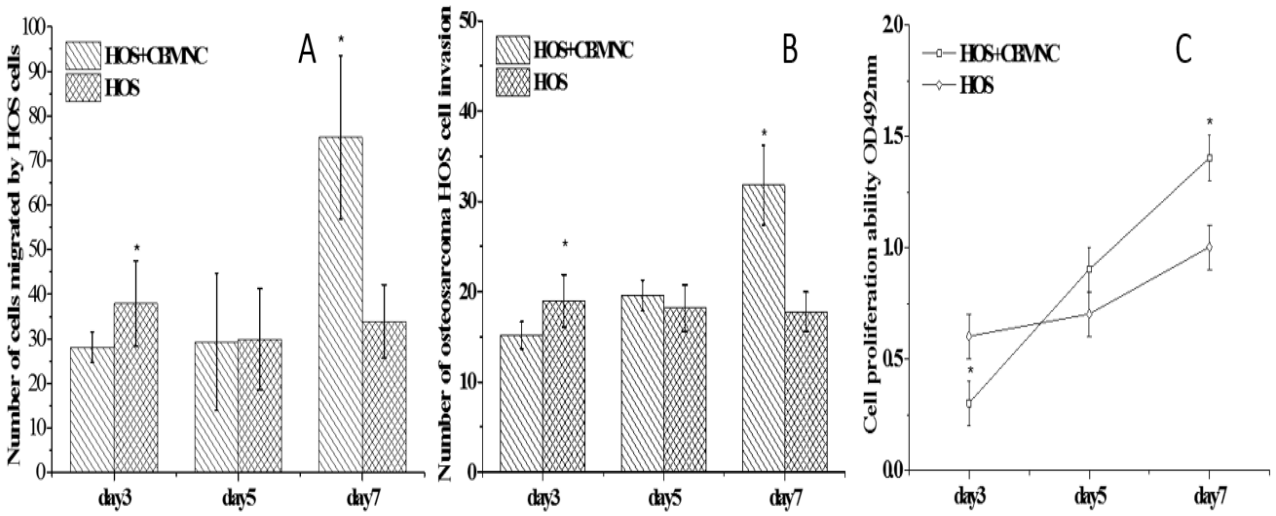

Fig. 4. *Migration (**A**), invasion (**B**) and proliferation (**C**) of HOS cells in the co-culture model.*

group at the same time point ($P < 0.05$). However, significant difference between the co-culture group and mononuclear cells in human umbilical cord blood (CBMNC) was only observed on the third day of culture ($P < 0.05$). Further analyses showed that the content of IL-6 and IL-10 in the co-culture group decreased over time. On the 5th and 7th day of co-culture, the content of IL-6 and IL-10 had decreased significantly ($P < 0.05$).

Effects of co-culture on the migration of HOS cells

The number of migrating HOS cells decreased in the early stage of co-culture. However, when the time of co-culture increased, the number of migrating HOS cells increased significantly (Fig. 3).

Migration (A), invasion (B) and proliferation (C) of HOS cells in the co-culture model are shown in Fig. 4. The number of HOS cells invading the lower chamber was lower in the co-culture group than that in the control group ($P < 0.05$). However, on the 5th day of culture, there was no significant difference in the number of invasive cells between the co-culture group and the HOS group ($P > 0.05$). Interestingly, on the 7th day of culture, the number of HOS cells

invading the lower chamber was significantly higher in the co-culture group than that in the control group ($P < 0.05$).

Effects of co-culture on the invasive ability of HOS cells

The number of invading HOS cells on days 3, 5 and 7 of culture was measured by the Transwell assay. The number of HOS cells invading the lower chamber was significantly lower in the co-culture group than that in the control group on the 3rd day of culture ($P < 0.05$). On the 5th day of culture, there was no significant difference in the number of invasive cells between the co-culture group and the control group ($P > 0.05$). However, on the 7th day of culture, the number of HOS cells invading the lower chamber was significantly higher in the co-culture group than that in the control group ($P < 0.05$).

Effects of co-culture on the proliferation of HOS cells

The D value of HOS cells in the co-culture system was measured by MTT assays. On the third day of co-culture, the proliferation of HOS cells in the co-culture group was significantly lower than that in the control group ($P < 0.05$). On day 7, the proliferation of HOS cells in the co-culture group was significantly enhanced ($P < 0.05$). It was further revealed that the proliferation ability of HOS cells in the co-culture model increased rapidly after the 5^{th} day, and significant difference was found on the 7^{th} day.

DISCUSSION

Containing many kinds of immune cells, such as MDSC, Treg, and Th17, the HOS microenvironment can regulate the development and metastasis of HOS cells (10). It was found that the number of immune cells decreased significantly over time, resulting in a large number of aggregates.

TGF-β, IL-6 and IL-10 not only play an important role in immune suppression, but also stimulate immune functions (11). The ELISA results of this study showed that the expression of the above three cytokines in the co-culture group was significantly higher than that in the control group, especially on the 3rd day of co-culture ($P < 0.05$). However, the concentration of these cytokines on the 5th and 7th day of co-culture decreased significantly, although the concentrations of IL-6 and IL-10 were still significantly higher than those in the control group.

Tumor invasion and metastasis require a series of complex steps (12). In this study, the invasive, migratory and proliferative ability of HOS cells showed the same trend during co-culture: the tumor cells were inhibited on day 3 of co-culture; no significant difference was observed between the control group and the co-culture group on day 5 of co-culture; on day 7 of co-culture, the migratory, invasive and proliferative ability of HOS cells in the co-culture group was significantly enhanced.

In conclusion, the co-culture of HOS cells and umbilical cord blood mononuclear cells significantly promoted the proliferation, migration and invasion of HOS cells by changing the levels of TGF-β and IL-6, which in turn exerted a great impact on the biological characteristics of the HOS cells.

ACKNOWLEDGEMENTS

This research was supported by grants from The National Natural Science Foundation of China (No. 81601878), The Zhejiang Medical and Health Science and Technology Program (No. 2016RCA016), and The Zhejiang Medical and Health Science Research Fund(No.2012KYA088).

REFERENCES

1. Moore DD, Luu HH. Osteosarcoma. Cancer Treat Res 2014; 162:65-92.
2. Kansara M, Teng MW, Smyth MJ, Thomas DM. Translational biology of osteosarcoma. Nat Rev Cancer 2014; 14(11):722-35.
3. Alfranca A, Martinez-Cruzado L, Tornin J, et al. Bone microenvironment signals in osteosarcoma development. Cancer Sci 2014; 105(2):159-67.
4. Zheng Y, Wang G, Chen R, Hua Y, Cai Z. Mesenchymal stem cells in the osteosarcoma microenvironment: their biological properties, influence on tumor growth, and therapeutic implications. Stem Cell Res Ther 2018; 9(1):22.
5. Sayour EJ, McLendon P, McLendon R, et al. Increased proportion of FoxP3+ regulatory T cells in tumor

infiltrating lymphocytes is associated with tumor recurrence and reduced survival in patients with glioblastoma. Cancer Immunol Immunother 2015; 64(4):419-27.

6. Bian Z, He Q, Wang X, Li M, Zhu L. Association of genetic polymorphisms with osteosarcoma risk: a meta-analysis. Int J Clin Exp Med 2015; 8(6):8317-28.
7. Gharibi A, La Kim S, Molnar J, et al. ITGA1 is a pre-malignant biomarker that promotes therapy resistance and metastatic potential in pancreatic cancer. Sci Rep 2017; 7(1):10060.
8. Liu C, Ma M, Zhang J, Gui S, Zhang X, Xue S. Galangin inhibits human osteosarcoma cells growth by inducing transforming growth factor-β1-dependent osteogenic differentiation. Biomed Pharmacother 2017; 89:1415-21.
9. Zhang H, Wu H, Zheng J, et al. Transforming growth factor β1 Signal is crucial for dedifferentiation of cancer cells to cancer stem cells in osteosarcoma. Stem Cells 2013; 31(3):433-46.
10. Hart KM, Byrne KT, Molloy MJ, Usherwood EM, Berwin B. IL-10 immunomodulation of myeloid cells regulates a murine model of ovarian cancer. Front Immunol 2011; 2:29.
11. Johannessen L, Sundberg TB, O'Connell DJ, et al. Small-molecule studies identify CDK8 as a regulator of IL-10 in myeloid cells. Nat Chem Biol 2017; 13(10):1102-8.
12. Yang Z, Li X, Yang Y, He Z, Qu X, Zhang Y. Long noncoding RNAs in the progression, metastasis, and prognosis of osteosarcoma. Cell Death Dis 2016; 7(9):e2389.

LETTER TO THE EDITOR

SOMATIC SYMPTOMS OF DEPRESSED OUTPATIENTS WITH RESIDUAL SYMPTOMS AFTER ACUTE PHASE TREATMENT IN CHINA: GENDER DIFFERENCES

XH. WANG[1], N. ZHAO[1], L. FENG[2], XQ. ZHU[2], WY. WU[3], G. WANG[2] and J. HU[1]

[1]Department of Psychiatry, the First Affiliated Hospital of Harbin Medical University, Harbin, China;[2]The National Clinical Research Center for Mental Disorders & Beijing Key Laboratory of Mental Disorders & Beijing Anding Hospital, Capital Medical University, Beijing, China; [3]Department of Psychiatry, Tongji Hospital of Tongji University, Shanghai, China

Received January 13, 2019 – Accepted February 26, 2019

To the Editor,

Depressed patients commonly suffer from somatic symptoms which complicate the diagnosis, prolong the depressive episode duration and intensify the severity of depression (1-2) . Somatic symptoms often reside even after appropriate treatment, leading to an increase in the recurrence rate and a decline in the remission rate of depression (3).

The therapeutic objectives in depression are to achieve symptom remission and functional recovery and return to mental and physical health (4). Incomplete remission is associated with increased risk of relapse and functional impairment (5). Most depressed patients still suffer residual symptoms after acute pharmacotherapy. The three most common residual symptoms are somatization, depression and anxiety. The unremitted depressed patients after treatment, especially those with more severe somatic symptoms, showed more clinical symptoms and poor quality of life (6).

Gender differences are prominent in depressed patients and are also found in somatic symptoms. Evidence suggests that depression accompanied by somatic symptoms may be a rooted psychosocial factor related to gender roles. Moreover, one study found that gender differences in somatic depression might account for the gender differences in almost all depressed patients (7).

To our knowledge, no study has assessed gender differences in residual somatic symptoms among depressed patients or somatic symptoms among different gender subgroups. Thus, our study was aimed to investigate gender differences in residual somatic symptoms among Chinese depressed patients after acute phase treatment.

MATERIALS AND METHODS

Subjects

Based on a cross-sectional design, 1,503 depressed outpatients (male/female, 559/944; age range 8-90 years) were recruited from 11 hospitals in China (The First Affiliated Hospital of Harbin Medical University, Harbin, Beijing Anding Hospital, Beijing.Tongji Hospital of Tongji University, Shanghai, Beijing Chao-Yang Hospital, Beijing, Beijing HuiLongGuan Hospital, Beijing, The First Hospital of Hebei Medical University, Hebei, The First Affiliated Hospital of Xi'an JiaoTong University, Xi'an, Affiliated Brain Hospital of Nanjing Medical University, Nanjing, Shanghai Mental Health Center, Shanghai, Shenzhen Kangning Hospital, Shenzhen, Guangdong Mental Health Center, Guangdong). One hundred and forty-three

Key words: depression; gender differences; residual somatic symptoms; PHQ-15

Corresponding Author:
Dr Jian Hu, Ph.D.,
Department of Psychiatry,
First Affiliated Hospital of Harbin Medical University
23 Youzheng Street,
Nangang District, Harbin, China.
e-mail: drhujiangbest1@163.com

0393-974X (2019)

patients were excluded due to inconsistent age criteria (n=9), mismatched treatment duration (n=60), no use of antidepressants (n=18), or incomplete data (n=56). The sociodemographic characteristics, history, clinical features, length and methods of treatment of depression were investigated. The participants who met the International Classification of Diseases (ICD)-10 for depressive episode or recurrent depressive disorder were treated for eight to twelve weeks. The main treatment was antidepressants, and the treatment duration interruption was no more than 2 weeks. The patients thought the disease had been recovered more than 50%. Exclusion criteria were primary clinical diagnosis of mania, bipolar disorder, schizophrenia, schizoaffective disorder, or other diseases associated with mental disorders.

All patients provided written informed consent to participate in the study. This project was approved by the Ethics Committee of each hospital.

Clinical ratings

The depression recovery was assessed by the Visual Analogue Scale (VAS) in which 0 = worst and 10 = best possible recovery (35). The patients were asked to draw a vertical line on the horizontal line based on the degree of recovery from depression. This would match the inclusion criterion that "patient thought the disease had been recovered more than 50%". The residual depressive symptoms were evaluated using the Quick Inventory of Depressive Symptomatology Self-Report Sixteen (QIDS-SR_{16}), in which QIDS-SR_{16} total score ≤ 5 and > 5 were classified as the non-RS group and the RS group, respectively (RS: residual symptoms). The somatic symptom severity was assessed using the 15-item Patient Health Questionnaire (PHQ-15) (36). Subjects were asked to rate the severity of each symptom over the last four weeks as 2, 1 or 0, which meant bothered a lot, a little, and not at all, respectively. The total score ranges from 0 to 30. The categories included minimal (PHQ-15 score=0–4), low (5–9), medium (10–14), and high (15–30) severity of somatic symptoms.

Statistical analysis

Initial analysis involved all subjects. The demographic and clinical data were described using standard deviation, means of mean and range or frequency and percentages. The percentage of the target variable was given by the 95% confidence interval (CI). Categorical variables were examined through *Chi*-squared tests or Fisher's exact test. Ridit analysis was used for two-way orderly variable. Variables that did not conform to normal distribution were assessed by Wilcoxon rank sum test. Differences between groups (male and female groups; RS group and non-RS group) were compared via independent samples *t*-tests. The PHQ-15 item score analysis between genders consisted of analysis of variance (ANOVA). In case of significance in ANOVA, age, years of education, medication time of this attack, history of physical diseases, and QIDS-SR_{16} total score were tested and added as covariates into the analysis model. When PHQ-15 total scores were included in the stepwise logistic regression analysis, the independent variables included age, time of drug treatment, recurrence of the disease, history of the past, and severity of QIDS-SR_{16}, and the ordinal dependent variable was the severity of PHQ-15. We identified the risk factors related to the severity of somatic symptoms. The statistical significance for all tests was set at $P<0.05$. All data were analyzed on the Statistics Analysis System (SAS 9.2).

RESULTS

Demographic data

A total of 1,503 patients, including 733 patients in the RS group and 770 cases in the non-RS group, were included. No significant gender differences were found between the RS and non-RS groups ($\chi^2=0.1493$, $P=0.6992$).

The characteristics of the RS group were compared. Significant difference was found between females and males in average age (44.11±14.84 *vs* 41.39±14.65, $P=0.0164$). Mean age at the first episode of depression was significantly lower for males than females ($P=0.0048$). Significantly fewer education years were found in females *vs* males ($P=0.0024$), but no significant gender differences were found age of onset of recurrent depression, number of past episodes, or medication time of this attack.

Comparison of the severity of somatic symptoms showed the proportion of somatic symptoms was significantly higher in the RS group than in the non-RS group (74.70% *vs* 24.69%), indicating the somatic symptoms of depression were more severe in the RS group.

Gender differences in PHQ-15 within the RS group

PHQ-15 scores were 5.29±4.32 among all patients and 7.52±4.48 in the RS group. The top five prevalent somatic symptoms in the RS group were fatigue (77.65%), sleeping trouble (68.53%), headache (55.29%), constipation (51.86%) and palpitation (48.73%).

Table I shows the PHQ-15 scores of the RS group compared between genders. Significant gender differences were found in abdominal pain and breathing trouble (P<0.05). These two symptoms were more severe in females than males according to the scores and 95%CIs. When age, years of education, medication time of this attack, history of physical diseases, and QIDS-SR16 total score were added as covariates into ANOVA, significant gender difference was still observed (*P*<0.05).

Gender differences in severity of residual somatic symptoms among age groups

A logistic model was established with the severity of PHQ-15 as the ordinal dependent variable, while age, medication time of this attack, recurrence of the disease, history of physical diseases, and severity of QIDS-SR_{16} as independent variables. *P* values of the Model Wald test score were less than 0.0001, which indicated significance of the model. The levels of PHQ-15, gender and the severity of QIDS-SR_{16} were all significantly different from the dependent variable, but no significant difference was found among the age groups

Logistic regression showed age did not significantly affect the total score of PHQ-15 when other factors were fixed (*P*>0.05). Further single-factor analysis showed differences in the number of residual symptoms and the severity of PHQ-15 among different male (or female) subgroups. In the female subgroups, a larger number of residual symptoms led to significantly higher severity of PHQ-15 in the age groups 18-30, 31-40 and 41-50 (*P*<0.05). In the male subgroups, only the 18-30 age group showed that the severity of PHQ-15 was more serious with the increased numbers of residual symptoms (Table II).

Table I. *Gender differences in PHQ-15 of patients with residual symptoms.*

Characteristic	Female		Male		T	*P*	95%CL
Abdominal pain	0.48	0.63	0.35	0.55	2.83	0.0048**	0.13[0.04，0.22]
Back pain	0.47	0.65	0.40	0.61	1.48	0.1386	0.07[-0.02,0.17]
Joint or limb pain	0.47	0.66	0.46	0.65	0.29	0.7688	0.01[-0.08,0.11]
Menstrual problems	0.34	0.28	-	-			
Headaches	0.70	0.67	0.66	0.70	0.66	0.5119	0.03[-0.07,0.14]
Chest pain	0.29	0.53	0.28	0.52	0.40	0.6921	0.02[-0.06,0.09]
Dizziness	0.56	0.63	0.58	0.67	-0.39	0.6939	-0.02[-0.12,0.08]
Fainting	0.08	0.28	0.08	0.28	-0.02	0.9823	0.00[-0.04,0.04]
Palpitations	0.61	0.65	0.53	0.64	1.66	0.0970	0.08[-0.01,0.18]
Breathing trouble	0.48	0.62	0.39	0.57	1.97	0.0494*	0.09[0.00,0.18]
Sexual pain/problems	0.15	0.42	0.17	0.47	-0.54	0.5923	-0.02[-0.08,0.05]
Diarrhea(constipation)	0.64	0.71	0.65	0.69	-0.18	0.8541	0.00[-0.11,0.10]
Gas or indigestion	0.56	0.65	0.52	0.67	0.68	0.4994	0.03[-0.06,0.13]
Fatigue	0.08	0.28	0.08	0.28	-0.02	0.9823	0.00[-0.04,0.04]
Sleeping trouble	0.90	0.74	1.00	0.74	-1.65	0.10	-0.09[-0.20,0.02]
Total score	7.71	4.63	7.20	4.18	1.48	0.1385	0.50[-0.16,1.18]

*Note: PHQ-15=Patient Health Questionnaire-15. *P<0.05, **P<0.01.*

Table II. *Differences in the number of residual symptoms and the severity of PHQ-15 among different male (or female) subgroups.*

Age (years)	PHQ-15 Total Score											
	Female						Male					
	5～9(Low)		10～14(Medium)		≥15(High)		5～9(Low)		10～14(Medium)		≥15(High)	
the numbers of residual symptoms	N	%	N	%	N	%	N	%	N	%	N	%
18～30												
≤5	19	85.71	3	14.29	0	0.00	13	92.86	1	7.14	0	0.00
6-7	31	79.49	4	10.26	4	10.26	28	80.00	6	17.14	1	2.86
≥8	20	47.62	13	30.95	9	21.43	12	50.00	8	33.33	4	16.67
Statistical test[a]	*Chi*-squared=11.4698		*P*=0.0032**				*Chi*-squared=8.9301		*P*=0.0115*			
31～40												
≤5	15	78.95	4	21.05	0	.00	15	93.75	1	6.25	0	0.00
6-7	37	78.72	7	14.89	3	6.38	23	88.46	2	7.69	1	3.85
≥8	17	54.84	5	16.13	9	29.03	21	72.41	4	13.79	4	13.79
Statistical test[a]	*Chi*-squared=9.4784		*P*=0.0087**				*Chi*-squared=4.0938		*P*=0.1291			
41～50												
≤5	22	78.57	5	17.86	1	3.57	7	87.50	1	12.50	0	0.00
6-7	28	73.68	6	15.79	4	10.53	12	70.59	4	23.53	1	5.88
≥8	11	47.83	4	17.39	8	34.78	15	71.43	2	9.52	4	19.05
Statistical test[a]	*Chi*-squared=8.3195		*P*=0.0156*				*Chi*-squared=2.5624		*P*=0.2777			
51～60												
≤5	29	87.88	4	12.12	0	0.00	8	88.89	1	11.11	0	0.00
6-7	42	79.25	7	13.21	4	7.55	18	81.82	3	13.64	1	4.55
≥8	12	63.12	4	21.05	3	15.79	7	100.00	0	0.00	0	0.00
Statistical test[a]	*Chi*-squared=4.9810		*P*=0.0829				*Chi*-squared=0.3108		*P*=0.8561			
＞60												
≤5	25	86.21	4	13.79	0	0.00	8	100.00	0	0.00	0	0.00
6-7	14	66.67	6	28.57	1	4.76	10	58.82	6	35.29	1	5.88
≥8	14	66.67	6	28.57	1	4.76	11	68.75	3	18.75	2	12.50
Statistical test[a]	*Chi*-squared=2.8421		*P*=0.2415				*Chi*-squared=1.4869		*P*=0.4755			

*Note: PHQ-15=Patient Health Questionnaire-15. [a]: Two-way ordered variables use Ridit analysis. *P<0.05, **P<0.01. Questionnaire-15.*P<0.05,**P<0.01.*

Gender differences in the severity of residual somatic symptoms in different treatment time and methods of patients with residual symptoms

No significant gender difference was found in the severity of somatic symptoms irrespective of treatment duration. However, in the female subgroups, the severity of somatic symptoms was significantly dependent on the treatment duration (*P*=0.0414). The longer treatment time led to severer residual somatic symptoms, while no identical findings were found in male subgroups.

The use of antidepressants (including those at present) since this time of depression was investigated. Comparison between genders in the RS group showed a gender difference in the use of antidepressants (*P*=0.0254) as more females were treated with mono-therapy (n=362, 78.02%), while more males were treated with two or more types of antidepressants (n=79, 29.37%). The patients were then divided into three groups of antidepressant treatments, including mono-therapy, combination of two or more reagents, and combination with antipsychotics/ benzodiazepines. The results showed the combination with antipsychotic or sedative hypnotics significantly reduced the severity of residual somatic symptoms in males (P=0.0102) (Table III).

DISCUSSION

We found residual symptoms to be common in

Table III. *Gender differences in the severity of somatic symptoms by different treatment time and different treatment methods.*

Treatment time and methods	Female			Male			Statistical test	
	5～9	10～14	≥15	5～9	10～14	≥15	χ^2	*P*
Treatment time (week)								
8	91(76.47)	18(15.13)	10(8.40)	60(76.92)	12(15.38)	6(7.69)	0.0327	0.9838
9	47(83.93)	5(8.93)	4(7.14)	23(100.00)	0(0.00)	0(0.00)	-	0.1929
10	63(68.48)	18(19.57)	11(11.96)	48(84.21)	8(14.04)	1(1.75)	6.3346	0.0421*
11	39(72.22)	9(16.67)	6(11.11)	25(73.53)	9(26.47)	0(0.00)	-	0.0984
12	95(66.43)	32(22.38)	16(11.19)	52(67.53)	13(16.88)	12(15.58)	1.5076	0.4706
Statistical test	*Chi*-squared=6.3683		*P*=0.0414*	*Chi*-Squared=4.3920		*P*=0.1112		
Treatment methods								
Methods 1	257(70.99)	69(19.06)	36(9.94)	106(55.79)	30(15.79)	13(6.84)	3.6609	0.3005
Methods 2	78(76.47)	13(12.75)	11(10.78)	35(44.30)	12(15.19)	6(7.59)	1.3306	0.7219
Statistical test	Fisher exact test		*P*=0.3359		*P*=0.7136			
Methods 3	51(41.80)	19(15.57)	12(9.84)	31（41.89）	9（12.16）	5（6.76）	1.4152	0.7020
Statistical test	Fisher exact test		*P*=0.0629		*P*=0.0102 *			

*Note: PHQ-15=Patient Health Questionnaire-15.*P<0.05,**P<0.01.*
Method 1: Mono-therapy. Method 2: Combined two or more antidepressants. Method 3:Anti depression drugs combined with antipsychotic drugs/benzodiazepines

depressed patients, as the incidence was 48.77% in the tested outpatients, consistent with the finding that only 47% of depressed patients achieved remission after six months of treatment (8).

We found females suffered more severe abdominal pain and breathing trouble than males, and the same results that females with abdominal pain are more depressed than males (9). The STAR*D study reported significantly higher rate of somatization disorder among depressed females (10). The exact reasons for this gender difference are still unknown and should be confirmed by further investigations.

Interestingly, our data showed females aged 18-50 years and males only 18-30 years had more severe residual somatic symptoms. Age is a crucial factor either for depression or the treatment effect (11). Moreover, focus should be on females between 18 and 50 since the less residual symptoms indicate the milder severity of somatic symptoms. Surprisingly, we found somatic symptoms of the females became increasingly severe with the prolonged treatment time. Not all patients are willing to reserve maintenance pharmacotherapy indefinitely, many females are more likely to adopt psychotherapy (12). The pressure sources from treatment may cause more somatic symptoms. Our results suggested drug combination can be recommended for male patients for lighter PHQ-15. The differences in the levels of hormone secretion and in the gender-related drug activity may cause gender difference in drug treatment.

In future, case-control and follow-up studies as well as objective assessment scales need to be added to solve the limitations of our study.

ACKNOWLEDGEMENTS

This work was supported by National Key Technology Research and Development Program of the Ministry of Science and Technology of China (2015BAI13B03); Beijing Municipal Administration

of Hospitals Clinical Medicine Development of Special Funding Support (ZY201403); Beijing health system high level health technical personnel training project (2013-2-001).

REFERENCES

1. Park SC, Sakong J, Koo BH, et al. Clinical significance of the number of depressive symptoms in major depressive disorder: results from the CRESCEND Study. J Korean Med Sci 2016; 31(4):617-22.
2. Leuchter AF, Husain MM, Cook IA, et al. Painful physical symptoms and treatment outcome in major depressive disorder: a STAR*D (Sequenced Treatment Alternatives to Relieve Depression) report. Psychol Med 2010; 40(2):239-51.
3. McMahon AB, Arms-Chavez CJ, Harper BD, LoBello SG. PHQ-8 minor depression among pregnant women: association with somatic symptoms of depression. Arch Womens Ment Health 2017; 20(3):405-9.
4. McIntyre RS. Using measurement strategies to identify and monitor residual symptoms. J Clin Psychiatry 2013; 74(Suppl 2):14-18.
5. Zhao N, Wang X, Wu W, et al. Gender differences in quality of life and functional disability for depression outpatients with or without residual symptoms after acute phase treatment in China. J Affect Disord 2017; 219:141-48.
6. Woo JM, Jeon HJ, Noh E, et al. Importance of remission and residual somatic symptoms in health-related quality of life among outpatients with major depressive disorder: a cross-sectional study. Health Qual Life Outcomes 2014; 12:188.
7. Silverstein B, Ajdacic-Gross V, Rossler W, Angst J. The gender difference in depressive prevalence is due to high prevalence of somatic depression among women who do not have depressed relatives. J Affect Disord 2017; 210:269-72.
8. Rossom RC, Solberg LI, Vazquez-Benitez G, Whitebird RR, Crain AL, Beck A, Unutzer J. Predictors of poor response to depression treatment in primary care. Psychiatr Serv 2016; 67(12):1362-67.
9. Bouchoucha M, Hejnar M, Devroede G, Babba T, Bon C, Benamouzig R. Anxiety and depression as markers of multiplicity of sites of functional gastrointestinal disorders: a gender issue? Clin Res Hepatol Gastroenterol 2013; 37(4):422-30.
10. Marcus SM, Young EA, Kerber KB, et al. Gender differences in depression: findings from the STAR*D study. J Affect Disord 2005; 87(2-3):141-50.
11. Delgadillo J, Moreea O, Lutz W. Different people respond differently to therapy: A demonstration using patient profiling and risk stratification. Behav Res Ther 2016; 79:15-22.
12. Garland A, Scott J. Cognitive therapy for depression in women. Psychiatr Ann 2002; 32(8):465-76.

LETTER TO THE EDITOR

T LYMPHOCYTE DEPENDENCE OF THE IMMUNE RESPONSE TO IMMUNOSUPPRESSIVE NEOANTIGEN-EXPOSING Fc FRAGMENTS OF IgG

E. STOLYAROVA[1], L. BEDULEVA[1,2,3], I. MENSHIKOV[1,2,3], A. SIDOROV[1] and T. KHRAMOVA[1,3]

[1]Department of Immunology and Cell Biology, Udmurt State University, Izhevsk, Russian Federation; [2]Novye Vakciny Ltd, Krasnoarmeyskaya, Izhevsk, Russian Federation; [3]Udmurt Federal Research Center, Ural Branch of the Russian Academy of Sciences, Izhevsk, Russian Federation

Received October 24, 2018 – Accepted March 8, 2019

To the Editor,

Our recent studies have identified a new factor in the negative immunoregulation that prevents experimental autoimmune diseases (1). This factor was shown to be anti-idiotypic antibodies to lymphocytes against autoimmune disease-inducing antigens; at the same time, it is specific for neoepitopes on papain Fc fragments of homologous IgG (1). Because of its specificity to Fc fragments, we designated this regulatory factor "regulatory rheumatoid factor" (regRF) (2). Immunization with IgG Fc fragments that expose epitopes recognized by regRF reduces collagen-induced arthritis (CIA) in rats (2). These characteristics indicate that regRF-producing lymphocytes may serve as a therapeutic biotarget, and the Fc fragments that expose epitopes recognized by regRF may be a promising therapeutic agent for rheumatoid arthritis. We noted that the regRF production induced by immunization with Fc fragments is always rapid and brief (2). RegRF peaks on day 7 post-immunization; by day 14 it has returned to the initial level. The characteristics of regRF production kinetics cannot be explained, because the mechanisms by which the system regulates autoimmunity with the involvement of regRF, particularly the mechanisms by which regRF production is activated, are unclear. They must be clarified in order to develop a strategy for vaccinating with IgG Fc fragments that expose epitopes recognized by regRF.

We hypothesize that the reason that IgG Fc fragments induce a rapid and brief response of regRF is that regRF-producing B lymphocytes are activated without T helper cell involvement. Fc fragments that bear epitopes recognized by regRF are therefore T-independent antigens. Since T-independent antigens are divided into type 1 and type 2 antigens, if indeed Fc fragments are T-independent, then the T-independent antigen type must also be determined.

MATERIALS AND METHODS

Animals

Wistar rats (8–10 weeks old) were obtained from the Stolbovaya breeding facility (Russia) and housed under standard laboratory conditions with food and water at a constant temperature of 20±5°C. Animal experiments were performed in accordance with THE European Commission Directive 86/609/EEC (European Convention for the Protection of Vertebrate Animals used for Experimental and other Scientific Purposes) and approved by the local

Key words: regulatory rheumatoid factor, Fc fragments of IgG, T-independent type 2 antigen

Corresponding Author:
Dr Elena Stolyarova,
Udmurt State University, 1,
Universitetskaya, Izhevsk,
426000, Russian Federation
Tel: +7(3412)916-426,
e-mail: shima12@yandex.ru

0393-974X (2019)

DISCLOSURE: ALL AUTHORS REPORT NO CONFLICTS OF INTEREST RELEVANT TO THIS ARTICLE.

animal care commission of Udmurt State University (protocol № 1801).

Administration of TNP-LPS, TNP-AECM-Ficoll, bovine collagen type II, and rat IgG Fc fragments, and Cyclosporine A (CsA)

Fc fragments of rat IgG were emulsified in incomplete Freund's adjuvant (IFA) (Sigma-Aldrich, St. Louis, MO, USA) and injected intradermally at a dose of 300μg/rat. TNP-LPS (LGC Biosearch Technologies) and TNP-AECM-Ficoll (LGC Biosearch Technologies) were injected intraperitoneally, at a dose of 50μg/rat and 25μg/rat, respectively. Collagen type II from bovine nasal septum (BC II) (Elastin Products Company, Inc., Owensville, MO, USA) was dissolved in acetic acid (0.1 mol/L) and then emulsified with the same volume of ice-cold IFA. Rats were injected intradermally at the tail base with BCII/adjuvant emulsion, 400 μg/rat. Rats that did not develop arthritis were given a second injection of 400μg/rat at week 10. Rats that developed arthritis but were in remission (9-10 weeks after BCII immunization) were given a second, identical dose of BCII.

Some of the immunized rats in each group received daily subcutaneous CsA (Sandimmune® Neoral®, Novartis Pharma AG, Switzerland) injections (25 mg/kg) for 5 days starting 1 day prior to immunization with antigen.

Determination of antibodies to TNP-LPS by ELISA

A plate (Corning 9018, Corning Incorporated, USA) was coated overnight at 4°C with 100 μl of TNP-LPS (LGC Biosearch Technologies) (50μg/ml in 0.15mol/L PBS). The plate was then washed with PBS containing 0.05% Tween 20 (PBS/Tween-20) and the was blocked with PBS containing 150 μl of 0.15mol/L PBS/5% powdered milk (neoFroxx GmbH, Einhausen, Germany)/0.05% Tween-20 for 1 h at room temperature (RT). Serum samples in serial dilution were added to the plate with the sorbed TNP-LPS and incubated overnight at 4°C. The plate was incubated with horseradish peroxidase-conjugated sheep anti-rat Ig (IgG, IgM, IgA) antibodies (IMTEK, Moscow, Russia) for 1 h at RT. The ELISA plate was then visualized by incubating 100 μl of the substrate mixture (5 ml of citrate buffered solution (pH 5.0)/3 mg ortho-phenylenediamine/15 μl 3% H_2O_2) at RT for 15-20 min. The reaction was stopped by the addition of 50 μl of 2 M sulfuric acid. Absorbance was read after 15 min at 492 nm.

Determination of antibodies to TNP-AECM-Ficoll by ELISA

A plate (Corning 9018, Corning Incorporated, USA) was coated overnight at 4°C with 50 μl of TNP-AECM-Ficoll (LGC Biosearch Technologies) (10μg/ml, 0.15mol/L PBS). The remaining steps were performed as indicated in the preceding section except that the serum samples were incubated for 1 h at RT.

Determination of anti-BCII antibodies by enzyme-linked immunosorbent assay (ELISA)

The procedure for determining antibodies to BCII was as described previously (1).

Measurement of regRF in rat serum

The regRF titer was determined in an agglutination test using rat IgG-loaded tanned human erythrocytes. Group 0 human erythrocytes (Republic Blood Transfusion Station, Izhevsk, Russia) were fixed with 1% glutaric dialdehyde. The erythrocytes were washed off, and incubated for 10 min with the same amount of tannin solution in PBS at RT. For sensitization, 4 mL of PBS (pH 6.4), 1 mL of a solution of 0.5mg/ml normal IgG from rat serum (Equitech Bio, Kerrville, TX, USA) in 0.9% NaCl, and 70 μl of the pelleted tanned erythrocytes were mixed. Incubation lasted for 20 min at RT; erythrocytes were washed with 0.15mol/L PBS containing 0.2% BSA. Two-fold serial dilutions of serum were prepared and put into wells in aliquots of 50 μl. The same amount of rat-IgG-loaded 1.5% erythrocyte suspension was then added. Agglutination results were read after 3 h.

Fc fragments of rat IgG

Fc fragments of rat IgG were obtained by the method described previously (2). The presence of neoepitopes recognized by regRF on Fc fragments were tested in the reaction of inhibition of regRF-induced agglutination of tanned erythrocytes loaded with rat IgG (2). RegRF-containing sera were

obtained from intact rats. Samples of Fc fragments at concentrations of 15.0 and 30.0 μg/well were mixed with regRF-containing serum and rat IgG-loaded tanned erythrocytes and incubated at 37°C. In addition, the presence of the epitopes on rat IgG Fc fragments was determined by their ability to induce production of regRF in intact rats. For this purpose, rats were immunized with Fc fragments at a dose of 400 μg in IFA. Blood levels of regRF were measured in the rats before immunization and on days 7 and 14 after immunization.

Isolation of mononuclear cells from red bone marrow (RBM) and production of B-lymphocyte-enriched RBM cell populations

RBM was extracted from the tibia and femur bones of intact rats under sterile conditions. The suspension of RBM cells was separated on a Ficoll (Paneco, Moscow, Russia) density gradient (1.077 g/cm^3) to obtain the mononuclear fraction.

Untouched B cells were obtained from the mononuclear fraction by immunomagnetic negative selection using an EasySep™ Rat B Cell Isolation Kit (STEMCELL Technologies, Inc., Cambridge, MA, USA). This antibody cocktail did not contain antibodies to any of the B-lymphocyte populations, including plasma cells.

Immunizing RBM cells with IgG Fc fragments and measuring regRF in RBM cell culture supernatant

Mononuclear cells (100 μl, 2x10^6 cells) or B lymphocytes (100 μl, 2-5x10^{5}cells) obtained from RBM of intact rats were cultivated in 1 ml RPMI-1640 medium (Paneco, Moscow, Russia) with added glutamine (0.3g/L) and gentamycin (120μg/ml) in the presence of rat IgG Fc fragments bearing epitopes recognized by regRF (100μg/well) in a 24-well plate (Costar 3524, Corning Incorporated, USA) for 4 days at 37°C in an atmosphere of 5% CO_2. Cells cultivated in the above-noted medium served as the control.

To determine the regRF level in the culture medium, samples were taken from the wells after 2 and 4 days of culture. The supernatant obtained after centrifugation was concentrated for 10 min at 1700 × *g* in concentrators (Amicon Ultra-0.5 mL Centrifugal Filters Ultracell 30K) (Merck Millipore Ltd, Ireland). The supernatant was condensed 7 times. The regRF titer in the supernatant was determined in an agglutination test using rat IgG-loaded tanned human erythrocytes. Since hemagglutination was used to measure regRF, we tested to determine whether the antibodies found in the supernatant were anti-erythrocyte. The supernatant of the culture of RBM cells cultured with and without Fc fragments did not induce agglutination of erythrocytes not loaded with IgG.

RESULTS

Time course of regRF and antibodies to T-independent and T-dependent antigens, including with cyclosporine A administration

To clarify whether Fc fragments of IgG are a T-dependent or T-independent antigen, we immunized rats with IgG Fc fragments and compared the resulting kinetics of regRF blood levels to those of the production of antibodies to known T-independent and T-dependent antigens (Fig. 1). For the T-independent antigens, we used TNP-LPS (T-independent type 1 (TI-1) antigen) and TNP-AECM-Ficoll (T-independent type 2 (TI-2) antigen). For the T-dependent antigen, we chose bovine collagen type II (BCII) for both the initial and repeat immunization of the rats.

In addition, we investigated the effect of cyclosporine A on regRF production and the immune response to T-dependent antigen and TI-1 and TI-2 antigens (Fig. 1). CsA is known to suppress the immune response to T-independent type 2 antigens and T-dependent antigens, but does not affect antibody production against T-independent type 1 antigens (3, 4). Therefore, a method for determining whether T-independent antigens are type 1 or type 2 is to examine the CsA sensitivity of the antibody production they induce.

Fig. 1a illustrates that the production of regRF induced by rat Fc fragments that bear epitopes recognized by regRF is transitory, peaking in the blood on day 7 post-immunization. CsA suppresses regRF production (Fig. 1a).

Antibodies to T-independent antigens (TNP-LPS and TNP-AECM-Ficoll) appeared in the blood as early as day 3 post-immunization, and over 14 days their level continued to increase (Fig. 1b and

1c, respectively). As expected, consistent with the findings of Higham et al. (4), CsA does not suppress the production of antibodies to TNP-LPS (TI-1 antigen) (Fig. 1b) but suppresses the production of antibodies to TNP-AECM-Ficoll (TI-2 antigen) (Fig. 1c).

Antibodies did not appear in the blood in response to primary immunization with the T-dependent antigen BCII until day 14 post-immunization (Fig. 1d). Their production was also sensitive to CsA.

Since regRF is always present in the blood of intact rats, and there are endogenous mechanisms that activate regRF-producing lymphocytes (5), the presence of memory cells may be the cause of the rapid regRF production in response to immunization with IgG Fc fragments. Therefore, we compared the kinetics of regRF with those of anti-BCII antibodies produced in response to a second BCII injection in rats that had previously been immunized with BCII. Some of these rats developed arthritis in response to the primary BCII immunization, while others were resistant. The rats that had developed arthritis were in remission when BCII was injected the second time, but antibodies to BCII remained in their blood (Fig. 1e). Fig. 1e shows that the second BCII administration did not alter the anti-BCII antibody levels in arthritic rats in remission, while administration of BCII with CsA increased the anti-

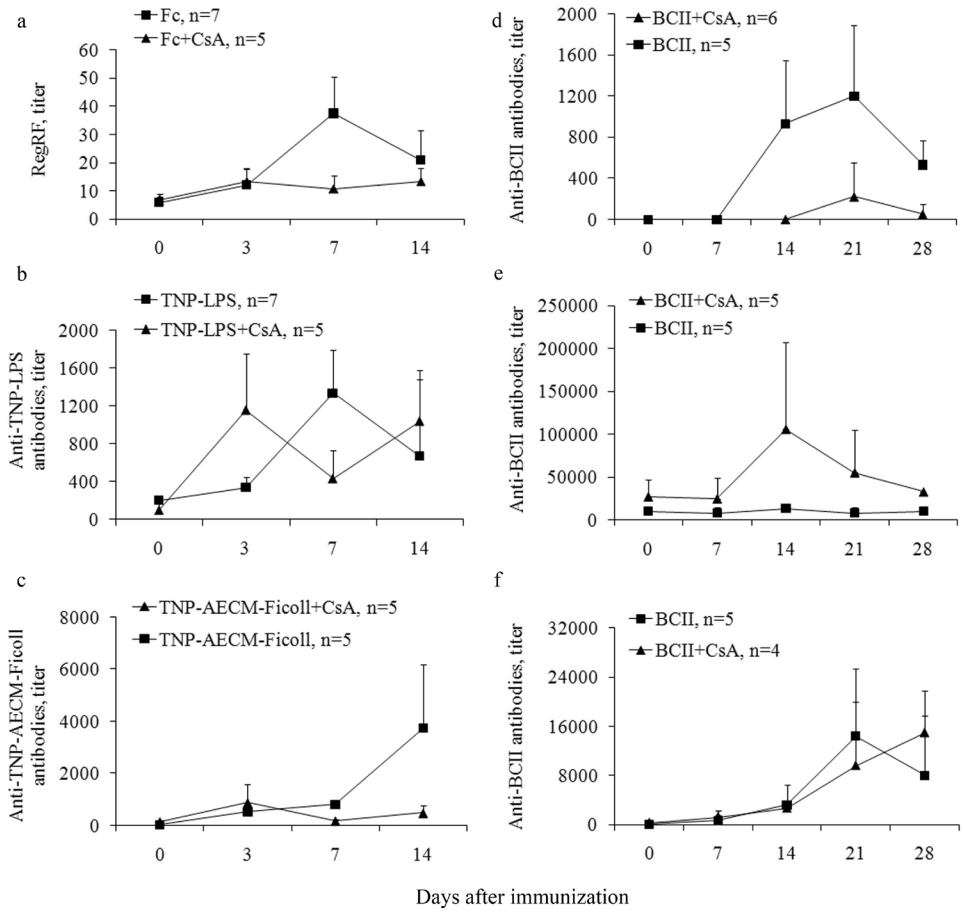

Fig. 1. *Time course of antibodies to T-independent and T-dependent antigens, including effect of cyclosporine A.* ***a)*** *Immunization with Fc fragments of rat IgG that bear epitopes recognized by regRF.* ***b)*** *Immunization with TNP-LPS (T-independent type 1 antigen).* ***c)*** *Immunization with TNP-AECM-Ficoll (T-independent type 2 antigen).* ***d)*** *Immunization with BCII. Primary immune response. Arthritis-resistant rats.* ***e)*** *Immunization with BCII. Secondary response. Arthritic rats in remission.* ***f)*** *Immunization with BCII. Secondary immune response. Arthritis-resistant rats. Results are presented as mean ± SD. n is the number of data in each point.*

BCII antibodies and exacerbated the arthritis.

In the arthritis-resistant rats, in response to the second immunization with BCII, the production of anti-BCII antibodies started on day 7 and peaked on day 21 (Fig. 1f), i.e., it developed faster than in response to the initial antigen administration (Fig. 1d), but the secondary immune response to BCII was not sensitive to cyclosporine A (Fig. 1f). Consequently, there was no similarity between the secondary immune response against BCII and the regRF response induced by Fc IgG fragments.

Generalizing the kinetics of antibodies to Fc fragments and to T-dependent and T-independent types 1 and 2 antigens leads us to conclude that the response of regRF-producing lymphocytes induced by Fc fragments is sensitive to CsA, as is the humoral immune response to T-independent type 2 antigen and the response to the initial administration of a T-dependent antigen. However, the rate of increase in blood levels of regRF induced by Fc fragments is comparable to the rate of increase in blood levels of antibodies to T-independent antigens. Thus, the kinetics of antibody production as an integral indicator of the humoral immune response suggest that homologous Fc fragments exposing epitopes recognized by regRF are a T-independent type 2 antigen.

Immunization of bone marrow cell cultures with Fc fragments of IgG exposing neoepitopes recognized by regRF

We next studied the ability of an RBM B lymphocyte culture to produce regRF when exposed to Fc fragments of IgG, with and without the presence of T cells.

Mononuclear cells isolated from RBM of intact rats were cultured for 4 days in the presence of Fc fragments of rat IgG. Several independently obtained samples of Fc fragments that expose epitopes recognized by regRF and several samples without such epitopes were investigated. RegRF levels in the culture supernatant of RBM mononuclear cells cultured with Fc fragments for 96 hours are shown in Fig. 2.

We found that Fc fragments that expose epitopes

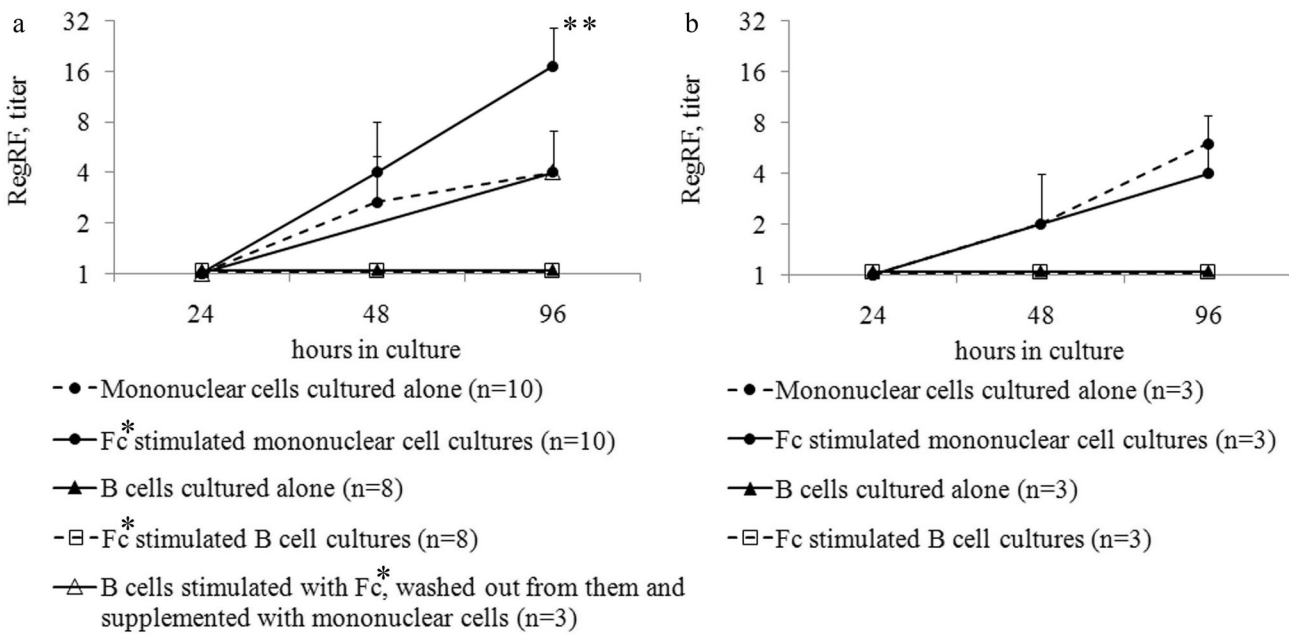

Fig. 2. *RegRF in the culture supernatant of RBM mononuclear cells and RBM B lymphocytes cultured with Fc fragments of rat IgG.* ***a****) Cells were cultured in the presence of Fc fragments (Fc*) exposing epitopes recognized by regRF.* ***b****) Cells were cultured in the presence of Fc fragments (Fc) that do not expose epitopes recognized by regRF. RBM was obtained from intact rats. Results are presented as mean ± SD. n is the number of independent cultures and independently obtained samples of Fc fragments; ** Statistically significant in relation to mononuclear cells cultured alone, P≤ 0.05 (Wilcoxon test).*

recognized by regRF induce production of regRF in RBM mononuclear cell cultures (Fig. 2a). RegRF is found in the culture supernatant starting at 48 hours, and its level increases through 96 hours. Production was detected in all of the subject rats (n=7).

B lymphocytes obtained from RBM mononuclear cells by depleting macrophages and T cells did not produce regRF upon stimulation with Fc fragments exposing epitopes recognized by regRF (Fig. 2a).

Thus, regRF-producing lymphocytes are present in the RBM of intact rats. To produce regRF, RBM lymphocytes require the assistance of T helper cells. It is well known that T helper cells or T cell replacement factors are needed for the production of antibodies to T-dependent antigens and to T-independent type 2 antigens (6). At the same time, regRF production occurred in poor media which contained neither serum nor mitogens, i.e., the factors needed for the production of antibodies to T-dependent antigens (7, 8). Therefore, the results of the culture study favor the T-independent nature of the regRF-specific antigen.

In turn, the T-independent type 2 nature of Fc fragments implies that T helper cells are not involved in the antigen-induced activation of regRF-producing B lymphocytes; however, T helper cells are required for regRF production. Therefore, antigen and T-helper cells were presented to the B lymphocytes separately. Firstly, B lymphocytes were incubated for 40 min at 37°C with Fc fragments of IgG bearing epitopes recognized by regRF. Next, the B lymphocytes were washed to remove the antigen-containing medium and mixed with RBM mononuclear cells (a source of T-helper cells and macrophages) obtained from the same rat. When mononuclear cells were added to stimulated B lymphocytes, regRF production was induced (Fig. 2a). This indicates that T helper cells assist regRF-producing B lymphocytes without entering into the cognate interaction typical of T-dependent antigens, and points to a TI-2-independent mechanism of activation for regRF-producing lymphocytes. Fc fragments not exposing epitopes recognized by regRF did not induce production of regRF in RBM mononuclear cell cultures (Fig. 2b).

Structure of rat IgG Fc fragments exposing immunosuppressive neoepitopes recognized by regRF

Since T-independent antigens have a distinct structure, our next step was to study the structure of the rat IgG Fc fragments that bear epitopes recognized by regRF. We previously elucidated some of the physicochemical properties and structural features

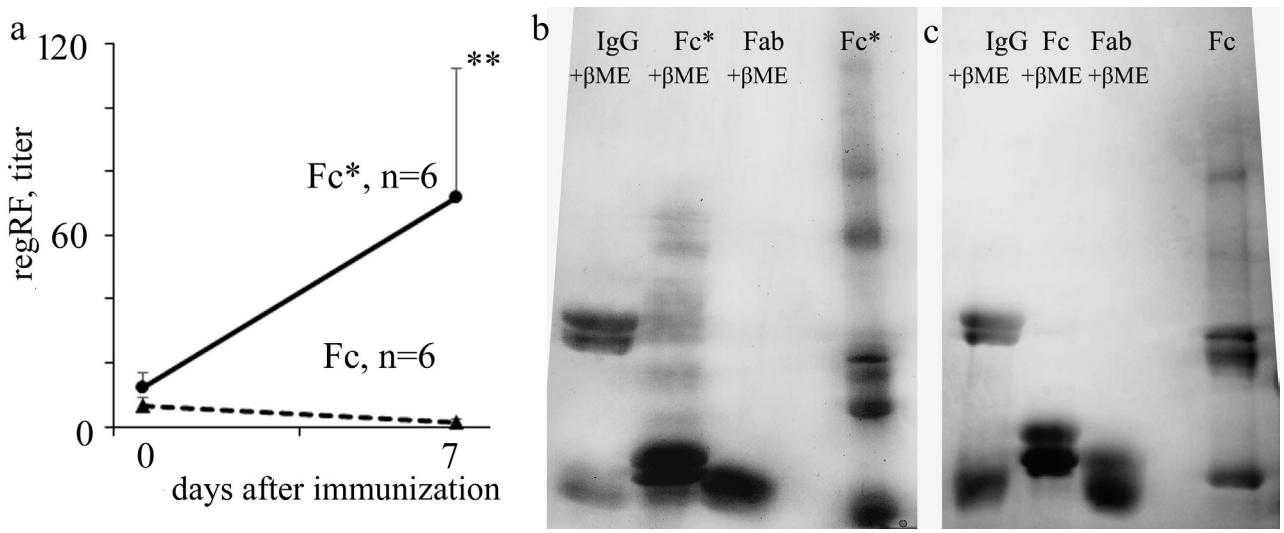

Fig. 3. *Fc fragments of rat IgG.* ***a****) Production of regRF in rats immunized with Fc fragments that expose or do not expose epitopes recognized by regRF.* ***b****) SDS-PAGE of Fc fragments (Fc*) exposing epitopes recognized by regRF.* ***c****) SDS-PAGE of Fc fragments (Fc) that do not expose epitopes recognized by regRF. 3–15% gradient gel. βME is beta-mercaptoethanol. ** Statistically significant in relation to day 0, P ≤ 0.05 (Wilcoxon test).*

of rat IgG Fc fragments exposing neoepitopes recognized by regRF (2). However, the question remains as to why some samples of Fc fragments bear epitopes and others do not, though they have all been obtained by the same method. In studying this issue, we detected distinguishing features of Fc fragments bearing epitopes recognized by regRF, and we present them here, since they allow us to understand to which antigen type the rat IgG Fc fragments bearing these epitopes belong.

Samples of rat IgG Fc fragments (Fig. 3a) that do and do not expose epitopes recognized by regRF were analyzed by electrophoresis in a polyacrylamide gel gradient under dissociating/reducing conditions. The results showed that the rat IgG Fc fragments bearing epitopes recognized by regRF form not only the typical bands in the 25 kDa range, but also numerous bands in the protein mobility range corresponding to a molecular weight of about 30 to 150 kDa (Fig. 3b). Fc fragments without epitopes recognized by regRF exhibit no such bands (Fig. 3c).

The bands characteristic of proteins with a molecular weight of 30-150 kDa (Fig. 3b) may have been formed by rat IgG Fc fragments that form polymers or aggregates via covalent bonds or hydrophobic interactions, respectively. Data indicating the presence of free sulfhydryl groups in the hinge of rat IgG Fc fragments obtained by papain proteolysis (2) support the theory that Fc fragments can polymerize. Interactions of cysteine residues in double-stranded Fc fragments or in the hinge region of a single-stranded Fc fragment may result in polymerization of Fc fragment molecules. Fc fragments can also form aggregates via hydrophobic interactions (9).

If the high-molecular structures of IgG Fc fragments are polymers, then they should not form bands at a molecular weight greater than 25 kDa in polyacrylamide gel under reducing conditions, since mercaptoethanol treatment breaks disulfide bonds. The existence of bands in the 30-150 kDa range (Fig. 3b) indicates that the IgG Fc fragments bearing epitopes recognized by regRF are not polymers formed via disulfide bonds, but are aggregates of IgG Fc fragments.

The size of these aggregates remains an open question. If 30-150 kDa is the true size of the structures formed by Fc fragments bearing epitopes recognized by regRF, then under gradient polyacrylamide gel dissociating conditions, such aggregates should be detected only in samples of fragments that bear the epitopes in question. However, there are bands in the area of 100 and 150 kDa under dissociating conditions in samples of Fc fragments both with and without the epitopes (Fig. 3, b,c). Therefore, the carriers of the epitopes recognized by regRF are not the structures weighing 100 and 150 kDa. We surmise that the true size of the Fc fragment aggregates is more than 300 kDa. Therefore, the rat Fc fragment aggregates remain at the gel entrance; when they are exposed to electric current, fragments separate from the aggregates. Since the aggregates are in reducing conditions, when they are exposed to the current, single-chain Fc fragments may separate from them, and the bands in the 30-150 kDa range might be formed by Fc strands weighing 25 kDa that enter the gel when exposed to the current after certain time intervals. Thus, Fc fragments of rat IgG bearing epitopes recognized by regulatory RF are high-molecular aggregates.

DISCUSSION

In-vivo experiments revealed that: i) the Fc fragments induce the same rapid humoral immune response in rats as do the T-independent antigens TNP-LPS and TNP-AECM-Ficoll; and ii) regRF production induced in rats by immunization with Fc fragments is sensitive to cyclosporine A, as is the production of antibodies to the TI-2 antigen TNP-AECM-Ficoll. Studies of regRF production in RBM cell cultures stimulated by Fc fragments demonstrated that B lymphocyte cultures produce regRF only in the presence of T helper cells and macrophages. It is known that TI-2 antigens are able to directly stimulate B lymphocytes, but for generating antibodies to TI-2 antigens a second signal provided by T helper cells is needed (6). Therefore, the *in-vitro* results do not contradict the hypothesis that Fc fragments of IgG bearing neoepitopes recognized by regRF are TI-2 antigens. Note that regRF production *in vitro* occurs

in poor culture medium which contains neither serum nor mitogens. Given that a primary antibody response *in vitro* to T-dependent antigens in cultures does not occur without mitogenic factors (7, 8), regRF production in a mitogen-free environment can be viewed as supporting the hypothesis that Fc fragments activate regRF-producing lymphocytes as T-independent antigens. Rat IgG Fc fragments bearing epitopes recognized by regRF are high-molecular aggregates, which makes them similar to TI-2 antigens, which are known to be multivalent antigens with a molecular weight of more than 100 kDa (6).

The purported T-independent nature of Fc fragments that induce regRF production implies that this antigen is incapable of forming immune memory. These results must be considered when developing a schedule for immunizing with Fc fragments in patients with autoimmune diseases.

ACKNOWLEDGEMENTS

All authors listed on the manuscript have contributed significantly to the experimental design, its implementation, and analysis and interpretation of the data. All authors were involved in the writing of the manuscript. We are grateful to Jennifer Guernsey for editorial assistance.

This work was supported by the Russian Foundation for Basic Research (grant numbers 18-315-00424, 16-34-60164 mol a dk) and Russian Federation Presidential Scholarship for young scientists and post-graduate students (No. SP-1630.2018.4).

REFERENCES

1. Beduleva L, Menshikov I, Stolyarova E, Fomina K, Lobanova O, Ivanov P, Terentiev A. Rheumatoid factor in idiotypic regulation of autoimmunity. Int J Rheum Dis 2015; 18:408-20.
2. Sidorov A, Beduleva L, Menshikov I, Terentiev A, Stolyarova E, Abisheva N. Fc fragments of immunoglobulin G are an inductor of regulatory rheumatoid factor and a promising therapeutic agent for rheumatic diseases. Int J Biol Macromol 2017; 95:938-45.
3. Kunkl A, Klaus GG. Selective effects of cyclosporine A on functional B cell subsets in the mouse.J Immunol 1980; 125(6):2526-31.
4. Higham AD, Sells RA, Marshall-Clarke S. Cyclosporin A has differential effects on the responses of murine B cells to TI antigens and B-cell mitogens. Immunology 1986; 59:203-7.
5. Stolyarova E, Beduleva L, Sidorov A, Menshikov I, Terentiev A, Vachrusheva K. The role of neutrophil proteases in LPS-induced production of regulatory rheumatoid factor that suppresses autoimmunity. Endocrine Metabolic Immune Disorders Drug Targets 2017; 17(1):71-7.
6. Jeurissen A, Ceuppens JL, Bossuyt X. T lymphocyte dependence of the antibody response to "T lymphocyte independent type 2" antigens. Immunology 2004; 111:1-7.
7. Coutinho A, Möller G. In vitro induction of specific immune responses in the absence of serum: requirement for nonspecific T or B cell mitogens. Eur J Immunol 1973; 9:531-37.
8. Burger M. An absolute requirement for 2-mercaptoethanol in the in vitro primary immune response in the absence of serum. Immunology 1979; 37:669-71.
9. Chennamsetty N, Helk B, Voynov V, Kayser V, Trout BL. Aggregation-Prone Motifs in Human Immunoglobulin G. J. Mol. Biol 2009; 391 404-13.

LETTER TO THE EDITOR

SALIVARY SECRETION IN PATIENTS WITH SCHIZOPHRENIA

E. VELASCO-ORTEGA[1], L. MONSALVE-GUIL[1], N. CASAS-BARQUERO[2], A. JIMENEZ-GUERRA[1], D. TORRES-LAGARES[1] and J. JOSE SEGURA-EGEA[1]

[1]Faculty of Dentistry, University of Seville, Seville, Spain; [2]Faculty of Dentistry, University of Seville, Seville, Spain

Received October 19, 2018 – Accepted March 12, 2019

To the Editor,

Poor oral health has long been documented among psychiatric patients (1-5). People with schizophrenia often have advanced oral diseases and receive less dental care that the general population (1-5). Salivary secretion flow rates in psychiatric patients have showed that mental illness and psychotropic medications used to treat the disorder can cause an important hyposalivation (2-5). Psychotropic medication may cause an important salivary gland hypofunction. Patient complaints of dry mouth are associated with a higher number of psychotropic drugs (5). Chronic administration of psychotropic medications may induce a reduced unstimulated salivary secretion flow by anticholinergic action and can also reflect the result of damage occurring in both the acinar and ductal compartments (5). Phenothiazines, atypical antipsychotics, benzodiazepines and antiparkinsonians drugs have been shown to cause hypofunction and xerostomia in patients with schizophrenia (2, 4-5). Antipsychotic medications (i.e. phenothiazines), by an anticholinergic action, cause a profound hyposalivation by blocking parasympathetic stimulation of the salivary glands. This oral adverse effect often is increased by the simultaneous administration of antiparkinsonian medication with anticholinergic action (5). Patients with schizophrenia with an important reduced salivary flow have rapid and progressive dental caries, and an intensification of periodontal disease (1-5). Furthermore, hyposalivation causes an important change in the oral environment and may increase the incidence of opportunistic oral infections such as candidiasis (1-5).

The aim of this study was to determine the whole salivary secretion flow rates in patients with schizophrenia compared with healthy control patients and to study the possible relationship between salivary secretion and different variables.

MATERIALS AND METHODS

This comparative study of unstimulated and stimulated whole salivary flow rates was conducted on two groups of subjects, patients with schizophrenia and healthy controls, who were selected with a random stratified method according to age and gender. The study was approved by the Research Ethics Committee of the University of Seville. All subjects gave informed, signed consent to participate in the study, or in the necessary cases, informed written consent was given by the family.

Patients with schizophrenia were selected from those attending at the Psychiatry Department of the University Hospital Virgen Macarena in the Faculty of Medicine of Seville, Spain. Diagnosis of schizophrenia was stablished

Key words: saliva, schizophrenia, whole salivary flow rate, mental disorders, salivary secretion, hyposalivation

Corresponding Author:
Prof. Eugenio Velasco Ortega,
Faculty of Dentistry,
University of Seville,
C/ Avicena s/n, 41009 Seville, Spain
Tel.: +34 954 481132
e-mail: evelasco@us.es

0393-974X (2019)

DISCLOSURE: ALL AUTHORS REPORT NO CONFLICTS OF INTEREST RELEVANT TO THIS ARTICLE.

according the international criteria of the American Psychiatric Association(6). The control group was selected from healthy subjects seeking dental treatment at the Faculty of Dentistry of Seville. Patients with systemic disease and/or taking any medication in the previous six months were excluded.

Demographic data of the patients with schizophrenia were obtained through interviews with the psychiatric staff, and similar information was gathered directly from the healthy control subjects. The demographic variables included age and gender. Psychiatric data were obtained by interviews with the psychiatry staff and review of the patients' medical charts. A suitable sample size was calculated to detect a difference of 0.75ml/min with a variation of 1.50ml/min, with an alpha error of 5% and a beta error of 20%, assuming a 15% loss (n = 50 per group).

Oral examination

Oral examination and saliva collection took place in the Faculty of Dentistry of Seville for healthy control patients and in the Psychiatry Department of University Hospital Virgen Macarena of Seville for patients with schizophrenia. The revisions were carried out by the same researcher. A new review was performed for every 10 patients to confirm the validity of the data collected (Kappa=0.88). Oral examination was determined according to criteria set by the World Health Organization (7). The decayed, missing and filled teeth (DMFT) score was used for the assessment of the dental status of patients. Community Periodontal Index (CPITN) was used for the assessment of periodontal status (7).

Salivary flow rates

Unstimulated and stimulated whole salivary flow rate (WSFR) samples were determined from the patients with schizophrenia and control patients according to the guidelines for collecting saliva provided by Navazesh, et al, (8). The collection of whole saliva was performed while participants were at rest in a quiet room. Saliva collection was performed between 9:00 AM and 12:00 PM to avoid diurnal variation. Each patient was requested not to eat, drink or perform oral hygiene or smoke 60 min before and during the collection of saliva. Five-minute samples were obtained under standardized conditions using expectoration technique for each subject. Unstimulated and stimulated WSFR was collected in plastic tubes from each patient. Stimulation was with a sugar-free, non-chewable, lemon-flavored candy.

Statistical analyses

Statistical analyses were carried with the SPSS Version 18.0 (SPSS Inc., Chicago, IL, USA). Descriptive statistics were used to report the general results of the study as mean ± standard deviation. *Chi*-squared test was used to analyse differences in proportions and the analysis of variance was ised for the detection of differences in means. Statistical significance was established at $p < 0.05$.

RESULTS

Fifty patients with schizophrenia were examined (39 males and 11 females) with a mean age of 39.9 years (range: 18-64 years) and 50 healthy control subjects (33 males and 17 females) with a mean age of 39.5 years (range: 20-67 years) (Table I). Differences in age (ANOVA; $p = 0.8542$) and gender (*chi*-squared test; $p = 0.18145$) between the two groups were not statistically significant.

All patients with schizophrenia were treated with two or more psychotropic drugs (mean: 3.9); 58% of the patients were taking more than four psychotropic medications. Phenothiazines (72%), atypical antipsychotics (60%), benzodiazepines (50%), antiparkinsonians (50%) and antidepressants (14%) were the psychotropic drugs mostly used. Twenty-nine patients with schizophrenia (58%) and 26 control subjects (52%) were smokers (Table I). Differences between groups were not statistically significant (*chi*-squared; $p = 0.12000$).

The number of carious teeth in both groups is presented in Table II. Differences were not statistically significant (ANOVA; $p= 0.18448$). Presence of root caries are shown in Table II, and these differences are significant (ANOVA; $p= 0.0002$). Periodontal conditions of both groups are shown in Table I. Differences were not statistically significant (*chi*-squared test; $p= 0.52132$). Oral mucosa lesions were significantly (*chi*-squared; $p=0.0000$) more prevalent in patients with schizophrenia (58%) compared with control patients (12%) (Table I). Moreover, oral candidiasis was, significantly (*chi*-squared; $p=0.0000$) more prevalent in patients with schizophrenia (46%) compared with control subjects (2%). Also, oral mucosa lesions were significantly higher (*chi*-squared; $p=0.00033$) in smoker patients with schizophrenia

Table I. *Distribution of patients according age, gender, smoking, dental and oral conditions.*

	Schizophrenia		Control		p
	n	%	n	%	
Age (years)					
< 35	13	26	19	38	NS
36-45	25	50	17	34	
>46	12	24	14	28	
Gender					
Males	39	78	33	66	NS
Females	11	22	17	34	
Smoking					
Smokers	29	58	26	52	NS
Nonsmokers	21	42	24	48	
Carious teeth (number)					
0-4	17	34	9	18	NS
5-9	16	32	21	42	
>10	17	34	20	40	
Root caries					
+	20	40	3	6	0.002
-	30	60	47	94	
CPITN					
Health	2	4	0	0	NS
Bleeding	2	4	1	2	
Calculus	26	52	34	68	
Shallow pockets	11	22	11	22	
Deep pockets	9	18	4	8	
Oral mucosa diseases					
+	29	58	6	12	<0.0001
-	21	42	44	88	
Oral candidiasis					
+	23	46	1	2	<0.0001
-	27	54	49	98	
Total	50	100	50	100	

NS: Not significant

Table II. *Mean unstimulated and stimulated whole salivary flow rates (ml/min) according to age, gender and smoking.*

	Unstimulated	Stimulated	Unstimulated	Stimulated
Age (years)				
< 35	0.27±0.21	0.74±0.80	1.23±1.36 $	2.85±4.33 $$
36-45	0.24±0.25	0.66±0.69	0.58±0.83 $	1.17±1.39 $$
>46	0.23±0.21	0.61±0.39	0.24±0.20 $	0.63±0.65 $$
Gender				
Males	0.33±0.28	0.86±0.86	0.76±0.21	1.74±3.07
Females	0.22±0.21	0.61±0.58	0.39±0.21	0.85±0.91
Smoking				
Smokers	0.23±0.21	0.66±0.63	0.60±0.97	1.30±2.20
Nonsmokers	0.26±0.25	0.68±0.67	0.66±0.93	1.58±2.95
Total	0.24±0.23*	0.67±0.65**	0.63±0.94*	1.44±2.57**

*All differences are not significant, except those marked with the same symbol: $, p=0.009; $$, p=0.0406; *, p=0.0057; **, p=0.0426.*

(79.3%) compared with non-smokers (28.6%).

A comparison of the mean whole salivary flow rates in each group revealed that the mean unstimulated flow rate was significantly (ANOVA; p=0.0057) lower in the schizophrenia group (0.24±0.23 ml/min) than in the control group (0.63±0.94 ml/min) (Table II). Moreover, the mean stimulated flow rate was significantly (ANOVA; p=0.0426) lower in the schizophrenia group (0.67±0.65 ml/min) than in the control group (1.44±2.57 ml/min).

The mean salivary flow rates in the schizophrenia group were decreasing with age in unstimulated and stimulated salivary flow. The mean salivary flow rates in the control group was decreasing significantly with age in unstimulated (ANOVA; p=0.0090) and stimulated (ANOVA; p=0.0406) salivary flow. The relationship between gender and salivary flow rate of unstimulated and stimulated whole saliva is shown in Table II. In both groups, whole saliva flow rates were lower in females than in males, but these differences were not statistically significant. Smoking-based differences in unstimulated and stimulated whole saliva flow rates are presented in Table II. In both groups, whole saliva flow rates were lower in smokers compared with non-smokers, but these differences were not statistically significant.

The relationship between psychotropic medications and salivary flow rates of unstimulated and stimulated whole saliva in patients with schizophrenia is shown in Table III. Whole salivary flow rates are lower in patients with schizophrenia that take more of four psychotropic medications. These differences were not statistically significant. However, in patients treated with antidepressants, the mean stimulated flow rate was significantly (ANOVA; p=0.0378) higher (1.14 ml/min) than the mean unstimulated flow rate (0.23 ml/min).

In both groups of patients, whole saliva flow rates

are decreasing while the number of caries teeth is increasing; but these differences are not statistically significant. Also, in both groups, the presence of root caries was related with a lower whole salivary flow, but these differences were not statistically significant. The relationship between whole salivary flow rates and periodontal status were not statistically significant. Moreover, the presence of oral diseases (candidiasis) was related with a lower whole salivary flow, but these differences were not statistically significant.

DISCUSSION

Our results shows that salivary flow rates were significantly diminished in patients with schizophrenia compared with control subjects. These results of the present study are in agreement with those of previous studies that reported a significant reduction in flow rates in patients with schizophrenia and other mental disorders (5). Pyschotropic medications have been reported to cause a decrease in unstimulated and stimulated salivary flow rates (2, 5, 9). In the present study, psychotropic medications can contribute to hyposalivation in schizophrenia patients and may explain the significant difference in salivary flow rate between schizophrenia patients and control subjects, especially in schizophrenia patients who take more than four psychotropic medications (Table III).

The subjects of this study with root caries present also a lower salivary secretion than those without root caries. A lower salivary flow may explain a higher incidence of smooth surface caries in schizophrenia patients compared with control patients (2, 5). Other factors associated with the high risk of caries in schizophrenia patients treated with antipsychotic medications are an excessive daily intake of sweets and less frequency of tooth brushing (10, 11). Oral mucosa diseases are most prevalent conditions in patients with schizophrenia (5, 9, 12). Side effects of the psychotropic medications must be considered as major factors related with soft tissues oral pathosis.
The results of the present study showed that the presence of oral diseases (i.e. candidiasis) was related with a lower unstimulated and stimulated whole salivary flow in both groups, especially in schizophrenia patients.

The present study indicates that patients with schizophrenia compared with control subjects showed a significantly decreased flow rate of unstimulated and stimulated whole saliva that is related with

Table III. *Mean unstimulated and stimulated whole salivary flow rates (ml/min) according to psychotropic medications.*

	Schizophrenia		
	Unstimulated	Stimulated	p
Number			
< 3	0.25±0.24	0.82±0.80	NS
>4	0.23±0.22	0.46±0.21	NS
Type			
Phenothiazines	0.24±0.22	0.67±0.61	NS
Atypical antipsychotics	0.28±0.23	0.64±0.62	NS
Benzodiazepines	0.27±0.21	0.84±0.81	NS
Antidepressants	0.23±0.08	1.14±0.43	0.037
Antiparkinsonians	0.24±0.24	0.78±0.69	NS
Others	0.20±0.22	0.58±0.44	NS
Total	0.24±0.23	0.67±0.65	NS

psychotropic medications and smoking habits, and these subjects are therefore predisposed to oral (i.e. candidiasis) and dental (i.e. caries) diseases.

REFERENCES

1. Velasco-Ortega E, Segura-Egea JJ, Córdoba-Arenas S, Jiménez-Guerra A, Monsalve-Guil L, López-López J. A comparison of dental status and treatment needs of older adults with and without chronic mental illness in Seville, Spain. Med Oral Patol Oral Cir Bucal 2013; 18:71-75.
2. Arnaiz A, Zumárraga M, Díez-Altuna I, Uriarte JJ, Moro J, Pérez-Ansorena MA. Oral health and the symptoms of schizophrenia. Psychiat Res 2011; 18:24-48.
3. Bertaud-Gounot V, Kovess-Masfety V, Perrus C, Trohel G, Richard F. Oral health status and treatment needs among psychiatric inpatients in Rennes, France: a cross-sectional study. BMC Psychiatry 2013; 13:227.
4. Velasco-Ortega E, Monsalve-Guil L, Ortiz-García I, Jiménez-Guerra A, López-López J, Segura-Egea JJ. Dental caries status of patients with schizophrenia in Seville, Spain: a case-control study. BMC Res Notes 2017; 10:50.
5. Hu KF, Chou YH, Wen YH, Hsieh KP, Tsai JH, Yang P, Yang YH, Lin CHR. Antipsychotic medications and dental caries in newly diagnosed schizophrenia; a nationwide cohort study. Psychiat Res 2016; 245:45-50.
6. American Psychiatric Association. Diagnostic and Statistical Manual of Mental Disorders. American Psychiatric Association. Washington DC, 2000.
7. World Health Organization. Oral Health Surveys-Basic Methods. WHO. Geneva, 1997.
8. Navazesh M, Kumar SK. Measuring salivary flow: challenges and opportunities. J Am Dent Assoc 2008; 139(suppl):35S-40S.
9. Bokor-Bratic M, Cankovic M, Dragnic N. Unstimulated whole salivary flow rate and anxiolytics intake are independently associated with oral *Candida* infection in patients with oral lichen planus. Eur J Oral Sci 2013; 121:427-33.
10. Tani H, Uchida H, Suzuki T, Shibuya Y, H. Shimanuki H, Watanabe K et al. Dental conditions in inpatients with schizophrenia: a large-scale multi-site survey. BMC Oral Health 2012; 12:32.
11. Grinshpoon A, Zusman SP, Weizman A, Ponizovsky AM. Dental health and the type of antipsychotic treatment in inpatients with schizophrenia. Is J Psychiatry Relat Sci 2015; 52:114-18.
12. Fratto G, Manzon L. Use of psychotropic drugs and associated dental diseases. Int J Psychiatr Med 2014; 48:185-97.

LETTER TO THE EDITOR

ASSOCIATION OF GPIa C807T POLYMORPHISM WITH UNEXPLAINED FEMALE INFERTILITY AND IVF IMPLANTATION FAILURE

K. KYDONOPOULOU[1], D. ROUSSO[2], G. ILONIDIS[1] and E. MANDALA[1]

[1]Fourth Department of Internal Medicine, Aristotle University of Thessaloniki, Hippokration General Hospital, Thessaloniki, Greece; [2]Third Department of Obstetrics and Gynecology, Aristotle University of Thessaloniki, Hippokration General Hospital, Thessaloniki, Greece

Received December 11, 2018 – Accepted March 13, 2019

To the Editor,

Glycoprotein Ia (GPIa), also known as integrin alpha 2 (ITGA2), together with GPIIa (ITGB1), form the heterodimer integrin α2β1. This complex is a major collagen receptor on the membrane of platelets, which is involved in thrombus formation through platelet adhesion and activation. A common variant of the *ITGA2* gene coding for GPIa is C807T polymorphism. The 807T allele has been associated with increased gene expression and receptor density, leading to increased collagen-induced platelet adhesion, or, according to a newly-proposed mechanism, increased mean platelet volume (1, 2). As a result, *ITGA2* 807T allele has been linked to arterial thrombosis risk, including myocardial infarction and stroke (3, 4).

Relatively recently, a few studies demonstrated association of integrin α2 with the complex interactions between the mother's side and the fetus during the implantation process, similarly to other molecules on the surface of platelets, such as integrin β3, platelet-endothelial cell adhesion molecule-1 (PECAM-1) and P-Selectin (5). Implantation failure is regarded as one of the multiple factors which are potentially responsible for unexplained female infertility. During the critical period of the "window of implantation", it has been shown that, among others, integrins may play an important role (6). Additionally, the suspected mechanism for placenta-mediated pregnancy complications is the defective placentation due to impaired feto-maternal blood flow and hemostatic imbalance. However, the role of thrombotic factors in problematic implantation is still debatable because of lack of clinical evidence (7).

The aim of this study was to examine whether *ITGA2* C807T polymorphism is associated with unexplained infertility in Greek women from the population of Northern Greece.

MATERIALS AND METHODS

A total of 222 Greek Caucasian women, living in Northern Greece, were enrolled in this case-control study. The group of patients included 115 women aged 25–48 years (BMI 19.1-29.9) presenting with unexplained infertility at the Hematology Outpatients Clinic, of the Fourth Department of Internal Medicine, of Aristotle University of Thessaloniki, in collaboration with the Third Department of Obstetrics and Gynecology, of Aristotle University of Thessaloniki. The control group, consisted of 107 fertile women aged 22-48 years (BMI 18.6-31.2) with normal conceptions and uncomplicated pregnancies, without any history of spontaneous abortions. Patient inclusion criteria were: i) primary infertility; ii) ≥12 months of regular intercourse; iii) no known infertility factors, including

Key words: ITGA2; GPIa; C807T polymorphism; unexplained infertility; implantation; thrombophilia, IVF

Corresponding Author:
Kydonopoulou Kyriaki, MSc,
Hippokration General Hospital,
49 Konstantinoupoleos str, 546 42,
Thessaloniki, Greece
Tel.: +302313312096 - fax: +302310992940
e-mail: kkydonopoulou@gmail.com

0393-974X (2019)

DISCLOSURE: ALL AUTHORS REPORT NO CONFLICTS OF INTEREST RELEVANT TO THIS ARTICLE.

male infertility, anatomic abnormalities of the uterus or fallopian tubes, infections, immunologic factors, abnormal levels of hormones, karyotype findings, Premature Ovarian Failure (POF), Polycystic ovary syndrome (PCOS), or endometriosis; iv) no other health issues, including diabetes mellitus, thyroid or cancer. In other words, a patient should have records of normal results for all examinations stated in Table I, based on their personal medical history, in order to be included in the present study.

Among the group of patients, a subgroup of 50 women had previously undergone IVF treatment without success due to implantation failure, according to their personal history.

Written informed consents were obtained from all participants and the study was approved by the Bioethics Committee of the Medical School of the Aristotle University of Thessaloniki and was conducted in accordance with the Declaration of Helsinki.

Peripheral whole blood was collected in EDTA tubes for both groups in the context of their visit in the clinic and a small fraction of this was donated for the present research. Genomic DNA was isolated using the QIAamp® DNA Blood Mini Kit (QIAGEN®, Hilden, Germany) according to the manufacturer's instructions. The *ITGA2* C807T variant was determined by PCR-RFLPs method (Polymerase Chain Reaction - Restriction Fragment Length Polymorphism), by using the protocol of Jorge Di Paola et al. (8). In more detail, the primer pair used for PCR amplification was i) 5' GATTTAACTTTCCCGACTGCCTTC 3' and ii) 5' CATAGGTTTTTGGGGAACAGGTGG 3'. The amplified target is 581-bp long and located within the intron following exon 7, where the polymorphism C807T lies. The PCR product contains a *Bgl II* restriction site only in the presence of the allele 807T. Following PCR amplification, the restriction enzyme *Bgl II* (ThermoScientific) was used for the digestion of the amplified segment after incubation at 37°C for approximately 16 hours, according to the manufacturer's instructions. The PCR product was then analyzed on a 2% agarose gel in 1x TE buffer, using staining with ethidium bromide and ultraviolet (UV) light for visualization. The 807 TT, CT and CC genotypes were determined by the different sizes of fragments detected on the gel, depending on whether the PCR product was fully, partially or not digested, respectively. Digestion is successful only in the presence of the 807T allele. Thus, CC genotype is determined by the presence of the amplified 581-bp segment that has not been digested; TT genotype is determined by the presence of the resulting 343-bp and 238-bp fragments after complete digestion of the amplified 581-bp segment; CT genotype is determined by the presence of both the undigested 581-bp and the digested 343-bp and 238-bp fragments (Fig. 1).

Table I. *List of required examinations in personal history records. All results should be normal, in order to determine unexplained female infertility and include a patient in the study.*

- ✓ **Anatomic:** uterus and fallopian tubes through ultrasound, hysteroscopy or hysterosalpingogram, as well as examination for endometriosis and PCOS
- ✓ **Hormonal:** LH, FSH, E2, progesterone, prolactin, AMH, 17-OHP, testosterone, T3, T4, FT3, FT4, TSH levels
- ✓ **Autoimmune:** antiphospholipid autoantibodies, antithyroid autoantibodies, antinuclear autoantibodies
- ✓ **Microbial:** *Mycoplasma genitalium, Chlamydia trachomatis, Neisseria gonorrhoeae*
- ✓ **Genetic:** Karyotype analysis
- ✓ **Male factor:** semen analysis, clinical, microbial and karyotype examination

PCOS: polycystic ovary syndrome; LH: Luteinizing hormone; FSH: follicle stimulating hormone; AMH: Anti-Müllerian hormone; E2: Estradiol; 17-OHP: 17-hydroxyprogesterone; FT3: free triiodothyronine; FT4: free thyroxine; TSH: Thyroid-stimulating hormone; T3: triiodothyronine; T4: thyroxine.

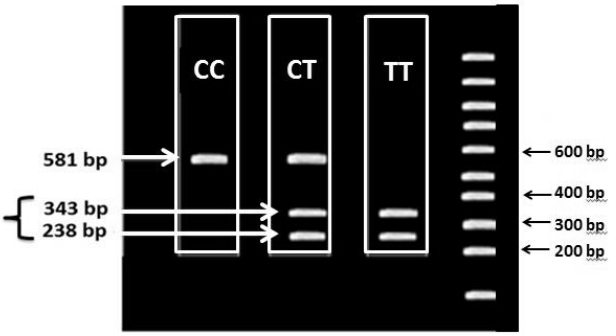

Fig. 1. *Representation of Bgl II digest of the amplified 581-bp PCR product. The first three lanes correspond to three patients with ITGA2 807 genotypes CC, CT and TT, respectively. The last lane corresponds to DNA ladder, used for comparison.*

Statistical analysis

The SPSS (version 17) software for Windows (SPSS Inc, Chicago, Illinois, USA) was used for statistical analysis. The results included categorical variables, which were reported as count and percentage and compared using the Pearson *chi*-squared test. The indication of statistical significance was set at a p value of ≤0.05, which corresponded to a probability of less than 0.05 that differences between patients and controls could be attributed to chance.

RESULTS

ITGA2 C807T genotype frequencies

Table II shows the genotype frequencies of the three *ITGA2* C807T genotypes for patients and controls. For women with unexplained infertility, 41.7% (48/115) were normal (CC), 50.4% (58/115) were heterozygous (CT) and 7.8% (9/115) were homozygous (TT). Among controls, genotype frequencies were 51.4% (55/107), 45.8% (49/107) and 2.8% (3/107), respectively. The differences between the two groups were not considered to be statistically significant (p=0.139>0.05).

Dominant and Recessive genetic models for ITGA2 C807T genotype frequencies

Two genetic models were employed for further data analyses (Table III). In the Dominant genetic model, heterozygotes and homozygotes were grouped together and compared to subjects with normal genotype. In the Recessive genetic model, normal and heterozygous genotypes were grouped together, versus the homozygous genotype.

Consequently, based on the Dominant genetic model, the difference between the study group and the controls was not found to be significant

Table II. *Comparison of the ITGA2 C807T genotype frequencies between female patients with unexplained infertility and controls.*

ITGA2 C807T genotype	Genotype frequency	
	Unexplained Infertility counts (%)	Control counts (%)
CC	48 (41.7%)	55 (51.4%)
CT	58 (50.4%)	49 (45.8%)
TT	9 (7.8%)	3 (2.8%)
Total counts	115	107
P value	0.139	

Table III. *Dominant and Recessive genetic models for ITGA2 C807T genotype frequencies. Comparison between unexplained infertility patients and controls.*

ITGA2 C807T genotype	DOMINANT MODEL Genotype Frequency		RECESSIVE MODEL Genotype Frequency	
	Unexplained Infertility counts (%)	Control counts (%)	Unexplained Infertility counts (%)	Control counts (%)
CC	48 (41.7%)	55 (51.4%)	106 (92.2%)	104 (97.2%)
CT	67 (58.3%)	52 (48.6%)		
TT			9 (7.8%)	3 (2.8%)
Total counts	115	107	115	107
P value	0.149		0.098	

Table IV. *Comparison between the subgroup of unexplained infertility patients with IVF implantation failure and controls: Dominant and Recessive genetic models for ITGA2 C807T genotype frequencies.*

ITGA2 C807T genotype	DOMINANT MODEL Genotype Frequency		RECESSIVE MODEL Genotype Frequency	
	IVF failure counts (%)	Control counts (%)	IVF failure counts (%)	Control counts (%)
CC	22 (44%)	55 (51.4%)	44 (88%)	104 (97.2%)
CT	28 (56%)	52 (48.6%)		
TT			6 (12%)	3 (2.8%)
Total counts	50	107	50	107
P value	0.387		0.021	

(p=0.149>0.05). In detail, 41.7% (48/115) of patients were CC and 58.3% (67/115) were either CT or TT. Whereas, in the control group, 51.4% (55/107) were normal, while 48.6% (52/107) were heterozygotes or homozygotes.

Similarly, in the Recessive genetic model, genotype differences between the two groups did not reach statistical significance (p=0.098>0.05). Among unexplained infertility patients, homozygotes accounted for 7.8% (9/115), and normal together with heterozygotes for 92.2% (106/115), respectively. Regarding controls, 2.8% (3/107) were homozygotes, while normal plus heterozygotes were 97.2% (104/107).

Subgroup of patients with IVF implantation failure

The study of the subgroup of patients with IVF implantation failure, under the Dominant genetic model, showed that 44% (22/50) of patients were normal, while homozygotes plus heterozygotes were 56% (28/50). Comparison of this subgroup of patients to controls, as described above, demonstrated no statistical significance (p=0.387>0.05) (Table IV).

However, under the Recessive genetic model, the difference between the subgroup of patients with IVF implantation failure and controls was statistically significant (p=0.021<0.05). In particular, homozygotes of this subgroup were 12% (6/50), whereas 88% (44/50) were either heterozygotes or normal.

DISCUSSION

This study does not support the association of *ITGA2* C807T polymorphism with unexplained infertility in Greek women. Interestingly, after focusing on the subgroup of patients with IVF implantation failure, differences were also insignificant under the Dominant genetic model, however, in contrast to the Recessive one, where our results confirmed the association.

Consequently, our results indicate association between IVF implantation failure in unexplained infertility and *ITGA2* 807 TT homozygosity. For this subgroup, the problem lies in unsuccessful implantation, which is the major concern regarding IVF outcome. The above-mentioned association is not confirmed in our whole group of patients, probably due to the fact that within the total group of unexplained infertility patients, for some women the problem possibly lies in other infertility aspects, other than or prior to implantation.

Previous studies have demonstrated that IVF implantation failure is a multifactorial condition (9). Moreover, the role of inherited thrombophilic factors has been examined, however it is still debatable (10). Nonetheless, recent studies indicate that the combination of *ITGA2* C807T with other platelet polymorphisms (GpIIIa PlA1/PA2, PECAM-1-C373G and P-Selectin-A37674C) is significantly associated with IVF implantation failure (11).

Regarding the limitations of the present study, one should bear in mind that the sample size, the study design and the inclusion criteria for female unexplained infertility are critical. In addition, different study populations and combinations of thrombophilic gene variants and other potential infertility factors are required to be examined. Ideally, 'omics' technology, and specifically 'reproductomics' is expected to be clinically useful for understanding

and treating implantation and endometrial receptivity issues (12).

REFERENCES

1. Kunicki TJ, Kritzik M, Annis DS, Nugent DJ. Hereditary variation in platelet integrin alpha 2 beta 1 density is associated with two silent polymorphisms in the alpha 2 gene coding sequence. Blood 1997; 89:1939-43.
2. Kunicki TJ, Williams SA, Nugent DJ, Yeager M. Mean platelet volume and integrin alleles correlate with levels of integrins α(IIb)β(3) and α(2)β(1) in acute coronary syndrome patients and normal subjects. Arterioscler Thromb Vasc Biol 2012; 32(1):147-52.
3. Antoniades C, Tousoulis D, Vasiliadou C, Stefanadi E, Marinou K, Stefanadis C. Genetic polymorphisms of platelet glycoprotein Ia and the risk for premature myocardial infarction: effects on the release of sCD40L during the acute phase of premature myocardial infarction. J Am Coll Cardiol 2006; 47(10):1959-66.
4. Wu G, Xi Y, Yao L, et al. Genetic polymorphism of ITGA2 C807T can increase the risk of ischemic stroke. Int J Neurosci 2014; 124:841-51.
5. Ivanov P, Tsvyatkovska T, Konova E, Komsa-Penkova R. Inherited thrombophilia and IVF failure: the impact of coagulation disorders on implantation process. Am J Reprod Immunol 2012; 68:189-98.
6. Lessey BA, Castelbaum AJ, Wolf L, et al. Use of integrins to date the endometrium. Fertil Steril 2000; 73(4):779-87.
7. Nelson SM, Greer IA. The potential role of heparin in assisted conception. Hum Reprod Update 2008; 14(6):623-45.
8. Di Paola J, Federici AB, Mannucci PM, Canciani MT, Kritzik M, Kunicki TJ, Nugent D. Low platelet alpha2beta1 levels in type I von Willebrand disease correlate with impaired platelet function in a high shear stress system. Blood 1999; 93(11):3578-82.
9. Vlachadis N, Vrachnis N, Economou E, Siristatidis C. Zooming in on the definition of 'recurrent implantation failure'. Reprod Biomed Online 2014; 29:144-45.
10. Di Nisio M, Rutjes AW, Ferrante N, Tiboni GM, Cuccurullo F, Porreca E. Thrombophilia and outcomes of assisted reproduction technologies: a systematic review and meta-analysis. Blood 2011; 118:2670-78.
11. Vlachadis N, Tsamadias V, Vrachnis N, Kaparos G, Vitoratos N, Kouskouni E, Economou E. Associations of combined polymorphisms of the platelet membrane glycoproteins Ia and IIIa and the platelet-endothelial cell adhesion molecule-1 and P-Selectin genes with IVF implantation failures. J Obstet Gynaecol 2017; 37(3):363-69.
12. Altmäe S, Esteban FJ, Stavreus-Evers A, et al. Guidelines for the design, analysis and interpretation of 'omics' data: focus on human endometrium. Hum Reprod Update 2014; 20(1):12-28.

LETTER TO THE EDITOR

CORRELATION BETWEEN THE PATHOGENESIS OF BRONCHIAL ASTHMA AND SERUM EXPRESSIONS OF IL-4, IL-12, IL-37 AND 25-(OH)D

YJ. JIANG

Department of Pediatrics, Cangzhou Central Hospital, Yunhe District, Cangzhou City, Hebei Province, China

Received January 16, 2019 – Accepted March 8, 2019

To the Editor,

Wheezing is a common symptom of respiratory diseases. A survey found that about 1/3 of all children had at least one episode of wheezing before reaching the age of 3, and about 1/2 of them had at least one episode of wheezing by the age of 6 (1, 2). Wheezing in children can be caused by different diseases, mainly including bronchiolitis, asthmatic bronchitis, and bronchial asthma. After treatment of wheezing children, the probability of recurrent attacks is about 40% and these children can eventually develop asthma (3). Although the pathogenesis of bronchial asthma remains unclear, it has been hypothesized that bronchial asthma is related to TH1/TH2 imbalance in the body (4, 5). In particular, IL-4 and IL-12 are the most representative molecules for Th2 and Th1 cells, respectively (6), while IL-37 exerts important anti-inflammatory and immunomodulatory effects (7, 8). As an important selective immunomodulatory molecule, vitamin D (Vit D) is implicated in the etiology of asthma (9, 10). In fact, most scholars believe that Vit D deficiency can reduce lung compliance and lead to immune dysfunction. As the serum form of Vit D, 25-(OH)D can reflect the nutritional status of Vit D in the body (11). In this study, the role of serum levels of IL-4, IL-12, IL-37 and 25-(OH)D in the pathogenesis of asthmatic diseases in children was investigated to provide a theoretical reference for early detection and treatment of bronchial asthma.

MATERIALS AND METHODS

Subjects

A total of 88 children were enrolled in the study, and were divided into an experimental group (72 children with bronchial asthma) and control group (16 healthy children, also called group D). The children in the experimental group were randomly selected from Cangzhou Central Hospital between October 2015 and October 2018, and they were divided into three subgroups: group A (patients with the first episode of wheezing at ≤ 3 years old); group B (patients with multiple episodes of wheezing at ≤ 3 years old); and group C (patients with multiple episodes of wheezing at > 3 years old). Informed consent was obtained from the arents of all children, and the protocol was approved by the ethics committee of Cangzhou Central Hospital.

Exclusion criteria: diseases that can cause wheezing; patients with congenital heart diseases, bronchial foreign body, bronchopulmonary dysplasia, and gastroesophageal reflux; children with other diseases of the immune system; patients not treated by hormone and immunosuppressant drugs within 2 weeks prior to the start of this study; patients taking Vit D supplementation.

Key words: bronchial asthma; interleukin-4; interleukin-12; interleukin-37, 25-hydroxy vitamin D

Corresponding Author:
Dr Yajing Jiang,
Department of Pediatrics,
Cangzhou Central Hospital, No. 16 Xinhua West Road,
Yunhe District, Cangzhou City, 061000,
Hebei Province, China
e-mail: jiangyajing0317@126.com

0393-974X (2019)

DISCLOSURE: ALL AUTHORS REPORT NO CONFLICTS OF INTEREST RELEVANT TO THIS ARTICLE.

Grouping

Group A: The patients experienced the first episode of wheezing at age ≤ 3 years, and the wheezing sound of expiratory asthma could be heard during the auscultation of the lungs. There were 20 cases in this group, including 10 males and 10 females, with an average age of 1.41±0.69 years;

Group B: The patients experienced 3 or more episodes of wheezing at an age of ≤ 3 years, and the wheezing sound of expiratory asthma could be heard during the wheezing attack. There were 18 cases in this group, including 9 males and 9 females, with an average age of 1.94±0.57 years;

Group C: The patients experienced 3 or more episodes of wheezing at an age of > 3 years, and the wheezing sound of expiratory asthma could be heard during the wheezing attack. There were 34 cases in this group, including 19 males and 15 females, with an average age of 6.04±1.63 years;

Group D: normal control group. The patients in this group had no history of infection, allergy, autoimmune disease, or immunodeficiency in the past 4 weeks, and no history of asthma or administration of hormones or immunosuppressants. There were 16 cases in this group, including 7 males and 9 females, with an average age of 5.44±1.52 years.

All subjects in these four groups were born at full term and the difference in the gender composition of different groups was not statistically significant (P>0.05).

Collection and preservation of specimens

Four ml of fasting venous blood was collected from each subject into a condensation vacuum blood collection tube. All samples were placed at room temperature for about 2-4 hours to achieve natural solidification before being centrifuged (Shaanxi Huanyu equipment Co., Ltd, China) for 20 min at 3000 r/min. Subsequently, 2 ml of the serum component was collected from each sample and placed in an Eppendorf (EP) tube. All EP tubes stored at -70°C before detecting the levels of IL-4, IL-12, IL-37, and 25-(OH)D.

Detection of serum levels of IL-4, IL-12 and IL-37

Before testing, the serum samples were restored to room temperature (18-25°C). An Enzyme Linked Immunosorbent Assay (ELISA) kit (Wuhan USCN Business Co., Ltd, China) was used to detect the levels of IL-4, IL-12, and IL-37 in serum samples according to the manufacturer's instructions. Blank control well (without sample and reaction reagent), standard well and sample well were set in the 96-well plate. In the experiment, 50 ul of S0-S5 standard solution was added into the bland control and standard wells, and the concentration was set as 0pg/ml, 3pg/ml, 6pg/ml, 12pg/ml, 24pg/ml, and 48pg/ml, respectively. On the coated plate of the enzyme label, 40 μl of the dilution of the sample was added into the sample well, and then 10 μl of the sample to be tested was added (the sample was finally diluted for 5 times). After the 96-well plate was sealed with the sealing film, it was incubated at 37°C for 30min. The concentrated washing solution was diluted with distilled water (30 times), and prepared for subsequent use. The sealing film was removed, and the liquid in the plate was sucked out and dried. Then, the washing solution which had been diluted with distilled water for 30 times was added into each well, and the washing liquid in the plate was removed after half a minute. The experimental steps above were repeated for 5 times. In addition to the blank wells, 50 μl of the enzyme labeling reagent was added to each of the remaining wells. The sealing film sealing plate was applied and placed in a thermostat at 37°C, for half an hour. The sealing film was removed, and the liquid was removed and dried. Then, the washing liquid which had been diluted with distilled water was placed in each well, and then left for 30 s before being discarded. The above steps were repeated 5 times, and pat dry treatment was performed; 50 μl of developer A and 50 μl of developer B were successively added to each well, and then gently shaken for even mixing, followed by development at 37°C in the dark for 15 min; 50 μl of the stop solution was added to each well to terminate the reaction. The absorbance (OD value) of each well was measured by a microplate reader at a wavelength of 450 nm.

Calculation and judgment of the results

The OD value of each standard product and sample to be tested minus the corresponding OD value of the blank well was defined as the actual OD value. The standard curve was plotted with standard sample concentrations as the abscissa of the coordinate axis, and OD values as the ordinate. Then, according to OD values of the sample, the corresponding concentration was calculated through the curve and multiplied by the dilution factor; alternatively, the linear regression equation of the curve was calculated by concentrations of the standard sample and OD values. The sample concentration was calculated based on OD

values of the sample and then multiplied by the dilution factor. The actual concentrations of IL-4, IL-12 and IL-37 were hence obtained.

The detection of 25 (OH) D

A 25-(OH)D detection kit (Shanghai Enzyme-linked Biotechnology Co., Ltd, China) was used to detect the level of 25-(OH)D in serum samples according to the manufacturer's instructions. In brief, 200 µl of a mixture containing the serum + a protein precipitation reagent + an internal standard was mixed with an extraction solvent to carry out the extraction process and collect the supernatant, which was then dried under nitrogen and reconstituted in a solution of 100 µl.

Statistical analysis

SPSS 17.0 statistical software was used for data analysis. Measurement data were tested for normality and homogeneity, and were then expressed as mean±standard deviation (x±s). A *chi*-squared test was used to compare gender composition in different groups. The comparison of measurement data satisfying the requirements of both normality and homogeneity was carried out using one-way analysis of variance (ANOVA), while the measurement data failing the above requirements were tested by rank sum tests. The correlation between two variables was analyzed by linear regression. The level of significance was set as a=0.05, and P<0.05 was considered statistically significant.

RESULTS

Comparison of serum levels of IL-4 among different groups

Serum levels of IL-4 in groups A, B, C and the control group D were 21.06±2.93 pg/ml, 23.88±3.91 pg/ml, 25.85±4.02 pg/ml, and 17.74±1.77 pg/ml, respectively. One-Way ANOVA with a completely random design was used to compare IL-4 levels among the four groups and the results showed significant difference (F: 40.407, P<0.01). Pairwise comparison among the groups showed that serum levels of IL-4 in groups A, B and C were significantly higher than those in the control group (P<0.001). In addition, the serum level of IL-4 in group B was significantly higher than that in group A (P=0.018), while no significant difference was found between groups B and C (P>0.05) (Fig. 1 and Table I).

Comparison of serum levels of IL-12 among different groups

Serum levels of IL-12 in group A, B, C and D were 30.68±3.65 pg/ml, 23.24±3.72 pg/ml, 22.60±2.24 pg/ml, and 33.35±2.40 pg/ml, respectively. One-Way ANOVA with a completely random design was used to compare IL-12 levels among the four groups and the results showed significant differences (F: 88.284,

Table I. *Different levels of serum IL-4,IL-12,IL-37 and 25-(OH)D among the four groups.*

Group	n	IL-4 (pg/ml)	IL-12(pg/ml)	IL-37(pg/ml)	25-(OH)D (ng/ml)
Group A	20	21.06±2.93	30.68±3.65	21.55±2.01	17.31±3.41
Group B	18	23.88±3.91	23.24±3.72	17.14±2.05	15.25±3.08
Group C	34	25.85±4.02	22.60±2.24	17.74±2.82	12.60±3.64
Group D	16	17.74±1.77	33.35±2.40	24.52±2.32	33.41±5.89
F		40.407	88.284	39.201	103
P		<0.01	<0.01	<0.01	<0.01

P<0.01). Pairwise comparison among the groups showed that the serum IL-12 levels in groups A, B and C were significantly lower than that in the normal control group D (P<0.001). In addition, the serum IL-12 level in group B was significantly lower than that in group A (P<0.001), while no significant difference was found between groups B and C (P>0.05), as shown in Fig. 1 and Table I.

Comparison of serum levels of IL-37 among different groups

Serum levels of IL-37 in group A, B, C and normal control group D were 21.55±2.01pg/ml, 17.14±2.05pg/ml, 17.74±2.82pg/ml, and 24.52±2.32pg/ml, respectively. One-Way ANOVA with a completely random design was used to compare IL-37 levels among the four groups and the results showed significant differences (F: 39.201 P<0.01). Pairwise comparison among the groups showed that the serum levels of IL-37 in groups A, B and C were significantly lower than that in normal control group D (P<0.001). In addition, the serum IL-37 level in group B was significantly lower than that in group A (P<0.001), while no significant difference was found between groups B and C (P>0.05), as shown in Fig. 1 and Table I.

Comparison of serum levels of 25-(OH)D among different groups

Serum levels of 25-(OH)D in groups A, B, C and D were 17.31±3.41ng/ml, 15.25±3.08ng/ml, 12.60±3.64ng/ml, and 33.41±5.89ng/ml, respectively. One-Way ANOVA with a completely random design was used to compare the levels of 25-(OH)D among the four groups and the results showed significant difference (F: 103.0, P<0.01). Pairwise comparison among the groups showed that the serum levels of 25-(OH)D in group A, B and C were significantly lower than those in the normal control group D (P<0.001). In addition, the serum level of 25-(OH)D in group C was significantly lower than that in group B (P=0.026), while no significant difference was found between group A and B (P>0.05), as shown in Fig. 1 and Table I.

Correlation analysis of IL-4, IL-12, IL-37, and 25-(OH)D

As shown in Fig.2, the serum level of IL-37 was negatively correlated with the expression of IL-4 (r: -0.549, P<0.001) but positively correlated with the expression of IL-12 (r: 0.847, P<0.001) and 25-(OH)D (r: 0.561, P<0.001). In addition, the serum level of 25-(OH)D was negatively correlated with the expression of IL-4 (r: -0.621, P<0.001) but positively correlated with the expression of IL-12 (r: 0.608, P<0.001), while

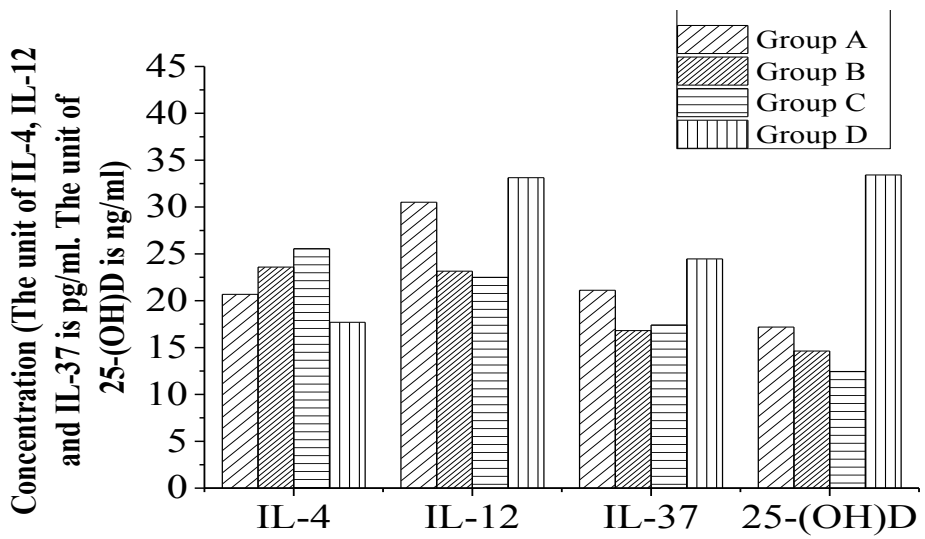

Fig. 1. *Levels of IL-4, IL-12, IL-37, and 25-(OH)D among the four groups.*

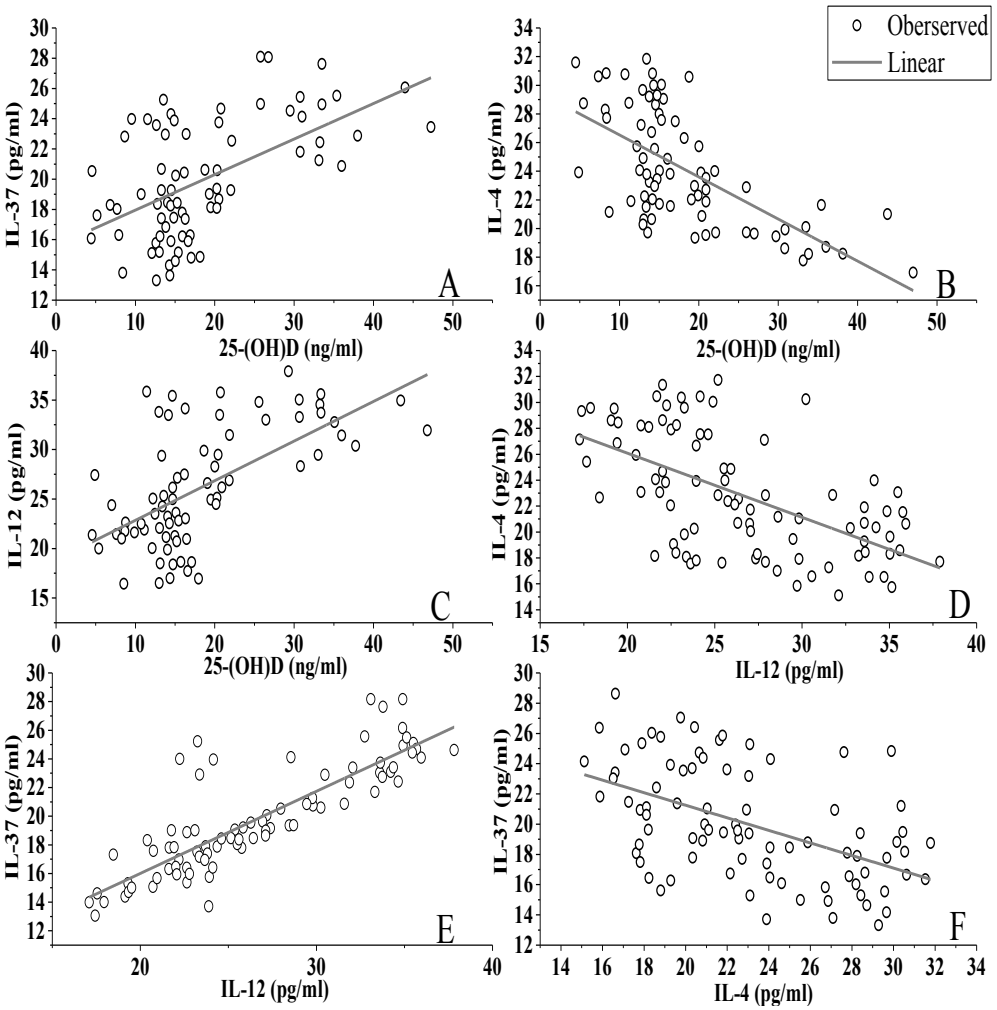

Fig. 2. *Correlation analysis of IL-4, IL-12, IL-37, and 25-(OH)D.* ***A)*** *the serum level of IL-37 was positively correlated with the level of 25-(OH)D;* ***B)*** *the serum level of IL-4 was negatively correlated with the level of 25-(OH)D;* ***C)*** *the serum level of IL-12 was positively correlated with the level of 25-(OH)D;* ***D)*** *the serum level of IL-4 was negatively correlated with the level of IL-12;* ***E)*** *the serum level of IL-37 was positively correlated with the level of IL-12;* ***F)*** *the serum level of IL-37 was negatively correlated with the level of IL-4).*

the serum level of IL-4 was negatively correlated with the expression of IL-12 (r: -0.589, P<0.001).

DISCUSSION

The mechanism underlying the pathogenesis of asthma remains unclear. It has been shown that the expression levels of IL-37 and Vit D are related to the onset of asthma (11). The results of this study showed that the serum levels of 25-(OH)D in group A and B were significantly lower than those in the normal control group D. Since the serum level of 25-(OH) D is negatively correlated with the level of IL-4 and positively correlated with the levels of IL-12 and IL-37, a decrease in the serum level of 25-(OH)D in peripheral blood may trigger asthmatic diseases by disrupting the dynamic balance between Th1/Th2. As a result, the production of such factors as IL-12 and IFN-γ of the Th1 subgroup was decreased, while the secretion of such factors as IL-4 and IL-10 of the Th2 subgroup was increased. Changes in the levels of these factors can disrupt the dynamic equilibrium of Th1/

Th2 to induce hyper reactivity and inflammation in the airway. In addition, the serum level of 25-hydroxy Vit D in group C was significantly lower than that in group B, suggesting that the serum level of 25-(OH)D decreased more significantly over age. Such results may be caused by a decreased level of outdoor activities and insufficient exposure to sunlight among children at the school age, suggesting that preschool and school children with wheezing should pay more attention to the supplementation of Vit D.

To sum up, bronchial asthma can occur in children of < 3 years old. In addition, during the first episode of wheezing in these children, there are already signs of Th1/Th2 imbalance along with typical asthmatic airway inflammation. Therefore, treatments should be carried out in these children as early as possible.

REFERENCES

1. Mummidi PS, Tripathy R, Dwibedi B, Mahapatra A, Baraha S. Viral aetiology of wheezing in children under five. Indian J Med Res 2017; 145(2):189-93.
2. Cohen RT, Pelton SI. Individual benefit vs societal effect of antibiotic prescribing for preschool children with recurrent wheeze. JAMA 2015; 314(19):20272-9.
3. Bannier MA, van de Kant KD, Jöbsis Q, Dompeling E. Biomarkers to predict asthma in wheezing preschool children. Clin Exp Allergy 2015; 45(6):1040-50.
4. Guo HW, Yun CX, Hou GH, et al. Mangiferin attenuates TH1/TH2 cytokine imbalance in an ovalbumin-induced asthmatic mouse model. PLoS One 2014; 9(6):e100394.
5. Wu Q, Tang Y, Hu X, Wang Q, Lei W, Zhou L, Huang J. Regulation of Th1/Th2 balance through OX40/OX40L signalling by glycyrrhizic acid in a murine model of asthma. Respirology 2016; 21(1):102-11.
6. Noble A, Thomas MJ, Kemeny DM. Early Th1/Th2 cell polarization in the absence of IL-4 and IL-12: T cell receptor signaling regulates the response to cytokines in CD4 and CD8 T cells. Eur J Immunol 2001; 31(7):2227-35.
7. Li C, Shen Y, Wang J, et al. Increased expression of IL-1R8 and a possible immunomodulatory role of its ligand IL-37 in allergic rhinitis patients. Int Immunopharmacol 2018; 60:152-59.
8. Filewod NC, Pistolic J, Hancock RE. Low concentrations of LL-37 alter IL-8 production by keratinocytes and bronchial epithelial cells in response to proinflammatory stimuli. FEMS Immunol Med Microbiol 2009; 56(3):233-40.
9. Hall SC, Agrawal DK. Vitamin D and bronchial asthma: an overview of data from the past 5 years. Clin Ther 2017; 39(5):917-29.
10. Smyk DS, Mavropoulos A, Mieli-Vergani G, Vergani D, Lenzi M, Bogdanos DP. The Role of Invariant NKT in Autoimmune Liver Disease: Can Vitamin D Act as an Immunomodulator? Can J Gastroenterol Hepatol 2018; 2018:8197937.
11. Pereda CA, Nishishinya MB. Is there really a relationship between serum vitamin D (25OHD) levels and the musculoskeletal pain associated with statin intake? A systematic review. Reumatol Clin 2016; 12(6):331-35.

LETTER TO THE EDITOR

PAI-1 and MASPIN GENE EVOLUTION ANALYSIS IN PLATEAU ZOKOR *(MYOSPALAX BAILEYI)*

SH. LI[1,2,4], B. XU[3], ZF. AN[2], ZJ. WANG[3], YX. LI[3], L.WEI[3] and DB. WEI[1,3]

[1]State Key Laboratory of Plateau Ecology and Agriculture, Qinghai University, Xining, Qinghai, China; [2]Research Center for High Altitude Medicine, Qinghai University, Xining, Qinghai, China; [3]College of Eco-Environmental Engineering, Qinghai University, Xining, Qinghai, China; [4]Department of Gastroenterology, Qinghai University Affiliated Hospital, Xining, Qinghai, China

Received February 25, 2019 – Accepted March 19, 2019

To the Editor,

Hypoxia is one of the most obvious environmental characteristics of the Qinghai-Tibet Plateau (1). Increasing tissue microvessel density is an important mechanism for plateau animals to adapt to the hypoxic environment (2). The plateau zokor (*Myospalax baileyi*) is a small local mammal of the Qinghai-Tibetan Plateau. They spend their whole life in sealed burrows with the characteristics of hypoxic and high carbon dioxide (3). The microvessel density (MVD) of *Spalax* in the hypoxic environment is significantly higher than that of Sprague-Dawley (SD) rats, while the expression level of *VEGF* decreases compared with SD rat under conditions of 6% O_2 for 4 h (4). This indicates that the expression pattern of angiogenesis in subterranean rodents is different from that of SD rats under hypoxia, which may be related to upregulated expression of angiogenic growth inhibitors (5).

PAI-1 and Maspin belong to the serine proteinase inhibitors (serpin) superfamily, which is mainly composed by vascular endothelial cells. The RSL of PAI-1binds with tissue plasminogen activator (t-PA) and urokinase-typeplasminogen activator (u-PA) to inhibit angiogenesis and metastasis by inhibiting protein hydrolysis, stable extracellular matrix (ECM) and reduced cell adhesion (6). Maspin binds to specific proteins by RSL to regulate cell movement and proliferation, inducing cell apoptosis and ultimately inhibiting angiogenesis (7). The expression level of PAI-1 and Maspin upregulates in hypoxia to inhibit the growth of capillaries (8). In this study, we used bioinformatics to analyze the evolution of PAI-1 and Maspin in plateau zokor in order to explore the effects of structural mutations on their functions and hypoxia on their expression.

MATERIALS AND METHODS

Sample collection and treatment

Plateau zokors were live-trapped in the Zongjiagou Region of Huangyuan County, Qinghai Province of China. Plateau zokors were divided into two groups: i) high altitude group zokors were captured at the altitude of 3,300 m, with the oxygen partial pressure of 14.13kPa and oxygen content of 193.4 g/m^3; ii) low altitude group zokors were captured in the Zongjiagou region and raised in Xining City, Qinghai Province of China at the altitude of 2,260 m for 8 days, with the oxygen partial pressure of 16.12kPa and oxygen content of 229.7g/m^3. Sprague-Dawley (SD) rats were bought from Lanzhou City, Gansu Province of China. Rats were divided into two groups: i) high altitude group rats were raised in the Zongjiagou region at the altitude of 3,300 m for 8 days; ii) low altitude group rats were in Xining City, Qinghai Province of China at the altitude of 2,260 m for

Key words: PAI-1; Maspin; evolutionary analysis; hypoxia; Plateau zokor (Myospalaxbaileyi)

Corresponding Author:
Dr Dengbang Wei,
State key laboratory of Plateau Ecology and Agriculture,
Qinghai University 10743, 251 Ningda Road,
Xining 810016, Qinghai, China
e-mail: weidengbang_qhu@163.com

0393-974X (2019)

8 days. The sample size was 8 for each group. All animals were anaesthetized with sodium pentobarbital (5%) and sacrificed using cervical dislocation immediately before dissection. Liver, lung, skeletal muscles tissues of plateau zokors were rapidly removed and quickly frozen in liquid nitrogen. RNA extraction, cDNA library construction and the next generation sequencing (NGS) and Isoform Sequencing (Iso-Seq) library construction were performed by Novogene Bioinformatics Technology Co. Ltd, Beijing, China. The NGS and Iso-Seq were sequenced on Illumina Hiseq 4000 and PacBio RSII platform, respectively. All procedures involved in the handling and care of the animals were in accordance with the China Practice for the Care and Use of Laboratory Animals and approved by the China Zoological Society (permit number: GB 14923-2010).

Construction of tree species from mtDNA data

Complete mitochondrial DNA (mtDNA) sequences for 24 mammalian species (including 14 Rodentia, 4 Lagomorpha and 6 other mammalian species served as Outgroup) were downloaded from NCBI (www.ncbi.nlm.nih.gov), including fourteen rodents, four Lagomorphas, four Artiodactylas and two Primates. The mtDNA phylogenetic trees were reconstructed using MrBayes 3.2.6. Bayesian inference (BI) with Markov-chain Monte Carlo (MCMC) sampling was performed by using MrBayes 3.2.6 to run for one million generations. We made two simultaneous runs, sampling trees in every 1,000 generations, with three heated and one cold chain to encourage swapping among the MCMC chains and avoid the analysis remaining in local rather than global optima. Model Test was used to select the optimal models based on the Akaike Information Criterion (AIC). Convergence of sampled parameters and potential autocorrelation (effective sampling size/ESS for all parameters>200) was investigated in Tracer 1.6 (http://tree.bio.ed.ac.uk/software/ tracer/). Additionally, the average SD of split frequencies between both runs were checked (<0.01). The Bayesian posterior probabilities were obtained from the 50% majority rule consensus of the post-burn-in trees sampled at stationarity, after removing the first 25% of trees as a "burn-in" stage.

PAI-1 and Maspin CDS sequence acquisition

The fasta format Triny gene in the NGS transcriptional databases and the flnc gene in the Iso-Seq Transcriptional databases were combined to build local databases , using ncbi-blast-2.7.1 program (https://ftp.ncbi.nlm.nih.gov/blast/executables/LATES T). The complete PAI-1 and Maspin coding sequences of *Nannospalax galili* were used as query sequences to find the homologous sequences or fragments by local blast. The fragments were resembled and translated by using Lesergene 7.0 program. Homologous tree with all sequences selected above was constructed by using MEGA 7.0 program. The sequence with the highest

Table I. *Likelihood values, parameter estimates, and sites under positive selection of PAI-1 and Maspin.*

Genes	**Model code**	Estimate of parameters	-In*L*[a]	Model comparison	Positively selected sites	2△In*L* (p-value)
PAI-1	**Branch-site Model**					
	Null A	p0= 0.780, p1=0.215, (p2+p3=0.005), ω0= 0.075, ω1= 1, ω2=1	-9485.35			
	Model A	p0= 0.780, p1=0.215, (p2+p3=0.005), ω0= 0.075, ω1= 1, ω2=1	-9481.34	Model A *vs* Null A	49 S, 67 S,73 A	0.20 (p=0.05)
Maspin	Null A	p0= 0.666, p1=0.067, (p2+p3=0.266),ω0= 0.069, ω1= 1, ω2=1	-6283.70			
	Model A	p0= 0.776, p1=0.075, (p2+p3=0.148), ω0= 0.073, ω1= 1, ω2=1	-6271.51	Model A *vs* Null A	292 E, 310 N , 340 G**, 346 H**, 352 R**, 374 P**	0 (p=1)

[a]*InL: log-likelihood score. *P > 0.95, **P > 0.99.*

homology of *Nannospalax galili* was selected as the coding sequence of target protein. Then the sequence was screened by DNAMAN version 9.0 (http://www.lynnon.com) from three Iso-Seq Transcriptional databases and one PacBio Transcriptional database, and the final Plateau zokor PAI-1 and Maspin sequence was selected. Complete PAI-1 and Maspin coding sequences for 23 mammalian species were downloaded from 23 available published mammalian genome sequences from NCBI (National Center for Biotechnology Information) (www.ncbi.nim.nih.gov).

Prediction on physicochemical properties and homology comparison

The physicochemical properties of PAI-1 and Maspin amino acid sequences were predicted by using the ProtParam tool (http://web.expasy.org/protparam/). Nucleotide sequences of each PAI-1 and Maspin and their deduced amino acid sequences were aligned separately by using ClustalW2 (http://www.ebi.ac.uk/Tools/msa/clustalw2) and MEGA 7.0. The maximal likelihood tree based on PAI-1 and Maspin coding sequences and amino acid sequences of 24 species was constructed by using MEGA 7.0.

Selection pressure analysis

The sequence alignment was obtained by using CluatalX1.81 and format conversion was performed with MEGA7.0 software. The maximum-likelihood method was used to estimate the positive sites by using branch-site models in Codeml from the PAML4.8 software package based on the 24 mammalian species tree. Positive selection was detected by using branch-site model A, in which it can vary among sites along specific lineages. The positively selected sites were identified by Bayes Empirical Bayes (BEB) analysis, and the significance of the likelihood ratio test (LRT) statistic was determined by *Chi*-squared test. The mtDNA Bayes tree, which well supported the phylogeny of Rodentia, Lagomorpha and Outgroup and proved its accuracy, was used as the input tree in this analysis.

Evolutionary or Parallel Analysis

The maximal likelihood tree based on PAI-1 and Maspin coding sequences of 24 species was used for evolutionary analysis. To infer convergent or parallel evolution sites of 24 species, ancestral sequences of PAI-1 and Maspin were reconstructed by Ancestors program

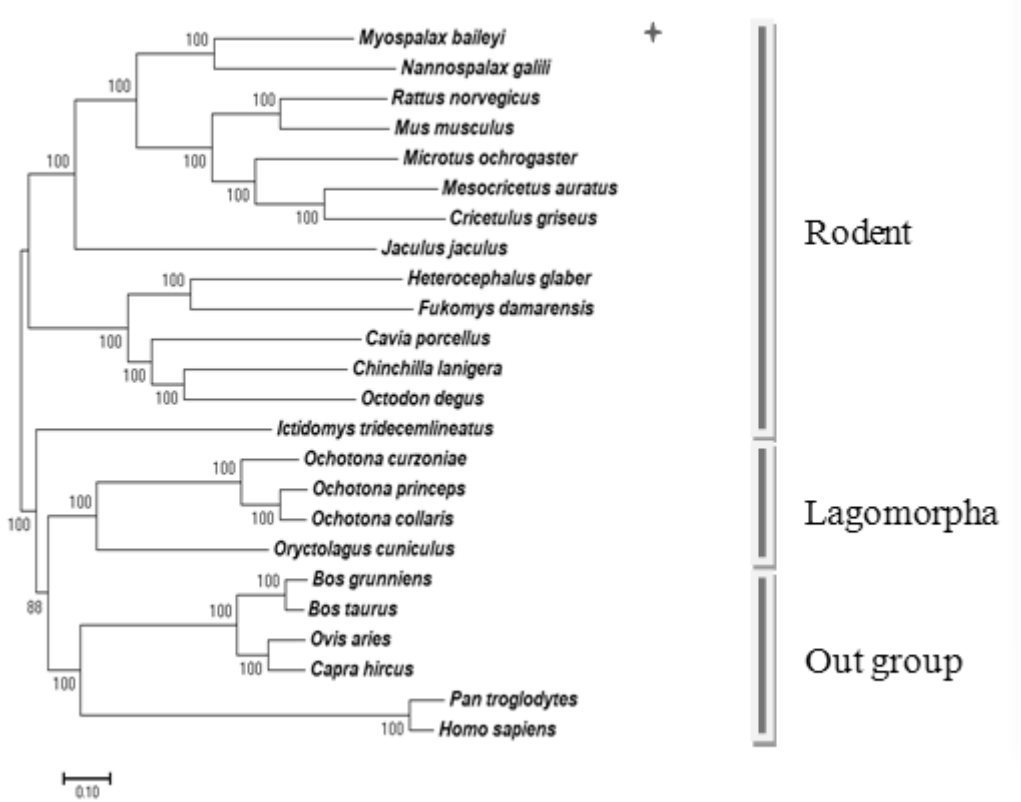

Fig. 1. *Phylogenetic tree of 24 mammals. Inferred by Bayesian inference under the GTR+I+G model (58). Posterior probabilities values (%) are indicated at the nodes. The branch of plateau zokor is indicated by the four-pointed star.*

in the MEGA 7.0 software. The posterior probabilities of the reconstructed ancestral sites were used to evaluate the accuracy of the reconstruction results. To avoid the interference of the ancestral locus polymorphism with the subsequent analysis, the site with posterior probability of less than 0.9 was excluded. Then we used the Jones-Taylor-Thornton (JTT) and Poisson amino acid substitution models to test whether the probabilities of observed convergent or parallel sites were significantly higher than expected by chance.

Evaluating the effects of the mutation sites on the function of PAI-1 and Maspin

The effects of convergent or parallel evolution sites on the function of PAI-1 and Maspinwere predicted by using 'Sorting Tolerant From Intolerant' (SIFT) algorithm. The PAI-1 sequence of *Mus musculus* (NP_032897.2) and Maspin sequence of *Mus musculus* (NP_033283.1) were used as a query sequence. Other parameters used default settings according to Kumar's studies.

The expression level of PAI-1 and Maspin by qRT-PCR

Total RNA was isolated from the liver, lung and skeletal muscle of *Myospalax baileyi* by trizol reagent (Invitrogen Corp, USA). RNA concentration and purity were assessed by Ultra Violet (UV) spectrophotometry (1.8<A260/A280<2.0). RNA integrity was checked by electrophoresis. Reverse transcription reaction was prepared to start from 3.8 μg of total RNA by using the First Strand cDNA Synthesis kit (Tiangen, China).

To make standard curves, 1 μL of first-strand cDNA was amplified with Premix Ex Taq Version Kit (TaKaRa Bio, Japan), and quantification of Polymerase Chain Reaction (PCR) products were used for plotting standard curves. The initial product concentration was set at 1 and standard curves were generated by using a 10-fold serial dilution ranging from 1 to 10^{-8}.

Quantitative Real-time Polymerase Chain Reaction (qRT-PCR) was performed by using the SYBR® Premix Ex Taq™ II (TaKaRa Bio, Japan) protocol on BIO-RAD, connecting real-time PCR detection system with cycling conditions of 95 for 3 min, followed by 40 cycles of 95 for 30 s and 60 for 30 s. β-actin was used as an internal control. The PCR primers for PAI-1 were 5'-AGCACAGTGAAGCAGGTGGACT-3' (sense) and 5'-GCTGCCGTCAGACTT GTGGAAA-3'(antisense), the amplicon length was 256 bp, and for Maspin were 5'-AGACAGACACCAAACCTGTGCA-3' (sense) and 5'-TGGACTCGTCCTCC ACATCCTT-3' (antisense), the amplicon length was 156bp; and for β-actin were 5'-TCACCAACTGGGACGATATG-3' (sense) and 5'-GTTGGCCTTAGGGTTCAG AG-3' (antisense), the amplicon length was 220bp. PAI-1 and Maspin mRNA level was normalized with β-actin mRNA to compensate for variations in initial RNA amounts. Normalization was carried out by dividing the logarithmic value of PAI-1 and Maspin and the logarithmic value of β-actin.

Statistical analysis

Statistical analysis was performed by one-way ANOVA analysis and Duncan's test by using SPSS 17.0 (SPSS Inc., Chicago, IL, USA). A value of $P < 0.05$ was considered statistically significant.

RESULTS

Construction of tree species from mtDNA data

For subsequent selection pressure analysis and evolutionary analysis, the mitochondrial genome DNA (mtDNA) sequences from 24 mammalian species were included in our study, Rodentia (*Mospalax baileyi,* NC_018098.1; *Nannospalax galili,* JN571132.1; *Rattus norvegicus,* KF011917.1; *Mus musculus,* J01420.1; *Microtus ochrogaster,* NC_027945.1; *Mesocricetus auratus,* EU660218.1; *Cricetulus griseus,* DQ390542.2; *Jaculusjaculus,* NC_005314.1; *Heterocephalus glaber,* HQ689652.1; *Fukomysdamarensis,* KT321364.1; *Caviaporcellus,* NC_000884.1; *Chinchilla lanigera,* NC_021386.1; *Octodon degus,* HM544134.1; *Ictidomystridecemlineatus,* NC_027278.1); Lagomorpha(*Ochotona curzoniae,* EF535828.1; *Ochotona princeps,* NC_005358.1; *Ochotona collaris,* AF348080.1; *Oryctolagus cuniculus,* NC_001913.1); Outgroup(*Bos grunniens,* AY684273.2; *Bos Taurus,* V00654.1; *Ovisaries,* KR868678.1; *Capra hircus,* KY305183.1; *Homo sapiens,* V00662.1; *Pan troglodytes,*NC_001643.1). Bayesian phylogenetic reconstruction based on the nucleotide sequences yielded a tree with a topology similar to the well-accepted mammal species tree according to published phylogenetic studies. Specifically, the Bayesian analysis

strongly supported the monophyly of the Rodentia and Lagomorpha [Bayesian posterior probability (BPP) =100%] (Fig.1).

Sequence homology alignment

Complete PAI-1 coding sequences for 23 mammalian species were downloaded from 23 available published mammalian genome sequences from NCBI (National Center for Biotechnology Information): *Nannospalaxgalili* (XM_008832312.2), *Rattus norvegicus* (NM_012620.1), *Mus musculus* (NM_00887 1.2), *Microtus ochrogaster* (XM_005361538.2), *Mesocricetus auratus* (XM_005 080401.3), *Cricetulus griseus* (XM_007637831.2), *Jaculusjaculus* (XM_004666293.1), *Heterocephalusglaber* (XM_004840153.2), *Caviaporcellus* (XM_003469906.2), *Chinchilla lanigera* (XM_00539 6870.2), *Ictidomystridecemlineatus* (XM_02172856 7.1), *Octodon degus* (XM_004630479.1), *Ochotona collaris* (XM_004587183.2), *Oryctolagus cuniculus* (XM_002722823.3), *Bos grunniens* (XM_019988055.1), *Bos Taurus* (NM_174137.2), *Ovisarie* (GQ855215.1), *Capra hircus*(XM_01 3976795.2), *Homo sapiens* (M16006.1), *Pan troglodytes*(XM_527841.4); PAI-1 consequences of *Fukomysdamarensis, Ochotona curzoniae*and *Ochotona princeps* were not found in NCBI.

Complete Maspin coding sequences for 23 mammalian species were downloaded from 23 available published mammalian genome sequences from NCBI (National Center for Biotechnology Information) (www.ncbi.nim.nih.gov): *Nannospalaxgalili* (XM_008840658.2), *Rattus norvegicus* (U58857.1), *Mus musculus*(U54705.1), *Microtus ochrogaster* (XM_005368727.1), *Mesocricetus auratus* (XM_005081451.3), *Cricetulus griseus* (XM_016965850.1), *Jaculusjaculus* (XM_004654793.1),*Heterocephalusglaber*(XM_02123 9269.1), *Fukomysdamarensis* (XM_019210780.1), *Caviaporcellus* (XM_003474063.2), *Chinchilla lanigera* (XM_013511244.1), *Octodon degus* (XM_004638257.1),*Ictidomystridecemlineatus* (XM_ 005323007.2), *Ochotona princeps* (XM_004579451.2), *Oryctolagus cuniculus* (XM_002713632.3), *Bos grunniens* (XM_005910186.2), *Bos Taurus* (NM_001098080.1), *Ovisarie* (XM_004 020573.3), *Capra hircus* (XM_005697305.3), *Homo sapiens* (U04313.1), *Pan troglodytes* (XM_001146935.4); Maspinconcequences of *Ochotona curzoniae and Ochotona collaris* were not found in NCBI.

In our study, PAI-1and Maspinsubunit in *Myospalaxbaileyi, Nannospalaxgalili, Rattus norvegicus* were analyzed. The coding sequence (CDS) of *Myospalaxbaileyi* and *Nannospalaxgalili* PAI-1 subunit were 1209 bp, encoding 402 amino acids, the molecular weight of the three species was about 45KDa. The coding sequence (CDS) of *Myospalax baileyi* and *Nannospalax galili* Maspin subunit was 1146 bp, encoding 381 amino acids.

Homology analysis results showed that the CDS of *Myospalaxbaileyi* PAI-1 nucleotide sequence was identified as 91.89%, 80.40%, 82.80%, 83.71%, 82.80%, 80.82%, 84.78% and 81.11%, and the amino acid sequence was identified as 91.79%, 76.62%, 82.59%, 81.59%, 79.85%, 78.37%, 83.83% and 79.11% with that of *Nannospalaxgalili, Heterocephalusglaber, Homo sapiens, Rattus norvegicus, Mus musculus, Cricetulus griseus, Mesocricetus auratus* and *Microtus ochrogaster*, respectively. Maspin nucleotide sequence was identified as 95.99%, 85.6%, 84.9%, 84.73%, 86.82%, 87.55%, 87.35% and 86.65%, and the amino acid sequence was identified as 95.54%, 88.45%, 87.66%, 86.09%, 88.71%, 90.05%, 89.76% and 88.45%. From the phylogenetic tree, we observed that plateau zokor had the highest homology with *Nannospalax galili*.

Selective pressure analysis

Selective pressure analysis has reflected that species are affected by the external environment, and site mutation may enhance the species' ability to adapt to the hypoxic environment effectively. To detect the positively selected sites of PAI-1 and Maspinin plateau zokor, we treated the plateau zokor branch as the foreground branch. Using the LRT test based on the branch-site model for PAI-1 and Maspingene, we observed that there are no positive selection sites in plateau zokor PAI-1, and there are four positive selection sites in plateau zokor Maspin. The mtDNA Bayes tree which was well-supported by the phylogeny of Rodentia, Lagomorpha and Outgroup was used as the input tree in this analysis (Table I).

Evolutionary analysis

Convergent or parallel evolution is strong evidence for adaptive evolution. To detect the convergent sites in subterranean rodents in response to hypoxia environments, we attempted to identify convergent changes by comparing ancestral and extend PAI-1 and Maspin protein sequences. We observed that four sites experienced parallel evolution on subterranean rodent branch of *Eospalax baileyi* and *Nannospalax galili*. The 111th, 172th, 179th and 334th positions of PAI-1 were lysine (K, Lys), serine (S, Ser), alanine (A, Ala) and aspartic (D, Asp) on the ancestral branch respectively, and the same replacement of glutamine (Q, Gln), lysine (K, Lys), threonine (T, Thr) andvaline (V, Val) was on the subterranean rodent branch of *Eospalax baileyi* and *Nannospalax galili*. A statistical test (29) showed that four parallel evolution sites were significantly greater than random expectations (P<0.01), indicating selection over chance (Fig. 2).

Evaluating the effects of the positive selection sites and parallel evolution sites on the function of PAI-1 and Maspin

According to the SIFT algorithm, if the score is less than 0.05, the amino acid mutation has an effect on the function of the protein, and vice versa. Our results showed that the parallel evolution site 334 Val had significant effects on the function of PAI-1. PAI-1 bound to t-PA and u-PA with RSL(amino acid 321-345) to inhibit plasminogen activation and protein hydrolysis that stabilized extracellular matrix, promoted the binding with low density lipoprotein receptor-like protein (LRP1) and inhibited the activation of matrix protease (MMP), thereby reducing the expression of vascular endothelial growth factor (VEGF) and blocking the aggregation of VEGF that bind with VEGFR-2 in extracellular matrix, which may directly inhibit the proliferation and angiogenesis of endothelial cells, and indirectly inhibit the adhesion between endothelial cells and matrix fibronectin (6).

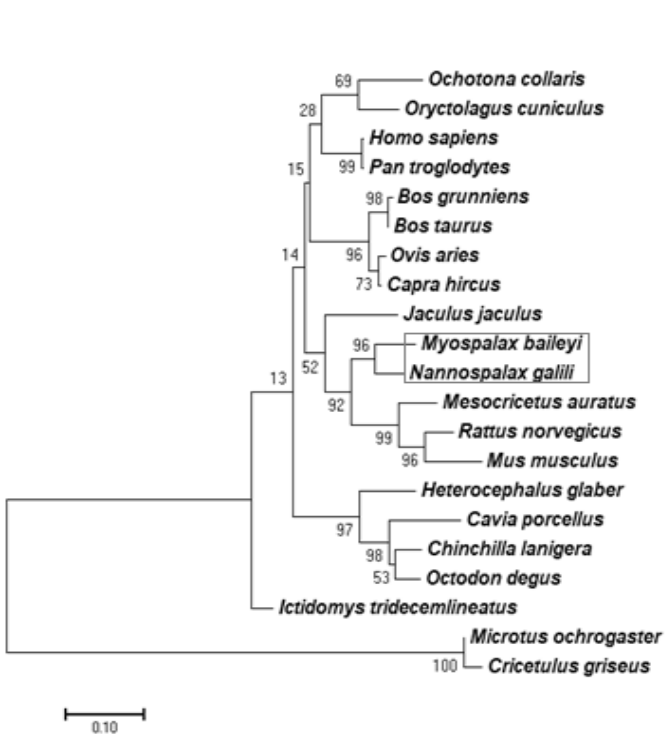

AA/Codon	AA/Codon	AA/Codon	AA/Codon
K/AAG	S/AGT	A/GCT	D/GAC
K/AAG	S/AGT	A/GCT	D/GAC
K/AAG	S/AGT	A/GCT	D/GAC
K/AAG	S/AGT	A/GCT	D/GAC
K/AAG	S/AGT	A/GCT	D/GAC
K/AAG	S/AGT	A/GCT	D/GAC
K/AAG	S/AGT	A/GCT	D/GAC
K/AAG	S/AGT	A/GCT	D/GAC
G/AAC	S/AGT	A/GCT	D/GAC
Q/CAG	K/AAA	T/ACT	V/GTC
Q/CAG	K/AAA	T/ACT	V/GTC
K/AAG	S/AGT	A/GCT	D/GAC
K/AAG	S/AGT	A/GCT	D/GAC
K/AAG	S/AGT	A/GCT	D/GAC
K/AAG	S/AGT	A/GCT	D/GAC
K/AAG	S/AGT	A/GCT	D/GAC
K/AAG	S/AGT	A/GCT	D/GAC
K/AAG	S/AGT	A/GCT	D/GAC
K/AAG	S/AGT	A/GCT	D/GAC
K/AAG	S/AGT	A/GCT	D/GAC

Fig. 2. *Convergent evolution sites of the PAI-1 sequence. Amino acids and codons of four sites are shown. Eospalax baileyi and Nannospalax galili are shown in the box*

The polar amino acid (Asp, D) mutated to non-polar amino acid (Val, V) in residue 334 in plateau zokor.

The positive selection sites (229 Glu, 346 His, 352 Arg and 374Pro) showed significant effects on the function of Maspin. Maspin is a tumor suppressor protein, which was bound to serine protease or cysteine protease by reactive site loop (amino acid 330-345) to reduce invasiveness, inhibit kinase-plasminogen system and promote endothelial cell apoptosis. According to activation of the apoptotic pathway of caspase-3 and bcl-2 genes, that induced apoptosis pathway activation and inhibited the matrix metalloprotease-2 (MMP-2) and kinase-plasminogen system to reduce the expression of vascular endothelial growth factor (VEGF) and microvessel density, and decreased angiogenesis ultimately (7). We found that the positions 229, 346, 352 and 374 of RSL region in SD rats were the polar amino acid without electrodes Gly (G), the negative electrodes polar amino acid Asp (D), the positive electrodes polar amino acid His (H) and the polar amino acid without electrodes Ser (S) respectively. In zokor the negative electrodes were polar amino acid Glu (E), the positive electrodes polar amino acid His (H), the positive electrodes polar amino acid Arg (R) and non-polar amino acid Pro (P), respectively. This may enhance the binding ability

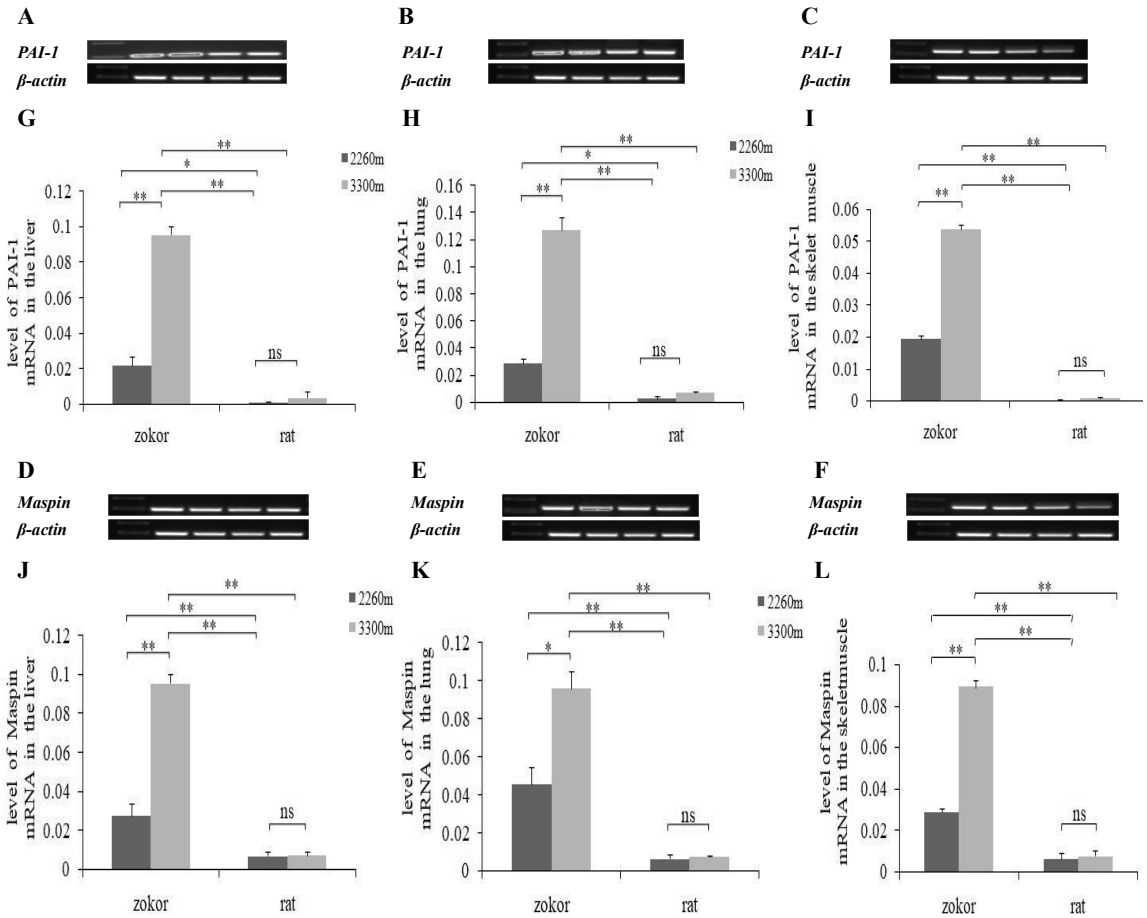

Fig. 3. *Quantification of PAI-1 and Maspin mRNA levels in tissues of plateau zokor and rat at different altitudes.* ***A-C)*** *Electrophoresis results of real-time PCR of PAI-1 and β-actin in plateau zokor and rat tissues.* ***D-F)*** *Electrophoresis results of real-time PCR of Maspin and β-actin in plateau zokor and rat tissues. Panels indicate liver (G), lung (H) and skeletal muscle (I) of PAI-1, and liver (J), lung (K) and skeletal muscle (L) of Maspin. M: marker; L: low-altitude group(2260 m); H: high-altitude group(3300 m);* ** *P<0.01;* **,P<0.05; ns: not significant(P>0.05). The sample size was 8 for each group.*

with protease by amino acid mutations and thus inhibit angiogenesis.

qRT-PCR analysis of PAI-1 and Maspin mRNA expression

The mRNA expression levels of PAI-1 and Maspin of plateau zokors and SD rats at 3,300 m and 2,260 m altitudes were examined in the liver, lung and skeletal muscle by qRT-PCR analysis. Studies found that the expression level of PAI-1 and Maspin was related to degree of hypoxia. Under normal conditions, PAI-1 and Maspin were expressed at low levels in most cells. When the oxygen content decreased, their expression levels increased gradually and inhibited the unrestricted increase of microvessel density in hypoxia environment (8). With the aggravation of hypoxia the balance of angiogenesis was broken in tumor cells, and the ratio of PAI-1 and Maspin with VEGF gradually decreased and microvessel density increased, which accelerated angiogenesis of tumor tissues. However, after overexpression of PAI-1 and Maspin, it was found that the vascular density in tumors decreased significantly, and the blood supply decreased, which resulted in the necrosis of tumor cells. For all tissues, the PAI-1 and Maspin of plateau zokor expression levels were significantly higher in the 3,300 m group than in the 2,260 m group($P < 0.01$); however, there was no difference between the 3,300 m and 2,260 m groups of SD rats in the three tissues. The relative expression levels of plateau zokors in the three tissues were significantly higher than that of SD rats in the 3,300 m and in the 2,260 m group($P< 0.05$), respectively (Fig. 3).

DISCUSSION

The plateau zokor is a rodent on the Qinghai-Tibet Plateau. Due to long-term living in hypoxia and high carbon dioxide environment, many genes of zokors have adaptive mutations to hypoxia (9).

Previous studies revealed that PAI-1 has a short span of activity with a t1/2 of ~2 h, however, the polar amino acids without electrode glutamine (Q) mutated to nonpolar amino acids proline (P) at position 324 that enhanced the half time to 180 h and the ability of binding to uPA, which reduced the degradation rate of extracellular matrix (10). By observing the spatial structure of Maspin in multiple tumor tissues, we found that the tumor cells' abilities of invasiveness, anti-apoptotic and angiogenesis were significantly enhanced after the non-polar amino acid proline (Pro, P) mutated to the polar amino acid without electrodes serine (Ser, S) at position 176, adjacent to the loop domain of the reaction site (10). This indicated that the polarity of amino acids abated in RSL could enhance the binding ability of PAI-1 to corresponding proteins. This viewpoint is consistent with our results.

P53 of plateau zokor is sensitive to environmental oxygen concentration. The expression level at 2,260 m was 80% lower than that at 3,300 m(11). PAI-1 and Maspin are the endogenous angiogenesis inhibitors identified in *p53* pathway, *p53* can positively stimulate the PAI-1 promoter sequences (-167~-125) and Maspin promoter sequences (-297~transcription initiation site), inhibiting angiogenesis by up-regulating their expression level (12).

In conclusion, the PAI-1 and Maspin genes in plateau zokors enhance the ability of inhibiting angiogenesis through site mutation and increase of the expression level.

ACKNOWLEDGEMENTS

This work was supported by the Natural Science Foundation of Qinghai Province (No.2016-ZJ-901).

REFERENCES

1. Lv YD, Huo ZH. Special environmental physiology. Military Medical Science Academy of the PLA Press 2005; 25-26 (in Chinese).
2. Zhang XZ, Guo SC, Dou YR. Progresses of hypoxia adaptation on plateau zokor. Life Science Research 2015; 19(6):554-58.
3. Wang ZW, Zeng JX, Han YC. Studies on gas metabolism of pika (*Ochotona*) and plateau zokor (*Myospalax baileyi*). Acta Zool Sin 1979; 25:75-84.
4. Avivi A, Resnick MB, Nevo E, Joel A, Levy AP. Adaptive hypoxic tolerance in subterranean mole rat *Spalax ehrenbergi*: the role of vascular endothelial growth factor. FEBS Lett 1999; 452:133-40.
5. Malik A, Korol A, Weber M, Hankeln T, Avivi A,

Band M. Transcriptome analysis of the spalax hypoxia survival response includes suppression of apoptosis and tight control of angiogenesis. BMC Genomics 2012; 13:615-35.

6. Wu JB, Strawn TL, Luo M, et al. Plasminogen activator inhibitor-1 inhibits angiogenic signaling by uncoupling vascular endothelial growth factor receptor-2-$\alpha_V\beta_3$ integrin cross-talk. Arterioscler Thromb Vasc Biol 2015; 35(1):111-20.
7. Jang HL, Nam E, Lee KH, Yeom S, Son HJ, Park C. Maspin polymorphism associated with apoptosis susceptibility and in vivo tumorigenesis. Int J Mol Med 2008; 22(3):333-38.
8. Amir S, Margaryan NV, Oderomarah V, Khalkhaliellis Z, Hendrix MJ. Maspin regulates hypoxia-mediated stimulation of uPA/uPAR complex in invasive breast cancer cells. Cancer Biol Ther 2005; 4(4):400-406.
9. Wang MY, Zhao Y, Zhang ST, Chen XQ, Du JZ. The regulation of expression for p53 and its target genes in simulate hypoxia. China J Appl Physiol 2013; 29:136-38.
10. Umekita Y, Hiipakka RA, Liao S. Rat and human maspins: structures, metastatic suppressor activity and mutation in prostate cancer cells. Cancer Lett 1997; 113:87-93.
11. An ZF, Zhao K, Wei LN, Wang ZJ, Li SH, Wei L, Wei DB. p53 gene cloning and response to hypoxia in the plateau zokor, Myospalax baileyi. Animal Biology 2018, DOI: 10.1163/15707563-18000004.
12. Resnick MA, Inga A. The expanding universe of p53 targets. Proc Natl Acad Sci USA 2003; 100:9934-39.

LETTER TO THE EDITOR

HIGH QUALITY NURSING OF CHILDREN WITH PNEUMONIA COMPLICATED WITH HEART FAILURE

SL. FU[1], CH. SUN[1], XX. SHANG[1] and XS. LIU[2]

[1]The Second Ward of Paediatric Department, The 2nd Affiliated Hospital of Harbin Medical University, Harbin, Heilongjiang, China; [2]Nursing Department, The 2nd Affiliated Hospital of Harbin Medical University, Harbin, Heilongjiang, China

Received January 29, 2019 – Accepted March 26, 2019

Children with severe pneumonia often have heart failure. This study explored the clinical effect of high quality nursing intervention on children with pneumonia complicated with heart failure. In the study, 96 children with pneumonia complicated with heart failure were selected and randomly divided into a conventional nursing group (n=48) and a high quality nursing group (n=48). Based on the conventional nursing, the children in one group were given high quality nursing, and comprehensive nursing was carried out in aspects such as respiratory tract, medication, psychology and diet. Then, the heart rate, respiratory rate, heart failure correction time, hospitalization time, cost and nursing satisfaction were compared between the two groups. The results showed that the heart rate of the high quality nursing group was 145.37±8.72 times/min and the respiratory rate was 45.65±6.08 times/min, which were significantly lower than those of the conventional nursing group (P<0.05). The correction time of heart failure was about 32 h in the high quality nursing group, and the length and cost of hospitalization were significantly lower than those in the conventional nursing group (P<0.05). The nursing satisfaction of the patients' family members in the high quality nursing group was also higher (P<0.05). This study shows that high quality nursing can promote the recovery of children with pneumonia complicated with heart failure, and is worth popularizing widely in clinics.a

To the Editor,

Pneumonia is a common disease in infants and young children, and is one of the main causes of death (1, 2), accounting for more than 14% of the deaths of under five year olds (3). The average treatment cost of pneumonia in children is 5722 yuan (4). Severe pneumonia is likely to cause heart failure (5), and its treatment is difficult. High quality nursing can improve the therapeutic effect of diseases. Li et al. (6) found that close observation of the condition of sick children in the nursing process, keeping the respiratory tract open, controlling the inflammatory reaction, and strengthening communication with the families of sick children could well promote the recovery of child patients. Xiang (7) studied 60 children and found that high quality nursing measures could significantly improve the nursing satisfaction of the family members and the clinical effect. Yan (8) found that 80 sick infants and young children recovered quickly and spent less time in hospital after high quality nursing intervention, which was significantly different from the control group. This study investigated the clinical effect of high quality

Key words: pediatric pneumonia; heart failure; conventional nursing; high quality nursing

Mailing address:
Dr Xuesong Liu,
Nursing department,
The 2nd Affiliated Hospital Harbin Medical University,
Harbin, Heilongjiang, 150086, China
e-mail: xuesongl_xs@126.com

0393-974X (2019)

nursing of children with pneumonia complicated with heart failure. The heart rate and respiratory rate after receiving nursing were compared to prove the value of high quality nursing, and this work provides some theoretical bases for its clinical promotion.

MATERIALS AND METHODS

General data

Ninety-six patients who were admitted to the second affiliated hospital of Harbin Medical University, Heilongjiang, China, between January 2017 and June 2018, and were confirmed with pneumonia complicated with heart failure were selected. Children with other severe complications were excluded. The research purpose and methods were explained to the families of the children, and the families signed informed consent. The observation record of the subjects started from the day of admission to the discharge day. They were randomly divided into a conventional nursing group and a high quality nursing group, with 48 cases in each group. There were 23 males and 25 females in the conventional nursing group (average age 1.6±0.8 years) with a disease course of 4.2±1.3 days. There were 27 males and 21 females in the high quality nursing group (average age 1.8±0.6 years) with a disease course of 3.9±1.2 days. There was no significant difference in general information between the two groups ($P > 0.05$), therefore the results were comparable.

Conventional nursing methods

Conventional nursing methods included giving the sick children vasoactive drugs, diuretic cardiac therapy, and appropriate oxygen intake. The nursing staff provided clean and tidy wards, which were regularly ventilated and disinfected, and adjusted with appropriate temperature and humidity, and made sure that the patients had enough sleep. The changes of vital signs in patients was given attention, and emergency preparation was made. The nursing staff were familiar with the usage and dosage of drugs and adverse reactions and closely observed the situation of children after medication. In addition, attention was paid to whether the respiratory tract was smooth or not and the family members of children were asked to provide more meals a day but less food at each.

High quality nursing methods

As well as conventional nursing, the high quality nursing group was also given the following attention.

The first measure was to fully understand the condition of illness. In order to provide better nursing for children, the nursing staff needed a full understanding of their conditions. After admission, the nursing staff recorded onset time, medical history and family medical history of the children and determined the pathogenesis. Symptoms such as cough and breathing were observed as well as whether there was diarrhea, vomiting and other phenomena and the growth of children and data such as heart rate and breathing frequency were recorded.

The second measure was high quality nursing for the respiratory tract. The oxygen demand of the heart of children with pneumonia complicated with heart failure was larger, therefore nursing staff took the respiratory tract nursing seriously. Children were arranged in different wards as far as possible to avoid cross infection and the wards were disinfected with ultraviolet ray every day. As the children were short of breath and easy to have respiratory tract secretion, ultrasonic atomization therapy was adopted to keep the respiratory tract unblocked (9). According to the symptoms, oxygen concentration was controlled lower than 40%, and the flow rate of oxygen was 0.5-1 L/min; the flow rate was adjusted in time when hypoxia improved.

Next was high quality nursing for psychology. According to the diagnosis result, the disease-related knowledge and precautions were explained to the children and their families to alleviate their tension and anxiety and increase the trust of children and their families in health care workers. If the children had the ability to understand, the caregiver could communicate with them in a gentle way. The nursing staff relaxed the children and relieved their pain and anxiety by means of storytelling. Appropriate measures were taken to divert the children's attention during injections to ensure the smooth progress of the treatment.

The fourth measure was high quality nursing for medication. The young children might have poisoning after medication because of the underdevelopment of the immune system, so medication was paid special attention to. Medication was conducted under the guidance of nursing staff, and the family members were forbidden to mix drugs. The dosage strictly followed the weight of the children, and the type and amount of drugs was adjusted by observing the changes of the signs and symptoms of the patients. After

the injection of digitalis preparation, the heart rate was tested. If the heart rate decreased to below 100/min, nursing staff stopped the medication immediately and reported to the attending physician for treatment. During the use of diuretics, the liquid inflow and outflow was recorded all day to evaluate the water electrolyte status. Children with emotional overreaction were given sedative drug treatment to prevent adverse symptoms.

The fifth measure was high quality nursing for diet. The children were fed with liquid and semi-liquid food which is easy to digested and has high nutrition. The intake of sodium salt was controlled (10). They were asked to drink a lot of water and have more meals a day but less food at each to avoid obstruction of breathing due to overeating. In order to prevent coughing, they were picked up when being fed. Children who were unable to eat were given intravenous injections to maintain their nutrition. They were encouraged and guided to eat potassium-containing foods such as bananas and milk.

The last measure was high quality nursing for special conditions. The first special condition was infection. Being bedridden for a long time might cause infection because of their weak immunity. Therefore, nursing staff guided and helped their family members to do cleaning. In order to prevent pressure sores, the pressed site of children with edema was regularly massaged. Special attention was paid to diet to prevent intestinal infections. The second special condition was high or low temperature. When the body temperature was too high, timely cooling treatment and sedation measures were adopted, and sufficient water was supplied. When the body temperature was lower than 35□, heat preservation and vital signs were paid attention to. The third condition was decreased cardiac output. The amount of activity was arranged according to different conditions of the children. Children with mild symptoms did some slight physical activities. Children with severe symptoms were asked to remain in bed and were treated by cardiac stimulants if necessary.

Observation index

i. Heart rate and breathing rate: The heart rate and breathing rate were measured by nursing staff 48 h after treatment.

ii. Heart failure correction time: Heart failure was considered being corrected when the heart rate stabilized at 120 ~ 160 times/min, breathing rate stabilized at 40 ~ 60 times/min, there was no murmur in the lung, and the growth of the liver stopped.

iii. Hospitalization time and hospitalization cost.

iv. Nursing satisfaction. Nursing satisfaction was investigated by a questionnaire with 5 questions which was answered by family members of the children. There were three options, satisfied, basically satisfied and unsatisfied, corresponding to 20 points, 15 points and 10 points; the total score was 100 points. The content of the questionnaire included:

Are you satisfied with the nursing staff's attitude?

Are you satisfied with the nursing staff's operation skill level?

Are you satisfied with the nursing staff's medication guidance?

Table I. *Comparison of heart rate and respiratory rate in children before and after treatment.*

		Conventional nursing group (n=48)	High quality nursing group (n=48)
Heart rate (times/min)	Before treatment	186.29±11.68	187.16±11.79
	After treatment	165.28±8.46*	145.37±8.72*#
Respiratory rate (times/min)	Before treatment	79.34±7.68	79.59±8.34
	After treatment	61.37±6.21*	45.65±6.08*#

** P < 0.05 compared to before treatment; # P < 0.05 compared to the conventional nursing group*

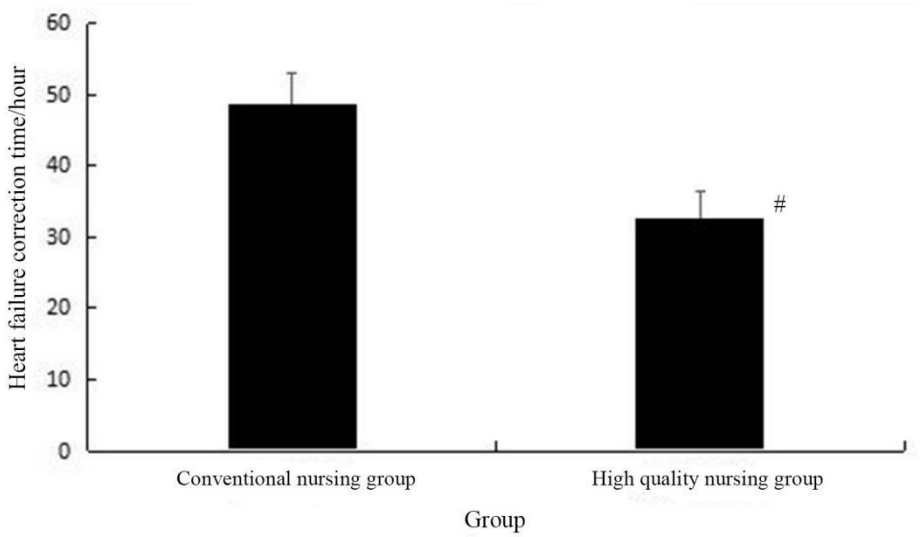

Fig. 1. *Comparison of heart failure correction time between the two groups.*

Table II. *Comparison of hospitalization time and costs between the two groups.*

	Conventional nursing group (n=48)	High quality nursing group (n=48)
Hospitalization time/hour	12.34±2.67	7.16±1.12#
Hospitalization cost/yuan	4203.87±330.63	3212.66±261.75#

 # P < 0.05 compared to the conventional nursing group.

Are you satisfied with the dietary guidance of nursing staff?

Are you satisfied with the nursing staff's treatment under special circumstances?

A total score between 75 points and 100 points was evaluated as satisfied, a total score between 50 points and 75 points was evaluated as basically satisfied, and a total score below 50 points was evaluated as unsatisfied.

Statistical method

SPSS17.0 was used for statistical analysis. Measurement data were expressed as and processed by *t*-test. Counting data were processed by χ^2. P<0.05 indicated that there was a significant difference.

RESULTS

Comparison of heart rate and respiratory rate

As seen in Table I, there was no significant difference in heart rate and respiratory rate between the two groups before treatment (P > 0.05). After treatment, the heart rate and respiratory rate of the sick children in both groups decreased significantly (P < 0.05). After treatment, the two groups were compared. The heart rate of the conventional nursing group was 165.28±8.46 times/min, which was significantly lower than 145.37±8.72 times/min in the high quality nursing group (P < 0.05). Similarly, the respiratory rate of the high quality nursing group was

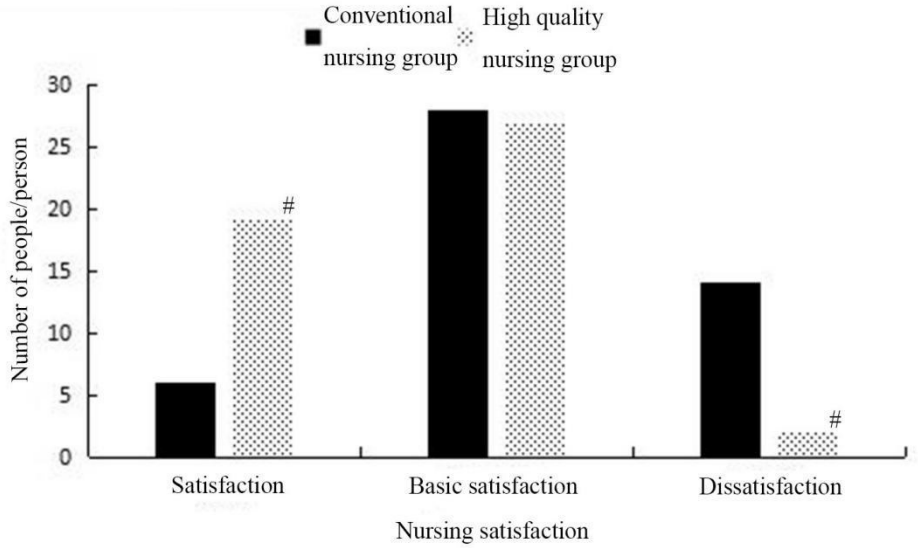

Fig. 2. *Comparison of nursing satisfaction between the two groups. #P < 0.05 compared to the conventional nursing group.*

45.65±6.08 times /min, which was significantly lower than that of the conventional nursing group (P < 0.05). The results showed that the sick children in the high quality nursing group recovered well under the care of nursing staff and the clinical effect of the high quality nursing group was better.

Comparison of heart failure correction time

Fig. 1 shows the comparison of the correction time of heart failure between the two groups. The heart failure symptoms of children in the conventional nursing group were corrected 48 hours after admission, while children in the high quality nursing group were corrected about 32 hours after admission, much earlier (P < 0.05). There was a significant difference between the two groups, which indicates that high quality nursing has a better clinical effect on pneumonia complicated with heart failure.

Comparison of hospitalization time and hospitalization cost

The hospitalization time of the high quality nursing group was 7.16±1.12 hours and the hospitalization cost was 3212.66±261.75 yuan, which were significantly lower than those of the conventional nursing group (P < 0.05) (Table II). This demonstrates that the recovery of the children under high quality nursing was faster. Hospitalization costs were lower because patients completed treatment in a shorter time and recovered faster. Shorter hospitalization time and lower hospitalization costs also proved the good effect of high quality nursing.

Comparison of nursing satisfaction

According to the nursing satisfaction (Fig. 2), the number of patients who were satisfied with the nursing in the high quality nursing group was 19, significantly higher than that in the conventional nursing group (P < 0.05), and the number of patients who were dissatisfied with the nursing in the high quality nursing group was 2, significantly lower than that in the conventional nursing group (P < 0.05). This indicated that the nursing effect of the high quality nursing group was better, so the satisfaction of the family members was higher.

DISCUSSION

Infantile pneumonia is a pulmonary inflammation caused by many pathogens or other factors, which can lead to cardiac hypoxia, myocardial contraction weakness, and increased heart burden. When cardiac output cannot meet the metabolic requirements of the body, congestion of the pulmonary or systemic

circulation will cause heart failure. In children, pneumonia complicated with heart failure has a fast onset and a high fatality rate. Clinical findings show that nursing has a great impact on the curative effect of infantile pneumonia.

Traditional routine nursing can play a role in the rehabilitation of children by diuresis, oxygen inhalation, keeping the ward clean and ensuring enough sleep. However, due to the age specificity of children and the difficulty of treatment of pneumonia complicated with heart failure, the role of traditional routine nursing is limited. High quality nursing is a more comprehensive nursing method on the basis of conventional nursing, which can provide all-round intensive care for children, giving considerate consideration to diet, medication, breathing and other aspects. According to the results of this study, there were significant differences in the heart rate, respiratory rate and heart failure correction time between the two groups ($P < 0.05$) and the children who received high quality nursing had shorter hospitalization, less costs ($P < 0.05$) and higher nursing satisfaction.

To sum up, the clinical effect of high quality nursing on children with pneumonia complicated with heart failure is obviously better than that of routine nursing. It can effectively alleviate the illness of children, improve the heart rate, respiratory and heart failure, improve the treatment effect, reduce hospital stay and expenses, and help children recover earlier.

REFERENCES

1. Komurian-Pradel F, Endtz H, Rakoto-Andrianarivelo M, et al. Severity of pneumonia in under 5-year-old children from developing countries: a multicenter, prospective, observational study. Am J Trop Med Hyg 2017; 97(1):68-76.
2. Zampoli M, Mukuddemsablay Z. Adenovirus-associated pneumonia in South African children: Presentation, clinical course and outcome. S Afr Med J 2017; 107(2):123.
3. Rodrigues CMC. Challenges of empirical antibiotic therapy for community-acquired pneumonia in children. Curr Ther Res Clin Exp 2017; 84:e7.
4. Li Y, An Z, Yin D, et al. Disease burden of community acquired pneumonia among children under 5 y old in China: A population based survey. Hum Vacc Immunother 2017; 13(3):1.
5. Corrales-Medina VF, Taljaard M, Yende S, et al. Intermediate and long-term risk of new-onset heart failure after hospitalization for pneumonia in elderly adults. Am Heart J 2015; 170(2):306-312.e6.
6. Li W, An X, Fu M, Li C. Emergency treatment and nursing of children with severe pneumonia complicated by heart failure and respiratory failure: 10 case reports. Exp Ther Med 2016; 12(4):2145-49.
7. Xiang XF. High quality nursing intervention experience of children with pneumonia complicated with heart failure. World Latest Med Inform 2017; 17(4):1-2.
8. Yan Y. Clinical nursing care of children with pneumonia complicated with heart failure. China Health Standard Manag 2017; 8(9):197-98.
9. Yang F. Oxygen-driving and atomized mucosolvan inhalation combined with holistic nursing in the treatment of children severe bronchial pneumonia. Pak J Pharm Sci 2015; 28(4 Suppl)):1477-80.
10. Zec SL, Selmanovic K, Andrijic NL, Kadic A, Zecevic L, Zunic L. Evaluation of drug treatment of bronchopneumonia at the pediatric clinic in Sarajevo. Med Arch 2016;70(3):177-81.

LETTER TO THE EDITOR

ADDITIONAL 4 CASES OF VALSARTAN/IRBESARTAN-INDUCED MELANOMAS?

G. TCHERNEV[1,2] and I. TEMELKOVA[1,2]

[1]Department of Dermatology, Venereology and Dermatologic Surgery, Medical Institute of Ministry of Interior (MVR), Sofia, Bulgaria; [2]Onkoderma- Clinic for Dermatology, Venereology and Dermatologic Surgery, Sofia, Bulgaria

Received March 6, 2019 – Accepted March 27, 2019

To the Editor,

The problematic with medically/drug-induced melanomas acquires increasingly widespread "popularity" and significance (1). Interesting is the fact that drug-induced melanomas occur or are clinically manifested only after defined but relatively equal or similar time intervals after systemic medication with sartans (1-3). Some of these lesions arise as *de novo* melanomas on intact skin (1), while others are based on the transformation of so-called melanocytic nevi or melanoma precursors (2-3). Despite skepticism among the medical community on the possible pathogenetic link between systemic medication and triggering of carcinogenesis, four new probable cases of cutaneous/ocular melanomas occurring during sartans (valsartan / irbesartan) treatment should/could not be ignored (4-7). It should be noted, even more disturbingly, that in one of them, during the long period of intake of sartans (17 years/regarding anamnestic data), in addition to melanoma, development of two additional types of cancers was observed - laryngeal squamous cell carcinoma and prostatic carcinoma (7). In such cases, the hypothesis should be expressed that long-term intake of sartans (valsartan /irbesartan) is likely to pose a risk of developing multiple cancers and probably carries the risk of developing multiple tumor diseases (7).

Some of the data described in the current literature (found by us in a short-term literature review) does not emphasize the concrete pathogenetic relationship between melanomas and sartan medication (ocular and metastatic), but they describe the parallel/possible or stepwise induction of cutaneous/ocular melanomas, which should be clarified (4-7). It is disturbing that one of these cases describes the presence of a much more aggressive simultaneous coexistence between sartans intake and development of three independent types of tumors (7). Even worse and severe than other mentioned cases for possible drug induced melanomas, is the fact that here it regards a metastatic type of melanoma (7).

It is precisely because of this fact that we should think seriously about the real, albeit unofficial at the moment, number of drug-induced melanomas. This reminds rather of the paraphrasing of George Bernard Shaw's thought : "You dream things; you say, "Why?" But I see things before my eyes; and I say "Why not?"

Another not less interesting fact at the moment is the universal and comprehensive voluntary recall for valsartan and irbesartan following the official realization of medical data on pathogenetically justified links between drug intake and tumor generation (and in particular melanomas) (1-3). The forthcoming, but also the already started retrospective analyses should focus on the triggering role of sartans not only

Key words: drug-induced melanoma; irbesartan; valsartan; drug related cancer; ocular melanoma

Corresponding Author:
Prof. Georgi Tchernev,
Department of Dermatology,
Venereology and Dermatologic Surgery
Medical Institute of Ministry of Interior (MVR),
General Skobelev 79, 1606 Sofia, Bulgaria
e-mail: georgi_tchernev@yahoo.de

0393-974X (2019)

DISCLOSURE: ALL AUTHORS REPORT NO CONFLICTS OF INTEREST RELEVANT TO THIS ARTICLE.

in melanoma patients but also in those with other types of tumors, such as renal, prostate or laryngeal carcinomas, for example (7, 8). Data from oncology dispensaries and oncology units would be a good starting point as a source of information concerning possible causally- related connections.

REFERENCES

1. Tchernev G, Temelkova I. Valsartan induced melanoma?! First description in medical literature! Open Access Maced J Med Sci 2018; 6(12):2378-80.
2. Tchernev G, Temelkova I. Drug induced melanoma: irbesartan induced cutaneous melanoma! First description in the world literature! Open Access Maced J Med Sci 2019; 7(1):114-16.
3. Tchernev G, Temelkova I. Irbesartan induced cutaneous melanoma! second case in the medical literature! Open Access Maced J Med Sci 2019; 7(1):121-23.
4. Kuint R, Lotem M, Neuman T, et al. Organizing pneumonia following treatment with pembrolizumab formetastatic malignant melanoma - A case report. Respir Med Case Rep 2017; 20:95-97.
5. Lin Y, Panarelli J. (2015 January/ February). Uveal melanoma masquerading as pigment dispersion syndrome. Challenging cases 2015; (1):39-41.
6. Miraldi V, Singh A, Jeng B, Oetting T. The whites of my eyes have turned blue! EyeNet Magazine/ Morning Rounds 2007(3): online content: https://www.aao.org/eyenet/article/whites-of-my-eyes-have-turned-blue
7. Genova P, Sorce M, Cabibi D, et al. Erratum to "Gastric and rectal metastases from malignant melanoma presenting with hypochromic anemia and treated with immunotherapy". Case Rep Oncol Med 2018; 2018:3142394.
8. Tomos I, Tsilika M, Aggelou E, Karageorgas T, Tsiodras S. An 80-year-old man with hemoptysis and unilateral patchy opacities. Chest 2018; 154(5):e135-38.

LETTER TO THE EDITOR

OPTIMIZED MID-LONG TERM MANAGEMENT OF KETOGENIC DIET IN CHILDREN WITH REFRACTORY EPILEPSY

GM. SHENG, P. YIN, M. LV, YH. ZHU, BM. LI, GF. LEI and H. LIU

Department of Pediatrics, Qilu Hospital of Shandong University, Ji'nan, China Received December

Received December 3, 2018 – Accepted March 28, 2019

To the Editor,

According to the International League Against Epilepsy (ILAE), intractable epilepsy is defined as failure of adequate attempts of two tolerated, appropriately chosen and used antiepileptic drug schedules (whether as monotherapies or in combination) to achieve sustained seizure freedom (1). Intractable epilepsy cases in childhood account for approximately 20-30% of all epileptic cases (2). The Ketogenic diet (KD) is one of the effective methods for the treatment of intractable epilepsy in children (3). In foreign countries, KD therapy has been used in treating intractable epilepsy for more than 90 years, while this was only started in 2004 in China (4). In China, KD therapy is affected by many factors. Determining how to timely and effectively manage children and the family in a mid-long term and improve the efficacy of KD and its compliance are the keys to ensure the smooth progress of KD. In the present study, the effect of KD on children with intractable epilepsy, the control rate of epilepsy and the influencing factors of compliance were first analyzed based on clinical data. Then, the problems that were found were discussed to find a solution, and mid-long term management plans were established. Subsequently, these patients were managed according to mid-long term management plans, and were evaluated.

MATERIALS AND METHODS

Subjects

This study was conducted in accordance with the Declaration of Helsinki and approved by the Ethics Committee of Qilu Hospital of Shandong University. Written informed consent was obtained from the patients or patients' parent/carer. Children with intractable epilepsy, who received KD therapy in our hospital from 2011 to 2015, were included in the present study. The basic management plan group comprised of 57 children (January 2011-August 2012), of whom 32 were boys and 25 were girls. The optimized management plan group comprised of 52 children (September 2012-April 2014), of whom 28 were boys and 24 were girls. All patients met the diagnostic criteria for intractable epilepsy established by the International League Against Epilepsy. Clinical epilepsy types include Doose syndrome, Dravet syndrome, L-G syndrome, infantile spasm and refractory epilepsy. Before enrollment, all patients had frequent epileptic seizures, which were not effectively controlled before the initiation of KD. Among the patients, the frequency of epileptic seizures was Dravet syndrome > 4 times/month, and the frequency of other types of epileptic seizures was > 7 times/week.

Inclusion criteria: intractable epilepsy patients under 14 years of age; patients who received KD treatment for the first time; patients whose parents provided a signed

Key words: ketogenic diet; children; refractory epilepsy; mid-long term management; efficacy assessment

Corresponding Author:
Hui Liu,
Department of Pediatrics,
Qilu Hospital of Shandong University,
No. 107 of Wenhua West Road,
Lixia District, Ji'nan 250012, China
Tel.: +86 18560086179 - Fax: +86 0531 82169114
e-mail: huiliudr@163.com

0393-974X (2019)

informed consent; the continuous treatment of KD lasted for more than 1-9 months; patients fulfilled the criteria in nine months of follow up.

Exclusion criteria: patients with metabolic disorders of fat and ketone body; patients with serious liver, kidney or pulmonary insufficiency; patients with long QT syndrome or serious cardiovascular diseases; patients with hyperlipidemia and urinary calculi (5).

In our study, patients who received mid-long term management of KD had more than three months of treatment and more than nine months of follow-up and management.

Research methods

KD management in the basic management plan group: Using the classic KD plan, fat: (carbohydrate + protein) = 4:1. Fasting lasted 21-27 hours. Children with KD were given laboratory and examination instructions by the physician on duty on the same day, and the dietician was responsible for formulating the meal plan and follow-up.

KD management in the optimized management plan group: Optimization of the KD management team: Professional nurses and follow-up nurses were included, and an information communication platform was constructed. The staffing included professional doctors, professional nurses, dieticians and follow-up nurses. The management system was formulated, and the workload was reasonably divided. Doctors were responsible for interpreting the condition and formulating the KD plan, while professional nurses were responsible for KD bed management, specimen collection and KD health education, and participated in the improvement and production of the KD diet. Dieticians were responsible for formulating the diet plan and food preparation adjustment, and teaching parents to use the food preparation software. Follow-up nurses were responsible for the short-term and long-term follow-up during the KD treatment, managing the equipment in the interview room and communicating with patients by telephone, network, QQ and WeChat.

Optimization of the KD scheme: Add 2:1 diet structure, use flexibly according to the specific situation of children. For patients of 6-18 months old, no fasting, transition from normal diet to KD; for patients of 18 months to 4 years old, fasting for 12 hours, KD ratio from 2:1; for patients of > age 4 years old, fasting for 15-18 hours, KD ratio from 2:1, water intake was no longer limited during fasting. The KD diet was modified with reference to the "ketogenic diet preparation software", and the individualized, dynamic and regionalized management of children with KD was carried out. Professional nurses and nutritionists helped parents perform the fine adjustment of KD. The diet was matched according to the geographical distribution characteristics and living habits of the disease population, and a suitable meal compound was sought according to local food sources and types in the resident region of the patient.

Optimization of health education and long-term follow-up system: Follow-up nurses were designated, follow-up indexes were divided, the methods of communication were determined, and the time of follow-up was fixed. A KD public lesson was held monthly to promote the families of children to exchange and encourage each other (6). Parents' daily records were established, and the parents were guided to closely observe and manage the situations of the epileptic seizures. Previous studies have revealed that recording the situations of epileptic seizures in the form of a diary was an extremely important method to monitor epileptic seizures (7, 8). Professional nurses were responsible for developing various food nutrition ingredient tables, including the "Reference Intake of Dietary Nutrients in Chinese Residents ", "the table of Components of Common Nutrient Extenders", and "the table of Components of Common Food and Some High-fat foods." These tables demonstrate the components and contents of various foods, and the requirements of people of various ages, which are convenient for parents.

Monitor and follow-up: During the KD treatment, blood glucose and blood ketone were daily monitored (q6h). The levels of blood glucose and ketone of patients were re-examined twice every week and both levels were maintained at 3-5 mmol/L after discharge. Blood and urine routine test, liver and renal function, blood fat, and uric acid were tested every month, in order to adjust KD treatment as precisely as possible. Data were acquired and statistically analyzed before treatment, and at months 1, 3, 6 and 9 post-treatment.

Evaluation indexes

The statistical data at different time periods of KD were compared between the basic management plan group and optimized management plan group. The effect of the mid-long term management of KD was evaluated through the

effective rate (refers to the rate of patients whose control of epileptic seizures was ≥50%) and compliance rate (refers to the proportion of children who continued to receive KD, accounting for the total children in this group). The evaluation of the curative effect of KD was based on the Engel classification: grade I, complete remission of seizure after treatment; grade II, after treatment, the reduction of the number of seizures was ≥90%; grade III, after treatment, the reduction of the number of seizures was ≥50%; grade IV, after treatment, the reduction of the number of seizures was <50%. After treatment, children who achieved grades I, II and III of the curative effect were regarded as effective, while children who achieved grade IV of the curative effect and children who withdrew from the treatment were regarded as ineffective (9). The effective rate of epilepsy control in this study was (GradI+ Grad II+ GradIII)/total ×100%.

Statistical analysis

The input and statistical analysis of all data were performed using statistical software package SPSS 16.0. Count data were compared using *Chi*-squared test. Fisher's exact probability was used for the relevant data, $P<0.05$ was considered statistically significant.

RESULTS

In our study, through our retrospective analysis in the basic management plan group, we found that at the initial phase of KD management, we did not set up an established team, and did not made an overall observation and follow-up scheme, the ratio of KD food was inflexible, the kinds of KD foods were very simple. We also observed common gastrointestinal side effects such as nausea, vomiting and constipation. The compliance of patients and their parents were not to our satisfaction; some of our patients ceased KD treatment for personal reasons. After we discovered such issues in the basic management plan group, we made our optimized mid-term management plans and gave the patients enrolled in the optimized management plan group an overall management. And we compared the results in the two groups.

Basic situation of children treated with KD

Differences in gender, onset age, course of the disease, age of KD, form of seizures, and drugs used at the beginning of KD between the optimized management plan group and basic management plan group were not statistically significant

Comparison of the effective rate of KD between the optimized management plan group and basic management plan group

The effective rate (control rate was >50%) of KD at the first, third, sixth and ninth month was 90.4%, 73.1%, 65.4% and 38.5%, respectively, in the optimized management plan group , and 63.2%, 45.6%, 38.6% and 21.1%, respectively, in the basic management plan group, and the differences between these two groups were statistically significant. Furthermore, the effective rates were significantly higher in the optimized management plan group than in the basic management plan group

According to the classification of the control rate of epilepsy, the proportion of children who achieved control grades I, II and III in the optimized management plan group was 19.2%, 30.8% and 40.4%, respectively, at the first month, 26.9%, 19.2% and 26.9%, respectively, at the third month, 32.0%, 11.5% and 21.2%, respectively, at the sixth month, and 21.2%, 9.6% and 7.6%, respectively, at the ninth month (Table I).

Comparison of the compliance rate of KD between the optimized management plan group and basic management plan group

The compliance rate of KD at the third, sixth and ninth months was 94.2%, 78.8% and 63.5%, respectively, in the optimized management plan group, and 82.5%, 47.4% and 28.1%, respectively, in the basic management plan group, and the differences between these two groups were statistically significant (Table II).

Comparison of blood biochemical indexes and side effects during KD treatment between the two groups

During KD treatment, blood glucose and ketones were monitored using peripheral blood during their hospital stay, and the levels of all maintained within 3-5 mmol/L. However, different degrees of adverse reactions were observed in both groups. The main adverse reactions were mainly vomiting, diarrhea,

Table I. *Engell classification of epilepsy control rate in two groups of KD children.*

Diet duration	Group	EngellI	EngellII	EngellIII	EngellIV	χ^2 value	*P* value
	Optimized management plan group	10(19.2)	16(30.8)	21(40.4)	4(9.6)		
1 months	Basic management plan group	9(15.7)	6(10.5)	20(35.1)	21(23.8)		0.003
	Optimized management plan group	14(26.9)	10(19.2)	14(26.9)	8(15.4)	17.2	
3 months	Basic management plan group	8(14.0)	4(7.0)	14(24.6)	21(36.8)	72	0.008
	Optimized management plan group	17(32.0)	6(11.5)	11(21.2)	7(13.5)		
6 months	Basic management plan group	9(15.7)	2(3.5)	11(19.3)	18(31.6)		0.003
	Optimized management plan group	11(21.2)	5(9.6)	4 (7.6)	13(25.0)	20.6	
9 month	Basic management plan group	7(12.2)	3(5.2)	2 (3.5)	4(10.5)	38	0.001

KD: ketogenic diet

Table II. *Comparison of the compliance rate of KD between the optimized management plan group and basic management plan group.*

	First month	Third month	Sixth month	Ninth month
Optimized management plan group (n=52)	52/52(100%)	49/52(94.2%)	41/52(78.8%)	33/52(63.5%)
Basic management plan group (n=57)	57/57(100%)	47/57(82.5%)	27/57(47.4%)	16/57(28.1%)
χ^2 value		3.589	11.48	13.76
P value		0.035	0.001	<0.001

KD: ketogenic diet

Table III. *Comparison of the main adverse reactions during KD treatment between the optimized management plan group and basic management plan group*

Adverse reactions	Optimized management plan group (times)	Basic management plan group (times)	χ^2 value	*P* value
Nausea,vomit,diarrhea,	11	28	9.258	0.002
Constipation	6	11	1.244	0.265
Hyperlipidemia	4	6	0.262	0.609
Hypoproteinemia	2	5	1.098	0.295
Urine crystallizes	1	0		
Renal calculus	0	1		
Fatty liver	0	1		

KD: ketogenic diet

constipation and hyperlipidemia, among which nausea, vomiting and diarrhea showed statistical differences between groups (χ^2=9.258, P=0.002, Table III).

The post-discharge monitoring results showed that the mean values of blood sugar and blood ketone in the two groups were maintained in the normal range. Liver function was normal at regular review in all the cases in this study, and no obvious abnormalities were found. However, there were six cases of hyperlipidemia and one case of fatty liver in the basic management plan group, and four cases of hyperlipidemia in the optimized management plan group.

DISCUSSION

Optimizing KD management scheme can improve epilepsy control rate. Suo et al. (4) reported that among the 317 children who were treated with KD, at three, six and 12 months of KD treatment, the rate of patients who achieved a >50% reduction in seizures was 35.0%, 26.2% and 18.6%, respectively, including 20.8%, 13.6% and 10.7% of patients without seizures. The result of the present study was higher than that reported by Suo et al. (4). In spite of this, the tendency of effective rate of epilepsy control were decreasing over time. Therefore, it is important to make long-term management strategies for KD treatment for those affected families.

Optimizing KD management can improve KD compliance. A summary of 10 studies in the literature on the KD treatment of children with intractable epilepsy, which was reported by Keene (10), revealed that children who underwent three, six and 12 months of treatment accounted for 79.9%, 60.6% and 35.9%. In this study, KD compliance was significantly improved. This is because we have formulated effective preventive measures and optimized the health education plan according to the main factors affecting compliance. Specifically, it includes discussing the expectations of KD with parents, not only to reduce seizures, but also to minimize drug treatment and improve cognition (11). The parents were informed at the same time that strict adherence to the diet is key to it being successful and effective, and the patients and their parents need to be patient and cooperative (12).

During treatment, adverse reactions were observed in both groups, mainly presenting with vomiting, nausea and diarrhea, however, these symptoms disappeared over time. We summarized the adverse effects in the starting phase of treatment, analyzing them and making strategies to avoid these adverse reactions, to achieve effective management.

ACKNOWLEDGEMENTS

This study was supported by multi-dimensional health analysis and intervention study of left-behind children in rural areas of Shandong Province underthe background of new era (No.: 18-ZZ-SH-04).

We appreciate the help from Dr Xiao-Fan Yang forthe improvement of our manuscript.

REFERENCES

1. Kwan P, Arzimanoglou A, Berg AT, et al. Definition of drug resistant epilepsy: consensus proposal by the ad hoc Task Force of the ILAE Commission on Therapeutic Strategies. Epilepsia 2010; 51:1069-77.
2. Ni FF, Li CR, Liao JX, Wang GB, Lin SF, Xia Y, Wen JL. The effects of ketogenic diet on the Th17/Treg cells imbalance in patients with intractable childhood epilepsy. Seizure 2016; 38:17-22.
3. Padmanabha H, Suthar R, Sankhyan N. Acta Neurol Scand. A randomized controlled trial of the ketogenic diet in refractory childhood epilepsy. Acta Neurol Scand 2018; 137:151.
4. Suo C, Liao J, Lu X, et al. Efficacy and safety of the ketogenic diet in Chinese children. Seizure 2013; 22:174-78.
5. Caraballo RH, Flesler S, Armeno M, et al. Ketogenic diet in pediatric patients with refractory focal status epilepticus. Epilepsy Res 2014; 108:1912-16.
6. Freeman JM, Kossoff EH, Freeman JB. The Ketogenic diet, a Treatment for Children and Others with Epilepsy M, 4th ed. New York: Demos Medical Publishing, 2009:65-66.
7. van der Louw E, van den Hurk D, Neal E, et al. Ketogenic diet guidelines for infants with refractory epilepsy. Eur J Paediatr Neurol 2016; 20:798-809.
8. Pires ME, Ilea A, Bourel E, et al. Ketogenic diet for infantile spasms refractory to first-line treatments: an

open prospective study. Epilepsy Res 2013; 105:189-94.
9. Engel JJ. Surgery for seizures. N Engl J Med 1996; 334:647-53.
10. Keene DL. A systematic review of the use of the ketogenic diet in childhood epilepsy. Pediatr Neurol 2006; 35:1-5.
11. Kossoff EH, Zupec-Kania BA, Auvin S, et al. Optimal clinical management of children receiving dietary therapies for epilepsy: Updated recommendations of the International Ketogenic Diet Study Group. Epilepsia Open 2018; 3:175-92.
12. Liao JX, Lan X. Implementation of ketogenic diet therapy in refractory epilepsies. Epilepsy J 2016; 2:111.

LETTER TO THE EDITOR

THE EFFECT OF ULINASTATIN, A BROAD-SPECTRUM PROTEASE INHIBITOR, ON THE EXPRESSION OF IL-6, CRP AND NGAL IN PATIENTS UNDERGOING GYNECOLOGICAL LAPAROSCOPIC SURGERY

WY. LI, RP. LI and YZ. GUO

Department of Gynaecology, Lanzhou University Second Hospital, Lanzhou City, China

Received January 16, 2019 - Accepted March 29, 2019

To the Editor,

Gynecological laparoscopic surgery has been widely used. Compared with traditional laparotomy, it is associated with a lower level of inflammatory response (1, 2). However, due to the use of CO to induce pneumoperitoneum in laparoscopic surgery, the establishment and removal of pneumoperitoneum may lead to stress and even ischemia-reperfusion injury in related tissues and organs (3). It has been reported that different anesthesia methods and drugs can alleviate post-operative stress (4). Therefore, intervention measures can be given before or during surgery to protect the immune function of patients. As a result, stimulation-induced stress in the body can be reduced to maintain the internal homeostasis and promote the postoperative recovery of patients.

As a broad-spectrum protease inhibitor purified from fresh urine of healthy adult males, ulinastatin can inhibit the activity of hydrolytic enzymes (5, 6), and stabilize cell membrane, inhibit the activity of lysosomal enzymes, block the release of inflammatory mediators, scavenge oxygen free radicals, and inhibit the synthesis of myocardial inhibitors, thus protecting endothelial cells, improving microcirculation and tissue perfusion, and protecting organs (7). Therefore, by detecting the change in the serum levels of interleukin-6 (IL-6), CRP (C-reactive protein) and NGAL (Neutrophil gelatinase-associated lipocalin) in patients undergoing gynecological laparoscopic surgery, this study aimed to clarify whether ulinastatin can protect renal function and reduce inflammatory stress in the body, thus providing a theoretical basis for the clinical application in the perioperative period.

MATERIALS AND METHODS

Patients

Fifty patients cases undergoing total laparoscopic hysterectomy and double appendix resection under general anesthesia in Lanzhou University Second Hospital from July 2017 to July 2018 were selected for the study. The patients were randomly divided into group A (ulinastatin group) and group B (control group), with 25 cases in each group. Group A were given 100 mg ulinastatin and 100 mL normal saline via 30 min of intravenous infusion before anesthesia, while group B were given 100 mL normal saline via 30 min of intravenous infusion before anesthesia. This study was approved by the Ethics Committee of Lanzhou University Second Hospital, and all patients and their families were informed of the purpose and significance of the study before the informed consent was signed.

Inclusion criteria: ASA grade I or II; age 40-65 years; weight 50-70 kg; height 155-170 cm; no immune system or inflammatory diseases.

Key words: ulinastatin; laparoscopic surgery; serum inflammatory factors; stress response

Corresponding Author:
Dr Yuzhen Guo,
Department of Gynaecology,
Lanzhou University Second Hospital,
No. 82 Cuiyingmen, Chengguan District,
Lanzhou, Gansu province, China
e-mail: guo_yuzhen2001@yeah.net

0393-974X (2019)

Exclusion criteria: abnormal cardiopulmonary function and biochemistry test results, allergic to ulinastatin, and open surgery.

Methods of anesthesia

After entering the operating room, patients were tested for ECG (electrocardiogram), SpO_2 (blood oxygen saturation) and BP (blood pressure) before an intravenous channel was established via artery puncture to induce local anesthesia with infusion of 1% lidocaine. During the infusion of 1% lidocaine, invasive arterial pressure was continuously monitored. Furthermore, the subjects in Group A received intravenous infusion of 200 mg ulinastatin (Guangdong Tianpu Biochemical and Pharmaceutical Co., Ltd., China) and l00 mL normal saline for 30 min before anesthesia, while the subjects in group B received intravenous infusion of 100 mL saline for 30 min before anesthesia. Subsequently, anesthesia was induced using 0.3-0.5 ug/kg of Sufentanil, 0.05 mg/kg of midazolam, 0.2-0.4 mg/kg of etomidate and 0.15 mg/kg of cis-atracurium. After the successful induction of anesthesia, a laryngeal mask (PenIon, SP2 anesthesia machine, Sleda Medical Supplies (Huizhou) Co., Ltd., China) was inserted into the larynx of the patient and connected to the anesthesia machine to initiate mechanical ventilation. During the operation, the oxygen flow rate was set to 1.5L/min, the tidal volume was set to 6-8mL/kg, and the respiratory rate was set to 10-14 times/min. Perioperative anesthesia was maintained by intravenous infusion of propofol (6mg/(kg·h)) and inhalation of sevoflurane (1-2%), supplemented with appropriate muscle relaxants and analgesics. During surgery, BP, HR (heart rate), and MAP (mean arterial pressure) were maintained within 30% of the baseline value, $P_{et}CO_2$ was maintained between 35 and 45 mmHg, and laparoscopic pneumoperitoneal pressure was maintained between 10 and 12 mmHg. Intravenous infusion during the perioperative period was carried out using 5mL/(kg·h) of sodium lactate Ringer's solution (JSCK, China). Subsequently, post-operative analgesia was carried out using patient-controlled intravenous analgesia (PCEA) with 100 mL of solution containing 100 ug sufentanil + l0 mg, Azasetron. During PCEA, the background dose was 1.5mL/h, the additional dose was 3.5mL/h, the locking time was 15 min, and the VAS (Visual Analogue Scale) score was maintained at < 3 points.

VAS pain scores: 0, no pain; 1-3, a tolerable mild pain that does not affect sleep; 4-6, a moderate pain that can affect sleep and should be treated; 7-10, a severe and intolerable pain that seriously affects sleep and appetite.

Sample collection

3-5 mL peripheral venous blood samples were collected from all subjects in the two groups at 3 time points: before surgery (T_0), at the end of surgery (T_1) and at 24 h after surgery (T_2). The serum levels of IL-6, CRP and NGAL in the peripheral venous blood samples were measured. The samples were conserved at -80°C until use.

Observational indicators

General data and surgery-related indicators: age, weight, height, surgery time, bleeding volume, and VAS scores on the first day after surgery (8). Perioperative monitoring indicators: MAP and HR were recorded before the induction of anesthesia, immediately after the insertion of laryngeal mask, at 10 min post-surgery, at 30 min post-surgery, and when the laryngeal mask was removed after the surgery. The parameters of arterial blood gas (pH, PaO_2, $PaCO_2$, HCO^{3-}, and K^+) were recorded at 30 min after surgery and analyzed. Peripheral venous blood samples collected at T_0, T_1 and T_2 were placed in heparin anticoagulant tubes, diluted with a PBS (Phosphate Buffer Saline) buffer (Semerfer, China) and centrifuged in a low-speed centrifuge (Type SC-04, Anhui Zhongke Zhongjia Scientific Instrument Co., Ltd., China). The serum levels of IL, CRP and NGAL were measured by double antibody enzyme-linked immunosorbent assay (ELISA). Detection kits for IL-6, CRP and NGAL (Shanghai Huzhen Industrial Co., Ltd., China) were used, respectively.

Samples were left at room temperature 4 h before detection. 100 µl sample dilution solution was added to each test well in the enzyme label plate, followed by 50 µl standard solution (containing reagents), negative and positive control, and serum samples to be tested, then incubated with an oscillator at room temperature for 2 h, and reacted with antigen and antibody, followed by washing three times. Then 200 µl ELISA was added, and the sample was again incubated at room temperature for 2 h. After washing, 200 µl of substrate was added, the sample was incubated in the dark for 30 min and then 50 ul termination solution was added. The absorbance value (OD value) of each well was measured by enzyme labeling instrument (Therm Company, USA). After establishing the standard curve, the levels of IL-6, CRP and NGAL in each sample were calculated.

Statistical analysis

SPSS20.0 statistical software was used for the statistical analysis. The measurement data were expressed by mean ± standard deviation. When the data conformed to normal distribution, an independent sample *t*-test was used for the comparison between the two groups, and a repeated variance measurement was used for the comparison at each time point. When the measurement data did not conform to normal distribution, a non-parametric rank sum test was used. $P < 0.05$ was used significant difference between the two groups.

RESULTS

Comparison of clinical data

The ages of patients in the two groups were 52.45±5.35 years and 52.23±5.14 years, respectively; height 159.56±3.9 cm and 159.16±4.86cm, respectively; and weight 61.01±4.52 kg and 61.44±4.99 kg, respectively. There was no significant difference in the three indexes between the two groups ($P > 0.05$). The surgery time was 81.4±15.3 min and 81.24±15.38 min, respectively. The perioperative bleeding volume was 78±14.05 ml and 78.1±13.87 ml, respectively. The daily VAS scores were 1.61±0.23 and 1.48±0.25, respectively. There was no significant difference in the three indexes between the two groups ($P > 0.05$).

Comparison of intraoperative hemodynamics and parameters of arterial blood gas

At time points before the induction of anesthesia, immediately after the insertion of laryngeal mask, 10 min after surgery, 30 min after surgery, and

Table I. *Comparison of MAP and HR at different time points between the two groups.*

Indicator	Group	Before the induction of anesthesia	Immediately after the insertion of laryngeal mask	10 min after surgery	30 min after surgery	During the post-operative removal of laryngeal mask
MAP (mmHg)	Group A	76.89±6.5	74.98±6.08	82.02±6.32	89.78±6.53	81.40±6.36
	Group B	77.01±7.21	75.22±6.38	82.78±6.77	89.89±6.95	81.42±6.89
	P	> 0.05	> 0.05	> 0.05	> 0.05	> 0.05
HR (bpm)	Group A	78.52±8.59	85.04±7.08	73.02±6.49	75.63±6.73	83.95±7.25
	Group B	78.98±8.90	85.43±8.02	73.98±7.93	76.36±6.94	82.16±6.89
	P	> 0.05	> 0.05	> 0.05	> 0.05	> 0.05

Table II. *Analysis and comparison of arterial blood gas parameters between the two groups at 30 min after surgery.*

Group	pH	PaO_2 (mmHg)	$PaCO_2$ (mmHg)	HCO_3^- (mmol/L)	K^+ (mmol/L)
Group A	7.45±0.04	355.31±20.36	37.98±3.02	22.05±2.59	3.79±0.19
Group B	7.29±0.02	357.38±21.58	38.03±3.24	22.79±2.04	3.48±0.18
P	> 0.05	> 0.05	> 0.05	> 0.05	> 0.05

during the post-operative removal of laryngeal mask, there was no significant difference between the two groups in terms of MAP and HR (P > 0.05), as shown in Table I.

There was no significant difference in the parameters of arterial blood gas between the two groups at 30 min after surgery (P > 0.05 (Table II).

Indicators of peripheral venous blood test

As shown in Fig. 1A, there was no significant difference in the levels of IL-6 at T0 between the two groups. Compared with T0, the level of IL-6 at T2 in the two groups increased significantly, and the increase was more significant than that in groups A and group B (p < 0.05).

There was no significant difference in CRP levels between the two groups at T0. Compared with T0, the CRP level of the two groups at T2 was significantly higher, and the CRP level of group B was significantly higher than that of group A (all P < 0.05) (Fig. 1B).

There was no significant difference in NGAL levels between the two groups at T0. Compared with T0, NGAL levels in both groups at T1 and T2 increased significantly, and the increase in group B was more significant than that in group A at the same time point (all P < 0.05) (Fig. 1C).

DISCUSSION

Postoperative stress is a normal physiological manifestation induced by many factors, however, excessive stress may lead to an increased perioperative risk (9). The main factors affecting the level of post-operative stress include the methods used to induce perioperative anesthesia, surgery and post-operative

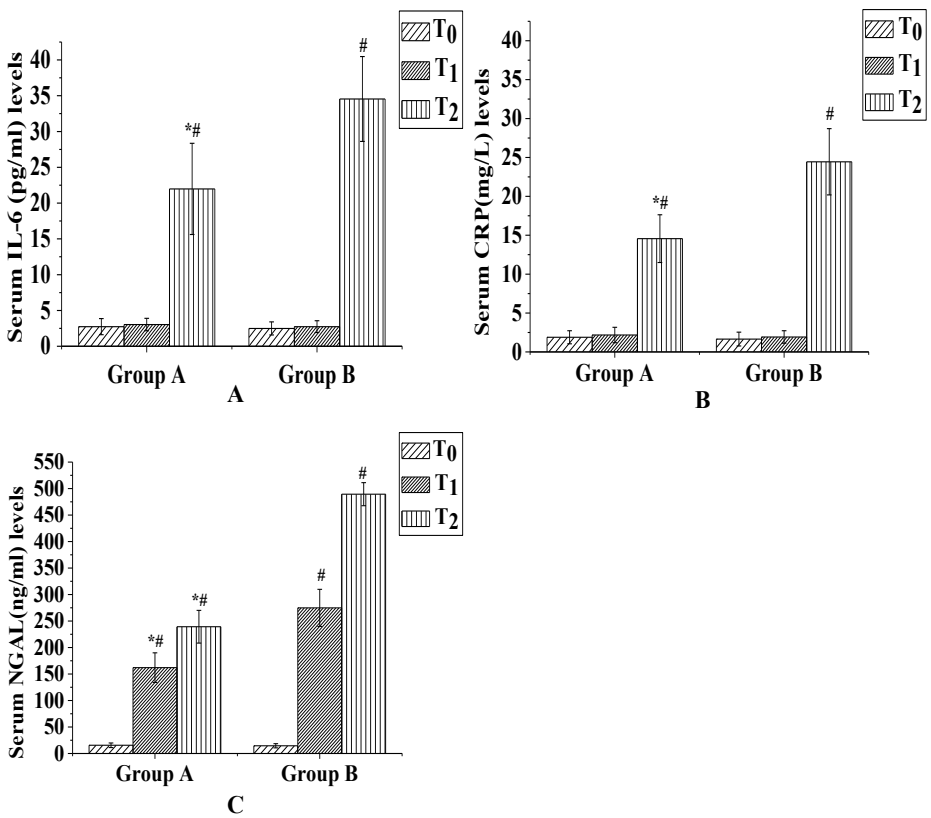

Fig. 1. *Comparison of serum levels of IL-6, CRP and NGAL between the two groups.* ***A)*** *comparison of serum IL-6 (pg/ml) levels between the two groups;* ***B)*** *comparison of serum CRP (mg/L) levels between the two groups;* ***C)*** *comparison of serum NGAL (ng/ml) levels between the two groups; compared with the control group, *P < 0.05; compared with preoperative, #P < 0.05.*

stimulation of pain. The impact of perioperative anesthesia and surgery on the stress of the two groups here could be neglected.

Laparoscopic surgery can affect post-operative recovery by causing pain in the abdomen, shoulder, back and ribs (10, 11). When patients receiving laparoscopic gynecological surgery under general anesthesia via the laryngeal mask were treated with intravenously controlled post-operative analgesia, their VAS scores were lower than 3. The effect of pain stimulation on the post-operative stress of the patients can be neglected here.

The serum levels of IL-6, CRP and NGAL in the ulinastatin group were lower than those in the control group. Therefore, it can be concluded that ulinastatin can be used in laparoscopic surgery to alleviate its adverse effects, reduce the production and release of pro-inflammatory cytokines, and prevent kidney injury.

In conclusion, preoperative use of ulinastatin can effectively reduce the level of stress by inhibiting the release of inflammatory cytokines, thus protecting the kidney and immune system of the body, improving the function of important organs, and promoting post-operative recovery.

REFERENCES

1. Querleu D, Leblanc E. Laparoscopic surgery for gynaecological oncology. Curr Opin Obstet Gynecol 2003; 15(4):309-14.
2. Angioli R, Terranova C, De Cicco Nardone C, et al. A comparison of three different entry techniques in gynecological laparoscopic surgery: a randomized prospective trial. Eur J Obstet Gynecol Reprod Biol 2013; 171(2):339-42.
3. Roy KK, Gc N, Singhal S, et al. Impact of energy devices on the post-operative systemic immune response in women undergoing total laparoscopic hysterectomy for benign disease of the uterus. J Turk Ger Gynecol Assoc 2018; 19(1):1-6.
4. Ezhevskaya AA, Mlyavykh SG, Anderson DG. Effects of continuous epidural anesthesia and postoperative epidural analgesia on pain management and stress response in patients undergoing major spinal surgery. Spine (Phila Pa 1976) 2013; 38(15):1324-30.
5. Tsujino T, Kawabe T, Omata M. Antiproteases in preventing post-ERCP acute pancreatitis. JOP 2007; 8(4 Suppl):509-17.
6. Chen CC, Wang SS, Lee FY. Action of antiproteases on the inflammatory response in acute pancreatitis. JOP 2007; 8(4 Suppl):488-94.
7. Jiang XM, Hu JH, Wang LL, Ma C, Wang X, Liu XL. Effects of ulinastatin on global ischemia via brain pro-inflammation signal. Transl Neurosci 2016; 7(1):158-63.
8. Knop C, Oeser M, Bastian L, Lange U, Zdichavsky M, Blauth M. [Development and validation of the Visual Analogue Scale (VAS) Spine Score]. Unfallchirurg 2001; 104(6):488-97.
9. Rettenmaier MA, Micha JP, Lopez KL, Wilcox AM, Goldstein BH. A prospective, observational trial assessing the efficacy of abdominal compression in reducing laparoscopic-induced shoulder pain. Surg Innov 2017; 24(6):552-56.
10. Barthelsson C, Sandblom G, Ljesevic-Nikoletic S, Hammarqvist F. Effects of intra-abdominally instilled isotonic saline on pain, recovery, and health-related quality-of-life following laparoscopic cholecystectomy: a randomized prospective double-blind controlled study. World J Surg 2015; 39(6):1413-20.
11. Ji M, Chen T, Wang B, et al. Effects of ulinastatin combined with mechanical ventilation on oxygen metabolism, inflammation and stress response and antioxidant capacity of ARDS. Exp Ther Med 2018; 15(6):4665-70.

LETTER TO THE EDITOR

PHOSPHATASE AND ACTIN REGULATOR 1 rs9349379 POLYMORPHISM IS ASSOCIATED WITH AN ELEVATED SUSCEPTIBILITY TO CORONARY ARTERY DISEASE: A META-ANALYSIS

X. SUN[1*], J. SUN[2*], D. ZHAO[1], Y. SONG[1] and L. YU[3]

[1]Department of Cardiovascular Medicine, Second Clinical Medical College of Inner Mongolia University for Nationalities, Inner Mongolia, China; [2]Department of Gynaecology and Obstetrics, Second Clinical Medical College of Inner Mongolia University for Nationalities, Inner Mongolia, China; [3]Department of Imaging, Second Clinical Medical College of Inner Mongolia University for Nationalities, Inner Mongolia, China

Received March 3, 2019 – Accepted March 29, 2019

[*] These authors contributed equally to this work

To the Editor,

Coronary artery disease (CAD) is the primary cause of mortality and morbidity worldwide (1-2), however, despite its high prevalence, its exact pathogenesis is still not fully understood.

Recently, a genome-wide association study (GWAS) conducted by the CARDIoGRAMplusC4D Consortium (3) found 46 genetic loci reaching genome-wide significance, including phosphatase and actin regulator 1 (*PHACTR1*) rs9349379 polymorphism. Since then, several genetic association studies have been performed on diverse populations to estimate potential associations between *PHACTR1* polymorphisms (rs9349379 and rs2026458) and CAD, with inconsistent results (4-6). Therefore, we conducted a meta-analysis of all relevant studies to more comprehensively analyze the effects of *PHACTR1* polymorphisms on individual susceptibility to CAD in a larger pooled population.

MATERIALS AND METHODS

We reported this meta-analysis as suggested by the Reporting Items for Systematic Reviews and Meta-analyses (PRISMA) guidelines (7).

Literature search and inclusion criteria

Eligible studies were retrieved from PubMed, Web of Science, Embase and CNKI using the following searching strategy: (phosphatase and actin regulator 1 OR PHACTR1) AND (polymorphism OR variant OR variation OR mutation OR genome-wide association study OR genetic association study) AND (coronary heart disease OR coronary artery disease OR angina pectoris OR acute coronary syndrome OR myocardial infarction). The initial search was conducted in November 2018 and the latest update was performed in February 2019. Moreover, we also screened the references of all retrieved articles to identify other potential relevant studies.

Included studies had to satisfy all the following criteria: i. genetic association studies about *PHACTR1* polymorphisms and CAD in human beings; ii. provide genotypic/allelic frequency of investigated polymorphisms in cases and controls; iii. full text in English or Chinese available. Studies were excluded if one of the following criteria was fulfilled: i. not about *PHACTR1* polymorphisms

Key words: phosphatase and actin regulator 1 (PHACTR1); polymorphisms; coronary artery disease (CAD); meta-analysis

Corresponding Author:
Dr L. Yu,
Department of Imaging, Second Clinical Medical College
Inner Mongolia University for Nationalities,
No. 81 Lincheng Road,
Inner Mongolia 022150, China.
e-mail: yulei88962@163.com

0393-974X (2019)

DISCLOSURE: ALL AUTHORS REPORT NO CONFLICTS OF INTEREST RELEVANT TO THIS ARTICLE.

and CAD; ii. studies that were not performed on human beings; iii. case reports or case series; iv. reviews, comments and conference presentations.

Data extraction and quality assessment

We extracted the following data from the included studies: the name of the first author, publication year, country and ethnicity of study subjects, sample size and genotypic/allelic distributions of *PHACTR1* polymorphisms in cases and controls. The probability value (*p* value) of Hardy-Weinberg equilibrium (HWE) was also calculated. When necessary, we wrote to the corresponding authors for extra information. We used the Newcastle-Ottawa scale (NOS) to assess the quality of eligible studies (8). This scale has a score range of zero to nine, and studies with a score of more than seven were thought to be of high quality. Data extraction and quality assessment were performed by two independent reviewers. Any disagreement between two reviewers was solved by discussion until a consensus was reached.

Statistical analyses

We used Review Manager Version 5.3.3 (The Cochrane Collaboration, Software Update) to conduct statistical analyses. We calculated odds ratios (ORs) and 95% confidence intervals (CIs) to estimate strength of associations in all possible genetic models, and *p* values ≤ 0.05 were considered to be statistically significant. All investigated *PHACTR1* polymorphisms contain a major allele (M) and a minor allele (m), the dominant comparison is defined as MM versus Mm + mm, recessive comparison is defined as mm *vs* MM +Mm, over-dominant comparison is defined as Mm *vs* MM + mm, and the allele comparison is defined as M *vs* m. I^2 statistics were employed to assess between-study heterogeneities. If I^2 was greater than 50%, random-effect models (REMs, Mantel–Haenszel method) would be used to pool the data on account of significant heterogeneities. Otherwise, fixed-effect models (FEMs, Mantel–Haenszel method) would be used for synthetic analyses. Subgroup analyses by ethnicity of participants were performed. Stabilities of synthetic results

Table I. *The characteristics of included studies.*

First author, year	Country	Ethnicity	Type of disease	Sample size	Genotype distribution		*P*-value for HWE	NOS score
					Cases	Controls		
rs9349379					AA/AG/GG			
Adlam 2019	UK	Caucasian	CAD	551/5697	277/234/40	2225/2606/866	0.024	7
Adlam 2019	UK	Mixed	CAD	504/1493	265/199/40	535/703/255	0.355	7
Assimes 2016	Taiwan	Asian	CAD	3133/5423	1635/1272/226	2650/2254/519	0.213	8
Chen 2019	China	Asian	CAD	332/119	165/134/33	34/60/25	0.877	7
Hager 2012	France	Caucasian	CAD	1523/426	NA	NA	NA	7
Hager 2012	France	Caucasian	CAD	2089/458	NA	NA	NA	7
Kiando 2016	France	Caucasian	CAD	1154/3895	555/486/113	1473/1831/591	0.574	7
Pérez-Hernández 2016	Mexico	Mixed	CAD	994/703	349/479/166	285/320/98	0.591	8
Xu 2017	China	Asian	CAD	200/200	NA	NA	NA	8
Zhao 2017	China	Asian	CAD	376/387	209/140/27	206/149/31	0.579	8
rs12526453					CC/CT/TT			
Chen 2019	China	Asian	CAD	332/119	83/164/85	45/46/28	0.021	7
Pérez-Hernández 2016	Mexico	Mixed	CAD	994/703	348/490/156	247/337/119	0.824	8

Abbreviations: CAD: Coronary artery disease; MI: Myocardial infarction; HWE: Hardy-Weinberg equilibrium; NOS: Newcastle-Ottawa scale

Table II. *Results of overall and subgroup analyses.*

Polymorphisms	Population	Sample size	Dominant comparison			Recessive comparison			Over-dominant comparison			Allele comparison		
			p value	OR (95%CI)	I^2	*p* value	OR (95%CI)	I^2	*p* value	OR (95%CI)	I^2	*p* value	OR (95%CI)	I^2
rs9349379	Overall	10856/18801	**0.004**	**1.39 (1.11-1.73)**	91%	**0.002**	**0.63 (0.48-0.84)**	85%	**0.03**	**0.89 (0.80-0.99)**	59%	**0.0002**	**1.30 (1.13-1.49)**	89%
	Caucasian	5317/10476	**<0.0001**	**1.54 (1.39-1.71)**	0%	**<0.0001**	**0.53 (0.38-0.73)**	63%	**0.001**	**0.84 (0.76-0.93)**	0%	**<0.0001**	**1.38 (1.30-1.48)**	50%
	Asian	4041/6129	0.08	1.37 (0.96-1.94)	82%	**0.02**	**0.68 (0.48-0.95)**	53%	0.19	0.95 (0.87-1.03)	29%	**0.03**	**1.27 (1.02-1.57)**	76%
rs2026458	Overall	1326/822	0.70	0.96 (0.76-1.20)	0%	0.36	0.76 (0.43-1.36)	82%	0.29	1.22 (0.85-1.75)	61%	0.49	1.11 (0.82-1.52)	73%

Abbreviations: OR: Odds ratio; CI: Confidence interval. The values in bold represent statistically significant differences between cases and controls.

were evaluated with sensitivity analyses, and publication biases were evaluated with funnel plots.

RESULTS

Characteristics of included studies

The initial literature search found 103 potential relevant articles. Among these articles, a total of 8 studies met the inclusion criteria and thus were included for pooled analyses (Fig. 1). The NOS score of eligible articles ranged from 7 to 8, which indicated that all included studies were of high quality. Baseline characteristics of included studies are shown in Table I.

Overall and subgroup analyses

The results of overall and subgroup analyses are summarized in Table I. To be brief, pooled analyses showed that rs9349379 polymorphism was significantly associated with CAD in overall population (dominant model: $p = 0.004$, OR = 1.39, 95%CI 1.11-1.73, $I^2 = 91\%$; recessive model: $p = 0.002$, OR = 0.63, 95%CI 0.48-0.84, $I^2 = 85\%$; over-dominant model: $p = 0.03$, OR = 0.89, 95%CI 0.80-0.99, $I^2 = 59\%$; allele model: $p = 0.0002$, OR = 1.30, 95%CI 1.13-1.49, $I^2 = 89\%$), and this significant finding was further confirmed in both Asians (dominant, recessive, over-dominant and allele models) and Caucasians (recessive and allele models). However, no positive findings were observed for rs2026458 polymorphism in overall and subgroup analyses.

Sensitivity analyses

We performed sensitivity analyses to test the

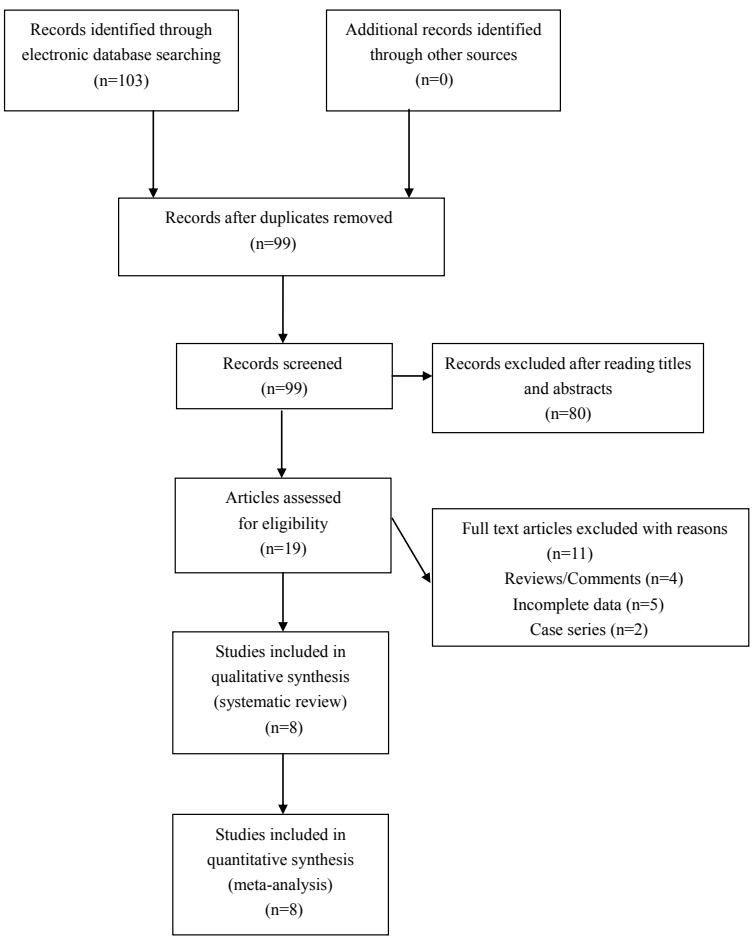

Fig. 1. *Flowchart of study selection .*

effects of individual study on pooled results. No altered results were observed in overall and subgroup comparisons, which indicated that our findings were statistically valid.

DISCUSSION

There are several notable points about this meta-analysis. Firstly, significant heterogeneities were detected in every genetic comparison of overall analyses, thus all analyses were performed with REMs. In further subgroup analyses by ethnicity, between study heterogeneities were significantly reduced, especially in Caucasians, which suggested that the magnitude of effects of rs9349379 polymorphism on individual susceptibility to CAD in Asians and Caucasians might be different, and the ethnic background of the study participants could partially explain the observed heterogeneities among the included studies. Secondly, it is worth noting that the rs9349379 polymorphism is an intronic variant (9-10), so theoretically it would not lead to alternations in gene expression or changes in protein structure, and we hypothesised that rs9349379 polymorphism may be linked to other *PHACTR1* polymorphisms or even linked to other unidentified genes, which could also impact individual susceptibility to CAD. Nevertheless, despite the above mentioned hypotheses, future experimental studies should try to determine the exact underlying mechanisms of our positive findings. Thirdly, the sample sizes of pooled analyses with regard to the rs2026458 polymorphism were still relatively small. Therefore, it is possible that our study was still not statistically adequate to detect the actual associations between *PHACTR1* polymorphisms and CAD, therefore, further studies with larger sample sizes still need to test these associations.

In conclusion, our meta-analysis suggested that *PHACTR1* rs9349379 polymorphism might affect individual susceptibility to CAD in both Asians and Caucasians. These results suggested that this polymorphism could be used to identify individuals at higher susceptibility to CAD. However, further well-designed experimental studies need to explore the underlying molecular mechanisms of our positive findings. Moreover, future investigations are also warranted to explore potential roles of other *PHACTR1* polymorphisms in the development of CAD.

REFERENCES

1. Moran AE, Forouzanfar MH, Roth G, et al. The Global Burden of Ischemic Heart Disease in 1990 and 2010: The Global Burden of Disease 2010 Study. Circulation 2014; 129:1493-501.
2. Global Burden of Disease Study 2013 Collaborators. Global, regional, and national incidence, prevalence, and years lived with disability for 301 acute and chronic diseases and injuries in 188 countries, 1990-2013: a systematic analysis for the Global Burden of Disease Study 2013. Lancet 2015; 386:743-800.
3. CARDIoGRAMplusC4D Consortium. Large-scale association analysis identifies new risk loci for coronary artery disease. Nat Genet 2013; 45:25-33.
4. Assimes TL, Lee IT, Juang JM, et al. Genetics of coronary artery disease in taiwan: a cardiometabochip study by the Taichi Consortium. PLoS One 2016; 11:e0138014.
5. Chen L, Qian H, Luo Z, et al. PHACTR1 gene polymorphism with the risk of coronary artery disease in Chinese Han population. Postgrad Med J 2019; doi: 10.1136/postgradmedj-2018-136298.
6. Hager J, Kamatani Y, Cazier JB, et al. Genome-wide association study in a Lebanese cohort confirms PHACTR1 as a major determinant of coronary artery stenosis. PLoS One 2012; 7: e38663.
7. Moher D, Liberati A, Tetzlaff J, Altman DG, PRISMA group. Preferred reporting items for systematic reviews and meta-analyses: the PRISMA statement. Ann Intern Med 2009; 151:264-9.
8. Stang A. Critical evaluation of the Newcastle-Ottawa scale for the assessment of the quality of nonrandomized studies in meta-analyses. Eur J Epidemiol 2010; 25:603-5.
9. Myocardial Infarction Genetics Consortium.. Genome-wide association of early-onset myocardial infarction with single nucleotide polymorphisms and copy number variants. Nat Genet 2009; 41:334-41.
10. Lu X, Wang L, Chen S, et al. Genome-wide association study in Han Chinese identifies four new susceptibility loci for coronary artery disease. Nat Genet 2012; 44:890-94.

LETTER TO THE EDITOR

PATHOGENESIS AND TISSUE TROPISM OF NEWCASTLE DISEASE VIRUS AND AVIAN INFLUENZA VIRUS (H9N2) IN SINGLE AND MIXED INFECTIONS

I. IRSHAD[1], A. ASLAM[1], M.Y. TIPU[1], K. ASHRAF[2], A. IRSHAD[3], S.F. REHMANI[4], I. AHMAD[1], S. RAO[5], T. BIBI[1] and G. MUSTAFA[1]

[1]Department of Pathology, University of Veterinary and Animal Sciences, Lahore-Pakistan; [2]Department of Parasitology, University of Veterinary and Animal Sciences, Lahore-Pakistan; [3]Centre of Excellence in Molecular Biology, University of the Punjab, Lahore-Pakistan; [4]Quality Operation Laboratory, University of Veterinary and Animal Sciences, Lahore-Pakistan; [5]Services Hospital Lahore-Pakistan

Received November 8, 2018 – Accepted March 28, 2019

To the Editor,

Newcastle disease (ND) and avian influenza (AI) are globally considered as a serious threat to the chicken and other avian species. The paramyxovirus type 1 and orthomyxovirus type A are RNA viruses, which cause ND and AI infection, respectively. Both of these infections are the main source of high economic losses in the poultry industry (1). Low pathogenic avian influenza viruses (LPAIVs) and high pathogenic avian influenza viruses (HPAIVs) are two main categories of avian influenza viruses (AIVs) in the chicken, which are classified on the basis of the existence of several basic amino acids at the hemagglutinin (HA) cleavage site and the virulence of the virus (2). Surface protein HA determines the pathogenicity of AIVs (3). For successful viral attachment and its replication in the host cell it is essential that HA protein be enzymatically cleaved into HA1 and HA2 (4). Cleavage of HA of HPAIVs requires furin and PC6, whereas cleavage of HA of LPAIVs needs proteases (trypsin like) released from intestinal and respiratory tissues (5). In case of Newcastle disease virus (NDV), severity of disease is based on the type of virus. Depending upon the fusion protein cleavage site and virulence of the virus, NDV is classified into virulent/severe (velogenic), moderate (mesogenic) and milder (lentogenic) forms. Velogenic and mesogenic are classified as virulent and lentognic as milder strains of NDV (6). A number of techniques are available for the detection of AIV and NDV from the tissue samples obtained from the infected birds. Identification of these viruses by using their reference antisera is one of the very important and reliable methods. Although molecular methods such as RT-PCR are being used for the quick detection of these viruses, immunohistochemistry (IHC) makes it easier to view tissue tropism of the viruses in the fixed tissues. Histopathology changes can be correlated with the results of IHC to determine the pathological changes in the cells with the presence of virus. The present study was designed to investigate the tissue tropism and pathogenesis of local field isolates of NDV and AIV (H9N2) on respiratory and lymphoid organs in single and mixed infection.

MATERIALS AND METHODS

Tissue samples (lungs, trachea, spleen, liver, proventriculus, cecal tonsils and intestine) of ND- and H9N2-suspected broiler birds were collected from the Punjab, Pakistan. These samples were triturated in phosphate buffered saline (PBS) mixed with antibiotics like penicillin (1000U/

Key words: Newcastle disease; avian influenza; H9N2; chicken, co-infection

Corresponding author:
Dr. Asma Irshad,
Centre of Excellence in Molecular Biology,
University of the Punjab,
Lahore, 54000-Pakistan
e-mail: asmairshad76@yahoo.com

0393-974X (2019)

mL) as well as streptomycin (1000U/mL). Each sample suspected for ND and H9N2 was inoculated in 9-10-day-old embryonated chicken eggs (specific NDV and AI antibodies free embryonated chicken eggs (ECE) via chorioallantoic membrane. Candling was carried out on the regular basis and embryos which died within 48 hours were discarded. The harvested fluid from embryos dead after 48 h was tested with spot hemagglutination (HA) assay, and the positive samples were subjected to hemeagglutination inhibition (HI) test to differentiate between ND and AI (H9N2). Primary monoclonal antibodies, raised in the rat against NDV and AIV (H9N2) were acquired from Pirbright Institute, UK to perform HI. NDV and AIV (H9N2) were further identified and differentiated through RT-PCR using specific primers. Embryo infectious dose 50 (EID50) of the selected NDV and AIV (H9N2) isolates was calculated using already derived equation (7).

Experimental design

Two hundred and ten day-old broiler-chicks were purchased from the local hatchery and reared at the University of Veterinary and Animal Sciences, Lahore. The status of maternal derived antibody titer against NDV and AIV (H9N2) was tested through enzyme linked immunosorbent assay (ELISA) on the same day. During the whole trial period, the birds were monitored two times a day on a daily basis. The birds were observed according to the procedures given by the Poultry Reference Center (PAS/PRC/035). The chicks were raised for 21 days without any vaccination. After that the chickens were divided into six groups, i.e. A, B, C, D, E and F containing 35 birds each. We used 10 EID50/dose/0.1mL in challenging the birds for NDV and H9N2. At the age of 21 days, the birds of group A were challenged with ND field virus ($10^{8.2}$/0.1mL/dose). Group B was challenged with H9N2 field virus ($10^{7.3}$/0.1mL/dose). Group C was challenged with both field isolates in sequence, i.e. ND ($10^{8.2}$/0.1mL/dose) and H9N2 ($10^{7.3}$/0.1mL/dose) at the 21st and 28th day of age, respectively. Group D was challenged with both field isolates in sequence, i.e. H9N2 ($10^{7.3}$/0.1mL/dose) and ND ($10^{8.2}$/0.1mL/dose) at the 21st and 28th day of age, respectively. Group E was challenged with both field isolates at the same time, i.e. H9N2 ($10^{7.3}$/0.1mL/dose) and ND ($10^{8.2}$/0.1mL/dose) at 21st day of age. Group F was kept as control. Supervision of the chickens was carried out on the regular basis to observe clinical-signs of each disease.

Histopathological examination

To observe various lesions, after sacrifice, trachea, lungs, thymus and spleen were collected from 10 birds of each group on 3rd, 5th, and 7th days post-infection (dpi). Organs were collected and fixed in 10% neutral buffered formalin (NBF) and processed by paraffin embedding technique for H & E staining and IHC (8).

Study of virus localization through immunohistochemistry

Tissue sections were cut from the paraffin blocks and placed on the positively charged slides (HistogripTM, Invitrogen cat. No.00805). For immunohistochemistry, SuperPicture™, Third Generation IHC Detection Kit (Invitrogen Cat. No.87-9673) was used according to the guidelines of the manufacturer.

Acquiring primary antibodies

Primary monoclonal antibodies, raised in the rat against NDV and AIV (H9N2) were acquired from Pirbright Institute, UK to perform IHC.

RESULTS

Clinical signs and gross lesions

None of the birds in any group showed signs of illness 24-hour post-infection (PI). From day 2 onward, the birds in Group A showed marked depression, loss of appetite, swelling of the head and diarrhea. Group B showed progressive depression and anorexia along with respiratory sound and excessive lacrimation. Groups C and D showed depression, anorexia, respiratory sounds, swelling of the head and diarrhea. Group E showed the most severe signs of lethargy, anorexia, nasal discharge, respiratory sounds and swelling of the head along with diarrhea while the birds of group F remained healthy. Ten birds from each group were sacrificed after 3rd, 5th and 7th days post-infection and examined; various lesions were observed in trachea, lungs, thymus and spleen in groups A, B, C, D and E. Ten birds from group F (control) were also sacrificed on 3rd, 5th and 7th day post-infection, but no lesions were observed on examination.

Histopathology

Histopathological lesions were observed in lymphoid and respiratory tissues on various days. These

lesions were present in the specific organ of a single bird or in the same organ of various birds of a particular group.

Trachea: Congestion was observed in the trachea of the birds of all challenged groups (A, B, C, D and E) sacrificed on 3rd, 5th and 7th dpi except in group A on 7th dpi and in group C on 3rd and 5th dpi. Infiltration of inflammatory cells was noticed in the birds of group A (3 dpi), B (5 dpi), D (3 and 5 dpi) and E (7 dpi). Necrosis was seen in group A (3 and 5 dpi), group C (7 dpi) and group E (5 and 7 dpi). Hemorrhages were noticed in the birds of groups A and E, sacrificed on 7th dpi (Table I).

Lungs: Congestion was detected in the lungs of the birds of challenged groups (A, B, C, D and E) sacrificed on 3rd, 5th and 7th dpi. Infiltration of inflammatory cells was noticed in group A (3 dpi), group B (3, 5 and 7 dpi), group D (5 and 7 dpi) and group E (3, 5 and 7 dpi). Necrosis was observed in group A on 3rd dpi. Atelectasis was seen in group A (3 and 5 dpi), C, D and E on 3rd, 5th and 7th dpi. Emphysema was observed in group A (5 and 7 dpi), B (7 dpi), C (3 dpi),

Table I. *Histopathological lesions/ changes and antigen detection through IHC in the respiratory and lymphoid organs of the birds sacrificed on 3rd, 5th and 7th dpi.*

Group	dpi	Histopathology																	Immunohistochemistry										
		Respiratory System									Lymphoid System								Virus	Respiratory System					Lymphoid System				
		Trachea				Lungs					Thymus				Spleen					Trachea		Lungs			Thymus			Spleen	
		Lesions				Lesions					Lesions				Lesions					Locations		Locations			Locations			Locations	
		Con	Inf	Nec	Hem	Con	Inf	Nec	Ate	Emp	Con	Inf	Hem	DL	Con	Nec	Hem	DL		Car	Muc	ATB	VAS	Par	LC	LM	BV	RP	WP	BV
A	3	+	+	+	-	+	+	+	+	-	+	+	+	+	+	+	+	-	N	+	-	+	-	+	+	+	+	+	+	+
	5	+	-	+	-	+	-	-	+	+	+	-	-	+	+	+	+	+	N	+	+	+	+	+	+	+	+	+	+	+
	7	-	-	-	+	+	-	-	-	+	+	-	-	-	-	-	-	-	N	+	+	+	+	+	+	+	+	+	+	+
B	3	+	-	-	-	+	+	-	-	-	+	-	-	-	+	-	-	-	A	+	+	+	-	+	-	+	-	+	-	+
	5	+	+	-	-	+	+	-	-	-	+	-	-	-	+	-	+	-	A	+	+	+	-	+	-	+	+	+	-	+
	7	+	-	-	-	+	+	-	-	+	+	-	-	-	+	-	-	-	A	+	-	+	+	+	-	-	+	+	-	-
C	3	-	-	-	-	+	-	-	+	+	-	+	+	-	+	-	+	+	N	+	-	+	+	+	+	+	+	+	-	-
																			A	+	+	+	+	+	+	+	-	+	+	+
	5	-	-	-	-	+	-	-	+	-	+	+	+	-	+	-	-	+	N	+	-	+	+	+	+	+	+	+	-	+
																			A	+	+	+	+	+	+	+	-	+	+	-
	7	+	-	+	-	+	-	-	+	-	+	-	+	-	+	-	-	+	N	+	-	+	-	+	+	+	+	+	-	-
																			A	+	+	+	+	+	+	+	-	+	+	-
D	3	+	+	-	-	+	-	-	+	-	-	-	-	-	+	-	-	+	N	+	-	+	-	+	+	+	+	+	-	-
																			A	-	+	+	+	-	-	+	+	+	+	+
	5	+	+	-	-	+	+	-	+	-	+	+	-	+	+	-	-	-	N	+	-	+	-	+	+	+	+	+	+	-
																			A	-	+	+	+	-	-	+	+	+	-	+
	7	+	-	-	-	+	+	-	+	+	+	+	-	-	+	-	-	-	N	+	-	+	-	+	+	+	+	+	-	-
																			A	-	+	+	+	-	-	+	-	+	+	-
E	3	+	-	-	-	+	+	-	+	-	+	-	+	-	-	-	-	-	N	+	-	+	+	+	-	+	+	+	-	-
																			A	+	+	+	+	+	-	+	+	+	-	-
	5	+	-	+	-	+	+	-	+	+	+	-	+	-	-	-	-	-	N	+	-	+	+	+	+	+	+	+	-	-
																			A	+	+	+	+	+	-	+	+	+	-	-
	7	+	+	+	+	+	+	-	+	-	+	-	-	-	+	-	-	-	N	-	-	+	+	+	+	+	+	+	-	+
																			A	-	+	+	+	+	+	+	+	+	-	-
F	3	-	-	-	-	-	-	-	-	-	-	-	-	-	-	-	-	-	N	-	-	-	-	-	-	-	-	-	-	-
																			A	-	-	-	-	-	-	-	-	-	-	-
	5	-	-	-	-	-	-	-	-	-	-	-	-	-	-	-	-	-	N	-	-	-	-	-	-	-	-	-	-	-
																			A	-	-	-	-	-	-	-	-	-	-	-
	7	-	-	-	-	-	-	-	-	-	-	-	-	-	-	-	-	-	N	-	-	-	-	-	-	-	-	-	-	-
																			A	-	-	-	-	-	-	-	-	-	-	-

Group A: Birds challenged with NDV on 3rd week, Group B: Birds challenged with H9N2 on 3rd week, Group C: Birds challenged with NDV on 3rd week and H9N2 on 4th week; Group D: Birds challenged with H9N2 on 3rd week and NDV on 4th week; Group E: Birds challenged with NDV and H9N2 simultaneously on 3rd week; Group F: No challenge was given (control). Con: congestion; Inf: infiltration of inflammatory cells; Nec: necrosis; Hem: hemorrhages; Ate: atelectasis; Emp: emphysema; DL: depletion of lymphocytes; Car: cartilage; Muc: mucosa; ATB: around tertiary bronchi; VAS: vasculature of air exchange spaces; Par: parenchyma; LC: lobular cortex; LM: lobular medulla; BV: blood vessels; RP: red pulp; WP: white pulp; dpi: days post-infection; N: NDV; A: AIV (H9N2). Dpi: days post-infection.

D (7 dpi) and E (5 dpi) (Table I).

Thymus: Congestion was observed in the thymus of the birds of group A, B, C, D and E sacrificed on 3rd, 5th and 7th dpi except in group C and D on 3rd dpi. Infiltration of inflammatory cells was seen in group A (3 dpi), C (3 and 5 dpi) and D (5 and 7 dpi). Hemorrhages were detected in group A (3 dpi), C (3, d and 7 dpi) and group E (3 and 5 dpi). Depletion of lymphocytes was noticed in group A (3 dpi) and D (5 dpi) (Table I).

Spleen: Congestion was observed in spleen in all challenged groups on 3rd, 5th and 7th dpi, except in group A on 7th dpi and in group E on 3rd and 5th dpi. Necrosis was seen in the birds of group A sacrificed on 3rd and 5th dpi. Hemorrhages were observed in group A (3 and 5 dpi), B (5 dpi) and C (3 dpi). Depletion of lymphocytes was seen in group A (5 dpi), C (3, 5 and 7 dpi) and D (3 dpi) (Table I). No lesions were observed in any bird of group F sacrificed on all post-infection days.

Immunohistochemistry

Immunohistochemistry was used to examine the tissue tropism of ND and AI (H9N2) viruses in birds challenged with single infection and with co-infection (NDV+H9N2). Localization of both viruses was examined in respiratory and lymphoid organs on different days post-infection.

Trachea: The cartilage of the trachea was positive for viral antigen NDV in birds of group A and H9N2 in group B on 3rd, 5th and 7th dpi. Mucosa of group A was positive for NDV on 5th and 7th dpi and of group B for H9N2 on 3rd and 5th dpi. Both antigens (NDV+H9N2) were detected in the cartilage of the trachea of groups C and E on 3rd, 5th and 7th dpi except in the birds of group E sacrificed on 7th dpi. Cartilage of the trachea in the birds of group D was positive for NDV and negative for H9N2 on 3rd, 5th and 7th dpi. Mucosa of the trachea was positive for H9N2 in group C, D and E on 3rd, 5th and 7th dpi (Table I).

Lungs: NDV and H9N2 were detected around the tertiary bronchioles of the lungs in group A and B respectively on 3rd, 5th and 7th dpi. Both viruses were detected around the tertiary bronchioles in co-infected groups, i.e. C, D and E on all post-infection (PI) sacrifice days. NDV and H9N2 were positive in group A (5th and 7th dpi) and B (7th dpi), respectively, in vasculature of air exchange spaces (VAES) of the lungs. NDV was positive in group C on the 3rd and 5th dpi while H9N2 was present in group C and D on 3rd, 5th and 7th dpi in VAES of the lungs. Both pathogens (NDV+H9N2) were positive in VAES of the lungs in the birds of group E sacrificed on 3rd, 5th and 7th dpi. NDV and H9N2 were present in the parenchyma of the birds of group A and B respectively on 3rd, 5th and 7th dpi. Only NDV was found positive in group D on 3rd, 5th and 7th dpi. Both viruses (ND+H9N2) were detected in the parenchyma of group C and E on 3rd, 5th and 7th dpi (Table I). No virus was detected in group F on all post-infection days.

Thymus: NDV was seen in the cortical lobules of the thymus of birds of group A and D on 3rd, 5th and 7th dpi. Both viruses (NDV+H9N2) were present in cortical lobules in group C on 3rd, 5th and 7th dpi. In group E, NDV was present on 5th dpi while both antigens were found on 7th dpi in lobules of cortex. In lobules of medulla, NDV and H9N2 were present in group A and group B, respectively, on all PI sacrifice days except H9N2 in group B on 7th dpi. Both antigens were present in co-infected groups C, D and E in lobules of medulla on 3rd, 5th and 7th dpi. In groups A and C, NDV was detected in the blood vessels on 3rd, 5th and 7th dpi. In blood vessels of group B, H9N2 was seen on 5th and 7th dpi. Both viruses were detected in the blood vessels of groups D and E on all post-infection sacrifice days except H9N2 in group D on 7th dpi (Table I).

Spleen: In the red pulp of spleen, NDV and H9N2 were detected in groups A and B respectively on 3rd, 5th and 7th dpi. Both pathogens were detected as positive in red pulp of all infected groups (A, B, C, D and E) on 3rd, 5th and 7th dpi. NDV was seen in white pulp of group A on 3rd, 5th and 7th dpi as well as in group D on 5th dpi. H9N2 virus was positive in white pulp of group C on 3rd, 5th and 7th dpi and in group D on 7th dpi. In blood vessels of the spleen, NDV was found positive in group A on 3rd, 5th and 7th dpi; in groups C and E on 5th and 7th dpi, respectively, whereas H9N2 was positive in group B on 3rd and 5th dpi and in group C on 3rd dpi as well as in group D on 3rd and 5th dpi (Table I). No virus was detected in group F.

DISCUSSION

In our study congestion, infiltration of inflammatory cells and necrosis were observed in the trachea of the ND infected group. In addition to these, emphysema was observed in the lungs of ND and co-infected groups. Both trachea and lungs were positive for NDV in immunohistochemical reactions. Similar results were reported in a study from Indonesia (9). In another study, congestion and leukocyte infiltration was observed in the trachea and lungs of H9 challenged birds on 5th dpi. Immunohistochemical positive staining was clearly observed in trachea and lungs on 5th dpi and 9th dpi. Congestion and infiltration of inflammatory cells in the trachea and lungs were noticed in both the studies on 5th dpi. In both studies, virus H9N2 was positive in trachea and lungs on 5th dpi when detected through IHC, though it was positive on 3rd dpi in our case, but in the other study no observation was recorded on 3rd dpi for H9N2. Hence, the findings of our study are in partial agreement with already reported study (10). The findings of our study are similar to a co-infection (NDV and H9N2) study conducted in Korea, it was observed that lungs were congested in ND alone, H9N2 alone and in H9N2+ND co-infected groups. Loss of lymphocytes in thymus and spleen were noted in ND alone and H9N2+ND co-infected groups (11). It can be inferred from the results of the current study that both LPAIV (H9N2) and virulent NDV cause lesions in various lymphoid and respiratory organs in single as well as co-infection, though lesions induced by LPAIV (H9N2) were mild in nature. More lesions were observed in virulent NDV-infected group (A), mostly mild lesions were observed in LPAIV (H9N2)-infected group (B). Relatively fewer lesions were observed in co-infected groups (C, D and E) compared to group A which shows that LPAIV (H9N2) have a negative effect on virulent NDV. There is no synergism for inducing lesions between LPAIV (H9N2) and virulent NDV. Furthermore, both viruses can be detected in these tissues on 3rd day post-infection through IHC.

ACKNOWLEDGEMENTS

The authors are grateful to the Higher Education Commission, Pakistan for support.

REFERENCES

1. Capua I, Alexander DJ. Avian influenza and Newcastle disease: a field and laboratory manual. Italy: Springer Verlag; 2009; 1-31.
2. Swayne DE, Suarez DL, Sims LD. Influenza. In: Diseases of Poultry. ed. Willey-Blackwell; Ames, Iowa 2013; p. 181-218.
3. Fouchier RA, Munster V, Wallensten A, et al. Characterization of a novel influenza A virus hemagglutinin subtype (H16) Obtained from black-headed gulls. J. Virol 2005; 79:2814-22.
4. Byrum BR, Slemons RD. Detection of proteolytic bacteria in the upper respiratory tract flora of poultry. Avian Dis 1995; 39:622-26.
5. Swayne DE, Suarrez DL. Highly pathogenic avian influenza. Rev Sci Tech Off Int Epiz 2000; 19:463-82.
6. Miller PJ, Koch G. Newcastle disease, other avian paramyxoviruses and avian metapneumovirus infections. In: Diseases of Poultry. ed.Wiley-Blackwell 2013; p. 89-138.
7. Reed LJ, Muench H. A simple method of estimating fifty per cent endpoints. Am J Epidemiol 1938; 27(3):493-97.
8. Afonina, I., X. N. Lim, et al. (2018). Planktonic interference and biofilm alliance between aggregation substance and endocarditis and biofilm associated pili in Enterococcus faecalis. J Bacteriol.
9. Etriwati, Raith D, Handharyani E, Setiyaningsih S. Pathology and immunohistochemistry study of Newcastle disease field case in chicken in Indonesia. Vet World 2017; 10(9):1066.
10. Subtain S, Chaudhry ZI, Anjum AA, Maqbool A, Sadique U. Study on pathogenesis of low pathogenic avian influenza virus H9 in broiler chickens. Pak J Zool 2011; 43(5).
11. Lee SM, Cho ES, Choi BH, Son HY. Clinical and pathological studies on co-infection of lowpathogenic avian influenza virus and Newcastle disease virus in the chicken. Korean J Vet Serv 2013; 36(3):163-69

LETTER TO THE EDITOR

CORRELATION BETWEEN THE SAP GENE OF *CANDIDA ALBICANS* AND ORAL LICHEN PLANUS

XH. YANG, HF. LI, FL. XING, MC. TAO and Y. CAO

Department of Dermatology and STD, Zhejiang Hospital of Traditional Chinese Medicine, Zhejiang Chinese Medical University, Hangzhou, China

Received January 25, 2019 – Accepted April 2, 2019

To the Editor,

Oral lichen planus (OLP) is a common oral mucosal disease (1), while Candidiasis is common in OLP patients (2). The clinical manifestations of OLP and oral candidiasis show certain similarities (3, 4), while antifungal therapies are effective in the treatment of some patients (5). Therefore, given the fact that the carrying rate and prevalence of Candida in OLP patients are significantly higher than those in normal healthy people, some scholars have hypothesised that there is a certain relationship between *Candida albicans* (*Candida a.)* and the occurrence of OLP (6). Recent studies have shown that *Candida a.* may act as a trigger or aggravating factor in the pathogenesis of OLP, while the secretion of exogenous enzymes plays an important role in the virulence and pathogenesis of OLP (7). Secreted aspartyl proteinase (SAP) is an acid proteinase secreted by *Candida a.*. To date, 10 different SAP genes have been identified, including the genes in the SAPl-3 and SAP4-6 subfamilies (8, 9). It has been shown that abnormal epithelial hyperplasia or malignant transformation of OLP is related to *Candida a.* infection (10). In this study, the expression of SAP gene in *Candida a.* carriers, *Candida a.* patients, OLP patients negative for Candida, OLP patients carrying *Candida a.*, and patients suffering both OLP and *Candida a.* was detected by RT-PCR. Subsequently, the relationship between SAP gene expression and *Candida a.* was analyzed and discussed to lay a solid theoretical basis to improve the clinical treatment of OLP.

MATERIALS AND METHODS

Subjects

The subjects of this study were from Zhejiang Hospital of Traditional Chinese Medicine between December 2015 and July 2018. None of the subjects had received antibiotics or hormones within 3 months prior to the start of the study. The subjects were divided into five groups: i) 20 *Candida a.* carriers, including 8 males and 12 females aged 18-76 years, were selected from scaling patients with no symptoms or signs of oral candidiasis. In addition, the fungal culture results of their saliva samples were 50-800 cfu/mL, and the presence of *Candida a.* in these subjects was confirmed by mycology; ii) 20 *Candida a.* patients, including 11 males and 9 females aged 24-67 years, were selected from patients with mucosal diseases. The fungal culture results of their saliva samples were more than 2000 cfu/mL and the presence of *Candida a.* in these subjects was confirmed by mycology; iii) 10 patients, including 2 males and 8 females aged 26-58 years, who were negative for Candida culture, were selected from OLP patients and their culture results of salivary fungi were negative; iv) 20

Key words: Candida albicans; SAP; lichen planus; expression of SAP9

Corresponding Author:
Dr Yi Cao,
Department of Dermatology & STD,
Zhejiang Hospital of Traditional Chinese Medicine,
Zhejiang Chinese Medical University,
YouDian Rd.54th, Hangzhou, 310006, China
e-mail: caoyi_zjcmu@163.com

0393-974X (2019)

OLP patients carrying *Candida a.*, including 9 males and 11 females aged 26-87 years, were selected and their fungal culture results of saliva samples were 50-800 cfu/mL. In addition, the presence of *Candida a.* in these subjects was confirmed by mycology; v) 20 patients suffering from both OLP and *Candida a.*, including 9 males and 11 females aged 31-81 years, were selected and their fungal culture results of saliva samples were more than 2000 cfu/mL. Exclusion criteria: patients with hypertension, diabetes mellitus, liver disease, hematological disease or HIV; those who had used immune preparations during the previous month; those who had acute infection history during the previous 3 months; those who were aged under 18 years or unable to cooperate; those who used antifungal agents or antibiotics. In addition, the presence of *Candida a.* in these subjects was confirmed by mycology. Furthermore, the presence of *Candida a.* was also detected by germ tube formation test, chlamydospore test, Candida chromogenic medium (CHROM agar Candida) identification, API20 system identification and 42°C growth test. The study was approved by the medical ethics committee of Zhejiang Hospital of Traditional Chinese Medicine and informed consent was signed by all patients.

Collection of saliva samples

Saliva samples were collected from 8 to 10 a.m. For two hours before saliva collection, the subjects were forbidden to smoke, drink water, eat, or brush their teeth. Before the

Table I. *Primer sequences and amplified fragments*

Gene name	Primer sequence	Amplified fragment	/bp
SAP1	Upstream	5'-TCAATCAATTTACTCTTTCCATTTCTAACA-3'	161
	Downstream	5'-CCAGTAGCATTAACAGGAGTTTTAATGACA-3'	
SAP2	Upstream	5'-AACAACAACCCACTAGACATCACC-3'	178
	Downstream	5'-TGACCATTAGTAACTGGGAATGCTTTAGGA-3'	
SAP3	Upstream	5'-CCTTCTCTAAAATTATGGATTGGAAC-3'	231
	Downstream	5'-TTGATTTCACCTTGGGGACCAGTAACATTT-3'	
SAP4	Upstream	5'-CATTCATTCCTTTAATACCGACTATC-3'	156
	Downstream	5'-GGTAACAAACCCTGTAGATCTTTTAAC-3'	
SAP5	Upstream	5'-TCCCCAGCATCTTCCCGCACT-3'	215
	Downstream	5'-TCAAACTCGGTAGCTTCGCCGC-3'	
SAP6	Upstream	5'-CATTCATTCCTTTAATACCGACTATC-3'	156
	Downstream	5'-GGTAACAAACCCTGTAGATCTTTTAAC-3'	
SAP7	Upstream	5'-GAAATGCAAAGAGTATTAGAGTTATTAC-3'	196
	Downstream	5'-GAATGATTTGGTTTACATCATCTTCAACTG-3'	
SAP8	Upstream	5'-TGCTGATAAATTGGCTGCTG-3'	281
	Downstream	5'-AGCCAACAGAATGGTGTTCC-3'	
SAP9	Upstream	5'-CGCTTATGATACCAGTGCCAT-3'	944
	Downstream	5'-GCGAAAGCAACAACCCATACAC-3'	
SAP10	Upstream	5'-AGCCCTCACACCCCCATTTCA-3'	815
	Downstream	5'-GGGGACTGTACTCAATGCCCCCT-3'	
ACT1	Upstream	A 5'-GGCTGGTAGAGACTTGACCAACCATTTG-3'	271
	Upstream	B 5'-GATTTTGTCTGAACGTGGTAACAG-3'	
	Downstream	5'-GGAGTTGAAAGTGGTTTGGTCAATAC-3'	

saliva samples were collected, the subjects first drank 100 mL of distilled water and sat on a chair slightly leaning forward while holding the measuring cup. Subsequently, their saliva was collected for 10 min and measured. A piece of pH test paper was then gently placed at the orifice of the submandibular gland for 5 sec, and the color change of the pH test paper was observed and recorded.

Extraction of Candida albicans RNA from saliva samples

Extraction of total RNA was carried out according to the manufacturer's instructions Trizol (TaKaRa Company, Japan). The saliva samples were divided into EP (Eppendorf) tubes, the bacteria were collected by centrifugation at 2,000 r/min and 4°C for 5 min. An appropriate amount of Trizol (1 mL) was added, mixed well, and stored at room temperature for 5 min. Chloroform (0.2 mL Trizol) was added and shaken upside down for 5 min at room temperature, followed by centrifugation for 15 min at 12,000 g and 4°C. The supernatant was absorbed into another centrifugal tube, and isopropanol of equal volume was added. After mixing upside down, it was maintained at room temperature for 10 min. After centrifugation for 10 min at 12,000g and 4°C, the supernatant was removed and 1mL 75% ethanol was added. After centrifugation for 5 min at 12,000 g and 4°C, the supernatant was removed, and dried for 5 min with an ultra-clean fan. Total RNA was dissolved in 20 μL DEPC water, and 5 μL total RNA A260/A280 (optical density, OD value) was measured by an ultraviolet spectrophotometer (Beijing Dafengrui Instrument Company, China). The purity was calculated and the experiment was carried out when the ratio was between 1.8 and 2.0.

Design and synthesis of primers

Sequences of target genes were obtained from the www.ncbi.nlm.nih.gov website. Primer premier 5 software was used to design primers and the synthesis of primers was carried out by Beijing Sanbo Yuanzhi Biotechnology Co., Ltd. (Table I). Actin (ACT) gene of *Candida a.* was selected as the positive control. In fact, ACT gene could not only amplify all test strains and standard strains to produce PCR products of the same size, but also confirm the presence of *Candida a.* by amplifying two pairs of Actin 1 (ACT1) primers.

Reverse transcription (RT) synthesis of cDNA

The expression of SAP1-10 and ACT1 (internal reference gene) in each sample was detected by RT-PCR, according to the manufacturer's instructions, of the RNA PCR kit 3.0 (AMV) kit (TaKaRa, Japan). RT-PCR was performed according to the instructions of TaKaRa RNA PCR kit 3.0 (AMV). Specific conditions were as follows: The RT reaction system was 20μL, which included 24.0 μL of MgCl, 2.0 μL of 10×RT buffer, 2 μL of dNTP mixture, 0.5 μL of Rnase inhibitors, 1 μL of AMV reverse transcriptase, 1 μL of Oligo dT adaptor primers, and 2 μL of sample RNA; the Rnase Freed H2O was finally added to reach 20 μL. The conditions of RT reaction were as follows: 30°C for 10 min; 42°C for 30 min; 99°C for 5 min; 5°C for 5 min.

Detection of the SAP1-10 expression in saliva samples by PCR

The reaction volume of SAP1-10 target fragments amplified by RT-PCR was 25 μL, which included 5 μL of 5×PCR buffer, 0.2 μL of TaKaRa Ex Taq HS, 0.5 μL of

Table II. *χ^2 test results in patients with Candida a. (A), OLP with Candida a. (B), Candida a. patients (C), OLP patients with candidiasis albicans (D), OLP patients carrying Candida a. (E) and OLP patients with candidiasis albicans (D).*

Groups	SAP1	SAP2	SAP3	SAP7	SAP8	SAP9	SAP10
A and B	-	-	-	χ^2=3.84 P=0.05	χ^2=7.66 P < 0.05	χ^2=1.44 P > 0.05	-
C and D	χ^2=1.40 P > 0.05	-	-	-	χ^2=1.604 P > 0.05	χ^2=12.13 P > 0.05	χ^2=1.406 P > 0.05
E and D	χ^2=18.5 P < 0.05	χ^2=4.901 P < 0.05	χ^2= 36.1 P < 0.05	χ^2=9.176 P < 0.05	χ^2=0 P > 0.05	χ^2=12.22 P < 0.05	χ^2=0.526 P > 0.05

forward primers, 0.5 μL of reverse primers, and 2.0 μL of cDNA; the reaction volume was 25 μL by adding 16.8 μL of sterilized distilled water. The reaction process of RT-PCR was as follows: denaturation at 94°C for 30 s, annealing at 62°C for 30 s, elongation at 72°C for 30 s, and elongation at 72°C for 10 min.

Statistical analysis

The experimental results were processed by SPSS 12.0 software. The measurement data were expressed as mean ± standard deviation. The counting data were tested by χ^2 test, and $P < 0.05$ indicated significant difference.

RESULTS

Expression of SAP in standard strains of Candida albicans and experimental samples

The amplification results of ACT and 10 SAP genes of standard strains of *Candida a.* were all positive (Fig. 1A). In particular, the saliva samples of 20 *Candida a.* carriers expressed SAP4-6 but not SAP1, SAP3, SAP8, SAP9 and SAP10 (Fig. 1B). In 20 saliva samples of Candida carriers, only some of the patients were positive for SAP2 and SAP7 gene expression: 14 were positive for SAP2, 4 were positive for SAP7, and the rest showed no SAP7 expression.

The results of ACT amplification in the saliva samples of *Candida a.* patients were all positive (Fig. 1C), confirming the presence of mRNA of *Candida a.* genes in the RNA extracted from the saliva samples. In addition, the positive amplification results of SAP2, SAP3, SAP4-6 and SAP7 were found in all 20 samples. Furthermore, 18 samples showed positive amplification of SAP1, 12 samples showed positive amplification of SAP8, 4 samples showed positive amplification of SAP9, and 6 samples showed positive amplification of SAP10.

The amplification results of ACT and 10 SAP genes in the saliva samples of lichen planus patients negative for *Candida a.* were all negative (Fig. 1D), confirming the absence of *Candida a.* in these samples. At the same time, the presence of non-

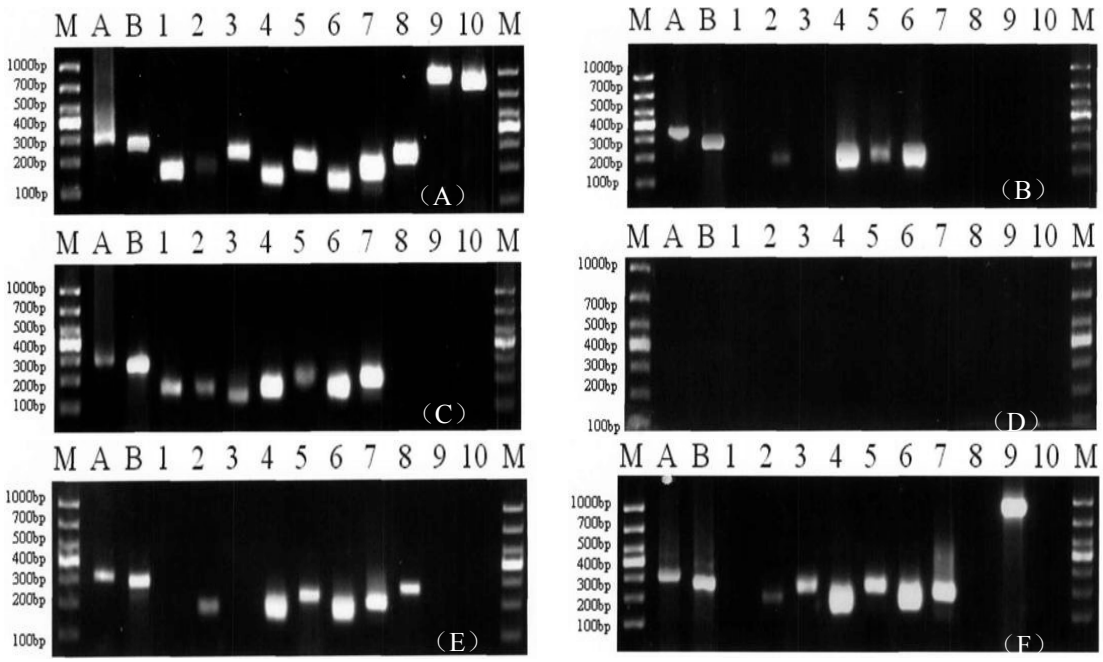

Fig. 1. *RT-PCR results of SAP.* ***A)*** *Candida a. standard strains;* ***B)*** *saliva samples of Candida a. carriers;* ***C)*** *saliva samples of Candida a. patients;* ***D)*** *Candida a. culture negative samples of OLP patients;* ***E)*** *saliva samples of OLP patients with Candida a.;* ***F)*** *saliva samples of OLP patients with Candida a. (M: Maker; A: ACT A, 304bp; B: ACT B, 271bp; 1: SAP1, 161bp; 2: SAP2, 178bp; 3: SAP3, 231bp; 4: SAP4, 156bp; 5: SAP5, 215bp; 6: SAP6, 156bp; 7: SAP7, 196bp; 8: SAP8, 281bp; 9: SAP9, 944bp; 10: SAP10, 815bp)*

specific RT-PCR amplification products in these samples also indicated the absence of cross-reaction with other RNA.

The results of ACT amplification in the saliva samples of OLP patients carrying *Candida a.* were all positive (Fig. 1E), confirming the presence of *Candida a.* genes in the extracted RNA samples. The positive amplification results of SAP 2 and SAP 4-6 were found in all 20 samples. In addition, only some of the patients showed positive expression of SAP7, SAP8 and SAP9 genes, including 11 samples showing positive amplification of SAP7, 8 samples showing positive amplification of SAP8, and 3 samples showing positive amplification of SAP9.

The results of ACT amplification in saliva samples of patients suffering from both lichen planus and *Candida a.* were all positive (Fig. 1F), confirming the presence of *Candida a.* genes in the extracted RNA. The positive amplification results of SAP2, SAP3, SAP4-6 and SAP7 were found in all 20 samples. In addition, only some of the patients were positive for SAP1, SAP8, SAP9 and SAP10 genes, including 14 samples showing positive amplification of SAP1, 7 samples showing positive amplification of SAP8, 15 samples showing positive amplification of SAP9, and 2 samples showing positive amplification of SAP10.

χ^2 test results of each experimental group

χ^2 test was performed between the following two groups: group A and group B (the *Candida a.* carriers *vs* OLP patients carrying *Candida a*), group C and group D (the *Candidiasis* patients *vs* OLP patients accompanied by *candidiasis*), and group E and group D (the OLP patients carrying *Candida a. vs* the OLP patients accompanied by *Candidiasis*). The results are shown in Table II. There was no significant difference in SAP9 expressions between group A and group B. The difference in SAP9 expressions between group C and group D, as well as that between group E and group D, suggested that SAP9 may also be involved in the pathogenesis of candidiasis in OLP patients.

Table II shows the results of χ^2 test performed comparing group A with group B, group C with group D, and group E with group D.

DISCUSSION

The expression of SAP in OLP patients has rarely been studied. This study found that no SAP gene was expressed in the saliva of OLP patients negative for Candida culture, confirming that the SAP gene is unique to *Candida a.* The expression of SAP in patients suffering from both lichen planus and *Candida a.* was more complex than that in healthy people carrying *Candida a.*. For example, the positive amplification results of SAP8 and SAP9 were not found in patients suffering from both lichen planus and *Candida a.*, while the difference of SAP expression between candidiasis albicans patients and patients suffering from both lichen planus and *Candida a.* was mainly manifested by differential expression of SAP1, SAP8, SAP9 and SAP10. In addition, the difference of SAP9 expression was statistically significant, indicating that the oral environment of OLP patients affected the characteristics of SAP expression.

According to previous research (11, 12), it was shown that SAP2 and SAP4-6 were frequently and highly expressed in SAP genes. In one study, there was no difference in SAP4-6 expression among different groups. Furthermore, the expression of SAP2 was only different between *Candida a.*-carrying OLP patients and patients suffering from both lichen planus and *Candida a.*, consistent with the role of SAP2 in adhesion. Moreover, SAP1 and SAP3 were not expressed in normal *Candida a.* carriers and OLP patients, while no difference was found between *Candida a.* patients and patients suffering from both lichen planus and *Candida a.*, nor was there any difference between *Candida a.*-carrying OLP patients and patients suffering from both lichen planus and *Candida a*. It was hypothesised that SAP2 and SAP4-6 might be involved in post-adhesion colonization, which was the prerequisite of bacterial pathogenesis. The expression of SAP7 was gradually increased in the order of *Candida a.* carriers, *Candida a.*-carrying OLP patients and patients suffering from both lichen planus and *Candida a.*, suggesting that SAP7 may be associated with the environmental factors of OLP patients and acts as an important contributing factor in the pathogenesis of

candidiasis. In addition, there was no difference in SAP9 expression between *Candida a.* carriers and *Candida a.*-carrying OLP patients. The difference in SAP9 expression between *Candida a.* carriers, candidiasis albicans patients, *Candida a.*-carrying OLP patients and patients suffering from both lichen planus and *Candida a.* suggested that SAP9 may also be involved in the pathogenesis of Candida in OLP patients. In this study, 2 samples expressing all SAP genes were derived from patients with erosive OLP. The causal relationship between the expression of SAP1-10 genes and the occurrence or development of erosive OLP remains to be further studied.

In conclusion, the SAP family plays a certain role in Candida infection of OLP patients. The characteristic expression of SAP9 in the saliva of OLP patients can help to maintain and strengthen the pathogenicity of *Candida a.* while promoting the onset and aggravation of OLP.

ACKNOWLEDGEMENTS

This work was supported by Nature Science Foundation of China (No. 81173271 and 81774313)

REFERENCES

1. Olson MA, Rogers RS 3rd, Bruce AJ. Oral lichen planus. Clin Dermatol 2016; 34(4):495-504.
2. Arora S, Verma M, Gupta SR, Urs AB, Dhakad MS, Kaur R. Phenotypic variability and therapeutic implications of Candida species in patients with oral lichen planus. Biotech Histochem 2016; 91(4):237-41.
3. Bokor-Bratic M, Cankovic M, Dragnic N. Unstimulated whole salivary flow rate and anxiolytics intake are independently associated with oral\r, Candida\r, infection in patients with oral lichen planus. Eur J Oral Sci 2013; 121(5):427-33.
4. Artico G, Freitas RS, Santos Filho AM, Benard G, Romiti R, Migliari DA. Prevalence of\r, Candida\r, spp. xerostomia, and hyposalivation in oral lichen planus-A controlled study. Oral Dis 2014; 20(3):e36-41.
5. Kragelund C, Kieffer-Kristensen L, Reibel J, Bennett EP. Oral candidosis in lichen planus: the diagnostic approach is of major therapeutic importance. Clin Oral Investig 2013; 17(3):957-65.
6. Simarkmattsson C, Eklund C. Reduced immune responses to purified protein derivative and Candida albicans in oral lichen planus. J Oral Pathol Med 2013; 42(9):691-97.
7. Pakshir K, Zomorodian K, Karamitalab M, Jafari M, Taraz H, Ebrahimi H. Phospholipase, esterase and hemolytic activities of Candida spp. isolated from onychomycosis and oral lichen planus lesions. J Mycol Med 2013; 23(2):113-18.
8. Pereira Tdos S, Silva Alves Jde F, Gomes CC, Rocha do Nascimento A, Stoianoff MA, Gomez RS. Kinetics of oral colonization by\r, Candida\r, spp. during topical corticotherapy for oral lichen planus. J Oral Pathol Med 2014; 43(8):570-75.
9. Staib P, Lermann U, Blass-Warmuth J, et al. Tetracycline-inducible expression of individual secreted aspartic proteases in Candida albicans allows isoenzyme-specific inhibitor screening. Antimicrob Agents Chemother 2008; 52(1):146-56.
10. Gainza-Cirauqui ML, Nieminen MT, Novak Frazer L, Aguirre-Urizar JM, Moragues MD, Rautemaa R. Production of carcinogenic acetaldehyde by Candida albicans from patients with potentially malignant oral mucosal disorders. J Oral Pathol Med 2013; 42(3):243-49.
11. Xu M, Liu J. [Immunoprotection by Sap2 and dendritic cells against systemic Candida albicans infection in mice]. Nan Fang Yi Ke Da Xue Xue Bao 2014; 34(7):1030-34.
12. Wu H, Downs D, Ghosh K, Ghosh AK, Staib P, Monod M, Tang J. Candida albicans secreted aspartic proteases 4-6 induce apoptosis of epithelial cells by a novel Trojan horse mechanism. FASEB J 2013; 27(6):2132-44.

LETTER TO THE EDITOR

ASSOCIATIONS BETWEEN VITAMIN D RECEPTOR GENETIC VARIATIONS AND LUNG CANCER: A META-ANALYSIS

Y. ZHAN, K. ABUDUWAILI, H. ZHU, C. LIU and X. WANG

Department of Pulmonary Medicine, The Affiliated Tumor Hospital of Xinjiang Medical University, Urumqi, China

Received Februay13, 2019 – Accepted March 4, 2019

To the Editor,

Lung cancer (LC) is the most common type of cancer in both males and females (1). In spite of rapid progress in chemotherapy and minimally invasive surgery achieved in the past few decades, LC is still the leading cause of cancer-related deaths in both sexes (2). However, despite its high prevalence, the pathogenesis of LC is still not fully understood.

Recently, there is accumulating evidence to support that vitamin D metabolic pathway might be involved in the pathogenesis of LC. Firstly, previous epidemical investigations found that vitamin D deficiency was a potential risk factor of multiple malignancies including LC, and the serum level of vitamin D was also correlated with disease severity (3-5). Secondly, several experimental studies showed that vitamin D had immune-regulatory, anti-proliferative and anti-angiogenic functions, which suggested that it might provide favorable protective effects against LC (6-8). It is well acknowledged that vitamin D exerts its biological functions by binding with vitamin D receptor (VDR). Consequently, it is possible that *VDR* variants, which may result in diminished function of vitamin D, may also be involved in the development of LC.

To date, some pilot studies have already investigated potential associations between *VDR* variants and LC. However, the results of these studies were conflicting, thus, we performed the present meta-analysis to obtain a more conclusive result.

MATERIALS AND METHODS

Literature search and inclusion criteria

This meta-analysis followed Preferred Reporting Items for Systematic Reviews and Meta-analyses (PRISMA) guideline (9). Potentially related literature published prior to January 2019 was retrieved from PubMed, Web of Science and Embase using the following searching strategy: (Vitamin D receptor OR VDR) AND (polymorphism OR variant OR variation OR mutation OR genotype OR allele) AND (lung OR pulmonary) AND (cancer OR carcinoma OR tumor OR oncology OR malignancy). We also checked the references of eligible articles to identify other potentially relevant studies.

To test the research hypothesis of this meta-analysis, the included studies met all the following criteria: i. case-control study on associations between *VDR* variants and LC; ii. provide genotypic frequency of investigated *VDR* variants in cases and controls; iii. full text in English available. Studies were excluded according to the following criteria: i. not relevant to *VDR* variants and LC; ii. *in vitro* studies or animal studies; iii. case reports or case series; iv. abstracts, reviews, comments, letters and conference presentations.

Key words: vitamin D receptor); gene variants; lung cancer; non-small cell lung cancer; meta-analysis

Corresponding Author:
Dr. Xiuli Wang,
Department of Pulmonary Medicine,
The Affiliated Tumor Hospital
Xinjiang Medical University, No. 789 Suzhou East Street,
Urumqi 830000, Xinjiang, China
e-mail: wangxiuli8896@163.com

0393-974X (2019)

For repeated reports, we only included the study with the largest sample size for analyses.

Data extraction and quality assessment

We extracted the following data from the included studies: (i) the name of the first author; (ii) publication time; (iii) country and ethnicity; (iv) sample size; and (v) genotypic distribution of *VDR* variants in cases and controls. The probability value (*p* value) of Hardy-Weinberg equilibrium (HWE) was also calculated. When necessary, we wrote to the corresponding authors for raw data. We used the Newcastle-Ottawa scale (NOS) to assess the quality of eligible studies (10). This scale has a score range of zero to nine, and studies with a score of more than seven were thought to be of high quality. Data extraction and quality assessment were performed by two independent reviewers. Any disagreement between two reviewers was solved by discussion until a consensus was reached.

Statistical analyses

We used Review Manager Version 5.3.3 (The Cochrane Collaboration, Software Update) to conduct statistical analyses. We calculated odds ratios (ORs) and 95% confidence intervals (CIs) to estimate strength of associations in all possible genetic models, and p values ≤ 0.05 were considered to be statistically significant. All investigated *VDR* polymorphisms contain a major allele (M) and a minor allele (m), and the definitions of all genetic comparisons were as follows, dominant comparison is defined as MM *vs* Mm + mm, recessive comparison is defined as mm *vs* MM +Mm, over-dominant comparison is defined as Mm *vs* MM + mm, and the allele comparison is defined as M *vs* m. Q test and I^2 statistic were employed to assess between-study heterogeneities. If p value of Q test was less than 0.1 or I^2 was greater than 50%, random-effect models (REMs) were used to pool the data. Otherwise, fixed-effect models (FEMs) were applied for synthetic analyses. Subgroup analyses by ethnicity of participants and type of disease were performed. Stabilities of synthetic results were evaluated with sensitivity analyses, and publication biases were evaluated with funnel plots.

RESULTS

Characteristics of included studies

We found 165 potential relevant articles among which, a total of 10 eligible studies were finally included for pooled analyses (Fig. 1). The NOS score of eligible articles ranged from 7 to 8, which indicated that all included studies were of high quality. Baseline characteristics of the included studies are shown in Table I.

Overall and subgroup analyses

Pooled overall analyses suggested that *VDR* rs1544410 (dominant model: $p = 0.01$, OR = 1.77, 95%CI 1.14-2.75; over-dominant model: $p = 0.02$, OR = 0.62, 95%CI 0.41-0.92; allele model: $p = 0.008$, OR = 1.59, 95%CI 1.13-2.25) and rs731236 (dominant model: $p = 0.04$, OR = 1.16, 95%CI 1.01-1.34; allele model: $p = 0.03$, OR = 1.13, 95%CI 1.01-1.26) variants were significantly associated with LC.

Further subgroup analyses by ethnicity revealed that rs7975232 (recessive model), rs1544410 (all genetic models) and rs731236 (dominant and allele models) variants were significantly associated with LC in East Asians. When we stratified data by type of disease, positive results were detected for rs1544410 (all genetic models) and rs731236 (dominant and allele models) variants in non-small cell lung cancer (NSCLC). No other positive findings were observed in overall and subgroup analyses (Table II).

Sensitivity analyses

Sensitivity analyses were performed to test stabilities of pooled results by excluding studies that violated HWE. No altered results were observed in overall and subgroup comparisons, which indicated that our findings were statistically stable.

Publication biases

We used funnel plots to assess publication biases. We did not find obvious asymmetry of funnel plots in any comparisons, which suggested that our findings were unlikely to be impacted by severe publication biases.

DISCUSSION

To the best of our knowledge, this is so far the most comprehensive meta-analysis on roles of VDR variants in LC, and our pooled analyses suggest that *VDR* rs7975232, rs1544410, and rs731236 variants were significantly associated with LC in East Asians, but not in Caucasians. There are two possible

Table I. *The characteristics of included studies.*

First author, year	Country	Ethnicity	Type of disease	Sample size	Genotype distribution		*P*-value for HWE	NOS score
					Cases	Controls		
ApaI rs7975232					AA/AC/CC			
Cai 2012	China	East Asian	NSCLC	144/142	76/63/5	74/60/8	0.353	8
Dogan 2009	Turkey	Caucasian	LC	137/156	44/64/29	58/76/22	0.716	8
Gromowski 2017	Poland	Caucasian	LC	823/919	236/412/175	235/500/184	0.005	8
Hou 2015	China	East Asian	NSCLC	288/284	142/116/30	136/100/48	<0.001	8
Kaabachi 2014	Tunisia	Caucasian	LC	240/280	101/118/21	100/134/46	0.922	7
Li 2013	China	East Asian	LC	72/67	49/19/4	30/28/9	0.550	8
Pan 2014	China	East Asian	NSCLC	62/70	33/24/5	36/25/9	0.178	7
Wei 2014	China	East Asian	LC	500/200	165/268/67	89/71/40	<0.001	8
Wu 2016	China	East Asian	NSCLC	426/445	140/191/95	142/214/89	0.607	8
Yang 2013	China	East Asian	NSCLC	105/71	62/41/2	38/29/4	0.613	8
BsmI rs1544410					AA/AT/TT			
Cai 2012	China	East Asian	NSCLC	144/142	134/10/0	124/18/0	0.420	8
Dogan 2009	Turkey	Caucasian	LC	137/156	57/60/20	45/86/25	0.131	8
Gromowski 2017	Poland	Caucasian	LC	810/916	330/388/92	384/410/122	0.449	8
Kaabachi 2014	Tunisia	Caucasian	LC	240/280	74/126/40	84/150/46	0.126	7
Wei 2014	China	East Asian	LC	500/200	353/147/0	102/98/0	<0.001	8
Wu 2016	China	East Asian	NSCLC	426/455	403/17/6	373/49/23	<0.001	8
Yang 2013	China	East Asian	NSCLC	105/71	99/6/0	62/9/0	0.568	8
FokI rs2228570					TT/TA/AA			
Gromowski 2017	Poland	Caucasian	LC	833/917	258/395/180	277/452/188	0.884	8
Kaabachi 2014	Tunisia	Caucasian	LC	240/280	134/90/16	116/134/30	0.342	7
Wu 2016	China	East Asian	NSCLC	426/445	166/192/68	160/204/81	0.261	8
TaqI rs731236					AA/AG/GG			
Cai 2012	China	East Asian	NSCLC	144/142	135/9/0	129/12/1	0.241	8
Dogan 2009	Turkey	Caucasian	LC	137/156	64/59/14	49/83/24	0.250	8
Gromowski 2017	Poland	Caucasian	LC	825/920	340/390/95	375/423/122	0.875	8
Hou 2015	China	East Asian	NSCLC	288/284	258/27/3	252/27/5	<0.001	8
Kaabachi 2014	Tunisia	Caucasian	LC	240/280	90/118/32	98/146/36	0.106	7
Pan 2014	China	East Asian	NSCLC	62/70	58/4/0	63/6/1	0.087	7
Wu 2016	China	East Asian	NSCLC	426/445	409/14/3	416/27/2	0.040	8
Yang 2013	China	East Asian	NSCLC	105/71	99/6/0	63/8/0	0.615	8

Abbreviations: LC: lung cancer; NSCLC: non-small cell lung cancer; HWE: Hardy-Weinberg equilibrium; NOS: Newcastle-Ottawa scale; NA: not available.

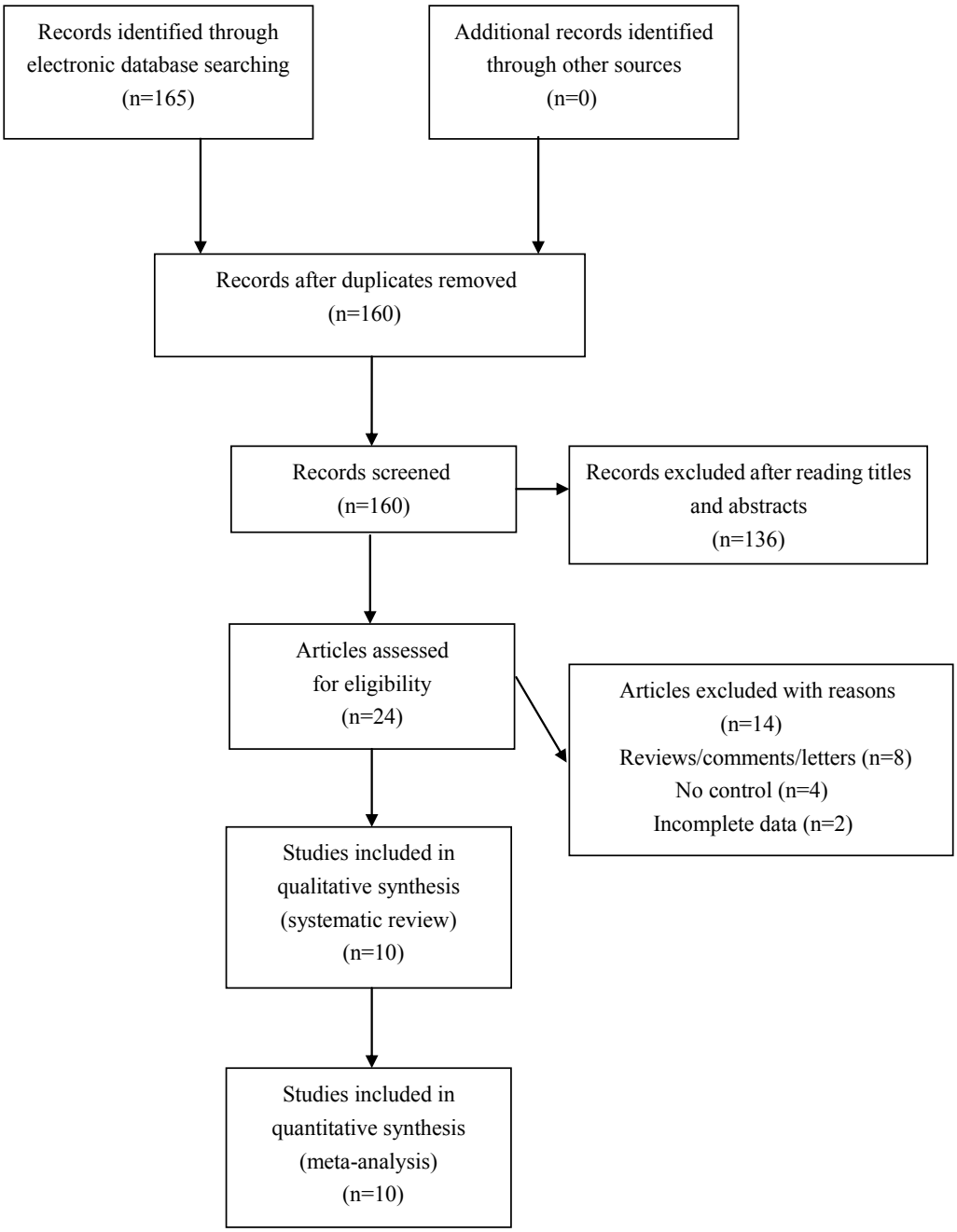

Fig. 1. *Flowchart of study selection for the present study.*

explanations for our positive findings. Firstly, genetic variations of the *VDR* gene may lead to alterations in gene expression or changes in VDR protein structure, which may subsequently affect biological functions of vitamin D and ultimately impact individual susceptibility to LC. Secondly, it is also possible that *VDR* variants may be linked to each other or even linked to other unidentified genes, which could also impact individual susceptibility to LC.

As with all meta-analysis, this study certainly has some limitations. Firstly, our results were based on unadjusted analyses, and we have to admit that lack of further adjusted analyses for potential confounding factors might impact the reliability of our findings (11). Secondly, associations between *VDR* variants and LC might also be modified by

Table II. *Results of overall and subgroup analyses.*

Polymorphisms	Population	Sample size	Dominant comparison		Recessive comparison		Over-dominant comparison		Allele comparison	
			P value	OR (95%CI)	*P* value	OR (95%CI)	*P* value	OR (95%CI)	*P* value	OR (95%CI)
ApaI rs7975232	Overall	2797/2634	0.51	1.07 (0.88-1.29)	0.08	0.78 (0.58-1.03)	0.75	1.04 (0.84-1.28)	0.19	1.09 (0.96-1.24)
	East Asian	1597/1279	0.67	1.06 (0.81-1.40)	**0.02**	**0.78 (0.63-0.96)**	0.61	1.09 (0.79-1.49)	0.25	1.07 (0.96-1.19)
	Caucasian	1200/1355	0.12	1.14 (0.97-1.36)	0.87	0.95 (0.54-1.69)	0.14	0.89 (0.76-1.04)	0.71	1.05 (0.82-1.35)
	NSCLC	1025/102	0.49	1.06 (0.89-1.27)	0.25	0.86 (0.67-1.11)	0.90	1.01 (0.76-1.04)	0.71	1.05 (0.82-1.35)
BsmI rs1544410	Overall	2362/2220	**0.01**	**1.77 (1.14-2.75)**	0.46	0.85 (0.55-1.31)	**0.02**	**0.62 (0.41-0.92)**	**0.008**	**1.59 (1.13-2.25)**
	East Asian	1175/868	**<0.001**	**2.67 (2.07-3.44)**	**0.005**	**0.27 (0.11-0.67)**	**<0.001**	**0.42 (0.32-0.54)**	**<0.001**	**2.38 (1.59-3.54)**
	Caucasian	1187/1352	0.44	1.13 (0.82-1.56)	0.44	1.13 (0.82-1.56)	0.67	0.94 (0.69-1.27)	0.40	1.05 (0.94-1.18)
	NSCLC	675/668	**<0.001**	**3.15 (2.15-4.63)**	**0.005**	**0.27 (0.11-0.67)**	**<0.001**	**0.39 (0.26-0.60)**	**<0.001**	**3.07 (2.17-4.36)**
FokI rs2228570	Overall	1499/1642	0.14	1.25 (0.93-1.67)	0.62	0.95 (0.79-1.15)	0.10	0.89 (0.77-1.02)	0.18	1.17 (0.93-1.47)
	Caucasian	1073/1197	0.29	1.34 (0.78-2.27)	0.60	0.86 (0.50-1.50)	0.21	0.80 (0.57-1.13)	0.37	1.22 (0.79-1.90)
TaqI rs731236	Overall	2227/2368	**0.04**	**1.16 (1.01-1.34)**	0.16	0.85 (0.68-1.07)	0.23	0.92 (0.80-1.06)	**0.03**	**1.13 (1.01-1.26)**
	East Asian	1025/1012	**0.04**	**1.42 (1.02-1.98)**	0.49	0.71 (0.27-1.88)	0.06	0.71 (0.50-1.01)	**0.03**	**1.41 (1.03-1.92)**
	Caucasian	1202/1356	0.22	1.22 (0.88-1.69)	0.20	0.86 (0.68-1.08)	0.66	0.97 (0.83-1.13)	0.11	1.10 (0.98-1.23)
	NSCLC	1025/1012	**0.04**	**1.42 (1.02-1.98)**	0.49	0.71 (0.27-1.88)	0.06	0.71 (0.50-1.01)	**0.03**	**1.41 (1.03-1.92)**

Abbreviations: OR: odds ratio; C: confidence interval; NA: not available; NSCLC: non-small cell lung cancer. The values in bold represent there is statistically significant differences between cases and controls. All investigated VDR polymorphisms contain a major allele (M) and a minor allele (m), and the definitions of all genetic comparisons were as follows: dominant comparison is defined as MM versus *Mm + mm, recessive comparison is defined as mm* vs *MM +Mm, over-dominant comparison is defined as Mm* versus *MM + mm, and the allele comparison is defined as M* versus *m.*

gene-gene and gene-environmental interactions. However, due to lack of raw data, we could not perform relevant analyses accordingly (11). Thirdly, only retrospective case-control studies were included in this meta-analysis, and thus direct causal relationship between the investigated variants and LC could not be established (12). On account of the above-mentioned limitations, our findings should be cautiously interpreted.

In conclusion, our meta-analysis suggested that *VDR* rs7975232, rs1544410 and rs731236 variants might serve as genetic biomarkers of LC in East Asians. However, further well-designed studies with larger sample sizes are still warranted to confirm our findings.

REFERENCES

1. Siegel RL, Miller KD, Jemal A. Cancer statistics, 2017. CA Cancer J Clin 2017; 67:7-30.
2. Ferlay J, Soerjomataram I, Dikshit R, et al. Cancer incidence and mortality worldwide: sources, methods and major patterns in GLOBOCAN 2012. Int J Cancer 2015; 136: E359-86.
3. Mondul AM, Weinstein SJ, Layne TM, Albanes D. Vitamin D and cancer risk and mortality: state of the science, gaps, and challenges. Epidemiol Rev 2017; 39:28-48.
4. Chen GC, Zhang ZL, Wan Z, et al. Circulating 25-hydroxyvitamin D and risk of lung cancer: a dose-response meta-analysis. Cancer Causes Control 2015; 26:1719-28.
5. Ma K, Xu W, Wang C, Li B, Su K, Li W. Vitamin D deficiency is associated with a poor prognosis in advanced non-small cell lung cancer patients treated with platinum-based first-line chemotherapy. Cancer Biomark 2017; 18:297-303.
6. Feldman D, Krishnan AV, Swami S, Giovannucci E, Feldman BJ. The role of vitamin D in reducing cancer risk and progression. Nat Rev Cancer 2014; 14:342-57.
7. Fleet JC, DeSmet M, Johnson R, Li Y. Vitamin D and cancer: a review of molecular mechanisms. Biochem J 2012; 441:61-76.
8. AlMatar M, AlMandeal H, Makky EA, Kayar B, Yarar E, Var I, Koksal F. The physiological/pathophysiological significance of vitamin D in cancer, cardiovascular disorders and beyond. Curr Drug Metab 2017; 18:207-24.
9. Moher D, Liberati A, Tetzlaff J, Altman DG, PRISMA group. Preferred reporting items for systematic reviews and meta-analyses: the PRISMA statement. Ann Intern Med 2009; 151:264-69.
10. Stang A. Critical evaluation of the Newcastle-

Ottawa scale for the assessment of the quality of nonrandomized studies in meta-analyses. Eur J Epidemiol 2010; 25:603-5.

11. Xie X, Shi X, Liu M. The Roles of TLR gene variants in atherosclerosis: a systematic review and meta-analysis of 35,317 subjects. Scand J Immunol 2017; 86:50-58.
12. Sun H, Li Q, Jin Y, Qiao H. Associations of tumor necrosis factor-α variants with the susceptibility of asthma: a meta-analysis. Exp Mol Pathol 2018; 105:411-66.

LETTER TO THE EDITOR

BASAL CELL CARCINOMA OF THE EYELID

D. BORRONI[1,2], M. PAREKH[3], C. ROCHA DE LOSSADA[4], S. ADATHILETHU[5], L. MARINO[1] and V. ROMANO[2]

[1]Department of Doctoral Studies, Riga Stradins University, Riga, Latvia; [2]Corneal and External Eye Service, St. Paul's Eye Unit, Royal Liverpool University Hospital, Liverpool, UK; [3]University College London - Institute of Ophthalmology, London, UK; [4]Department of Ophthalmology, Regional University Hospital of Malaga, Malaga, Spain; [5]University of Liverpool, School of Medicine, Liverpool, UK

Received February 17, 2019 – Accepted March 13, 2019

To the Editor,

Basal cell carcinomas (BCC) are the most common malignant tumors in the world, and 4.3 million cases of BCC are diagnosed in the United States every year. They represent 20% of eyelid tumors and 90% of eyelid malignancies (1). The purpose of this article is to present two cases with stage IV BCC (Fig. 1A) and infiltrated BCC (Fig. 1B). In both cases, a total destruction of the left side of the face was observed with open communication with the frontal sinus of the frontal bone reaching maxillary sinus. Loss of periocular tissues was observed with damage of approximately 95% of left nasal skin. Although both the patients complained of discomfort for 2-3 years, they never visited a tertiary care center for the treatment due to fear of consulting a doctor, which is usually observed in the patients residing in the Latvian rural areas where the medicare education is poor. It was extremely difficult to convince the patients to undergo medical treatment, as they were afraid to consult doctors. Although histopathology (1), microsurgical excision, hedgehog inhibitors, beam radiation (2), vismodegib, radiotherapy, imiquimod, eyelid reconstruction and exenteration (2) are known for diagnosis and treatment, unfortunately only palliative care was advised.

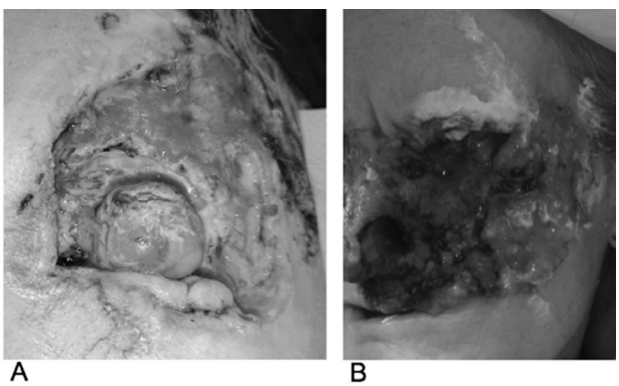

Fig. 1. ***A)*** *Stage IV basal cell carcinoma in a 58-year-old Male with advanced involvement of the left periorbital skin.* ***B)*** *Infiltrated basal cell carcinoma in a 62-year-old female with completely degraded orbit and loss of left eye including 95% involvement of the nasal skin.*

REFERENCES

1. Shi Y, Jia R, Fan X. Ocular basal cell carcinoma: a brief literature review of clinical diagnosis and treatment. Onco Targets Ther 2017; 10:2483-89.
2. Kakkassery V, Heindl LM. SOP - Standarized procedures in diagnostics and therapies of periocular basal cell carcinoma. Klin Monbl Augenheilkd 2017. doi: 10.1055/s-0043-120086.

Key words: basal cell carcinoma; eyelid

Corresponding Author:
Davide Borroni, MD
St. Paul's Eye Unit, Corneal and External Eye Service,
Royal Liverpool University Hospital
Prescot St, Liverpool L7 8XP, UK
Tel.: +44 7384726941
e-mail: info.borroni@gmail.com

0393-974X (2019)

DISCLOSURE: ALL AUTHORS REPORT NO CONFLICTS OF INTEREST RELEVANT TO THIS ARTICLE.

LETTER TO THE EDITOR

CHARACTERIZATION OF microRNA IN THE FOLLICULAR FLUID OF PATIENTS UNDERGOING ASSISTED REPRODUCTIVE TECHNOLOGY

L. MENCAGLIA[1], M. CERBONESCHI[2,3], F. CIOCIOLA[1], S. RICCI[1], I. MANCIOPPI[1], V. AMBROSINO[1], C. FERRANDI[4], F. STROZZI[4], P. PIFFANELLI[4] and A. GRASSELLI[5]

[1]Azienda USL Sud Est, Regione Toscana Centro di PMA Ospedale Santa Margherita La Fratta Cortona, Arezzo, Italy; [2]NEXT Genomics Srl, Prato, Italy; [3]Department of AgriFood Production and Environmental Sciences (DISPAA), University of Florence, Sesto Fiorentino (Florence), Italy; [4]PTP Science Park, Lodi, Italy; [5]IBSA Farmaceutici Italia Srl, Medical Scientific Division, Lodi, Italy

Received September 12, 2018 – Accepted February 18, 2019

To the Editor,

Female fertility plays a decisive role in the reproduction of mammals, with related issues that include oocyte or embryo quality, establishment of pregnancy, and the physiology of the tissues that contribute to reproduction and metabolic disorders associated with reproductive failure. Although reproductive failure may be attributed to various factors in different species, female infertility is largely controlled by a number of molecular signals that can be regulated in a cycle- and tissue-dependent manner (1).

Evaluation of embryonic potential is key to the fine-tuning of pre-implant diagnoses to reduce reproductive failure rates in patients undergoing assisted reproductive technology (ART) (2,3). Even in patients younger than 35 years, alterations in the number of chromosomes (aneuploidy) in embryos generated *in vitro* are common, in most cases resulting in a lack of implantation (1, 4). MicroRNAs (miRNAs) are single-stranded RNA molecules known to regulate gene expression at the transcriptional level of approximately 30% of human genes (5). A given miRNA may have different target messenger RNAs and each of these can be regulated by different miRNAs. A single miRNA can modulate the expression of multiple molecular pathways and ultimately cell functions, including the development of the follicle, oocyte maturation, preimplantation changes and embryo implantation (1, 5, 6).

While the role of miRNAs in female infertility has not yet been fully clarified, there is evidence that miRNAs have indicative functions in pregnancy and may have potential as markers of pregnancy failure and complications (7).

Therefore, this study aimed to identify and characterize miRNAs present in the follicular fluid of women undergoing intracytoplasmic sperm injection (ICSI) in order to evaluate the presence of miRNAs potentially predictive of pregnancy outcome and to compare the expression of these miRNAs in study populations.

MATERIALS AND METHODS

Study design

This retrospective monocentric study was performed from April 2014 to end February 2015 at the USL SUDEST

Key words: micro RNA; follicular fluid; assisted reproductive technology; pregnancy outcome

Corresponding Author:
Luca Mencaglia, MD
Department of Physiopathology of Reproduction,
USL Sud Est Toscana, Loc La Fratta 145,
52044 Cortona, Italy
Tel.: +39 0575 639278 - Fax: +39 0575 639275
e-mail: luca.mencaglia@uslsudest.toscana.it

0393-974X (2019)

Tuscany Region, PMA Center of the Santa Margherita Hospital La Fratta Cortona (AR), Italy. The Area Vasta Sudest C.E.A.V.S.E. ethics committee approved the protocol and all patients signed an informed consent. This study was performed according to the guidelines of the Standards for Reporting of Diagnostic Accuracy Studies (STARD) (http://www.equator-network.org/reporting-guidelines/stard).

Participants and in vitro fertilization protocol

Patients who met the following inclusion criteria were consecutively enrolled: females aged 18-38, basal follicle stimulating hormone (FSH) <10 IU/L, estradiol <80 pg/mL, absence of genetic abnormalities in their family history, presence of normal uterine cavity and normal thyroid function.

Exclusion criteria were: prior established poor response to gonadotropin stimulation (poor responders), ovarian hyperstimulation history (OHSS), polycystic ovary syndrome, stage III and IV endometriosis, dysthyroidism, cancer, renal or hepatic impairment and any other clinical condition judged incompatible with the present study.

Only patients with normal seminal parameters according to WHO 2010 were selected for the study. The patient population observed was homogeneous regarding the factors that could potentially influence the biological processes observed (age, smoking status, indication for infertility treatment).

A total of 40 female ICSI patients were enrolled in the last quarter of 2015. For ovarian stimulation, 20 patients were treated with purified FSH, according to the long-acting protocol: Suprefact (buserelin, Sanofi)/Fertipeptil (triptorelin, Ferring) and Fostimon (urofollitropin, IBSA Pharmaceuticals Italia). The duration of gonadotropin treatment was approximately 11 days at varying doses ranging from 1500 to 3000 IU. The other 20 patients were treated according to the long-acting protocol with GnRh analogue agonist (buserelin, Sanofi)/Fertipeptil (triptorelin, Ferring)/Decapeptyl 3.75 (triptorelin, IPSEN) and Gonal F (follitropin alfa, Merck Serono SpA) or Puregon (follitropin beta, Merck Sharp and Dohme). The duration of treatment with gonadotropin was approximately 11 days, at doses ranging from 1300 to 3300 IU.

RNA extraction

At the time when oocytes were collected (pick-up) follicular fluid was also isolated, immediately frozen in liquid nitrogen and stored for subsequent miRNA analysis. Samples were initially identified as "P" when referring to follicular fluids derived from patients treated with "purified" hormone (urofollitropin), or identified as "R" when referring to samples derived from patients treated with the "recombinant" hormone (alfa or beta follitropin).

Follicular fluid samples were subjected to the following treatments:

i. Gradient extraction of blood and cell debris from follicular fluid by centrifugation at 12,000 g.

ii. Total miRNA purification from follicular fluid was performed by NucleoSpin miRNA (Macherey-Nagel) according to the manufacturer's protocol.

iii. Quantification and quality assessment of purified miRNA was performed using the RNA chip kit and the Agilent Bioanalyzer tool (Bioanalyzer 2100, Agilent Technologies, CA, USA).

Library generation and next generation sequencing

miRNA libraries required for sequencing were set up following Illumina's "TruSeq small RNA" protocol. The protocol was optimised for 1 µg of total RNA in 5 µl nuclease free water. Deep sequencing analysis was then performed on HiSeq2000 (Illumina) using the 50SR protocol.

Bioinformatics and statistical analysis of sequencing data

The quality of raw sequence reads was checked using FastQC v0.11.2 (https://www.bioinformatics.babraham.ac.uk/projects/fastqc/). Illumina raw sequences were quality filtered and adapter trimmed using Trimmomatic software v.0.32. Each read was processed and trimmed with a cut-off value for the minimum base quality set at 15 (Phred score) over 4 bases sliding window. Trimmed sequences were used for small-RNA quantification and discovery with the Mirdeep2 software. Known human small-RNA (mature and precursors) were downloaded from the miRbase database (http://www.mirbase.org/) and used for comparison.

Both novel (i.e., previously undiscovered) and known small-RNA were used to quantify reads counts for each sample using Mirdeep2 utilities. This pipeline produced a simple list for each sample of small-RNA IDs and the relative abundance of mapping reads, and these counts files were then submitted for downstream statistical analysis.

For mature miRNA expression profiles, statistical analyses were performed using R statistical software and edgeR package that allows differential expression analysis of RNA-seq expression profiles with biological replication. Only genes having at least one count per million over at least three samples were selected to filter low expressed genes. The filtered counts were normalized using the edgeR TMM method and the comparisons among sample groups were performed using the edgeR statistical exact test. Lists of statistically relevant miRNAs for the differential expression among the two experimental conditions (R and P) were generated and filtered using a Benjamini–Hochberg FDR adjusted P-value <0.05.

Target analysis for novel miRNAs identified with Mirdeep2 was performed using MirTarget (http://mirdb.org/miRDB/index.html) and NCBI-Blast searches with optimized parameters for short query sequences (blastn-short).

Statistical analysis

Descriptive analyses were performed. The distribution of each variable was evaluated by the Kolmogorov-Smirnov test. The prevalence of patients in each subgroup was compared by the Fisher-Yates test. Comparison of variables among different groups was performed by *t*-test when they showed normal distribution, whereas Mann-Whitney or Kruskal-Wallis tests were applied for not-normally distributed parameters. Post-hoc tests were performed by the Dunnet test. Parameters were compared by Spearman's correlation coefficient. For all comparisons, a p-value <0.05 was considered statistically significant.

Statistical analysis was performed using the 'Statistical Package for the Social Sciences' software for Macintosh (version 21.0; SPSS Inc., Chicago, IL, USA).

RESULTS

Baseline demographic and clinical characteristics of the patients is presented in Table I. Individual samples of follicular fluid derived from 40 patients who underwent ICSI were initially collected and analyzed. Applying a pre-determined cut-off of 500K sequences to allow for poor sequencing during the deep sequencing analysis, 10 samples were eliminated: 5 from group P and 5 from group R, reducing the experimental sample to the data of only 30 patients (15 samples each). The 30 included patients had a mean age of 33.3 years (32.5 years in group P and 34.1 years in group R, respectively).

Sequencing data for the 30 selected samples were then subjected to a first quantitative analysis of global miRNA expression (MDS plot, Fig. 2). From this analysis similarity ratios emerged, regardless of the type of FSH with which patients were treated (P = Purified *vs* R = Recombinant). Furthermore, the analysis highlighted a set of samples that were very closely related based on the global expression profile of miRNAs, regardless of the FSH formulation used by patients.

Analysis P vs R

Global sequencing of miRNAs obtained from the two groups of 15 samples (P, R) were then subjected to a differential statistical analysis with the aim of evaluating the presence of miRNAs differentially expressed within the two P and R groups

Differential analysis highlighted 23 miRNAs that were statistically significant in a confidence interval greater than 95% (FDR, correct P value). The outcome of the mirDeep2 analysis on the two treatment groups, which encompass miRNAs sequenced in all samples, regardless of their expression level in the two groups, identified a total of 252 miRNAs differentiated between the two treatment groups. A total of 23 miRNAs showed a statistically significant change in their expression levels between the two groups (FDR <0.5%).

Of the 23 miRNAs selected for their expression pattern, 18 represent "novel" miRNAs and are significantly up-regulated only in the purified FSH (P) group; for 4 of the 5 known miRNAs, a significant down regulation was observed in the group of follicular fluid samples derived from women treated with recombinant FSH.

The target genes of 5 "known" miRNAs were identified using the miRbase miRNA database. Target genes of the 18 "new" miRNAs were identified using two different strategies: "MirTarget", a miRDB online software tool, and BLAST analysis in NCBI (data not shown).

Our analysis, supported by the experimental data of Lin et al. (8), showed that there was no difference

Table I. *Patient baseline and clinical characteristics.*

Patient Code	Age (years)	Cause of infertility	BMI (kg/m^2)	FSH (mIU/mL)	Estradiol (pg/mL)	Suppression	GnRh analogue / agonist	Total dose (mg)	Cycle Outcome
Purified follicle stimulating hormone group									
12746	34	Idiopathic	25	0.3	OK	Suprefact	Fostimon	2175	Negative
13866	37	Idiopathic	24	7.0	21	Fertipeptil	Fostimon	2175	Negative
14108	36	Male (mild)	26	0.3	OK	Fertipeptil	Fostimon	2175	Positive
14295	29	Male (mild)	22	6.6	34	Fertipeptil	Fostimon	1650	Positive
12553	40	Male (mild) and Tubal		6.5		Fertipeptil	Fostimon	1575	Positive
13368	40	Idiopathic		9.2		Fertipeptil	Fostimon	2025	Positive
13488	32	Endometriosis		7.0		Suprefact	Fostimon	2325	Negative
15292	31	Male	25	7.7	52	Suprefact	Fostimon	2850	Negative
14324	40	Idiopathic		7.4	50	Suprefact	Fostimon	2475	Interrupted (lack of fertility)
13549	32	Tubal		6.5		Suprefact	Fostimon	2475	Negative
14282	37	Male	28	7.5	52	Suprefact	Fostimon	2475	Positive
14553	27	Male and Female		5.3		Suprefact	Fostimon	1875	Interrupted (hyperstimulation)
15250	35	Tubal	21	6.6	101	Suprefact	Fostimon	2250	Negative
14442	32	Male	22	4.9		Suprefact	Fostimon	1500	Positive
14110	38	Endometriosis	25	7.6	45	Suprefact	Fostimon	2175	Negative
Recombinant follicle stimulating hormone group									
13432	33	Idiopathic		5.0		Suprefact	Puregon	3300	Negative
13061	32	Male				Suprefact	Gonal F	1000	Positive
9179	24	Idiopathic		5.5		Suprefact	Gonal F	1725	Positive
13332	38	Male (mild)	36	5.0		Suprefact	Puregon	3600	Negative
14009	38	Male (mild)	27	7.4		Suprefact	Gonal F	3300	Biochemical pregnancy
11985	38	Male				Suprefact	Puregon	3300	Negative
14823	27	Male (mild)				Decapeptyl 3.75	Gonal F	1675	Interrupted (hyperstimulation)
15153	34	Ovulatory endocrine		7.9		Fertipeptil	Gonal F	1950	Positive
14052	38	Mixed		9.1	49	orgalutran	Puregon	3300	Negative
883	40	Tubal		6.1	55	Suprefact	Gonal F	2475	Negative
13436	35	Idiopathic		6.7	91	Suprefact	Puregon	2200	Positive
9708	33	Ovulatory endocrine				Decapeptyl 3.75	Gonal F	1350	Interrupted (high risk)
12276	39	Tubal		7.9		Fertipeptil	Gonal F	2175	Negative
15110	39	Idiopathic				Suprefact	Gonal F	2175	Positive

BMI: body mass index; FSH: follicle stimulating hormone

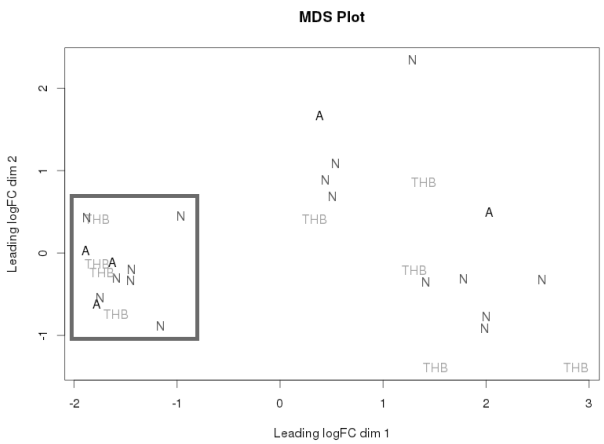

Fig. 1. *MDS plot intracytoplasmic sperm injection (ICSI). The distance/proximity of the samples is indicative of their diversity/resemblance to the total expression of miRNAs. Close by samples show very similar expression profiles, while distant samples show substantial differences between them. The letter "N" indicates the patients in whom the absence of pregnancy has been observed; "A" biochemical pregnancy and "THB" live newborn (take home baby). Grey square groups identify a set of samples with similar total levels of miRNA expression.*

Table II. *Follicular fluid samples evaluated.*

Purified follicle stimulating hormone group			Recombinant follicle stimulating hormone group		
Code	Pregnancy outcome	Pregnancy tag	Code	Pregnancy outcome	Pregnancy tag
P1	Absence	N	R1	Absence	N
P2	Abortion	A	R2	Live birth	THB
P3	Live birth	THB	R4	Live birth	THB
P4	Live birth	THB	R5	Absence	N
P7	Live birth	THB	R7	Biochemical	A
P8	Live birth	THB	R8	Absence	N
P9	Absence	N	R10	Live birth	THB
P10	Absence	N	R11	Live birth	THB
P11	Absence	N	R13	Absence	N
P12	Absence	N	R14	Absence	N
P13	Biochemical	A	R15	Absence	N
P15	Absence	N	R16	Live birth	THB
P16	Absence	N	R17	Absence	N
P17	Abortion	A	R18	Absence	N
P19	Absence	N	R19	Abortion	A

Follicular fluid samples evaluated after the bioinformatic quality check of microRNA sequencing. The column "Code" refers to the original classification of patients in the Purified versus Recombinant (P vs R) contrast study; "Pregnancy outcome" and "Pregnancy tag" to the final outcome of each pregnancy. Samples labeled as "N" indicate those in which the absence of pregnancy was observed; "A" biochemical pregnancies but with no later evolution; and "THB" for live newborns ("take-home baby").

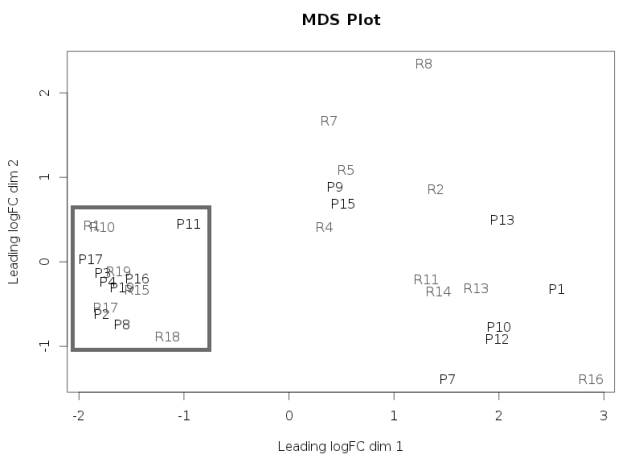

Fig. 2. *MDS plot of FSH treatment. The distance/proximity of the samples is indicative of their diversity/resemblance at the total expression level of miRNAs, regardless of experimental design (P vs. R). Closely related samples show very similar expression profiles, while distant samples display substantial differences among them. With R are highlighted samples for the "recombinant" group, P depicted codes for the "purified" group. A square identifies a set of samples with similar total levels of miRNA expression.*

Table III. *Significantly up-regulated MiRNAs and their association with pregnancy outcome.*

miRNAs associated with negative pregnancy outcome			
Micro ID	Log FC	FDR	P-value
Novel:17_14495	5.940	1.46×10^{-2}	1.96×10^{-5}
Novel:22_24557	9.041	2.06×10^{-2}	8.40×10^{-5}
Novel:16_11171	6.308	2.06×10^{-2}	1.06×10^{-4}
Novel:1_21252	4.365	2.06×10^{-2}	1.37×10^{-4}
Novel:X_47984	4.146	2.06×10^{-2}	1.39×10^{-4}
Novel:20_22416	4.865	3.05×10^{-2}	2.79×10^{-4}
hsa-mir-375	3.463	3.05×10^{-2}	2.88×10^{-4}
Novel:11_2815	3.759	3.07×10^{-2}	3.31×10^{-4}
hsa-mir-3679	4.070	3.64×10^{-2}	4.42×10^{-4}
Novel:X_46609	4.177	4.18×10^{-2}	6.06×10^{-4}
Novel:8_43470	4.912	4.18×10^{-2}	6.20×10^{-4}
miRNAs associated with positive pregnancy outcome (born alive)			
Micro ID	Log FC	FDR	P-value
Novel:15_9638	4,597	1.03×10^{-2}	1.39×10^{-5}
hsa-mir-615	2.917	1.06×10^{-2}	2.85×10^{-5}
Novel:4_31392	4.214	2.27×10^{-2}	1.62×10^{-4}
Novel:17_13367	3.600	2.27×10^{-2}	2.1×10^{-4}
Novel:14_8898	3.005	2.27×10^{-2}	2.24×10^{-4}
Novel:14_8888	4.599	2.27×10^{-2}	2.62×10^{-4}
Novel:14_8095	4.599	2.27×10^{-2}	2.64×10^{-4}
Novel:X_46609	-5.930	2.27×10^{-2}	2.74×10^{-4}
hsa-mir-1243	3.028	2.27×10^{-2}	2.75×10^{-4}
Novel:13_7643	4.154	2.4×10^{-2}	3.23×10^{-4}
Novel:17_12935	3.263	2.84×10^{-2}	4.22×10^{-4}

between pregnancy outcome and the different FSH formulations, likely due to the small number of samples.

Based on the results obtained (Fig. 2), we decided to re-evaluate the expression of the miRNA by reclassifying the original samples not by pharmacological treatment (FSH-P *vs* FSH-R), but on the basis of the results of treatment. Samples were then labeled as "N" indicating those in which the absence of pregnancy has been observed; "A" biochemical pregnancies but with no later evolution and "THB" live newborns ("take-home baby") (Table II).

Comparative analysis was carried out as follows:

i. N *vs* A + THB

ii. THB *vs* A + N

This new analysis allowed characterization of the subgroup that was initially identified in the P *vs* R analysis, revealing that 73% of the samples refer to biochemical pregnancy or absence of pregnancy. The distance/proximity of the samples, indicative of their diversity/resemblance to the total expression of miRNAs is summarized in Fig. 1.

Follicular fluid miRNAs associated with negative pregnancy outcome

A further evaluation of miRNA expression was then performed using data on pregnancy results by using contrast analysis N *vs* A + THB and THB *vs* N + A.

The analysis between groups N and A + THB highlighted a new set of 11 statistically significant miRNAs (FDR <0.5%), which are reported in Table III.

These 11 miRNAs are significantly up-regulated in the group associated with negative pregnancy outcome. None of these belong to the "novel" miRNA significantly up-regulated exclusively in the purified FSH group (P). Based on these data, it can be stated that the increase in expression levels of miRNAs included in Table III correlates with a "negative pregnancy" phenotype. Therefore, an increase in the relative amount of these miRNAs within follicular fluid could be associated with a low probability of pregnancy.

Follicular fluid miRNAs associated with positive pregnancy outcome

Table III also shows the other 11 miRNAs with a significant difference in their expression levels (FDR <0.5%) between THB and N + A groups.

Differential analysis revealed 10 miRNAs that have been significantly up-regulated in the group were associated with live born babies, three of which belong to the "novel" miRNAs significantly up-regulated exclusively in the purified FSH (P) treated group. The miRNA Novel: X_46609 was reported in Table III with an inverse outcome: up-regulated in the case of negative pregnancy and down-regulated in the case of positive pregnancy outcome, as expected. Based on these data, it can be stated that an increase in the expression levels of miRNAs reported in Table III correlates with the "live birth" phenotype. Therefore, an increase in the relative amount of these miRNAs within the follicular fluid could be indicative of a high probability of positive pregnancy outcome.

DISCUSSION

Initially it was thought that miRNAs only existed in the cellular microenvironment and were not present in extracellular spaces. However,

recent studies have now detected extracellular (EC) miRNAs in a wide range of biological fluids, including follicular fluid (9-12). Follicular fluid is produced by both the transmission of blood plasma substances that cross the blood follicular barrier and by the secretory actions of granulosa and thecal cells (12), and miRNAs within follicular fluid may reflect the follicular microenvironment and determine the quality of oocytes. The expression patterns of EC miRNAs in follicular fluid have been shown to be linked to the physiological state of the ovary, and may be associated with age-related reduction in ovarian function and subsequent infertility (11, 12).

A functioning and healthy oocyte is essential for the successful fertilization and consequent *in vitro* embryo development, and EC miRNAs may be ideal biomarkers to assess oocyte quality because they are widely expressed in serum and follicular fluid or secreted into culture media via oocytes and embryos.

Our study enabled us to identify 23 miRNAs differentially expressed between the two groups (P *vs* R FSH), including a cluster of 18 "novel" miRNAs. Eleven miRNAs were associated with a negative pregnancy outcome, while 11 others were associated with a positive pregnancy outcome and live birth of a newborn. Furthermore, target genes of five miRNAs were also found to be differentially expressed in follicular fluid samples. All miRNAs were found to be overexpressed in the group associated with a negative pregnancy outcome.

The limitations of our study were the small number of subjects involved and the retrospective design. However, our findings are of interest and justify and stimulate further investigations to improve our understanding of the role of miRNA in pregnancy. In future, identifying the presence or overexpression of these miRNAs in follicular fluid, may represent a useful predictive marker of positive pregnancy outcome ("take-home babies").

ACKNOWLEDGEMENTS

The authors would like to thank Colin G. Egan, PhD (CE Medical Writing, Pisa, Italy) and Carmen Innes, an independent Medial Writer on behalf of Springer Healthcare, who provided skillful editorial assistance. This study was sponsored by IBSA Farmaceutici Italia Srl.

CONFLICT OF INTEREST STATEMENT

A.G. is an employee of IBSA Farmaceutici Srl. The authors declare that they have no other relationships or activities that could appear to have influenced the submitted work.

REFERENCES

1. Tesfaye D, Salilew-Wondim D, Gebremedhn S, et al. Potential role of microRNAs in mammalian female fertility. Reprod Fertil Dev 2016; 29(1):8-23.
2. Li J, Liu D, Wang J, et al. Meta-analysis identifies candidate key genes in endometrium as predictive biomarkers for clinical pregnancy in IVF. Oncotarget 2017; 8(60):102428-36.
3. Wells D. Mitochondrial DNA quantity as a biomarker for blastocyst implantation potential. Fertil Steril 2017; 108(5):742-47.
4. Capalbo A, Rienzi L, Cimadomo D, et al. Correlation between standard blastocyst morphology, euploidy and implantation: an observational study in two centers involving 956 screened blastocysts. Hum Reprod 2014; 29(6):1173-81.
5. Catalanotto C, Cogoni C, Zardo G. MicroRNA in control of gene expression: An overview of nuclear functions. Int J Mol Sci 2016; 17(10):pii: E1712.
6. Eisenberg I, Kotaja N, Goldman-Wohl D, Imbar T. microRNA in human reproduction. Adv Exp Med Biol 2015; 888353-87.
7. Zhao Z, Zhao Q, Warrick J, et al. Circulating microRNA miR-323-3p as a biomarker of ectopic pregnancy. Clin Chem 2012; 58(5):896-905.
8. Lin L, Du T, Huang J, Huang LL, Yang DZ. Identification of differentially expressed microRNAs in the ovary of polycystic ovary syndrome with hyperandrogenism and insulin resistance. Chin Med J (Engl) 2015; 128(2):169-74.
9. Chen X, Ba Y, Ma L, et al. Characterization of microRNAs in serum: a novel class of biomarkers for diagnosis of cancer and other diseases. Cell Res 2008; 18(10):997-1006.
10. Chim SS, Shing TK, Hung EC, et al. Detection

and characterization of placental microRNAs in maternal plasma. Clin Chem 2008; 54(3):482-90.
11. Diez-Fraile A, Lammens T, Tilleman K, et al. Age-associated differential microRNA levels in human follicular fluid reveal pathways potentially determining fertility and success of in vitro fertilization. Hum Fertil (Camb) 2014; 17(2):90-98.
12. Sohel MM, Hoelker M, Noferesti SS, et al. Exosomal and non-exosomal transport of extracellular microRNAs in follicular fluid: Implications for bovine oocyte developmental competence. PLoS One 2013; 8(11):e78505.

LETTER TO THE EDITOR

NOMA: A REAPPRAISAL IN WESTERN COUNTRIES - ARE HIV-NEGATIVE IMMUNOCOMPETENT ADULT PATIENTS SAFE?

M. MASCITTI[1], A. BARLATTANI[2], L. TOGNI[1], F. SAMPALMIERI[1], G. FAVIA[3], L. LO MUZIO[4] and A. SANTARELLI[1,5]

[1]Department of Clinical Specialistic and Dental Sciences, Marche Polytechnic University, Ancona, Italy; [2]Department of Clinical Sciences and Translational Medicine, Tor Vergata University, Roma, Italy; [3]Department of Interdisciplinary Medicine, Complex Operating Unit of Odontostomatology, "Aldo Moro" University, Bari, Italy; [4]Department of Clinical and Experimental Medicine, University of Foggia, Foggia, Italy; [5]National Institute of Health and Science of Aging, INRCA, Ancona, Italy

Received September 27, 2018 – Accepted January29, 2019

To the Editor,

Noma is an ancient Greek term referring to a gangrenous disease that destroys soft and hard tissues of oral and perioral structures (1). This disease has been known since ancient times and persisted in Europe until World War 2 (2), while in the present day it is almost exclusively found in sub-Saharan Africa. It most commonly affects children under 16 years of age with compromised health conditions, due to malnutrition, poor oral hygiene, and other diseases (3).

Exact incidence and prevalence are not well established due to the difficulty in obtaining reliable data from the most affected areas (4). Literature data estimate that 770,000 people are affected by Noma sequelae, with a global incidence of approximately 30-40,000 cases, predominantly in African countries (4).

The pathogenesis of Noma can be divided into 3 stages: the "staging period", the "infection period", and the "invasive-destruction stage". In the "staging period" there is a weakening of the local defences due to several risk factors, leading to the formation of an ulcer. The "infection period" is characterized by the presence of a trigger microorganism that infects both the ulcer and the surrounding tissues, resulting in oral mucositis that is characterised by polymicrobial growth. Finally, in the invasive-destruction stage, a gangrenous infection develops and invades the facial tissues (1). The prognosis is poor without treatment, due to development of sepsis that determines the death of 90% of these patients within 2 weeks (5), while the mortality rate with treatment is about 10-20% (6). Adults are rarely affected by Noma, mainly immunocompromised patients, such as HIV-positive subjects or cancer patients undergoing chemotherapy (7).

In developed countries, sporadic cases of Noma occur in HIV-positive patients as oral opportunistic infection. In this work we report 3 cases of Noma referred to the Complex Operating Unit of Odontostomatology, involving HIV-negative Caucasian women in Italy.

For all three patients, written informed consent was obtained, and the study was conducted in accordance with the "Ethical Principles for Medical Research Involving Human Subjects" statement of the Helsinki Declaration.

Key words: noma; cancrum oris; immunocompetent patient; type 2 diabetes mellitus

Corresponding Author:
Prof. Andrea Santarelli,
Via Tronto 10,
60126 Ancona, Italy
Tel.: +39 071 2206226
Fax: +39 071 2206221
e-mail: andrea.santarelli@staff.univpm.it

0393-974X (2019)

DISCLOSURE: ALL AUTHORS REPORT NO CONFLICTS OF INTEREST RELEVANT TO THIS ARTICLE.

Case 1

A 75-year-old woman was referred for a painful ulcer in the cheek mucosa, which prevented her from feeding properly. She reported a 7-day burning pain inside the mouth at right cheek and mandibular regions, followed after 3 days by ulceration and swelling. The patient noticed weight loss in the previous 2 weeks. Her medical history was significant for diverticular disease and the use of Lactulose to treat constipation.

Physical examination showed the presence of moderate swelling and redness of the right cheek, near the mandibular angle. The neck was soft without evidence of lymphadenopathy, tenderness or erythematosus changes in the skin. A 2.5 x 2 cm non-bleeding ulcer in the right cheek was found, with soft borders and superficial gangrenous aspects (Fig. 1). The patient had a maxillary removable dental prosthesis and poor oral hygiene (Plaque Control Record (PCR) of 75%, Gingival Index (GI) of 2.0,

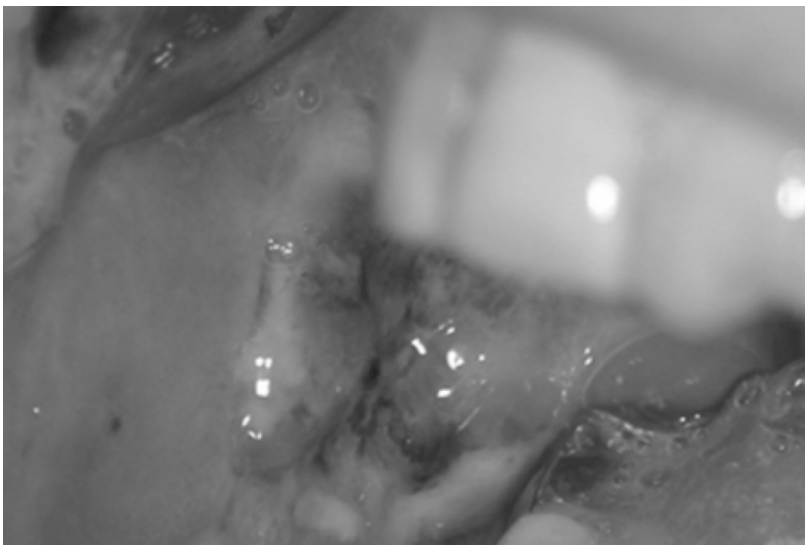

Fig. 1. *Case 1: Large ulceration of the right cheek mucosa with superficial necrotic-gangrenous aspects.*

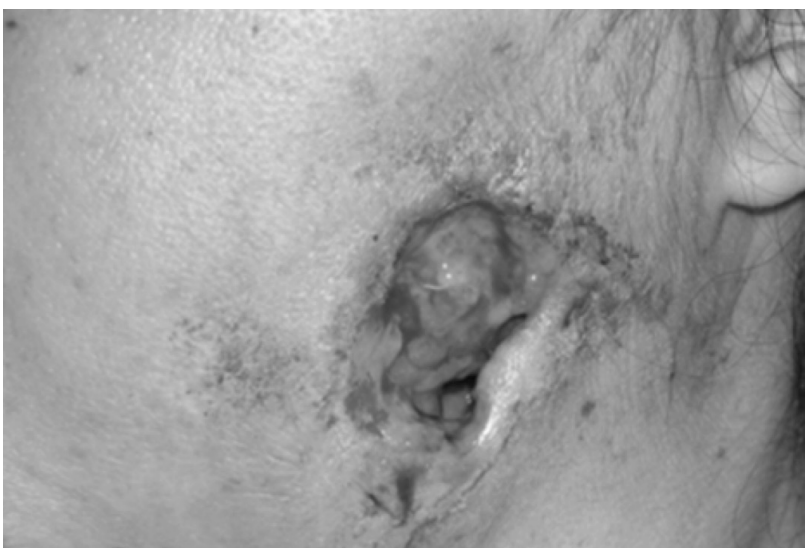

Fig. 2. *Case 2: Wide loss of substance near the mandibular angle with a clear exposure of masseter muscle.*

and large calculus deposits). Two biopsy samples were taken from the ulcer borders and processed for histological analysis, bacterial isolation, and susceptibility testing to antibiotic agents.

Histology was unremarkable, showing acute and chronic inflammatory infiltrates, with granulocyte infiltration near the necrotic sites. Microbiological culture results revealed the presence of *Candida spp.* and non-specific gram-negative cocci infection.

Routine laboratory tests showed mild anaemia (haemoglobin 11.5 g/dL), haematocrit level of 36%, normal ferritin blood level, low transferrin saturation level, borderline levels of sodium and potassium, and low albumin (3 g/dL). Nutritional assessment revealed a weight of 58 kg (BMI of 22) and a recent weight loss of about 2 kg. Biochemical data showed erythrocyte sedimentation rate (ESR) of 40 mm/hr and C-reactive protein (CRP) of 8.8 mg/L. Mini Nutritional Assessment (MNA) was administered to the patient, showing the presence of risk of malnutrition.

After tissue and blood sample collection, empirical antibiotic and antifungal therapy was started (IV infusion of cephalosporin for 3 g/dayand oral nystatin, 600,000 IU, 4 times a day). Oral hygiene regimen was based on saline and peroxide rinses, and chlorhexidine-based solution. Local wound care consisted of a daily irrigation with a solution of rifampicin, saline and hydrogen peroxide. Due to the general conditions of the patient, nasogastric tube feeding was started to ensure adequate intake of micronutrients and calories. Oral feeding was resumed after clinical improvement. The oral ulcer had not progressed to perforation and started to heal in the following days. The recovery was complete after a week, and the patient was discharged in good condition. Follow-up visits were made every 3 months for 2 years, showing no recurrences.

Case 2

A 43-year-old woman was referred for a painful ulcer in the cheek mucosa. The patient reported a 10-day burning pain in the molar region, with inflammation and swelling of the mandibular left posterior region. The inflammation has spread to the cheek, followed after 4 days by ulceration with spontaneous skin drainage. She reported a slight weight loss, due to the difficulties in chewing and swallowing. Her medical history was significant for diabetes mellitus (DM) under treatment with oral antihyperglycemic agents. The patient was a "light smoker" (<10 cigarettes/day), and overweight (BMI of 26.6).

Physical examination showed the presence of moderate swelling of the left cheek and a 3 x 2 cm non-bleeding ulcer with soft borders (Fig. 2). The neck was soft without evidence of lymphadenopathy, tenderness or erythematosus changes in the skin. Oral examination revealed a 3.5 x 2.5 cm non-bleeding ulcer, with exposure of the masseter muscle. The patient had poor oral hygiene (PCR of 70%, GI of 3.0, slight calculus deposits) and chronic generalized periodontitis. Two biopsy samples were taken from the ulcer borders: histological analysis and microbiological culture test revealed non-specific features, as in Case 1. Routine blood tests showed a mild neutrophilic leucocytosis, ESR of 50 mm/hr and CRP of 10 mg/L. DM was poorly controlled (blood glucose levels of 210 mg/dL and HbA1c of 7.5%).

Empirical antimicrobial therapy was carried out with antibiotic and antifungal therapy for 1 week, consisting in amoxicillin 3 g/day, metronidazole 1.5 g/day, doxycycline 200 mg/day and fluconazole 300 mg/day. In the following 2 weeks, the antibiotic therapy was changed to amoxicillin 2 g/day and metronidazole 500 mg/day. As with Case 1, a strict oral hygiene regimen and a local wound care were performed, and a wound impermeable dressing was placed over the defect. Moreover, nasogastric tube feeding was started due to difficulty chewing and swallowing. The patient was hospitalized for 2 weeks, and antibiotic therapy was continued for another week. The patient showed marked improvement in the following days, and she was able to resume normal oral feeding. The patient was discharged after complete recovery, and follow-up visits were made every week for 1 month, followed by a visit every 3 month for 1 year, showing no recurrences. Reconstructive surgery will be planned to correct the aesthetic deficit caused by the scar formation.

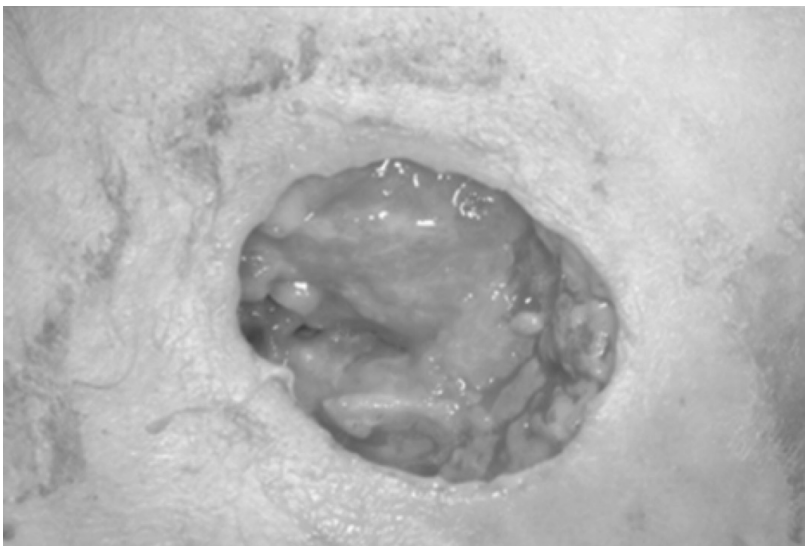

Fig. 3. *Case 3: Loss of substance near the right mandibular angle with exposure of soft surrounding tissues.*

Case 3

A 36-year-old woman was referred for a painful swelling of the right mandibular area, causing eating difficulties accompanied by weight loss. The patient reported a 5-day burning pain in right mandibular region, accompanied by the appearance of a bluish area on the skin, followed after 4 days by ulceration. The patient reported a weight loss of 3 kg over the past 2 weeks, due to several medical reasons.

Medical history revealed that the patient suffered from acute gastroenteritis 2 weeks before the onset of oral symptoms. In particular, she reported a 5-day history of self-limited watery diarrheal illness, with nausea, anorexia, and mild fever. Moreover, the patient reported dental extraction of the first mandibular right molar 5 days before the onset of oral symptoms. The patient was overweight (BMI of 26.8) and had quit smoking about 1 year previously.

Physical examination showed the presence of moderate swelling of the right mandibular angle and a 4 x 3 cm non-bleeding ulcer with soft borders (Fig. 3). Clinical examination of the neck was unremarkable. A large bleeding ulcer (3.5 x 3 cm) was present near the right mandibular angle. The patient had poor oral hygiene (PCR of 80%, GI of 3.0, large calculus deposits) and chronic generalized periodontitis. Two biopsy samples were taken from the ulcer borders: histological analysis and microbiological culture test revealed non-specific features, as in Case 1. Routine laboratory tests showed mild neutrophilic leucocytosis, ESR of 45 mm/hr and CRP of 11 mg/L, hypokalaemia (3.0 mEq/l), and borderline sodium levels.

Empirical antimicrobial therapy was carried out with antibiotic and antifungal therapy for 1 week, following the same protocol used in Case 2. As with the previous case, strict oral hygiene regimen and local wound care were performed, and a wound impermeable dressing was placed over the defect. Moreover, nasogastric tube feeding was started due to difficulty chewing and swallowing and continued until clinical improvement. The patient remained hospitalized for 2 weeks and was treated with the same therapeutic regimen used in Case 2. Follow-up visits were made every week for 1 month, followed by a visit every 3 months for 1 year, showing no recurrences. As for the previous case, reconstructive surgery will be planned to correct the aesthetic deficit caused by the scar formation.

DISCUSSION

Noma is exceptionally rare in developed countries, and has been associated with predisposing conditions such as HIV infection, chronic malnutrition, and poor oral health (8). A multifactorial origin model

has been proposed, in which the weakening of the immune system is responsible for the formation of the oral lesion (1). While Noma cases among immunodeficient patients is rising, we reported 3 cases in immunocompetent women with some degree of malnutrition, although only in Case 1 it was demonstrated. Despite different clinical conditions, the onset of Noma seems to suggest that these patients shared a transient immune dysfunction (ID). Case 2 was the second case reported in literature with Noma and DM (9). People with DM are more susceptible to developing oral health problems, and the ID of oral tissues alters the response to infections (10). It is possible that diabetes-related ID creates the conditions for development of Noma. In Case 3 the untreated gastroenteritis caused severe debilitation and possible micronutrient deficiencies, although no specific analyses were conducted. For this reason, it can be assumed that the patient health status, combined with the poor oral hygiene, led to Noma. *P. intermedia* and *F. necrophorum* are suspected to play a key role in the development of Noma, although not all cases showed the presence of these pathogens (11, 12). Moreover, premature ulceration and possible mistakes made in managing the tissue samples may have killed the specific anaerobic flora. In these cases, non-specific gram-negative cocci were found, while the presence of *Candida spp.* could indicate a possible superinfection. Diagnosis of Noma is based on clinical manifestations, although histopathological and microbiological examinations can be useful to rule out other diseases (1). After nasogastric nutrition all the patients showed rapid improvement, suggesting that malnutrition could lead to Noma also in developed countries. Noma could be result of weakened immune system due to predisposing conditions and associated infections (1). However, in our series it was not possible to identify specific infections. In one case, the ID and delayed healing of oral mucosa as result of DM could have led to Noma (9). Further studies are necessary to investigate the role of malnutrition and other risk factors in the pathogenesis of Noma in HIV-negative adult patients.

REFERENCES

1. Enwonwu CO, Falkler WA, Idigbe EO. Oro-facial gangrene (noma/cancrum oris): pathogenetic mechanisms. Crit Rev Oral Biol Med 2000; 11:159-71.
2. Adelsberger L. Medical observations in Auschwitz concentration camp. Lancet 1946; 1:317-19.
3. Enwonwu CO. Epidemiological and biochemical studies of necrotizing ulcerative gingivitis and noma (cancrum oris) in Nigerian children. Arch Oral Biol 1972; 17:1357-71.
4. Fieger A, Marck KW, Busch R, Schmidt A. An estimation of the incidence of noma in north-west Nigeria. Trop Med Int Health 2003; 8:402-7.
5. Bourgeois DM, Leclercq MH. The World Health Organization initiative on noma. Oral Dis 1999; 5:172-74.
6. Farley E, Lenglet A, Ariti C, et al. Risk factors for diagnosed noma in northwest Nigeria: A case-control study, 2017. PLoS Negl Trop Dis 2018; 12:e0006631.
7. Feller L, Altini M, Chandran R, et al. Noma (cancrum oris) in the South African context. J Oral Pathol Med 2014; 43:1-6.
8. Chidzonga MM. Noma (cancrum oris) in human immunodeficiency virus/acquired immune deficiency syndrome patients: report of eight cases. J Oral Maxillofac Surg 1996; 54:1056-60.
9. Evans LM, Lane H, Jones MK. Cancrum oris in a Caucasian male with Type 2 diabetes mellitus. Diabet Med 2001; 18:246-48.
10. Gurav AN. Management of diabolical diabetes mellitus and periodontitis nexus: Are we doing enough? World J Diabetes 2016; 7:50-66.
11. Masipa JN, Baloyi AM, Khammissa RA, Altini M, Lemmer J, Feller L. Noma (cancrum oris): a report of a case in a young AIDS patient with a review of the pathogenesis. Head Neck Pathol 2013; 7:188-92.
12. Santarelli A, Mascitti M, Rubini C, et al. Active inflammatory biomarkers in oral lichen planus. Int J Immunopathol Pharmacol 2015; 28:562-68.

LETTER TO THE EDITOR

SPONTANEOUS HEMOPERITONEUM IN A PREGNANCY WITH ENDOMETRIOSIS

M.G. PORPORA[1], A. TICINO[1], I. PIACENTI[1], S. SIMONETTI[1], M.P. NUSINER[1], L. MANGANARO[2] and P. BENEDETTI PANICI[1]

[1]Department of Maternal and Child Health and Urology, University of Rome "Sapienza", Policlinico "Umberto I" Rome, Italy; [2]Department of Radiological, Oncological, and Pathological Sciences, Sapienza University of Rome, Policlinico Umberto I, Rome, Italy

Received November 2, 2018 – Accepted February 12, 2019

To the Editor,

The protective effect of pregnancy on endometriosis is well known, but complications related to the pregnant state, such as hemoperitoneum, uroperitoneum and bowel perforation may occur (1). Spontaneous haemoperitoneum during pregnancy (SHiP) is a very rare condition associated with high fetal and maternal risks (2). The etiology is still unknown but endometriosis seems to be a major risk factor (3). The incidence of SHiP in women affected by endometriosis is about 0.4%, but the small number of cases reported in the literature limits the interpretation of data (4). Up to now, 64 cases have been reported (5). Controlled ovarian hyperstimulation in assisted reproductive techniques (ART) seems to increase the occurrence and severity of SHiP (5). Most cases occur in the third trimester of pregnancy (6). Diagnosis of SHiP is difficult due to the absence of symptoms, and in the majority of cases diagnosis is achieved only at surgery (7). We present a case of SHiP in a woman with endometriosis, whose diagnosis of SHiP was possible only intraoperatively.

Case Report

A 29-year-old gravida 0 para 0 patient was admitted with abdominal pain at 31 weeks of a naturally conceived pregnancy. She had a diagnosis of a left ovarian endometrioma of 40 mm in diameter, found at a vaginal ultrasound examination during a gynecological control performed 3 months before pregnancy. She was already hospitalized at 26 weeks of pregnancy in another hospital for suspected renal colic and she received antibiotic therapy and a complete corticosteroid cycle (two doses of 12 mg betamethasone administered 24 hours apart) to induce fetal lung maturity.

On admission to our hospital, the patient's main symptom was a severe stabbing pelvic pain and uterine contractile activity. Physical examination of the abdomen did not reveal rebound, and normal bowel sounds were present, Murphy's and Giordano's signs were negative. The pain was diffuse and increasing. She had no dysuria, constipation or diarrhea, but she complained of nausea and vomiting starting 3 hours earlier. The patient's vital signs were: blood pressure 130/80 mmHg, pulse 110 beats/minute, respiratory rate 15 breaths/minute, temperature 36.5°C. Obstetric examination showed normal external genitalia, regular vagina, absence of bleeding, a slightly soft, closed, shortened cervix, a uterus normal for 31 weeks of pregnancy, and apparently intact membranes. Fetal assessment confirmed a normal singleton

Key words: spontaneous hemoperitoneum; pregnancy; endometriosis

Corresponding Author:
Dr Ilaria Piacenti,
Department of Maternal and Child Health and Urology,
University of Rome "Sapienza", Policlinico "Umberto I"
Viale del Policlinico 155, 00100, Roma, Italy
Tel.: +39 3384068727
e-mail: ilaria_piacenti@libero.it

0393-974X (2019)

pregnancy with a regular left-located placenta and a normal amniotic fluid volume, the cervical length was 28 mm. Cardiotocography (CTG) showed a fetal normoreactive pattern and the presence of uterine contractile activity. Complete laboratory work-up and urinalysis were performed. Her laboratory tests showed hemoglobin 10.4g/dL, 17870/μL leukocytes and 238000/μL platelets. Coagulation test, metabolic hepatic panel and urinalysis were negative. Because of the presence of uterine contractile activity, the patient was administered tocolysis with a bolus iv injection of 6.75 mg of atosiban and a rescue dose of betamethasone (12 mg, 1 intramuscular vial) for fetal lung maturation.

After two hours, CTG showed repeated late decelerations and the patient complained of worsening of pain. An emergency caesarean section (CS) was performed. At the opening of the abdomen a massive hemoperitoneum was found in the peritoneal cavity. About 1500 mL of blood was aspirated from the abdominal cavity. Pelvic exploration revealed numerous and voluminous clots mixed with blood, mainly attached to the omentum and an active bleeding from a ruptured left endometriotic cyst and endometriotic foci. The left fallopian tube and ovary were attached to the left side of the uterine wall. The right fallopian tube and ovary appeared normal. The uterus was full of blood and fibrin; focal adenomyosis was observed, but the uterine outline appeared intact. Hysterotomy and amniorrhexis were rapidly performed. A healthy female baby was delivered; her weight was 1.795 kg and the Apgar scores were 7 and 8 at the first and fifth minute, respectively.

After closing the cesarean breach, the uterus was well contracted. Coagulation of the bleeding ovarian cyst wall and of peritoneal lesions was performed using electrocoagulation. A drainage tube was placed in the peritoneal cavity before closing the abdominal wall to monitor possible further bleeding. Histological examination of the placenta showed an extensive hemorrhagic infarction on the maternal face of 6 cm, normal umbilical cord and normal membranes. In the post -operative period the patient continued antibiotic therapy started during the CS and received antithrombotic therapy with daily subcutaneous injection of enoxaparin 4000 IU for 14 days. Postoperative laboratory results showed hemoglobin 8.3 g/dL on the first post-operative day and 7 g/dL after 5 days when she was discharged from the hospital. Oral iron therapy for one month was prescribed. The baby had an uneventful course in neonatal intensive care and was discharged one month after birth. Two years later the patient underwent laparoscopy for persistent pelvic pain. Surgery showed extensive pelvic adherences, diffuse peritoneal endometriosis and a nodule of deep infiltrating endometriosis (DIE). A careful adhesiolysis and coagulation of endometriotic foci and removal of the DIE lesion were performed. Currently the patient is taking 0.02 mg of ethinylestradiol/3 mg of Drospirenone and she is in good health.

The patient signed written informed consent for the treatment and to the publication of this case report.

DISCUSSION

SHiP is a very rare condition associated with high fetal and maternal risk, resulting in 26% of perinatal mortality and 1.7% of maternal mortality according to Lier et al. (8), whereas Brosens et al. reported 36% and 4%, respectively (7). Endometriosis represents a major risk factor for SHiP. Sixty-four cases of SHiP have been described in the literature: 24 patients with endometriosis, pregnant after ART; 20 women with endometriosis who conceived naturally and 20 women without endometriosis (5). Lier et al. reported a diagnosis of endometriosis in 71% of SHiP (8). In two-thirds of the cases, endometriosis was diagnosed before pregnancy (2). Most cases of SHiP occur in the third trimester (6), out of labor in 61%, during labor in 18% and after delivery in 21% (3). The pathophysiology of hemoperitoneum in the presence of endometriosis is still unclear. It is possible that endogenous progesterone stimulation of preexisting endometriotic implants induces decidualization of ectopic endometrium and bleeding from decidualized endometriosis lesions. The fall of progesterone levels, especially at the end of pregnancy, activates the apoptotic process, cell death and bleeding (9). Other hypothesized mechanisms are: a) invasion of the adjacent vessels by endometriotic foci; b) bleeding from utero-ovarian vessels that appear friable due

to chronic inflammation typical of the disease; and c) increased tension to the vessels due to adhesions when the uterus is enlarged during pregnancy, causing elevated intraluminal pressure until rupture (10).

The source of bleeding in cases of SHiP may not be easily recognizable. The bleeding was described as venous, arterial or unknown in 80%, 16% and 4% of cases, respectively. Rupture of utero-ovarian veins, erosion of uterine artery by endometriosis, rupture of ovarian endometrioma, and invasion of the ovarian hilum by endometriotic implants have all been described as the cause of SHiP (7). SHiP due to rupture of utero-ovarian vessels is reported to occur most commonly in the third trimester and during labor, possibly due to increased intra-abdominal pressure during labor or maneuvers such as vomiting, straining during defecation, etc. In 90% of cases, the bleeding originates from the posterior side of the uterus, the parametrium and/or uterosacral ligaments (7). Deep endometriosis infiltrating the parametrium involving the uterine artery is a possible cause of the bleeding (11). In the literature, there is only one reported case of massive haemoperitoneum from endometriosis involving the fallopian tube occurring in a pregnant woman. The authors hypothesized that decidualization of the vascular endometriotic implant on the tube could have weakened the tubal wall. As the uterus enlarged, there may have been excessive traction on the severely adherent decidualized tube, causing it to rupture and leading to massive hemoperitoneum (12). *In-vitro* fertilization (IVF) in women with severe endometriosis may be an additional risk factor for maternal complications. Ueda et al. reported one case of abscess formation and one case of rupture in the group of patients with endometriomas who underwent IVF (13). A series of recent reports have drawn attention to a possible link between IVF carried out in women with endometriosis and SHiP. Controlled ovarian hyperstimulation plus embryo transfer may increase the severity or incidence of SHiP, especially in moderate and severe endometriosis. High non-physiological progesterone levels early in the pregnancy achieved after ovarian stimulation can accelerate or exacerbate the process of decidualization (5). Diagnosis of SHiP is difficult and rarely made preoperatively due to non-specific symptoms, possible confounding obstetric and surgical conditions and the need for immediate surgical intervention. Women with SHiP present sub-acute abdominal pain accompanied by decreased levels of hemoglobin until signs of hypovolemic shock and fetal distress occur. Ultrasound examination is useful to diagnose and quantify the extent of bleeding (2). The differential diagnosis is: placental abruption (the most common), uterine rupture, preterm birth, abdominal pregnancy, ruptured appendix, HELLP syndrome, spleen or liver rupture and perforated gastric ulcer (14). MRI lacks specificity and can be hampered by the presence of the gravid uterus and poor compliance of the patient. Management of SHiP depends on the clinical presentation, the severity of hemorrhage and the gestational age. Expectant management can be considered in the absence of hypovolemic shock or fetal distress or in the post-partum period, but surgery is often unavoidable and laparotomy is the first-choice treatment. Lier et al. reported surgery performed in 95% of patients, 70% for maternal reasons, 4% for fetal distress and 26% for a combination of both. Expectant management was applied only in 5% of cases. The authors did not find an association between severity of bleeding and the stage of endometriosis (2). Brosens et al. reviewed 25 cases of SHiP and in all cases ultrasound examination failed to diagnose intraperitoneal bleeding (7). Other authors describe a non-specific MRI diagnosis showing a fluid-fluid level in the pelvis. Hemoperitoneum could not be excluded but a definitive cause was not identified until laparotomy (12, 15). Surgery is useful to establish the presence of endometriosis as a cause of bleeding. Biopsy and histological confirmation are recommended (2). However peritoneal endometriotic implants undergo decidualization during pregnancy, losing their pigmentation and therefore they are often missed at laparotomy. A reported successful continuation of pregnancy was observed in 15% of cases, but the rate of preterm birth was high (50-70% of cases) (3, 8). Recurrence of SHiP was described in 8% of patients, during pregnancy or post-partum period, but it was not surgically confirmed in all cases (2). In the present case, SHiP was diagnosed only intraoperatively during an emergency caesarean section performed for abnormal fetal heartbeat at

cardiotocography. Due to the absence of specific symptoms and the difficulty in performing ultrasound because of poor patient compliance, a preoperative diagnosis was not achieved. Moreover, uterine contractile activity represented a confounding factor in our case. Placental abruption was suspected. Placental abruption could be considered a differential diagnosis but also a concomitant condition in women affected by endometriosis and/or adenomyosis, probably due to aberrant uterine contractility, alteration of the junctional zone and subsequent placental disorders (16). In fact, in our case surgery confirmed the bleeding of endometriotic foci and ovarian endometrioma, and histological examination showed placental abruption, both possible causes of uterine contractile activity. This case shows that the clinical approach to SHiP can be problematic. As the frequency of pregnancy in patients with endometriosis is increasing, it is important to be aware of this possible severe complication. The physician should consider SHiP as a differential diagnosis in all pregnant women with abdominal pain and decreased hemoglobin levels. In conclusion, women with endometriosis should be informed of the possible risks of maternal and obstetrical complications during pregnancy.

REFERENCES

1. Glavind MT, Møllgaard MV, Iversen ML, et al. Obstetrical outcome in women with endometriosis including spontaneous hemoperitoneum and bowel perforation: a systematic review. Best Pract Res Clin Obstet Gynaecol 2018; 51:41-52.
2. Lier MCI, Malik RF, Ket JCF, et al. Spontaneous hemoperitoneum in pregnancy (SHiP) and endometriosis e a systematic review of the recent literature. Eur J Obstet Gynecol Reprod Biol 2017; 219:57-65.
3. Passos F, Calhaz-Jorge C, Graca LM. Endometriosis is a possible risk factor for spontaneous hemoperitoneum in the third trimester of pregnancy. Fertil Steril 2008; 89:251-52.
4. Katorza E, Soriano D, Stockheim D, et al. Severe intraabdominal bleeding caused by endometriotic lesions during the third trimester of pregnancy. Am J Obstet Gynecol 2007; 197(5):501. e1e4.
5. Brosens IA, Lier MC, Mijatovic V, et al. Severe spontaneous hemoperitoneum in pregnancy may belinked to in vitro fertilization in patients with endometriosis: a systematic review. Fertil Steril 2016; 106 (3):692-703.
6. Lier MCI, Brosens IA, Mijatovic V, et al. Decidual bleeding as a cause of spontaneous hemoperitoneum in pregnancy and risk of preterm birth. Gynecol Obstet Invest 2017; 82(4):313-21.
7. Brosens IA, Fusi L, Brosens JJ. Endometriosis is a risk factor for spontaneous hemoperitoneum during pregnancy. Fertil Steril 2009; 92(4):1243-45.
8. Lier M, Malik RF, van Waesberghe J, et al. Spontaneous haemoperitoneum in pregnancy and endometriosis: a case series. BJOG 2017; 124(2):306-12.
9. Brosens JJ, Gellersen B. Death or survival—progesterone-dependent cell fate decisions in the human endometrial stroma. J Mol Endocrinol 2006; 36:389-98.
10. Leone Roberti Maggiore U, Ferrero S, Mangili G, et al. A systematic review on endometriosis during pregnancy: diagnosis, misdiagnosis, complications and outcome. Hum Reprod Update 2016; 22(1):70-103.
11. Stochino Loi E, Darwish B, Abo C, et al. Recurrent hemoperitoneum during pregnancy in large deep endometriosis infiltrating the parametrium. J Minim Invasive Gynecol 2016; 23(4):643-46.
12. Aggarwal I, Tan P, Mathur M. Decidualised fallopian tube endometriotic implant causing spontaneous haemoperitoneum in a twin pregnancy. BMJ Case Rep 2014. doi:10.1136/bcr-2014-205317.
13. Ueda Y, Enomoto T, Miyatake T, et al. A retrospective analysis of ovarian endometriosis during pregnancy. Fertil Steril 2010; 94:78-84.
14. Aziz U, Kulkarni A, Lazic D, et al. Spontaneous rupture of the uterine vessels in pregnancy. Obstet Gynecol 2004; 103(5 Pt 2):1089-91.
15. Cozzolino M, Corioni S, Maggio L, Sorbi F, Guaschino S, Fambrini M. Endometriosis-related hemoperitoneum in pregnancy: a diagnosis to keep in mind. Ochsner J 2015; 15(3):262-64.
16. Brosens I, Brosens JJ, Fusi L, Al-Sabbagh M, Kuroda K, Benagiano G. Risks of adverse pregnancy outcome in endometriosis. Fertil Steril 2012; 98 (1):30-35.

LETTER TO THE EDITOR

MULTIDISCIPLINARY APPROACH WITH BILATERAL SINUS-LIFT AND FULL-MOUTH IMPLANTOLOGY IN PATIENTS WITH SEVERE SINUSITIS

A. PACIFICI[1], A. POLIMENI[1], A. BANZI[2] and L. PACIFICI[1]

[1]Department of Oral and Maxillofacial Sciences, Sapienza University of Rome, Italy; [2]Banzi Healthcare, Pieve di Cento, Bologna, Italy

Received February 2, 2019 – Accepted February 20, 2019

To the Editor,

Sinusitis is an acute or chronic inflammation of the paranasal sinuses, sustained by infective processes developed on the mucosa. In some specific forms, it may cause severe impairment of the local response to medical and dental therapies. Maxillary sinusitis is a challenging pathology affecting the good results after oral implantology procedures (1).

Recently, several authors have studied the main pathways of sinusitis, trying to understand the overall mechanisms leading to hypertrophy and tissue loss around the sinus membrane. The high number of co-factors able to influence the local environment is worthy of investigation as they trigger the behaviour of different cell populations (2-5), such as local and systemic factors leading to oxidative stress (6-9), infection (10), oncogenic factors (11) or systemic and syndromic diseases (12).

Sinusitis and implant surgery

The literature shows that maxillary sinusitis is mainly unilateral: clinical signs and diagnostic and therapeutic measures of sinusitis are highly customized according to each patient's requirements. Maxillary sinusitis may be the direct consequence of dislocation or migration of dental implants in the nasal cavities or in the maxillary sinus. The migration of dental implants into maxillary sinus is an uncommon event that may occur. In case of maxillary sinusitis, scarce alveolar bone density, high incidence of masticatory force in posterior region, and a compromised clinical picture can be found, which lead to failure of implant-supported rehabilitation (13). In such cases when a dental implant migrates into the maxillary sinus, it should be immediately extracted, as it may cause sinusitis or further migrate to other paranasal sinuses (14).

The multidisciplinary approach with bilateral sinus-lift and full-mouth implantology in patients with severe sinusitis is a topic that has been widely discussed in the current literature; several authors have tried to analyse the relationship between dental implants and some radiological modifications of the maxillary sinus; the results mainly show that the correct placement of implants does not seem to be associated with severe sinusitis. However, also in a considerable number of patients, radiological alterations of the paranasal sinuses were observed. Thus, it is important to plan assessment of the prosthetic and peri-implant procedures.

In our technical note, we reviewed the main literature related to the above topic, highlighting the appropriate treatments to manage patients with maxillary sinusitis during oral rehabilitation: we reported the exemplificative case of a female patient with severe periodontitis and sinusitis, requiring teeth extraction and implant surgery.

Key words: dental implants; sinus lift; sinusitis; oral pathology

Corresponding Author:
Prof. Luciano Pacifici,
Department of Oral and Maxillofacial Sciences,
Sapienza University of Rome,
Rome, Italy
e-mail: prof.lucianopacifici@libero.it

0393-974X (2019)

DISCLOSURE: ALL AUTHORS REPORT NO CONFLICTS OF INTEREST RELEVANT TO THIS ARTICLE.

Case report

A 43-year-old female referred to a dental surgeon after several relapses of abscesses in the maxillary region. After X-ray examination and clinical assessment, the patient was diagnosed with a high horizontal bone loss, monolateral acute sinusitis, decay associated to oral granulomas, and an overall inflammatory condition in both maxillary bones (Fig. 1). The patient reported pain and bleeding in the previous 2 weeks, moreover, she was under pharmacological treatment for psychological disease. The surgeon planned to do massive teeth extraction, a bilateral sinus lift and full-mouth implant-supported rehabilitation. The patient gave informed signed consent for this publication.

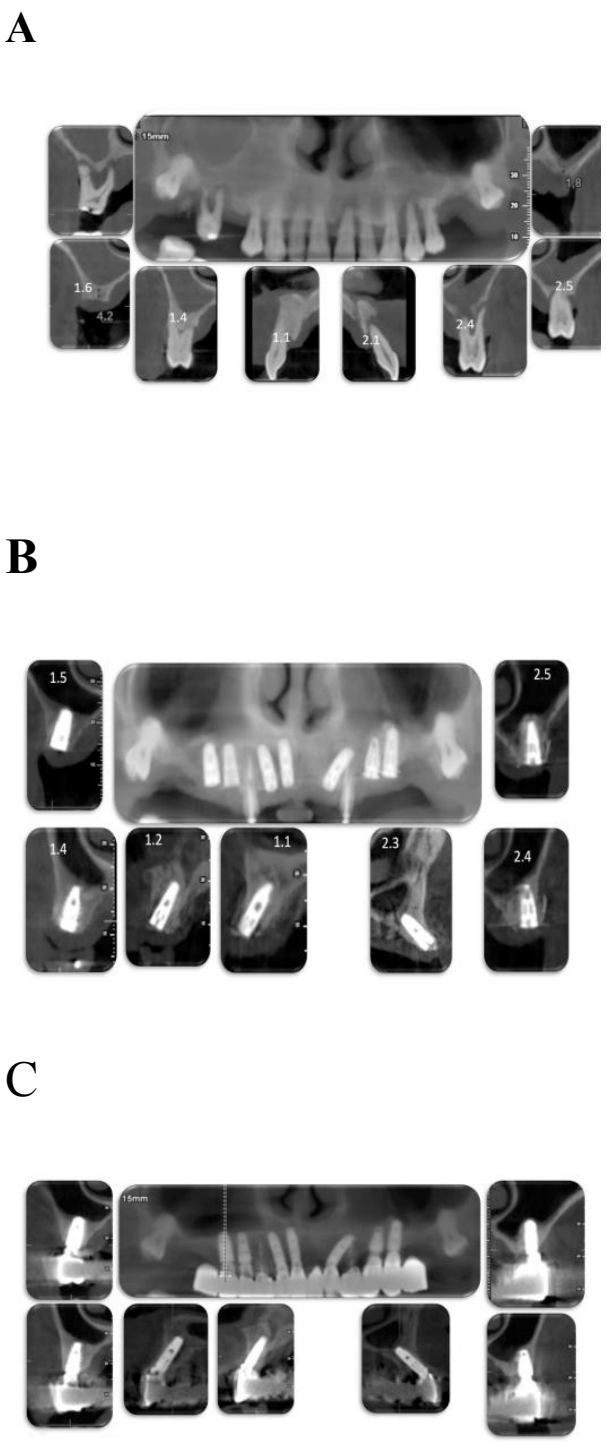

Fig. 1. *Case-report: **A**)before treatment; **B**) 10-month follow-up; **C**) 24-month follow-up.*

After several teeth extractions, each inflammatory site was treated. Sinusitis was treated with antibiotic and anti-inflammatory administration. A bilateral sinus-lift with trans-crestal approach was performed. After healing of regenerated maxillary bone, 7 implants (3P and EV, B&B Dental Evolution, Italy) were placed in order to rehabilitate the whole maxillary arch (Fig. 2).

The implants were properly loaded with full-arch prosthesis, a slight and well supported cantilever and residual wisdom teeth in both the upper sides. After 24 months, the regenerated bone appeared to be healthy and mature, showing also a good integration between implants and peri-implant bone. Sinus was completely free from any residual sign of inflammation, and implantology did not affect the Schneiderian membrane in any way (Fig. 3).

DISCUSSION

The maxillary sinus bone grafting or sinus lift procedure has proven to be a predictable and relatively safe procedure over time. This surgical technique allows the reconstruction of the atrophic posterior maxilla, in order to replace the missing posterior maxillary teeth with implant-supported restorations. The complications of this surgical procedure are reported below, and can include acute maxillary sinusitis, wound dehiscence, and Schneiderian membrane perforations, with scattering of the grafting material in the sinus cavities.

Several studies conducted on patients who performed maxillary sinus elevation and simultaneous implant placement, using the minimally invasive antral membrane balloon elevation (MIAMBE)

Table I. *Overall analysis of different scientific contributions on implant surgery in sinus-related complications.*

Authors	Paper	Scientific Journal	Aim	Conclusions
Grygorov S, Poberezhnik G, Grygorova A.	Actual issues of odontogenic maxillary sinusitis (review).	Georgian Medical News	Causes and treatment of odontogenic maxillary sinusitis	Dental treatment may resolve the odontogenic sinusitis.
Conforte JJ, Ponzoni D.	Sinusitis Due to the Presence of a Dental Implant Inside the Maxillary Sinus.	Journal of Craniofacial Surgical	Implant migrations	Sinusitis after the surgery.
Furuya Y, Norizuki Y, Yajima Y.	A Case of Simultaneous Ectopic Tooth Extraction and Removal of Migrated Dental Implant from Maxillary Sinus.	The Bulletin of Tokyo Dental College	Implant removal issue	Implant removal should be considered.
Kfir E, Goldestein M, Abramovitz I, Mazor Z, Kfir V, Kaluski E	The effects of sinus membrane pathology on bone augmentation and procedural outcome using minimal invasive antral membrane balloon elevation.	Journal of Oral Implantology	Zygomatic implant rehabilitation and sinusitis	Maxillary sinus elevation and simultaneously implants placement and the thickening of the sinus membrane cause acute sinusitis.
Kozuma A et al.	Preoperative chronic sinusitis as significant cause of postoperative infection and implant loss after sinus augmentation from a lateral approach.	Oral Maxillofac Surgical	Main causes of postoperative infection and implant loss	Preoperative chronic sinusitis could be a significant cause of postoperative infection and implant loss
Anavi Y, Allon DM , Avishai G , Calderon S.	Complications of maxillary sinus augmentations in a selective series of patients.	Oral Surgery, Oral Medicine, Oral Pathology, Oral Radiology	Correlation between the increase of the maxillary sinus with the sinusitis.	Strong correlation between implant insertion, bone loss, atrial sinus elevation and sinusitis
De Jong MA, Rushinek H, Eliashar R.	Removal of dental implants displaced into the maxillary sinus: A case series. 2016;9(4):427-433.	European Journal *of* Oral Implantology.	Migration of displaced implants causing secondary sinusitis	Removal of the implant resolves sinusitis

method, showed that a consequential thickening of the sinus membrane may cause a massive sinusitis (15).

Among intra/postoperative complications of sinus augmentation from a lateral approach, postoperative infection and implant loss are particularly important because they have irreversible consequences. In a study conducted in 2017, 109 (121 sinuses, 252 implants) patients were included. The purpose of that study was to determine the causes of postoperative infection and implant loss after a lateral approach and to determine the appropriate prophylaxis and therapy. Postoperative infection and implant loss occurred in 8/121 sinuses (6.6%). Infection had the strongest correlation to preoperative chronic sinusitis ($p = 0.007$), followed by timing of implant insertion. Implant loss had the strongest correlation to preoperative chronic sinusitis ($p = 0.007$), followed by sex, diabetes, postoperative use of dentures, and intraoperative perforation of the sinus membrane. Preoperative chronic sinusitis could be a significant cause of postoperative infection and implant loss when using sinus augmentation from a lateral approach. For appropriate prophylaxis and therapy, it is necessary to diagnose the presence of chronic sinusitis that should be treated with appropriate methods prior to sinus augmentation (16).

Although sinus lift is known to be as a safe and reliable technique, acute sinusitis is a possible complication which must be managed immediately, in order to reduce the risk of further complications, such as pansinusitis, osteomyelitis of the maxillary bone, or the spreading of the infection in the infratemporal space or orbital cavity. To minimize risks, caution must be taken with all the steps of the procedure, in order not to obliterate the ostium, impairing maxillary sinus clearance. The typical clinical signs of infection are pain, inflammation, tumefaction and rhinorrhoea (17).

Different opinions were reported from different

groups regarding the potential correlation between the increasing of the maxillary sinus volume and maxillary sinusitis. Certainly, there are several contras. One study on patients hospitalized for a failed lateral-approach maxillary sinus augmentation, performed by a dental practitioner, with or without simultaneous implant placement, reported that 26 out of 34 implants were lost, and 7 of them were displaced into the sinus. All patients reported maxillary sinusitis, and 2 also had inflammation of other paranasal sinuses (18).

Migration of displaced implants and mucosal changes may occur over a short period, eventually causing secondary sinusitis. The implant must be removed surgically. Surgery should be as close as possible to displacement in order to minimise mucosal inflammation and prevent unnecessary manipulation during surgical removal (19).

There are several studies on sinusitis, dental implants and related issues, and often have contrasting conclusions. It is recommended to use clinical, radiographic and tomographic examinations before any assessment: the implant insertions after maxillary sinus lift do not have specific contraindications, as substantially demonstrated (Table I). The presence of active maxillary sinusitis, on the contrary, causes implant failure, as well as inflammatory acute phenomena leading to severe bone resorption.

ACKNOWLEDGEMENTS

The Authors wish to acknowledge Sapienza University for technical support.

REFERENCES

1. Grygorov S, Poberezhnik G, Grygorova A. Actual issues of odontogenic maxillary sinusitis. Georgian Med News 2018; 276:46-50.
2. Paduano F, Marrelli M, Palmieri F, Tatullo M. CD146 expression influences periapical cyst mesenchymal stem cell properties. Stem Cell Rev 2016; 12(5):592-603.
3. Paduano F, Marrelli M, Amantea M, et al. Adipose tissue as a strategic source of mesenchymal stem cells in bone regeneration: a topical review on the most promising craniomaxillofacial applications. Int J Mol Sci 2017; 18(10).
4. Gronthos S, Mankani M, Brahim J, Robey PG, Shi S. Postnatal human dental pulp stem cells (dpscs) in vitro and in vivo. Proceedings of the National Academy of Sciences of the United States of America 2000; 97:13625-30
5. Miura M, Gronthos S, Zhao M, Lu B, Fisher LW, Robey PG, Shi S. SHED: stem cells from human exfoliated deciduous teeth. Proc Natl Acad Sci 2003; 100:5807-12.
6. Tatullo M, Simone GM, Tarullo F, et al. Antioxidant and antitumor activity of a bioactive polyphenolic fraction isolated from the brewing process. Sci Rep 2016; 6:36042.
7. Tatullo M, Marrelli M, Scacco S, et al. Relationship between oxidative stress and "burning mouth syndrome" in female patients: a scientific hypothesis. Eur Rev Med Pharmacol Sci 2012 Sep;16(9):1218-21.
8. Tatullo M, Gentile S, Paduano F, Santacroce L, Marrelli M. Crosstalk between oral and general health status in e-smokers. Medicine (Baltimore) 2016; 95(49):e5589.
9. Marrelli M, Gentile S, Palmieri F, et al. Correlation between Surgeon's experience, surgery complexity and the alteration of stress related physiological parameters. PLoS One 2014; 9(11):e112444.
10. Marrelli M, Tatullo M, Dipalma G, Inchingolo F. Oral infection by Staphylococcus aureus in patients affected by White Sponge Nevus: a description of two cases occurred in the same family. Int J Med Sci 2012; 9(1):47-50.
11. Tatullo M, Marrelli M, Amantea M, Paduano F, Santacroce L, Gentile S, Scacco S. Bioimpedance detection of oral lichen planus used as preneoplastic model. J Cancer 2015; 6(10):976-83.
12. Inchingolo F, Tatullo M, Abenavoli FM, et al. Non-syndromic multiple supernumerary teeth in a family unit with a normal karyotype: case report. Int J Med Sci 2010; 7(6):378-84.
13. Conforte JJ, Ponzoni D. Sinusitis due to the presence of a dental implant inside the maxillary sinus. J Craniofac Surg 2018; 29(6):e591.
14. Furuya Y, Norizuki Y, Yajima Y. A case of simultaneous ectopic tooth extraction and removal of migrated dental implant from maxillary sinus. Bull Tokyo Dent Coll 2015; 56(4):253-8.

15. Kfir E, Goldestein M, Abramovitz I, Mazor Z, Kfir V, Kaluski E. The effects of sinus membrane pathology on bone augmentation and procedural outcome using minimal invasive antral membrane balloon elevation. J Oral Implantol 2014; 40(3):285-93.
16. Kozuma A, Sasaki M, Seki K, Toyoshima T, Nakano H, Mori Y. Preoperative chronic sinusitis as significant cause of postoperative infection and implant loss after sinus augmentation from a lateral approach. Oral Maxillofac Surg 2017; 21(2):193-200.
17. Chirilă L, Rotaru C, Filipov I, Săndulescu M. Management of acute maxillary sinusitis after sinus bone grafting procedures with simultaneous dental implants placement – a retrospective study. BMC Infect Dis 2016; 16(1):94
18. Anavi Y, Allon DM, Avishai G, Calderon S. Complications of maxillary sinus augmentations in a selective series of patients. Oral Surg Oral Med Oral Pathol Oral Radiol Endod 2008; 106(1):34-8
19. De Jong MA, Rushinek H, Eliashar R. Removal of dental implants displaced into the maxillary sinus: A case series. Eur J Oral Implantol 2016; 9(4):427-33.

LETTER TO THE EDITOR

FUNCTIONALIZATION OF SCAFFOLDS WITH NaOH-BASED SOLUTION CAN IMPROVE BONE REGENERATION

A. PACIFICI[1], A. POLIMENI[1], A. BANZI[2] and L. PACIFICI[1]

[1]Department of Oral and Maxillofacial Sciences, Sapienza University of Rome, Italy; [2]Banzi Healthcare, Pieve di Cento, Bologna, Italy

Received February 3, 2019 – Accepted March 12, 2019

All the Authors contributed equally to this work

To the Editor,

Background

Among the numerous types of materials used in medical applications, titanium and its alloys provide many advantages, such as excellent biocompatibility, high strength-to-weight ratio, lower elastic modulus, and superior corrosion resistance, required for dental and orthopaedic implants. For these reasons titanium is a promising material for bone substitution, while its bio-inert property results in demand of modifications to improve the osteointegration capacity.

The formation of a biologically active layer on the surface of an artificial material is an essential requirement to bond the implant to living bone in a body environment. It has been reported that after NaOH- and heat-treatment, titanium metal and titanium alloys form a biologically active bone-like apatite layer on its surface (1); in a living body, the apatite layer bond to and integrate with bone. It is believed that apatite establishment on the metal surface is induced by amorphous sodium titanate formation after the NaOH and heat treatments, especially when it could be converted into anatase (mineral form of titanium dioxide). Indeed bone-bonding ability of NaOH-treated titanium metal can be further enhanced if the sodium titanate on its surface is converted into anatase by a method such as the water and subsequent heat treatments.

For the NaOH treatment, the titanium substrates should be immersed in NaOH aqueous solution at 60°C for 24 h. After this, the metal substrates are washed and immersed in ultra-pure water for various periods up to 48 h at 80°C and then heated up to 600°C for 1 h, and then allowed to cool in the Ni-Cr electric furnace.

The NaOH treatment determines the formation of amorphous sodium titanate on a metal surface, and the release of sodium ions that by a mechanism of ion exchange with the hydronium ions present in the surrounding fluid results in the formation of Ti-OH (anatase) groups on its surface. The Ti-OH groups induce apatite nucleation, and the increasing pH of the fluid, induced by the released sodium ions, further accelerate apatite formation. After apatite nuclei formation, they grow spontaneously by consuming the calcium and phosphate ions from the surrounding body fluid that is highly supersaturated in respect to the apatite or other biomaterials (2).

Alternatively, it has been proposed to create "hybrid scaffolds" carrying the mechanical stability of metal fused with osteointegration capacity and osteoinductivity of other bio-active materials.

Key words: dental implants; NaOH functionalization; scaffolds; polymeric biomaterials

Corresponding Author:
Dr. Andrea Pacifici,
Department of Oral and Maxillofacial Sciences,
Sapienza University of Rome,
Rome, Italy
e-mail: dott.andreapacifici@libero.it

0393-974X (2019)

DISCLOSURE: ALL AUTHORS REPORT NO CONFLICTS OF INTEREST RELEVANT TO THIS ARTICLE.

Examples of these biomaterials have been widely described, focusing on several methods used for the functionalization of porous bioactive surfaces by NaOH after a superficial treatment. In recent years, polymeric and composite scaffolds with several types of reinforcement have been engineered to include specific morphological and chemical signals capable of mimicking the biological structure of the extracellular matrix of the tissue to be replaced. Various bioabsorbable synthetic polymers or biopolymers have been merged or combined with the aim of developing complex and smart scaffolds with different mechanical skills and biological safety. The main process technologies have been tested in recent years and optimized for the production of personalized scaffolds able to ensure high morphological complexity and appropriate degradation properties.

In perspective, new manufacturing methods can be further implemented through the integration of the processes already studied in order to more effectively reproduce the structural and functional complexity of the natural tissue during the initial phases of regeneration.

Rapid prototyping technology has been used to fabricate porous three-dimensional (3D) scaffold in several reports. 3D scaffold plotting system (SPS) technology has been applied to design a scaffold with reproducible porosity and well-defined 3D structures, treated with NaOH to fabricate the biomimetic surface. The dispensing material used is mainly the polycaprolactone (PCL), ejected via dispenser of SPS. The 3D scaffolds are formed by Layer-by-layer deposition of PCL. Scaffolds are further treated and functionalized in NaOH solutions for several hours to fabricate biomimetic surface (3).

Additive manufacturing (AM) is characterized by the production of constructs through the accumulation and the union of layers of material to obtain a desired physical model. Several AM processes are currently available, such as stereolithography (SLA), selective laser sintering (SLS) and fused deposition modelling (FDM).

These production processes are designed for their potential commercial applications in the electronics sector (resistors and sensors), automotive, communication, but also and especially in the medical sector with the production of dental fixtures, customized prostheses for patients and tissue scaffolds for engineering and regenerative medicine. The AM therefore allows to produce medical devices with an accurate control and layout of the material.

Fused deposition modelling (FDM) is the most common and less-expensive 3D printing technology. This technology is used for a wide variety of purposes thanks to the accessibility of personal 3D printing devices. In this technique, a thermoplastic filament is passed through a heated print head and is deposited on the construction platform layer by layer, until the required object is formed. FDM printers are available that can use a wide variety of materials and can print at high resolutions. FDM printers can host more than one printhead and, therefore, can print multiple types of one material at a time.

3D bioresorbable scaffolds consist of different biomaterials: the most used couplings are made from 80% PCL and 20% TCP (poly (ε-caprolactone)-tricalcium phosphate). Usually, scaffolds have been used for bone regeneration purposes. Pre-treatment of the PCL-TCP scaffolds with NaOH improves porosity values, pore sizes and the surface roughness: these parameters can be varied according to treatment time and concentration (4).

Several authors performed novel surface modification techniques for adding micro- and nano-structure on a PCL scaffold to create an implant with local drug delivery functionality. Scaffolds have often been used to release stem cells or drugs: the drug release experiment provided information about a stronger long-term binding of drugs to the scaffold previously treated (5).

FDM is able to design constructs made with biomaterials quickly, accurately, with excellent mechanical properties and with relatively low costs. There are several biocompatible polymers and composites that can be used for the accurate production of porous structures. The most used polymers for the FDM process are based on PLA and PCL and are widely used for different biomedical applications thanks to their biocompatible and biodegradable properties. Material combinations, such as PCL/chitosan or PCL/β-TCP (β tricalcium

phosphate) are also used in the FDM process to improve the bioactive properties of the scaffolds. Several studies have evaluated the FDM technique, demonstrating the absence of alterations in the biocompatibility or in the osteogenic behaviour of the polymers used. In particular, the production of PLA discs by using FDM techniques have been largely studied. The *in-vitro* investigations with osteoblasts showed no cytotoxic effects, making such technique safe and reliable, furthermore, FDM would seem not to alter the biocompatibility of PLA, both alone or in combination with other polymers (6).

3D printing using FDM allows the production of constructs for bone tissue engineering applications. In particular, a guide for the design of PCL/β-TCP structures were provided, demonstrating the feasibility of single-piece structures that integrate multiple porosity. Potentially this paves the way towards the development of new prostheses, such as specific implants, not only for the patient but also for the different type of bone (7). Three-dimensional NaOH-treated PLGA scaffolds are used also for articular cartilage reconstruction. For this purpose, PLGA scaffolds are modified via chemical etching techniques using 1 N NaOH for 10 min. Hydrolytic degradation of PLGA by NaOH determines a more hydrophilic surface, alters porosity and confers a greater degree of nanometer roughness.

CONCLUSION

Summarizing the main information reported in our article, NaOH is widely used in the assembly and in the functionalization of bio-active scaffold for clinical applications with particular regard to regenerative medicine. From several studies, it emerged that repairing techniques of bone defects with PCL scaffolds containing chitosan and manufactured by melt stretching and multilayer deposition (MSMD) are less effective than PCL scaffolds containing tricalcium phosphate and manufactured by the molten deposition modelling (FDM) technique. This shows how the FMD technique is useful for better bone regeneration.

The use of biological scaffolds composed of decellularized extracellular matrix (ECM) has been proposed in recent studies for the osteo-inductivity and the great ability of these materials to induce osteogenic differentiation of human mesenchymal stem cells (hMSCs) (8). There are several ways to use functionalized scaffolds and stem cells or other drugs (9) properly delivered, such as for syndromic patients with functional minus in their body (10), infectious diseases to be treated locally (11, 12), local administration of therapies (13) with benefits on the systemic health (14) and several other uses, depending highly on the experience of clinicians (15).

More in detail, we can choose the best approach to functionalise implant surfaces in one (or more) of the following strategies: NaOH treatment of titanium implants, followed by immersion in ultra-pure water and heating in a Ni-Cr electric furnace; the effect will be to stimulate the formation of apatite on the surface of the metal. Apatite coating stimulates the bonding with the bone surrounding the implantation site and new bone formation. Pre-treatment of PCL scaffold and of PCL-TCP 3D scaffolds is used to fabricate a biomimetic surface, where porosity values, pore sizes and the surface roughness can be varied according to treatment time and NaOH concentration. Chemical PLGA scaffold treatment with NaOH determines the hydrolytic degradation of PLGA in a more hydrophilic surface, alters porosity and confers a greater degree of nanometer roughness. Therefore, PLGA can be used to try a functionalization of the implant surface. NaOH is also used for the neutralization of pre-digested bone ECM samples and to determine the formation of hydrogel in the presence of high phosphate salt solutions. Finally, we could add NaOH to other widely used biomaterials such as hydrogels, PLA-PGA microparticles with high-porosity, or other similar biomatrices for tissues engineering purposes.

ACKNOWLEDGEMENTS

The Authors want to acknowledge Sapienza University for technical support.

REFERENCES

1. Kim HM, Miyaji F, Kokubo T, Nakamura T. Effect

of heat treatment on apatite-forming ability of Ti metal induced by alkali treatment. J Mater Sci Mater Med. 1997; 8(6):341-47.
2. Perniconi B, Coletti D, Aulino P, et al. Muscle acellular scaffold as a biomaterial: effects on C2C12 cell differentiation and interaction with the murine host environment. Front Physiol 2014; 5:354.
3. Marrelli M, Pujia A, Palmieri F, et al. Innovative approach for the in vitro research on biomedical scaffolds designed and customized with CAD-CAM technology. Int J Immunopathol Pharmacol 2016; 29(4):778-83.
4. Tarafder S, Bose S. Polycaprolactone-coated 3D printed tricalcium phosphate scaffolds for bone tissue engineering: in vitro alendronate release behavior and local delivery effect on in vivo osteogenesis. ACS Appl Mater Interfaces 2014; 6(13):9955-65.
5. Paduano F, Marrelli M, Alom N, Amer M, White LJ, Shakesheff KM, Tatullo M. Decellularized bone extracellular matrix and human dental pulp stem cells as a construct for bone regeneration. J Biomater Sci Polym Ed 2017; 28(8):730-48.
6. Bruyas A, Lou F, Stahl AM, Gardner M, Maloney W, Goodman S, Yang YP. Systematic characterization of 3D-printed PCL/β-TCP scaffolds for biomedical devices and bone tissue engineering: influence of composition and porosity. J Mater Res 2018; 33(14):1948-59
7. Aulino P, Costa A, Chiaravalloti E, et al. Muscle extracellular matrix scaffold is a multipotent environment. Int J Med Sci 2015; 12(4):336-40.
8. Paduano F, Marrelli M, White LJ, Shakesheff KM, Tatullo M. Odontogenic Differentiation of Human Dental Pulp Stem Cells on Hydrogel Scaffolds Derived from Decellularized Bone Extracellular Matrix and Collagen Type I. PLoS One 2016; 11(2):e0148225.
9. Tatullo M, Simone GM, Tarullo F, et al. Antioxidant and Antitumor Activity of a Bioactive Polyphenolic Fraction Isolated from the Brewing Process. Sci Rep 2016; 6:36042.
10. Inchingolo F, Tatullo M, Abenavoli FM, et al. Non-syndromic multiple supernumerary teeth in a family unit with a normal karyotype: case report. Int J Med Sci 2010;7(6):378-84.
11. Marrelli M, Tatullo M, Dipalma G, Inchingolo F. Oral infection by Staphylococcus aureus in patients affected by White Sponge Nevus: a description of two cases occurred in the same family. Int J Med Sci 2012; 9(1):47-50.
12. Tatullo M, Marrelli M, Amantea M, Paduano F, Santacroce L, Gentile S, Scacco S. Bioimpedance Detection of Oral Lichen Planus Used as Preneoplastic Model. J Cancer 2015; 6(10):976-83.
13. Tatullo M, Marrelli M, Scacco S, et al. Relationship between oxidative stress and "burning mouth syndrome" in female patients: a scientific hypothesis. Eur Rev Med Pharmacol Sci. 2012; 16(9):1218-21.
14. Tatullo M, Gentile S, Paduano F, Santacroce L, Marrelli M. Crosstalk between oral and general health status in e-smokers. Medicine (Baltimore) 2016; 95(49):e5589.
15. Marrelli M, Gentile S, Palmieri F, Paduano F, Tatullo M. Correlation between Surgeon's experience, surgery complexity and the alteration of stress related physiological parameters. PLoS One 2014; 9(11):e112444.

LETTER TO THE EDITOR

EFFECT OF ACTIVATED CHARCOAL PROBIOTIC TOOTHPASTE CONTAINING *LACTOBACILLUS PARACASEI* AND XYLITOL ON DENTAL CARIES: A RANDOMIZED AND CONTROLLED CLINICAL TRIAL

A. BALLINI[1*], S. CANTORE[1,2,3*], R. SAINI[4], F. PETTINI[4], E.A. FOTOPOULOU[5], S.R. SAINI[4], I.P. GEORGAKOPOULOS[4,5], G. DIPALMA[4*], C. GARGIULO ISACCO[4,6*] and F. INCHINGOLO[4*]

[1]Department of Basic Medical Sciences, Neurosciences and Sense Organs, University of Bari Aldo Moro, Bari, Italy; [2]POLYPHENO S.r.l., Accredited Spin Off, University of Bari Aldo Moro, Bari, Italy; [3]Sorriso & Benessere Ricerca e Clinica S.r.l., Bari, Italy; [4]Department of Interdisciplinary Medicine, School of Medicine, University of Bari Aldo Moro, Bari, Italy; [5]Dentist Education Institute, Athens, Greece; [6]Human Stem Cells Research Center, Ho Chi Minh City, Vietnam

Received February 14, 2019 – Accepted March 12, 2019

*These Authors contributed equally to this work

To the Editor,

In the oral cavity, there is an imbalance between the loss and gain of the minerals; as a result, mutually with the cariogenic bacteria, dental caries emerges (1). Dental caries begins and advances with the colonization of *Streptococcus mutans* (*S. mutans*) and similar predisposing factors, which influence the human-oral micro flora (2, 3). As stated in recent findings, the oral microbial ecology is modulated for the rationale of being able to control the dental diseases that emerge due to microbial activity.

The concept of probiotics dates back to 1908, when Noble Prize winner Eli Metchnikoff suggested that the long life of Bulgarian peasants resulted from their consumption of fermented milk products. The oral cavity is a confined compartment within the human body i.e. anatomically, the oral cavity is connected to the nasopharynx, the larynx, the tonsils, the middle ear through the Eustachian tube and the gastrointestinal tract. Physiologically it is connected to the whole body and thus, the oral cavity is influenced by and influences general health. The encouraging effects of probiotics (i.e. *Lactobacillus*) in different fields of healthcare have resulted recently also in their introduction for oral healthcare (4).

To prevent caries, the use of xylitol is approved by the American Academy of Paediatric Dentistry (AAPD) (5). The fact that xylitol products have bacteriostatic effect on *S. mutans* has been documented in clinical trials (4, 6).

Moreover, the literature is currently lacking in studies evaluating the effects of toothpastes with activated charcoal, xylitol, or xylitol-probiotics on *S. mutans* in the saliva of young patients (aged 18-25 years). The purpose of the present study was to evaluate the beneficial efficacy of activated charcoal probiotic toothpaste, containing both *L. paracasei* and xylitol, on dental caries.

Keywords: Lactobacillus paracasei*, activated charcoal, probiotics, tooth paste, xylitol*

Corresponding Author:
Dr. Andrea Ballini,
University of Bari Aldo Moro,
P.zza Giulio Cesare, 11,
70124, Bari, Italy
Tel./fax: +39 0805448514.
e-mail: andrea.ballini@me.com

0393-974X (2019)

DISCLOSURE: ALL AUTHORS REPORT NO CONFLICTS OF INTEREST RELEVANT TO THIS ARTICLE.

MATERIALS AND METHODS

The present study was conducted at the Dental Unit (Dentist Education Institute) of the City Unity College, Greece in collaboration with the University of Bari Aldo Moro, Italy. All eligible subjects were given information on the products and the purpose of the study and gave an informed consent, in accordance with the ethical principles originating in the Declaration of Helsinki and consistent with good clinical practices. The patients received a verbal description of the clinical protocol.

In order to have unbiased and accurate clinical data, a double-blind protocol for enrolment of the patients in terms of treatment plan and further categorization into the study group was performed for 24 healthy subjects patients aged between 18 and 40 years.

Study subjects

Prior the study period, the volunteers received an oral soft and hard tissue examination and a professional scaling and polishing to remove all calculus, plaque and extrinsic tooth staining to get the baseline score to nil. This was performed using hand instruments, mechanical scalers, rotating brushes with polishing paste, and dental floss in the interproximal areas. All candidates were screened for suitability by the research team. Selection criteria was a dentition with ≥20 evaluable teeth (minimum of five teeth per quadrant), no oral lesions, no severe periodontal problems (no probing depth ≥5 mm), and no removable prostheses or orthodontic bands or appliances.

All the subjects were advised to brush twice daily for 5 minutes with modified bass method technique (the technique was demonstrated to each subject), and similar medium bristle tooth brushes were provided to each of the subjects during the study course to maintain standardization and tooth paste. The subjects were then categorized into two treatment regimes in groups I and II (12 each).

Group I (n = 12): Hyperbiotics activated charcoal probiotic toothpaste containing *L. paracasei* and xylitol (Hyperbiotics, USA).

Group II (n = 12): Non-active tooth paste (Non-marketed formulation).

Clinical parameters evaluated by the same blinded trained examiner at baseline (prior oral hygiene procedures) and at 90 days were the following: extrinsic tooth stain score (SI) and the oral hygiene index (OHI) (7-9). Stain was evaluated using the following criteria and codes for intensity: 0= no stain present with the natural tooth coloration; 1= slim stain; 2= clearly visible stain, orange to brown; 3= dark stain, dark brown to black, on the basis of Discoloration Index proposed by Lobene (1968) (8) and modified by Macpherson, et al. (2000) (9).

A

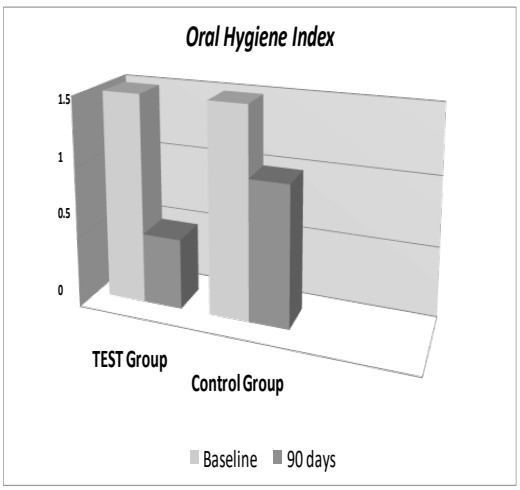

B

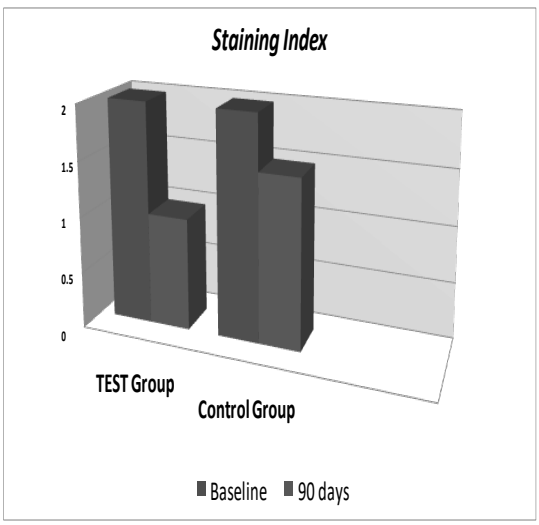

Fig. 1. ***A-B)*** *Clinical index results before and after the study period.*

All the clinical parameters, were assessed by a trained experienced dental examiner under standard dental office and light source conditions. Moreover, for plaque detection, a disclosing agent (erythrosine) was used to disclose the plaque during the examination.

Bacterial sample analysis

The levels of *S. mutans* were evaluated at the baseline and after 90 days from enrolment. The participants were instructed not to eat or drink for 2 hours before collection saliva and to brush their teeth only once in the morning on the day of the sample collection. 2 ml of stimulated saliva were collected into a sterile plastic cup for 5 min during paraffin-wax chewing. The saliva was transferred to a selective culture medium in glass tubes and then was incubated at 37°C for 48 h. After incubation, the colony forming units score of *S. mutans* was obtained by comparing the test strip with an evaluation chart provided by the manufacturer. The results were presented in qualitative form only, following the study design.

In vitro analysis

Non-carious extracted teeth were included for the study. Attrided, abraded, hypoplastic, fractured, malformed, restored, endodontically treated teeth, and teeth extracted from patients with systemic diseases which could cause variation in salivary flow, tooth formation, and maturation were excluded from the study. Each tooth was longitudinally sectioned, using a diamond disc. All specimens were immersed in demineralizing solution for 3 days, after which the depth of demineralization was measured under the confocal microscope. The samples were subjected to the surface treatments and hyperbiotics: Activated Charcoal Probiotics Tooth Paste was applied on sections and left undisturbed for 5 min. Finally, all specimens were immersed in artificial saliva with pH 7.2 for 3 days. The artificial saliva solution was replaced each day. The sections were observed under a confocal microscope and the remineralization measured as unit values.

Statistical analysis

All data were collected and statistically evaluated. The statistical analyses were performed by using Statistical Package for Social Sciences (SPSS for Windows, Version 11.5, Chicago, Ill, USA) software.

RESULTS

All subjects (N = 24) completed the trial, and there were no missing values. No adverse events or side effects were reported or observed. All the clinical parameters were recorded of both the groups during

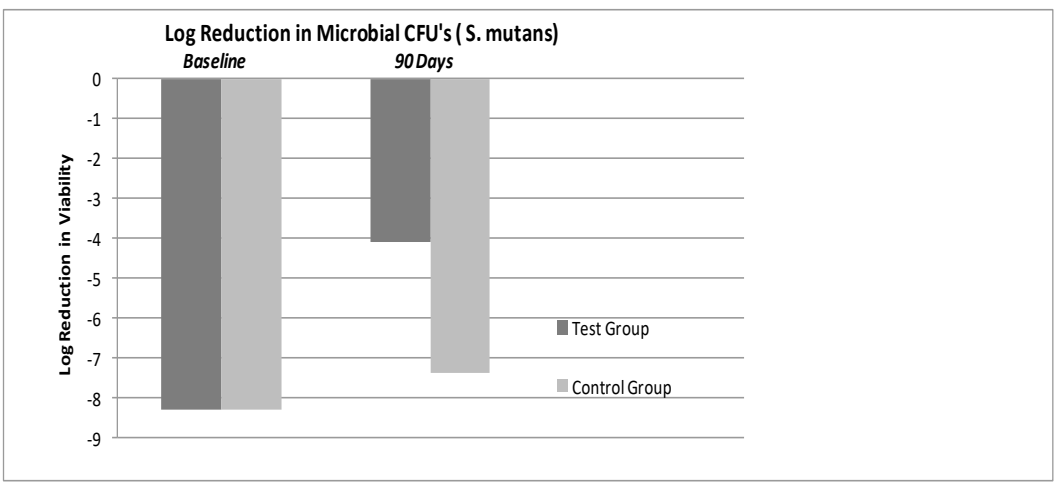

Fig. 2. *Bacterial salivary analysis.*

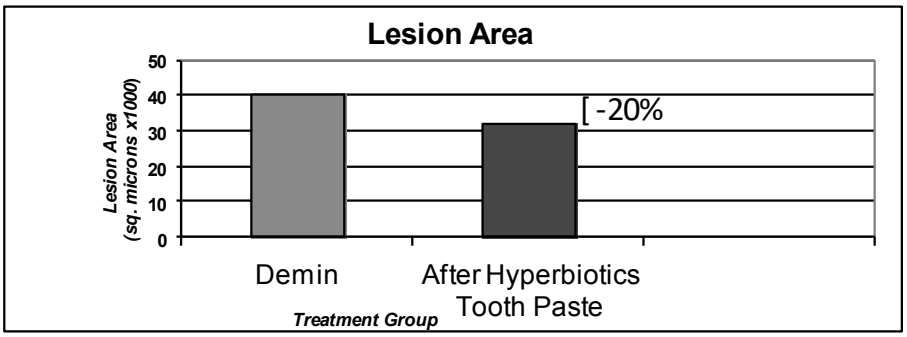

Fig. 3. *Demineralization/remineralisation analysis.*

the study at baseline (TO) and at the end of study, at 90 days (T1), respectively. The clinical scores for the test and control groups at baseline and at the end of the experimental study period are shown in Fig. 1 (A-B), showing a reduction of 76% from baseline in the test group, compared to control group (33% from baseline) for OHI and a reduction of 52% from baseline in the test group, compared to the control group (23% from baseline) for SI. The colony-forming units of total *S. mutans* bacteria in the saliva of subjects at baseline and at 90 days are reported in Fig. 2, showing a load reduction of 55% from baseline in the test group compared to the control group (15% from baseline). Moreover, confocal microscope analysis showed a re-mineralization of around 20% of the enamel treated surface (Fig. 3 A-B).

Large variations in inter- and intra-individual measurements were observed. Both the examinations (clinical and laboratory) showed a significant improvement from the baseline. These results support that hyperbiotics, activated charcoal probiotic toothpaste, worked significantly to improve all the clinical parameters and to promote remineralization and decrease *S. mutans* bacterial activity.

DISCUSSION

Demineralization–remineralization is a dynamic process, and there is always a battle between them. Both processes can occur on the hard tissue surface to some extent. Therefore, the main aim would be to maintain the environment that prevents demineralization but encourages remineralisation (10, 11). Combining different beneficial ingredients into one, such as hyperbiotics, activated charcoal probiotics toothpaste (*L. paracasei* and xylitol), would surely facilitate daily oral hygiene procedures and the remineralization process. In addition, the data indicated that the experimental therapy with probiotics and xylitol resulted in significant short-term improvements in clinical parameters, in accordance with the international scientific literature (2-6).

With a similar study design, Vivekananda et al. (12) recently demonstrated the plaque inhibition, anti-inflammatory and anti-microbial effects of *Lactobacillus* during non-surgical therapy and the maintenance phase of periodontal treatment. The study period was 42 days and the participants took tablets containing *Lactobacilli* or the corresponding placebo tablets twice daily from day 21 to day 42 in a split-mouth design protocol. At day 42, all clinical indexes were significantly reduced by scaling and root planning plus administration of a probiotic agent.

The results in the present study suggest that a probiotic intervention with activated charcoal probiotics toothpaste (Hyperbiotics, USA) could be a beneficial tool in oral health. This approach may provide a valuable addition or alternative to the armamentarium of treatment options for oral hygiene practices. On the one hand, the tested probiotics, and in lesser amount, its xylitol-content, seem to be as effective in reducing salivary *S. mutans* levels. On the other hand, it also

facilitates the daily remineralization process to prevent dental erosion. Their constant long-term application is thus recommended to prevent dental caries.

REFERENCES

1. Cantore S, Ballini A, Mori G, et. al. Anti-plaque and antimicrobial efficiency of different oral rinses in a 3-day plaque accumulation model. J Biol Regul Homeost Agents 2016; 30:1173-78.
2. Inchingolo F, Dipalma G, Cirulli N, et. al. Microbiological results of improvement in periodontal condition by administration of oral probiotics. J Biol Regul Homeost Agents 2018; 32:1323-28.
3. Tatullo M, Gentile S, Paduano F, Santacroce L, Marrelli M. Crosstalk between oral and general health status in e-smokers. Medicine (Baltimore) 2016; 95:e5589.
4. Cantore S, Ballini A, De Vito D, et. al. Clinical results of improvement in periodontal condition by administration of oral probiotics. J Biol Regul Homeost Agents 2018; 32:1329-34.
5. American Academy on Pediatric Dentistry. Guideline on xylitol use in caries prevention. Pediatr Dent 2011; 33:157-60.
6. Ballini A, Cantore S, Fotopoulou EA, et al. Combined sea salt-based oral rinse with xylitol in orthodontic patients: clinical and microbiological study. J Biol Regul Homeost Agents 2019; 33:263-68.
7. Greene JC, Vermillion Jr. The Simplified Oral Hygiene Index. J Am Dent Assoc 1964; 68:7-13.
8. Lobene RR. Effect of dentifrices on tooth stains with controlled brushing. J Am Dent Assoc 1968; 77:849-55.
9. Macpherson LM, Stephen KW, Joiner A, Schafer F, Huntington E. Comparison of a conventional and modified tooth stain index. J Clin Periodontol 2000; 27:854-9.
10. Abou Neel EA, Aljabo A, Strange A, et al. Demineralization–remineralization dynamics in teeth and bone. Int J Nanomedicine. 2016; 11:4743-63.
11. Grassi FR, Pappalettere C, Di Comite M, et al. Effect of different irrigating solutions and endodontic sealers on bond strength of the dentin-post interface with and without defects. Int J Med Sci 2012; 9:642-54.
12. Vivekananda MR, Vandana KL, Bhat KG. Effect of the probiotic Lactobacilli reuteri (Prodentis) in the management of periodontal disease: a preliminary randomized clinical trial. J Oral Microb 2010; 2:5344-52.

LETTER TO THE EDITOR

COMPARATIVE PROTEOMIC ANALYSIS BETWEEN THE GINGIVAL CREVICULAR FLUID AND THE CORRESPONDING PERIODONTAL POCKET: A PRELIMINARY STUDY

C. BERTOLDI[1], S. BERGAMINI[1], M. FERRARI[2], M. LALLA[3], E. BELLEI[1], S. SPINATO[2], A. TOMASI[1] and E. MONARI[1]

[1]Department of Surgery, Medicine, Dentistry and Morphological Sciences with Transplant Surgery, Oncology and Regenerative Medicine Relevance, University of Modena and Reggio Emilia, Modena, Italy; [2]Private Practice, Modena, Italy; [3]Department of Economics Marco Biagi, University of Modena and Reggio Emilia, Modena, Italy

Received January 25, 2019 – Accepted March 12, 2019

To the Editor,

Periodontal disease is characterized by gingival inflammation, clinical attachment loss, and alveolar bone resorption (1, 2). The combined effect of microbial aggression and inflammatory/immune response causes periodontal attachment loss and the formation of periodontal pockets and gingival recessions (1-3).

To date, the diagnosis of periodontitis is established mainly by clinical criteria based on the use of a periodontal probe to detect attachment loss and pockets, which are the clinical expression of periodontal diseases. (4). The pathogenesis of periodontitis has not yet been properly defined. Further advances in our understanding of mechanisms of homeostasis and responses to trauma and infection of periodontal tissues will likely require a more sophisticated analyses, including a complete list of the proteins expressed in periodontal pockets (5-7).

Most proteomic analyses regarding periodontal diseases have been performed on saliva or crevicular fluid samples, peripheral blood or periodontal plaque samples. However, very few studies were directly performed on the periodontal pocket, which is the key lesion that defines periodontal disease diagnosis (7-8).

Some proteins and cytokines have been individually proposed as the main actors involved in the pathogenetic basis of the periodontal lesion, so becoming the main cause of periodontal disease. However, it is now clear that the periodontal damage that generates periodontal pockets is not caused by a single molecule, but by changes occurring in a complex molecular network (6, 7). Periodontal surgery is necessary to harvest and study the periodontal pocket tissue and to reliably explain the pathogenesis and the diagnostic way of the periodontal disease. Therefore, biological samples, such as gingival crevicular fluid (GCF), saliva, and peripheral blood, among others, are more easily available in a less invasive way; nevertheless, it is not known whether these compartments have the same molecular network as the periodontal pocket. The aim of this study was to compare the proteomic profile of interproximal pocket tissues with that of gingival crevicular fluid (GCF), and to analyze whether they show a significant similarity in the proteomic profile.

Key words: gingival crevicular fluid; inflammation; periodontal disease; periodontal poket tissue; proteomic

Corresponding Author:
Prof. Carlo Bertoldi,
Dipartimento Chirurgico, Medico,
Odontoiatrico e di Scienze Morfologiche
con Interesse Trapiantologico, Oncologico e di Medicina Rigenerativa,
Università di Modena e Reggio Emilia,
Via del Pozzo 71, 41124, Modena, Italy
Tel.: +39 0594224101 - Fax: +39 0594224795
e-mail: carlo.bertoldi@unimore.it

0393-974X (2019)

MATERIALS AND METHODS

This clinical study was performed at the Modena University Hospital (Periodontology Unit of Dentistry and Oral-Maxillofacial Surgery). The patients considered in this perspective study signed informed consent detailing all procedures of the treatment, as requested by the Helsinki protocols. The study was approved, and supervised by the local ethics committee of the Health Service of the Emilia-Romagna region (University-Hospital of Modena- protocol nr. 3968/2017, registration nr. 315/17). Subjects who were included suffered from moderate or severe periodontal disease assessed according the current diagnostic criteria (4) and who needed additional surgical therapy after completion of the cause-related therapy. Furthermore, the patients had to satisfy the following systemic and local inclusion criteria: absence of relevant medical conditions (2, 9), aged over 18 years, non-pregnant or lactating, non-smokers and without history of alcohol abuse. The full-mouth plaque score (FMPS) and the full-mouth bleeding score (FMBS) had to be maintained ≤25% (4 aspects per tooth).

Study design

Six weeks after the end of cause-related therapy, at baseline, immediately before the periodontal surgery, GCS, samples were taken over a 30-second period by means of filter paper strips (Wathman, USA) positioned in the gingival sulcus correspondent to periodontal pockets considered. The samples were immediately stored at -80°C in sealed Eppendorf tubes. The periodontal pocket tissue, harvested during surgery, was likewise stored at -80°C.

The protein extraction from GCF and periodontal pockets was performed as previously described (7). The protein content determination and 1-DE analysis were performed as previously described (7).

The Coomassie-stained gel images were acquired using a GS-800 Calibrated Densitometer (Bio-Rad) that converts signals from biological samples into digital data and display the data in the form of a gray scale. The specific software "Quantity One" (Bio-Rad version 4.6.7) was used for the 1-DE image analysis; this software detects increased or decreased proteins bands on the basis of staining intensity. The total intensity of the protein band is obtained by the sum of the intensities of all the pixels that make the band, and the signal intensity is expressed as optical density (OD). The detected bands were cut manually by the gel and subjected to the "in-gel" digestion for the subsequent MS analysis as previously described by Monari et al. (7).

ESI-Q-ToF LC MS analysis

Tryptic digest was treated as previously described (7), then mass spectrometry (MS) data processing was carried out. Protein-identification band lists were generated using MASCOT search engine (http://mascot.cigs.unimo.it/mascot) against the UniProt Knowledgebase database (UniProt.org), specifying parameters described previously (7). Proteins were identified with at least 2 or more significant peptide sequences and with the highest score hits among MASCOT search results.

Statistical analysis

The primary outcomes of this study were: qualitative and quantitative protein band comparison between GCF and pocket tissue in every patient. Secondary outcome was the evaluation of the possibility that there are protein bands able to influence significantly the behavior of other protein bands. Statistical analysis was performed using the parametric correlation and regression test to study the connection between GCF and pocket tissue proteome in every patient. The correlation and regression test between all protein bands obtained was mathematically analyzed by multivariate analysis, using a "stepwise" statistical method, in order to select the possible independent variables and to analyze possible correlation between the different protein amounts resulted.

For all measured variables, the null hypothesis (H_0) of no correlation among protein band was rejected for a critical significance level of $p < 0.05$.

RESULTS

Four patients, 2 males and 2 females, aged 33-48 years (mean ± SD, 40.7±6.6 years) fulfilled the entry criteria to the retrospective study. The protein content GCF and pocket tissue extracts were respectively 3.2±0.94μg/μL and 3.05±1.93 μg/μL.

The image analysis software program (QuantityOne) found almost the same protein expression profile between GCF and pocket tissue in each patient with 12 bands detected in each case.

The relative amount of each protein band was

expressed as a percentage of the full amount of proteins found in each GCF, and pocket tissue sample. The mean amount (mean ± SD) of each band in relation to the total protein content resulted 1.44±1.40% in GCF and 1.33±0.62% in pocket tissue in the first patient, 1.03±0.14% in GCF and 1.25±0.57% in pocket tissue in the second patient, 1.04±0.13% in GCF and 1.49±1.09% in pocket tissue in the third patient and 1.06±0.13% in GCF and 1.77±1.78% in pocket tissue in the fourth patient.

The correlation and regression test performed to analyze the connection between the quantitative proteomic profile of GCF and pocket tissue in each patient resulted not significant for correlation considered in all four patients ($p \geq 0.05$). The multivariate analysis applied to analyze possible correlation between the different protein bands showed that just one band was gave a significant correlation between GCF and pocket tissue proteome in each patient ($p=0.008$). MS analysis then showed that such band was formed by K immunoglobulin. This association consists in a direct correlation between GCF and pocket proteome profile.

DISCUSSION

The current pathogenetic models did not capture the dynamic nature of the biological parameters that may accelerate or dampen the changes occurring during periodontal disease, which include, among others, innate differences among subjects and changes in environmental factors. A modern pathogenic model has to consider several levels of homeostatic regulators, and thus has to incorporate data from genes, proteins, and metabolites. Then, such data must build a model based upon a multilevel framework that includes disease-initiating and -resolving mechanisms, which, in turn, are regulated by innate and environmental factors (6, 7). The tissue resorption or regeneration depends on a large number of variables both in animals and human beings (10-12). In this regard, the study of periodontal disease pathogenesis through a minimally invasive system, in a simple way, carried out in a short time and by a limited use of means, would be very advantageous. Planning a study that compares sick patients to healthy ones, and that regards a high number of observations, would likely lead to significant diagnostic developments in a short time. GCF is indeed considered the most promising source of disease indicators as it offers great potential in reflecting the ongoing response generated by cells and tissues in the periodontium (5). However, obtaining GCF may be technically difficult (difficulty in accessing all tooth sites, salivary contamination or bleeding from the sites, etc.), and thus it appears that this approach is quite complicated to implement clinically.

Saliva is more readily available and easier to collect than GCF (5). However, saliva is less representative of the proteomic network that characterizes periodontal disease than GCF as it contains a lot of other material that can interfere with the analysis. Thereby, saliva represents a more comprehensive appraisal of whole oral health status, opposed to the site-specific characteristics of GCF analysis (5). However, a site-specific analysis, i.e., in the periodontal pocket, is necessary to understand exactly the changes in the molecular network that are responsible for the pathogenesis of periodontal disease. The periodontal pocket is the clinical expression of periodontal diseases. Therefore, the biomolecular arrangement in the periodontal pocket tissue is conceptually the closest biological environment we know to the pathogenic process that produces periodontal disease. The gingival sulcus is the anatomical structure closest to the periodontal pocket that can be analyzed in a minimally invasive way. Öztürk et al. (8) studied the gingival tissue, the GCF, saliva and serum in subjects with chronic periodontitis, aggressive periodontitis and non-periodontitis control subjects. Subjects with chronic periodontitis and generalized aggressive periodontitis exhibited significantly higher L-plastin gene expression in gingival tissue and GCF than subjects in the control group, but there was no statistically significant difference between serum and salivary L-plastin levels among the three study groups.

In the present study, a network of 12 protein bands was considered in gingival tissue and in the GCF. A similar distribution of bands was observed between periodontal pocket tissue and GCF, but no statistical

quantitative correlation resulted between the gingival pocket tissue and GCF. Even if the qualitative data of the proteomic distribution detected in the tissue of the periodontal pocket resulted similar to that found in the GCF, there was no statistical correlation between the gingival tissue and the GCF. It can therefore be assumed that the protein network proper of the periodontal pocket did not influence significantly the protein network of the GCF with the only exception of a band corresponding to K immunoglobulin.

In conclusion, we think that it is unrealistic to consider a single protein as a reliable biomarker of a complex pathology such as periodontal disease. Even if within the limits of a preliminary study, we believe that the periodontal pocket and the GCF are similar in their proteomic network, and that the GCF does not seem suitable to adequately study the pathogenesis of periodontal disease.

REFERENCES

1. Bertoldi C, Pellacani C, Lalla M, Consolo U, Pinti M, Cortellini P, Cossarizza A. Herpes Simplex I virus impairs regenerative outcomes of periodontal regenerative therapy in intrabony defects: a pilot study. J Clin Periodontol 2012; 39:385-92.
2. Bertoldi C, Zaffe D, Generali L, Lucchi A, Cortellini P, Monari E. Gingival tissue reaction to direct adhesive restoration: A preliminary study. Oral Dis 2018; 24:1326-35.
3. Bertoldi C, Bencivenni D, Lucchi A, Consolo U. Augmentation of keratinized gingiva through bilaminar connective tissue grafts: a comparison between two techniques. Minerva Stomatol 2007; 56:3-20.
4. Caton JG, Armitage G, Berglundh T, et al. A new classification scheme for periodontal and peri-implant diseases and conditions - Introduction and key changes from the 1999 classification. J Periodontol 2018; 89(S1):S1-S8.
5. Giannobile WV. Salivary diagnostics for periodontal diseases. J Am Dent Assoc 2012; 143(10 Suppl):6S-11S.
6. Bertoldi C, Bellei E, Pellacani C, et al. Non-bacterial protein expression in periodontal pockets by proteome analysis. J Clin Periodontol 2013; 40:573-82.
7. Monari E, Cuoghi A, Bellei E, et al. Analysis of protein expression in periodontal pocket tissue: a preliminary study. Proteome Sci 2015; 13:1-11.
8. Öztürk VÖ, Emingil G, Osterwalder V, Bostanci N. The actin-bundling protein L-plastin: a novel local inflammatory marker associated with periodontitis. J Periodont Res 2015; 50:337-46.
9. Bertoldi C, Balli F, Tanza D, Bertolani P, Chiarini L. Experimentation and clinical analysis of the interrelationships between dental damage and celiac disease. Minerva Stomatol 1995; 44:395-405.
10. Bertoldi C, Pradelli JM, Consolo U, Zaffe D. Release of elements from retrieved maxillofacial plates and screws. J Mater Sci Mater Med 2005; 16:857-61.
11. Consolo U, Bertoldi C, Zaffe D. Intermittent loading improves results in mandibular alveolar distraction osteogenesis. Clin Oral Implants Res 2006; 17:179-87.
12. Bertoldi C, Zaffe D. In vivo comparison of two bone substitutes in the distal femur of the rabbit. Int J Oral Maxillofac Implants 2012; 27:119-27.

JOURNAL OF BIOLOGICAL REGULATORS & HOMEOSTATIC AGENTS Vol. 33, no. 3, 987-989 (2019)

LETTER TO THE EDITOR

PERIODONTAL NEOFORMATIONS AND MYOCARDITIS ONSET: IS IT MORE THAN A SIMPLE COINCIDENCE?

F.M. ABENAVOLI[1], A.D. INCHINGOLO[2], A.M. INCHINGOLO[2], G. DIPALMA[2] and F. INCHINGOLO[2]

[1]Department of Maxillofacial Surgery, "San Pietro" Hospital, Fatebenefratelli, Rome, Italy; [2]Department of Interdisciplinary Medicine, University of Bari, Bari, Italy

Received February 14, 2019 – Accepted March 22, 2019

To the Editor,

Medicine is a heterogeneous science with several branches, all closely connected to each other. Human tissues may be influenced by a high number of factors able to modify the local environment, thus triggering the behaviour of different cell populations (1-4). Local and systemic factors may concur to impair oxidative stress values (5-8), and the most frequent co-factors acting on tissues are infections (9), some oncogenic factors (10) or systemic and syndromic diseases (11).

Oral cavity is one of the first gates to the human body; it is not unusual to observe first signs of systemic pathologies developing in the oral cavity (12), and the tight correlations between oral and systemic diseases are useful to ensure early diagnosis and a better prognosis. Currently, there is a wide knowledge on periodontal disease as a co-factor in the pathogenesis of several cardiovascular pathologies: periodontal disease significantly influences the risk of developing cardiovascular pathologies (10-12). However, to date, no association has been reported in the scientific literature on the role of odontogenic cysts as a possible cause of myocarditis.

MATERIALS AND METHODS

We investigated the hypothetical association among some dental-related pathologies and the onset of some acute cardiological diseases. To better describe our null hypothesis, here we report the clinical case of a 43-year-old male with no clinical history of severe diseases. The patient gave his informed consent prior to the inclusion in this report. The entire observational report was carried out under the ethical and legal principles applied to research with human subjects.

The reported subject had not travelled to any foreign country during the previous 6 months. He came to the dentist for moderate pain of the left mandible and fever. During the clinical visit, the patient revealed that he was aware of the presence of a huge odontogenic cyst affecting the left side of the mandible. Despite the presence of such cyst, the patient refused any surgical treatment, because of low symptomatology.

To treat any potential odontogenic bacterial infection, a cycle of antibiotic therapy was administered. After few days from our first diagnosis, the patient referred to be suffering from severe fatigue, with diffuse chest pain and severe difficulty in breathing. Hematological tests showed a slight increase in white cell values, and a high increase of inflammation-related markers (Reactive Protein-C and VES). The new diagnosis, after a deep clinical evaluation, was acute myocarditis.

Key words: periodontitis; myocarditis; inflammation; cardiovascular diseases

Corresponding Author:
Prof. Francesco Inchingolo,
D.I.M., Department of Interdisciplinary Medicine,
University of Bari,
Bari, Italy
e-mail: francesco.inchingolo@uniba.it

0393-974X (2019)

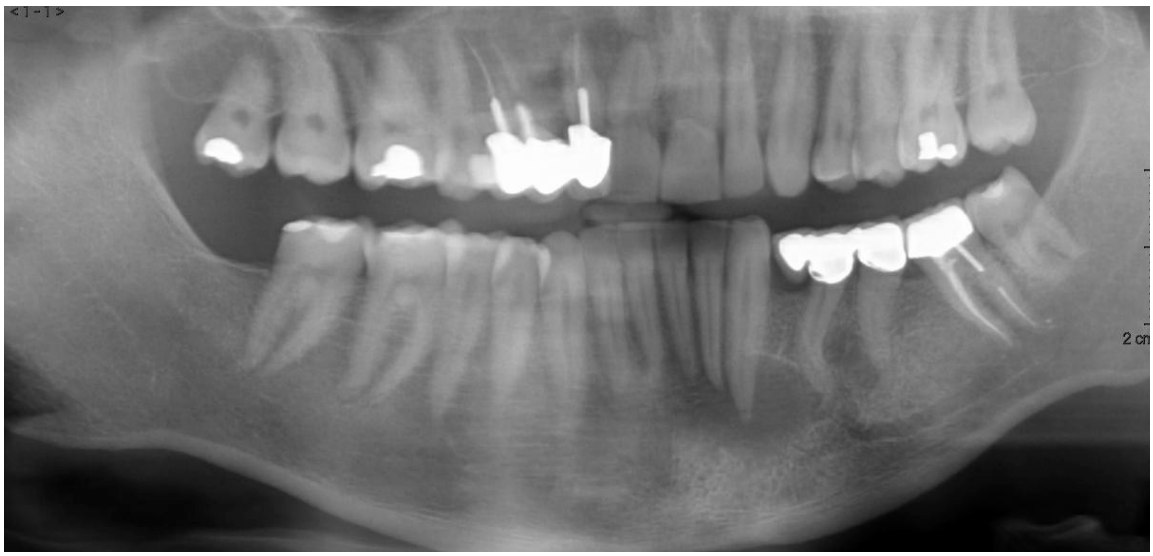

Fig. 1. *Orthopanoramic X-ray with the cystic neoformation involving teeth 3.1, 3.2, 3.3 and 3.5.*

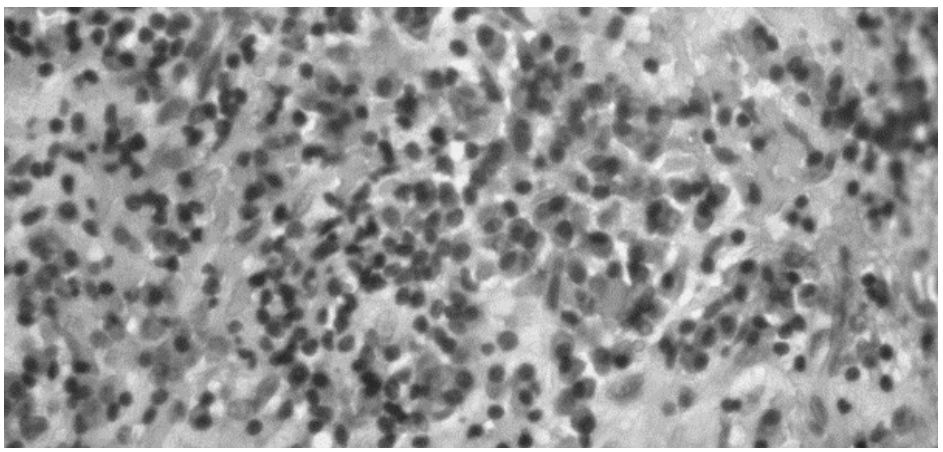

Fig. 2. *Histology section of the cystic lesion with numerous inflammatory cells.*

The new therapeutic approach was based on a multi-drug therapy *per os*, associated with intravenous antibiotics. aAter this cycle of therapy, the clinical evolution seemed to be quite favorable.

The onset of the acute myocarditis was the reason to be able persuade our patient to finally undergo surgical eradication of the cystic neoformation.

RESULTS

The orthopanoramic X-ray (Fig. 1) clearly showed a radiotransparent neoformation, which involved the roots of incisive and canine teeth located in the third quadrant. We performed oral surgery to remove the cyst, and surgical endodontics to restore the compromised root apices.

The histology carried out on the cyst, showed a diffuse infiltration of inflammatory cells. Inflammatory cells were detected around the fibrous capsule of the cyst, mainly consisting of fibroblast-like cells along with infiltrating lymphocytes, monocytes and few polymorphonucleates. (Fig. 2).

DISCUSSION

Periodontitis has been widely reported to be closely related to cardiovascular diseases. In our letter, we argue a new intriguing hypothesis: in fact, we hypothesize that odontogenic cysts may also be considered as a potential cause of myocarditis.

Despite our letter being only a communication, we suggest that dentists or maxillofacial surgeons should be well informed about this association. Patients with local mandibular pain, and a history of odontogenic cyst should be immediately evaluated for an appropriate antibiotic systemic therapy to avoid possible cardiological complications.

REFERENCES

1. Paduano F, Marrelli M, Palmieri F, Tatullo M. CD146 expression influences periapical cyst mesenchymal stem cell properties. Stem Cell Rev 2016; 12(5):592-603.
2. Paduano F, Marrelli M, Amantea M, et al. Adipose tissue as a strategic source of mesenchymal stem cells in bone regeneration: a topical review on the most promising craniomaxillofacial applications. Int J Mol Sci 2017; 18(10).
3. Tatullo M, Simone GM, Tarullo F, et al. Antioxidant and antitumor activity of a bioactive polyphenolic fraction isolated from the brewing process. Sci Rep 2016; 6:36042.
4. Tatullo M, Marrelli M, Scacco S, et al. Relationship between oxidative stress and "burning mouth syndrome" in female patients: a scientific hypothesis. Eur Rev Med Pharmacol Sci 2012; 16(9):1218-21.
5. Tatullo M, Gentile S, Paduano F, Santacroce L, Marrelli M. Crosstalk between oral and general health status in e-smokers. Medicine (Baltimore) 2016; 95(49):e5589.
6. Marrelli M, Gentile S, Palmieri F, Paduano F, Tatullo M. Correlation between Surgeon's experience, surgery complexity and the alteration of stress related physiological parameters. PLoS One 2014; 9(11):e112444.
7. Marrelli M, Tatullo M, Dipalma G, Inchingolo F. Oral infection by Staphylococcus aureus in patients affected by White Sponge Nevus: a description of two cases occurred in the same family. Int J Med Sci 2012; 9(1):47-50.
8. Tatullo M, Marrelli M, Amantea M, et al. bioimpedance detection of oral lichen planus used as preneoplastic model. J Cancer 2015; 6(10):976-83.
9. Inchingolo F, Tatullo M, Abenavoli FM, et al. Non-syndromic multiple supernumerary teeth in a family unit with a normal karyotype: case report. Int J Med Sci 2010; 7(6):378-84.
10. Inchingolo F, Tatullo M, Abenavoli FM, et al. Non-Hodgkin lymphoma affecting the tongue: unusual intra-oral location. Head Neck Oncol 2011; 3:1.
11. Inchingolo F, Tatullo M, Abenavoli FM, et al. Oral piercing and oral diseases: a short time retrospective study. Int J Med Sci 2011; 8(8):649-52.
12. Inchingolo F, Tatullo M, Marrelli M, et al. Clinical trial with bromelain in third molar exodontia. Eur Rev Med Pharmacol Sci 2010; 14(9):771-74.

LETTER TO THE EDITOR

ALLOPURINOL, FUROSEMIDE AND A PHYTOTHERAPEUTIC AGENT (BAZOTON UNO) REVERSE P-GLYCOPROTEIN-MEDIATED DOXORUBICIN RESISTANCE IN HUMAN UTERINE SARCOMA MES-SA/Dx5 CELLS: A NOVEL THERAPEUTIC PERSPECTIVE

A. ANGELINI[1,2], M.A. CENTURIONE[3], R. DI PIETRO[1] and L. CENTURIONE[1]

[1]Department of Medicine and Aging Science, School of Medicine and Health Science University of Chieti-Pescara, Italy; [2]Research Center on Aging and Translational Medicine (Ce.S.I. Met), "G. D'Annunzio" University of Chieti-Pescara, Italy; [3]Institute of Molecular Genetics, National Research Council, Unit of Chieti, Italy

Received October 29, 2018 – Accepted March 27, 2019

To the Editor,

Multidrug resistance (MDR) is still one of the major obstacles of cancer chemotherapeutic treatment (1). The major mechanism for development of MDR is the overexpression of P-glycoprotein (Pgp), a member of the ATP-binding cassette family. To overcome drug resistance, it is essential to find chemo-sensitizer agents able to inhibit the Pgp function, thus reversing MDR. However, several side effects limit their clinical applicability (2). Therefore, several nontoxic natural compounds have been selected *in vitro* (3). In this context, we previously reported the effectiveness of several natural Pgp inhibitors such as flavonoids, honokiol and theobromine (4-6). Cancer patients with tumor lysis syndrome (TLS), an acute cell lysis caused by chemotherapy and radiation therapy (7), usually present metabolic disorders and acute renal failure. We investigated the chemo-sensitizer effects of two synthetic drugs, allopurinol and furosemide, commonly used during chemotherapy (8) and a phytotherapeutic agent, Bazoton uno (*Urtica dioica*) (9). We assessed Pgp activity in a human resistant sarcoma cell line (MES-SA/Dx5) that expresses high levels of Pgp (100-fold) and is resistant to doxorubicin (doxo) (10). MES-SA/dx5 cells were treated with various doxo concentrations (2, 4 and 8 μM), alone or in combination with different concentrations of the three drugs analyzed, clinically achievable in human serum, measuring intracellular doxo accumulation and cytotoxicity. In addition, we determined the production of the reactive oxygen species (ROS). In this study, we used *in vitro* concentrations of allopurinolo, furosemide and Bazoton uno similar to those obtained in human plasma when standard oral dose was administered. We used concentrations of doxo, similar to those obtained in the blood of patients undergoing chemotherapy. The results were compared to those obtained with verapamil (ver), a calcium blocker, used as positive control.

MATERIALS AND METHODS

Chemicals

Doxorubicin (doxorubicin hydrochloride), verapamil and allopurinol, furosemide, 2',7'-dichlorofluorescein diacetate (DCF-DA), dithionitrobenzoic acid (DTNB) and

Key words: P-glycoprotein, allopurinol, furosemide, Bazoton uno, MDR, MES-SA/Dx5 cells

Corrisponding Author:
Dr Antonio Angelini,
Università "Gabriele D'Annunzio",
Centro di Scienze dell'Invecchiamento (Ce.S.I-Me.T),
Via dei Vestini, 31 - 66013 Chieti, Italy
Tel./Fax: +39 0871 541420.
e-mail: aangelini@unich.it

0393-974X (2019)

DISCLOSURE: ALL AUTHORS REPORT NO CONFLICTS OF INTEREST RELEVANT TO THIS ARTICLE.

dimethyl sulfoxide (DMSO) were obtained from Sigma-Aldrich Co. (St Louis, MO, USA). Cytotoxicity detection Kit^{plus} LDH was also purchased from Sigma-Aldrich Co. (St Louis, MO, USA). Bazoton uno was purchased from Abbott (Erbofarma; M896). All chemicals and drugs were freshly dissolved before use except for doxorubicin and Bazoton uno, which were stored separately in a stock solution (1 mM in PBS and 4.6mg/ml in 20% methanol, respectively) at -20° C in the dark.

Tissue culture

The doxo-resistant human uterus sarcoma cell line MES-SA/Dx5 was obtained from the European Collection of Cell Cultures (cat. 95051031; Salisbury, UK) and grown in 25 cm^2 plastic culture flasks (Iwaki Company, Japan) containing 15 ml McCoy's 5a medium (Sigma-Aldrich) supplemented with 10% heat-inactivated foetal bovine serum (Sigma-Aldrich), 2 mM L-glutamine, penicillin (1000U/ml) and streptomycin (100µg/ml) in a humidified atmosphere of 95% air and 5% CO_2 at 37°C. Cells at 70-80% confluence were sub-cultured every 3-4 days after treatment with 0.05% trypsin and 0.02% EDTA in Ca^{++} and Mg^{++} free 1X phosphate buffered saline (PBS). Cells were periodically checked for Mycoplasma contamination.

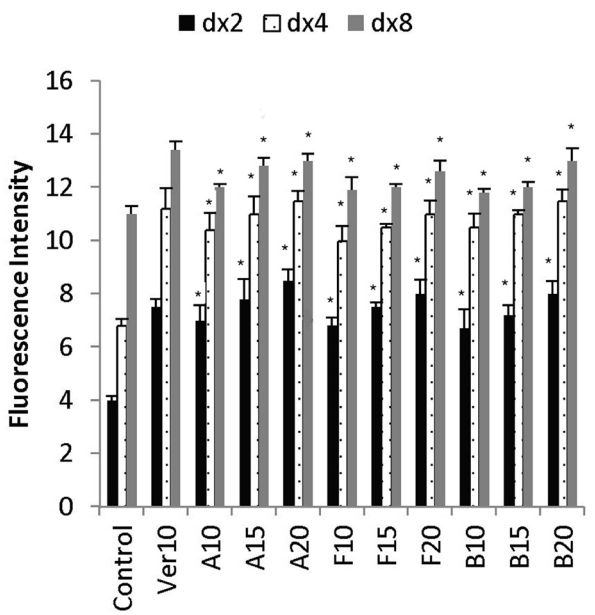

Fig. 1. *The effects of Allopurinol, Furosemide, and Bazoton uno on doxo accumulation in MES-SA/Dx5 cell line. Cells were pre-treated with: Verapamil (10 µM); Allopurinol (10, 15, 20 µM); Furosemide (10, 15, 20 µM) and Bazoton uno (10, 15, 20 µg) for 24 h at 37°C. Thereafter three different concentrations of doxo (2, 4, 8 µM) were added and incubated for 3 h at 37°C. Fluorescence intensity of doxo was then measured and results were expressed as the mean ± SD of three different experiments compared to the mean fluorescence of un-pre-treated control cells. All bars were significant ($p<0.05$) (asterisks) when compared to control (doxo alone).*

Bazoton uno extraction

Pills of 459 mg each of Bazoton uno contained a methanolic extract of stinging nettle root with an active ingredient ratio of 7.1-14.3:1. This ratio was similar to that obtained from a methanolic extract of about 1 Kg of dried stinging nettle roots. Each Bazoton uno pill was homogenized by using a laboratory mortar mixer and transferred to a beaker with a magnetic mixer. Then, a solution of extractant (20% methanol) was added and stirred with a mechanical stirrer at room temperature. After 4 h the supernatant was separated from the solid phase, and the residue was re-extracted under the same conditions. After completion of the extraction process, the extracts obtained were combined and centrifuged at 10,000 rpm for 10 min at 4°C to separate any precipitated material that could interfere with *in vitro* growth assays. The supernatant was then filtered through a 0.22-µm nylon filter (Millipore), transferred to vials and stored at -20°C until use.

Determination of intracellular accumulation of doxorubicin

MES-SA-Dx5 cells were seeded on 24-well culture dishes at a density of 1.0x10^5 cells/well (Corning-Costar Corp., Corning New York) and incubated for 72 h in growth medium alone at 37°C in an atmosphere containing 5% CO_2 and 95% air to allow cell attachment. At confluence, cells were washed three times with PBS at 37°C and allopurinol 10, 15 and 20 µM corresponding to 0.65, 1.9, 2.55µg/ml, furosemide 10, 15 and 20 µM corresponding to 3.4; 5.0; 6.67µg/ml or Bazoton uno extract (10, 15, and 20µg /ml) were added to triplicate wells and incubated at 37°C. After incubation for 24 h all pre-treated cells were exposed to three different doxo concentrations (2, 4 and 8 µM) and the monolayer cultures were then incubated for 3 h at 37°C. In these experiments ver at 10 µM concentration was used as a positive control drug. All values were averaged from three wells for each experiment. Then, wells were rinsed with ice-cold PBS (pH 7.4) to stop doxo accumulation. Thereafter

cells were solubilized with 4 M NaOH (250 µl) for 2 h and neutralized with 2 M HCl (500 µl). Concentration of doxo was determined fluorimetrically (excitation, 475 nm; emission, 580 nm) with a fluorescence spectrophotometer (Perkin Elmer LS 45). The accumulated amount of doxo inside cancer pre-treated (with the allopurinolo, furosemide and Bazoton uno or ver) cells was expressed as a percentage of doxo retention in doxo alone control cells at the selected concentrations (2, 4 and 8 µM) and was calculated as: doxo accumulation (%) = 100 x (F treated – F control) / F treated, where F treated = mean fluorescence of wells treated with allopurinol, furosemide, Bazoton uno or ver prior treatment with doxo; F control = mean fluorescence of wells treated with doxo alone.

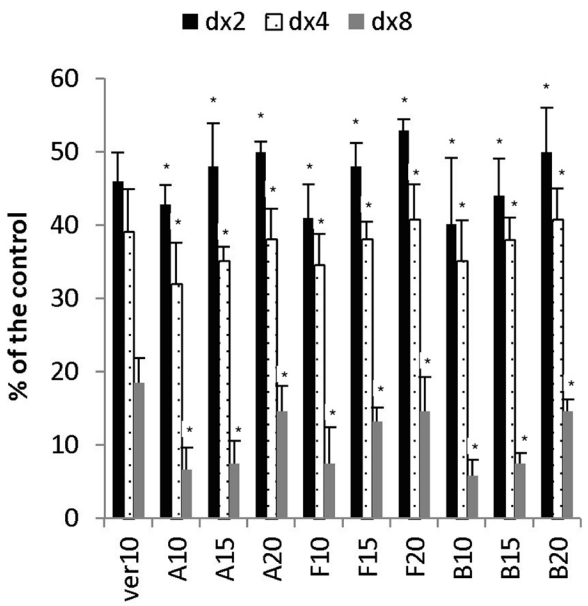

Fig. 2. *Mean percentage of increase in intracellular doxo accumulation in MES-SA/Dx5 resistant cells pre-treated for 24 h at 37°C with Verapamil (10 µM); Allopurinol (10, 15, 20 µM), Furosemide (10, 15, 20 µM) and Bazoton uno (10, 15, 20 µg) in combination with three different doxo concentration (2, 4, 8 µM) compared to untreated cells (doxo alone). All bars were significant when compared to control ($p<0.05$) (asterisks). Data represents the mean ± SD obtained from at least three independent observations.*

Assay of LDH activity

Lactic acid dehydrogenase (LDH) is a stable cytoplasmatic enzyme present in all cells. It is rapidly released into the cell culture supernatant when the plasma membrane is damaged. Damage of the plasma membrane or cell death was evaluated by measuring the amount of intracellular enzyme LDH released into the medium after treatment with drugs. An increase in the number of dead cells results in an increase of LDH activity in the culture supernatant proportional to the number of MES-SA/dx5 lysed cells. LDH activity was measured spectrophotometrically using a Cytotoxic Detection Kit^{plus} (Sigma-Roche) according to instructions of the manufacturer with some modifications. Briefly, cells were plated into 96-well microplates (Iwaki Company, Japan) at a density of 1.0 x10^4 cells/well in growth medium. Cells were incubated in an atmosphere of 5% CO_2 at 37°C for 24 h to allow adhesion to the wells. Cell viability was determined by cultivation of MES-SA/Dx5 cells with different concentrations of doxo (2, 4, and 8 µM) in absence or presence of allopurinol (10, 15 and 20 µM), furosemide (10, 15 and 20 µM) or Bazoton uno (10 µg, 15 µg and 20 µg) for 100µl/well. The active substance of Bazoton uno for 10, 15 and 20 µM ranged from a minimum of 0.7, 1.07, 1.42 µg, respectively, to a maximum of 1.42, 2.14 and 2.86 µg, respectively. Cells were then incubated at 37°C for 72 h. MES-SA/Dx5 cells incubated with medium alone were used as negative control for optical density (OD). Doxo (2, 4 and 8 µM) with 10 µM ver was used as positive control. The cytotoxicity of each drug itself was also measured. Reaction mixture was subsequently added to each well in the 96 well plate and incubation for 30 min was performed at room temperature in the dark. The reaction was stopped with Stop solution and OD value was quantified on a Spectra max 190 microplate spectrophotometer reader (Molecular Devices) at the wavelength of 490 nm. Each experiment was performed in triplicate. The percentage of cell growth inhibition was evaluated as: 100 (OD treated well - OD control well) x OD control well, where OD treated wells corresponded to the mean absorbance values of cells pre-treated with allopurinol, furosemide and Bazoton uno or ver, whereas OD control wells corresponded to the mean absorbance values of untreated malignant cells.

Determination of intracellular ROS

The contents of the intracellular generation of ROS

induced by allopurinol, furosemide and Bazoton uno were determined by using the fluorogenic reagent DFC-DA. Briefly, MES-SA/Dx5 cells were seeded on 24-well culture dishes at a density of 1 x 10^4 cells/well and incubated at 37°C in 5% CO_2 as above for 48 h. After this period the cells were treated with three different concentrations of allopurinol (10, 15 and 20 μM), furosemide (10, 15 and 20 μM), Bazoton uno (10, 15, 20 μg), or ver (10 μM) as control for 24 h at 37°C. Thereafter cells were washed three times with PBS and suspended with PBS containing 20 μM DCF-DA and incubated for 45 min at 37°C. DCF-DA is a cell permeable, non-fluorescent probe that is separated by nonspecific cellular esterase inside cells to non-fluorescent DCFH and oxidized by ROS to a fluorescent product dichlorofluorescein (DCF). Fluorescence intensity is proportional to the amount of oxidant species produced by the cells. For ROS determinations, the cells were washed with PBS and solubilized with 250 μl of 4 M NaOH for 2 h and neutralized with 500 μl of 2 M HCl. Measurements

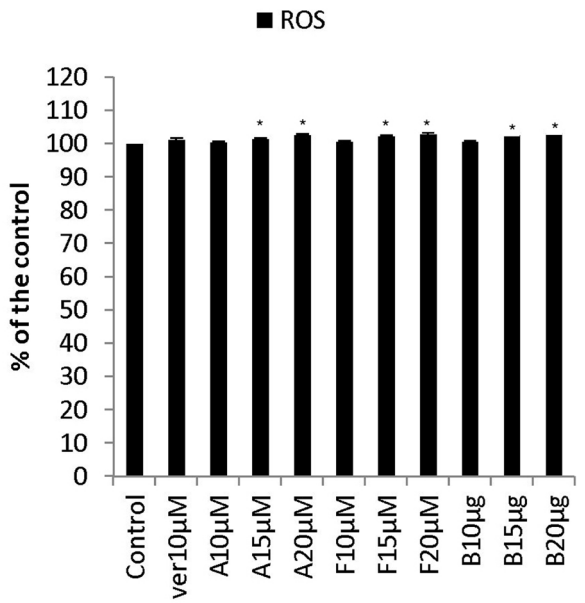

Fig. 3. *Effects of Verapamil (10 μM); Allopurinol (10, 15, 20 μM), Furosemide (10, 15, 20 μM) and Bazoton uno (10, 15, 20 μg) on redox status. ROS production was evaluated after 24 h incubation of the MES-SA/Dx5 cells at 37°C. Cells treated with medium alone were used as control (100%). Results were expressed as a percentage of control. Data are means ± SD of three experiments. No significant increase of ROS was observed at 10 μM concentration for all compounds, while at 15 μM and 20 μM significant differences were observed for all compounds when compared to control (p<0.05) (asterisks).*

spectrofluorimeter (Perkin Elmer LS 45; excitation at 485 nm and emission at 530 nm). Cells containing medium alone were used as control. Intracellular ROS levels (DCF) were recalculated respect to control expressed as percentages.

Statistical analysis

The results were expressed as mean ±SD and analyzed for statistical significance with the Student's *t*-test between doxo alone treated control and the three drug treatment samples. P-values of <0.05 were considered significant.

Variant analysis was carried out using Excel model.

RESULTS

Effects of allopurinol, furosemide and Bazoton uno on doxo accumulation in MES-SA/dx5 cells

As shown in Fig. 1, pre-incubation of cancer cells for 24 h at 37°C with various concentrations of allopurinol, furosemide and Bazoton uno significantly increased the doxo concentration capacity at all doxo concentrations when compared to those cultures treated with doxo alone (p<0.05). In particular, the mean percentage of doxo accumulation capacity after exposure at 2 μM concentration of doxo in presence of allopurinol, furosemide and Bazoton uno at 10, 15 and 20 μM were 42.8±2.6; 48±5.9; 50±1.4 and 41±4.5; 48±3.2; 52.9±1.5; and 40.2±8.9; 44±5; 50±6, respectively, while in combination with 4 μM doxo concentration were 32±5.6; 35.2±1.8; 38.1±4.1; and 34.6±4.2; 38.1±2.3; 40.8±4.7; and 35.2±5.4; 38±3; 40.8±4.2, respectively, while with 8 μM doxo percentages were 6.7±2.9; 7.5±3; 14.6±3.4; and 7.5±4.9; 13.2±1.9; 14.6±4.6; and 5.8±2.2; 7.5±1.3; 14.6±1.6, respectively. The values of ver (10 μM) used in combination with 2, 4 and 8 μM doxo were 46±3.9; 39.1±5.8 and 18.5±3.3, respectively. All values were significant compared to control cells (p<0.05).

Effects of allopurinol, furosemide and Bazoton uno on doxo cytotoxicity in MES-SA/dx5 cells

As shown in Table I, the three compounds associated with doxo had significantly enhanced growth inhibitory effects on MES-SA/dx5 cells after 72 h incubation at 37°C at all doxo concentrations when compared with control cells treated with doxo

alone ($p<0.05$). In fact, growth inhibition using 2, 4 and 8 μM doxo concentrations in the presence of allopurinol (10, 15 and 20 μM) showed increases of 1.32; 1.66; 1.92-fold (allopurinol plus dx2); 1.18; 1.3; 1.4-fold (allopurinol plus dx4) and 1.31; 1.39; 1.52-fold (allopurinol plus dx8), respectively, whereas in combination with furosemide (10, 15 and 20 μM) increases of 1.3; 1.56; 1.62-fold (furosemide plus dx2) and 1.1; 1.17; 1.34-fold (furosemide plus dx4) and 1.24; 1.34; 1.43-fold (furosemide plus dx8), respectively, were observed. In presence of Bazoton uno (10, 15 and 20 μM), however, results showed increases of 1.36; 1.6; 1.9-fold (Bazoton uno plus dx2) and 1.17; 1.3; 1.38-fold (Bazoton uno plus dx4) and 1.28; 1.46; 1.5-fold (Bazoton uno plus dx8), respectively, when compared to the corresponding cells treated with doxo alone. Furthermore, results normalized for toxicity of compounds themselves reported in Fig. 2 show that Bazoton uno was able to significantly increase cytotoxicity at 10, 15 and 20 μM concentrations in combination with all doxo concentrations up to 30% ($p<0.05$). No cytotoxic effect of methanol of cell proliferation was observed (data not shown).

Effects of allopurinol, furosemide and Bazoton uno on ROS production in MES-SA/Dx5 cells

The effects of the three compounds and ver on cellular ROS production in MES-SA/Dx5 cells are shown in Fig. 3. No significant increase of ROS production was observed after treatment of MES-SA/Dx5 cells with all compounds at 10 μM concentrations ($p< 0.05$) compared to corresponding control cultures (medium alone). In contrast, a significant increase in ROS production was observed when cancer cells were treated with higher concentrations of all compounds (15 and 20 μM).

Table I. *Cytotoxic effects of doxo alone and in combination with the diuretics or ver in MES-SA/Dx5 cells.*

	Control	cyto%	doxo2μM	cyto%	doxo4μM	cyto%	doxo8μM	cyto%
Medium	1.12±0.04							
doxo2μM	1.29±0.01	14.9±3.7						
doxo4μM	1.37±0.02	22.5±5.6						
doxo8μM	1.41±0.01	25.6±5.4						
Ver10μM	1.18±0.06	4.41±3.8	1.4±0.03	25.3±7	1.51±0.01	35.1±5.9	1.6±0.02	43.1+4.5
A10μM	1.16±0.02	3.57±1	1.34±0.04	19.7±7.9	1.42±0.05	26.5±6.1	1.5±0.05	33.5±1
A15μM	1.2±0.05	6.2±1	1.4±0.05	24.6±0.63	1.44±0.06	29±0.8	1.53±0.02	35.6±3.2
A20μM	1.23±0.02	11.5±4.1	1.44±0.05	28.4±1	1.48±0.03	31.7±2.6	1.56±0.03	38.8±2.9
F10μM	1.16±0.02	3.4±3	1.35±0.04	20.8±3.7	1.4±0.01	25±5	1.48±0.02	31.8±3.4
F15μM	1.17±0.01	4.5±3.2	1.38±0.03	23.4±2.3	1.42±0.02	26.5±5.1	1.51±0.04	34.4±2.3
F20μM	1.2±0.05	8.7+5.3	1.4±0.04	24.3±4.4	1.46±0.02	30.3±4.9	1.52±0.03	35.9±4.5
B10μg	1.16±0.02	3.5±1	1.35±0.04	20.4±1.4	1.42±0.01	26.4±4.5	1.49±0.03	32.9±2.7
B15μg	1.15+0.05	4.5±2	1.4±0.02	25.3±5.3	1.48±0.02	29.4±5.1	1.54±0.04	37.6±1.6
B20μg	1.25±0.04	9.5±2.3	1.44±0.01	28.8±4.8	1.49±0.07	31.1±2.1	1.56±0.02	39.5±3.5

DISCUSSION

The use of inhibitors of drug transporters is a promising strategy to improve drug availability in cancer cells and to make chemotherapy more effective. In this study we showed that exposure of Pgp overexpressing human sarcoma MES-SA/dx5 cells to two synthetic compounds such as allopurinol and furosemide and a herbal extract, Bazoton uno, at *in vivo* achievable concentrations (11, 12), leads to the increase of doxo accumulation (up to 40%), when compared to untreated control cultures (without drugs) at all doxo concentrations used (2, 4, and 8 μM) (Fig. 1). However, highest increase of doxo retention was obtained using a lower doxo concentration in combination with higher concentrations of drugs. These results are consistent with an increased sensitivity of doxo resistant sarcoma cells toward doxo treatment, as measured by LDH test. As shown in Table I, all compounds increase cytotoxic effects of doxo in cancer cells at all concentrations, but this increase was higher at the lowest molar concentration (2 μM). Therefore, all compounds at lower doxo concentrations might antagonize MDR Pgp-mediated through competitive inhibition of the Pgp activity, resulting in a decrease in efficiency of the transport of doxo out of cells. These results were also in agreement with the assessment of the intracellular redox status (Fig. 3). In conclusion, our results demonstrated that allopurinol, furosemide and Bazoton uno, at therapeutic dosages, alone or in combination with doxo, were able to interfere with Pgp activity, rendering MDR cells susceptible to anticancer drugs. However, Bazoton uno had little cytotoxic activity and was as effective as synthetic drugs. Further studies are needed to verify the effectiveness of this compound, *in vitro* and *in vivo*. Nevertheless, the combination of anticancer drugs with Bazoton uno or its derivatives could represent a potential safe treatment for cancer patients with Pgp-mediated MDR.

ACKNOWLEDGEMENTS

We are grateful to Dr Giuliano Ciofani and Dr Domenico De Cesare for their technical assistance.

REFERENCES

1. Chen Z, Shi T, Zhang P, et al. Mammalian drug efflux transporters of the ATP binding cassette (ABC) family in multidrug resistance: A review of the past decade. Cancer Lett 2016; 370:153-64.
2. Binkhathlan Z, Lavasanifar A. P-glycoprotein inhibition as a therapeutic approach for overcoming multidrug resistance in cancer: current status and future perspectives. Curr Cancer Drug Targets 2013; 13:326-46.
3. Amaral L, Spengler G, Molnar J. Identification of important compounds from natural sources that have activity against multidrug-resistant cancer cell lines: effects on proliferation, apoptotic mechanism and the efflux pump responsible for multi-resistance phenotype. Anticancer Res 2016; 36:5665-72.
4. Angelini A, Di Ilio C, Castellani ML, Conti P, Cuccurullo F. Modulation of multidrug resistance P-glycoprotein activity by flavonoid and honokiol in human doxorubicin-resistant sarcoma cells (MES-SA/Dx5): implications for natural sedatives as chemosensitizing agents in cancer therapy. J Biol Regul Homeost Agents 2010; 24:197-205.
5. Angelini A, Conti P, Ciofani G, Cuccurullo F, Di Ilio C. Modulation of multidrug resistance P-glycoprotein activity by antiemetic compounds in human doxorubicin-resistant sarcoma cells (MES-SA/Dx5): implications on cancer therapy. J Biol Regul Homeost Agents 2013; 27:1029-37.
6. Angelini A, Ciofani G, Conti P. Antipsychotics reverse P-Glycoprotein-mediated doxorubicin resistance in human uterine sarcoma MES-SA/Dx5 cells: a novel approach to cancer chemotherapy. J Biol Regul Homeost Agents 2015; 29:357-65.
7. Mirrakhimov AE, Voore P, Khan M, Ali AM. Tumor lysis syndrome: A clinical review. World J Crit Care Med 2015; 4:130-38.
8. Goldman SC, Holcenberg JS, Finklestein JZ, et al. A randomized comparison between rasbucase and allopurinol in children with lymphoma or leukemia at high risk for tumor lysis. Blood 2001; 97:2998-3003.
9. Safarinejad MR. Urtica dioica for treatment of benign prostatic hyperplasia: a prospective, randomized double-blind, placebo-controlled, crossover study. J

Herb Pharmacotherapy 2005; 5:1-11.
10. Wesolowska O, Paprocka M, Koziak J, Motohashi N, Dus D, Michalak K. Human sarcoma cell lines MES-SA and MES-SA/Dx5 as a model for multidrug resistance modulators screening. Anticancer Res 2005; 25:383-89.
11. Nakajima A, Oda S, Yokoi T. Allopurinol induces innate responses through mitogen-activate protein kinase signalling pathways in HL-60 cells. J Appl Toxicol 2016; 36:1120-28.
12. Van Wart SA, Shoaf ES, Mallikaarjun S, Mager DE. Population-based meta-analysis of furosemide pharmacokinetics. Biopharm Drug Dispos 2014; 35:119-33.

JOURNAL OF BIOLOGICAL REGULATORS & HOMEOSTATIC AGENTS Vol. 33, no. 3, 999-1003 (2019)

LETTER TO THE EDITOR

SERUM BIOMARKERS FOR SEPSIS IN CHILDREN WITH FEBRILE NEUTROPENIA AND CANCER

A. RUGGIERO[1*], K. POCINO[2*], M. CATALANO[1], P. MAURIZI[1], M. D'AMBRA[1], D. RIZZO[1], S. TRIARICO[1], G. ATTINÀ[1], S. MASTRANGELO[1] and E.D. CAPOLUONGO[2]

[1]Pediatric Oncology Unit, Fondazione Policlinico A. Gemelli IRCCS - Università Cattolica Sacro Cuore, Rome, Italy; [2]Institute of Clinical Biochemistry, Fondazione Policlinico A. Gemelli IRCCS - Università Cattolica Sacro Cuore, Rome, Italy

Received November 18, 2018 – Accepted April 1, 2019

[*]These Authors contributed equally to this work

To the Editor,

The National Institute for Health and Care Excellence (NICE) defines febrile neutropenia or "neutropenic sepsis" as a patient with an absolute neutrophil count (ANC) <0.5 x 109/L and temperature >38°C or signs and symptoms of sepsis (1). Prompt diagnosis to rule out or confirm acute bacterial infection and response to established antimicrobial therapy are critical to the treatment and prognosis of patients with febrile neutropenia following chemotherapy for malignancy (2). Whilst in the majority of febrile episodes no causal infection is identified, 10-20% are secondary to a bloodstream infection. A positive blood culture is the gold standard for the diagnosis of infection; however, this examination requires time and it is not able to distinguish sepsis from colonisation. The markers usually adopted in the clinical practice are fever, leukocytosis, C-reactive protein (CRP), and procalcitonin (PCT) (3). CRP is an acute phase α-globulin produced by the liver, and it increases in the 24-48 hours after the onset of inflammation. At present, there are still no objective outcome-based clinical trial data to justify using CRP values alone (4). PCT is released by parenchymal tissues after an inflammatory reaction and bacterial endotoxins. In sepsis, PCT starts to increase after three hours and remains elevated throughout the episode (5). The aim of this study was to assess whether blood levels of calprotectin and presepsin were superior prognostic markers for febrile neutropenia compared with the serum levels of CRP and PCT. Calprotectin is mainly exhibited in the cytoplasm of neutrophils as a result of activation, it has an antibacterial, apoptosis-inducing and chemotactic role, and it increases during infectious and inflammatory status (6). Presepsin is the soluble form of CD14, produced by monocytes and macrophages, which recognises and induces phagocytosis of Gram-negative bacteria. Some clinical trials showed that the level of soluble CD14 increased significantly in patients with sepsis compared with healthy people, and the levels were related to the severity and prognosis of the disease (7-9). Presepsin is characterised by fast kinetics: the activation time from the onset of a bacterial or fungal event is two hours, with a peak concentration at three hours. The plasma half-life of this molecule is 4-5 hours. Thus, it is an early biomarker for diagnosis of sepsis (10).

Key words: sepsis; febrile neutropenia; procalcitonin; presepsin; children

Corresponding Author:
Antonio Ruggiero, MD
Pediatric Oncology Unit, Fondazione Policlinico A. Gemelli IRCCS, Università Cattolica Sacro Cuore
Largo A. Gemelli 8, 00168 Rome, Italy
Tel.: +39 06 30155165 - Fax: +39 06 3052751
e-mail: antonio.ruggiero@unicatt.it

0393-974X (2019)

DISCLOSURE: ALL AUTHORS REPORT NO CONFLICTS OF INTEREST RELEVANT TO THIS ARTICLE.

MATERIALS AND METHODS

Patient characteristics

The study was conducted at the Pediatric Oncology Unit, Fondazione Policlinico A. Gemelli IRCCS – Università Cattolica Sacro Cuore of Rome, Italy from January to December 2014. We evaluated data collected from patients admitted due to a febrile episode during a period of hematologic toxicity following a chemotherapy course. Twenty-five patients with solid tumors or hematological malignancies were enrolled in this prospective cohort study. Thirty-nine episodes of febrile neutropenia were registered. Neutropenia was defined as ANC < $0.5x10^9$/L at the onset of the fever. Fever was referred to an axillary body temperature ≤ 38.5°C in 1 measurement or ≥ 38°C in 2 or more measurements in a 4-hour period. Blood specimens were collected on the first, third and fifth day of fever. Presepsin, calprotectin, PCT and CRP were measured. In addition to this, 30 healthy subjects similar for age and sex to the patients were assessed as controls for the study.

Only patients with the following characteristics were enrolled: presence of a central venous catheter; in a hematologic toxicity period after chemotherapy; suffering from an episode of febrile neutropenia. For every patient two sets of blood cultures were taken on admission from a peripheral vein and all lumens of central venous catheters, along with urgent full blood count, urine analysis and urine culture, and a throat swab before empirical broad-spectrum antimicrobial therapy was started.

According to microbiological and clinical findings, episodes of febrile neutropenia were divided into two groups: group 1, febrile episodes with negative blood culture (CN), absence of signs of sepsis and of clinically/microbiologically documented local infection; group 2, febrile episodes with positive blood culture (CP) or a clinical diagnosed sepsis.

This study was approved by the Ethics Committee of our institution. An informed consent was obtained from all patients.

Sampling and laboratory analysis

Blood was collected into test tubes, 2 mL, then it was

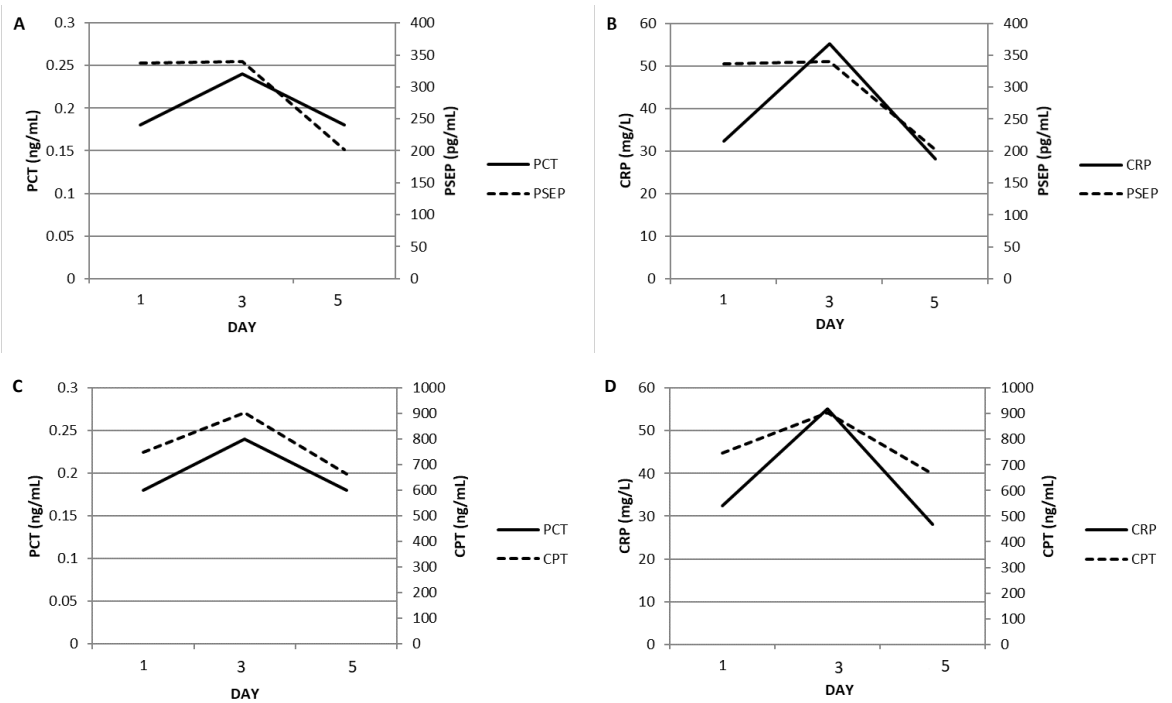

Fig. 1. *Trends of serum markers.* ***A)*** *PCT (continuous line)* vs *PSEP (dashed line);* ***B)*** *CRP (continuous line)* vs *PSEP (dashed line);* ***C)*** *PCT (continuous line)* vs *CPT (dashed line);* ***D)*** *CRP (continuous line)* vs *CPT (dashed line). Abbreviations. PCT: procalcitonin; PSEP: presepsin; CRP: C-reactive protein; CPT: calprotectin.*

centrifuged at 3700 rpm for 15 min and the serum was stored at -80°C for subsequent analysis. CRP and PCT were measured immediately with the ECLIA method on a Roche Cobas 8000 analytical platform (Mannheim, Germany), presepsin with ECLIA tests through the PATHFAST Presepsin tool (Medience Mitsubishi Chemical Corporation, Japan) and calprotectin with ELISA Calprest Eurospital (Trieste, Italy).

Statistical analysis

Continuous variables are expressed as median with ranges in brackets or Mean ± Standard Deviation. Differences of continuous variable were assessed by Mann-Whitney U test. For statistical analysis SPSS 15.0 version was used (Chicago, Illinois, USA). P-values equal to or less than 0.05 were considered significant.

RESULTS

A total of 25 patients were enrolled in our study, and a total of 39 febrile neutropenia episodes were considered evaluable. Group 1 included 25 episodes of febrile neutropenia, while 14 episodes were reported in group 2. The isolated pathogens from blood cultures were *Staphylococcus hominis*, *Sphingomonas p*., *Klebsiella p*., *Pseudomonas a*., *Enterococcus f*., *Staphylococcus h*. and *Candida p*.

The details of serum marker concentrations over febrile neutropenia days are shown in Table I.

The median value of presepsin on the first day of febrile neutropenia in CN patients (337 pg/mL, 113-1035) and in CP patients (373 pg/mL, 169-943), was significantly higher than in controls (99.7 pg/mL, 58.2-197) (P<0.001). The median values of PCT on the first day of febrile neutropenia in CN patients (0.13 ng/mL, 0.10-0.27) and in CP patients (0.13 ng/mL, 0.05-0.41), were significantly higher than in controls (0.02 ng/mL, 0.0-0.03) (P<0.001).

To investigate the influence of the sampling time on the dynamics of presepsin and PCT, the serum levels of these two markers were compared against the sample collection time. When compared with controls, presepsin and PCT were significantly higher at onset, on the third and fifth day compared with controls (P<0.001). The median value of presepsin was 237 pg/mL (125-779) and 175 pg/mL (83.5-603) in CN patients, and 374 pg/mL (105-499) and 277 pg/mL (142-1158) in CP patients on the third and fifth day, respectively. In both cases the concentrations decreased over 5 days.

Likewise, the median value of PCT was 0.18 ng/mL (0.09-1.30) and 0.12 ng/mL (0.08-0.64) in CN patients, and 0.23 ng/mL (0.09-0.80) and 0.14 ng/mL (0.06-0.73) in CP patients on the third and fifth day,

Table I. *Concentrations of serum markers on days 1, 3, 5 during febrile episodes. CRP: C-reactive protein; PCT: procalcitonin; PSEP: presepsin; CP: culture positive; CN: culture negative.*

	CRP Day 1	CRP Day 3	CRP Day 5	PCT Day 1	PCT Day 3	PCT Day 5	PSEP Day 1	PSEP Day 3	PSEP Day 5
		mg/L			ng/mL			pg/mL	
Total episodes	32.4 (0.09-184.3)	55.1 (0.1-287.5)	28.1 (0.07-214.2)	0.18 (0.05-1.18)	0.24 (0.09-39.34)	0.18 (0.06-6.86)	337 (113-1035)	340 (105-1017)	202 (83.5-1158)
CP episodes	28.7 (10.5-184.3)	54.2 (10.2-206.2)	28.8 (0.34-214.2)	0.13 (0.05-0.41)	0.23 (0.09-0.80)	0.14 (0.06-0.73)	373 (169-943)	374 (105-499)	277 (142-1158)
CN episodes	31.4 (0.09-119.7)	24.2 (0.1-147.5)	8.7 (0.07-115.3)	0.13 (0.10-0.27)	0.18 (0.09-1.30)	0.12 (0.08-0.64)	337 (113-1035)	273 (125-779)	175 (83.5-603)
Episodes of mucositis	37.9 (10.5-184.3)	57.6 (3.62-206.2)	43.6 (0.34-214.2)	0.20 (0.05-1.06)	0.28 (0.09-1.11)	0.22 (0.06-0.73	322 (169-943)	340 (105-771)	270 (120-1158)
Healthy controls		2.3 (0.05-3.0)			0.02 (0.0-0.03)			99.7 (58.2-197)	

respectively. In the subgroup of patients who also presented a mucositis, the trends of serum marker were the same of the above-mentioned groups (Table I).

In addition, we analysed the performance of the other two markers, CRP and calprotectin, on days 1, 3 and 5. The median concentration of CRP was already high on day 1, 32.4 mg/L (0.09-184.3). It then increased on day 3, 55.1 mg/L (0.1-287.5) and decreased on day 5, 28.1 mg/L (0.07-214.2) (Table I) without statistically significant differences between groups. Even the calprotectin mean values were very high on day 1 (747±803 ng/mL), they decreased on day 3 (904±1878 ng/mL), and were even more reduced on day 5 (665±766 ng/mL).

DISCUSSION

In this study, we measured and compared 4 blood infection indicators to understand which one is the most useful in guiding clinicians for the most appropriate treatment for febrile neutropenia. In Fig. 1 presepsin and calprotectin are compared individually to PCT and CRP. Fig. 1A shows that PCT and presepsin concentrations were both high on day 1, with an increase on day 3 and a decrease on day 5. In addition to this, while median PCT levels on day 1 are still below the range for sepsis (<0.5 ng/mL), presepsin has already reached range values indicative of sepsis (>200 pg/mL). In 34 out of 39 episodes, the concentrations of presepsin on the first day of febrile neutropenia were between 200 and 1000 pg/mL. This increase is also described by Koh et al. (11), and is an indication of high sensitivity for infection. Fig. 1B shows the same trend for both CRP and presepsin markers, although the increase of presepsin is earlier than CRP. The decrease of presepsin on day 5 is greater than CRP, suggesting a response to antibiotics, with persistence of the inflammatory disease. Fig. 1C shows the same trend of PCT and calprotectin concentrations over 1 to 5 days. Over 5 days, PCT decreases more than calprotectin during antibiotic treatment, due to infection remission. The calprotectin instead remains at higher values on day 5 as for ongoing inflammation. Finally, by comparing the measurements of CRP and calprotectin (Fig. 1D), calprotectin was higher than CRP on day 1, but both concentrations decreased from day 3 to day 5.

The results did not allow us to discriminate significantly between CP and localised infection, as was also seen in the report by Urbonas et al. (12). Furthermore, the median serum concentration of presepsin on day 1 was higher in CP febrile episodes when compared with the CN group, although this did not show a statistically significant difference (P=0.05). However, it is possible that an insufficient number of cases may have led to the lack of statistical significance. In this study, we observed that during febrile neutropenia, presepsin levels increased significantly earlier than PCT levels. Furthermore, Endo et al. (10) reported a lower specificity and sensitivity of PCT compared with presepsin, for the diagnosis of bacterial infections. Moreover, our data show a rapid decrease of presepsin levels in CN episodes during the first 5 days, suggesting remission from infection. This information would allow the clinician to stop earlier antibiotic treatment in patients who no longer needed it.

In conclusion, presepsin was shown to be a more useful marker of early sepsis than PCT, and while serum calprotectin has an important antimicrobial role, CRP is useful for monitoring the response to antibiotic therapy.

REFERENCES

1. Bate J, Gibson F, Johnson E, Selwood K, Skinner R, Chisholm J; National Institute for Clinical Excellence. Neutropenic sepsis: prevention and management of neutropenic sepsis in cancer patients (NICE Clinical Guideline CG151). Arch Dis Child Educ Pract Ed 2013; 98:73-75.
2. Ruggiero A, Rizzo D, Attinà G, et al. Phase I study of temozolomide combined with oral etoposide in children with recurrent or progressive medulloblastoma. Eur J Cancer 2010; 46(16):2943-49.
3. Wu CW, Wu JY, Chen CK, et al. Does procalcitonin, C-reactive protein, or interleukin-6 test have a role in the diagnosis of severe infection in patients with febrile neutropenia? A systematic review and meta-analysis Support Care Cancer 2015; 23:2863-72.
4. Jaye DL, Waites KB. Clinical applications of C-reactive protein in pediatrics. Pediatr Infect Dis J 1997; 16:735-46.
5. Agarwal S, Akbas N, Soundar EP, Gonzalez G,

Devaraj S. Validation of the procalcitonin (PCT) assay: Experience in a pediatric hospital. Clin Biochem 2015; 48:886-90.

6. Stríz I, Trebichavský I. Calprotectin - a pleiotropic molecule in acute and chronic inflammation. Physiol Res 2004; 53:245-53.
7. Zou Q, Wen W, Zhang XC. Presepsin as a novel sepsis biomarker. World J Emerg Med 2014; 5:16-19.
8. Romualdo LG, Torrella PE, González MV, et al. Diagnostic accuracy of presepsin (soluble CD14 subtype) for prediction of bacteremia in patients with systemic inflammatory response syndrome in the Emergency Department. Clin Biochem 2014; 47:505-508.
9. Olad E, Sedighi I, Mehrvar A, Tashvighi M, Fallahazad V, Hedayatiasl A, Esfahani H. Presepsin (scd14) as a marker of serious bacterial infections in chemotherapy induced severe neutropenia. Iran J Pediatr 2014; 24:715-22.
10. Endo S, Suzuki Y, Takahashi G, et al. Usefulness of presepsin in the diagnosis of sepsis in a multicenter prospective study. J Infect Chemother 2012; 18:891-97.
11. Koh H, Aimoto M, Katayama T, et al. Diagnostic value of levels of presepsin (soluble CD14-subtype) in febrile neutropenia in patients with hematological disorders. J Infect Chemother 2016; 22:466-71.
12. Urbonas V, Eidukaitė A, Tamulienė I. The predictive value of soluble biomarkers (CD14 subtype, interleukin-2 receptor, human leucocyte antigen-G) and procalcitonin in the detection of bacteremia and sepsis in pediatric oncology patients with chemotherapy-induced febrile neutropenia. Cytokine 2013; 62:34-37.

JOURNAL OF BIOLOGICAL REGULATORS & HOMEOSTATIC AGENTS Vol. 33, no. 3, 1005-1009 (2019)

LETTER TO THE EDITOR

ANTI-CALCULUS EFFICACY OF PERIOGEN® ORAL RINSE IN GINGIVITIS PATIENTS

A. BALLINI[1*], S. CANTORE[1,2,3*], G. DIPALMA[4*], D. DE VITO[1], R. SAINI[4], S.R. SAINI[4], P. GEORGAKOPOULOS[5], C. GARGIULO ISACCO[4,6*] and F. INCHINGOLO[4*]

[1] Department of Basic Medical Sciences, Neurosciences and Sense Organs, University of Bari Aldo Moro, Bari, Italy; [2]POLYPHENO S.r.l., Accredited Spin Off, University of Bari Aldo Moro, Bari, Italy; [3]Sorriso & Benessere Ricerca e Clinica S.r.l., Bari, Italy; [4]Department of Interdisciplinary Medicine, School of Medicine, University of Bari Aldo Moro, Bari, Italy; [5]Dentist Education Institute, Athens, Greece; [6]Human Stem Cells Research Center, Ho Chi Minh City, Vietnam

Received March 19, 2019 – Accepted April 12, 2019

[*]These Authors contributed equally to the work

To the Editor,

Dental calculus is calcified dental plaque, composed primarily of calcium (Ca) and phosphorous (P) ions deposited between and within remnants of formerly viable microorganisms (1). In a healthy oral environment, saliva is supersaturated with Ca and P levels, however, without precipitation. Nonetheless, when this equilibrium is disturbed, dental calculus is formed enhanced by elevated salivary pH (2). Dental calculus is formed with four different crystals of Ca–P, brushite, octa Ca–P, hydroxyapatite and whitlockite, in which the most abundant crystals are the hydroxyapatite and octa Ca–P, which can lead to gingivitis and periodontitis (3).

In populations that practice regular oral hygiene and with access to regular professional care, supra-gingival dental calculus formation is restricted to tooth surfaces adjacent to the salivary ducts (4). Supra-gingival calculus formation can be controlled by chemical mineralization inhibitors, applied in toothpastes or mouth rinses. These agents act to delay plaque calcification, keeping deposits in an amorphous non-hardened state to facilitate removal with regular hygiene. Clinical efficacy for these agents is typically assessed as the reduction in tartar area coverage on the teeth between dental cleaning (5). This mineralization of dental plaque can be delayed by the presence of crystallization inhibitors, such as pyrophosphate (6).

The purpose of the present study was to evaluate the anti-calculus efficiency of a mouthwash containing a combination of sodium tripolyphosphate, tetrapotassium pyrophosphate, sodium bicarbonate and citric acid (Periogen®) in patients affected with gingivitis.

MATERIALS AND METHODS

The present study was conducted at the Dental Unit (Dentist Education Institute) of the City Unity College, Greece, from October 2018 to January 2019 in collaboration with the University of Bari Aldo Moro, Italy. In order to have the unbiased and accurate clinical data, a double-blind protocol for enrolment of the patients in terms of treatment plan and further categorization in the study group was carried out for a total of 30 gingivitis

Key words: salivary calcium, salivary phosphorus, dental calculus, plaque index, anti-calculus mouthwash

Corresponding Author:
Dr. Andrea Ballini,
University of Bari Aldo Moro,
P.zza Giulio Cesare, 11,
70124, Bari, Italy
Tel./fax: +39 0805448514.
e-mail: andrea.ballini@me.com

0393-974X (2019)

DISCLOSURE: ALL AUTHORS REPORT NO CONFLICTS OF INTEREST RELEVANT TO THIS ARTICLE.

patients (from moderate to severe) between the ages of 18 and 40 years. All eligible subjects were given oral information about the products and the purpose of the study and gave an informed consent, in accordance with the ethical principles originating in the Declaration of Helsinki and consistent with good clinical practices.

Prior to the study period, the volunteers received an oral soft and hard tissue examination and a professional scaling and polishing to remove all calculus, plaque and extrinsic tooth stains. This was performed using hand instruments, mechanical scalers, rotating brushes with polishing paste, and dental floss in the interproximal areas. All candidates were screened for suitability by the research team. Selection criteria was a dentition with ≥20 evaluable teeth (minimum of five teeth per quadrant), no oral lesions, no severe periodontal problems (no probing depth ≥5 mm), and no removable prostheses or orthodontic bands or appliances. Persons allergic to several mouthwash components were excluded from the study. All the subjects were advised to brush twice daily for 5 minutes using a modified bass method technique (technique demonstrated to each subject), and similar medium bristle toothbrushes and toothpaste were provided to each of the subjects during the study course to maintain standardization.

The subjects were then categorized into two treatment regimes, groups I and II (15 subjects in each). All of the mouth rinse bottles had similar appearance. Periogen® was pre-reconstructed by the investigators and then delivered to the subjects in an anonymous bottle.

Group I (n = 15): Oral rinse containing sodium tripolyphosphate, tetrapotassium pyrophosphate, sodium bicarbonate and citric acid (Periogen®);

Group II (n = 15): Placebo oral rinse (physiologic saline solution with no mouthwash active principles added).

Subjects in both groups were instructed to rinse their mouth with 10 ml of mouthwash daily after breakfast and and after lunch for 90 days (twice for the first 60 days, than once per day for the following 30 days) for at least 1 min and not to rinse with water thereafter and for the following 30 min. All bottles with mouthwash were pre-weighed. All participants were instructed to refrain from using any other means of oral hygiene during the experimental period. Written instructions were provided explaining how to use the mouthwash. Rinsing was performed at home without supervision. To check for compliance, subjects were asked to note the times of day when they rinsed (1).

Clinical parameters evaluated by the same blinded trained examiner at baseline (prior oral hygiene procedures) and at 90 days were Calculus, Plaque and Oral Hygiene Index-simplified scores, according, respectively, to Silness-Löe, and Greene and Vermillion (1-7). All the clinical parameters were assessed by a trained experienced dental examiner under standard dental office and light source conditions. Moreover, for plaque/calculus detection, a disclosing agent (ultraviolet-induced fluorescence: fluorescein dye) was used to disclose the plaque during the examination. All measurements were carried out under the same conditions by the same blinded investigator. All returned mouthwash bottles were weighed to calculate the amount of mouth rinse used and to check for compliance.

Saliva collection

In addition to the clinical study, a laboratory study was also performed. Unstimulated, directly expectorated, whole saliva samples were collected in clean, dry, sterile graduated 5-mL test tubes. Participants were instructed not to consume food (neither solids nor liquids) 2 h before sampling and were asked to rinse their mouth with distilled water 10 min prior to collection. The subjects were asked to allow saliva (at least 3 mL) to drool from the oral cavity into the sterile test tube. The subjects were refrained from talking and asked to drop the head down and not to cough up mucus as saliva was collected. The subjects were then asked to let the saliva pool in their floor of the mouth to their maximum extent and then expectorate into the collecting vessel till the desired quantity was collected. Samples from all the participants were collected between 10:00 am and 11.30 am, 2 h after the last meal, to standardize the collection according to the circadian rhythm. The saliva was then transported to the laboratory within 1 hour where it was stored at -20°C. The test tube was then centrifuged at 3000 rpm for 5 min to remove the particulates in the collected saliva. Estimation of calcium and phosphorus was made using a commercial kit.

Statistical analysis

All data were collected and statistically evaluated. The statistical analyses were performed by using Statistical Package for Social Sciences (SPSS for Windows, Version 11.5, Chicago, Ill) software.

RESULTS

All subjects (N = 30) completed the trial, and there were no missing values. The amounts of mouthwashes used indicated good compliance with the instructions. No adverse events or side effects were reported or observed.

All the clinical parameters, were recorded for both groups during the study at baseline (TO) and at the end of study, at 90 days (T1). The clinical scores for the test and control groups at baseline and the end of the experimental study period are shown in Fig. 1 A-C.

It is very interesting that both the mean salivary calcium and the mean phosphorus content in the test group were found to be lower when compared to the control group (Fig. 2 A-B).

The clinical scores for the test and control groups at baseline and the end of the experimental study period are shown in Fig. 1 A-C, showing a reduction of 60% from baseline in the test group, compared to the control group (40% from baseline) for the Oral Hygiene Index and a reduction of 50% from baseline in the test group, compared to the control group (25% from baseline) for Plaque index, and a reduction of 70% from baseline in the test group, compared to the control group (30% from baseline) for Calculus index. The Ca and P in the saliva of subjects at baseline and at 90 days intervals are reported in Fig. 2, showing a reduction of 33% and 37%, respectively, from baseline in the test group, compared to the control group (5% and 3% from baseline).

DISCUSSION

In oral diagnostics there is a great challenge to establish biomarkers for screening and evaluating the

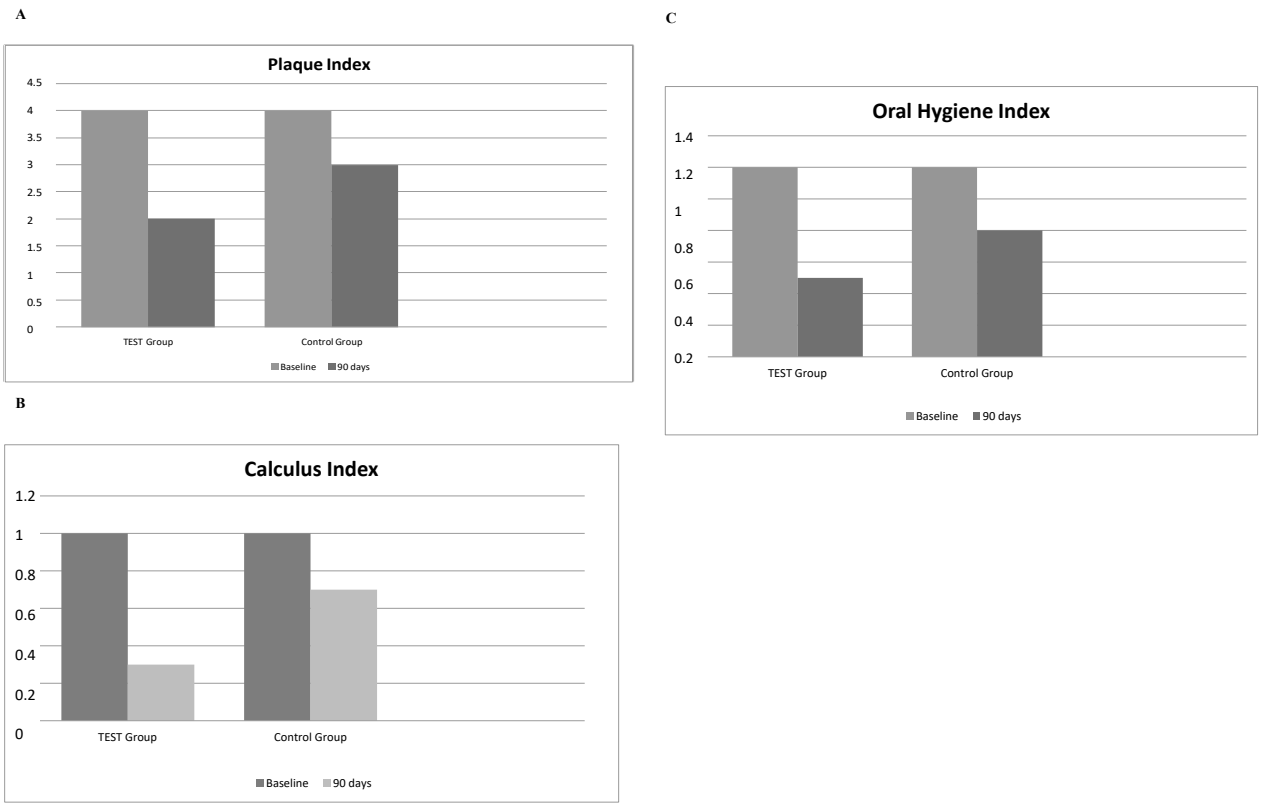

Fig. 1. *Clinical index results before and after the study period: plaque index (**A**) Calculus Index (**B**) and Oral Hygiene Index-simplified (**C**) scores.*

A

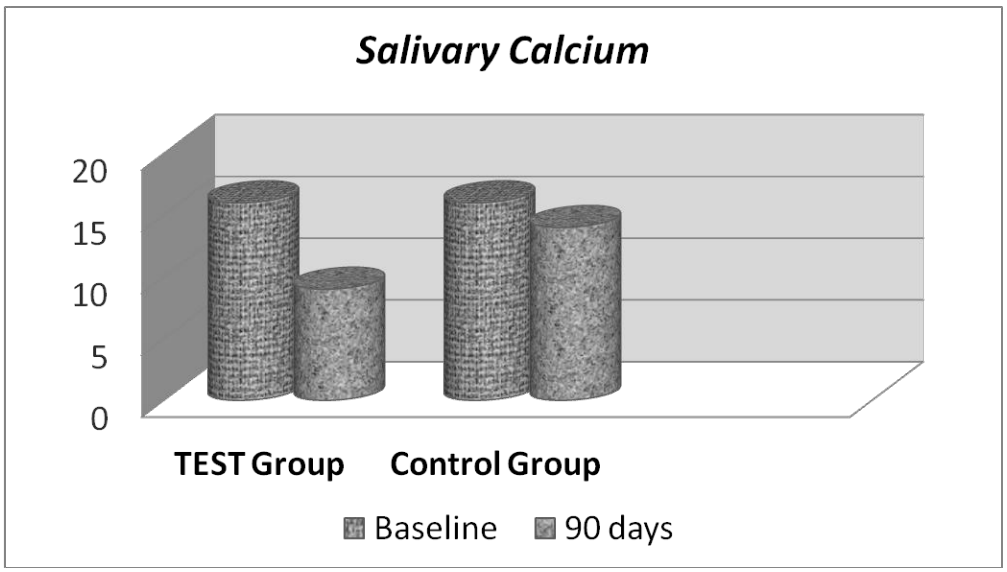

B

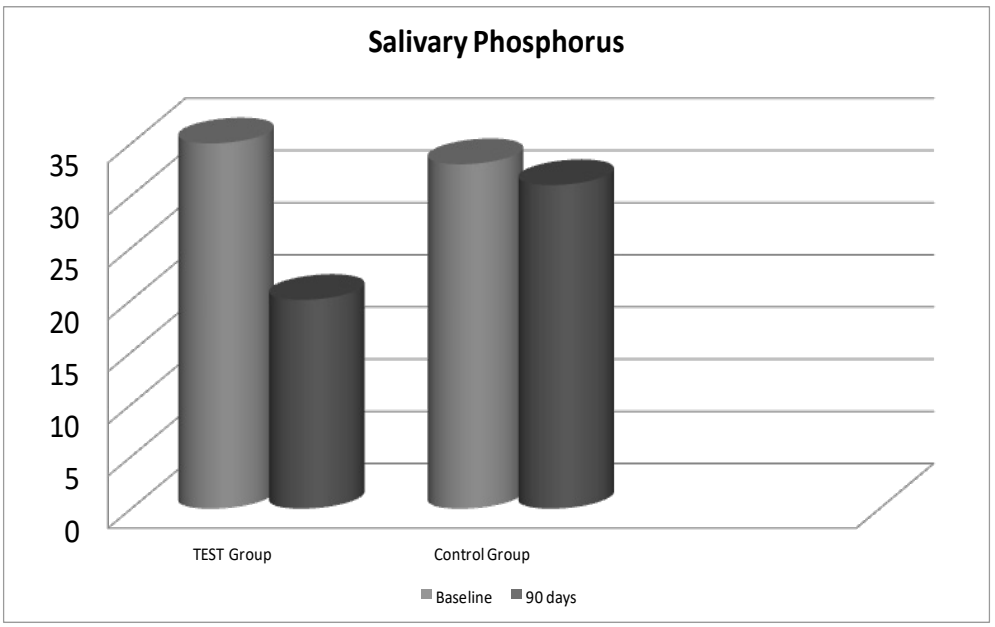

Fig. 2. *Estimation of salivary calcium (**A**) and phosphorus (**B**) before and after the study period.*

disease activity. Biomarkers can also serve as a useful tool to evaluate the efficacy of the therapy. This study was conducted through careful sample collection and laboratory analysis resulting in significant data supporting the usefulness of Periogen® (1).

Low salivary buffering capacity, and low Ca and P levels show a pronounced link to increased caries. Preservation of the equilibrium between demineralization and remineralization depends on the ionic concentration of Ca and P in saliva which, in turn, is influenced also by alkaline phosphatase levels (7-10).

In the present study, when salivary inorganic Ca and P levels were compared in patients with gingivitis

and the control group, the results were statistically highly significant, showing a reduction in the both clinical indexes and levels of Ca and P in test patients when compared to healthy controls. These results support that Periogen®, delaying the mineralization of dental plaque by the presence of crystallization inhibitors, such sodium tripolyphosphate, tetrapotassium pyrophosphate, sodium bicarbonate and citric acid, worked significantly to decrease all the clinical and biomarkers parameters.

The use of mouthwashes such as Periogen® can aid to support the adequate level of Ca and P that are responsible for the significant deposition of these minerals in plaque that deeply reduces the development of gingivitis in the adjacent enamel.

This being a short-term study, the results can be used as baseline data for future studies with similar study design. However, the clinical interpretation of results obtained in this case-control study should be further substantiated incorporating a larger sample size in order to conclude the specific role played by saliva as a host-protective factor in gingivitis patients.

REFERENCES

1. Cantore S, Ballini A, Mori G, et al. Anti-plaque and antimicrobial efficiency of different oral rinses in a 3-day plaque accumulation model. J Biol Regul Homeost Agents 2016; 30:1173-78.
2. Inchingolo F, Dipalma G, Cirulli N, et al. Microbiological results of improvement in periodontal condition by administration of oral probiotics. J Biol Regul Homeost Agents 2018; 32:1323-28.
3. Ballini A, Cantore S, Farronato D, et al. Periodontal disease and bone pathogenesis: the crosstalk between cytokines and porphyromonas gingivalis. J Biol Regul Homeost Agents 2015; 29:273-81.
4. Inchingolo F, Ballini A, Cagiano R, et al. Immediately loaded dental implants bioactivated with platelet-rich plasma (PRP) placed in maxillary and mandibular region. Clin Ter 2015; 166:e146-52.
5. Cantore S, Ballini A, De Vito D, et al. Clinical results of improvement in periodontal condition by administration of oral probiotics. J Biol Regul Homeost Agents 2018; 32:1329-34.
6. Ballini A, Cantore S, Fotopoulou EA, et al. Combined sea salt-based oral rinse with xylitol in orthodontic patients: clinical and microbiological study. J Biol Regul Homeost Agents 2019; 33:263-68.
7. Grassi FR, Pappalettere C, Di Comite M, et al. Effect of different irrigating solutions and endodontic sealers on bond strength of the dentin-post interface with and without defects. Int J Med Sci 2012; 9:642-54.
8. Foti C, Sforza V, Rizzo C, et al. Cutaneous manifestations of Mycobacterium gordonae infection described for the first time in Italy: a case report. Cases J 2009; 2:6828.
9. Cicinelli E, Ballini A, Marinaccio M, Poliseno A, Coscia MF, Monno R, De Vito D. Microbiological findings in endometrial specimen: our experience. Arch Gynecol Obstet 2012; 285:1325-29.
10. Pettini F, Savino M, Corsalini M, Cantore S, Ballini A. Cytogenetic genotoxic investigation in peripheral blood lymphocytes of subjects with dental composite restorative filling materials. J Biol Regul Homeost Agents 2015; 29:229-33.

LETTER TO THE EDITOR

A TECHNICAL NOTE FOR THE USE OF SMALL-DIAMETER CANNULA FOR LIPOASPIRATION TECHNIQUE IN AESTHETIC RECONSTRUCTIVE POST-ONCOLOGICAL SURGERY

F.M. ABENAVOLI[1], A.D. INCHINGOLO[2], A.M. INCHINGOLO[2], G. DIPALMA[2] and F. INCHINGOLO[2]

[1]Department of Maxillofacial Surgery, "San Pietro" Hospital, Fatebenefratelli, Rome, Italy; [2]Department of Interdisciplinary Medicine, University of Bari, Bari, Italy

Received April 1, 2019 – Accepted April 17, 2019

To the Editor,

Skin cancer basal cell carcinoma (BCC) is a quite common lesion with a worldwide annual incidence between 3% and 8%. BCCs have been recently renamed as 'Keratinocyte cancer': this term also includes the cutaneous squamous cell carcinoma (cSCC), thus representing more than 90% of malignant skin tumours (1).

The increasing of BCC may be related to some environmental factors which are able to trigger changes in several tissues, also through activation of local stem cells (2, 3), leading to abnormalities in the physiology of epithelium. Oxidative stress (4, 5), infections, systemic factors (6, 7), chronic traumatisms (8) and preneoplastic lesions (9) are the most influencing factors leading to oncological transformation of a healthy tissue.

Tissue reconstruction should be even biologically driven: to date, scientific literature has reported several biomimetic scaffolds usable in reconstructive surgery, such as biomatrices (10-12) and biomaterials, even if the success rate strongly depends on the surgeon's experience in these specific surgical procedures.

Nowadays, the naso-genial flap is one of the safest and usable flaps for the reconstruction of the labial and nasal region after the invasive surgery aimed to a full BCC excision; in fact, the proximity of this flap to the area to be treated, the similar colour of the skin and the technical possibility to perform a single-time surgery to both harvest the flap and remove the lesion in the area to be then reconstructed, make it highly preferred by surgeons. The close angular artery is able to ensure an adequate perfusion in the flap zone, allowing the flap to be properly mobilized. The only drawback may be represented by the need to leave a small amount of subcutaneous tissue *in situ*, in order not to compromise the proper vascularization of the flap.

In this protocol, however, patients may experience an aesthetic issue, represented by an important swelling along the flap. In such cases, an appropriate pharmacological therapy may reduce the swelling in the area of the flap: however, in this context, in order to prevent the most severe swelling, we started to use a novel method using the small-diameter cannula for a lipoaspiration technique (SDCL). The SDCL technique consists of a few simple passages: firstly, surgeons should correctly mark the area of the flap, and an infiltration with local anaesthetic should be performed around the marked area. After few minutes, through a minimal incision in the peripheric

Key words: lipoaspiration; adipose-based scaffold; inflammation; tissue regeneration

Corresponding Author:
Prof. Francesco Inchingolo,
D.I.M.,
Department of Interdisciplinary Medicine,
University of Bari,
Bari, Italy
e-mail: prof.inchingolo@libero.it

0393-974X (2019)

DISCLOSURE: ALL AUTHORS REPORT NO CONFLICTS OF INTEREST RELEVANT TO THIS ARTICLE.

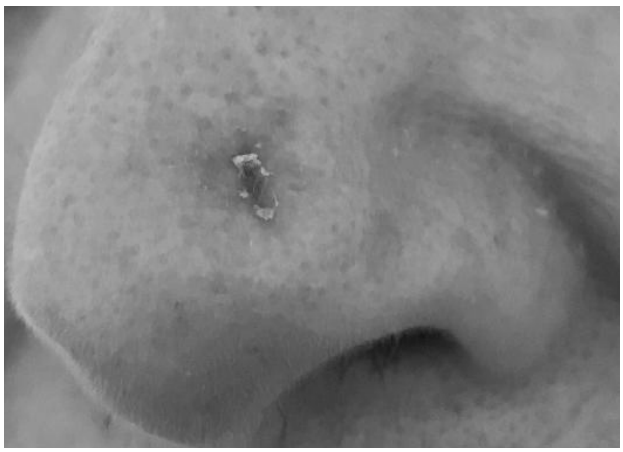

Fig. 1. *Preoperative basal cell lesion of the nose.*

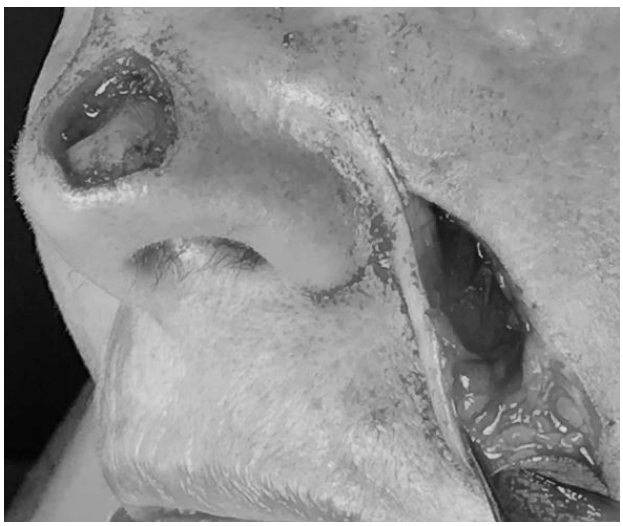

Fig. 2. *Incision of the flap: the presence is evident of a reduced thickness of subcutaneous adipose tissue.*

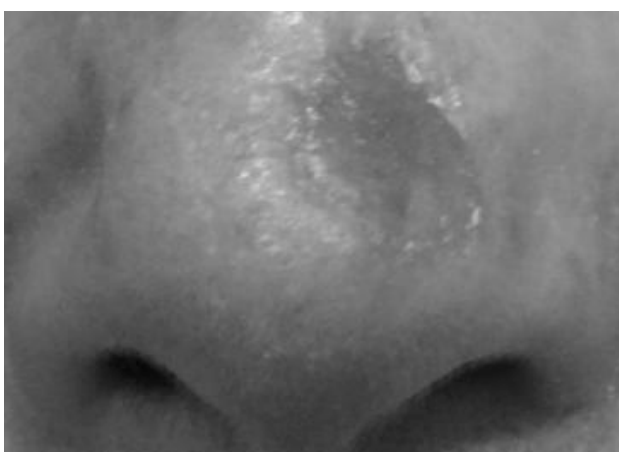

Fig. 3. *Eight-month post-surgery follow-up.*

area of the flap, the surgeon should gently enter with the cannula and start to aspirate with a small-sized syringe: after sufficient adipose thickness has been obtained, the flap is excised as usually described in scientific literature, and finally the flap is repositioned and fixed with internal stitches.

Case report

We report the case of a 67-year-old patient with basal cell lesion at the tip of the nose (Fig. 1). After the removal of the entire lesion, the SDCL technique was performed. A slight liposuction was carried out just under the flap area, and finally the flap was used together with adipose support (Fig. 2), after a superficial disepithelization; the flap was located in a dorsal pocket, in order to avoid any visible incision on the side of the nose. The clinical and aesthetical results after 8 months were extremely satisfactory (Fig. 3). Despite reporting only 1 case, we can assure that this technique is effective and useful for several types of surgical reconstruction.

The patient gave informed, signed consent for this case report to be published.

Conclusion

The correct use of SDCL technique will allow the surgeons to use the subcutaneous adipose tissue in order to obtain a novel adipose-based scaffold, highly compatible with the area in which the flap us to be placed. This technique will ensure reduced swelling, faster post-surgery follow-up, and a better aesthetic result.

REFERENCES

1. Sánchez G, Nova J, Rodriguez-Hernandez AE, et al. Sun protection for preventing basal cell and squamous cell skin cancers. Cochrane Database Syst Rev 2016; 7:CD011161.
2. Paduano F, Marrelli M, Palmieri F, Tatullo M. CD146 expression influences periapical cyst mesenchymal stem cell properties. Stem Cell Rev 2016; 12(5):592-603.
3. Paduano F, Marrelli M, Amantea M, et al. Adipose tissue as a strategic source of mesenchymal stem cells in bone regeneration: a topical review on the most promising craniomaxillofacial applications. Int

J Mol Sci 2017; 18(10).
4. Tatullo M, Marrelli M, Scacco S, et al. Relationship between oxidative stress and "burning mouth syndrome" in female patients: a scientific hypothesis. Eur Rev Med Pharmacol Sci 2012; 16(9):1218-21.
5. Tatullo M, Gentile S, Paduano F, Santacroce L, Marrelli M. Crosstalk between oral and general health status in e-smokers. Medicine (Baltimore) 2016; 95(49):e5589.
6. Inchingolo F, Tatullo M, Abenavoli FM, et al. Non-syndromic multiple supernumerary teeth in a family unit with a normal karyotype: case report. Int J Med Sci 2010; 7(6):378-84.
7. Inchingolo F, Tatullo M, Abenavoli FM, Marrelli M, Inchingolo AD, Inchingolo AM, Dipalma G. Non-Hodgkin lymphoma affecting the tongue: unusual intra-oral location. Head Neck Oncol 2011; 3:1.
8. Inchingolo F, Tatullo M, Abenavoli FM, et al. Oral piercing and oral diseases: a short time retrospective study. Int J Med Sci 2011; 8(8):649-52.
9. Tatullo M, Marrelli M, Amantea M, Paduano F, Santacroce L, Gentile S, Scacco S. Bioimpedance detection of oral lichen planus used as preneoplastic model. J Cancer 2015; 6(10):976-83.
10. Inchingolo F, Tatullo M, Marrelli M, et al. Regenerative surgery performed with platelet-rich plasma used in sinus lift elevation before dental implant surgery: an useful aid in healing and regeneration of bone tissue. Eur Rev Med Pharmacol Sci 2012; 16(9):1222-26.
11. Aulino P, Costa A, Chiaravalloti E, et al. Muscle extracellular matrix scaffold is a multipotent environment. Int J Med Sci 2015; 12(4):336-40.
12. Inchingolo F, Tatullo M, Marrelli M, et al. Clinical trial with bromelain in third molar exodontia. Eur Rev Med Pharmacol Sci 2010; 14(9):771-74.